Stable isotopes analysis to assess abiotic and biotic remediation of groundwater polluted by chlorinated methanes

Diana Rodríguez Fernández

2018

STABLE ISOTOPES ANALYSIS TO ASSESS ABIOTIC AND BIOTIC REMEDIATION OF GROUNDWATER POLLUTED BY CHLORINATED METHANES

STABLE ISOTOPES ANALYSIS TO ASSESS ABIOTIC
AND BIOTIC REMEDIATION OF GROUNDWATER
POLLUTED BY CHLORINATED METHANES

Diana Rodríguez Fernández
PhD thesis 2018

ACCES
PROHIBIT
ZONA
CONTAMINADA

Diana Rodríguez Fernández

Departament de Mineralogia, Petrologia i Geologia aplicada
Facultat de Ciències de la Terra

UNIVERSITAT DE BARCELONA

MAiMA
ISÒTOPS ESTABLES I MINERALOGIA

UNIVERSITAT DE BARCELONA

Facultat Ciències de la Terra

Departament de Mineralogia, Petrologia i Geologia Aplicada

STABLE ISOTOPES ANALYSIS TO ASSESS ABIOTIC

AND BIOTIC REMEDIATION OF GROUNDWATER

POLLUTED BY CHLORINATED METHANES

Tesi doctoral presentada per:

Diana Rodríguez Fernández

Per aspirar a l'obtenció del títol de doctora per la Universitat de Barcelona amb Menció Internacional.

Tesi realitzada en el marc del Programa de Doctorat de Ciències de la Terra, sota la co-direcció de la Dra. Mònica Rosell Linares i la Dra. Cristina Domènech Ortí, i tutoritzada pel Dr. Albert Soler i Gil

Dra. Mònica Rosell Linares   **Dra. Cristina Domènech Ortí**

Dr. Albert Soler i Gil

Aos meus avós

AGRADECEMENTOS/AGRAïMENTS/AGRADECIMIENTOS/ACKNOWLEDGEMENTS

Gracias a la beca de Formación de Profesorado Universitario FPU2012/01615 del Ministerio de Educación, Cultura y Deporte que me ha permitido realizar la tesis, así como también a las ayudas para Estancias Breves asociadas a esta beca que sufragaron la estancia en Múnich. Gracias también a la Fundación Pedro i Pons 2014 por costear la estancia en Neuchâtel.

Gràcies a les meves directores de tesi, la Dra. Cristina Domènech i la Dra. Mònica Rosell, per les encertades correccions, suggeriments i aportacions realitzades al llarg de tota la tesi que han permès que aquest treball de recerca s'hagi pogut dur a terme. Gràcies pel suport científic i acadèmic ofert i per la paciència i perseverança demostrada i inculcada en tot moment, sobretot durant les llargues reunions i els llargs processos de publicació dels articles. Gràcies també per les paraules d'ànim i per tots aquells moments que m'han ajudat a créixer com a persona.

Dr. Albert Soler, gràcies per donar-me l'oportunitat de realitzar aquesta tesi en el grup MAIMA així com per haver confiat en mi per a la col·laboració en projectes tant públics com d'empresa privada. Gràcies per poder haver participat en la docència de les pràctiques de l'assignatura de Mineralogia del primer curs d'Enginyeria Geològica, que ha format part de la meva formació dintre de les beques FPU (Formació de Professorat Universitari, Ministerio de Educación, Cultura y Deporte) i APIF (Ajuts de Personal Investigador en Formació, UB).

Gràcies al Departament de Mineralogia, Petrologia i Geologia Aplicada de la Facultat de Ciències de la Terra per tots aquests anys.

Gràcies al personal dels Centres Científics i Tecnològics de la Universitat de Barcelona, en concret al de l'àrea de Cromatografia de gasos – Espectrometria de masses aplicada, pels serveis oferits. En concret agraeixo l'ajuda rebuda per la Dra. Pilar Teixidor, la Lourdes Berdie, la Pilar Rubio, l'Anna Navarro, l' Asunción Marin i per la Sete.

Gracias a la Dra. Clara Torrentó por su gran apoyo durante toda la tesis, ya sea a través de la ayuda técnica y científica recibida como a través de la humanidad y empatía que me ha demostrado en todo momento. En concreto, querría agradecerle tanto el alojamiento como la ayuda personal y científica que me ofreciste durante la estancia en la *Université de Neuchâtel*, como también tu disponibilidad ya sea para rescatarme de un bloqueo en medio de una pista de esquí en los Alpes, para tomar una cerveza o para viajar en tren (casi) todos los fines de semana de la estancia visitando ciudades helvéticas. ¡Todo ello es uno de los mejores recuerdos de la tesis!

Gracias a Alba Grau, Rosana Margalef y Edson Plasencia por haber realizado este recorrido viviendo una experiencia similar.

celebrated my birthday in a Vietnamese restaurant with some of the work colleagues: you made those days nicer. Thanks Dr. Alice Badin and Dr. Violaine Poisin for your kind treatment, the meals and trips around the country and especially the sled adventures! Thanks to Dr. Hunkeler and the rest of group members for the great farewell lunch with breathtaking views.

Me gustaría agradecer el apoyo a todos aquellos que me escucharon y con los que compartí algún momento en estos últimos años. Gracias Mònica Torres por ser tan generosa y un ejemplo de bondad y fortaleza para mí, gracias Lidia Butjosa por estar siempre dispuesta a ayudar y por ser compañera de viajes metafóricos y reales (a Galicia, a Sant Joan con Sergi, a Múnich, a Edimburgo, ...y los que te rondaré!). Gracias Itxaso Ruiz por tu optimismo y tus palabras llenas de una visión positiva de la vida que siempre refrescan; gracias Enrique Torres y Luz Gomis por ser inspiración y homólogos de 'viaje'. Sunna Farriol y Alís, junto con Enrique, gracias por el fantástico verano de 2017 en Mallorca en el que todos fuimos una familia y, con vuestro permiso, un poco papás de Alís. Aquel Julio recordé la bonita experiencia que fue estudiar geología precisamente por la gente que me fui encontrando por el camino y lo mejor es que el sentimiento y la cercanía que tuvimos no se ha perdido y podemos seguir haciendo 'salidas de campo' juntos a pesar de encontrarnos lejos. ¡Porque hacen falta más personas como vosotr@s!

Gracias también a David Candami, Katia, Enric, Sandra Amores, Helena y Òscar por vuestro tiempo, palabras y momentos vividos.

Mercè, gràcies per ensenyar-me sempre una altra visió de les coses, una perspectiva sempre agitadora per on seguir indagant, t'agraeixo l'oportunitat d'haver-te pogut conèixer i gaudir de la companyia de la teva família, la Sira, la Carla, la Paola i el Michele tant sigui a una calçotada, una castanyada estiuenca, durant un estiu a Mallorca, a Galiza o en un aniversari sorpresa.

Gracias Leti y Laia por seguir ahí después de tantos años de alegrías y tristezas. Laia gracias por ser siempre tan generosa y buena consejera y hacer posible que los 600 km que duraron 10 años se borraran de un plumazo gracias a ti, haciendo más fácil el final de la tesis. Siempre te estaré agradecida.

Gracias, gracias y mil gracias a todos aquellos que en algún momento os habéis preocupado durante el transcurso de la tesis (coma ti Cris!) e a os Xarelos por facer dos 'braus' o mellor de cada ano.

Cati y Félix, gracias por las escapadas a Bilbo o los momentos en el Galicia que me revitalizan, por hacerme sentir como en casa. Ramón e Amadora, polos anos que compartimos, pola risa e polo que significades para Igor.

Use, Sara y Sergio gracias por esas visitas a Xares o las escapadas rurales, me alegro de formar parte de vuestra familia. Sergio (tato), me alegro de haber vivido juntos momentos vitales para cada uno.

Carlos, Èlia, Júlia, Llúcia i Ot, la vostra gran família de petits m'ha donat molts bons moments com a padrina privilegiada que han donat aire a èpoques difícils ja sigui pujant a la Mola, al Matagalls o ensenyant minerals a marrecs de 3 anys. Gràcies per preguntar i per inspirar.

Gracias papá e mamá por ser un referente de persoas traballadoras e de dignidade. Abuela gracias, porque ti es un exemplo de alegría 'porque sí', porque sufro tanto o terte lonxe e me das tanta paz o terte cerca. Non podo dicir nada mais que vos quero muto.

Igor, gracias por tu amor incondicional, por tu infinita generosidad, por tu bondad, por tu alegría, por tus abrazos y por haber experimentado mis emociones como tuyas durante todo el transcurso. Muchas gracias por ser mi ilustrador (con todas las acepciones posibles) de cabecera.

Table of contents

Table of figures

List of Tables

Abstract

Carbon tetrachloride (CT) and chloroform (CF) are chlorinated methanes (CMs) which have been released to the environment for decades owing to scarce waste management. Since they are dense non-aqueous phase liquids (DNAPLs), CMs migrate downwards and reach groundwater constituting a contamination source. Thus, this pollution requires a thoughtful monitoring and treatment since CT and CF are toxic and predicted to be carcinogenic substances (IARC, 2017).

Although CT and CF are considered quite persistent in aquifers, they undergo abiotic and biotic natural attenuation. This degradation occurs mainly through reductive pathways under anoxic conditions, but CF oxidative microbial cometabolism could be also plausible (Cappelletti et al., 2012; Penny et al., 2010). Hence, CMs transformation processes are expected under field conditions. Òdena field site (Barcelona, Spain) is polluted by CMs among other volatile organic compounds (VOCs) due to industrial activity during the 70s and 80s. Chlorinated ethenes (CEs) degradation was detected in the fractured aquifer by carbon isotope ($\delta^{13}C$) enrichment over time (Palau et al., 2014b). CF alkaline hydrolysis (AH) was also revealed by $\delta^{13}C$ monitoring in the interception trenches filled with construction wastes (pH ~12) built in the unsaturated zone after 2005 source removal, whereas the cause of CT $\delta^{13}C$ enrichment over time in these trenches remains unknown (Torrentó et al., 2014).

Induced reactions bear potential to overcome the challenges derived from the slow degradation rates of CMs natural attenuation. Biostimulation, zero valent iron permeable reactive barriers (Fe(0)-PRB) or those made of other reducing agents are receiving increasing attention as alternative remediation strategies. However, *in situ* chemical oxidation (ISCO) and alkaline hydrolysis are techniques of interest only for CF as a result of the high oxidation state of carbon in CT.

Compound specific isotopic analysis (CSIA) is a useful tool to evaluate the efficiency of both CMs natural attenuation and induced strategies in the field. CSIA not only verifies that the concentration decrease is due to reactive processes (instead of dispersion or dilution) but also permits quantification. Moreover, dual isotope plots in which shifts in isotope values of one element are plotted against those of a second element, allow distinction between different CMs reaction mechanisms by means of specific slopes (Λ). Thus, laboratory CMs degradation experiments under controlled conditions are required to gain understanding of the expected isotopic changes in the field and to evaluate whether it is feasible to quantitatively detect degradation. Although relatively new, Cl-CSIA for CEs and chlorinated ethanes has been gradually incorporated in the last 6 years in combination with consolidated C-CSIA. However, Cl-CSIA was only used in few laboratory experiments for CF and the method was not validated for any CMs prior to this thesis.

Abstract/Resumen

The main aims of this thesis have been to better understand CMs natural attenuation together with potential CMs remediation strategies to improve the assessment of CMs fate in Òdena site and, by extension, in other polluted sites all over the world. These goals were addressed primarily by C-CSIA and Cl-CSIA, among other techniques. Prior to their use in laboratory or field samples, Cl-CSIA method has been developed and evaluated for CT and CF by both, gas chromatography-isotope ratio mass spectrometry (GC-IRMS) and by gas chromatography-quadrupole mass spectrometry (GC-qMS validated in an interlaboratory comparison) through an international collaboration (*Helmholtz Zentrum München* and *Université de Neuchâtel*) during different thesis stays.

Three relevant abiotic CF transformation mechanisms were studied in batch experiments: oxidation by heat-activated persulfate (abbreviated as PS); AH and reductive dechlorination by Fe(0), obtaining similar Λ values for PS and AH (17±2, 13.0±0.8) which are distinguishable from reductive dechlorination (8±2).

CT and CF degradation by Fe(0) and Fe-bearing minerals (pyrite (Py, FeS_2) and magnetite (Mag, Fe_3O_4) in the presence of $FeCl_2$) were carried out in laboratory experiments at pH 7 and 12 simulating groundwater in the saturated zone and in alkaline interception trenches in the unsaturated zone of Òdena site, respectively. CF hydrogenolysis to dichloromethane (DCM) by milli-sized Fe(0) was characterized at both pHs, whereas CF degradation by Fe-bearing minerals was only identified at pH 12. In this case, AH was hypothesized since no VOCs by-products were detected except for DCM only with Py, evidencing CF hydrogenolysis. CT degradation by both Fe(0) and Fe-bearing minerals was confirmed at pH 12, whereas at pH 7, CT degradation was only obtained by nano-sized Fe(0) and Py. pH did not affect Λ values of CT and CF degradation by Fe(0) nor CT degradation by Py. CT thiolytic reduction to carbon disulphide (CS_2) occurred in parallel to CT hydrogenolysis in experiments with Py at both pH values, showing different Λ values to net CT hydrogenolysis by Fe(0), but similar Λ values to CT reduction by Mag at pH 12. These differences provide good chances to detect these pathways in the field.

Additionally, CT and CF microcosm experiments were performed separately for each compound by using slurry from one of the most polluted wells in Òdena site (S3). Biotically-mediated CT hydrogenolysis was confirmed in the microscoms. Biostimulation with vitamin B_{12} catalyzed CT biodegradation and stimulates CF biodegradation, the latter not observed without B_{12}. For both target compounds, no relevant accumulation of other chlorinated compounds neither CS_2 was detected with B_{12}. CT experiments with B_{12} might be linked to a major activity of *Pseudomonas stutzeri* able to reduce CT to CO_2. *Acidovorax, Ancylobacter* and *Pseudomonas* were the most metabolically active genera observed in the experiments, whereas commonly found organo-halide respiring bacteria, *Dehalobacter* and *Desulfitobacterium,* were below 0.1% of relative abundance. The Λ of CF biodegradation by B_{12} (7±1) was similar to that reported for CF reductive dechlorination by Fe(0) (hydrogenolysis plus reductive elimination) (8±2). Λ of CT biodegradation without B_{12} showed no difference to CT hydrogenolysis by Fe(0) which indicates

the same pathway. Furthermore, Λ of CT degradation was statistically different despite their 95% of confidence interval (CI) with and without B_{12} (5±1 *vs.* 6.1±0.5, respectively), indicating possible influence of other reduction processes different from CT hydrogenolysis. $\delta^{13}C$ enrichment of CEs, once CMs were completely degraded by B_{12}-catalyzed biotic reactions, confirmed CMs inhibition of CEs degradation.

The obtained laboratory data improved the knowledge on CMs degradation processes and established the basis applicable in multi-contaminant polluted sites like Òdena. A long-term monitoring to study 2005 source's removal effects on groundwater CMs has been performed from 2002 to 2014. Through by-products and C-CSIA monitoring, CMs transformation processes over time have been confirmed. The source's removal was inefficient since active CMs leaching was proved in the outskirts of the dismantled wastewater pipe and in the wastewater tank. Nevertheless, by-products and Λ studies disclosed CT and CF reduction processes precisely in those areas. In contrast, in former disposal pit source, where removal was more efficient, isotopic values unveiled a migration of the focus downstream as well as an influence of hydrolysed CF coming from the alkaline trench and/or CF oxidation processes in the saturated zone of this area.

To sum up, this thesis has provided progress in Cl-CSIA methodology for CMs and new compelling C and Cl-isotope laboratory data related with CT and CF degradation processes. These data combined with other microbial and geochemical tools have allowed the discrimination of CMs degradation processes at field scale and are promising for monitoring the efficiency of remediation strategies in other polluted sites. The routine use of Cl-CSIA analyses are worthwhile for further research together with well-stablished C-CSIA. Moreover, the up-scale application and evaluation of studied CMs remediation techniques such as biostimulation by economical B_{12} sources in combination or not with Fe(0) or Fe-bearing minerals (which implies mining wastes revalorization) are challenges ahead.

Resumen

El tetracloruro de carbono (CT) y el cloroformo (CF) son compuestos orgánicos que pertenecen al grupo de los metanos clorados (CMs) los cuales han sido vertidos descontroladamente al medio ambiente durante décadas debido a la escasa gestión y tratamiento de residuos. Puesto que son disolventes más densos que el agua, una vez vertidos, estos contaminantes migran en profundidad hasta las aguas subterráneas creando frecuentes fuentes de contaminación ambiental que, por su persistencia, constituyen un riesgo para la salud pública. Por lo tanto, este tipo de contaminación requiere de un seguimiento exhaustivo, así como de hallar tratamientos específicos debido a que el CT y el CF son consideradas substancias tóxicas y carcinogénicas (IARC, 2017).

Aunque el CT y el CF son persistentes en acuíferos, estos compuestos experimentan atenuación natural tanto biótica como abiótica. Los CMs se degradan principalmente a través de mecanismos de reducción bajo condiciones anóxicas, aunque la oxidación microbiana del CF por cometabolismo también es un proceso de degradación potencial (Cappelletti et al., 2012; Penny et al., 2010). Por consiguiente, se esperan procesos de transformación de los CMs en emplazamientos contaminados. El enclave contaminado de Òdena (Barcelona) se encuentra afectado tanto por CMs como por otros compuestos orgánicos volátiles (VOCs, por sus siglas en inglés) debido a actividad industrial en los años 70 y 80. La degradación de etenos clorados (CEs por sus siglas en inglés) en este acuífero fracturado fue detectada ya que se observó un enriquecimiento isotópico del carbono (δ^{13}C) a lo largo del tiempo (Palau et al., 2014b). La presencia de hidrólisis alcalina (AH, por sus siglas en inglés) del CF fue también revelada mediante el seguimiento de la δ^{13}C del CF en las rasas de intercepción de agua de lluvia creadas con residuos de la construcción (pH~12) en la zona no saturada, una vez que se extrajeron las fuentes de contaminación en 2005. Sin embargo, aún se desconoce el motivo del enriquecimiento de la δ^{13}C del CT a lo largo del tiempo en estas rasas (Torrentó et al., 2014).

Para mejorar las limitaciones de los potenciales procesos de atenuación natural de los CMs y hacerlos más eficientes, se pueden usar diferentes técnicas de remediación inducida. La bioestimulación y el uso barreras reactivas permeables de Fe(0) o construidas con otros agentes reductores son de creciente interés. La oxidación química in situ (ISCO) y la AH son técnicas de remediación abiótica pertinentes únicamente para el CF, debido al alto estado de oxidación del carbono en el CT.

El análisis isotópico de compuesto específico (CSIA por sus siglas en inglés) es una herramienta muy útil para evaluar la eficiencia tanto de la atenuación natural de los CMs como la de las estrategias de remediación aplicadas en emplazamientos contaminados. El método de CSIA no solo verifica, mediante el seguimiento de la composición isotópica a lo largo del tiempo, que la disminución de la concentración de los CMs sea debida a procesos reactivos (*vs.* otros no destructivos, como por ejemplo la dispersión o la dilución), sino que también permite la cuantificación del alcance de la degradación del contaminante. Asimismo, los

gráficos binarios de isótopos, en los que los cambios isotópicos de un elemento se grafican respecto al de un segundo elemento de la molécula estudiada, permiten la discriminación entre diferentes vías de degradación de los CMs, a través de la obtención de pendientes específicas de cada mecanismo (Λ). Para aplicar el CSIA con tales fines, deben realizarse previamente experimentos de laboratorio bajo condiciones controladas para estudiar las reacciones de degradación de los CMs. De este modo es posible evaluar de forma fiable los cambios isotópicos esperados en el campo y, por lo tanto, conocer si se puede detectar de forma cuantitativa la degradación, así como también, estudiar la viabilidad de los potenciales tratamientos. El CSIA del carbono (C-CSIA) está ampliamente consolidado para el análisis de VOCs. El CSIA del Cl (Cl-CSIA) ha sido extensamente usado en los últimos años para los CEs y los etanos clorados. Sin embargo, el Cl-CSIA solamente ha sido aplicado en algún experimento para el CF y no ha sido utilizado previamente para el CT. Por consiguiente, el método de Cl-CSIA no había sido evaluado ni validado pormenorizadamente para ningún CMs antes de la presente tesis.

Los principales objetivos de esta tesis son la adquisición de un mejor conocimiento de los procesos de atenuación natural de los CMs a través de experimentos de laboratorio, así como también de las potenciales estrategias de remediación de éstos, con el fin de aplicar dichos avances en emplazamientos tales como el de Òdena. El C-CSIA y el Cl-CSIA han sido las herramientas de seguimiento principales de los estudios realizados, aunque se han utilizado otras técnicas geoquímicas y microbiólogas dando un carácter pluridisciplinar a la tesis. Previamente al uso del método de Cl-CSIA en los CMs de las muestras de laboratorio y campo, se ha desarrollado y validado el método para el CT y CF con un cromatógrafo de gases acoplado a un espectrómetro de relación isotópica (GC-IRMS) y con un cromatógrafo de gases acoplado a un espectrómetro de masas cuadrupolo (GC-qMS, siendo la metodología para este último comparada en un interlaboratorio). Este desarrollo se ha llevado a cabo en colaboración con grupos de investigación internacionales (*Helmholtz Zentrum Müenchen* y *Université de Neuchâtel*) durante las tres estancias del doctorado.

Han sido estudiados tres mecanismos diferentes de transformación abiótica del CF en experimentos batch: oxidación por persulfato activado térmicamente (abreviado como PS); AH y decloración reductiva del CF con Fe(0). Se han obtenido valores similares de Λ del CF para PS y AH (17±2 y 13.0±0.8, respectivamente) que se pueden distinguir de la decloración reductiva (8±2).

Se han realizado experimentos de degradación de CT y CF con Fe(0) y minerales de hierro (pirita (Py, FeS_2) y magnetita (Mag, Fe_3O_4)), estos últimos con la presencia de $FeCl_2$ a pH 7 y pH 12, simulando el agua subterránea de la zona saturada y la de las rasas de intercepción alcalinas de la zona no saturada de Òdena, respectivamente. Se detectó hidrogenólisis del CF a diclorometano (DCM) mediante Fe(0) de tamaño milimétrico para ambos valores de pH, mientras que la degradación del CF por minerales de hierro solo fue identificada a pH 12. En este último caso, se hipotetiza la existencia de AH ya que no se

detectan VOCs como productos, salvo cierta acumulación de DCM con Py, lo que evidenciaría hidrogenólisis solo en el experimento con Py. La degradación del CT, mediante Fe(0) o minerales de hierro, ha sido confirmada a pH 12. Sin embargo, a pH 7 la degradación del CT solo ha sido confirmada con Fe(0) nanométrico y Py. Se ha observado la existenia paralela de reducción tiolítica del CT a CS_2 e hidrogenólisis del CT a CF en ambos valores de pH, dando lugar ambos procesos a un valor de Λ diferente al obtenido para la hidrogenólisis neta del CT con Fe(0) y similar al de la reducción del CT con Mag a pH 12. De esta manera, se evidencia el potencial para detectar y diferenciar estos procesos en el campo mediante gráficos binarios de isótopos C-Cl. Así mismo, se deduce que el pH no afecta al valor de Λ de la degradación del CT ni del CF mediada por el Fe(0), ni a la degradación del CT por acción de la Py o del Fe(0).

Adicionalmente, se han realizado experimentos de microcosmos con CT y CF, separadamente, con lodo del fondo de uno de los pozos más contaminados de Òdena (S3). Se ha confirmado una biodegradación natural de CT siguiendo la vía de hidrogenólisis a CF. La bioestimulación con vitamina B_{12} ha catalizado la degradación de CT y estimulado la biodegradación del CF, siendo la última inexistente sin la presencia de B_{12}. Para ambos compuestos, no se detecta una acumulación de compuestos clorados ni de CS_2 en los tratamientos con B_{12}. La ausencia de acumulación de CF con la adición de B_{12} durante la degradación de CT puede estar relacionada con una mayor actividad de la especie *Pseudomonas stutzeri* detectada más activa en esos tratamientos y capaz de reducir el CT a CO_2. Los géneros más metabólicamente activos en los tratamientos del microcosmos *son Acidovorax, Ancylobacter* and *Pseudomonas* son, mientras que bacterias ampliamente conocidas como decloradoras (como *Dehalobacter* y *Desulfitobacterium*), se encuentran por debajo de un 0.1% de abundancia relativa. El valor de Λ para la biodegradación del CF (solo detectada con la adición de B_{12}, 7±1) es similar al registrado para la decloración reductiva del CF con Fe(0) (8±2), el cual incluye hidrogenólisis y eliminación reductiva. El valor de Λ de la biodegradación del CT sin la vitamina B_{12} y el de la hidrogenólisis neta del CT por Fe(0) no muestran diferencia estadística, lo cual confirma la misma vía para ambos experimentos. También cabe destacar que los valores de Λ de la degradación del CT con y sin B_{12} son estadísticamente diferentes (5±1 *vs.* 6.1±0.5), respectivamente, a pesar de su similitud a juzgar por su intervalo de confianza del 95%. Este hecho indicaría una posible influencia de otros procesos de reducción del CT diferentes a la hidrogenólisis cuando la vitamina B_{12} está presente. Por último, añadir que este estudio de microcosmos revela un enriquecimiento en ^{13}C de los CEs, una vez los CMs son totalmente degradados mediante reacciones bióticas catalizadas por la B_{12}, lo cual confirma la inhibición que ejercen los CMs en la degradación de los CEs.

Considerando todo lo anteriormente mencionado, el conjunto de datos obtenido en los experimentos sienta las bases para un mejor conocimiento de la atenuación natural e inducida de los CMs aplicable a nivel práctico en acuíferos contaminados por múltiples contaminantes como el citado de Òdena. De esta forma, ha sido llevado a cabo un estudio a largo plazo (del 2002 al 2014) del efecto de la remoción de las fuentes de contaminación de CMs en 2005 en

las aguas subterráneas del emplazamiento monitorizado de Òdena. A través del seguimiento de la concentración de los CMs y sus productos de degradación, así como del C-CSIA de los CMs, se han sido confirmado procesos de transformación de estos contaminantes a lo largo del tiempo. La remoción de las fuentes de contaminación se considera ineficiente dado que se han detectado procesos de lixiviado de CMs tanto en la zona no saturada alrededor del conducto de transporte de aguas residuales que fue desmantelado, como también entorno al tanque de almacenamiento subterráneo. No obstante, los productos de degradación y el estudio de los valores de Λ han evidenciado procesos de reducción del CT y del CF en ambas áreas. Por otro lado, en la zona donde se realizaron vertidos al aire libre sí se ha detectado una remoción eficiente de la fuente de contaminación y los valores isotópicos han revelado una migración del foco aguas abajo, así como también, cierta influencia de CF afectado por AH en las zanjas de intercepción y/o por procesos de oxidación del CF en la zona saturada de esta área.

Para concluir, subrayar que esta tesis proporciona avances en la metodología de Cl-CSIA de los CMs, así como nuevos datos isotópicos de carbono y cloro para caracterizar procesos de degradación del CT y del CF. Estos datos combinados con otras técnicas geoquímicas y microbiológicas permiten discriminar y evaluar de forma pluridisciplinar procesos de atenuación natural en emplazamientos contaminados, así como realizar un asesoramiento y seguimiento de la eficiencia de las potenciales técnicas de remediación de CMs aquí descritas por parte de consultorías ambientales y administraciones. El uso rutinario del método de Cl-CSIA en los CMs es prometedor para futuras investigaciones y proyectos de remediación, paralelamente al ya consolidado C-CSIA. La implementación y evaluación de las técnicas de remediación de CMs a escala de campo, como la bioestimulación a través de fuentes económicas de $B_{12,}$ en combinación o no con el uso de Fe(0) o minerales de hierro a través de la puesta en valor de residuos mineros, son desafíos a corto plazo.
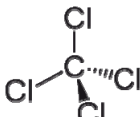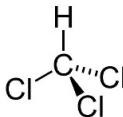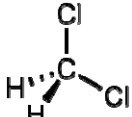
1. Introduction

1.1 State of the art

1.1.1 Clorinated methanes and their environmental impact

The chlorinated methanes (CMs) carbon tetrachloride (CT), chloroform (CF) and dichloromethane (DCM), are volatile organic compounds (VOCs) commonly found as pollutants in groundwater as a consequence of releases from chemical manufacturing processes or accidental spills (Zogorski et al., 2006). CT was used as a cleaning solvent, degreaser, fungicide and refrigerant which is now prohibited, whereas CF was used as an anesthetic and chemical precursor to nowadays banned refrigerants such as chlorodifluoromethane (HCFC-22) due to its ozone depletion and high global warming potential (Watts et al., 2004). CF is also added in pesticide formulations, used as a solvent, cleaning agent, in fire extinguishers, and in the rubber industry (Cappelletti et al., 2012). However, natural sources of CT and CF such as marine algae in oceans, volcanic emissions or fungi in soil have been reported (Haselmann et al., 2000, 2002; Laturnus et al., 2000; Penny et al., 2010; Cappelletti et al., 2012). DCM is a common by-product of CF hydrogenolysis, but it has been also widely used at many industrial processes as solvent, propellant, degreaser and postharvest fumigant among other applications (Shestakova and Sillanpää, 2013).

Table 1. Physicochemical properties on CT, CF and DCM

	CT	CF	DCM
Molecular structure			
Chemical formula	CCl_4	$CHCl_3$	CH_2Cl_2
Molecular weight (g/mol)	153.8	119.4	84.9
Density (g/cm^3 at 20 ºC)	1.59	1.49	1.33
Solubility in water (mg/L at 20 ºC)	800	8000	13700
Boiling point (ºC)	76.5	61.2	39.8
logK$_{oc}$	1.69-2.16	1.44-2.79	1.68

CMs are dense non-aqueous-phase liquids (DNAPLs) and due to their physicochemical properties with low water solubility, moderate volatility and low tendency to sorb to soil organic carbon, both compounds have high mobility in aquifers (Table 1). These properties make them diffuse rapidly into the unsaturated zone easily spreading the pollution which tend to accumulate at the bottom of aquifers representing an environmental challenge (Pankow and Cherry, 1996). This fact is especially critical in fractured aquifers which allows unrestricted DNAPLs downward movement whereas hamper a straightforward control of the plume location.

A clear probe of their mobility and ubiquity is that CF was the most frequently detected VOC in groundwater in a study performed in the United States with more than 5,000 samples

(3,497 of wich from aquifers) (Zogorski et al., 2006) (see Figure 1). This survey showed that VOC mixtures are commonly found in polluted sites, being the chlorinated ethenes (CEs, such as PCE, TCE) and CF mixture among the most regularly detected. The chlorinated hydrocarbons represents 8-9% of the main pollutant groups found in polluted sites from Catalunya from 2012 to 2016 which is in the EU average in 2011 (Figure 2).
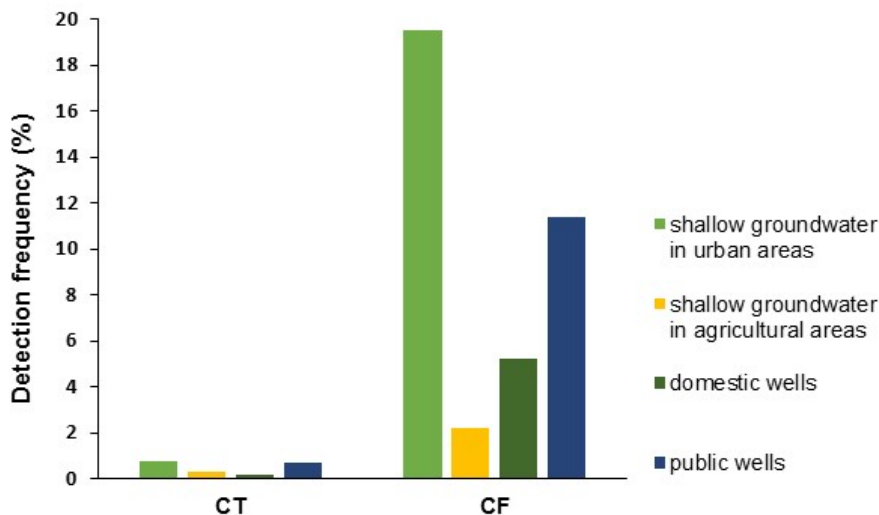
Figure 1. Detection frequency (%) at an assessment level of 0.2 µg/L of CT (carbon tetrachloride) and CF (chloroform) in 847 samples in shallow groundwater (screened near the top of the water table, Squillace et al., 2004) in urban areas, 723 samples in shallow groundwater in agricultural areas, 2401 samples of domestic wells, and 1096 samples in public wells in the United States. Created after Zogorski et al. (2006).

According to the International Agency for Research on Cancer (IARC, 2017), CT and CF are classified as possibly (and DCM as probably) carcinogenic substances to humans. Moreover, on a 2-year basis, the Agency for Toxic Substances and Disease Registry (ATSDR) revises and publishes a list of prioritization of substances based on a combination of their frequency, toxicity, and potential for human exposure at National Priority List (NPL) sites in United States. In accordance to the last ATSDR 2017 Substance Priority List, CF is ranked in the 11th position whereas CT ranks 50th, CT by-product carbon disulphide (CS_2) is positioned in the number 186 and DCM is not even listed. Apart from toxic and carcinogenic effects, CT has also harmful consequences for the stratospheric ozone (Penny et al., 2010) and this is the reason why after Montreal Protocol its use was phased-out by 2010 (United Nations Environment Programme, 2006), although it is still produced as intermediate for other chemical compounds (Penny et al., 2010).

On its side, European Union (EU) established in the Directive 2008/105/EC the water quality standards of 12, 2.5 and 764 µg/L for CT, CF and DCM, respectively (European Union, 2008). However, the Catalan Water Agency (ACA) (2007) established different limits (30, 210 and 17 µg/L, respectively), as values for intervention in polluted sites since this is the estimated concentration entailing a risk to potential users.
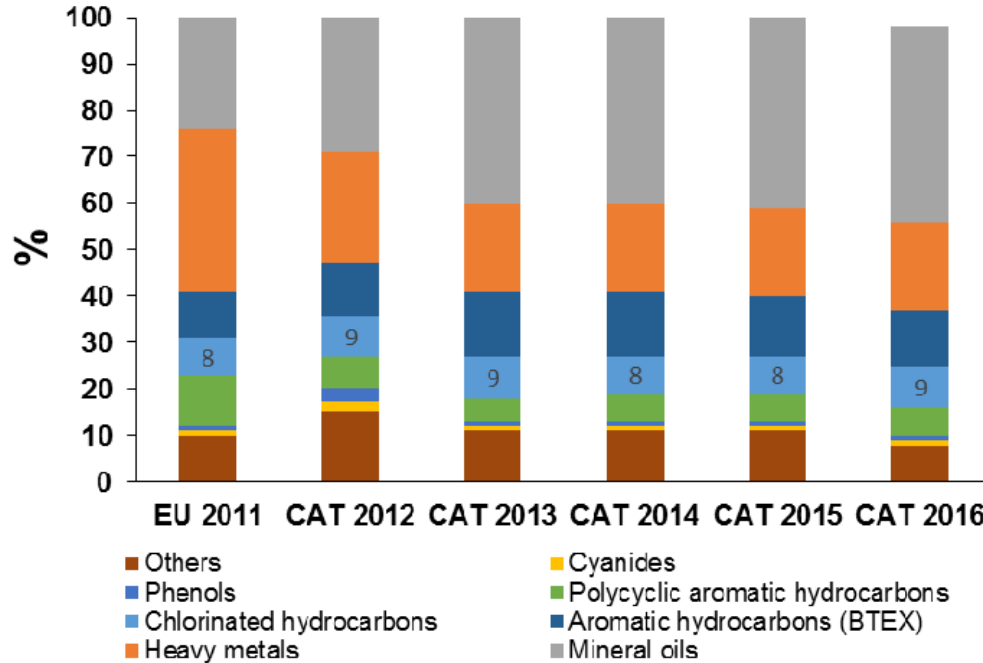
Figure 2. Percentage (%) of the main pollutants found in soils of polluted sites from Catalunya in the last years (referred as 'CAT year') compared to the average of European Union in 2011 (referred as 'EU 2011') (created after data from *Agència de Residus de Catalunya* (ARC), 2012, 2013, 2014, 2015, 2016). The % of the chlorinated hydrocarbons is specified in the corresponding bar.

Therefore, research on CMs degradation is essential in order to enforce the law regarding the maximum permitted CMs concentrations in groundwater, which are widely spilled worldwide.

1.1.2 Natural attenuation of chlorinated methanes: degradation pathways

The CT molecule has a tetrahedral symmetry. Due to the absence of a C-H bond and the presence of four highly polarized C-Cl bonds, a radical reaction is necessary for the cleavage of C-Cl bond (Table 1). There are no known organisms that metabolically degrade CT. Under anoxic conditions, microbial CT degradation appears to be a non-specific co-metabolic reaction. Enrichment cultures or consortia capable of CT degradation have been reported, but few have been taxonomically characterized (Penny et al., 2010). They are mainly methanogens, sulfate reducers and acetogens or methoanogenic archaea.

Thiol compounds (e.g. H_2S), biogenic iron species, electron transfer mediators such as cobalamin (vitamin B_{12}) and other reducing agents like Fe(0), pyrite (Py, FeS_2), magnetite (Mag, Fe_3O_4) and goethite (α-$Fe^{3+}O(OH)$) may help in the reductive dechlorination of CT (Penny et al., 2010). In fact, iron minerals and/or zero-valent metals have been proven to mediate both CT and CF reduction abiotically at laboratory scale (e.g. Matheson and Tratnyek, 1994; Támara and Butler, 2004; Feng and Lim, 2005; Zwank et al., 2005; He et al., 2015; Lee et al., 2015). Therefore, CMs degradation can be either abiotically or biotically-catalyzed.

The main CT reductive pathways are summarised in Figure 3 and, except pathway 5, all of them are biotic and abiotically described. In CT hydrogenolysis (pathway 1), after a first electron transfer, a hydrogen replaces a chlorine leading to CF and subsequently DCM (Figure 3). In alternative pathways, after the transfer of two electrons, subsequent hydrolysis leads to hydrolytic substitution producing CO, formate, and CO_2 (hydrolytic reduction, pathway 3), or to thiolytic substitution leading to CS_2 (thiolytic reduction, pathway 4). Finally, CT reduction by *Pseudomonas stutzeri* strain KC deserves special mention since leads to CO_2 as the main product without CF formation, but with phosgene and thiophosgene as toxic intermediates (pathway 5) (Lewis and Crawford, 1995). Specifically, B_{12} catalyzed CT biodegradation to CO, CO_2 or CS_2 (hypothetically by pathways 3 and 4) whereas CF becomes a minor product, possibly because B_{12} stimulates further CF degradation (Cappelletti et al., 2012).

Microbial CF degradation takes place under both oxic and anoxic conditions. Although CF biodegradation was mainly reported by cometabolism, *Dehalobacter* and *Desulfitobacterium* genus can dechlorinate CF to DCM by dehalorespiration. This CF dehalorespiration has been identified to be mediated by *ctrA* gene in *Desulfitobacterium* sp. strain PR (Ding et al., 2014) and by *cfrA* in *Dehalobacter* sp. (Tang and Edwards, 2013). Under anoxic conditions, CF can be degraded by dehalorespiration and co-metabolic hydrogenolysis to DCM (pathway 1, Figure 3); by reductive elimination to CH_4 (pathway 2), and by reduction followed by hydrolysis and final oxidation to CO and CO_2 (pathway 3). Under oxic conditions, cometabolic reactions performed by monooxygenases transform CF to CO_2 and chloride ion (pathway 6) (Cappelletti et al., 2012). DCM, CF by-product, is also a source of carbon and energy for microbial growth under both oxic and anoxic conditions (e.g. Kayser et al., 2002; Firsova et al., 2010; Trueba-Santiso et al., 2017).

CT and CF inhibit the activity of microbial respiration of chlorinated ethanes and ethenes of some well-known *Dehalococcoides* and *Desulfitobacterium* species by enzyme competition or through inhibition of the metabolic processes (Cappelletti et al., 2012; Futagami et al., 2013). Moreover, CT and CF can inhibit each other biodegradation (Grostern et al., 2010; Lima and Sleep, 2010; Justicia-Leon et al., 2014).
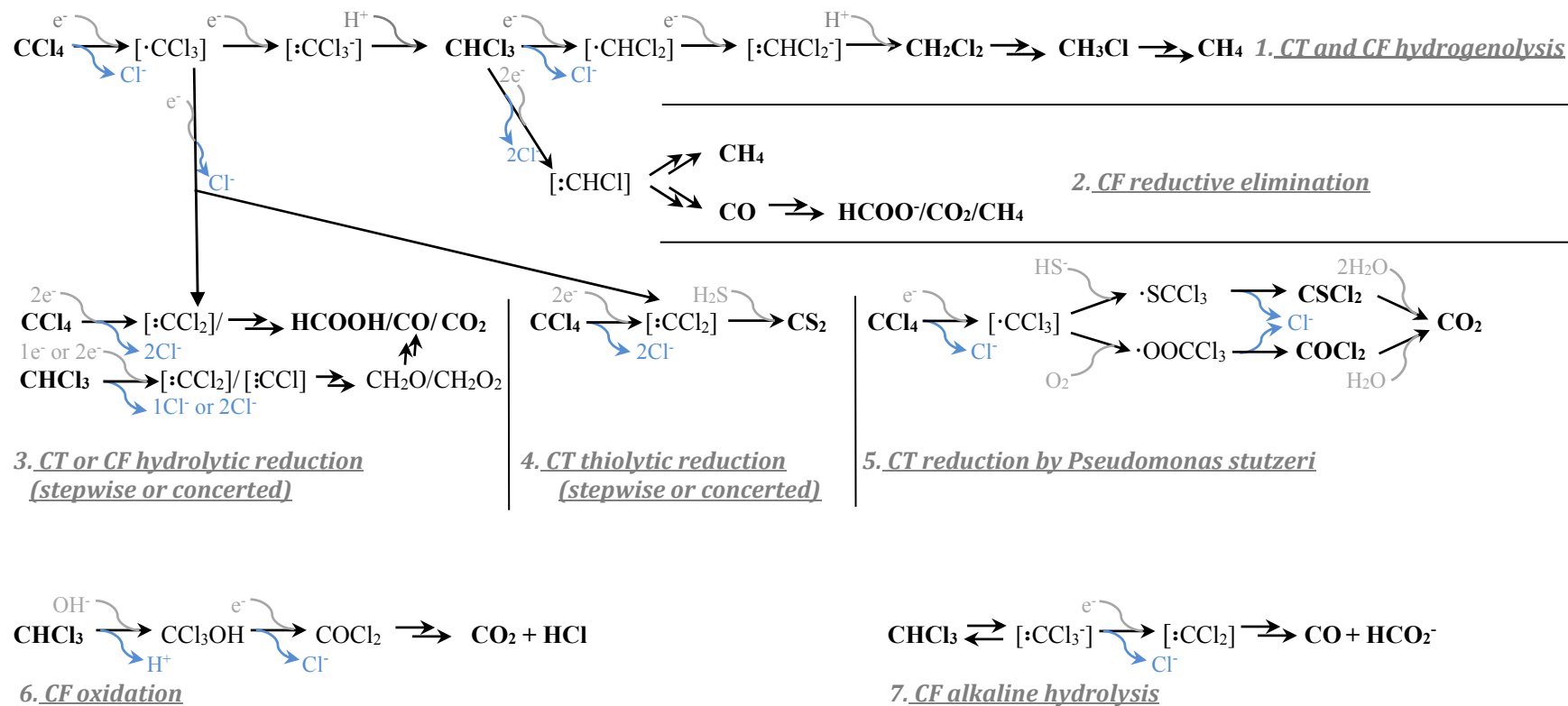
Figure 3. Hypothetical CT (carbon tetrachloride, CCl_4) and CF (chloroform, $CHCl_3$) reductive pathways (nº 1 to 5) (Lewis and Crawford, 1995; Field and Sierra-Alvarez, 2004; Song and Carraway, 2006; Penny et al., 2010; Cappelletti et al., 2012), CF oxidation by persulfate pathway (nº 6) (Pohl et al., 1977) and CF alkaline hydrolysis pathway (nº 7) (Skell and Hauser, 1945). Double arrow means that several steps are omitted to simplify.

1.1.3 Remediation strategies of chlorinated methanes

1.1.3.1 Abiotic remediation techniques

Only few field *in situ* applications of abiotic remediation techniques are reported for CMs. Within them, the following can be highlighted:

<u>Oxidation</u>

The degradation of CMs by *in situ* chemical oxidation (ISCO) using common oxidants such as permanganate, iron-activated persulfate (PS), ozone, hydrogen peroxide, or Fenton's Reagent is in general much less effective than for CEs (Huling and Pivetz, 2006). This is due to the high oxidation state of carbon in CT and CF. Nevertheless, due to the presence of a C-H bond in CF in contrast to CT (Table 1), thermally activated PS is an efficient CF oxidant since strongly oxidizing sulfate radical and other reactive intermediates are generated at neutral pH (Huang et al., 2005; Waldemer et al., 2007; Tsitonaki et al., 2010) (pathway 6, Figure 3).

<u>Alkaline hydrolysis</u>

CF can be degraded to CO and formate through alkaline hydrolysis (AH) (pathway 7, Figure 3) (Hine, 1950). This reaction is the basis of a remediation technology in which CF polluted groundwater is forced to react with concrete-based construction wastes (Torrentó et al., 2014). However, CT hydrolysis is pH independent and extremely slow (Jeffers et al., 1989), not being suitable as a remediation strategy.

<u>Reduction by Fe(0) and Fe-bearing minerals</u>

The permeable reactive barrier (PRB) technology is described as an effective passive remediation technique to decontaminate groundwater of a diversity of chlorinated organic and inorganic compounds commonly by the passage of the polluted flow through the barrier containing a reactive material (O'Hannesin and Gillham, 1998; U.S. EPA, 2008). The most widely used material in PRBs is Fe(0) since it is a strong reducing agent, cheaper and less harmful than other zero-valent metals (Vodyanitskii, 2014). For this reason, this remediation strategy has been successfully proven at field sites contaminated by chlorinated aliphatic hydrocarbons (CAHs) especially with CEs (He et al., 2015) but not extensively applied in the case of CMs. CMs reductive dechlorination by Fe(0) has been proved only at laboratory scale (Matheson and Tratnyek, 1994;Támara and Butler, 2004; Feng and Lim, 2005; He et al., 2015; Lee et al., 2015).

Some Fe-bearing minerals can be formed over time in these Fe(0) PRBs, affecting CMs degradation by reducing their effectiveness, such as in the case of Mag, or by promoting it, like in the case of FeS (Obiri-Nyarko et al., 2014). As long-term evolution of PRBs is not fully understood, it would be interesting to better assess the role in the field of these ubiquitous Fe-bearing minerals derived from Fe(0) or those naturally occurring such iron sulfides, iron oxides and green rusts besides the biogenic minerals function in CMs degradation. In fact, CMs degradation by mackinawite ($(Fe,Ni)_{1+x}S$, x=0-0.07), FeS, Py, pyrrhotite ($Fe_{1-x}S$, x=0-0.2), green rust (green crystalline compounds containing Fe(II), Fe(III), HO^- and another anions) and Mag

was detected in the laboratory, mostly characterised in terms of kinetics and by-products formation. However, only few studies have isotopically evaluated CMs degradation by Fe-bearing minerals (Elsner et al., 2004; Zwank et al., 2005) which is required to decide if they can be potentially used as efficient reducing agents for CMs degradation in PRBs, enhanced reductive dechlorination (ERDs) systems and bioreactors (He et al., 2015). These minerals could be recycled from mining and industrial wastes.

1.1.3.2 Bioremediation techniques

Bioremediation consists on the use of microorganisms to convert pollutants to less harmful compounds in contaminated sites. There exist different types of bioremediation: 1) monitored natural attenuation (MNA) which is based on the reliance that physical, chemical, or biological mechanismst act, favourably without human intervention, to reduce the mass, toxicity, mobility, volume, or concentration of contaminants in groundwater and achieving site-specific remediation objectives within a reasonable timeframe (Declercq et al., 2012); 2) biostimulation, when energy sources are deliberately altered to increase organisms activity; or 3) bioaugmentation, when selected organisms are added to improve the biodegradation capacity because natural microbial population is incapable of performing required pollutant transformation or an increase of the biodegradation rates is pursued (Stroo, 2010).

Dispersion, dilution, sorption, volatilisation, and (bio)chemical stabilisation are mechanism capable of acting as natural attenuation processes. However, biodegradation is frequently considered to be the primary mechanism for pollutants attenuation (Declercq et al., 2012). MNA is more cost-effective than other active remediation, although it requires appropriate quantification and evaluation over time (Wiegert et al., 2012).

Biostimulation has been demonstrated as an effective method of degrading CMs among other CAHs because enhances *in situ* anaerobic bioremediation with relatively low cost comparing to other remediation strategies (Henry, 2010). Moreover, biostimulation increases desorption or dissolution of chlorinated solvents in the aquifer matrix from the DNAPL, in contrast to other methods which previously require dissolution (for further *ex-situ* treatments), and it is efficient for several co-contaminants at the same time. On the other hand, biostimulation is not an instantaneous process and some on site-specific limitations such as low permeability or highly heterogeneous conditions constrains its application (Henry, 2010). Specifically for CMs, literature reports some laboratory experiments that were done to stimulate their *in situ* natural attenuation. It was reported that the addition of vitamin B_{12} enhances anaerobic CT and CF biotransformation to non-harmful by-products (Becker and Freedman, 1994; Hashsham et al., 1995; Guerrero-Barajas and Field, 2005a, 2005b), although this product distribution depends on the reductant used in the system to reduce the Co(III) in the B_{12} to Co(I). The major advantages of a B_{12}-catalyzed system in comparison with the sole use of anaerobic bacteria are the faster degradation rate, no need of addition of an extraneous carbon source and no restriction in the pollutant's concentration range to be treated (Guo and Chen, 2018).

The occurrence of above-mentioned well-known degrader species like *Pseudomonas stutzeri, Desulfitobacterium* and *Dehalobacter* is favourable and a basis for further CMs biostimulation techniques. If these species were not present or MNA have not been proved, bioaugmentation strategies can then be an option as shown by satisfactory results in different pilot-scale studies of CT-polluted sites by the addition of *Pseudomonas stutzeri* KC (Pfiffner, 2000; Dybas et al., 1998; 2002).

However, before designing a bioremediation strategy a thoughtful understanding on the biogeochemical and hydrogeological conditions of the aquifer (Henry, 2010) besides the study of the active microbial populations by RNA is mandatory in order to tailor the remediation to the needs of each site. RNA-based analyses provide more insights into active biologic processes than potential physiologic or genetic capability alone as DNA studies do (Yargicoglu and Reddy, 2015). Next-Generation Sequencing (NGS) technologies, such as MiSeq, have prompted a shift towards high-throughput methods for characterizing both total and metabolically active (16S rRNA from active ribosomes and total RNA, analysed from synthesized cDNA) microbial communities (Pelissari et al., 2017).

Coupling bioremediation and ISCO is feasible and provide extensive and cost-effective treatment but requires a thorough understanding of the chemical oxidation impact on subsequent microbial activity. For example, the high sulfate concentrations that remain following PS oxidation can stimulate sulfate-reducing bacteria, which might, in turn, be capable of CMs degradation or at least promote appropriate redox conditions for organohalide-respiring bacteria (OHRB) (Sutton et al., 2011).

Moreover, when Fe(0) reacts with water in PRBs also leads to the formation of hydrogen (H_2) supporting the growth of hydrogenotrophic microorganisms that can further influence the degradation of the barriers target compound (Novak et al., 1998; Gregory et al., 2000; Weathers and Parkin, 2000; Rosenthal et al., 2004; Xiu et al., 2010; Lojkasek-Lima et al., 2012). Specifically, bioaugmentation by *Dehalobacter*-containing mixed cultures was proved to considerably increase CF removal rates in reactive Fe(0) PRBs in laboratory experiments (Lee et al., 2015). Fe(0) and a OHRB combination has been also proposed to degrade certain CAHs resistant to Fe(0) such as 1,2-dichloroethane or DCM and to overcome the inhibition of OHRB by CAHs degradable by Fe(0) (CT and CF) (Koenig et al., 2016). However, the impact on bacterial activity and growth of Fe(0) related to toxic effects but also with the creation of suitable conditions for their activity is not fully understood (Xie et al., 2017).

The application of a combined active indigenous community study and the isotopic approach (explained in the following section 1.1.4.) has been suggested as relevant for evidencing and monitoring degradation processes (Hunkeler et al., 2011) and understanding and designing combined or not remediation strategies.

1.1.4 Compound specific isotope analysis (CSIA)

Stable isotope techniques are based on the fact that for each target element there exist, at least, two stable isotopes in nature with different natural abundances. When organic pollutants are degraded, the ratio of these stable isotopes changes and the degradation extent can be quantified by this change (Hunkeler et al., 2008). Delta notation (δ) (Eq. 1) is used to standardize isotopic experimental data, by expressing the relative difference between the ratio of the heavy (h) and light (l) isotopes of an element E from a compound in a sample, i.e. $R(^hE/^lE)_{comp}$, with respect to an international standard, i.e. $R(^hE/^lE)_{std}$ (Elsner et al., 2012). International standards for chlorinated compounds are Vienna Pee Dee Belemnite for carbon ($δ^{13}C_{VPDB}$) and the international Standard Mean Ocean Chloride (V-SMOC) for chlorine ($δ^{37}Cl_{SMOC}$).

$$\delta^h E_{comp} = \frac{R\left(^hE/^lE\right)_{comp} - R\left(^hE/^lE\right)_{std}}{R\left(^hE/^lE\right)_{std}} = \frac{R\left(^hE/^lE\right)_{comp}}{R\left(^hE/^lE\right)_{std}}$$

Eq. 1

Compound Specific Isotope Analysis (CSIA) is a technique able to isolate organic analytes from mixtures and determine the stable isotope ratio of the target element for one of the analytes (Elsner et al., 2012). The method consists of a gas chromatograph (GC) that separates different VOCs due to their different rate of progression, coupled to an isotope ratio mass spectrometer (IRMS) that transform carbon atoms from the organic molecules into CO_2 (GC-IRMS) (Hunkeler et al., 2008) (Figure 4A). Carbon isotopic composition analysis ($δ^{13}C$) has been commonly applied in VOCs-polluted sites for identifying sources of contamination and assessing transformation processes since the late 90s (Hunkeler et al., 1999; Sherwood Lollar et al., 1999). The latest method's developments allowed chlorine isotope analyses in VOCs ($δ^{37}Cl$). The performance of online measurements of chlorine isotopes in VOCs, without laborious offline conversion of the analyte to CH_3Cl and subsequent analyses in a dual inlet IRMS (Holt et al., 1997) was achieved by Shouakar-Stash et al. (2006) and Sakaguchi-Söder et al. (2007). A GC connected to IRMS or to a qMS (quadrupole mass spectrometer) detectors can be used for chlorine isotope analyses (Shouakar-Stash et al., 2006; Sakaguchi-Söder et al., 2007) (Figure 4B,C). The alternative strategy by GC and H_2-induced high temperature conversion (Hitzfeld et al., 2011; Renpenning et al., 2015) still presents some challenges. The GC-IRMS and GC-qMS methods were improved and used specially for chlorinated ethenes and ethanes (Aeppli et al., 2010b; Jin et al., 2011; Palau et al., 2014a, 2014c). However, despite chlorine isotopes measurements for CF were reported (Breider and Hunkeler, 2014), they were not systematically validated for CMs as it was done previously for TCE (Bernstein et al., 2011).
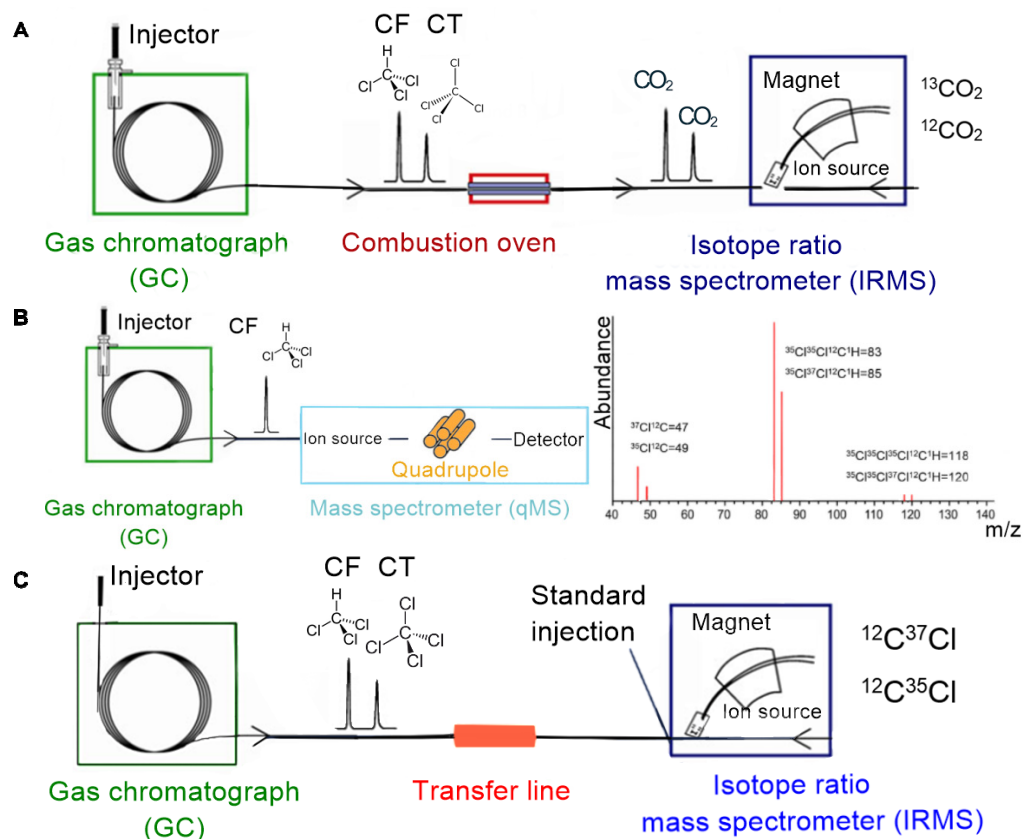
Figure 4. GC-IRMS equipment for carbon isotope analysis (A); and GC-qMS (B) and GC-IRMS (C) for chlorine isotope analysis modified after Elsner et al. (2012).

CSIA has been applied in environmental forensics to elucidate contaminant sources and to distinguish among different contaminant spills (Nijenhuis et al., 2016). The premise for its usefulness is that those VOCs from different sources should be of consistently different isotopic composition. The traditional approach of monitoring parental compound and by-product concentration does not offer reliable information in environmental forensics since concentrations can vary for several reasons (dilution, dispersion, phase-transfer processes); the same by-products may come from different parental compounds or reactions; gas by-products have limited solubility in water and are difficult to measure in environmental samples (i.e. CO, CO_2, CH_4); or compounds can be both parental and by-products (i.e. CF, DCM). CSIA not only allows pollutant monitoring in groundwater during natural or induced degradation processes but also its quantification (Hunkeler et al., 2008; Elsner et al., 2012). However, these CSIA applications in field studies require previous laboratory experiments to understand beforehand VOCs transformation reactions and the associated isotopic fractionation values (ε) and, hence, to ascertain if isotopic changes will be quantitatively detected in the field.

The extent of a VOC transformation based on stable isotope ratios requires the determination of isotopic fractionation (ε) following the Rayleigh approach (Eq. 2), where δ_0 and δ_t are isotope values in the beginning (t=0) and at a given time (t), respectively, and f is the fraction of substrate remaining at time t. Isotope signatures are usually reported in per mil (‰)

using the delta notation relative to the international standards which are V-PDB and V-SMOC for carbon and chlorine, respectively (Shouakar-Stash et al., 2006, Elsner 2012).

$$\ln\left(\frac{\delta_t + 1}{\delta_0 + 1}\right) = \varepsilon \times \ln f$$

<div align="right">Eq. 2</div>

There are only few studies providing carbon isotopic fractionation values for CMs (ε_C). ε_C values of -27.5±0.9‰ and -4.3±0.5‰ were reported for CF biodegradation by two strains of *Dehalobacter* sp. (CF50 and UNSWDH consortium, respectively) (Chan et al., 2012; Lee et al., 2015) and a value of -29±2‰ was found for CF abiotic degradation by Fe(0) (Lee et al., 2015). ε_C values ranged from -32 to -10.8‰ for CT abiotic degradation by Fe-bearing minerals and Zn(0) (Elsner et al., 2004; Zwank et al., 2005; Vanstone et al., 2008; Neumann et al., 2009) and a ε_C of −53±3‰ was found for CF AH (Torrentó et al., 2014). However, no ε_C values for CT biodegradation neither chlorine isotopic fractionation values (ε_{Cl}) of CMs were reported so far.

Isotope fractionation is not directly linked to the effect on isotopes only in reacting bonds, but it reflects the average behavior of isotopes in a molecule (Elsner et al., 2012). However, it is possible to quantify the kinetic isotope effect (KIE) that corresponds to the reactions rate (*k*) at the specific site of the studied reaction (chemical bond change) reflecting the relative stability of bonds formed by the heavy ($^h k$) *vs.* light stable isotopes ($^l k$) of the target element (Eq. 3).

$$KIE_E = \frac{^l k}{^h k}$$

<div align="right">Eq. 3</div>

The apparent kinetic isotope fractionation effect (AKIE) can be also experimentally determined. AKIE contains information of isotope sensitive mode of bond cleavage and all the prior steps (Nijenhuis and Richnow, 2016). Carbon and chlorine AKIE values are calculated following Eq. 4, where *n* is the number of atoms of the considered element in the molecule, *x* is the number of these atoms located at the reactive site/s, and *z* is the number of atoms located at the reactive site/s and being in intramolecular competition. The uncertainty of the AKIE is estimated by error propagation in Eq. 4.

$$AKIE_E \approx \frac{1}{1 + \left(\frac{z \times n}{x} \times \frac{\varepsilon_E}{1000}\right)}$$

<div align="right">Eq. 4</div>

AKIE would express KIE in homogenous reactions but AKIE can be smaller than KIE in complex enzymatic reactions or when they are diffusion-controlled due to masking effects (Elsner et al., 2005; Nijenhuis and Richnow, 2016). Secondary kinetic isotope effects are found when adjacent bonds affect the rate of the target bond cleavage in the rate-determining step of a reaction. These secondary kinetic isotope effects are detected when both AKIE is higher than the KIE or when AKIE can be calculated in an element not directly involved in the studied

reaction bond cleavage, indicate that (Nijenhuis and Richnow, 2016). These effects are usually much smaller than primary kinetic isotope effects.

When isotope values of different elements of the same target compound can be measured, information about the reaction mechanism is provided. Different reaction mechanisms are expected to have different slopes (Λ) in dual isotope plots. In this kind of plots, masking effects can be cancelled out because they are supposed to affect in the same extent both elements, showing one of the advantages of 2D-CSIA approach over AKIE studies. Moreover, 2D-CSIA with carbon and chlorine isotope analyses have allowed more precise identification of pollutants' origin and fate as dual isotope slopes (Λ) reflect ongoing degradation mechanisms and can be compared with characteristic slopes from laboratory studied reactions (Hunkeler et al., 2009). In addition, a source of contamination that aged would undergo fractionation processes in the unsaturated zone distinctly or not that those occurred in the saturated zone (Jeannottat and Hunkeler, 2012, 2013) and, thus, it would hamper reliable degradation processes discrimination. Therefore, if original pure phase is not available, the study and comparison of isotope values from wells located in sources (Wiegert et al., 2012) with those of commercial solvents (Imfeld et al., 2008; Palau et al., 2014b) is strongly advisable. Some drawbacks appear when two different degradation pathways involve the same reaction mechanism at the first determining step, if the isotope effects of the two elements do not proceed in an identical way (Nijenhuis and Richnow, 2016) such as when two different species that are known to follow the same pathway give different slope due to differences in the enzymatic process (Palau et al., 2017b). In those cases complementary tools become crucial to validate interpretation of 2D-CSIA analysis. This multiple isotope approach has been applied successfully to CEs (Wiegert et al., 2012, 2013; Kuder et al., 2013; Badin et al., 2014; 2016; Kaown et al., 2014; Palau et al., 2014b; Audí-Miró et al., 2015; Doğan-Subaşı et al., 2017; Gafni et al., 2018; Heckel et al., 2018) and chlorinated ethanes (Palau et al., 2016 ; 2017b). At the time of starting the present thesis, only one study monitoring CT degradation with δ^{13}C (Kirtland et al., 2003) and two articles for CF, which use δ^{13}C to confirm CF degradation (Hunkeler et al., 2005) and to monitor a CF remediation treatment by AH in Òdena site (Spain) (Torrentó et al., 2014) were reported as field studies about CMs, but to the best of our knowledge, there were not dual isotope studies of CMs.

As several processes could be responsible of VOCs degradation, the choice of the correct ε value is not straightforward; therefore, the use of the indigenous ε obtained by microcosms experiments is advisable. The degradation extent (D in %) can be calculated using the expression derived from the Rayleigh equation (Eq. 5), where δ_0 and δ_t are isotope values at the beginning (t=0) and at a given time (t), respectively and ε is the isotope fractionation of the transformation reaction under consideration (Eq. 2).

$$D(‰) = \left[1 - \left(\frac{\delta_t + 1000}{\delta_0 + 1000}\right)^{\frac{1000}{\varepsilon}}\right] \times 100$$

<div align="right">Eq. 5</div>

Moreover, for a given process assumed responsible for CMs degradation, it is possible to calculate the weighted average of the CMs isotope signature of one of its elements (e.g. $\delta^{13}C_{SUM}$). For instance, weighted average of carbon assuming a hydrogenolysis process would be calculated according to Eq. 6 (Hunkeler et al., 1999; Aeppli et al., 2010a) where x is the molar fraction of each compound relative to the total molar CMs mass from those isotopic values that are available in each case. The uncertainty of $\delta^{13}C_{SUM}$ was determined by error propagation in Eq. 6. When $\delta^{13}C_{SUM}$ does not remain constant, it suggests further degradation of the considered by-products or that different/s pathway/s from the considered hydrogenolysis are taking place.

$$\delta^{13}C_{SUM} \ (‰) = x_{CT} \times \delta^{13}C_{CT} + x_{CF} \times \delta^{13}C_{CF} + x_{DCM} \times \delta^{13}C_{DCM}$$

<div align="right">Eq. 6</div>

Frequently, several pathways do occur simultaneously during a target VOC degradation along a flowpath or due to the activity of different degraders in a mixed culture. Pathway-specific contributions of two pathways in the total degradation may be estimated using the expression derived by Van Breukelen (2007) (Eq. 7), where F is the distribution of pathways 1 and 2; ε_C and ε_{Cl} are the C and Cl isotope fractionation values of the two pathways, respectively and Λ is the observed dual C-Cl isotope slope for a target pollutant due to the two processes.

$$F_1 = \frac{\Lambda\varepsilon_2^{Cl} - \varepsilon_2^C}{(\varepsilon_1^C - \varepsilon_2^C) - \Lambda(\varepsilon_1^{Cl} - \varepsilon_2^{Cl})} \times 100 \ (\%)$$

<div align="right">Eq. 7</div>

1.1.5 Study site

Òdena field site (at 50 km from Barcelona city) (Figure 5) is a clear example of a multi-contaminant polluted site. The groundwater is polluted by a mix of pollutants ranging from CAHs (chlorinated ethenes, ethanes and methanes) and chlorobenzenes to pesticides and BTEXs coming from the spills and wastes of a chemical plant located in the site and active from 1975 to 1985. The studied aquifer is an unconfined fractured bed constituted with limestones and alternating argillaceous limestone, sandstones and microconglomerates beds with low permeability basically through fractures and fissures. These lithologies belong to Igualada fm., member of an Eocene transgression period (Figure 5). Quaternary sandy-silt deposits, soil and anthropogenic fill overlap the above-mentioned unit. Contaminant concentration was screened using a photo-ionization detector (PID) to depths up to 3 meters below ground surface (mbgs) across the contaminated site. High VOCs concentrations were found around the wastewater tank, the former disposal pit (>1500 mg/L of VOCs) and in the soil of the surrounding area of the chemical plant (>1000 mg/L of VOCs) (Torrentó et al., 2014). The main former sources of pollution were the underground wastewater tank, the disposal pit and abandoned barrels at the factory (Figure 5C) (Palau et al., 2014b).

During the 2002 to 2005 period, the barrels, underground tank and pit areas were sampled for concentration and $\delta^{13}C$ analyses of CEs and CMs. In 2005 the barrels and the wastewater pipe system were dismantled and 2000 t of polluted soil from the tank and pit areas were removed.

In parallel, ten multilevel wells were installed, in collaboration with ACA and the Catalan Waste Agency (*ARC*), for monitoring the pollution in the aquifer of the site (Figure 5C). This monitoring led to two doctoral thesis in *Mineralogia aplicada i geoquímica de fluids* (MAG) research group focused on CEs degradation in the saturated zone (Marchesi, 2010; Palau, 2008). The comparison of $\delta^{13}C_{PCE}$, $\delta^{13}C_{TCE}$ and $\delta^{13}C_{sum}$ (including $\delta^{13}C_{cDCE}$) between potential sources and multilevel wells allowed the differentiation between two plumes (around pit area and tank area, respectively) in the fractured bedrock aquifer. VOCs concentrations and the $\delta^{13}C$ study showed source mixing along the two plumes, negligible PCE and TCE biodegradation at potential sources prior to the removal and the absence of PCE and TCE degradation around pit area (S1 and S4 wells) (Figure 5C) while degradation was detected for these compounds in tank area (S3, S6 and S10 wells) (Palau et al., 2014b). Nevertheless, CMs were not specifically studied in the saturated zone of Òdena site.

In the unsaturated zone, two interception trenches with a total depth of 6.5 m were built in 2006 in the empty space of former tank and pit sources. They were filled with concrete-based aggregates from construction wastes (named as pit trench and tank trench, respectively (Figure 5D). Rainwater lixiviates are retained in the unsaturated zone and infiltrate to trenches where alkaline conditions are achieved and AH takes place allowing CF degradation, evidenced by $\delta^{13}C$ shifts in CF over time in field samples and laboratory experiments (Torrentó et al., 2014). In contrast, detected shifts in $\delta^{13}C$ of CT in field trenches were not attributed to CT alkaline

hydrolysis according to CT experiments performed with concrete (Torrentó et al., 2014), in agreement with the slow reaction rates anticipated for CT hydrolysis at environmental temperatures (Jeffers et al., 1989). Therefore, it was hypothesized that Fe-bearing materials from used construction wastes in trenches at pH 12 might play an important role in CT degradation (Torrentó et al., 2014).
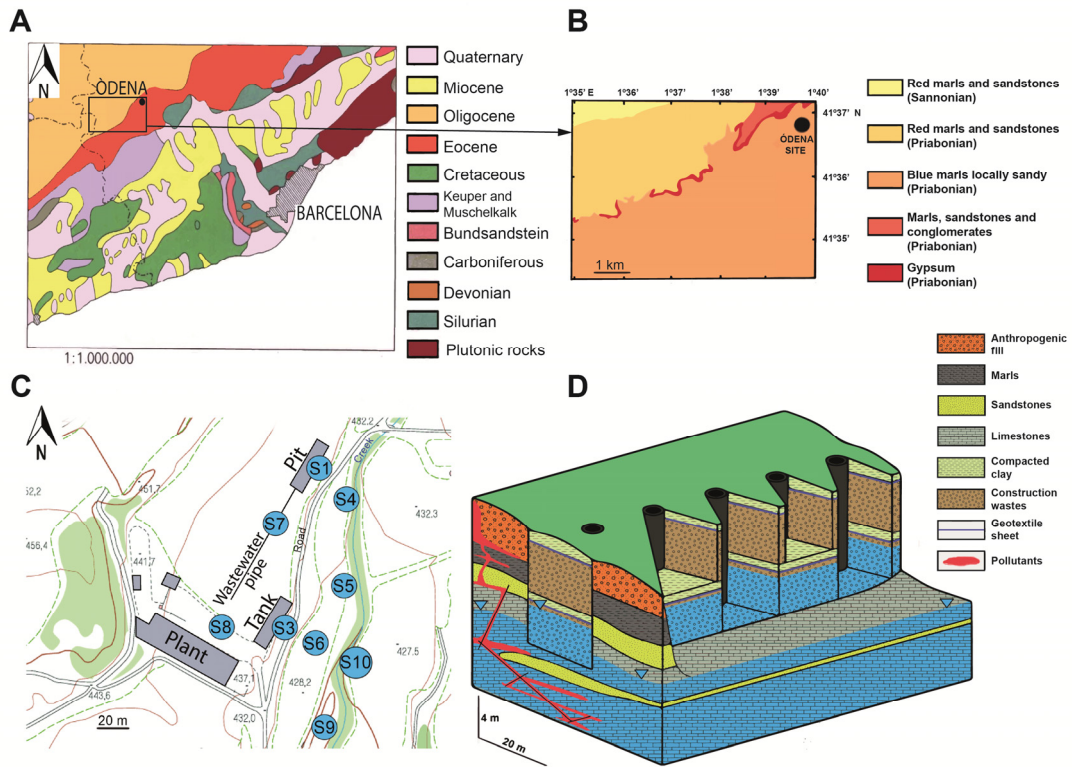
Figure 5. A) Regional geology of Òdena site. B) Detail of the Eocene-Oligocene geology. C) Topographic map of Òdena site and groundwater monitoring wells network (named as 'S#'), industrial plant and former tank, pit and wastewater pipe location. D) Scheme of trenches built after soil from tank and pit sources were removed in 2005.

1.2 Objectives

This thesis aims at improving the knowledge of the degradation processes (natural and induced remediation strategies) of CT and CF in the laboratory scale to be further applied in field sites, such as in Òdena site, where pollution by CMs is a matter of concern. This purpose is sought primarily by means of compound specific isotope characterization of these degradation processes by $\delta^{13}C$ and $\delta^{37}Cl$ analyses of the target compounds.

In order to achieve this main objective, the following specific objectives were defined:

Concerning methodology, the overall goal is to develop compound-specific chlorine isotope analysis (Cl-CSIA) of CT and CF by both gas chromatography-isotope ratio (GC-IRMS) and GC-quadrupole mass spectrometry (GC-qMS) by:

- o choosing the best fragment ions and acquisition parameters for optimum performance in each instrument;

- o validating Cl-CSIA methodology in an interlaboratory comparison exercise performed in international experienced laboratories (Institute of Groundwater Ecology of the *Helmholtz Zentrum München*, Germany, and *Centre d'hydrogéologie et de géothermie*, *Université de Neuchâtel*, Switzerland) with the same type of GC-qMS instrument; and,

- o comparing the precision and trueness of both methods and laboratories.

Concerning laboratory experiments, the main objective is to use Cl-CSIA and C-CSIA to assess CT and CF degradation processes in a set of laboratory experiments which are aimed at:

- o exploring the different CF reaction mechanisms potentially existing in contaminated sites by studying the kinetics of these reactions and characterizing their ε_C and ε_{Cl} and their dual C-Cl isotope patterns ($\Lambda = \delta^{13}C$ *vs.* $\delta^{37}Cl$);

- o assessing and distinguishing different anaerobic CT and CF natural or induced abiotic reductive degradation reactions by Fe(0) and Fe-bearing minerals at different pHs representative of groundwater and alkaline interception trenches of Òdena site and seeing the possible pH effect by studying their kinetics and characterizing as well, their ε_C, ε_{Cl} and dual C-Cl isotope patterns; and,

- o evaluating the anaerobic CT and CF biodegradation potential of indigenous microbiota from Òdena site together with the biostimulation effects of B_{12} addition in microcosm batch experiments. These experiments will allow determining the potential biodegradation reactions' kinetics, ε_C, ε_{Cl} and dual C-Cl isotope patterns along with the active microbial population, through RNA-based next generation sequencing (NGS), and the effect of different B_{12}/CM ratios on the population.

The selected experiments to achieve those objectives are:

o CF degradation experiments following three relevant transformation mechanisms: oxidative C-H bond cleavage by heat-activated persulfate (PS), alkaline hydrolysis (AH) at pH 12 and C-Cl bond cleavage by reductive dechlorination by Fe(0);

o CT and CF reduction reactions by using batch experiments with Fe(0) as well as with Fe(II) sorbed in Py and Mag at two different pH values (7 and 12)

o microcosm studies of CT and CF natural attenuation and biostimulation by B_{12} under anoxic conditions with slurry of Òdena site.

Concerning field application, the principal aim is to test dual $\delta^{13}C$ and $\delta^{37}Cl$ approach application in the complex Òdena field site for:

o identifying original source/s and potential changes in aged-sources;

o studying if sources removal in 2005 was efficient in long-term perspective;

o uncovering CMs active leaching zones;

o confirming if CT and CF natural attenuation processes have taken place in Òdena site over time; and,

o discriminating among different degradation processes of CT and CF in the studied wells through dual C-Cl isotope patterns ($\Lambda=\delta^{13}C$ *vs.* $\delta^{37}Cl$) and quantify when possible their maximum degradation extent.

1.3 Publications derived from this thesis

A total number of five scientific articles have resulted from the work of this thesis, all published in international peer-reviewed science citation index (SCI) journals with high impact factors. These five publications are grouped in the Annex of this document, summarised in Table 2 and briefly described in this section.

Table 2. Summary of the publications derived from this thesis and the SCI journals rank according to Web Of Science, WOS (Thomson Reuters).

Article	Reference	Quartile and category	Impact factor
Article 1	Heckel, B., Rodríguez-Fernández, D., Torrentó, D., Meyer, A., Palau, J., Domènech, C., Rosell, M., Soler, A., Hunkeler, D., Elsner, D., 2017. Compound-specific chlorine isotope analysis of tetrachloromethane and trichloromethane by GC-IRMS *vs*. GC-qMS: Method development and evaluation of precision and trueness. Anal. Chem. 89, 3411–3420. doi: 10.1021/acs.analchem.6b04129	Q1, Analytical chemistry	6.32 (2016)
Article 2	Torrentó, C., Palau, J., Rodríguez-Fernández, D., Heckel, B., Meyer, A., Domènech, C., Rosell, M., Soler, A., Elsner, M., Hunkeler, D., 2017. Carbon and chlorine isotope fractionation patterns associated with different engineered chloroform transformation reactions. Environ. Sci. Technol. 51, 6174–6184. doi:10.1021/acs.est.7b00679	Q1, Environmental chemistry	6.198 (2016)
Article 3	Rodríguez-Fernández, D., Heckel, B, Torrentó, C., Meyer, A., Elsner, M., Hunkeler,D., Soler, A., Rosell, M, Domènech, C. 2018. Dual element (C-Cl) isotope approach to characterize abiotic reactions of chlorinated methanes by Fe(0) and by Fe(II) on iron minerals at neutral and alkaline pH. Chemosphere, 206, 447-456. doi: 10.1016/j.chemosphere.2018.05.036	Q1 Environmental science	4.2 (2016)
Article 4	Rodríguez-Fernández, D., Torrentó, C., Guivernau, M., Viñas, M., Hunkeler, D., Soler, A., Domènech, C., Rosell, M., 2018. Vitamin B_{12} effects on chlorinated methanes-degrading microcosms: Dual isotope and metabolically active microbial populations assessment. Sci. Total Environ. 621, 1615–1625. doi:10.1016/j.scitotenv.2017.10.067	Q1, Environmental science	4.9 (2016)
Article 5	Rodríguez-Fernández, D., Torrentó, C., Palau, J., Marchesi, M., Soler, A., Hunkeler, D., Domènech, C., Rosell, M. Unraveling long-term source removal effects and chlorinated methanes natural attenuation processes by C and Cl stable isotopic patterns at a complex site. *Submitted to* Sci. Total Environ.	Q1 Environmental science	4.9 (2016)

Figure 6 summarizes the relationship among the different research tasks performed during this thesis.
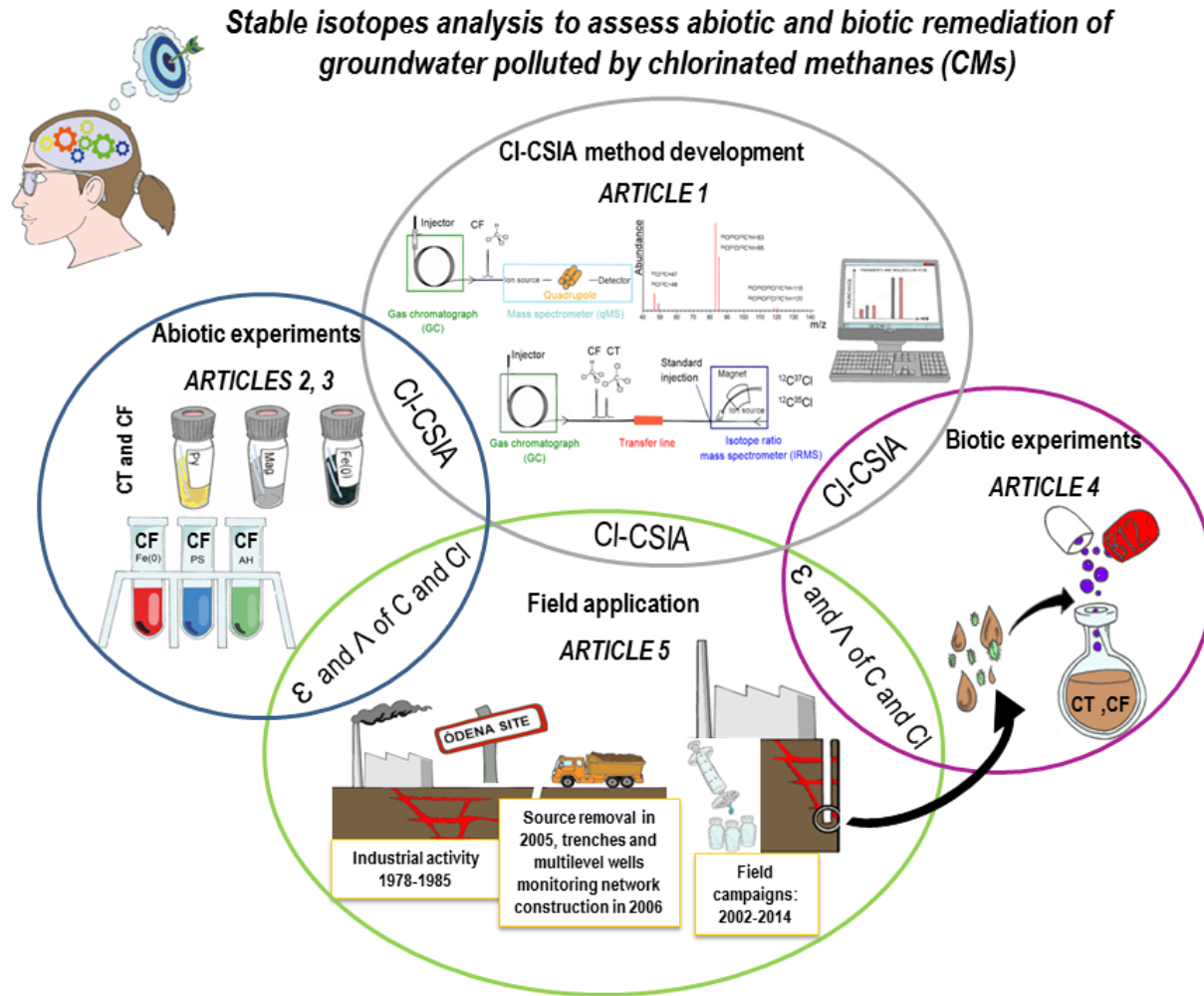
Figure 6. Infographic of the thesis research.

Other contributions presented in conferences related with this thesis are reviewed in Table 3.

Table 3. Summary of the main contributions to conferences in the thesis framework.

Rosell, M.; Rodríguez-Fernández, D.; Torrentó, C.; Palau, J.; Marco-Urrea, E.; Domènech, C.; Soler, A. Compound Specific Isotope Analysis (CSIA) from characterising contaminants degradation pathways to food authenticity. 40th International Conference on Environmental & Food Monitoring (ISEAC-40). (Santiago de Compostela, Spain), 2018. Oral.

Himi,M; Rodríguez-Fernández, D.; Folch, A.; Domènech, C.; Rosell, M.; Otero, N.; Lovera, R.; Palau, J.; Fernàndez-Garcia, D.; Casas, A.; Rivero, L.; Soler, A. Hydrogeological and Geophysical Characterization of Fractured Aquifer of Òdena (Barcelona, Catalunya).Near Surface Geoscience (Malmö, Sweden), 2017. Poster

Soler, A.; Rosell, M.; Otero, N.; Domènech, C.; Palau, J.; Audí-Miró, C.; Rodríguez-Fernández, D. *L'anàlisi isotòpica de compostos orgànics específics (CSIA) com a eina per identificar fonts de contaminació i avaluar els processos de (bio) degradació en emplaçaments contaminats Jornada Tècnica R+D+I en l'aplicació de tecnologies de descontaminació del subsòl. Casos pràctics* (Barcelona, Spain), 2017 Oral

Rosell, M.; Audí-Miró, C.; Rodríguez-Fernández, D.; Palau, J.; Domènech, C.; Soler, A. Compound Specific Isotope Analysis (CSIA) as a successful tool to assess source identification and (bio)degradation processes of organic groundwater contaminants in field studies. International Meeting on New Strategies in Bioremediation Processes. BioRemid2017 (Granada, Spain), 2017. Oral

Rodríguez-Fernández, D.; García-Moliner, D.; Bagaria-Rovira, F.; Soler, A.; Rosell, M.; Domènech, C. Assessing chloromethanes abiotic reductive dechlorination by pyrite and magnetite at neutral and alkaline conditions
2nd European Mineralogical Conference, emc2016 (Rimini, Italy), 2016. Poster

Rodríguez-Fernández, D.; Rosell, M.; Domènech, C.; Torrentó, C.; Palau, J.; Soler, A. Assessment of indigenous chloromethanes biodegradation potential and vitamin B_{12} effects in microcosm experiments.10th ISEB conference, organized by the International Society for Environmental Biotechnology (Barcelona, Spain), 2016. Oral

Rodríguez-Fernández, D.; Folch, A.; Himi, M.; Domènech, C.; Rosell, M., Otero, N., Lovera, R.; Palau, J.; Fernàndez-Garcia, D.; Casas, A.; Soler, A. *Caracterización hidrogeológica del acuífero fracturado bajo el emplazamiento monitorizado de Òdena (Barcelona, Cataluña). 50 Aniversario CIHS 1966-2016* (Barcelona, Spain), 2016. Poster

Rodríguez-Fernández, D.; Rosell, M.; Domènech, C.; Torrentó, C.; Palau, J.; Soler, A. C and Cl-CSIA for elucidating chlorinated methanes biotic and abiotic degradation at a polluted bedrock aquifer. AIG-11, 11th Applied Isotope Geochemistry (BRGM, Òrleans, France), 2015. Oral

Folch, A.; Pijuan G.; Rodríguez-Fernández, D.; Rosell, M.; Domènech, C.; Fernández-García, Daniel; Soler, A. *Caracterización hidrogeológica y modelización hidrodinámica del emplazamiento monitorizado de Òdena (Barcelona. II Congreso ibérico de las aguas subterráneas* (Valencia, Spain), 2014. Poster

Guivernau ,M; Viñas, M; Rodríguez-Fernández, D.; Torrentó, C; Domènech, C.; Soler, A; Rosell, M. Unraveling microbial community interactions in a chlorinated VOC polluted aquifer harboring natural attenuation processes. DehaloCon conference (Jena, Germany), 2014. Poster

Rodríguez-Fernández, D.; Torrentó, C.; Rosell, M.; Audí-Miró, C.; Soler. Evaluating potential chlorinated methanes degradation mechanisms and treatments in interception trenches filled with concrete-based construction wastes. EGU2014 (Viena, Austria), 2014. Poster

Rodríguez-Fernández, D.; Rosell, M.; Torrentó, C.; Audí-Miró, C.; Marchesi, M.; Palau, J.; Otero, N.; Soler. Long-term monitoring of the evolution of the chlorinated VOCs pollution in a fractured bedrock aquifer using CSIA. AIG10, 10th Applied Isotope Geochemistry (Budapest, Hungary), 2013. Poster

Rosell, M.; Torrentó, C.; Rodríguez-Fernández, D.; Audí-Miró, C.; Marchesi, M.; Palau, J.; Guivernau, M.; Viñas, M.; Otero, N.; Soler, A. Multiple evidences of chlorinated methanes natural attenuation in a complex polluted aquifer. AIG10, 10th Applied Isotope Geochemistry (Budapest, Hungary), 2013. Oral

Rodríguez-Fernández, D. ; Rosell, M. ; Torrentó, C. ; Audí-Miró, C. ; Marchesi, M. ; Guivernau, M.; Viñas, M.; Otero, N.; Albert Soler, A. Unravelling chlorinated methanes degradation processes in a complex polluted aquifer by isotopic and molecular tools. Isotopes 2013. Isotopes effects across disciplines (Sopot, Poland), 2013. Poster

Rosell, M.; Torrentó, C.; Audí-Miró, C.; Rodríguez-Fernández, D.; Marchesi, M.; Palau, J.; Aravena, R.; Viñas, M.; Otero, N.; Soler, A. Assessment of remediation strategies in an aquifer polluted by chlorinated organic compounds at a former production site. Aquaconsoil (Barcelona, Spain), 2013. Oral

1.3.1 ART. 1 Cl-CSIA method development

This first article is focused on the development of the analytical methodology for Cl-CSIA in both CT and CF in two different mass spectrometers (GC-qMS and GC-IRMS) and on the interlaboratory comparison of the method by using GC-qMS. This reserch represents a necessary first step prior to the use of both methods in CT and CF remediation studies at laboratory and field scale. The method tests were partially performed during a three months stay in 2014 of Diana Rodríguez-Fernández in the Institute of Groundwater Ecology of the *Helmholtz Zentrum München* (IGOE, Munich, Germany) and during two different stays in 2015 in the *Centre d'hydrogéologie et de géothermie*, *Université de Neuchâtel* (CHYN, Neuchâtel, Switzerland). The main analyses and the analytical methods used in each article are detailed in Table 4. Diana Rodríguez-Fernández was totally involved in Cl-CSIA method development for GC-qMS during the stays in *Université de Neuchâtel*. To compare the trueness of both methods and laboratories, samples from CT and CF degradation experiments were analysed in both laboratories and then calibrated against two isotopically different reference standards for each compound. As $\delta^{37}Cl$ analyses of CF were already performed in *Université de Neuchâtel*, although without a thorough method development, the available standards of that laboratory were used (Breider, 2013). However, a previous work of collecting different commercial brands of CT and analysing their $\delta^{37}Cl$ signature was required in order to perform a two-point calibration for Cl-CSIA method covering a wide range of $\delta^{37}Cl$ values to arrive at reliable $\delta^{37}Cl_{SMOC}$ signatures (Ebert et al., 2017). CT diffusion-controlled vaporization experiments was performed by the PhD student at the Universitat de Barcelona (UB) thanks to the advice and supervision of Dr. Jordi Palau (see Annex A, CT diffusion-controlled vaporization experiments) for generating higher differences in the isotope values of the commercial samples. CT formate experiments were performed entirely by Benjamin Heckel. CF experiments with Fe(0) at pH 12 were perfomed entirely by Diana Rodríguez-Fernández during the stay in Institute of Groundwater Ecology of the *Helmholtz Zentrum München* and the C-CSIA of CF in those samples were performed by Diana Rodríguez-Fernández in the Scientific and Technological Centers of Universitat de Barcelona (CCiT-UB). The results and discussion showed in the article was done through an equally contribution of both Benjamin Heckel and Diana Rodríguez-Fernández.

This article has been also included in Bejamin Heckel's thesis.

1.3.2 ART. 2 Abiotic CF reference reactions

This article is an advance in the knowledge of the different CF transformation mechanisms. It investigated for the first time the isotope fractionation of C and Cl for three different relevant transformation mechanisms trough batch experiments. The studied transformation reactions have been: oxidative C−H bond cleavage using heat-activated PS, transformation under alkaline conditions (pH ~ 12) and reductive C− Cl bond cleavage by milli-sized Fe(0). For more experiments details see Article 2.

The CF reaction by milli-sized Fe(0) at pH 7 was conducted entirely by the PhD student in the Institute of Groundwater Ecology of the *Helmholtz Zentrum München* during the three-month thesis stay, where Cl-CSIA was also performed, but the C-CSIA of CF and daughter products of those samples were performed by Diana Rodríguez-Fernández in the CCiT-UB (Table 4). CF reactions with AH and PS were performed at UB by Dra. Clara Torrentó where Diana Rodríguez-Fernández contributed with C-CSIA analyses and Dr. Jordi Palau with Cl-CSIA in *Université de Neuchâtel* (Table 4).

Diana Rodríguez-Fernández has contributed both in results discussion and in the wording of this article.

Table 4. Summary of the main analyses, the analytical method used, and the location of the latter, for the five articles derived from this thesis. Among the used analytical methods, Diana Rodríguez-Fernández directly performed those analyses flagged by an asterisk (*).

Analyses	Analytical method	Location	Article
VOCs concentration	GC-qMS	*Helmholtz Zentrum München (IGOE)*	1,3
	HS-GC-TOF-MS*	*Helmholtz Zentrum München (IGOE)*	2,3
	HS-GC-MS*	CCiT-UB	2,3,4,5
C-CSIA	SPME-HS-GC-IRMS*		1,2,3,4,5
	Direct gas injection by GC-IRMS	*Helmholtz Zentrum München (IGOE)*	3
Cl-CSIA	GC-qMS*	*Université de Neuchâtel, CHYN*	1,2,3,4,5
	GC-IRMS	*Helmholtz Zentrum München (IGOE)*	1,2,3
Total bacterial population	DNA and 16S rRNA extraction for DGGE analyses and deep microbial assessment by Illumina (Miseq) high-throughput sequencing	GIRO Joint Research Unit IRTA-UPC	4
Metabolically active populations			
cfrA gene expression			
Specific surface area/ Particle size distribution/image scanning	BET/photon correlation spectroscopy/ SEM coupled with energy-dispersive X-ray*	CCiT-UB	3
Anions and cations total concentrations	ICP-OES, ICP-MS, Tritation, HPLC		4,5
Eh and pH	Eh and pH sensors*		2,3,4,5

Equipment abbreviations correspond to gas chromatography (GC)-quadrupole mass spectrometer (qMS); headspace (HS)- GC-coupled to a time-of-flight (TOF)-MS; solid-phase micro-extraction (SPME)-HS-GC coupled to an isotope ratio mass spectrometer (IRMS); denaturing gradient gel electrophoresis (DGGE), Brunauer–Emmett–Teller method (BET), scanning electron microscope (SEM), inductively coupled plasma optical emission spectrometry (ICP-OES), inductively coupled plasma mass spectrometry (ICP-MS), high-performance liquid chromatography (HPLC).

1.3.3   ART. 3 Abiotic chlorinated methanes degradation

In this article, CT and CF abiotic reactions with Fe(0) and with Fe(II) sorbed on Py and Mag at pH 7 and pH 12 under anoxic conditions were studied in laboratory batch experiments to distinguish potential natural attenuation processes and/or characterize remediation strategies. These experiments were named as 'pollutant_mineral/aq/Co _pHvalue', being 'pollutant' CT or CF; 'mineral' means $FeCl_2$ and Mag or Py; 'aq' means only $FeCl_2$ presence; CO, only buffered solution; and pHvalue, 7 or 12 (for more details of each experiment see Article 3, Table 1). The study was addressed primarily by monitoring parental and by-products concentration and C and Cl-CSIA of VOCs. Diana Rodríguez-Fernández conducted all the experiment except that of CT degradation by Fe(0) which was done by Benjamin Heckel in the Institute of Groundwater Ecology of the *Helmholtz Zentrum München.* Diana Rodríguez-Fernández analysed the concentration and C-CSIA of VOCs in the CCiT-UB, while Cl-CSIA were done during the thesis stays both at *Université de Neuchâtel* by GC-qMs and in the Institute of Groundwater Ecology of the *Helmholtz Zentrum München* by GC-IRMS.

Diana Rodríguez-Fernández has led the results discussion and the article wording*.*

1.3.4   ART. 4 Biotic chlorinated methanes degradation

This article is focused on studying the CT and CF anaerobic natural attenuation in the slurry of a well located in one of the former sources of pollution in Òdena site (S3 well, Figure 5. These experiments were named as 'pollutantw/oB', being pollutant CT or CF. In addition, different biostimulation scenarios with vitamin B_{12} were conducted named as 'B_{12}/pollutant' (B_{12}/pollutant ratio of 0.01 and 0.1). The study was performed in terms of parental and by-products concentrations, carbon and Cl-CSIA of VOCs and active microbial community through 16S rRNA (RNA/DNA-based) MiSeq high-throughput sequencing. Microcosm experiments were conducted by Diana Rodríguez-Fernández in the CCiT-UB where concentration and C-CSIA of VOCs were also analysed, whereas Cl-CSIA were done at *Université de Neuchâtel* by Diana Rodríguez-Fernández during the two thesis stays in this research institute (Table 4). The microbial population analyses were carried out by the GIRO Joint Research Unit IRTA-UPC (Table 4). To our knowledge, the dual carbon-chlorine isotope data from field-derived CT and CF microcosms of this thesis are the first obtained.

Diana Rodríguez-Fernández has led the results discussion and the article wording.

1.3.5   ART. 5 Chlorinated methanes degradation: field study

This last article studies the degradation of CMs in a field scale. It puts forward for the first time the application of the new abiotic and biotic CT and CF degradation insights, including the application of 2D-CSIA approach obtained in laboratory experiments into real field samples.

Apart from samples taken from 2002 to 2005 in sources prior to their removal, field campaigns in Òdena were performed by MAG research group from 2006 to 2014. This thesis research was directly involved in the last two campaigns (March 2013 and November 2014): in their organization, performance and in the analytical measurements specified in Table 4.

Additionally, the compilation of data set, treatment, interpretation and discussion of these two field campaigns and the previous ones were also performed during this thesis. In March 2013 and November 2014 campaigns, a dual isotope approach was possible as a result of the Cl-CSIA method development.

This paper studies the efficiency of pollution source's removal and their long-term effects on CMs in groundwater concentrations, the finding of CMs active leaching zones, the detection of CMs natural attenuation and the evaluation of the potential of dual C and Cl isotope approach to identify CMs degradation pathways at sites with complex mixtures such that of Òdena are studied. To achieve fulfil these challenges, the wells located downgradient the main pollution sources in Òdena site are studied in terms of CMs and their by-products concentration, C and Cl isotopic composition evolution and redox shifts over time. C-CSIA were done in CCIT-UB and Cl-CSIA, in *Université de Neuchâtel* during the thesis stays.

Diana Rodríguez-Fernández has led the results discussion and the article wording.

2. Results

2.1 ART.1 Cl-CSIA method development

For GC-IRMS analysis, masses of m/z= 47 and 49 (CCl fragment) were recorded for both CT and CF since they correspond to half of the masses for which the IRMS instrument is configured. Regarding the study of acquisition parameters of compound-specific chlorine isotope analysis in the CG-qMS, the plot of standard deviation (SD) against different ions pairs and dwell times (Article 1, Fig. 2A) revealed that the most precise result for both CT and CF in the GC-qMS from Munich (GC-qMS-1) was the recording of two ions with a dwell time of 70 ms. However in GC-qMS from Neuchâtel (GC-qMS-2) the method published by Breider and Hunkeler (2014) was followed (50 ms).

The precision, defined as the closeness of agreement among a set of results, of CT measurements was studied in both instruments. For the GC-IRMS, at low amplitudes (100 mV) the CT showed SD of ±0.6‰ (n=10), whereas at signals (>1 V) the SD became smaller (±0.1‰, n=60) (Article 1, Fig. 3A). On the other hand, the interlaboratory comparison between both GC-qMSs showed similar results and it revealed that only above an area of 30 million TIC (total ion count) SDs of ±0.6 to 0.4‰ (n=13) were achieved (Article 1, Fig. 3B). In contrast to CT, CF showed a strong-amount-dependency by the GC-IRMS (Article 1, Fig. 4A) and SDs were also amount-dependent by both GC-qMSs, being higher (±1.0‰ *vs.* ±0.4‰) at lower concentrations (0.24-0.36 mg/L *vs.* 1.2-2.4 mg/L) (Article 1, Fig. 5A), although SDs were better for GC-IRMS (< ±0.5 at 2.5 ng on column *vs.* >±1 for the same amount) (Article 1, Fig. 5B).

However, unlike the observed linearity of precision, no amount-dependency was observed for the trueness (defined as the closeness of the mean of a set of measurement results to the true value) of $\delta^{37}Cl$ values of CT neither for CF on both GC-qMSs (Article 1, Fig. 3B and 5A). Trueness of CT and CF $\delta^{37}Cl$ values by both instruments was studied in samples of different experiments which gave rise to remarkable fractionation providing a reliable range of $\delta^{37}Cl$ values. Samples of the CT experiment with sodium formate without external standard normalization to international V-SMOC scale differ 5‰ at the initial isotope value from normalized one and showed differences of 0.5‰ in the isotopic fractionation values (ε) between normalized and those non-normalized values (Article 1, Fig. 6A). Moreover, when uncorrected $\delta^{37}Cl$ values from different experiments are plotted against those corrected by two-point calibration relative to V-SMOC, the obtained slopes (m) for both studied GC-qMS instruments deviate from unity, especially for CF (m(Munich)=1.6 and m(Neuchâtel)=1.9 (Article 1, Fig. 6B). However, these slopes values showed small variations for different measurement days over long time periods (Article 1. Fig. 6C).

Finally, when two-point calibration is performed, extremely close ε values for CT (CT sodium formate experiments, Figure 7A) and remarkably similar Λ values for CF ($\Delta\delta^{13}C/\Delta\delta^{37}Cl$) were found for both GC-qMS-1 and GC-IRMS (CF experiments with Fe(0) at pH 12, Figure 7B).
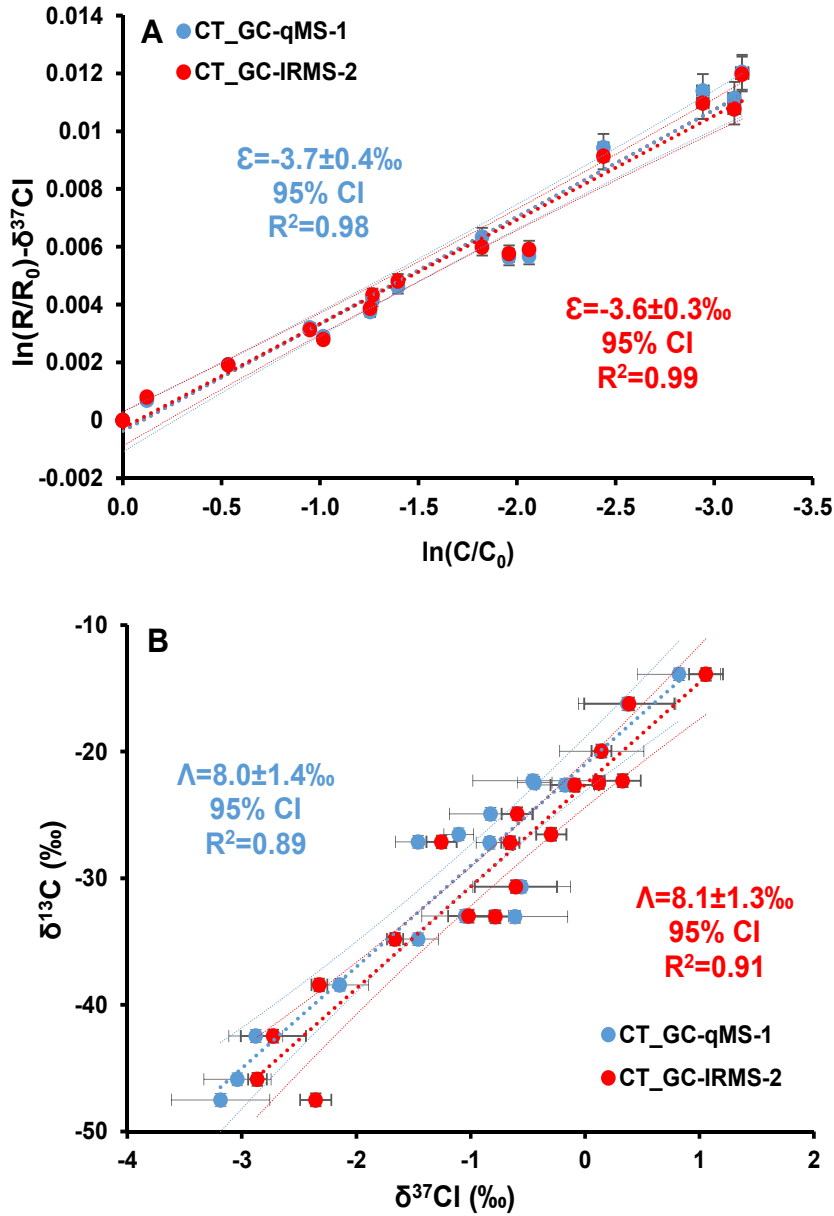
Figure 7. A) Logarithmic plot according to Rayleigh equation (Eq. 2) of chlorine isotope ratios of CT in sodium formate experiments from GC-qMS and GC-IRMS from Munich after two-point calibration. B) Dual element isotope plot ($\delta^{13}C$ *vs.* $\delta^{37}Cl$) of CF degradation with Fe(0) at pH 12 and the comparison of regressions from GC-qMS and GC-IRMS chlorine isotope data (four measurements were conducted for each data point).

2.2 ART. 2 Abiotic CF reference reactions

CF oxidation by heat-activated PS showed a 90% of CF removal after 6 days in experiments with a molar ratio of PS/CF of 40/1 (Article 2, Fig. 1A) following a pseudo-first-order kinetics with k'=0.40±0.06 d^{-1} (R^2=0.96, Article 2, supplementary information (SI), Fig. S1). Chlorine was released into solution but other by-products or intermediates were not detected by GC/MS. The carbon (ϵC_{CF}) and chlorine (ϵCl_{CF}) fractionation values were -8±1‰ and -0.44±0.06‰, respectively (Table 5). The corresponding AKIE$_C$ value (Eq. 4, n=x=z=1 in all reactions of this section) for this reaction was 1.008±0.001 and the value for AKIE$_{Cl}$, 1.00045±0.00004 (Eq. 4, n=x=3, z=1). The dual carbon-chlorine isotope pattern for oxidation ($\Lambda=\Delta\delta^{13}C/\Delta\delta^{37}Cl$) was 17±2 (Table 5, Figure 8B).

CF transformation under alkaline conditions (pH~12) showed 85% of CF concentration after 35 days (Article 2, Fig. 1B) following a pseudo-first-order kinetics with k'=0.052±0.008d^{-1} (R^2=0.92, Article 2, SI, Fig. S1) agreeing with previous reported values (Torrentó et al., 2014). Potential degradation by-products were not analyzed. For CF AH, the obtained fractionation values were ϵC_{CF}= -57±5‰ and ϵCl_{CF}=-4.4±0.4‰ (Table 5). The corresponding AKIE$_C$ value was 1.061±0.006 and the value for AKIE$_{Cl}$, 1.0133±0.0004 (Eq. 4, n=x=z=3). Λ value was 13.0±0.8 (Table 5, Figure 8A).

CF transformation study by milli-sized Fe(0) at pH 6.2±0.2 revealed a 84% of CF removal after 50 hours. Although iron surface passivation might have increased reaction half-lives and deviations from pseudo-first-order kinetics at later stages of a reaction, a k' of 0.07±0.01 h^{-1} (R^2=0.93, Article 2, SI, Figure S1) was obtained which corresponds to the calculated value of k_{SA}=2.1±0.4 x 10^{-2} L m^{-2} d^{-1}. Free chlorine and up to 2.4% DCM yield were detected as by-products. The obtained CF fractionation values were ϵC_{CF}= -33±11‰ and ϵCl_{CF}=-3±1‰ (Table 5). The corresponding AKIE$_C$ was 1.034±0.012 and AKIE$_{Cl}$, 1.008±0.001 (Eq. 4, n=x=z=3). Λ value was 8±2 (Table 5, Figure 8B).

Table 5. Comparison of Ɛ and AKIE values for C and Cl isotopes in the different CT and CF degradation studies performed during this thesis. CF oxidation involves a C-H bond cleavage and the rest of reactions, a C-Cl bond cleavages n.m.: not measured. n=x=z=1 in Eq. 4 for $AKIE_c$ in both CT and CF; n=x=3 and z=1 for $AKIE_{Cl}$ in CF oxidation and z=3 in the rest of CF reactions; n=x=z=4 for $AKIE_{Cl}$ in all CT reactions.

Compound	Experiment	Degradation pathway	ε_{bulkC} (‰) ± 95%CI	$AKIE_C$	ε_{bulkCl} (‰) ± 95%CI	$AKIE_{Cl}$	$\Lambda \approx \varepsilon_C/\varepsilon_{Cl}$	Reference
CF	Heat-activated persulfate	Oxidation	-8 ± 1	1.008 ± 0.001	-0.44 ± 0.06	1.00045 ± 0.00004	17 ± 2	Article 2
CF	pH ~12	Alkaline hydrolyisis	-57 ± 5	1.061 ± 0.006	-4.4 ± 0.4	1.0133 ± 0.0004	13.0 ± 0.8	
CF	Abiotic Fe(0) pH 7	Hydrogenolysis ± reductive elimination	-33 ± 11	1.034 ± 0.012	-3 ± 1	1.008 ± 0.001	8 ± 2	
CF	Abiotic Fe(0) pH 12	Hydrogenolysis ± reductive elimination	-20 ± 9	1.020 ± 0.009	-2 ± 1	1.006 ± 0.001	8 ± 1	Article 3
CF	Abiotic Py at pH 12	Hydrogenolysis ± reductive elimination and partly by AH?	-20 ± 7	1.020 ± 0.007	n.m.			
CF	Biotic (field slurry) with vitamin B_{12}	Hydrogenolysis ± reductive elimination	-14 ± 4	1.014 ± 0.002	-2.4 ± 0.4	1.0072 ± 0.0004	7 ± 1	Article 4
CT	Nano-sized Fe(0) at pH 7 and pH 12	Hydrogenolysis	-3.7 and -3.4	1.0037 and 1.0034	-0.58 and -0.55	1.00233 and 1.00220	5.8 ± 0.4 and 6.1 ± 0.5	Article 3
CT	Aqueous $FeCl_2$ at pH 12	Hydrogenolysis	-3 ± 3	1.003 ± 0.003	Low regression	High confidence interval		
CT	Py at pH 7	Hydrogenolysis and thiolytic reduction	-5 ± 2	1.005 ± 0.002	-1.5 ± 0.4	1.0060 ± 0.0004	2.9 ± 0.5	
CT	Py pH 12	Hydrogenolysis and thiolytic reduction	-4 ± 1	1.004 ± 0.001	-0.9 ± 0.4	1.0036 ± 0.0004	3.7 ± 0.9	
CT	Mag at pH 12	Hydrogenolysis and hydrolytic reduction?	-2 ± 1	1.002 ± 0.001	-0.8±0.2	1.0032 ± 0.0002	2 ± 1	
CT	Biotic (field slurry)	Hydrogenolysis among other reductions	-16 ± 6	1.016 ± 0.001	-6 ± 3	1.023 ± 0.003	6.1 ± 0.5	Article 4
CT	Biotic (field slurry) with vitamin B_{12}	Reduction processes	-13 ± 2	1.013 ± 0.003	-4 ± 2	1.015 ± 0.002	5 ± 1	
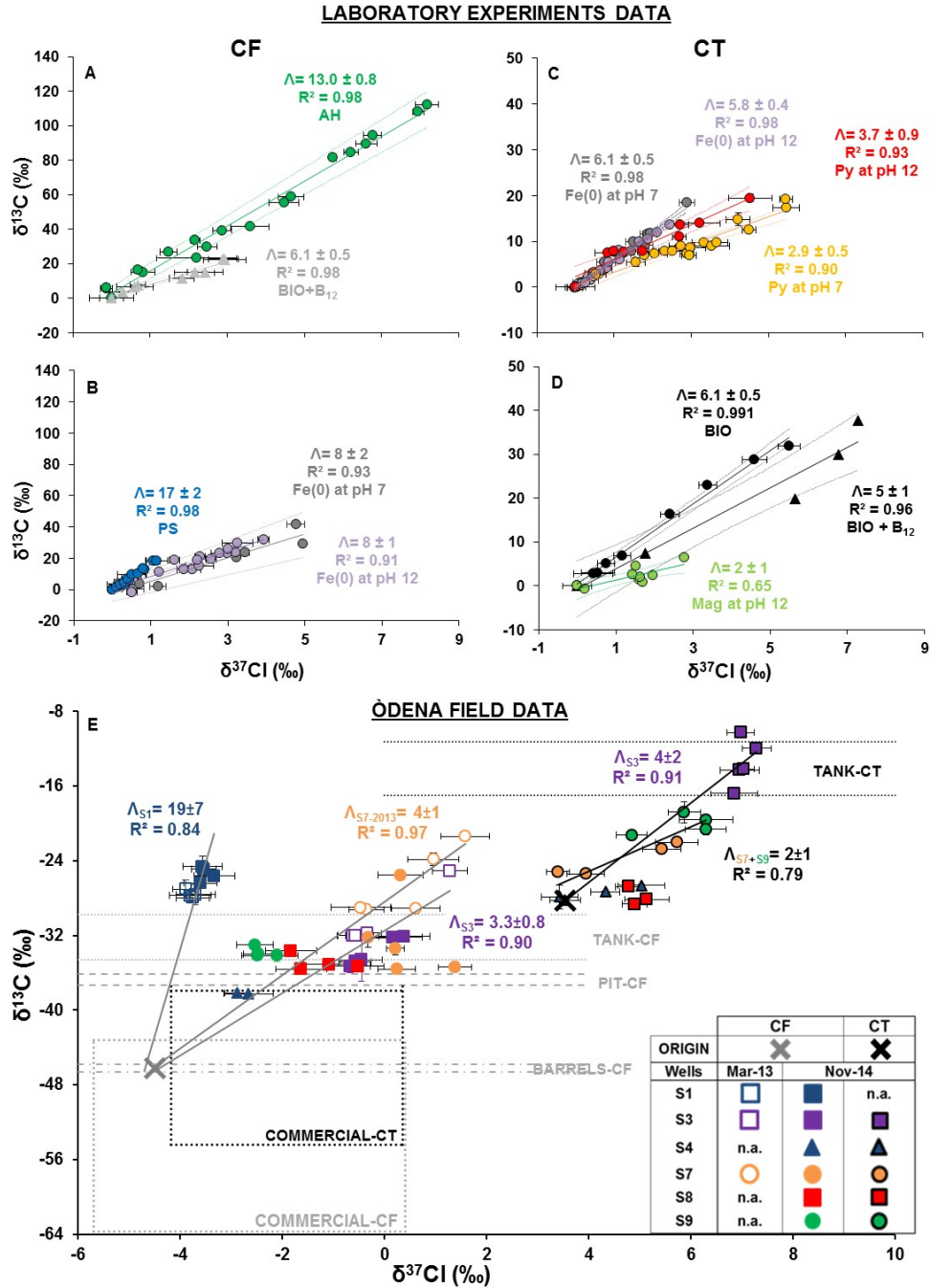
Figure 8. CF and CT C-Cl isotope slopes obtained from all the experiments of this thesis: A) slopes (Λ) obtained for CF AH (Article 2) and CF biodegradation with B_{12} (BIO+B_{12}, Article 4); B) Λ obtained for CF oxidation by PS (Article 2) and CF reduction by Fe(0) at pH 7 and 12 (Article 3); C) Λ, for CT reduction by Fe(0) at pH 7 and 12 and pyrite (Py) at both mentioned pH values (Article 3); D) Λ of CT biodegradation without and with B_{12} (BIO and BIO + B_{12}, Article 4) and CT degradation by magnetite (Mag) at pH 12 (Article 3). E) C-Cl isotope plot of the field site. $\delta^{13}C$ (‰) of the sources (barrels, pit and tank) sampled prior to their removal and isotopic values of commercial substances are represented in black and grey dashed lines for CT and CF, respectively. Error bars show uncertainty in $\delta^{13}C$ and $\delta^{37}Cl$ values. The CT and CF slopes of wells are shown (Λ_{well}) with respect to the specified origin (Article 5).

2.3 ART. 3 Abiotic chlorinated methanes reactions

Measured initial concentrations were lower than expected in some experiments (Article 3, Fig. 3A,D and 4A,D) while pH remained constant (SD<0.5) for the major part of them. Regarding experiments with Fe(0) (Fe(0) experiments), CT concentration decreased below detection limit after 4 h, following a pseudo-first-order kinetic law of $K_{SA}=(4.9\pm0.6)\times10^{-2}$ Lm^{-2} h^{-1} at pH 7 and of $(4.4\pm0.1)\times10^{-2}$ $Lm^{-2}h^{-1}$ at pH 12 (Article 3, SI, Table S1). Significant shifts in $\delta^{13}C_{CT}$ and $\delta^{37}Cl_{CT}$ resulted in similar ϵC_{CT} (-3.7±0.1, R^2=0.995 and -3.4±0.1, R^2=0.993) at pH 7 and 12 after 99.4‰ and 98.6% removal, respectively. Similarly, comparable ϵCl_{CT} were obtained (-0.58±0.04, R^2=0.98 and -0.55±0.03, R^2=0.98) at pH 7 and pH 12, respectively (Table 5). Consequently, corresponding CT $AKIE_C$ values (Eq. 4, x=z=1 in all experiments) were similar for both pH values (1.0037±0.0001, pH 7; 1.0034±0.0001, pH 12), as also happens for $AKIE_{Cl}$ values (Eq. 4, x=z=4 for CT in all CT experiments): 1.0023±0.0004, pH 7; and 1.00220±0.00003, pH 12 (Table 5). CF (representing 45-56% of initial CT) and DCM (up to 0.3% of initial CT) were detected as by-products at both pH values (Article 3, Fig.1) as it was previously observed in literature (Feng et al., 2008; Helland et al., 1995; Lien et al., 2007; Song and Carraway, 2006; Támara and Butler, 2004). However, a thorough study of by-product distribution was not the aim of this study since only VOCs were analyzed but gases (CO_2, CO, CH_4) were not examined. The difference between the final $\delta^{13}C_{SUM}$ (Eq. 6) with respect to the initial $\delta^{13}C_{SUM}$ (only considering CT and CF as by-product) was of only 1.5‰ at pH 7 but of 35‰ at pH 12, indicating in the first case, the absence of by-product formation other than CF and no further CF degradation during 3.5 h. However, Λ values obtained at pH 7 and 12 were similar (6.1±0.5, R^2=0.98, and 5.8±0.4, R^2=0.98, respectively) (Figure 8C). In addition, experiments with milli-sized Fe(0) and CF at pH 12 were also carried out to complement the data at pH 7 obtained in Article 2 and to improve the knowledge on the behavior of this common by-product and parental compound. Relevant $\delta^{13}C_{CF}$ shifts of 17.6‰ after 9 days confirmed degradation in the CF control experiment (without Fe(0)) at pH 12. In Fe(0) experiments at pH 12, CF concentration also decreased with fluctuations that caused poor correlations in K_{SA} and ϵ calculations (Article 3; SI table S1 and S4) showing low DCM accumulation (≤0.3 % yield after 9 days) and a Λ of 8±1 (R^2=0.91) (Table 5, Figure 8C).

Regarding experiments with Mag and 0.6 mM of aqueous $FeCl_2$ (Mag experiments), no significant $\delta^{13}C$ shifts were detected neither in CT nor in CF experiments at pH 7 (Article 3, Fig. 3B). Conversely, in analogous CT and CF experiments at pH 12, concentration decreased following a pseudo-first-order law (Article 3, SI, Table S3) and degradation was confirmed by significant $\Delta\delta^{13}C$ and $\Delta\delta^{37}Cl$ (Article 3, Fig. 3). The obtained ϵ values and corresponding AKIEs of CT and CF degradation by Mag at pH 12 are summarized in Table 5. The CF yield was up to 38% for CT degradation with Mag at pH 12 and the corresponding Λ value was 2±1 although with poor linear regression (R^2=0.65) (Table 5, Figure 8D).

Regarding experiments with Py and 0.6 mM of aqueous $FeCl_2$ (Py experiments), CT underwent degradation at both studied pH conditions but CF was only degraded at pH 12. In all

cases, degradation was confirmed by enrichment in ^{13}C and ^{37}Cl (Article 3, Fig. 4) following pseudo-first-order-rates of parental concentration decrease (Article 3, SI, Table S3). Obtained ε values and corresponding AKIEs are listed in Table 5. CF and CS_2 were detected as CT degradation by-products with Py at both pH values and especially at pH 12 very enriched $\delta^{13}C_{CS2}$ values (+28.8‰) with respect to the initial $\delta^{13}C_{CT}$ were detected after 46 h (Article 3, Fig.4). On the other hand, DCM, although with low yield (only up to 6%), was the single detected product for CF degradation by Py at pH 12. Similar Λ values at both pH conditions for CT degradation by Py were obtained (Λ=2.9±0.5, R^2=0.9 for pH 7 and Λ=3.7±0.9, R^2=0.93 for pH 12) (Table 5, Figure 8C).

2.4 ART. 4 Biotic chlorinated methanes degradation

In autoclaved slurry controls, CF and CT concentration fluctuated (Article 4 Fig. 1) but any increase in the by-products concentration neither any shift in $\delta^{13}C$ nor in $\delta^{37}Cl$ signatures ($\delta^{13}C_{CF}$=−41.7±0.3‰, n=9; $\delta^{37}Cl_{CF}$=−2.6±0.1‰, n=3; $\delta^{13}C_{CT}$=−40.4±0.8‰, n=19; $\delta^{37}Cl_{CT}$=−0.8±0.1‰, n=4) (Article 4 Fig. 2) was not detected.

In the CF microcosm without added B_{12}, although CF concentration fluctuated (Article 4, SI, Fig. 1A), $\delta^{13}C_{CF}$ did not vary significantly (−40.8±0.8‰, n=7) (Article 4, SI, Fig. 2A). On the other hand, in the presence of B_{12} (0.01B/CF treatment), a CF concentration decrease (Article 4, SI, Fig. 1B) was accompanied by significant $\delta^{13}C$ and $\delta^{37}Cl$ enrichment ($\Delta\delta$ of 23 and 3‰, respectively, after 376 days). In the 0.1B/CF treatment, with more B_{12}, CF was completely consumed before 72 days (Article 4, Fig. 1C), not allowing isotope measurements. Transient DCM accumulation was detected only in 0.01B/CF around 200 days (Article 4, SI, Fig. A3B).

In the CT microcosm without B_{12}, the decrease of CT concentration (Article 4, Fig. 1D) was accompanied by significant $\Delta\delta^{13}C$ and $\Delta\delta^{37}Cl$ (up to 32‰ and 6‰ after 376 days, respectively, Article 4, Fig. 2C) and CF was yielded as a by-product. A complete CT consumption was observed with B_{12} after 110 and 72 days for 0.01B/CT and 0.1B/CT treatments, respectively (Article 4, Fig.1E–F). Both CT treatments showed significant and similar $\delta^{13}C$ and $\delta^{37}Cl$ enrichment trends (Article 4, Fig. 2C, D). In the 0.01B/CT treatment, the CF concentration increased over time as a by-product (Article 4 Fig. 1E), whereas in the 0.1B/CT treatment, a decrease in the CF concentration was detected (Article 4 Fig. 1F).

Pseudo-first rate constant values of CMs concentration removal kinetics (k') ranged from 0.003±0.001 to 0.08±0.06 d^{-1} for CF and from 0.005±0.002 to 0.06±0.07d^{-1} for CT (ARTICLE 4, SI, Fig. A4).

$\Delta\delta^{13}C$ of the background PCE and cDCE was up to 11.6 and 5.3‰, respectively, in 0.1B/pollutant experiments when the CT and CF concentrations decreased to levels under the detection limit. Conversely, $\delta^{13}C_{PCE}$ remained constant (−26.6±0.1‰) if CF was still in solution in the 0.1B/CF treatment (Article 4, Fig. 3).

Isotopic fractionation values were ϵC_{CF}=-14±4‰ and ϵCl_{CF}=-2.4±0.4‰ with B_{12}; ϵC_{CT}=-16±6 and ϵCl_{CT}=-6±3 with B_{12} and ϵC_{CT}=-13±2‰ and ϵCl_{CT}=-4±2‰ without B_{12} (Table 5). AKIE calculations were done assuming one C-Cl bond cleavage and the above-mentioned ϵ values ($R^2 \geq 0.9$) were used (Article 4, Table 3, Fig. A8). Obtained values are also listed Table 5. *Acidovorax, Ancylobacter* and *Pseudomonas* were the most metabolically active genera identified, being the last two denitrifying genera. However, commonly found OHRB such as *Dehalococcoides, Sulfurospirillum, Geobacter, Desulfosporosinus, Dehalobacter* and *Desulfitobacterium* were below 0.5% relative abundance in any of the sampled times for CT nor CF treatments.

Λ value for CF biodegradation (only detected with B_{12}, 7±1) was similar to that for CF hydrogenolysis in combination with reductive elimination by Fe(0) (8±2) and statistically different (ANCOVA, p<0.0001) from the CF alkaline hydrolysis or oxidation (13.0±0.8, 17±2) obtained in ARTICLE 2 (Table 5, Figure 8A,B). CF hydrogenolysis was supported by temporary DCM accumulation and possibly further degradation by species like *Ancylobacter dichloromethanicus*. Λ values for CT were statistically different (ANCOVA p=0.02) with and without B_{12} (5±1 *vs.* 6.1±0.5), respectively (Table 5, Figure 8D).

2.5 ART. 5 Chlorinated methanes degradation: field study

The $\delta^{13}C_{CT}$ of the wastewater tank source in 2003 and 2004 (no other sources were available), prior to 2005 source's removal, were was above the range of commercial CT values (Article 5, Table 1). In contrast, $\delta^{13}C_{CF}$ value of the barrels was within the range of commercial CF, whereas those values from tank and pit were much more enriched (Article 5, Table 1).

S1 and S4 wells (Figure 5) are influenced by pit source according to groundwater flowpath described previously by Palau et al. (2014b). Along all the campaigns, only two $\delta^{13}C_{CT}$ values could be measured in S1, a well located in the former disposal pit, being one of them (-30.0±0.5‰) the most depleted observed within all sampling wells and sampling campaigns. CF was the most abundant CMs in S1 (Article 5, Fig. 2) and $\delta^{13}C_{CF}$ values from this well were more enriched than sources and commercial values (Article 5, Fig. 3) evidencing CF fractionation processes. Eh conditions in S1 were controlled by the Fe system in 2006 and 2007 but they evolved towards more oxidizing conditions in the last campaigns (Article 5, SI, Fig. A1). Regarding S4, total CMs concentrations in March 2013 and November 2014 were the highest measured ever in the equivalent depth of the upstream well S1 during studied campaigns along with the presence of higher proportion of CT (Article 5, Fig. 2) and less degraded CT and CF isotopic compositions (Article 5, Fig. 3). The dual C-Cl isotope plot of CF obtained in March 2013 and November 2014 is shown in Figure 8E and it is compared with previously reported Λ values for different degradation mechanisms studied during this thesis. A CF slope for S1 of Λ=19±7 (R^2=0.84) was obtained using the most depleted C and Cl isotopic values ever found in the field (-46.2‰ and -4.5‰) and considering certain enrichment in the initial $\delta^{37}Cl_{CF}$.

S3 and S6 wells belong to tank source's influence area (Figure 5). S3 is placed in the former tank source, and reached CMs concentrations close to 350 μM in November 2010 (Article 5, Fig. 2). CMs concentration showed different trends along the S3 profile, it decreased over time in the upper parts whereas fluctuated in the deepest, while CF was the most abundant CMs in all studied depths and along time (Article 5, Fig. 2). Higher DCM amounts, up to 102 μM and CS_2 up to 0.8 μM, were found in this well in contrast to the rest of wells. Unlike S1, $\delta^{13}C_{CT}$ values were far from commercial solvent compositions in S3 and fell into tank source values (Article 5, Fig. 3). Both $\delta^{13}C_{CT}$ and $\delta^{37}Cl_{CT}$ values of S3 well were the most enriched ones of all sampling wells (Article 5, Fig. 3). Different $\delta^{13}C_{CT}$ enrichment trends were detected in depth and over time in S3, although the Eh was steadily controlled by the Fe system over time (Article 5, SI, Fig. A1). $\delta^{13}C_{CF}$ values were within the limits found for the tank and pit sources, except for the deepest parts which had the most enriched values of the well (Article 5, Fig. 3). The only available $\delta^{13}C_{DCM}$ values in S3 were located in the deepest levels and are similar to those found in sources (Article 5, Table 1). Dual C-Cl slope of CT from S3 well during March 2013 and November 2014 (Λ=4.3±0.7, R^2=0.88) was calculated taking the most depleted values (S4) as origin. CF Λ of S3 (Λ=3.3±0.8, R^2=0.90) was calculated using the same origin than for S1 (Figure 8E). Downstream, in S6 well CMs concentration was lower than ever in S3 and decreased during the studied time being CF the most abundant CMs (Article 5, Fig. 2). There

were few $\delta^{13}C_{CT}$ values available in S6 also far from CF commercial values and similar to those from tank source in 2003 and 2004, but it is not possible to determine when or where CT degradation processes occurred (Article 5, Fig. 2). $\delta^{13}C_{CF}$ values in S6 fluctuated and could be attributable to high CT degradation in S3- S6 area, but this hypothesis could not be confirmed with the existing data.

Wells S7 and S8 were both located along the wastewater pipe and the industrial plant building facilities (Figure 5). S8 well is the closest to the chemical plant (Figure 4) and showed low CMs concentrations which not clearly decreased during the studied period and with CF always more abundant than CT (Article 5, Fig. 2). Eh fluctuated between values controlled by N and Fe system (Article 5, SI, Fig. A1). $\delta^{13}C_{CT}$ values from S8 well were one of the most depleted values of the field site together with those of S1 and S4 and fluctuated around 4‰ (Article 5, Fig. 3). $\delta^{13}C_{CF}$ values were close to pit and tank sources and underwent more than a 10‰ decrease from March 2013 to November 2014. In contrast, the highest CMs concentration of Òdena site in the studied period was found in the upper part of S7 well (Article 5, Fig. 2). CMs concentration increased over time achieving a maximum value of 632 μM in November 2014 in the upper parts (Article 5, Fig. 2). Relevant $\delta^{13}C_{CT}$ and $\delta^{13}C_{CF}$ fluctuations were detected (Article 5, Fig. 3). Since both S7 and S9 wells had similar slope, their CT data from 2013 and 2014 were combined and a Λ of 2±1 (R^2=0.8) was obtained. Regarding CF, taking the same origin for the slope than for S3 and S1, the obtained Λ for March 2013 in S7 was 4±1 (R^2=0.97).

S9 is the furthest well downstream from the chemical plant (Figure 5). Although legal concentration boundaries of the Catalan Water Agency (ACA) and those from the European Union 2008/105/CE are surpassed, CMs natural attenuation processes were detected. Conversely, in the S10 well, which is located downstream S6 and on the other side of the creek (Figure 5), the CMs concentration was low and only slightly above the EU limits.

3. Partial discussions

3.1 ART.1 Cl-CSIA method development

The CF strong amount-dependency (linearity) by GC-IRMS was solved by an amplitude correction with a negative factor which takes into account the amount-dependency of the postulated 'crossover interference' when H-containing fragment ions $[^{13}C^{1}H^{35}Cl]^{+}$ falls into the same cup than $[^{12}C^{37}Cl]^{+}$. This interference is higher when the number of ions is low since the lower the collisions, the lesser the H atoms transferred to other non-analyzed ions are. The absence of amount-dependency observed for the trueness of $\delta^{37}Cl$ values of CT and CF on both GC-qMS instruments might be attributed to the fact that both, CT and CF, have one kind of predominating ions, which means that mass spectra exclusively rise to the fragment of mass m/z=117 and 119 (121 to a lesser extent) for CT and m/z=83 and 85 for CF.

Large differences in ε values were detected between sample values corrected to V-SMOC scale and those uncorrected, as well as deviation from unity was identified in slopes resulting from plotting uncorrected $\delta^{37}Cl$ values *vs.* corrected values in both studied GC-qMSs, especially for CF. Therefore, these observations highlight the need of two-point calibration by standards bracketing a range of different chlorine isotope values.

Strong agreement of GC-qMS and GC-IRMS results for both CT and CF (i.e. conformity in Λ±95%CI, ε values as well as their associated good linear regressions) indicate that excellent trueness and precision can be achieved by both studied methods. This confirms that they are reliable and can be indistinctly used in terms of precision and trueness.

3.2 ART. 2 Abiotic CF reference reactions

Regarding mechanistic considerations of the three studied reactions, $AKIE_C$ of heat-activated PS reaction with CF was in agreement with oxidative cleavage of a C-H bond for both abiotic (1.008-1.015) and biotic (1.001-1.044) reactions (Article 2, SI, Table S2). The small detected $AKIE_{Cl}$ value (1.00045±0.0004) evidenced a secondary isotopic effect in the expected oxidative reaction more than a C-Cl bond cleavage per se.

In contrast, AKIEs for CF AH were consistent with a C-Cl bond cleavage (Article 2, SI, Table S2). A stepwise elimination mechanism has been considered more plausible than one-step nucleophilic substitution mechanism for this reaction. By the interaction of several factors, there was not statistically difference between Λ of CF oxidation and that of CF AH (ANCOVA, p=0.2) (Figure 8B). Although $AKIE_c$ values were different since different bond cleavages are involved (C-H *vs.* C-Cl, respectively), $AKIE_{Cl}$ values were similar because in the case of the AH they corresponded to primary effects of a C-Cl bond cleavage, and in the case of oxidation, they corresponded to a secondary isotopic effect.

$AKIE_C$ value of CF reductive dechlorination was within values reported for C-Cl reductive cleavage in literature (Article, SI, Table S2) and similar to that obtained by Lee et al. (2015). $AKIE_{Cl}$ value was also similar to biotic and abiotic reductive dechlorination. Therefore, a C-Cl cleavage was proved. The slope observed during CF reductive dechlorination by Fe(0) was significantly different from that of CF oxidation by thermally activated PS and CF AH (p<0.0001) (Figure 8A,B).

3.3 ART. 3 Abiotic chlorinated methanes reactions

The lower or fluctuating concentrations observed in some experiments were attributed to sorption of pollutants on non-reactive sites of initial or newly formed solid phases (Burris et al., 1995; 1998, Kim and Carraway, 2000; Song and Carraway, 2006).

CF accumulation in CT batches at pH 7 with Fe(0) and Py evidenced hydrogenolysis. By contrast, Mag did not degraded CT at pH 7 under experimental conditions. This could explain the decrease in degradation efficiency of aged Fe(0) PRBs (Vodyanitskii, 2014), in which some oxide minerals such as Mag may form onto Fe(0) surface. While only CT hydrogenolysis to CF occurs with Fe(0), the CS_2 together with CF yield in CT experiments with Py at pH 7 revealed thiolytic reduction in parallel to CT hydrogenolysis. This was confirmed by different CT Λ values (2.9±0.5 *vs.* 6.1±0.5, Py and Fe(0) respectively at pH 7) (Figure 8C).

On the other hand, at pH 12, all CT experiments (i.e. with Fe(0), Py and Mag) underwent hydrogenolysis to CF, and only Py experiments showed (as at pH 7) CS_2, evidencing parallel CT thiolytic reduction. Since different reactions are present as it was evidenced by different by-products formation, Λ values of CT with minerals at pH 12 (Mag, 2±1, and Py, 3.7±0.9) are substantially different from that of CT degradation with Fe(0) (5.8±0.4) (Figure 8C,D). Although in CT degradation by Mag at pH 12 only CF was detected as VOC by-product, the reported Λ value differs from that of CT hydrogenolysis. Hydrolytitc reduction to CO (non-analyzed by-product) is suggested in this case according to literature (Danielsen and Hayes, 2004). Variation of pH did not significantly affect the Λ values of CT degradation by Fe(0) nor by Py. This would confirm that pH affects intermediate radical compounds rather than the initial rate-limiting step (Zwank et al., 2005).

CF degradation was only detected by Fe(0) at pH 7. However, at pH 12, CF was degraded in all the studied experiments. Similarly to CT, when comparing the Λ of CF degradation by Fe(0) at pH 7 (8±2) (Article 2) and that at pH 12 (8±1) (obtained here in Article 3) it follows that pH does not affect this reaction neither. In Fe(0) at pH 12, CF hydrogenolysis seems the main reaction and CF AH (13.0±0.8) is considered negligible, as it was confirmed also by assessing the distribution (F, Eq. 7) of AH and dechlorination by Fe(0) following Van Breukelen (2007) and $\mathcal{E}$ data of AH from Article 2. When combining the data of CF degradation by Fe(0) at pH 7 and pH 12, the Λ value is not significantly different (ANCOVA, p=0.05065) from that of CF reaction in model systems for outer-sphere single electron transfer (OS-SET) (Heckel et al., 2017) which suggests that OS-SET is involved in the first rate-limiting step of the concerted C-Cl bond cleavage. The moderate DCM accumulation in CF degradation by Fe(0) at pH 12 and slower CF consumption than at pH 7 by Fe(0), could be explained by Fe(0) surface passivation due to Fe-oxyhydroxides precipitation which is enhanced at alkaline pH (Farrell et al., 2000; Támara and Butler, 2004). In contrast to Fe(0), in CF experiments with Mag and $FeCl_2$ at pH 12, CF fractionation was revealed and it was attributed to AH since no VOCs were detected. Conversely, DCM was yielded in CF experiments with Py, evidencing hydrogenolysis

which cannot be discarded to occur in parallel to AH that is a reaction expected under experimental conditions and during the studied experiment time (Torrentó et al., 2014). However, AH cannot be confirmed since $\delta^{37}C_{CF}$ values of these experiments were not available.

Finally, it is important to highlight that in all experiments at both pH values where degradation was reported by Fe(0) or iron minerals, AKIEs values (Table 5) were below 50% of Streitwieser limit for C-Cl bon cleavage (KIE$_C$=1.057, KIE$_{Cl}$=1.013) and also below all reported values for abiotic and biotic reductive dechlorination of chlorinated compounds (Article 3, Table S2) indicating mass transfer masking effects. Thus, the pollutant is rapidly reduced when contacting a reducing agent, being the diffusion of CT through the solution the rate-limiting step rather than the C-Cl bond cleavage (Arnold et al., 1999). These masking effects affect carbon and chlorine CT fractionation to the same extent, and, thus, in the C-Cl dual plot these effects cancel out.

3.4 ART. 4 Biotic chlorinated methanes degradation

Autoclaved slurry controls discarded volatile losses and abiotic degradation processes due to B_{12}. CF biodegradation only occurred in the microcosms with added B_{12}, whereas CT degradation occurred in both without and with B_{12} experiments, being accelerated in the latter. Thus, B_{12} exerts a catalytic effect on CT and CF degradation and it induced, in turn, CEs degradation as it was confirmed by $\delta^{13}C$ enrichment once CMs concentrations were decreased below inhibitory limits for CEs degraders.

Regarding mechanistic considerations, the obtained $AKIE_C$ values (Table 5) are much below the realistic value of 50% bond cleavage (1.029) (Elsner et al., 2005) showing masking effects but within the range of those obtained for CF microbial reductive dechlorination (1.004–1.028) (Article 4, SI, Table A7). The $AKIE_{Cl}$ of the 0.01B/CF treatment was lower than both the Streitwieser limit for KIE_{Cl} (1.013) for a C-Cl bond cleavage and the theoretical revised value (1.019) (Paneth, 1992), but it was closer to 50% of the Streitwieser limit (1.0065) (Elsner et al., 2005), in contrast to the $AKIE_C$. However, since both elements should be affected by masking to the same extent, this dissimilarity between elements with respect to 50% Stretweiser limit, revealed that chlorine secondary isotopic effects are expected to be present although they are masked. On the other hand, the $AKIE_{Cl}$ value of CTw/oB treatment was much above the before-mentioned theoretical maximum KIE_{Cl} values expected on a C-Cl bond cleavage. This could be explained by important secondary isotopic effects (Świderek and Paneth, 2012), experimental values exceeding theoretical values or by the cleavage of two C-Cl bonds concurrently with only one C-Cl bond cleavage (Elsner et al., 2004). In contrast, the $AKIE_{Cl}$ of CT biodegradation with B_{12} (1.015±0.002) was similar to the expected KIE_{Cl} values for a C-Cl bond cleavage which is still indicative of chlorine secondary isotopic effect (it is higher than the 50% Stretweiser limit) but lower than without B_{12}. Thus, mechanistic differences were revealed by the $AKIE_{Cl}$ study between the CT natural attenuation and B_{12} catalyzed CT reactions. They could be related to i) the fact that the derived $AKIE_{Cl}$ might be a weighted average of the kinetic effects of different proportions of competing parallel mechanisms (e.g. one *vs.* two C-Cl bond cleavages, leading to $\cdot CCl_3$ *vs.* $:CCl_2$ respectively, Figure 3), which is typical from mixed cultures containing several species capable of distinct pollutant degradation (Nijenhuis and Richnow, 2016) or ii) to dissimilarities in rate-determining steps preceding C-Cl bond cleavage related to rate limitations in biological systems (e.g. extracellular processes like those reported in *Pseudomonas stutzeri*).

With regard to pathways, CF reductive dechlorination was confirmed and CF hydrolytic reduction or oxidation processes were discarded by the 2D-CSIA approach. On the other hand, several reductive pathways might be competing in the CT treatments since: different $AKIE_{Cl}$ values were disclosed; no CF accumulation was observed when B_{12} was added, probably linked to a major activity of *Pseudomonas stutzeri* in B_{12} treatments (species which is reported capable of CT reduction to non-chlorinated products, Figure 3); and different Λ values were found for CT B_{12} amended and unamended treatments.

3.5 ART. 5 Chlorinated methanes degradation: field study

The study of the δ^{13}C values of CT and CF from 2002 to 2005 of the potential sources of pollution suggested that CMs fractionation processes had started during the industrial process, and/or in the wastewater tank source during the industrial activity and/or after the plant closure (1985), especially for CT. In this context and after studying every single well in depth and over time, some δ^{13}C values from pit source's influence area (S1 and S4 wells) were disclosed as the less enriched values of the field, and in the case of CF, these values were most similar ones to commercial values. In addition, higher CMs concentrations in S4 than in the upstream S1 in March 2013 and November 2014 together with higher CT proportion and more depleted δ^{13}C values in S4 evidenced a detachment of the pollution plume downgradient from S1 to S4 as a consequence of the removal of the source. Only certain CF degradation processes were visible in this S1-S4 plume.

As regards tank's source influence area study (Figure 5C), differences in CMs concentration behavior in depth and over time in S3 well could be explained by a migration of the pollution from the upper unsaturated zone downwards to deepest zones of the S3 through the fracture network. Moreover, different δ^{13}C enrichment trends in depth and over time in S3 would support CT degradation processes inducing δ^{13}C$_{CT}$ enrichment parallel to CT incomings from the remaining pollution in soil from unsaturated zone or from upstream trench, which are in hydraulic connectivity through fractures, and causing δ^{13}C$_{CT}$ depletion. Furthermore, CF degradation processes were clearly detected in the deepest part of S3, while in the rest of depths, CF isotopic signature was probably a mixture of CF degradation and the continuous inputs of CF as by-product of CT degradation or as incoming pollution. CMs degradation in tank source's influence area (S3 and S6 wells) is evidenced by much lower CMs concentration in the downstream S6 well, and δ^{13}C enrichment processes in S3 under appropriate Eh conditions.

Similarly to S3 well, leaching from the unsaturated zone was also revealed for S8 and specially in S7 well where the highest CMs amounts were ever found. This indicated insufficient source removal not only in tank source but also along the wastewater pipe and plant facilities (Figure 5C). Nevertheless, natural attenuation processes were glimpsed in both wells, especially for CT in S7 well.

Regarding the 2D-CSIA approach, the CT slope of S3 (4±2 Figure 8E) was statistically similar to the slope of CT net hydrogenolysis (5.8±0.4) and also similar to Λ from CT natural attenuation in microcosms performed with the slurry of the deepest parts of this well (6.1±0.5) (Figure 8C,D). Thus, the highest CT degradation extent in S3 well in the studied period, and calculated according to the detected pathway was 72±11%. In contrast to CT, for a reliable CF 2D-CSIA study, a predominance of CF as a parental compound was argued and the CF slope of S3 was found more similar to reduction processes than to CF oxidation or hydrolysis (Figure 8A,B,E). The hydrogenolysis CMs in S3 is supported by closed/similar isotopic balance (δ^{13}C$_{SUM}$) at different depths at certain times (i.e. Mar-13). However, fluctuation of δ^{13}C$_{SUM}$ of S3

over time might be indicative of the presence of other volatile by-products which were not taken into account in the $\delta^{13}C_{SUM}$ calculations belonging to the hydrogenolysis chain itself (such as DCM which was found in high amounts in S3, chloromethane or CH_4) or to other parallel reductive pathways such as contribution of CT thiolytic or hydrolytic reduction (Figure 3) which is in turn backed up by Λ values comparison of S3 with Fe-bearing minerals slopes and high CS_2 amounts found in S3 when compared to the rest of the wells. These CT and CF reductive processes are in accordance with the steadily Eh values controlled by the Fe system (Article 5, SI, Fig. A1). In the S7 well, CMs degradation was detected and supported by appreciable decrease in Eh values with depth evidencing appropriate redox conditions. The CT slope of combined data of S7 and S9 wells was statistically similar to CT hydrogenolysis combined with thiolytic reduction (2.9±0.5) (Figure 8C,E). According to these pathways, the highest CT degradation extent in S7 well was 84±6%. The CF slope of S3 well in Mar-13 is closer to CF reduction processes than to CF oxidation or AH (Figure 8A,B,E). The coincidence of $\delta^{13}C_{SUM}$ values in S3 and S7 wells together with that of the tank (Article 5, SI, Fig. A2) pointed to a similar composition of the original mixture of spilled CMs. Finally, the $\delta^{13}C_{SUM}$ evolution over time towards more depleted values confirmed leaching in both S3 well and in the upper parts of S7.

On the other hand, the CF slope of S1 was coherent with CF oxidation (Λ=17±2) but also with CF AH (Λ=13.0±0.8) (ANCOVA, p>0.05) (Figure 8A,B,E) which would be supported by the evolution from reducing to oxidizing conditions over time along with documented open-air spills in the pit source area (Palau et al., 2014b), while CF affected by AH could also come from the upstream alkaline trench hydraulically connected with the saturated zone (Torrentó et al., 2014). However, further research is required for distinguishing the predominant CF process.

4. General discussion

After having developed the Cl-CSIA method in terms of the optimization of acquisition parameters in CG-qMS instruments and its validation in an interlaboratory comparison, and after having also evaluated its precision and trueness it was concluded that there was an excellent agreement between GC-IRMS and GC-qMS for CT and CF provided that two reference standards with large differences in $\delta^{37}Cl$ values are needed for true results. Thus, both techniques can be indistinctly used for laboratory and field data analysis (Article 1).

Abiotic CF degradation was characterized in the laboratory for three relevant different transformation mechanisms: oxidation with heat-activated PS, AH and reductive dechlorination (Article 2). The obtained Λ for CF reductive dechlorination is different from both CF oxidation and CF AH, which allow distinction between aerobic and anaerobic CF processes or the detection of the extent of degradation if two CF competing pathways occur at a field site either simultaneously or subsequently (Eq. 7) (Van Breukelen, 2007) (e.g. ISCO *vs.* natural dechlorination). In particular, the CF reductive dechlorination (including hydrogenolysis and reductive elimination) was further studied under different conditions (pH 7 and pH 12 which are representative of groundwater and alkaline interception trenches in Òdena, respectively) and by using different reducing-agents (Fe(0), Py and Mag, the last two amended with $FeCl_2$) that could also be naturally present in field sites (Article 3). At pH 7, only Fe(0) was effective to dechlorinate CF to DCM. Conversely, CF degradation was detected in all experiments at pH 12 and it was attributed to AH although with Py presence, CF dechlorination to DCM was also distinguished. On the other hand, CF degradation was confirmed to be biotically-mediated in microcosm experiments from Òdena site but only in the presence of B_{12} and without relevant VOCs accumulation. Well-known OHRB such as *Dehalococcoides, Sulfurospirillum, Geobacter, Desulfosporosinus, Dehalobacter,* and *Desulfitobacterium* spp. were not metabolically active in any of CT neither CF microcosms' treatments. On the contrary, *Pseudomonas, Acidovorax and Ancylobacter* were the most metabolically active genera in all treatments where CMs degradation was detected. The Λ value from CF degradation biotically-mediated by B_{12} treatment (Article 4) had not significant statistically difference to that for abiotic CF reductive dechlorination by Fe(0) (ANCOVA, p>0.05) (Article 3), being postulated CF hydrogenolysis and reductive elimination as predominant pathways in both cases. The presence of only punctual DCM formation in CF biotically-mediated degradation by B_{12}, could be explained by the detected activity of species (*Ancylobacter dichloromethanicus*) capable of DCM dechlorination that along with the addition of B_{12}, stimulates CF reductive elimination to CO and CO_2 as reported in literature (Cappelletti et al., 2012). Other reaction mechanisms such as CF oxidation or net hydrolysis were discarded when comparing the Λ of these reactions (Articles 2, 3) with that of CF biotically-mediated degradation (Article 4) since they are significantly different (ANCOVA, p<0.001). Those 2D-CSIA slopes obtained in abiotic and biotic CF experiments allowed the assessment of CF natural attenuation processes of Òdena field site in 2013 and 2014 (Figure 8). CF oxidation processes and/or transport of CF affected by AH from upstream

interception trenches to downstream wells were identified in former pit source area (S1 well) (Article 5). Nevertheless, in S3 and S7 wells (representative of former tank and wasterwater pipe sources, respectively), dual CF Λ values from 2013 and 2014 statistically deviates from reference slopes obtained in laboratory experiments. This lack of match could be due to little contribution of CF as by-product of CT hydrogenolysis (see below) and to the contribution of the detected leachates of CF from the unsaturated zone probably affected by fractionation processes (i.e. CF diffusion) different from those transforming CF in the saturated zone. Hence, source's removal in S3 and S7 areas was revealed inefficient by leaching detection, unlike S1 zone. Despite the lack of match with CF reference slopes, CF Λ of S3 and S7 wells are closer to CF reduction slopes than to that found representative of CF degradation processes in S1 well.

Since CT reduction is the expected predominant reaction mechanism for this target compound due to the high oxidation state of carbon, abiotic (Article 3) and biotically-mediated (Article 4) CT reduction processes were studied during this thesis. Abiotic CT reduction processes by Fe(0) and Fe(II) on Py and Mag at neutral and alkaline pH conditions were investigated (Article 3). At pH 7, only Fe(0) and Py experiments produced CT degradation by net CT hydrogenolysis in the former, and both by CT hydrogenolysis combined with CT thiolytic reduction in the latter. At pH 12, the same processes and Λ values than at pH 7 were obtained for Fe(0) and Py. CT degradation by Mag was due to hydrogenolysis (detection of CF as by-product) while CF was not degraded by Mag at pH 7. CT hydrolytic reduction is suggested in parallel with detected CT hydrogenolysis by Mag according to literature (Danielsen and Hayes, 2004). This hypothesis is also consistent with different Λ values found for Mag (2 ± 1, $R^2=0.65$) and net hydrogenolysis by Fe(0) (5.8 ± 0.4 $R^2=0.98$ at pH 12), while similar Λ to that of combined CT hydrogenolysis with CT thiolytic reduction by Py (3.7 ± 0.9, $R^2=0.93$) (which share the same initial mechanism Figure 3) were uncovered. On the other hand, microcosm experiments from S3 well revealed natural CT hydrogenolysis to CF (Article 4) with no statistically significant difference (ANCOVA, p>0.05) to Λ of net CT hydrogenolysis by Fe(0) (Article 3). The B_{12} presence catalyzed CT biotically-mediated degradation and, differently to without B_{12} addition, it did not produce nor CF neither other VOCs by-products. Dissimilarities as that of by-products yield were also detected by $AKIE_{Cl}$ besides in Λ terms since, despite both CT biotically-mediated degradation processes have similar Λ values when 95%CI are taken into account, they showed significant statistically difference. These differences among CT biotic experiments could be correlated with major *Pseudomonas stutzeri* activity with B_{12}, since this bacterium is capable of readily transform CT to CO_2; and also major *Ancylobacter dichloromethanicus* activity, which might explain the absence of CF neither DCM detection (Firsova et al., 2010) in B_{12} amended experiments. Thus, Λ values could support an initial step of two electrons transfer, in parallel to one electron transfer, since CT biotically-mediated degradation by B_{12} has no statistically significant difference (p>0.05) with CT degradation by Py where CT hydrogenolysis and CT thiolytic reduction occur simultaneously (Article 3). In addition, although CT biotically-mediated degradation by B_{12} showed statistically significant difference compared to CT degradation by Mag at pH 12, the obtained p=0.03 value is close to the boundary between

being statistically significant and non-statistically significant (p=0.05), hence further research is needed in this respect. CS_2 accumulation confirming thiolytic reduction was not detected in any microcosm treatment, but this compound could have been also further degraded (Cox et al., 2013). In any case, the observed Λ flattening with the B_{12} addition will indicate an initial mechanism parallel to and different from that of CT net hydrogenolysis which is expected to be similar to CT hydrolytic or thiolytic reduction.

In all CT laboratory experiments, masking effects were detected especially by $AKIE_C$ values when they were compared with Streitwieser limit of KIE_C. In Fe(0) and Fe-bearing minerals abiotic experiments, masking effects were also evidenced by $AKIE_{Cl}$, indicative of diffusion-controlled reactions. Thus, Ɛ and reaction rates of these reactions should be taken with caution for estimates of degradation extent. However, these masking affects affected C and Cl the same extent, thus, in the 2D-CSIA plot these effects cancel out. In biotically-mediated treatments, the $AKIE_{Cl}$ values were much above the KIE_{Cl} (CT without B_{12}) or similar to it (CT with B_{12}), which could be associated with secondary kinetic isotopic effects or with cleavage of two C-Cl bonds (e.g. by CT thiolytic or hydrolytic reduction) simultaneously (or not) to only one C-Cl bond cleavage (CT hydrogenolysis). Furthermore, a chlorine secondary kinetic isotopic effect was also evinced in CF oxidation reaction where the initial bond cleavage is C-H, since a low $AKIE_{Cl}$ value was obtained.

Through the application of the newly acquired insights in Òdena site the CT characterization was satisfactorily accomplished (Article 5*)*. Isotopic mass balances of tank source (S3 well) and of distant sources (S7 well) evidenced a similar composition of the original mixture of spilled CMs. The pollutant focus detachment and migration downstream (indicative of efficient source removal) in pit source influence area were detected after studying the evolution of CMs $\delta^{13}C$ and detecting low CT concentrations. Conversely, as it was above-mentioned, in tank and wastewater pipe areas active CMs leaching was detected with CMs concentrations exceeding the legal limits. Encouragingly, different CT degradation processes were evidenced in these areas by dual isotope approach. The CT Λ value from the well S3 fitted with that of net CT hydrogenolysis obtained by Fe(0) and, hence, also with CT biotically-mediated degradation experiments performed with the slurry of this well, being CT biodegradation to CF a main transformation process in this well. Nevertheless, isotopic mass balances of S3 well and high presence of CS_2 revealed that parallel CT reducing processes accompanying CT hydrogenolysis could have been taking place on tank source's influence area. Whereas in S7 and S9 wells, obtained Λ values pointed to hydrogenolysis combined with thiolytic reduction.

After having detected the remaining active sources in Òdena site and the main CMs degradation processes in each area with a discretized study in every single well, remediation processes should be applied. For that purpose a hydrogeological characterization was preliminary performed in collaboration with the group of *Geologia Econòmica, Ambiental i Hidrologia* (UB) and the *Grup d'Hidrologia Subterrània* (UPC-CSIC) (see Annex H for further details) before future remediation actions take place.

5. Conclusions

This doctoral thesis has improved the knowledge on the degradation processes (both natural and induced remediation strategies) of CT and CF from the laboratory to the field scale taking the monitored contaminated Òdena site as application example. This aim has been sought primarily by means of compound specific isotope analysis of $\delta^{13}C$ and $\delta^{37}Cl$.

The development of Cl CSIA of CT and CF has been achieved demonstrating excellent agreement between GC-IRMS and by GC-qMS, being the latter validated through an interlaboratory comparison. Reliable results can be obtained provided that two reference standards calibrated relative to V-SMOC and bracketing a large range of different chlorine isotope values are used.

Detected isotopic shifts of the studied reactions are significant and, therefore, trustworthy signs for detecting CMs degradation in the field according to EPA guidelines (Hunkeler et al., 2008).

CT reductive reactions by Fe(0), Py and Mag are diffusion-controlled since remarkable mass transfer masking effects were evidenced by AKIEs values.

CT and CF are reduced by Fe(0) following a hydrogenolysis (+ reductive elimination in the case of CF) at both studied pH values (7 and 12). CF degradation experiments by Fe(0) at pH 12 showed that AH was negligible since Λ values by Fe(0) differed from that of CF AH. However, CF AH has been suggested as the main process at pH 12 in Fe-bearing experiments being ineffective for CF degradation at pH 7.

Parallel pathways to CT hydrogenolysis like hydrolytic and thiolytic reduction in Mag at pH 12 and in Py at both pH values, respectively, were derived from CS_2 accumulation in the case of Py and by the significant differences at both pHs between the Λ values of the these minerals and that of CT net hydrogenolysis by Fe(0).

pH affects primarily intermediate radical reactions (e.g. [$\cdot CCl_3$]) rather than the initial rate-limiting step since CT removal at pH 7 and 12 by Fe(0) and by Py resulted in very similar ϵ, AKIEs and Λ values.

Mag and Py are effective minerals for abiotic CT remediation strategies, especially under alkaline conditions, at which the accumulation of harmful by-products is avoided since further degradation of CS_2 and CF was evidenced by $\delta^{13}C$. Therefore, 2D-CSIA can be used for CT pathway identification in Òdena alkaline trenches. On the other hand, under aquifer conditions (pH 7), the use of these minerals for cost-effective PRB-building requires to ensure subsequent CF and CS_2 elimination under aquifer conditions, for instance by coupling biodegradation.

In microcosm experiments of Òdena site, B_{12} catalyzed CT biodegradation and made possible the CF biodegradation to non-chlorinated VOCs. B_{12} is a promising biostimulation strategy appropriate in complex multi-contaminant polluted sites since it allows sequential

pollutant degradation, minimizing CF inhibition issues in CEs inasmuch as CEs degradation was confirmed by $\delta^{13}C$ monitoring once CMs were degraded.

CMs hydrogenolysis by Fe(0) is similar to that found for CF biodegradation with B_{12} and to that reported for biotically-mediated CT degradation without B_{12}. However, differences were detected in CT natural attenuation *vs.* B_{12}-catalyzed reactions due to CT different weighted average of the kinetic effects of competing parallel mechanisms, dissimilarities in rate-determining steps and/or rate limitations in biological reactions were revealed by $AKIE_{Cl}$ and Λ values.

Acidovorax, Ancylobacter, and *Pseudomonas* were the most metabolically active genera in the studied experiments, whereas the role of well-known the OHRB *Dehalobacter* and *Desulfitobacterium* was negligible. The key finding of the natural occurrence of *Pseudomonas stutzeri* and their relative abundance rise by the addition of B_{12} makes feasible CMs remediation mediated by this species in Òdena site since it has been already successfully proved as bioaugmentation for CT remediation (reviewed in Penny et al. (2010)). In addition, the presence of metabolically active denitrifying genera (*Pseudomonas, Rhizobium,or Acidovorax*) which are linked to CT and CF biodegradation raises interest in the study of the co-metabolism of both pollutants as a potential bioremediation strategy.

The 2D-CSIA approach could be used to distinguish between aerobic and anaerobic CF natural attenuation pathways or to estimate the different contribution of applied CF remediation strategies such as ISCO *vs. in situ* bioremediation based on significant differences between Λ values of CF oxidation and CF reductive dechlorination. However, the distinction between CF oxidation and AH requires complementary tools to 2D-CSIA due to their strong Λ slope similarity.

The application of CSIA in Òdena site revealed that aged sources should be taken with caution since CMs could have underwent isotope fractionation after their disposal and wrong conclusions can be drawn, e.g. during pathways discrimination. CMs long-term monitoring disclosed that source removal was more effective in pit source's influence area in contrast to tank and wastewater pipe zones where CMs leaching prevailed. Nonetheless, 2D-CSIA isotope plots unveiled different natural attenuation pathways: CF oxidation or AH in pit area and potential CT and CF reduction processes in tank and wastewater pipe. CT degradation extent by reduction reached over 90%. Further remediation strategies are required to avoid both leaching and the exceeding of lawful concentration downstream.

Thus, a comprehensive study of CMs degradation processes was previously performed in the laboratory by combining C and Cl CSIA with other geochemical and biological techniques. This synergetic approach has shown great potential to identify CMs degradation pathways at field sites with complex mixtures and high heterogeneity, providing that a critical study in every single well is necessary for a conducive diagnosis, and is promising for a better interpretation of coupled remediation strategies.

6. Future work

The achievement in the GC-qMS of a precision as good as for GC-IRMS should be a short-term scientific challenge in order to routinely use both instruments to distinguish different pollutant sources, to detect degradation in field samples and to distinguish the degradation pathways in samples in a wide range of concentrations. The implementation of the Cl-CSIA method in the CCiT-UB is currently under way for its use as a basis routine after the experience gained during this thesis. In addition, the development and evaluation of the Cl-CSIA method for DCM would be an interesting future challenge for the scientific community. Cl-CSIA implementation for DCM requires the search of two commercial standards with large differences in $\delta^{37}Cl$ values or the application of pure-phase enrichment experiments as the CT diffusion experiments made in this thesis. Moreover, the development and optimization of the hydrogen isotope analysis of CF for a 3D-CSIA approach (such as recently made for 1,2-DCA, (Palau et al., 2017a) would be of interest to distinguish CF oxidation from CF AH.

Future laboratory studies that would follow up these thesis outcomes would be the attainment of pure CT hydrolytic and CT thiolytic reactions for their characterization based in by-products, isotopes, and especially in Λ calculation, in order to gain a better mechanistic understanding and an improved assessment of the contribution of parallel CT reactions like those produced by Mag and Py. Detection of degradation intermediates by high-resolution mass spectrometry, radical trap experiments and mass balance deficit analysis in combination with an isotopic study have been found to be useful to gain insights for conflicting CEs mechanisms (Heckel et al., 2018) and, thus, they could be also applied to CMs.

Furthermore, the combination of stable isotope probing (SIP) and phospholipid fatty acids (PLFA) or nucleic acids studies which can track the incorporation of isotopically-labeled compounds into microbial biomass should be used in new microcosms experiments of different field site's wells to determine the exact CMs pathway and which microorganisms are likely involved (Yargicoglu and Reddy, 2015). Additionally, the isolation of the *Pseudomonas stutzeri* from the mixed culture of S3 and the subsequent study to get the specific Ɛ and Λ values of CT biodegradation by this species would be essential to disclose the reaction mechanism and to assess the contribution of *Pseudomonas stutzeri* in CT natural attenuation or in bioremediation strategies. In addition, the development of Cl-CSIA for CMs allows the future 2D-CSIA study of reported CF dechlorination by *Dehalobacter* and *Desulfitobacterium* (Tang and Edwards, 2013; Ding et al., 2014) for gaining understanding on their CF degradation mechanisms. CF degradation by *Dehalobacter* was only assessed by C-CSIA up to now, and the corresponding $Ɛ_C$ values are one order of magnitude different between the two studied strains (Chan et al., 2012; Lee et al., 2015), therefore, the 2D-CSIA study would shed light on these dissimilarities.

After the work performed at laboratory scale and the confirmation of the effectiveness of 2D-CSIA approach for CMs degradation study at field scale, it would be necessary starting an up-scaling study, e.g. meso-scale, for testing the feasibility of each CMs remediation strategy or

the combination of them (i.e. biostimulation, the use of recycled Fe-bearing materials/minerals in PRBs and CF oxidation) previously to their final application and monitoring in field sites. In the case of Fe(0) and Fe-bearing minerals application for *in situ* remediation, the potential adverse effects that Fe could have on indigenous microbial communities should be also studied not only at laboratory scale but also at pilot-scale. For instance, it was found that Fe(0) only has a transient effect on *Pseudomonas stutzeri*, species found in S3 microcosms (Saccà et al., 2014). This up-scaling study would be useful also to prove the combination of C and Cl-CSIA approach with other techniques like: active microbial population assessment; the use of PLFA as biomarkers; field redox study; $\delta^{34}S$ signature of sulfate derived from PS after the ISCO application, etc. as tools for detecting, monitoring and distinguishing natural or/and induced degradation.

Since both saturated and non-saturated zones (the latter referred to alkaline interception trenches) are currently studied in Òdena, the best CMs remediation strategy which perfectly fits in both conditions should be evaluated. In the non-saturated zone at pH 12, CF degradation by AH has been already proved in trenches, but the process responsible for CT fractionation remains unknown (Torrentó et al., 2014). The Λ values of CT from trenches should be compared with those obtained in this thesis by Fe(0), Mag and Py, and with that of above-mentioned suggested experiments to study other CT net processes and to unravel whether CT degradation is due to the Fe-bearing minerals detected in the gravels from construction wastes used in the trench (Annex H, poster EGU).

Regarding the saturated zone at neutral pH, the potential for CMs biodegradation should be examined in different areas previously to choose the most appropriate treatment, for instance by assessment of the active microbial population in the most polluted wells of Òdena site, to detect bacteria capable of VOCs dechlorination, as it was confirmed in S3 well's microcosm. Target functional genes should be studied in polluted wells (apart from S3) and where leaching is still active (e.g. in S7 and S8) to detect their degradation potential. Interesting genes to be sought are *cfrA,* responsible of CF dechlorination to DCM by *Dehalobacter* (as well as of 1,1,1-trichloroethane dechlorination to dichloroethane) (Tang and Edwards, 2013), although it was not detected in S3; *ctrA* of *Desulfitobacterium* (Ding et al., 2014) and *pdt*c gene which is the cluster for biosynthesis of PDTC, that is the excreted metal chelator involved in CT degradation and identified as siderophore of *Pseudomonas stutzeri* KC (reviewed in Penny et al., (2010)). As Òdena is a multi-contaminated site, a sequential treatment would be required to ensure CEs degradation once CMs will be degraded to overcome inhibition issues. Thus, the activity of chloroethene-reductive dehalogenases encoding genes (*bvcA, vcrA* and *tceA*) and the specific 16Sr RNA *Dehalococcoides* gene (*Dhc*) should be also studied. According to currently available information, different *in situ* treatments should be applied in each well. Since CF oxidation processes in S1 were detected, they could be enhanced by ISCO application. Nonetheless, CF reduction was detected in S3 and S7, therefore, although ISCO application would be also suitable for CF, biostimulation or abiotically reduction by nano-sized Fe(0) injections would be a better remediation strategy in these wells to reduce high CT contents. In

addition, B_{12} was identified also as an efficient alternative for CMs as well as CEs degradation. Further research is needed to test cheaper B_{12} sources, since although small molar ratios are necessary, its use is costly; and also to clarify the potential inhibition or toxic effects of literature reported B_{12}-related intermediates (phosgene, thiophosgene) on the degradation of CMs or other co-contaminants. New strategies in genetic engineering are used in the industry to commercially produce vitamin B_{12} through microbial fermentation since several organisms can naturally produce it. Moreover, the immobilization of B_{12} to solid supports can allow retention of the enzyme within a reactor system. This method has been tested, instead of using insoluble B_{12}, because it offers much higher surface concentration and enables the separation from the polluted stream for its reuse. These findings provide foundation for more efficient, economical and long-lasting systems but additional research is needed since their preparation is complicated (Guo and Chen, 2018).

7. Bibliography

Aeppli, C., Hofstetter, T.B., Amaral, H.I.F., Kipfer, R., Schwarzenbach, R.P., Berg, M., 2010a. Quantifying in situ transformation rates of chlorinated ethenes by combining compound-specific stable isotope analysis, groundwater dating, and carbon isotope mass balances. Environ. Sci. Technol. 44, 3705–3711. doi:10.1021/es903895b

Aeppli, C., Holmstrand, H., Andersson, P., Gustafsson, Ö., 2010b. Direct compound-specific stable chlorine isotope analysis of organic compounds with quadrupole GC/MS using standard isotope bracketing. Anal. Chem. 82, 420–426. doi:10.1021/ac902445f

Agència catalana de l'aigua (ACA), 2007. Valors genèrics per a la restauració d'aigües subterrànies en emplaçaments contaminats per fonts d'origen puntual. Barcelona.

Agència de Residus de Catalunya (ARC), 2012. Programa de gestió de residus industrials de Catalunya (PROGRIC) 2007-2012. Barcelona.

Agència de Residus de Catalunya (ARC), 2013. Memòria Agència de Residus de Catalunya. Barcelona.

Agència de Residus de Catalunya (ARC), 2014. Memòria Agència de Residus de Catalunya. Barcelona.

Agència de Residus de Catalunya (ARC), 2015. Memòria Agència de Residus de Catalunya. Barcelona.

Agència de Residus de Catalunya (ARC), 2016. Memòria Agència de Residus de Catalunya. Barcelona.

Arnold, W.A., Ball, W.P., Roberts, A.L., 1999. Polychlorinated ethane reaction with zero-valent zinc: pathways and rate control. J. Contam. Hydrol. 40, 183–200. doi:10.1016/S0169-7722(99)00045-5

Audí-Miró, C., Cretnik, S., Torrentó, C., Rosell, M., Shouakar-Stash, O., Otero, N., Palau, J., Elsner, M., Soler, A., 2015. C, Cl and H compound-specific isotope analysis to assess natural *versus* Fe(0) barrier-induced degradation of chlorinated ethenes at a contaminated site. J Hazard Mater 299, 747–754. doi:10.1016/j.jhazmat.2015.06.052

Badin, A., Buttet, G., Maillard, J., Holliger, C., Hunkeler, D., 2014. Multiple dual C-Cl isotope patterns associated with reductive dechlorination of tetrachloroethene. Environ. Sci. Technol. 48, 9179–9186. doi:10.1021/es500822d

Badin, A., Broholm, M.M., Jacobsen, C.S., Palau, J., Dennis, P., Hunkeler, D., 2016. Identification of abiotic and biotic reductive dechlorination in a chlorinated ethene plume after thermal source remediation by means of isotopic and molecular biology tools. J. Contam. Hydrol. 192, 1–19. doi:10.1016/j.jconhyd.2016.05.003

Becker, J.G., Freedman, D.L., 1994. Use of cyanocobalamin to enhance anaerobic biodegradation of chloroform. Environ. Sci. Technol. 28, 1942–1949. doi:10.1021/es00060a027

Bernstein, A., Shouakar-stash, O., Ebert, K., Laskov, C., Hunkeler, D., Jeannottat, S., Sakaguchi-Söder, K., Laaks, J., Jochmann, M.A., Cretnik, S., Jager, J., Haderlein, S.B., Schmidt, T.C., Aravena, R., Elsner, M., 2011. Compound-specific chlorine isotope analysis: a comparison of gas chromatography/isotope ratio mass spectrometry and gas chromatography/quadrupole mass spectrometry methods in an interlaboratory study. Anal. Chem. 83, 7624–7634. doi:dx.doi.org/10.1021/ac200516c

Breider, F., 2013. Investigating the origin of chloroform in soils and groundwater using carbon and chlorine stable isotopes analysis. Thesis. *Université de Neuchâtel*, Switzerland.

Breider, F., Hunkeler, D., 2014. Investigating chloroperoxidase-catalyzed formation of chloroform from humic substances using stable chlorine isotope analysis. Environ. Sci. Technol. 48, 1592–1600. doi:dx.doi.org/10.1021/es403879e

Burris, D.R., Campbell, T.J., Manoranjan, V.S., 1995. Sorption of trichloroethylene and tetrachloroethylene in a batch reactive metallic iron-water system. Environ. Sci. Technol. 29, 2850–2855. doi:10.1021/es00011a022

Burris, D.R., Allen-King, R.M., Manoranjan, V.S., Campbell, T.J., Loraine, G.A., Deng, B., 1998. Chlorinated ethene reduction by cast iron: sorption and mass transfer. J. Environ. Eng. 124, 1012–1019. doi:10.1061/(ASCE)0733-9372(1998)124:10(1012)

Cappelletti, M., Frascari, D., Zannoni, D., Fedi, S., 2012. Microbial degradation of chloroform. Appl. Microbiol. Biotechnol. 96, 1395–1409. doi:10.1007/s00253-012-4494-1

Chan, C.C.H., Mundle, S.O.C., Eckert, T., Liang, X., Tang, S., Lacrampe-Couloume, G., Edwards, E.A., Sherwood Lollar, B., 2012. Large carbon isotope fractionation during biodegradation of chloroform by *Dehalobacter* cultures. Environ. Sci. Technol. 46, 10154–10160. doi:10.1021/es3010317

Cox, S.F., McKinley, J.D., Ferguson, A.S., O'Sullivan, G., Kalin, R.M., 2013. Degradation of carbon disulphide (CS_2) in soils and groundwater from a CS_2-contaminated site. Environ. Earth Sci. 68, 1935–1944. doi:10.1007/s12665-012-1881-y

Danielsen, K.M., Hayes, K.F., 2004. pH dependence of carbon tetrachloride reductive dechlorination by magnetite. Environ. Sci. Technol. 38, 4745–4752. doi:10.1021/es0496874

Declercq, I., Cappuyns, V., Duclos, Y., 2012. Monitored natural attenuation (MNA) of contaminated soils: State of the art in Europe-A critical evaluation. Sci. Total Environ. 426, 393–405. doi:10.1016/j.scitotenv.2012.03.040

Ding, C., Zhao, S., He, J., 2014. A *Desulfitobacterium* sp. strain PR reductively dechlorinates both 1,1,1-trichloroethane and chloroform. Environ. Microbiol. 16, 3387–3397. doi:10.1111/1462-2920.12387

Doğan-Subaşı, E., Elsner, M., Qiu, S., Cretnik, S., Atashgahi, S., Shouakar-Stash, O., Boon, N., Dejonghe, W., Bastiaens, L., 2017. Contrasting dual (C, Cl) isotope fractionation offers potential to distinguish reductive chloroethene transformation from breakdown by permanganate. Sci. Total Environ. 596–597, 169–177. doi:10.1016/j.scitotenv.2017.03.292

Dybas, M.J., Barcelona, M., Bezborodnikov, S., Davies, S., Forney, L., Heuer, H., Kawka, O., Mayotte, T., Sepúlveda-Torres, L., Smalla, K., Sneathen, M., Tiedje, J., Voice, T., Wiggert, D.C., Witt, M.E., Criddle, C.S., 1998. Pilot-scale evaluation of bioaugmentation for in-situ remediation of a carbon tetrachloride-contaminated aquifer. Environ. Sci. Technol. 32, 3598–3611. doi:10.1021/es980200z

Dybas, M.J., Hyndman, D.W., Heine, R., Tiedje, J., Linning, K., Wiggert, D., Voice, T., Zhao, X., Dybas, L., Criddle, C.S., 2002. Development, operation, and long-term performance of a full-scale biocurtain utilizing bioaugmentation. Environ. Sci. Technol. 36, 3635–3644. doi:10.1021/es0114557

Ebert, K.A., Laskov, C., Elsner, M., Haderlein, S.B., 2017. Calibration bias of experimentally determined chlorine isotope enrichment factors: the need for a two-point calibration in compound-specific chlorine isotope analysis. Rapid Commun. Mass Spectrom. 31, 68–74. doi:10.1002/rcm.7752

Elsner, M., Haderlein, S.B., Kellerhals, T., Luzi, S., Zwank, L., Angst, W., Schwarzenbach, R.P., 2004. Mechanisms and products of surface-mediated reductive dehalogenation of carbon tetrachloride by Fe(II) on goethite. Environ. Sci. Technol. 38, 2058–2066. doi:10.1021/es034741m

Elsner, M., Zwank, L., Hunkeler, D., Schwarzenbach, R.P., 2005. A new concept linking observable stable isotope fractionation to transformation pathways of organic pollutants. Environ. Sci. Technol. 39, 6896–6916. doi:10.1021/es0504587

Elsner, M., Jochmann, M.A., Hofstetter, T.B., Hunkeler, D., Bernstein, A., Schmidt, T.C., Schimmelmann, A., 2012. Current challenges in compound-specific stable isotope analysis of environmental organic contaminants. Anal. Bioanal. Chem. 403, 2471–2491. doi:10.1007/s00216-011-5683-y

European Union, 2008. Directive 2008/105/CE related to the rules of environmental quality within water policies, Official Journal of the European Union.

Farrell, J., Kason, M., Melitas, N., Li, T., 2000. Investigation of the long-term performance of zero-valent iron for reductive dechlorination of trichloroethylene. Environ. Sci. Technol. 34, 514–521. doi:10.1021/es990716y

Feng, J., Lim, T.T., 2005. Pathways and kinetics of carbon tetrachloride and chloroform reductions by nano-scale Fe and Fe/Ni particles: Comparison with commercial micro-scale Fe and Zn. Chemosphere 59, 1267–1277. doi:10.1016/j.chemosphere.2004.11.038

Feng, J., Zhu, B., Lim, T.T., 2008. Reduction of chlorinated methanes with nano-scale Fe particles: Effects of amphiphiles on the dechlorination reaction and two-parameter regression for kinetic prediction. Chemosphere 73, 1817–1823. doi:10.1016/j.chemosphere.2008.08.014

Field, J.A., Sierra-Alvarez, R., 2004. Biodegradability of chlorinated solvents and related chlorinated aliphatic compounds. Rev. Environ. Sci. Biotechnol. 3, 185–254. doi:10.1007/s11157-004-4733-8

Firsova, J.E., Doronina, N. V, Trotsenko, Y.A., 2010. Analysis of the key functional genes in new aerobic degraders of dichloromethane. Mikrobiologiya 79, 72–78. doi:10.1134/S0026261710010091

Futagami, T., Fukaki, Y., Fujihara, H., Takegawa, K., Goto, M., Furukawa, K., 2013. Evaluation of the inhibitory effects of chloroform on ortho-chlorophenol- and chloroethene-dechlorinating *Desulfitobacterium* strains. AMB Express 3, 1–8. doi:10.1186/2191-0855-3-30

Gafni, A., Lihl, C., Gelman, F., Elsner, M., Bernstein, A., 2018. $\delta^{13}C$ and $\delta^{37}Cl$ isotope fractionation to characterize aerobic *vs* anaerobic degradation of trichloroethylene. Environ. Sci. Technol. Lett. acs.estlett.8b00100. doi:10.1021/acs.estlett.8b00100

Gregory, K.B., Mason, M.G., Picken, H.D., Weathers, L.J., Parkin, G.F., 2000. Bioaugmentation of Fe(0) for the remediation of chlorinated aliphatic hydrocarbons. Environ. Eng. Sci. 17, 169–181. doi:10.1089/ees.2000.17.169

Grostern, A., Duhamel, M., Dworatzek, S., Edwards, E.A., 2010. Chloroform respiration to dichloromethane by a *Dehalobacter* population. Environ. Microbiol. 12, 1053–1060. doi:10.1111/j.1462-2920.2009.02150.x

Guerrero-Barajas, C., Field, J.A., 2005a. Riboflavin- and cobalamin-mediated biodegradation of chloroform in a methanogenic consortium. Biotechnol. Bioeng. 89, 539–550. doi:10.1002/bit.20379

Guerrero-Barajas, C., Field, J.A., 2005b. Enhancement of anaerobic carbon tetrachloride biotransformation in methanogenic sludge with redox active vitamins. Biodegradation 16, 215–228. doi:10.1007/s10532-004-0638-z

Guo, M., Chen, Y., 2018. Coenzyme cobalamin: biosynthesis, overproduction and its application in dehalogenation—a review. Rev. Environ. Sci. Bio/Technology. doi:10.1007/s11157-018-9461-6

Haselmann, K.F., Ketola, R.A., Laturnus, F., Lauritsen, F.R., Grøn, C., 2000. Occurrence and formation of chloroform at Danish forest sites. Atmos. Environ. 34, 187–193. doi:10.1016/S1352-2310(99)00279-4

Haselmann, K.F., Laturnus, F., Grøn, C., 2002. Formation of chloroform in soil. A year-round study at a Danish spruce forest site. Water. Air. Soil Pollut. 139, 35–41. doi:10.1023/A:1015896719508

Hashsham, S.A., Scholze, R., Freedman, D.L., 1995. Cobalamin-enhanced anaerobic biotransformation of carbon tetrachloride. Environ. Sci. Technol. 29, 2856–2863. doi:0013-936XJ95/0929-2856$09.00/0

He, Y.T., Wilson, J.T., Su, C., Wilkin, R.T., 2015. Review of abiotic degradation of chlorinated solvents by reactive iron minerals in aquifers. Groundw. Monit. Remediat. 35, 57–75. doi:10.1111/gwmr.12111

Heckel, B., Cretnik, S., Kliegman, S., Shouakar-Stash, O., McNeill, K., Elsner, M., 2017. Reductive outer-sphere single electron transfer is an exception rather than the rule in natural and engineered chlorinated ethene dehalogenation. Environ. Sci. Technol. 51, 9663–9673. doi:10.1021/acs.est.7b01447

Heckel, B., McNeill, K., Elsner, M., 2018. Chlorinated ethene reactivity with vitamin B_{12} is governed by cobalamin chloroethylcarbanions as crossroads of competing pathways. ACS Catal. 8, 3054–3066. doi:10.1021/acscatal.7b02945

Helland, B.R., Alvarez, P.J.J., Schnoor, J.L., 1995. Reductive dechlorination of carbon tetrachloride with elemental iron. J. Hazard. Mater. 41, 205–216. doi:10.1016/0304-3894(94)00111-S

Henry, B.M., 2010. Biostimulation for anaerobic bioremediation of chlorinated solvents, in: Stroo, H.F., Ward, C.H. (Eds.), In Situ Remediation of Chlorinated Solvent Plumes. doi:10.1007/978-1-4419-1401-9

Hine, J., 1950. Carbon dichloride as an intermediate in the basic hydrolysis of chloroform. A mechanism for substitution reactions at a saturated carbon atom. J. Am. Chem. Soc. 72, 2438–2445. doi:10.1021/ja01162a024

Hitzfeld, K.L., Gehre, M., Richnow, H.H., 2011. A novel online approach to the determination of isotopic ratios for organically bound chlorine, bromine and sulphur. Rapid Commun. Mass Spectrom. 25, 3114–3122. doi:10.1002/rcm.5203

Holt, B.D., Sturchio, N.C., Abrajano, T.A., Heraty, L.J., 1997. Conversion of chlorinated volatile organic compounds to carbon dioxide and methyl chloride for isotopic analysis of carbon and chlorine. Anal. Chem. 69, 2727–2733. doi:10.1021/ac961096b

Huang, K.C., Zhao, Z., Hoag, G.E., Dahmani, A., Block, P.A., 2005. Degradation of volatile organic compounds with thermally activated persulfate oxidation. Chemosphere 61, 551–560. doi:10.1016/j.chemosphere.2005.02.032

Huling, S.G., Pivetz, B.E., 2006. In-Situ Chemical Oxidation-Engineering issue. EPA/600/R-06/072. U.S. Environmental Protection Agency Office of Research and Development, National Risk Management Research Laboratory: Cincinnati, OH.

Hunkeler, D., Aravena, R., Butler, B.J., 1999. Monitoring microbial dechlorination of tetrachloroethene (PCE) using compound-specific carbon isotope ratios: Microcosms and field experiments. Environ. Sci. Technol. 33, 2733−2738. doi:10.1021/es981282u

Hunkeler, D., Aravena, R., Berry-Spark, K., Cox, E., 2005. Assessment of degradation pathways in an aquifer with mixed chlorinated hydrocarbon contamination using stable isotope analysis. Environ. Sci. Technol. 39, 5975–5981. doi:10.1021/es048464a

Hunkeler, D., Meckenstock, R.U., Lollar, B.S., Schmidt, T.C., Wilson, J.T., 2008. A Guide for assessing biodegradation and source identification of organic ground water Contaminants using Compound Specific Isotope Analysis (CSIA), EPA.

Hunkeler, D., Van Breukelen, B.M., Elsner, M., 2009. Modeling chlorine isotope trends during sequential transformation of chlorinated ethenes. Environ. Sci. Technol. 43, 6750–6756. doi:10.1021/es900579z

Hunkeler, D., Abe, Y., Broholm, M.M., Jeannottat, S., Westergaard, C., Jacobsen, C.S., Aravena, R., Bjerg, P.L., 2011. Assessing chlorinated ethene degradation in a large scale contaminant plume by dual carbon-chlorine isotope analysis and quantitative PCR. J. Contam. Hydrol. 119, 69–79. doi:10.1016/j.jconhyd.2010.09.009

Imfeld, G., Nijenhuis, I., Nikolausz, M., Zeiger, S., Paschke, H., Drangmeister, J., Grossmann, J., Richnow, H.H., Weber, S., 2008. Assessment of in situ degradation of chlorinated ethenes and bacterial community structure in a complex contaminated groundwater system. Water Res. 42, 871–882. doi:10.1016/j.watres.2007.08.035

International Agency for Research on Cancer, IARC Monographs on the Evaluation of Carcinogenic Risks to Humans. [WWW Document], 2017. URL http://monographs.iarc.fr/ENG/Classification/latest_classif.php (accessed 11.14.17).

Jeannottat, S., Hunkeler, D., 2012. Chlorine and carbon isotopes fractionation during volatilization and diffusive transport of trichloroethene in the unsaturated zone. Environ. Sci. Technol. 46, 3169–3176. doi:10.1021/es203547p

Jeannottat, S., Hunkeler, D., 2013. Can soil gas VOCs be related to groundwater plumes based on their isotope signature? Environ. Sci. Technol. 47, 12115–12122. doi:10.1021/es4010703

Jeffers, P.M., Ward, L.M., Woytowltch, L.M., Wolfe, N.L., 1989. Homogeneous hydrolysis rate constants for selected chlorinated methanes, ethanes, ethenes, and propanes. Environ. Sci. Technol. 23, 965–969. doi:10.1021/es00066a006

Jin, B., Laskov, C., Rolle, M., Haderlein, S.B., 2011. Chlorine isotope analysis of organic contaminants using GC-qMS: method optimization and comparison of different evaluation schemes. Environ. Sci. Technol. 45, 5279–5286. doi:10.1021/es200749d

Justicia-Leon, S.D., Higgins, S., Mack, E.E., Griffiths, D.R., Tang, S., Edwards, E.A., Löffler, F.E., 2014. Bioaugmentation with distinct *Dehalobacter* strains achieves chloroform detoxification in microcosms. Environ. Sci. Technol. 48, 1851–1858. doi:10.1021/es403582f

Kaown, D., Shouakar-Stash, O., Yang, J., Hyun, Y., Lee, K.K., 2014. Identification of multiple sources of groundwater contamination by dual isotopes. Groundwater 52, 875–885. doi:10.1111/gwat.12130

Kayser, M.F., Ucurum, Z., Vuilleumier, S., 2002. Dichloromethane metabolism and C1 utilization genes in *Methylobacterium* strains. Microbiology 148, 1915–1922. doi:10.1099/00221287-148-6-1915

Kim, Y.H., Carraway, E.R., 2000. Dechlorination of pentachlorophenol by zero valent iron and modified zero valent irons. Environ. Sci. Technol. 34, 2014–2017. doi:10.1021/es991129f

Kirtland, B.C., Aelion, C.M., Stone, P.A., Hunkeler, D., 2003. Isotopic and geochemical assessment of in situ biodegradation of chlorinated hydrocarbons. Environ. Sci. Technol. 37, 4205–4212. doi:10.1021/es034046e

Koenig, J.C., Boparai, H.K., Lee, M.J., O'Carroll, D.M., Barnes, R.J., Manefield, M.J., 2016. Particles and enzymes: Combining nanoscale zero valent iron and organochlorine respiring bacteria for the detoxification of chloroethane mixtures. J. Hazard. Mater. 308, 106–112. doi:10.1016/j.jhazmat.2015.12.036

Kuder, T., Van Breukelen, B.M., Vanderford, M., Philp, P., 2013. 3D-CSIA: Carbon, chlorine, and hydrogen isotope fractionation in transformation of TCE to ethene by a *Dehalococcoides* culture. Environ. Sci. Technol. 47, 9668–9677. doi:10.1021/es400463p

Laturnus, F., Lauritsen, F.R., Grøn, C., 2000. Chloroform in a pristine aquifer system: Toward an evidence of biogenic origin. Water Resour. Res. 36, 2999–3009. doi:10.1029/2000WR900194

Lee, M., Wells, E., Wong, Y.K., Koenig, J., Adrian, L., Richnow, H.H., Manefield, M., 2015. Relative contributions of *Dehalobacter* and zerovalent iron in the degradation of chlorinated methanes. Environ. Sci. Technol. 49, 4481–4489. doi:10.1021/es5052364

Lewis, T.A., Crawford, R.L., 1995. Transformation of carbon tetrachloride via sulfur and oxygen substitution by *Pseudomonas* sp. strain KC. J. Bacteriol. 177, 2204–2208. doi:10.1128/jb.177.8.2204-2208.1995

Lien, H.-L., Jhuo, Y.-S., Chen, L.-H., 2007. Effect of heavy metals on dechlorination of carbon tetrachloride by iron nanoparticles. Environ. Eng. Sci. 24, 21–30. doi:10.1089/ees.2007.24.21

Lima, G. da P., Sleep, B.E., 2010. The impact of carbon tetrachloride on an anaerobic methanol-degrading microbial community. Water. Air. Soil Pollut. 212, 357–368. doi:10.1007/s11270-010-0350-z

Lojkasek-Lima, P., Aravena, R., Shouakar-Stash, O., Frape, S.K., Marchesi, M., Fiorenza, S., Vogan, J., 2012. Evaluating TCE abiotic and biotic degradation pathways in a permeable

reactive barrier using compound specific isotope analysis. Ground Water Monit. Remediat. 32, 53–62. doi:10.1111/j1745

Marchesi, M., 2010. Stable isotopes for monitoring chemical oxidation and natural attenuation of groundwater contaminated by organic compounds: laboratory and field studies. Thesis. *Universitat de Barcelona*, Barcelona.

Matheson, L.J., Tratnyek, P.G., 1994. Reductive dehalogenation of chlorinated methanes by iron metal. Environ. Sci. Technol. 28, 2045–2053. doi:10.1021/es00061a012

Neumann, A., Hofstetter, T.B., Skarpeli-Liati, M., Schwarzenbach, R.P., 2009. Reduction of polychlorinated ethanes and carbon tetrachloride by structural Fe(II) in smectites. Environ. Sci. Technol. 43, 4082–4089. doi:10.1021/es9001967

Nijenhuis, I., Renpenning, J., Kümmel, S., Richnow, H.H., Gehre, M., 2016. Recent advances in multi-element compound-specific stable isotope analysis of organohalides: Achievements, challenges and prospects for assessing environmental sources and transformation. Trends Environ. Anal. Chem. 11, 1–8. doi:10.1016/j.teac.2016.04.001

Nijenhuis, I., Richnow, H.H., 2016. Stable isotope fractionation concepts for characterizing biotransformation of organohalides. Curr. Opin. Biotechnol. 41, 108–113. doi:10.1016/j.copbio.2016.06.002

Novak, P.J., Daniels, L., Parkin, G.F., 1998. Enhanced dechlorination of carbon tetrachloride and chloroform in the presence of elemental iron and *Methanosarcina barkeri*, *Methanosarcina thermophila*, or *Methanosaeta concillii*. Environ. Sci. Technol. 32, 1438–1443. doi:10.1021/es970785h

O'Hannesin, S.F., Gillham, R.W., 1998. Long-term performance of an *In Situ* "Iron Wall" for remediation of VOCs. Ground Water 36, 164–170. doi:10.1111/j.1745-6584.1998.tb01077.x

Obiri-Nyarko, F., Grajales-Mesa, S.J., Malina, G., 2014. An overview of permeable reactive barriers for in situ sustainable groundwater remediation. Chemosphere 111, 243–259. doi:10.1016/j.chemosphere.2014.03.112

Palau, J., 2008. Aplicación de la composición isotópica del carbono de compuestos orgánicos volátiles en acuíferos contaminados por disolventes clorados. Thesis. *Universitat de Barcelona*, Barcelona.

Palau, J., Cretnik, S., Shouakar-Stash, O., Höche, M., Elsner, M., Hunkeler, D., 2014a. C and Cl isotope fractionation of 1,2-dichloroethane displays unique $\delta^{13}C/ \delta^{37}Cl$ patterns for

pathway identification and reveals surprising C−Cl bond involvement in microbial oxidation. Environ. Sci. Technol. 48, 9430–9437. doi:10.1021/es5031917

Palau, J., Marchesi, M., Chambon, J.C.C., Aravena, R., Canals, À., Binning, P.J., Bjerg, P.L., Otero, N., Soler, A., 2014b. Multi-isotope (carbon and chlorine) analysis for fingerprinting and site characterization at a fractured bedrock aquifer contaminated by chlorinated ethenes. Sci. Total Environ. 475, 61–70. doi:10.1016/j.scitotenv.2013.12.059

Palau, J., Shouakar-Stash, O., Hunkeler, D., 2014c. Carbon and chlorine isotope analysis to identify abiotic degradation pathways of 1,1,1-trichloroethane. Environ. Sci. Technol. 48, 14400–14408. doi:10.1021/es504252z

Palau, J., Jamin, P., Badin, A., Vanhecke, N., Haerens, B., Brouyère, S., Hunkeler, D., 2016. Use of carbon - chlorine dual isotope analysis to assess the degradation pathways of 1,1,1-trichloroethane in groundwater. Water Res. 92, 235–243. doi:10.1016/j.watres.2016.01.057

Palau, J., Shouakar-Stash, O., Hatijah Mortan, S., Yu, R., Rosell, M., Marco-Urrea, E., Freedman, D.L., Aravena, R., Soler, A., Hunkeler, D., 2017a. Hydrogen isotope fractionation during the biodegradation of 1,2-dichloroethane: Potential for pathway identification using a multi-element (C, Cl, and H) isotope approach. Environ. Sci. Technol. 51, 10526–10535. doi:10.1021/acs.est.7b02906

Palau, J., Yu, R., Hatijah Mortan, S., Shouakar-Stash, O., Rosell, M., Freedman, D.L., Sbarbati, C., Fiorenza, S., Aravena, R., Marco-Urrea, E., Elsner, M., Soler, A., Hunkeler, D., 2017b. Distinct dual C-Cl isotope fractionation patterns during anaerobic biodegradation of 1,2-dichloroethane: potential to characterize microbial degradation in the field. Environ. Sci. Technol. 51, 2685–2694. doi:10.1021/acs.est.6b04998

Paneth, P., 1992. How to measure heavy atom isotope effects: general principles, in: Buncel, E., Saunders, W.H.J. (Eds.), Isotopes in Organic Chemistry. Elsevier, New York, p. 1992.

Pankow, J.F., Cherry, J.A., 1996. Dense chlorinated solvents and other DNAPLs in groundwater. History, behavior and remediation, Waterloo P. ed. Portland, OR.

Pelissari, C., Guivernau, M., Viñas, M., de Souza, S.S., García, J., Sezerino, P.H., Ávila, C., 2017. Unraveling the active microbial populations involved in nitrogen utilization in a vertical subsurface flow constructed wetland treating urban wastewater. Sci. Total Environ. 584–585, 642–650. doi:10.1016/j.scitotenv.2017.01.091

Penny, C., Vuilleumier, S., Bringel, F., 2010. Microbial degradation of tetrachloromethane: mechanisms and perspectives for bioremediation. FEMS Microbiol. Ecol. 74, 257–275. doi:10.1111/j.1574-6941.2010.00935.x

Pfiffner, S.M., 2000. Bioaugmentation potential at a carbon tetrachloride contaminated site, in: 2nd International Conference on Remediation of Chlorinated and Recalcitrant Compounds. Monterey, CA, pp. 389–394.

Pohl, L.R., Bhooshan, B., Whittaker, N.F., Krishna, G., 1977. Phosgene: a metabolite of chloroform. Biochem. Bioph. Res. Co. 79, 684–691. doi:10.1016/0006-291X(77)91166-4

Renpenning, J., Hitzfeld, K.L., Gilevska, T., Nijenhuis, I., Gehre, M., Richnow, H.H., 2015. Development and validation of an universal interface for compound-specific stable isotope analysis of chlorine (^{37}Cl/^{35}Cl) by GC-high-temperature conversion (HTC)-MS/IRMS. Anal. Chem. 87, 2832–2839. doi:10.1021/ac504232u

Rosenthal, H., Adrian, L., Steiof, M., 2004. Dechlorination of PCE in the presence of Fe0 enhanced by a mixed culture containing two *Dehalococcoides* strains. Chemosphere 55, 661–669. doi:10.1016/j.chemosphere.2003.11.053

Saccà, M.L., Fajardo, C., Martinez-Gomariz, M., Costa, G., Nande, M., Martin, M., 2014. Molecular stress responses to nano-sized zero-valent iron (nZVI) particles in the soil bacterium *Pseudomonas stutzeri*. PLoS One 9, 3–9. doi:10.1371/journal.pone.0089677

Sakaguchi-Söder, K., Jager, J., Grund, H., Matthäus, F., Schüth, C., 2007. Monitoring and evaluation of dechlorination processes using compound-specific chlorine isotope analysis. Rapid Commun. Mass Spectrom. 21, 3077–3084. doi:10.1002/rcm.3170

Sherwood Lollar, B., Slater, G.F., Ahad, J., Sleep, B., Spivack, J., Brennan, M., MacKenzie, P., 1999. Contrasting carbon isotope fractionation during biodegradation of trichloroethylene and toluene: Implications for intrinsic bioremediation. Org. Geochem. 30, 813–820. doi:10.1016/S0146-6380(99)00064-9

Shestakova, M., Sillanpää, M., 2013. Removal of dichloromethane from ground and wastewater: A review. Chemosphere 93, 1258–1267. doi:10.1016/j.chemosphere.2013.07.022

Shouakar-Stash, O., Drimmie, R.J., Zhang, M., Frape, S.K., 2006. Compound-specific chlorine isotope ratios of TCE, PCE and DCE isomers by direct injection using CF-IRMS. Appl. Geochemistry 21, 766–781. doi:10.1016/j.apgeochem.2006.02.006

Skell, P.S., Hauser, C.R., 1945. The mechanism of β-elimination with alkyl halides. J. Am. Chem. Soc. 67, 1661–1661. doi:10.1021/ja01226a013

Song, H., Carraway, E.R., 2006. Reduction of chlorinated methanes by nano-sized zero-valent iron. Kinetics, pathways and effect of reaction conditions. Environ. Eng. Sci. 23, 272–284. doi:10.1089/ees.2006.23.272

Squillace, P.J., Moran, M.J., Price, C. V., 2004. VOCs in shallow groundwater in new residential/commercial areas of the United States. Environ. Sci. Technol. 38, 5327–5338. doi:10.1021/es0349756

Stroo, H.F., 2010. Bioremediation of chlorinated solvent plumes, in: Stroo, H.F., Ward, C.H. (Eds.), In Situ Remediation of Chlorinated Solvent Plumes. doi:10.1007/978-1-4419-1401-9

Sutton, N.B., Grotenhuis, J.T.C., Langenhoff, A.A.M., Rijnaarts, H.H.M., 2011. Efforts to improve coupled in situ chemical oxidation with bioremediation: A review of optimization strategies. J. Soils Sediments 11, 129–140. doi:10.1007/s11368-010-0272-9

Świderek, K., Paneth, P., 2012. Extending limits of chlorine kinetic isotope effects. J. Org. Chem. 77, 5120–5124. doi:10.1021/jo300682f

Támara, M.L., Butler, E.C., 2004. Effects of iron purity and groundwater characteristics on rates and products in the degradation of carbon tetrachloride by iron metal. Environ. Sci. Technol. 38, 1866–1876. doi:10.1021/es0305508

Tang, S., Edwards, E.A., 2013. Identification of *Dehalobacter* reductive dehalogenases that catalyse dechlorination of chloroform, 1,1,1-trichloroethane and 1,1-dichloroethane. Phil. Trans. R. Soc. B 368, 20120318. doi:10.1098/rstb.2012.0318

Torrentó, C., Audí-Miró, C., Bordeleau, G., Marchesi, M., Rosell, M., Otero, N., Soler, A., 2014. The use of alkaline hydrolysis as a novel strategy for chloroform remediation: The feasibility of using construction wastes and evaluation of carbon isotopic fractionation. Environ. Sci. Technol. 48, 1869–1877. doi:10.1021/es403838t

Trueba-Santiso, A., Parladé, E., Rosell, M., Lliros, M., Mortan, S.H., Martínez-Alonso, M., Gaju, N., Martín-González, L., Vicent, T., Marco-Urrea, E., 2017. Molecular and carbon isotopic characterization of an anaerobic stable enrichment culture containing *Dehalobacterium* sp. during dichloromethane fermentation. Sci. Total Environ. 581–582, 640–648. doi:10.1016/j.scitotenv.2016.12.174

Tsitonaki, A., Petri, B., Crimi, M., Mosbaek, H., Siegrist, R.L., Bjerg, P.L., 2010. In situ chemical oxidation of contaminated soil and groundwater using persulfate: a review. Crit. Rev. Environ. Sci. Technol. 40, 55–91. doi:10.1080/10643380802039303

U.S. EPA, 2008. Field application of a permeable reactive barrier for treatment of arsenic in ground water (EPA 600/R-08/093). Ada, OK.

United Nations Environment Programme, 2006. Production and consumption of ozone depleting substances under the Montreal Protocol: 1986–2004. Nairobi, Kenya.

Van Breukelen, B.M., 2007. Extending the Rayleigh equation to allow competing isotope fractionating pathways to improve quantification of biodegradation. Environ. Sci. Technol. 41, 4004–4010. doi:10.1021/es0628452

Vanstone, N., Elsner, M., Lacrampe-Couloume, G., Mabury, S., Sherwood Lollar, B., 2008. Potential for identifying abiotic chloroalkane degradation mechanisms using carbon isotopic fractionation. Environ. Sci. Technol. 42, 126–132. doi:10.1021/es0711819

Vodyanitskii, Y.N., 2014. Effect of reduced iron on the degradation of chlorinated hydrocarbons in contaminated soil and ground water: A review of publications. Eurasian Soil Sci. 47, 119–133. doi:10.1134/S1064229314020136

Waldemer, R.H., Tratnyek, P.G., Johnson, R.L., Nurmi, J.T., 2007. Oxidation of chlorinated ethenes by heat-activated persulfate: Kinetics and products. Environ. Sci. Technol. 41, 1010–1015. doi:10.1021/es062237m

Watts, P. Long, G. Meek, M.E., 2004. Chloroform: International Program of Chemical Safety (IPCS) Concise international chemical assessment document 58, World Health Organization, Geneva.

Weathers, L.J., Parkin, G.F., 2000. Toxicity of chloroform biotransformation to methanogenic bacteria. Environ. Sci. Technol. 34, 2764–2767. doi:10.1021/es990948x

Web of Science, WOS Thomson Reuters [Web], 2018. URL https://apps-webofknowledge-com.sire.ub.edu/

Wiegert, C., Aeppli, C., Knowles, T., Holmstrand, H., Evershed, R., Pancost, R.D., Macháčková, J., Gustafsson, Ö., 2012. Dual carbon-chlorine stable isotope investigation of sources and fate of chlorinated ethenes in contaminated groundwater. Environ. Sci. Technol. 46, 10918–10925. doi:10.1021/es3016843

Wiegert, C., Mandalakis, M., Knowles, T., Polymenakou, P.N., Aeppli, C., Macháčková, J., Holmstrand, H., Evershed, R.P., Pancost, R.D., Gustafsson, O., 2013. Carbon and chlorine isotope fractionation during microbial degradation of tetra- and trichloroethene. Environ. Sci. Technol. 47, 6449–6456. doi:10.1021/es305236y

Xie, Y., Dong, H., Zeng, G., Tang, L., Jiang, Z., Zhang, C., Deng, J., Zhang, L., Zhang, Y., 2017. The interactions between nanoscale zero-valent iron and microbes in the subsurface environment: A review. J. Hazard. Mater. 321, 390–407. doi:10.1016/j.jhazmat.2016.09.028

Xiu, Z. ming, Jin, Z. hui, Li, T. long, Mahendra, S., Lowry, G. V., Alvarez, P.J.J., 2010. Effects of nano-scale zero-valent iron particles on a mixed culture dechlorinating trichloroethylene. Bioresour. Technol. 101, 1141–1146. doi:10.1016/j.biortech.2009.09.057

Yargicoglu, E.N., Reddy, K.R., 2015. Review of biological diagnostic tools and their applications in geoenvironmental engineering. Rev. Environ. Sci. Biotechnol 14, 161–194. doi:10.1007/s11157-014-9358-y

Zogorski, J.S., Carter, J.M., Ivahnenko, T., Lapham, W.W., Moran, M.J., Rowe, B.L., Squillace, P.J., Toccalino, P.L., 2006. The quality of our nation's waters - Volatile organic compounds in the nation's ground water and drinking-water supply wells, U.S. Geological Survey Circular 1292.

Zwank, L., Elsner, M., Aeberhard, A., Schwarzenbach, R.P., 2005. Carbon isotope fractionation in the reductive dehalogenation of carbon tetrachloride at iron (hydr)oxide and iron sulfide minerals. Environ. Sci. Technol. 39, 5634–5641. doi:10.1021/es0487776

Annex A. CT diffusion-controlled vaporization experiment.

Two-point calibration Cl-CSIA covering a wide range of δ^{37}Cl values was necessary to arrive at reliable δ^{37}Cl$_{SMOC}$ signatures of CMs, as it was already confirmed for chlorinated ethenes (Ebert et al., 2017). A maximum δ^{37}Cl difference of 4.5‰ was measured within the CT standards from different commercial brands collected during this thesis: -4.11±0.07‰ (n=2) for a standard from Fluka (USA) and +0.27±0.08‰ (n=2) for a standard from Panreac (Spain).

In order to get two standards covering a wider range of δ^{37}Cl-CT signatures, a CT diffusion-controlled vaporization experiment through a porous media was proposed by Dr. Jordi Palau using the most ^{37}Cl enriched commercial standard (Panreac). The feasibility of this option for enriching CT standards was studied in advance in terms of the expected $\Delta\delta^{37}$Cl of CT and the required time to obtain this $\Delta\delta^{37}$Cl.

Cl isotope fractionation is expected to occur as a result of a combination of fractionation due to vaporization (by CT−vapor equilibration) and due to CT diffusion (Jeannottat and Hunkeler, 2012). According to Jeannottat and Hunkeler (2012), effective Cl isotope fractionation factors for pairs of isotopologues (α Eff) can be expressed assuming slow vaporization by Eq. A1.

$$\alpha_{\text{Eff}}^{ITL} = \alpha_{\text{Eqm}}^{ITL} \times \alpha_{\text{Diff}}^{ITL}$$

Eq. A1

where α Eqm is the fractionation factor for CT−vapor equilibration and α Diff for diffusion given by Eq. A2, where D_h and D_l are the diffusion coefficient for heavy and light isotopologues, respectively; MW$_l$ is the molecular weight of the light molecule; MW$_h$, the molecular weight of the heavy molecule; and MW$_{air}$, the molecular weight of air (28.8 g/mol in this case). Considering the isotopologue pair with none ($[^{12}C^{35}Cl_4]^+$, m/z=152) and one ($[^{12}C^{35}Cl_3^{37}Cl]^+$, m/z=154) heavy Cl isotope, a value of α Diff = 0.99896 was found, which is equivalent to ε_{Cl} = (α-1) ×1000=-1.03‰.

$$\alpha_{\text{Diff}}^{ITL} = \frac{D_h}{D_l} = \sqrt{\frac{(\text{MW}_h + \text{MW}_{\text{air}}) \times \text{MW}_l}{(\text{MW}_l + \text{MW}_{\text{air}}) \times \text{MW}_h}}$$

Eq. A2

The expected $\Delta\delta^{37}$Cl can be calculated by using the estimated ε for chlorine following the Rayleigh equation (Eq. A3) where δ_0 and δ_t are isotope values in the beginning (t=0) and at a given time (t), respectively, and f is the fraction of substrate remaining at time t. Isotope signature is reported in ‰ using the delta notation relative to the international standards which is V-SMOC for chlorine (Shouakar-Stash et al., 2006). A 95% removal of CT by diffusion-controlled vaporization (remaining fraction, f=C/C$_0$= 0.05) would result in a Cl isotope shift of $\Delta\delta^{37}$Cl=+3.1‰.

Annex A

$$\ln\left(\frac{\delta_t + 1}{\delta_0 + 1}\right) = \varepsilon \times \ln f$$

<div align="right">Eq. A3</div>

For assessing the experimental time required for reaching f=0.05, the Fick's law for onr (spatial) dimension is applied (Eq. A4). The Fick's law relates the diffusive flux to the concentration under the assumption of steady state. It postulates that the flux goes from regions of high CT concentration to regions of low CT concentration.

$$J = -D_v \times \frac{dC_S}{dz}$$

<div align="right">Eq. A4</div>

In Eq. A4 J is the diffusive flux (mol/(s×cm²)), D_v is the effective diffusion coefficient (cm²/s), C_S is the concentration expressed as the amount of CT per unit of volume (mol/cm³) and z is the length of the diffusion path (cm).

C_S (mols/s) can be obtained after assuming CT as an ideal gas and applying the ideal gas law (Eq. A5) and considering 1 m³ of volume.

$$n = \frac{PV}{RT}$$

<div align="right">Eq. A5</div>

where n is the CT amount (mol), P is the CT vapour pressure (0.14 atm, following Antoine equation of $\log_{10}P$=A-B(T+C) with values obtained in NIST, https://webbook.nist.gov/), V is the CT volume (m³), R is the ideal, or universal, gas constant (8.2057$10^{-5}$ m³×atm/K×mol), and T is temperature (K).

The effective diffusion coefficient of CT in a porous media (D_v) can be obtained using the modification of the Millington & Quirk relationship done by Dragun (1988)), where T is the media tortuosity; Φ is the media porosity and Φ_B is porosity affected by sealed porous, and D is the CT molecular diffusion coefficient.

$$D_v = T \times (\Phi - \Phi_B) \times D$$

<div align="right">Eq. A6</div>

Figure A1 shows the experimental device used for the diffusion-controlled vaporization experiments. The device was filled with non-consolidated silica coarse sand (Sigma Aldrich, USA), with the following characteristics: T ranged from 0.6 and 0.7 (an average of 0.66 was considered), a Φ value of 0.43 was considered (Sanders, 1998), Φ_B was assumed to be negligible and D value for CT in air was 0.0828 cm²/s (Lugg, 1968). The length of the diffusion path was 12 cm and the radius of the circular area of diffusion, 9.5 cm.
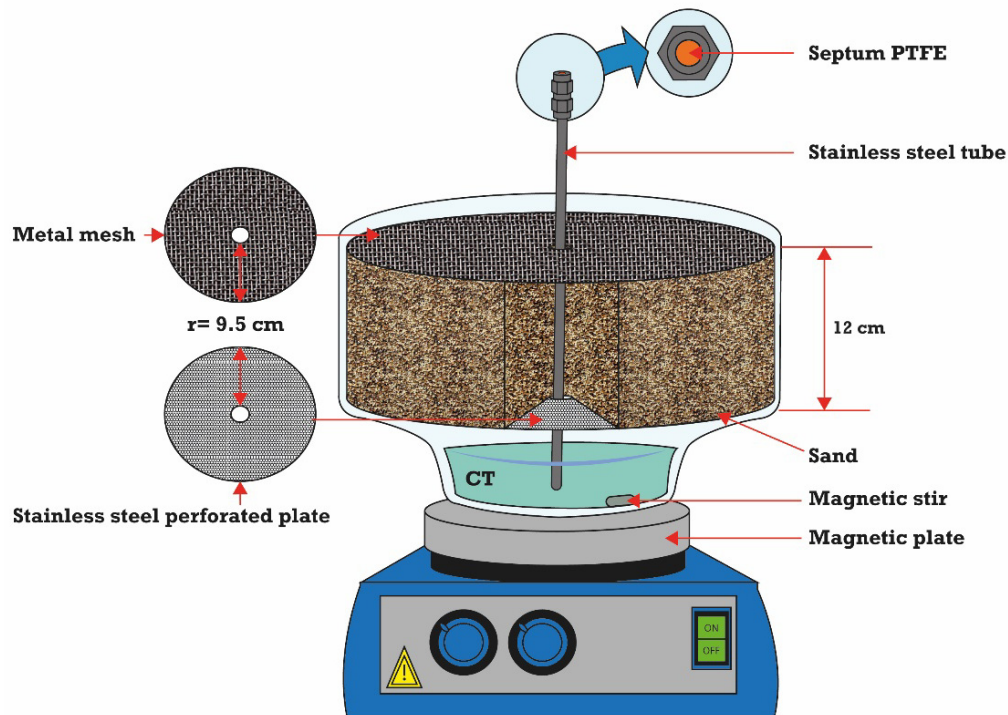
Figure A1. Scheme of the CT diffusion-controlled vaporization experiment

The experiment was performed at 25ºC. For the experimental system, the diffusive flux of CT through the experimental area (283.5 cm^2) was 3.39×10^{-6} mols CT/s (0.52 mg CT/s). Considering a CT initial volume of 1 L, the time for reaching f=0.05 was calculated to be 35.23 days. Therefore, the experiment duration was found as feasible.

The device was placed on an analytical balance and it was weighted at each sampling time in order to know whether the estimation of the reaction kinetics was accurate aiming at obtaining at least around 40 mL in the final sampling point. Moreover, the CT liquid phase was sampled periodically in order to assess the isotope fractionation (ε) associated to diffusion (Figure A2). Results show that CT diffusion followed a normal isotope fractionation for Cl but inverse for C (Figure A2), similar to the results of Jeannottat and Hunkeler (2012) for TCE diffusion-controlled vaporization in column experiments.

After 95% of CT removal, a total $\delta^{37}Cl$ shift was $\Delta\delta^{37}Cl$ ~2‰. The experimental $\Delta\delta^{37}Cl$ (~2‰) was lower than that expected theoretically (3.1‰), fact that has been already detected for chlorine in TCE (Jeannottat and Hunkeler, 2012) and for C and H in MTBE (Kuder et al., 2009).
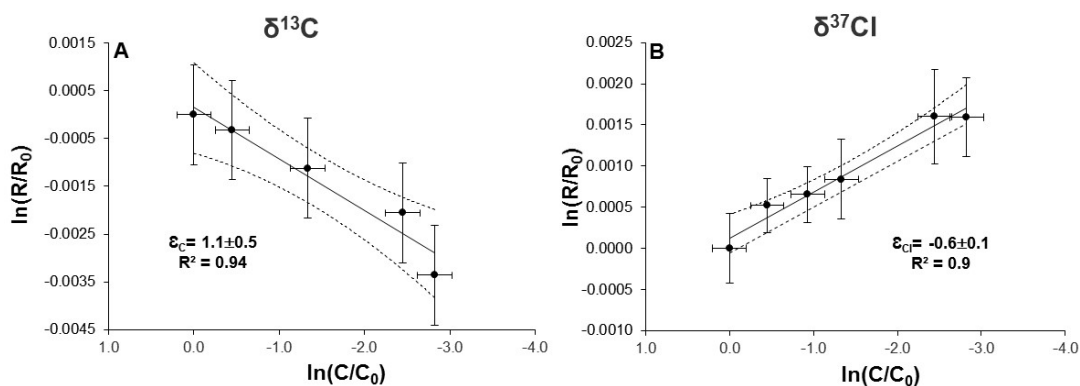
Figure A2. Logarithmic plots according to Rayleigh equation (Fig. A3) of carbon (A) and chlorine (B) isotope ratios during CT diffusion experiment. Obtained ℰC and ℰCl values are given. Dashed lines represent 95% confidence interval of the linear regression. Error bars display the uncertainty calculated by error propagation including uncertainties in concentration (SD=5%) and isotope measurements (0.5‰ for $\delta^{13}C$ and the corresponding SD value for $\delta^{37}Cl$ data point).

These standards were referenced to V-SMOC (‰) by the University of Delaware following the method of Holt et al. (1997). Therefore, this new produced ^{37}Cl-enriched standard (+1.98±0.10‰, n=2) and the most depleted commercial standard (-4.11±0.07‰ from Fluka) were used as CT standards for two-point calibration schemes for the determination of accurate and reliable $\delta^{37}Cl_{SMOC}$ signatures of experimental and field samples.

References Annex A

Dragun, J., 1988. The soil chemistry of hazardous materials. Silver Spring, Maryland: The Hazardous Materials Research Institute.

Ebert, K.A., Laskov, C., Elsner, M., Haderlein, S.B., 2017. Calibration bias of experimentally determined chlorine isotope enrichment factors: the need for a two-point calibration in compound-specific chlorine isotope analysis. Rapid Commun. Mass Spectrom. 31, 68–74. doi:10.1002/rcm.7752

Holt, B.D., Sturchio, N.C., Abrajano, T.A., Heraty, L.J., 1997. Conversion of chlorinated volatile organic compounds to carbon dioxide and methyl chloride for isotopic analysis of carbon and chlorine. Anal. Chem. 69, 2727–2733. doi:10.1021/ac961096b

Jeannottat, S., Hunkeler, D., 2012. Chlorine and carbon isotopes fractionation during volatilization and diffusive transport of trichloroethene in the unsaturated zone. Environ. Sci. Technol. 46, 3169–3176. doi:10.1021/es203547p

Kuder, T., Philp, P., Allen, J.O.N., 2009. Effects of volatilization on carbon and hydrogen isotope ratios of MTBE. Environ. Sci. Technol. 43, 1763–1768. doi:10.1021/es802834p

Lugg, A., 1968. Diffusion coefficients of some organic and other vapors in air. Anal. Chem. 40. doi: 10.1021/ac60263a006

Sanders, L.L., 1998. A manual of field hydrogeology. Prentice-Hall, Inc., New Yersey.

Shouakar-Stash, O., Drimmie, R.J., Zhang, M., Frape, S.K., 2006. Compound-specific chlorine isotope ratios of TCE, PCE and DCE isomers by direct injection using CF-IRMS. Appl. Geochemistry 21, 766–781. doi:10.1016/j.apgeochem.2006.02.006

Annex B. Article 1. Cl-CSIA method development

Heckel, B., Rodríguez-Fernández, D., Torrentó, D., Meyer, A., Palau, J., Domènech, C., Rosell, M., Soler, A., Hunkeler, D., Elsner, D., 2017. Compound-specific chlorine isotope analysis of tetrachloromethane and trichloromethane by GC-IRMS *vs*. GC-qMS: Method development and evaluation of precision and trueness. Anal. Chem. 89, 3411–3420. doi: 10.1021/acs.analchem.6b04129.

Compound-Specific Chlorine Isotope Analysis of Tetrachloromethane and Trichloromethane by Gas Chromatography-Isotope Ratio Mass Spectrometry vs Gas Chromatography-Quadrupole Mass Spectrometry: Method Development and Evaluation of Precision and Trueness

Benjamin Heckel,[†] Diana Rodríguez-Fernández,[‡] Clara Torrentó,[§] Armin Meyer,[†] Jordi Palau,[§,‡]
Cristina Domènech,[‡] Mònica Rosell,[‡] Albert Soler,[‡] Daniel Hunkeler,[§] and Martin Elsner[*,†,⊥]

[†]Institute of Groundwater Ecology, Helmholtz Zentrum München, Ingolstädter Landstrasse 1, 85764 Neuherberg, Germany
[‡]Grup de Mineralogia Aplicada i Geoquímica de Fluids, Departament de Mineralogia, Petrologia i Geologia Aplicada, Facultat de Ciències de la Terra, Universitat de Barcelona (UB), C/Martí i Franquès, s/n 08028, Barcelona, Spain
[§]Centre d'Hydrogéologie et de Géothermie (CHYN), Université de Neuchâtel (UNINE), Rue Emile-Argand 11, Neuchâtel 2000, Switzerland

⑤ Supporting Information

ABSTRACT: Compound-specific chlorine isotope analysis of tetrachloromethane (CCl_4) and trichloromethane ($CHCl_3$) was explored by both, gas chromatography-isotope ratio mass spectrometry (GC-IRMS) and GC-quadrupole MS (GC-qMS), where GC-qMS was validated in an interlaboratory comparison between Munich and Neuchâtel with the same type of commercial GC-qMS instrument. GC-IRMS measurements analyzed CCl isotopologue ions, whereas GC-qMS analyzed the isotopologue ions CCl_3, CCl_2, CCl (of CCl_4) and $CHCl_3$, $CHCl_2$, CHCl (of $CHCl_3$), respectively. Lowest amount dependence (good linearity) was obtained (i) in H-containing fragment ions where interference of ^{35}Cl- to ^{37}Cl-containing ions was avoided; (ii) with tuning parameters favoring one predominant rather than multiple fragment ions in the mass spectra. Optimized GC-qMS parameters (dwell time 70 ms, 2 most abundant ions) resulted in standard deviations of 0.2‰ ($CHCl_3$) and 0.4‰ (CCl_4), which are only about twice as large as 0.1‰ and 0.2‰ for GC-IRMS. To compare also the trueness of both methods and laboratories, samples from CCl_4 and $CHCl_3$ degradation experiments were analyzed and calibrated against isotopically different reference standards for both CCl_4 and $CHCl_3$ (two of each). Excellent agreement confirms that true results can be obtained by both methods provided that a consistent set of isotopically characterized reference materials is used.
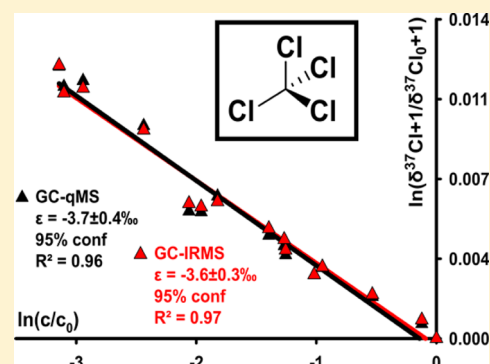
C hlorinated methanes such as trichloromethane ($CHCl_3$) and tetrachloromethane (CCl_4) have been used as dry cleaning agents, solvents and for the production of chlorofluorocarbons. As a consequence of accidents and inadvertent handling, spills of these chemicals have led to groundwater and soil contaminations. Because of their potential to cause cancer and chronic diseases, both compounds have received attention as notorious legacy chemicals at contaminated sites.[1,2]

To characterize on-site contamination and to explore best remediation strategies, compound-specific isotope analysis (CSIA) offers the possibility to distinguish chemically identical contamination sources by their isotope values and to quantify transformation of chlorinated solvents by the observation of degradation-induced changes in these isotope ratios.[3,4] While the ability to derive both lines of evidence is limited if isotope ratios of only one element are measured, the possibilities of CSIA are magnified when analyzing isotopic information from several elements.[5-8] Specifically, as shown for chlorinated

ethylenes, analysis of carbon and chlorine isotopes makes it possible to create dual element isotope plots offering the opportunity to distinguish sources more confidently, to detect degradation, and importantly to investigate different transformation mechanisms.[9-16] For CCl_4 and $CHCl_3$ this perspective became achievable by the introduction of viable approaches for compound-specific chlorine isotope analysis of organic compounds.[17-19] Traditionally, the analysis of chlorine isotopes does not only require dedicated instrumentation but also time-demanding offline preparation, such as analyte conversion to CH_3Cl.[20,21] Subsequently, CH_3Cl can be measured on a dual-inlet gas isotope ratio mass spectrometer (DI-IRMS). This so-called offline method for chlorine isotope

analysis was established by Holt et al.[22] Another possibility is the conversion to cesium chloride for thermal ion mass spectrometry analysis[23] or the atomization of compounds in an inductively coupled plasma followed by multicollector MS.[24,25] A breakthrough for compound-specific chlorine isotope analysis by continuous flow ("online") measurements without laborious offline preparation was accomplished by Shoukar Stash et al.[21] and Sakaguchi-Soder et al.[26] Chlorine isotope analysis was performed on original target analyte molecules of tetrachloroethylene (PCE) and trichloroethylene (TCE) eluting from the gas chromatographic separation. Measurements rely on molecular ions, or fragment ions, generated in the ion source of an IRMS[21] or qMS.[26] In 2010, Aeppli et al.[27] obtained chlorine isotope ratios for PCE, PCP, and DDT using this GC-qMS approach. To improve the qMS measurements of PCE and TCE, Jin et al.[28] optimized the method and compared different evaluation schemes. Palau et al. investigated for the first time 1,2-dichloroethane[11] and 1,1,1-trichloroethane.[29] Chlorine isotope measurements for $CHCl_3$ were reported but not yet systematically validated by Breider and Hunkeler.[30] Hitzfeld et al.[31] and Renpenning et al.[32] introduced yet an alternative and potentially improved strategy to measure chlorine, bromine, and sulfide isotopes. In their studies, GC separation was followed by H_2-induced high temperature conversion (HTC) to HCl, HBr, or H_2S, respectively, and subsequent qMS[31] or IRMS[32] analysis. While this approach represents a universal strategy irrespective of target compound structure, memory effects, and short reactor lifetimes are presently reported to limit HTC applications.[32] Consequently, analyses of unconverted target analytes by GC-IRMS[21] or GC-qMS[26] are the current methods of choice. They represent an emerging opportunity for field studies and mechanistic investigations that is far from being explored. Specifically, current applications are restricted for several reasons. On the one hand, parameters for GC-qMS and GC-IRMS analyses must be carefully validated for each new target compound[33] and the choice of adequate analyte/fragment ions to achieve optimum performance (sensitivity, linearity) in isotope analysis is still an open question.[28] On the other hand, interlaboratory comparisons show that the use of two isotopically distinct isotopic reference materials of each target compound are necessary to ensure comparable results in different laboratories.[11,33,34] Comparisons between the performance of GC-qMS and GC-IRMS using the same reference materials are highly desirable yet limited to a few comparative studies.[11,33]

In this study we, therefore, optimized and carefully evaluated compound-specific chlorine isotope analysis for two new important target compounds, $CHCl_3$ and CCl_4, by both GC-IRMS and GC-qMS, with a particular focus on the comparison of precision and trueness for both approaches. Also, we focused on the question whether rules of thumb can be derived to choose the best analyte/fragment ions for optimum performance (sensitivity, linearity) of isotope analysis. We evaluated the performance using reference material with independently determined isotope ratios as well as with samples from degradation experiments to investigate if measured shifts in isotope ratios and enrichment factors are consistent among methods. In addition, GC-qMS methods were validated in an interlaboratory comparison between Munich and Neuchâtel.

■ EXPERIMENTAL SECTION

Chemicals. All chemicals in this study were used as received: $CHCl_3$ (Fluka), CCl_4 (Panreac), sodium formate (HCOONa, Merck), cast iron (92% Gotthart Maier Metallpulver GmbH), dibasic anhydrous sodium phosphate (Na_2HPO_4, Panreac AppliChem), sodium hydroxide (NaOH, Baker), hydrochloric acid (HCl, 32 wt %, Sigma-Aldrich).

Abiotic Degradation of CCl_4 with Sodium Formate. A volume of 10 μL of CCl_4 was dissolved in 35 mL of degassed ultrapure water by vigorous stirring for 24 h in a 40 mL vial. The reaction was started inside an anoxic chamber with the addition of 1 g of sodium formate. The vial was closed with a mininert valve (Supelco) and constantly stirred with a magnetic stir plate. Seven samples were taken over a time course of 7 h. For each time point, 0.5 mL was removed from the reaction mixture and diluted in 7 mL of hydrogen peroxide solution (1%), and 1 mL of subsamples were immediately taken from this solution to analyze concentrations and chlorine isotope values. One experimental replicate was performed with 2 g instead of 1 g of sodium formate and was analyzed in the same way.

Abiotic Degradation of $CHCl_3$ with Cast Iron at pH 12. The cast iron was washed with 0.1 M HCl for an hour, rinsed, and dried overnight to activate the surface.[35] The surface of the activated iron was determined by the BET (Brunauer–Emmett–Teller) method as 1.624 ± 0.007 m^2 g^{-1}. The 42 mL vials (20 reaction vials, 12 blank vials) were wrapped in aluminum foil to inhibit photoreaction and 2 g of cast iron were added to each vial. Subsequently, a buffer solution of pH 12 was added until nearly no headspace was left. To start the reaction, pure $CHCl_3$ was added to reach a concentration of 100 mg/L. During the whole reaction vials were placed on a horizontal shaker (IKA KS 260 BASIC, Stanfen, Germany). Samples were taken over 9 days, and for each time point one vial was sacrificed. To stop the reaction, 0.2 μm filtration and subsequent neutralization by acetic acid was done. Samples were frozen[36] in 10 mL vials until analyses for concentrations, carbon and chlorine isotope ratios.

Stable Carbon Isotope Analysis by GC-C-IRMS. Carbon isotope analyses of $CHCl_3$ were performed in the Centres Científics i Tecnològics at the Universitat de Barcelona (CCiTUB) according to the method described elsewhere[37] by using a Thermo Finnigan Trace GC Ultra instrument coupled via a GC-Isolink interface to a Delta V Advantage isotope ratio mass spectrometer (Thermo Scientific GmbH, Bremen, Germany). The GC was equipped with a Supelco SPB-624 column (60 m × 0.32 mm × 1.8 μm, Bellefonte, PA). The GC program started at 60 °C for 5 min, the GC was heated to 165 °C at a rate of 8 °C/min, then heated to 220 °C at 25 °C/min, and finally held at 220 °C for 1 min. A split ratio of 1:5 was used at an injector temperature of 250 °C. Helium (5.0) served as a carrier gas (2.2 mL min^{-1}). The chlorinated methanes were extracted from aqueous samples by automated headspace solid-phase microextraction (HS-SPME) using a 75 μm Carboxen-PDMS fiber (Supelco, Bellefonte, PA) and a TriPlus autosampler equipped with a SPME holder (Thermo Fisher Scientific, Waltham). Samples were extracted at a constant agitation rate (600 rpm) for 20 min at 40 °C. After extraction, the SPME fibers were desorbed at 250 °C for 5 min in the GC injector. The analytical uncertainty (2σ) of carbon isotopic measurements never exceeded ±0.5‰. A pulse of CO_2 as monitoring gas was introduced at the beginning and at the end of each run. For carbon, the monitoring gas had been calibrated beforehand so that values are stated relative to the international reference material Vienna Pee Dee Belemnite (VPDB) on the international per mille scale. Moreover, several
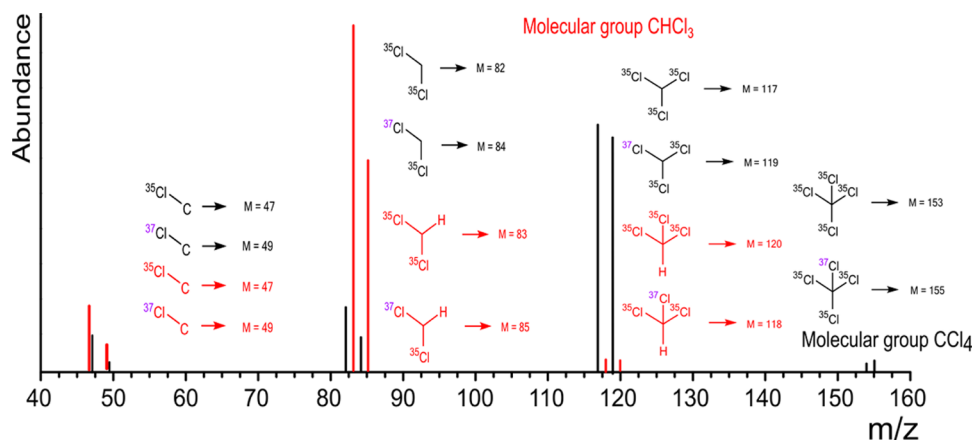
Figure 1. Mass spectra of the isotopologue ion peaks of CCl_4 (in black) and $CHCl_3$ (in red) in analysis by GC-qMS.

$CHCl_3$ aqueous control standards were prepared daily at the same concentration range than the samples from a pure in-house standard of known carbon isotopic composition ($\delta^{13}C$) and analyzed on the same days as the samples to ensure accuracy of the isotopic measurements and to correct slight carbon isotopic fractionation induced by the HS-SPME preconcentration technique.[38] The $\delta^{13}C$ of this pure $CHCl_3$ standard ($-48.96 \pm 0.04‰$) was determined previously using a Flash EA1112 (Carlo-Erba, Milano, Italy) elemental analyzer (EA) coupled to a Delta C IRMS (Thermo Fisher Scientific, Bremen, Germany) through a Conflo III interface (Thermo Finnigan, Bremen, Germany) using six international reference materials (NBS 19, IAEA-CH-6, USGS40, IAEA-600, IAEA-CH-7, L-SVEC) with respect to the VPDB standard, according to Coplen et al.[39] All the controls injected together with the present samples had an average $CHCl_3$-$\delta^{13}C$ value of $-50.0 \pm 0.3‰$ ($n = 15$).

Stable Chlorine Isotope Analysis by GC-IRMS in Munich. GC-IRMS analysis of CCl_4 and $CHCl_3$ was conducted by recording the masses $m/z = 47$ and 49 (CCl fragment), which correspond to half of the masses for which the IRMS instrument is specifically configured (98, dichloroethene molecular ion; 94, double dechlorinated tetrachloroethene fragment ion). The GC-IRMS system (Thermo Scientific) consisted of a Trace GC that was connected via a transfer line to a MAT 253 IRMS equipped with a dual inlet system. The gas chromatograph was operated with He carrier gas (5.0) at 1.4 mL/min and contained a 30 m VOCOL column (Supelco) with 0.25 mm inner diameter and a film thickness of 1.5 μm. The GC program started at 60 °C for 2 min, followed by a temperature ramp of 8 °C/min to 165 °C and of 25 °C/min to 220 °C (held for 1 min). The 1 mL gas phase was injected from 10 mL headspace vials that contained 1 mL of aqueous sample and that had previously been equilibrated for 5 min at 40 °C. Injection was performed in split mode (1:10 split ratio) at 220 °C through a split/splitless injector. No difference was observed in isotope values obtained with a split ratio of 1:10 compared to 1:20 (data not shown).

To provide an anchor between individual measurements, pulses of a monitoring gas of CCl_4 and $CHCl_3$ were introduced via the dual inlet system at the beginning and the end of each measurement. Monitoring gas was never adjusted to sample concentration, but instead the amount dependency ("linearity") of isotope measurements was carefully investigated using external standards (see below). In addition, to convert delta values relative to the international reference Standard Mean Ocean Chloride (SMOC), a two point calibration was performed with external standards of CCl_4 and $CHCl_3$. These external standards were placed into daily measurement sequences in the following way. At the beginning of a sequence, 10 injections of the first standard and four injections of the second standard were performed with different headspace volumes. This resulted in a series of amplitudes that allowed evaluating the linearity of the method and, if necessary, performing an amplitude correction. After that, duplicate measurements of both standards were introduced after every 10 sample injections to enable a drift correction accounting for slow outgassing of the CCl_4 monitoring gas from the reference bellow of the IRMS. The measurement sequence was, finally, concluded by quadruplicate measurements of both standards with the same concentration and headspace volumes. Values of the external standards (after amplitude and drift correction) were plotted against their values on the SMOC scale and sample measurements were evaluated using the intercept and the slope of this regression (again, after amplitude and drift correction). The chlorine isotope signatures ($\delta^{37}Cl$) of the external CCl_4 standards were $+1.98 \pm 0.1‰$ ($n = 2$) and $-4.11 \pm 0.07‰$ ($n = 2$), as characterized at the University of Delaware (Newark, DE) and those of the external $CHCl_3$ standards were $-3.02 \pm 0.17‰$ ($n = 17$) and $-5.4 \pm 0.3‰$ ($n = 8$), as characterized in Waterloo (Isotope Tracer Technologies Inc., Waterloo, Canada), in both cases by IRMS after conversion to CH_3Cl.[22]

Concentration and Stable Chlorine Isotope Measurements with GC-qMS. GC-qMS measurements for analysis of CCl_4 and $CHCl_3$ concentrations and chlorine isotope values were performed in Munich (GC-qMS-1) and Neuchâtel (GC-qMS-2). A summary of instrument parameters in the GC-qMS-1 and GC-qMS-2 setups can be found in the Supporting Information (Table S1). The isotope data from both qMS were also corrected by a two-point calibration with the external standards mentioned above. For each run, four samples of both standards with the same concentration were measured at the beginning, two after every 10 measurements and again four at the end to enable a drift correction. In contrast to GC-IRMS, an amplitude ("linearity") correction was not necessary, because we did not observe an amount-dependency (for further discussion see the Results section below). The data acquisition frequency was chosen such that 15−25 data points are obtained across the chromatographic peaks (Agilent GC/

MSD ChemStation and Instrument Operation, Course Number H4043A Volume I, page 100). This requires around 3 measurement cycles/s corresponding to a total scan time for each cycle of around 300 ms. A suitable dwell time is then obtained by dividing this time interval by the number of ions (n) analyzed. Reasonable dwell times were calculated in milliseconds.

$$\text{dwell time} = \frac{300}{n+1} \tag{1}$$

In this study, the dwell time was varied around this typical value.

Evaluation of Chlorine Isotope Data. Instrument isotope values for chlorine and carbon measurements by IRMS were in a first step derived from the instrument's software, where samples were evaluated relative to a monitoring gas in each run. For the calculation of chlorine isotope values eq 2 was used:

$$\delta^{37}Cl_{compound} = \frac{(^{37}Cl/^{35}Cl)_{compound} - (^{37}Cl/^{35}Cl)_{ref}}{(^{37}Cl/^{35}Cl)_{ref}}$$
$$= \frac{R_t}{R_{ref}} - 1 \tag{2}$$

where values are given in per mille For example, a value of 10 ‰ indicates that a substance contained 10 per mille (or one percent) more $^{37}Cl/^{35}Cl$ than the compound to which it was compared. An analogous equation applies with $^{13}C/^{12}C$ for carbon.

For chlorine isotope measurements by GC-qMS-1, we tested settings with different numbers of ion pairs and different dwell times (i.e., 2, 4, and 6 ions and dwell times between 40 and 100). The molecular ion peaks and fragment ion peaks of CCl_4 and $CHCl_3$ are shown in Figure 1. The masses 119/117, 84/82, and 49/47 were chosen for CCl_4 and 120/118, 85/83, and 49/47 for $CHCl_3$. For the evaluation of selected-ion monitoring (SIM) measurements relying on only two ions we chose the peak intensities of the two most abundant fragment ions (m/z 83 and 85) for $CHCl_3$ and (m/z 117, 119) for CCl_4. These ion couples correspond to the isotopologue pairs ($[^{35}Cl_2{}^{12}CH]^+$ and $[^{35}Cl^{37}Cl^{12}CH]^+$) and ($[^{35}Cl_3{}^{12}C]^+$ and $[^{35}Cl_2{}^{37}Cl^{12}C]^+$), respectively.[27] The isotope ratio was obtained from the ratio of these isotopologues according to eqs 3 and 4.[40]

For the fragment ions m/z 83 and 85 of $CHCl_3$ the equation applies

$$R = \frac{^{37}Cl}{^{35}Cl} = \frac{^{37}p}{^{35}p} = \frac{k}{(n-k+1)} \frac{^{35}Cl_{(k)}{}^{35}Cl_{(n-k)}}{^{37}Cl_{(k-1)}{}^{35}Cl_{(n-k+1)}}$$
$$= \frac{1}{2} \frac{^{85}I}{^{83}I} \tag{3}$$

where ^{37}p and ^{35}p are the probabilities of encountering ^{37}Cl and ^{35}Cl, n is the number of Cl atoms in the fragment (here, 2), k is the number of ^{37}Cl isotopes in the "heavy" isotopologue (here, 1), $^{37}Cl_{(k)}{}^{35}Cl_{(n-k)}$ and $^{37}Cl_{(k-1)}{}^{35}Cl_{(n-k+1)}$ represent the isotopologues containing k and $(k-1)$ heavy isotopes (here, $[^{35}Cl^{37}Cl^{12}CH]^+$ and $[^{35}Cl_2{}^{12}CH]^+$), respectively, and I indicates the ion peak intensities. An analogous equation applies to the fragment ions m/z 117 and 119 ($[^{35}Cl_2{}^{37}Cl^{12}C]^+$ and $[^{35}Cl_3{}^{12}C]^+$ of CCl_4, respectively):

$$R = \frac{^{37}Cl}{^{35}Cl} = \frac{^{37}p}{^{35}p} = \frac{k}{(n-k+1)} \frac{^{35}Cl_{(k)}{}^{35}Cl_{(n-k)}}{^{35}Cl_{(k-1)}{}^{35}Cl_{(n-k+1)}}$$
$$= \frac{1}{3} \frac{^{119}I}{^{117}I} \tag{4}$$

with $n = 3$ and $k = 1$. Values calculated this way were subjected to a calibration with the external standards as described above (measured values of standards were plotted against their values on the SMOC scale, sample measurements were subsequently evaluated using the intercept and the slope of this regression). Resultant values were reported in the δ-notation in parts per thousand relative to the international Standard Mean Ocean Chloride (SMOC) standard.

In contrast, for evaluation of the 4 and 6 ion settings for CCl_4 and $CHCl_3$, the modified multiple ion method was used.[28] Equations 5 and 6 show the corresponding expressions for $CHCl_3$.

Four ions:

$$R_{CHCl_3} = aR_{F1}^{CHCl_3} + bR_{F2}^{CHCl_3}$$
$$a = \frac{I_{85} + I_{83}}{(I_{85} + I_{83}) + (I_{49} + I_{47})}$$
$$b = \frac{I_{49} + I_{47}}{(I_{85} + I_{83}) + (I_{49} + I_{47})} \tag{5}$$

Six ions:

$$R_{CHCl_3} = aR_M^{CHCl_3} + bR_{F1}^{CHCl_3} + cR_{F2}^{CHCl_3}$$
$$a = \frac{I_{120} + I_{118}}{(I_{120} + I_{118}) + (I_{85} + I_{83}) + (I_{49} + I_{47})}$$
$$b = \frac{I_{85} + I_{83}}{(I_{120} + I_{118}) + (I_{85} + I_{83}) + (I_{49} + I_{47})}$$
$$c = \frac{I_{49} + I_{47}}{(I_{120} + I_{118}) + (I_{85} + I_{83}) + (I_{49} + I_{47})} \tag{6}$$

where R_M is the isotope ratio of the molecular group, R_{F1} of fragment 85/83 and R_{F2} of the fragment 49/47 (eq 3). For a quantitative evaluation of degradation experiments, isotopic enrichment factors (ε) were determined according to the Rayleigh equation[41,42]

$$\ln\left(\frac{\delta^{37}Cl + 1}{\delta^{35}Cl_0 + 1}\right) = \varepsilon \ln f \tag{7}$$

where $\delta^{37}Cl_0$ is the chlorine isotope value at time zero, $\delta^{37}Cl$ is the chlorine isotope value at time t, and f is the residual fraction of the substrate (i.e., the concentration at time t divided through the concentration at time zero). The isotopic enrichment factor expresses the difference in reaction rates of molecules containing light and heavy isotopes, respectively, where a value of, e.g., -3.5‰ indicates that heavy isotopologues reacted by 3.5‰ more slowly than light isotopologues.

■ RESULTS AND DISCUSSION

Acquisition Parameters for GC-qMS Analysis. A crucial parameter for chlorine isotope measurements on a GC-qMS is the optimum configuration in SIM mode. On the one hand,

instrument fluctuations and also "isotope swings" (i.e., changing isotope values over a chromatographic peak) are better accounted for when measurements jump quickly back and forth between masses. On the other hand, each mass is analyzed more precisely when recorded over a longer time. Finally, different masses can be selected to derive isotope values (see Figure 1). In a first step it was, therefore, our aim to find the optimal choice of ions and dwell times. As described in detail above, we evaluated the most abundant ions method (eqs 3 and 4) plus dwell times of 100, 70, or 50 ms, on the one hand, and the multiple ion method (eqs 5 and 6) for 4 and 6 ions with dwell times of 60 and 40 ms, respectively, on the other hand. For each configuration, 25 identical aqueous samples with concentrations of 1–5 mg/L were measured and the resultant standard deviations were plotted in Figure 2A (after
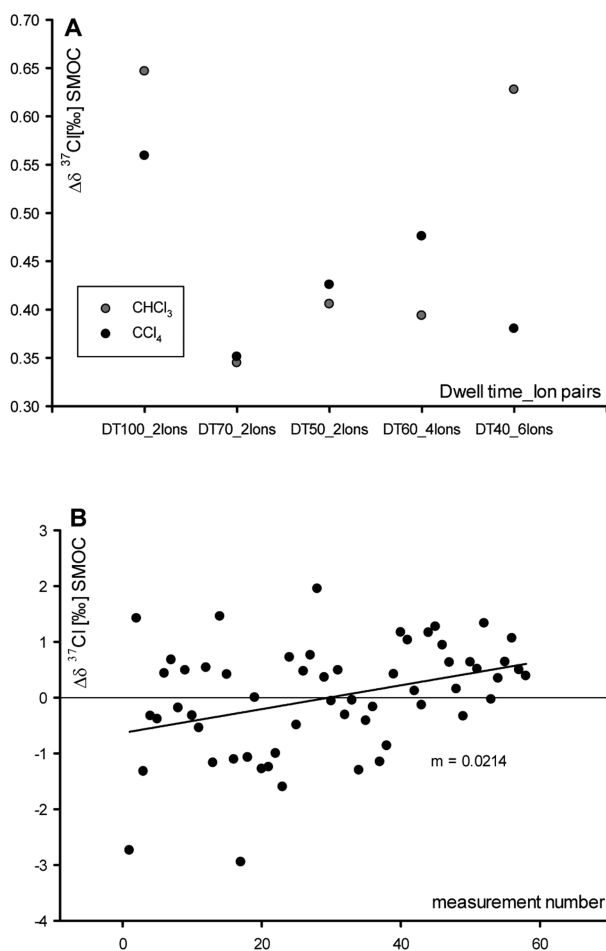
Figure 2. (A) Standard deviation ($n = 25$) of $\delta^{37}Cl$ of CCl_4 and $CHCl_3$ with different ion pair/dwell time settings measured on GC-qMS-1. Delta values (in per mille) are calibrated against SMOC. (B) $\delta^{37}Cl_{CCl4}$ measurements with dwell times of 70 ms and 2 ions in per mil and calibrated against SMOC, indicating a small drift over time for CCl_4 in GC-qMS-1.

two-point calibration against the international standard SMOC to convert instrument readings into per mille units of the δ-scale). This plot of precision versus instrument configuration showed that the recording of 2 ions with a dwell time of 70 ms gave the most precise results for both CCl_4 and $CHCl_3$, with a low standard deviation of around 0.35 per mille. Consequently, we used this setting for all subsequent evaluations in GC-qMS-1. In Neuchâtel (GC-qMS-2), the method already established

for $CHCl_3$ by Breider and Hunkeler,[27] using the two most abundant ions and 50 ms as dwell time, was followed.

Figure 2B gives an example of CCl_4 standard measurements over time (60 measurements in a range of 1–25 mg/L) showing a small drift, which occurs with increasing measurement number. We observed such a shift in nearly all measurements and a corresponding drift correction was applied, both in GC-qMS-1 as well as in GC-IRMS measurements. To this end, a linear regression similar to Figure 2B was performed from external standards analyzed along the sequence. Subsequently, the regression parameters were used to correct isotope values of samples.

Amount Dependency ("Linearity") of Chlorine Isotope Analysis of CCl_4 by GC-qMS and GC-IRMS. To determine the precision of CCl_4 measurements on the GC-IRMS instrument, we analyzed 70 standards in a range of 0.03–2.6 mg/L. Even at the lowest amplitude (100 mV), CCl_4 measurements had a standard deviation of only ±0.6‰ ($n = 10$) and at signals greater than 1 V a very small standard deviation of ±0.1‰ ($n = 60$) was accomplished (Figure 3A). No amount dependency of the trueness (i.e., the target value) was detected, which is consistent with results obtained previously with chlorinated ethylenes on the GC-IRMS system.[33] Figure 3B shows the precision of CCl_4 measurements by GC-qMS.

For signals of small areas below 10 million TIC (total ion count), chlorine isotope values of GC-qMS-1 measurements showed a rather low precision (±3‰). Above an area of 30 million, in contrast, standard deviations of ±0.6 to 0.4‰ ($n = 13$) were obtained, which represent an excellent precision for a GC-qMS.[33] In support of these data, an interlaboratory comparison using the same type of GC-qMS gave identical results in Neuchâtel for the GC-qMS-2 (Figure 3B). Therefore, even though standard deviations (i.e., the precision) were clearly affected by the injected amount, the target value (i.e., the trueness) appeared to be hardly amount-dependent in both laboratories. This is in remarkable contrast to previous TCE measurements with GC-qMS,[33] where the concentrations of external standards had to be adjusted to sample concentrations for accurate chlorine isotope analysis by GC-qMS. To compare the precision of GC-IRMS and GC-qMS, the same standard and concentration range (on-column amounts) was measured on the three instruments (Figure 3C). Here, the x axis displays the amount of analyte that, after accounting for the split flow in the injector, reaches the chromatographic column and is measured at the ion source. This amount is also reflected in the signal amplitudes of Figure 3A,B.

Amount Dependency ("Linearity") of Chlorine Isotope Analysis of $CHCl_3$ by GC-IRMS. Chlorine isotope measurements of $CHCl_3$ by GC-IRMS were conducted identically, meaning that, like for CCl_4, also the fragment masses 49 and 47 were recorded on the GC-IRMS (corresponding to $[^{12}C^{37}Cl]^+$ and $[^{12}C^{35}Cl]^+$ in both cases). Figure 4A shows that, in contrast to CCl_4, for $CHCl_3$ a strong amount-dependency of isotope values was observed, which could be taken into account by an amplitude correction. We attribute this observation to the fact that, besides the fragment $[^{12}C^{37}Cl]^+$, also the fragment $[^{13}C^1H^{35}Cl]^+$ fell on the detector cup that analyzed the mass 49 (Figure 4B). Therefore, as the number of ions increased, also the probability of collisions increased so that more H atoms were stripped from the $[^{13}C^1H^{35}Cl]^+$ fragment and were transferred to other ions (which were not analyzed) and therefore the interference by

A. Dependence of IRMS Raw Data on the Choice of Ions

$m = 0.00027$ ‰/mV
$R^2 = 0.97$

● Fragments 49/47
▲ Fragments 50/48
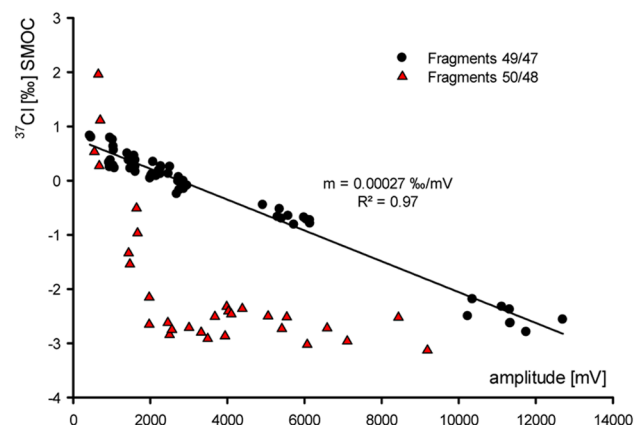
B. Possibility of Interfering Masses

| Textbook example of linearity correction (H₃-Factor) | Analogous to H₃-case Linearity correction neccesary | No Interference Good Linearity |
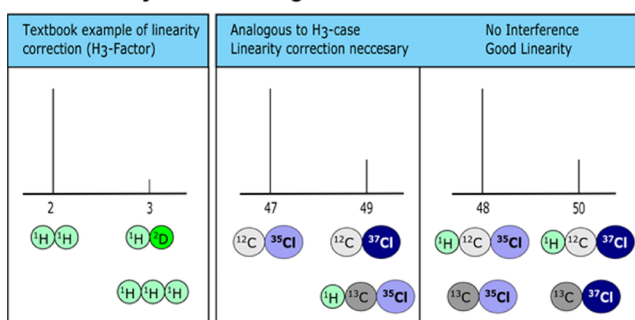
Figure 4. (A) Chlorine isotope values of $CHCl_3$ in dependence on increasing amplitudes on the GC-IRMS (fragments 49/47, 60 data points; fragments 50/48, 30 data points). (B) "Crossover interference" where ions containing a light isotope (^{35}Cl or ^1H) contribute to the mass of a heavy isotope (^{37}Cl or ^2H). This interference is dependent on intermolecular proton transfer in the ion source of the GC-IRMS and, hence, amount-dependent. Such interference is possible for the masses $m/z = 3$ ($^1H_3^+$ vs $^1H^2H$, left) and $m/z = 49$ ($^{37}Cl^{12}C$ vs $^{35}Cl^{13}C^1H$, center) but not for mass 50 (right).

Figure 3. (A) Precision of chlorine isotope measurements vs signal amplitude of CCl_4 measured by GC-IRMS (70 data points). (B) Precision of chlorine isotope measurements of CCl_4 on GC-qMS-1 and GC-qMS-2 in dependence on signal intensity, where $\delta^{37}Cl_{CCl4}$ (calibrated to SMOC scale) of the two most abundant ions are plotted against area (from 119 + 117 ions; GC-qMS-1: 58 data points; GC-qMS-2: 50 data points). (C) Comparison of the precision of chlorine isotope analysis by GC-IRMS vs GC-qMS-1 and GC-qMS-2 in dependence on the mass of analyte (CCl_4) on column.

$[^{13}C^1H^{35}Cl]^+$ decreased. The phenomenon is well-known from H-measurements where hydrogen atoms are transferred to H_2 molecules creating ions of the mass H_3^+ that are detected together with $[^2H^1H]^+$. In both cases the probability of H transfer increases with the amount of analyte molecules in the ion source. However, while in the case of hydrogen, more

collisions create more H_3^+ ions and, hence, increase the interference, in the case of $CHCl_3$ more collisions decreased the number of $[^{13}C^1H^{35}Cl]^+$ ions so that the interference became smaller. For hydrogen isotope measurements, the problem is circumvented by a linear correction of the amount-dependency, i.e., determination of a (positive) H_3-factor. Following an analogous strategy, we introduced an amplitude correction with a negative factor to take into account the amount-dependency of the interference by $[^{13}C^1H^{35}Cl]^+$. This amplitude correction did not require additional analytical effort because external standards needed to be measured anyways, and an injection of different amounts of headspace from the same standard was sufficient to calibrate for the amount-dependency according to Figure 4A (see the Experimental Section above).

Our hypothesis of this "crossover interference" (where ions containing a light isotope (^{35}Cl) contributed to the mass of a heavy isotope (^{37}Cl)) is confirmed by analysis of the fragment masses 50 and 48 of $CHCl_3$, which did *not* show a mass dependency between 2000 to 12000 mV. Figure 4B illustrates the underlying reason: unlike in the case of mass 49 and 47, there is no possibility for ions containing ^{35}Cl to contribute to the mass recorded for ions containing heavy isotopes, $^{37}Cl^{12}CH$ (note that ^2H is of too low abundance for $^{35}Cl^{13}C^2H$ to make a difference). Since in the case of chloroform, the sensitivity of

measurements of the masses 50 and 48 was 2.5 times lower and standard deviation was worse compared to masses 49 and 47, we nevertheless decided against measurements of the masses 50 and 48 and rather performed an amplitude correction on the masses 49 and 47. Figure 5B illustrates the resulting linearity demonstrating that, after correction, excellent accuracy could be obtained.

Amount Dependency ("Linearity") of Chlorine Isotope Analysis of CHCl₃ by GC-qMS. To accomplish a similar method comparison of GC-IRMS and GC-qMS as for CCl_4, $CHCl_3$ standards were measured again by both GC-qMS instruments in Munich and Neuchâtel (Figure 5A). As in the case of CCl_4, standard deviations were amount-dependent ranging from ±1.0‰ (low concentrations of 0.24−0.36 mg/L, n = 20) to ±0.4‰ (higher concentrations of 1.2−2.4 mg/L, n = 15). On the one hand, the low standard deviations for GC-qMS are remarkable. On the other hand, however, Figure 5B illustrates that GC-IRMS still showed better precision, especially when on-column amounts of samples became smaller.

In contrast to the amount-dependency of precision, no amount-dependency was observed for the trueness of chlorine isotope values of CCl_4 and $CHCl_3$ on both GC-qMS (Figure 3B and 5A). This can partly be explained by the fact that masses of fragment ions of the type $CHCl_x^+$ were analyzed, where "crossover interferences" as in Figure 4B can be avoided. However, amount dependencies of mean values did occur on some instruments in previous analysis of TCE[43] despite the fact that also there, only the fragments with hydrogen atoms were measured (e.g., TCE mass 97/95 "$C_2HCl_2^+$") and not those without (e.g., TCE mass 96/94 "$C_2Cl_2^+$"). It is important to understand the reasons for this poor linearity. Since "crossover interferences" are not a possible explanation, Figure 5C explores an additional factor.

Expected isotope fractionation trends in Figure 5C predict that the isotope ratios of molecular and fragment ions should be more stable if the respective ion pair is the predominant one in a given mass spectrum, i.e., to the very left of the reactant (molecular ion) curve or to the very right of the product (fragment ion) curve. The reason is that these are the locations where the slope of the isotope fractionation graph is shallowest (i.e., least sensitive to changes in the extent of fragmentation). Indeed, we found that the relative peak intensities in mass spectra differed significantly between chlorinated methanes and TCE (Figure 5C). Measuring all three compounds with the same ion source settings showed for each chlorinated methane mainly one fragment but three fragments of similar intensity for TCE. Hence, the "lesson learned" from this observation is that instruments should be tuned for either soft ion source settings which preserve mainly the original molecule or for strong ion source fragmentation which ideally leads to one predominant fragment.

Trueness of Chlorine Isotope Analysis of CCl₄ and CHCl₃ by GC-qMS and GC-IRMS. While Figures 3, 4, and 5 illustrate the methods' performances in terms of precision, the trueness requirements of both methods can only be tested with samples that include a range of isotope values. Therefore, for each substance one degradation experiment was conducted. CCl_4 was reduced with sodium formate and $CHCl_3$ with zerovalent iron. Both reactions gave rise to pronounced chlorine isotope fractionation, which is a necessary precondition for reliable investigations of trueness over a representative range of δ values. Figure 6A shows changes in isotope values

A. Area Dependence of qMS Measurements
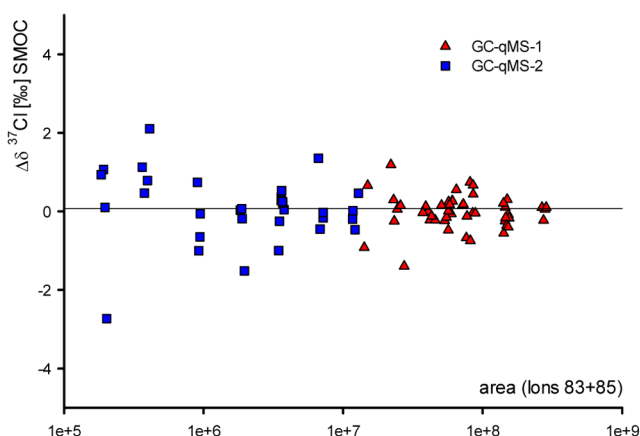
B. Amount Dependence of qMS and IRMS Measurements
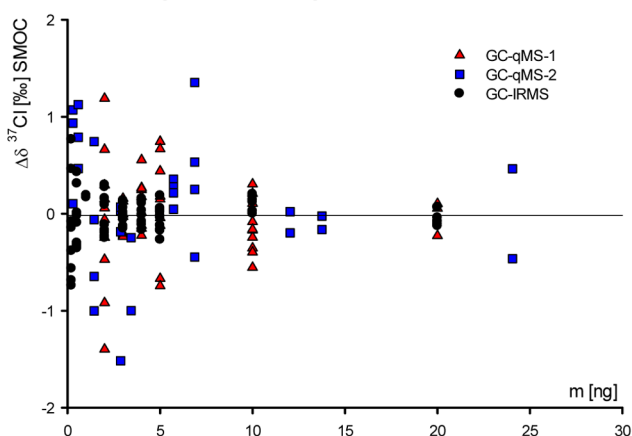
C. Choice of Fragments for Robust Ion-Source Isotope Fractionation
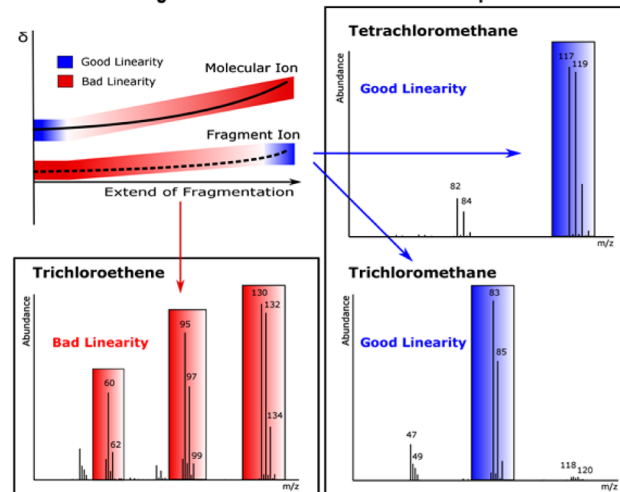
Figure 5. (A) Interlaboratory comparison of $CHCl_3$ measurements on GC-qMS-1 and GC-qMS-2, where the $\delta^{37}Cl_{CHCl_3}$ (calibrated to SMOC scale) of the two most abundant ions are plotted against area (from 83 + 85 ions) readings (GC-qMS-1, 51 data points; GC-qMS-2, 32 data points). (B) Comparison of the precision of chlorine isotope analysis by GC-IRMS (after amplitude correction) vs both GC-qMS in dependence on the mass of analyte ($CHCl_3$) on column (IRMS, 60 data points). (C) Expected isotope fractionation trends of molecular and product ions (see, e.g., ref 44) predict that isotope values are not amount dependent if one kind of ion predominates (either parent or product). Mass spectra of $CHCl_3$ and CCl_4 illustrate that, indeed, CCl_4

Figure 5. continued

gives almost exclusively rise to the fragment of mass $m/z = 117/119/121$ and $CHCl_3$ almost exclusively to that of $m/z = 83/85$. This contrasts with ionization of TCE, where several fragments of similar intensity are formed under identical tune settings.

during the degradation of CCl_4 with sodium formate determined by GC-qMS-1. The figure illustrates the importance of a two-point standard calibration. On the one hand, without an external standard that projects instrument values on the international SMOC scale, the start isotope value would be wrong by 5‰ precluding comparisons between laboratories. On the other hand, however, the data show that a two-point calibration is important to quantify changes in isotope values relative to this starting value, as demonstrated by a difference of 0.5‰ in the enrichment factor ε (Figure 6A). The underlying reason for this is illustrated in Figure 6B which shows isotope data obtained from degradation experiments for CCl_4 and $CHCl_3$. In this figure, uncorrected "instrument" chlorine isotope values determined by GC-qMS are plotted against corrected ones by a two-point calibration relative to SMOC. The deviation of the slopes from unity and the differences between compounds and laboratories strongly emphasize the need of calibration by two characterized compound-specific isotope standards for chlorine isotope measurements. The effect is particularly pronounced for $CHCl_3$, where the isotope values would be strongly overestimated without a standard correction (m(Munich) = 1.6 and m(Neuchâtel) = 1.9). These slopes show even small variations between measurement days (or sequence number, Figure 6C) over a period of half a year for CCl_4 and 2 years for $CHCl_3$. For CCl_4, the average slopes were 0.91 ± 0.03 in Munich and 1.06 ± 0.02 in Neuchâtel, whereas for $CHCl_3$ average slopes were 1.6 ± 0.2 and 1.8 ± 0.2, respectively. With a two-point calibration, in turn, reliable results were obtained by GC-qMS for CCl_4, as evidenced by the strong agreement of GC-qMS-1 versus GC-IRMS results shown in Figure 7A, indicating that excellent trueness can be achieved by both methods. Good agreement was also accomplished for $CHCl_3$ degradation with iron, as shown in Figure 7 where results of chlorine isotope values measured on both instruments were combined with carbon isotope values analyzed by GC-C-IRMS in a dual element isotope plot. Very good agreement of linear regressions performed on GC-qMS vs GC-IRMS, both regarding the slope and 95% confidence intervals, confirms that both methods are able to deliver precise and true results.

◼ CONCLUSION

With its enabling role for dual element isotope studies, compound-specific chlorine isotope analysis can greatly increase the identification of groundwater contamination sources and the elucidation of pollutant transformation pathways, and the dual element approach may be a game changer in the assessment of contaminated sites. However, chlorine CSIA has been validated for only a handful of compounds, and systematic method comparisons have been rare. This study contributes to closing this gap by validating, on the one hand, the method for $CHCl_3$ and CCl_4 as important environmental contaminants. On a more fundamental (and general) level, it highlights factors that may lead to strong amount dependence (poor linearity) of chlorine isotope values: (i) protonation of ions containing ^{13}C and ^{35}Cl that may
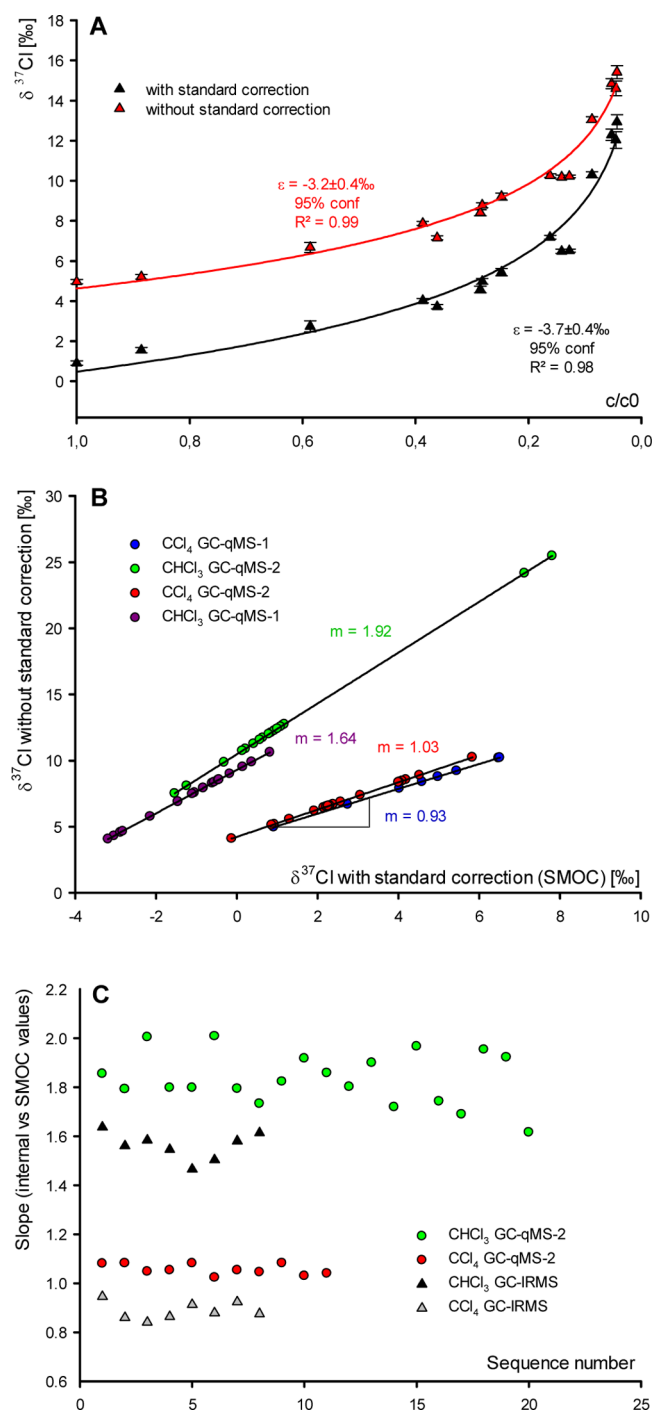
Figure 6. (A) CCl_4 degradation with sodium formate measured at the GC-qMS-1. (Four measurements were conducted for each data point.) Calibration of isotope values by external standards is not only necessary to fix the start chlorine isotope value to the SMOC scale but also to obtain true enrichment factors. (B) Comparison of chlorine isotope values of $CHCl_3$ and CCl_4 from degradation experiments determined with and without correction in two different sequences from GC-qMS-2 and GC-qMS-1. (C) Plot of slope vs sequence number for CCl_4 and $CHCl_3$ from Munich and Neuchâtel shows small variations for different measurement days over longer time periods.

contribute to the mass off ^{37}Cl ions; and (ii) deviation from "ideal" fragmentation conditions where multiple fragment ions rather than one predominant ion are formed. This insight will
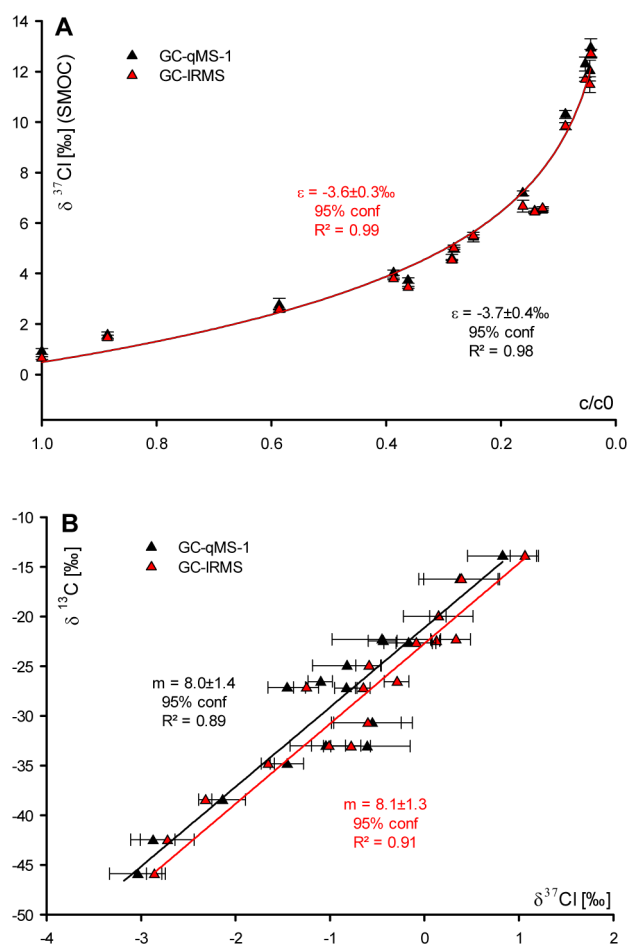
Figure 7. (A) Comparison of $\delta^{37}Cl_{CCl4}$ results against remaining fraction in sodium formate experiments from GC-IRMS and GC-qMS-1 after two-point calibration. (Four measurements were conducted for each data point) (B) Dual element isotope plot of $CHCl_3$ degradation with metallic iron at pH 12 and comparison of regressions from GC-qMS-1 and GC-IRMS chlorine isotope measurements. (Four measurements were conducted for each data point).

be valuable to guide future method developments also for other target compounds.

On the other hand, our study systematically addresses the question of trueness: whether accurate results are obtained by different methods (GC-qMS vs GC-IRMS) in different laboratories. Our results show indeed that measurements of $CHCl_3$ and CCl_4 on a GC-qMS are a very promising alternative if no GC-IRMS is available. Especially at higher concentrations (1.2−2.4 mg/L) isotope measurements with a low standard deviation and a high trueness can be obtained ($\Delta\delta^{37}Cl = 0.2−0.6‰$). In turn, the possibility to measure chlorine isotope values of $CHCl_3$ and CCl_4 on a GC-IRMS can provide the extra precision that may be critical to distinguish different sources of groundwater contaminations and to detect the onset of degradation in field samples. Finally, our results stress the importance of a two-point calibration with compound-specific chlorine isotope standards bracketing a range of different chlorine isotope values. For true results, the need must, therefore, be addressed for standards with large differences in chlorine isotope values.

ASSOCIATED CONTENT

Supporting Information

The Supporting Information is available free of charge on the ACS Publications website at DOI: 10.1021/acs.analchem.6b04129.

Overview of the setup of GC-qMS-1 (Munich) and GC-qMS-2 (Neuchâtel) instruments (PDF)

AUTHOR INFORMATION

Corresponding Author

*Phone: +49 89 3187 2565. E-mail: martin.elsner@helmholtz-muenchen.de.

ORCID

Jordi Palau: 0000-0001-9492-7306
Martin Elsner: 0000-0003-4746-9052

Present Address

⊥M.E.: Chair of Analytical Chemistry and Water Chemistry, Technical University of Munich, Marchioninistrasse 17, D-81377 Munich, Germany

Author Contributions

The manuscript was written through contributions of all authors. All authors have given approval to the final version of the manuscript.

Notes

The authors declare no competing financial interest.

REFERENCES

(1) Wiedemeier, T. H.; Rifai, H. S.; Newell, C. J.; Wilson, J. T. *Natural Attenuation of Fuels and Chlorinated Solvents in the Subsurface*; John Wiley & Sons: New York, 1999.

(2) Hunkeler, D.; Meckenstock, R. U.; Sherwood Lollar, B.; Schmidt, T.; Wilson, J.; Schmidt, T.; Wilson, J. *A Guide for Assessing Biodegradation and Source Identification of Organic Ground Water Contaminants using Compound Specific Isotope Analysis (CSIA)*; PA 600/R-08/148, December 2008; www.epa.gov/ada, U.S. EPA, Oklahoma, 2008.

(3) Meckenstock, R. U.; Morasch, B.; Griebler, C.; Richnow, H. H. *J. Contam. Hydrol.* **2004**, *75*, 215−255.

(4) Blessing, M.; Schmidt, T. C.; Dinkel, R.; Haderlein, S. B. *Environ. Sci. Technol.* **2009**, *43*, 2701−2707.

(5) Mancini, S. A.; Ulrich, A. E.; Lacrampe-Couloume, G.; Sleep, B.; Edwards, E. A.; Sherwood Lollar, B. *Appl. Environ. Microbiol.* **2003**, *69*, 191−198.

(6) Kuder, T.; Wilson, J. T.; Kaiser, P.; Kolhatkar, R.; Philp, P.; Allen, J. *Environ. Sci. Technol.* **2005**, *39*, 213−220.

(7) Kuntze, K.; Kozell, A.; Richnow, H. H.; Halicz, L.; Nijenhuis, I.; Gelman, F. *Environ. Sci. Technol.* **2016**, *50*, 9855−9863.

(8) Penning, H.; Sorensen, S. R.; Meyer, A. H.; Aamand, J.; Elsner, M. *Environ. Sci. Technol.* **2010**, *44*, 2372−2378.

(9) Cretnik, S.; Thoreson, K. A.; Bernstein, A.; Ebert, K.; Buchner, D.; Laskov, C.; Haderlein, S.; Shouakar-Stash, O.; Kliegman, S.; McNeill, K.; Elsner, M. *Environ. Sci. Technol.* **2013**, *47*, 6855−6863.

(10) Renpenning, J.; Keller, S.; Cretnik, S.; Shouakar-Stash, O.; Elsner, M.; Schubert, T.; Nijenhuis, I. *Environ. Sci. Technol.* **2014**, *48*, 11837.

(11) Palau, J.; Cretnik, S.; Shouakar-Stash, O.; Höche, M.; Elsner, M.; Hunkeler, D. *Environ. Sci. Technol.* **2014**, *48*, 9430−9437.

(12) Kuder, T.; van Breukelen, B. M.; Vanderford, M.; Philp, P. *Environ. Sci. Technol.* **2013**, *47*, 9668−9677.

(13) Wiegert, C.; Aeppli, C.; Knowles, T.; Holmstrand, H.; Evershed, R.; Pancost, R. D.; Macháčková, J.; Gustafsson, Ö. *Environ. Sci. Technol.* **2012**, *46*, 10918−10925.

(14) Hunkeler, D.; Abe, Y.; Broholm, M. M.; Jeannottat, S.; Westergaard, C.; Jacobsen, C. S.; Aravena, R.; Bjerg, P. L. *J. Contam. Hydrol.* **2011**, *119*, 69−79.

(15) Badin, A.; Broholm, M. M.; Jacobsen, C. S.; Palau, J.; Dennis, P.; Hunkeler, D. *J. Contam. Hydrol.* **2016**, *192*, 1−19.

(16) Wiegert, C.; Mandalakis, M.; Knowles, T.; Polymenakou, P. N.; Aeppli, C.; Macháčková, J.; Holmstrand, H.; Evershed, R. P.; Pancost, R. D.; Gustafsson, Ö. *Environ. Sci. Technol.* **2013**, *47*, 6449−6456.

(17) vanWarmerdam, E. M.; Frape, S. K.; Aravena, R.; Drimmie, R. J.; Flatt, H.; Cherry, J. A. *Appl. Geochem.* **1995**, *10*, 547−552.

(18) Zwank, L.; Berg, M.; Elsner, M.; Schmidt, T. C.; Schwarzenbach, R. P.; Haderlein, S. B. *Environ. Sci. Technol.* **2005**, *39*, 1018−1029.

(19) Shouakar-Stash, O.; Frape, S. K.; Drimmie, R. J. *J. Contam. Hydrol.* **2003**, *60*, 211−228.

(20) Holt, B. D.; Heraty, L. J.; Sturchio, N. C. *Environ. Pollut.* **2001**, *113*, 263−269.

(21) Shouakar-Stash, O.; Drimmie, R. J.; Zhang, M.; Frape, S. K. *Appl. Geochem.* **2006**, *21*, 766−781.

(22) Holt, B. D.; Sturchio, N. C.; Abrajano, T. A.; Heraty, L. J. *Anal. Chem.* **1997**, *69*, 2727−2733.

(23) Numata, M.; Nakamura, N.; Koshikawa, H.; Terashima, Y. *Environ. Sci. Technol.* **2002**, *36*, 4389−4394.

(24) Van Acker, M.; Shahar, A.; Young, E. D.; Coleman, M. L. *Anal. Chem.* **2006**, *78*, 4663−4667.

(25) Zakon, Y.; Halicz, L.; Gelman, F. *Anal. Chem.* **2014**, *86*, 6495−6500.

(26) Sakaguchi-Soder, K.; Jager, J.; Grund, H.; Matthaus, F.; Schuth, C. *Rapid Commun. Mass Spectrom.* **2007**, *21*, 3077−3084.

(27) Aeppli, C.; Holmstrand, H.; Andersson, P.; Gustafsson, O. *Anal. Chem.* **2010**, *82*, 420−426.

(28) Jin, B.; Laskov, C.; Rolle, M.; Haderlein, S. B. *Environ. Sci. Technol.* **2011**, *45*, 5279−5286.

(29) Palau, J.; Shouakar-Stash, O.; Hunkeler, D. *Environ. Sci. Technol.* **2014**, *48*, 14400−14408.

(30) Breider, F.; Hunkeler, D. *Environ. Sci. Technol.* **2014**, *48*, 1592−1600.

(31) Hitzfeld, K. L.; Gehre, M.; Richnow, H.-H. *Rapid Commun. Mass Spectrom.* **2011**, *25*, 3114−3122.

(32) Renpenning, J.; Hitzfeld, K. L.; Gilevska, T.; Nijenhuis, I.; Gehre, M.; Richnow, H. H. *Anal. Chem.* **2015**, *87*, 2832−2839.

(33) Bernstein, A.; Shouakar-Stash, O.; Ebert, K.; Laskov, C.; Hunkeler, D.; Jeannottat, S.; Sakaguchi-Soder, K.; Laaks, J.; Jochmann, M. A.; Cretnik, S.; Jager, J.; Haderlein, S. B.; Schmidt, T. C.; Aravena, R.; Elsner, M. *Anal. Chem.* **2011**, *83*, 7624−7634.

(34) Schimmelmann, A.; Qi, H.; Coplen, T. B.; Brand, W. A.; Fong, J.; Meier-Augenstein, W.; Kemp, H. F.; Toman, B.; Ackermann, A.; Assonov, S.; Aerts-Bijma, A. T.; Brejcha, R.; Chikaraishi, Y.; Darwish, T.; Elsner, M.; Gehre, M.; Geilmann, H.; Gröning, M.; Hélie, J.-F.; Herrero-Martín, S.; Meijer, H. A. J.; Sauer, P. E.; Sessions, A. L.; Werner, R. A. *Anal. Chem.* **2016**, *88*, 4294−4302.

(35) Slater, G.; Sherwood Lollar, B.; Allen King, R.; O'Hannesin, S. F. *Chemosphere* **2002**, *49*, 587−596.

(36) Elsner, M.; Couloume, G. L.; SherwoodLollar, B. *Anal. Chem.* **2006**, *78*, 7528−7534.

(37) Torrentó, C.; Audí-Miró, C.; Bordeleau, G.; Marchesi, M.; Rosell, M.; Otero, N.; Soler, A. *Environ. Sci. Technol.* **2014**, *48*, 1869−1877.

(38) Palau, J.; Soler, A.; Teixidor, P.; Aravena, R. *Journal of Chromatography A* **2007**, *1163*, 260−268.

(39) Coplen, T. B.; Brand, W. A.; Gehre, M.; Groning, M.; Meijer, H. A. J.; Toman, B.; Verkouteren, R. M. *Anal. Chem.* **2006**, *78*, 2439−2441.

(40) Elsner, M.; Hunkeler, D. *Anal. Chem.* **2008**, *80*, 4731−4740.

(41) Rayleigh, J. W. S. *Philos. Mag.* **1896**, *42*, 493−498.

(42) Hoefs, J. *Stable Isotope Geochemistry*; Springer-Verlag: Berlin, Germany, 1997.

(43) Bernstein, A.; Shouakar-Stash, O.; Ebert, K.; Laskov, C.; Hunkeler, D.; Jeannottat, S.; Sakaguchi-Söder, K.; Laaks, J.; Jochmann, M. A.; Cretnik, S.; Jager, J.; Haderlein, S. B.; Schmidt, T. C.; Aravena, R.; Elsner, M. *Anal. Chem.* **2011**, *83*, 7624−7634.

(44) Hunkeler, D.; Elsner, M. In *Environmental Isotopes in Biodegradation and Bioremediation*; Aelion, C. M., Hohener, P.; Hunkeler, D., Aravena, R., Eds.; CRC Press: Boca Raton, FL, 2010.

ASSOCIATED CONTENT

SUPPORTING INFORMATION FOR

Compound-specific Chlorine Isotope Analysis of Tetrachloromethane and Trichloromethane by GC-IRMS vs. GC-qMS: Method Development and Evaluation of Precision and Trueness

Benjamin Heckel[a], Diana Rodríguez-Fernández[b], Clara Torrentó[c], Armin Meyer[a], Jordi Palau[c], Cristina Domènech[b], Mònica Rosell[b], Albert Soler[b], Daniel Hunkeler[c], Martin Elsner[a]

[a]Institute of Groundwater Ecology, Helmholtz Zentrum München, Ingolstädter Landstrasse 1, 85764 Neuherberg Germany

[b]Grup de Mineralogia Aplicada i Geoquímica de Fluids, Departament de Mineralogia, Petrologia i Geologia Aplicada, Facultat de Geologia, Universitat de Barcelona (UB), C/ Martí i Franquès, s/n -08028 Barcelona, Spain

[c]Centre d'hydrogéologie et de géothermie (CHYN), Université de Neuchâtel (UNINE), Rue Emile-Argand 11, Neuchâtel 2000, Switzerland

SUMMARY:

3 pages, 2 tables

	qMs-1 Munich CCl$_4$	qMs-1 Munich CHCl$_3$	qMs-2 Neuchâtel CCl$_4$	qMs-2 Neuchâtel CHCl$_3$
Instrument manufacturer	Agilent	Agilent	Agilent	Agilent
GC	7890A (Agilent)	7890A (Agilent)	7890A (Agilent)	7890A (Agilent)
qMs	5975C qMS (Agilent)	5975C qMS (Agilent)	5975C qMS (Agilent)	5975C qMS (Agilent)
m/z	119 & 117	83 & 85	119 & 117	83 & 85
	most abundant fragments from fragment group II	most abundant fragments from fragment group I	most abundant fragments from fragment group II	most abundant fragments from fragment group I
EI (eV)	70	70	70	70
Dwell time (msec)	70	70	50	50
Flow (mL min)	1.4	1.4	1.2	1.2
Split	1:10	1:10	1:20	1:20
Column	Vocol column (30 m x 0.25 mm ID × 0.25 µm, Supelco)	Vocol column (30 m x 0.25 mm ID × 0.25 µm, Supelco)	DB-5 column (30 m x 0.25 mm ID × 0.25 µm, Agilent)	DB-5 column (30 m x 0.25 mm ID × 0.25 µm, Agilent)
Temperature program	start at 60°C (2 min), 8°C/min to 165°C (0 min), temperature ramp of 25°C/min to 220°C (1 min)	start at 60°C (2 min), 8°C/min to 165°C (0 min), temperature ramp of 25°C/min to 220°C (1 min)	start at 70°C (2 min), 20°C/min to 230°C (0 min)	start at 70°C (2 min), 20°C/min to 230°C (0 min)
Injection temperature	250°C	250°C	250°C	250°C
Injection technique	automated HS	automated HS	automated HS	automated HS
Injection vial	10mL (9ml Headspace + 1mL liquid)	10mL (9ml Headspace + 1mL liquid)	20mL (5ml Headspace + 15mL liquid)	20mL (5ml Headspace + 15mL liquid)
Agitator temperature	40°C	40°C	60°C	60°C
Autosampler	CombiPal (CTC Analytics)	CombiPal (CTC Analytics)	CombiPal (CTC Analytics)	CombiPal (CTC Analytics)
Peak integration	ChemStation Integrator	ChemStation Integrator	ChemStation Integrator	ChemStation Integrator
Software	ChemStation E.02.02.1431	ChemStation E.02.02.1431	ChemStation E.02.01.1177	ChemStation E.02.01.1177
Two-point calibration curve slope	0.91 ±0.03	1.6 ± 0.2	1.06 ±0.02	1.8 ± 0.2
m= number of x-y pairs of calibration curve	30	30	25	52
Concentration range	60-2600 µg/L	60-2400 µg/L	5-200 ug/L	10-840 ug/L

Table S1: Setup of GC-qMS-1 (Munich) and GC-qMS-2 (Neuchâtel)

	IRMS	IRMS
	CCl$_4$	CHCl$_3$
Instrument manufacturer	Thermo Fisher Scientific	Thermo Fisher Scientific
GC	Thermo Trace GC	Thermo Trace GC
IRMS	MAT 253	MAT 253
m/z	49 & 47	49 & 47
Flow (mL min)	1.4	1.4
Split	1:10	1:10
Column	Vocol column (30 m ×0.25 mm ID × 0.25 μm, Supelco)	Vocol column (30 m × 0.25 mm ID × 0.25 μm, Supelco)
Temperature program	start at 60°C (2 min), 8°C/min to 165°C (0 min), of 25°C/min to 220°C (1 min)	start at 60°C (2 min), 8°C/min to 165°C (0 min), of 25°C/min to 220°C (1 min)
Injection temperature	230°C	230°C
Injection technique	automated HS	automated HS
Injection vial	10mL (9ml Headspace + 1mL liquid)	10mL (9ml Headspace + 1mL liquid)
Agitator temperature	40°C	40°C
Autosampler	PAS Technology	PAS Technology
Peak integration	ISODAT 3.0	ISODAT 3.0
Software	ISODAT 3.0	ISODAT 3.0
Two-point calibration curve slope	0.87 ±0.02	1.5 ± 0.2
m= number of x-y pairs of calibration curve	20	20
Concentration range	20-2600 μg/L	20-2400 μg/L

Table S2: Setup of GC-IRMS (Munich)

Erratum of Heckel, B., Rodríguez-Fernández, D., Torrentó, D., Meyer, A., Palau, J., Domènech, C., Rosell, M., Soler, A., Hunkeler, D., Elsner, D., 2017. Compound-specific chlorine isotope analysis of tetrachloromethane and trichloromethane by GC-IRMS *vs*. GC-qMS: Method development and evaluation of precision and trueness. Anal. Chem. 89, 3411–3420. doi: 10.1021/acs.analchem.6b04129.

In Fig. 1 (page 3413) M=118 must be 120 and M=120 must be 118 in molecular group of CF as follows:
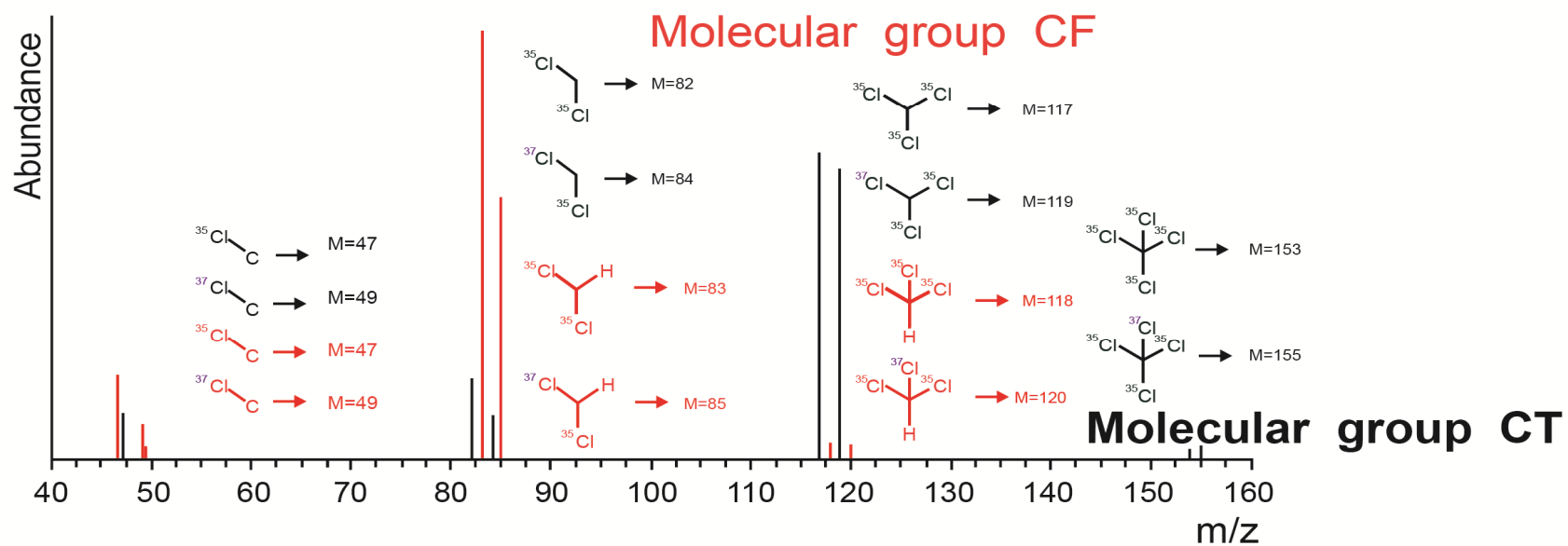
In page 3415, the citation Breider and Hunkeler[27] must be Breider and Hunkeler [30].

Annex C. Article 2. Abiotic CF reference reactions

Torrentó, C., Palau, J., Rodríguez-Fernández, D., Heckel, B., Meyer, A., Domènech, C., Rosell, M., Soler, A., Elsner, M., Hunkeler, D., 2017. Carbon and chlorine isotope fractionation patterns associated with different engineered chloroform transformation reactions. Environ. Sci. Technol. 51, 6174–6184. doi:10.1021/acs.est.7b00679.

Carbon and Chlorine Isotope Fractionation Patterns Associated with Different Engineered Chloroform Transformation Reactions

Clara Torrentó,[*,†,‡] Jordi Palau,[†,‡] Diana Rodríguez-Fernández,[‡] Benjamin Heckel,[§] Armin Meyer,[§] Cristina Domènech,[‡] Mònica Rosell,[‡] Albert Soler,[‡] Martin Elsner,[§,⊥] and Daniel Hunkeler[†]

[†]Centre for Hydrogeology and Geothermics, Université de Neuchâtel, 2000 Neuchâtel, Switzerland

[‡]Grup de Mineralogia Aplicada i Geoquímica de Fluids, Departament de Mineralogia, Petrologia i Geologia Aplicada, Facultat de Ciències de la Terra, Martí Franques s/n, Universitat de Barcelona (UB), 08028 Barcelona, Spain

[§]Institute of Groundwater Ecology, Helmholtz Zentrum München, 85764 Neuherberg, Germany

[⊥]Chair of Analytical Chemistry and Water Chemistry, Technical University of Munich, Marchioninistrasse 17, D-81377 Munich, Germany

S *Supporting Information*

ABSTRACT: To use compound-specific isotope analysis for confidently assessing organic contaminant attenuation in the environment, isotope fractionation patterns associated with different transformation mechanisms must first be explored in laboratory experiments. To deliver this information for the common groundwater contaminant chloroform (CF), this study investigated for the first time both carbon and chlorine isotope fractionation for three different engineered reactions: oxidative C−H bond cleavage using heat-activated persulfate, transformation under alkaline conditions (pH ∼ 12) and reductive C−Cl bond cleavage by cast zerovalent iron, Fe(0). Carbon and chlorine isotope fractionation values were −8 ± 1‰ and −0.44 ± 0.06‰ for oxidation, −57 ± 5‰ and −4.4 ± 0.4‰ for alkaline hydrolysis (pH 11.84 ± 0.03), and −33 ± 11‰ and −3 ± 1‰ for dechlorination, respectively. Carbon and chlorine apparent kinetic isotope effects (AKIEs) were in general agreement with expected mechanisms (C−H bond cleavage in oxidation by persulfate, C−Cl bond cleavage in Fe(0)-mediated reductive dechlorination and E1$_{CB}$ elimination mechanism during alkaline hydrolysis) where a secondary AKIE$_{Cl}$ (1.00045 ± 0.00004) was observed for oxidation. The different dual carbon-chlorine ($\Delta\delta^{13}$C vs $\Delta\delta^{37}$Cl) isotope patterns for oxidation by thermally activated persulfate and alkaline hydrolysis (17 ± 2 and 13.0 ± 0.8, respectively) vs reductive dechlorination by Fe(0) (8 ± 2) establish a base to identify and quantify these CF degradation mechanisms in the field.
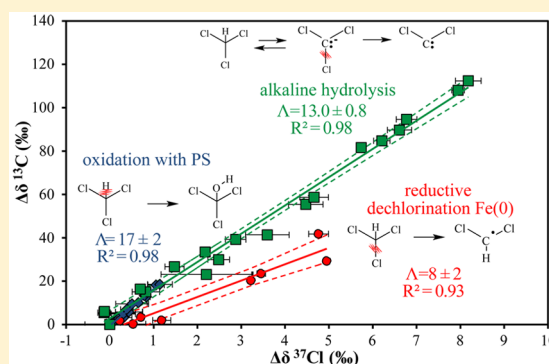
1. INTRODUCTION

Chloroform (CF) is both an anthropogenic environmental contaminant widely distributed around the world as well as a natural compound formed in various aquatic and terrestrial environments.[1−3] CF of anthropogenic origin has been extensively used as degreasing agent and as a precursor to Teflon and various refrigerants and was historically used in medicine as anesthetic. It is formed as oxidation byproduct during drinking water treatment[4] and may form as a daughter product of carbon tetrachloride (CT) dehalogenation at contaminated sites. As a result, CF is one of the most frequently detected volatile organic compounds (VOCs) in groundwater.[5] Taking into account its high ecotoxicity,[6] CF prominently ranks among the halogenated VOCs on the Agency for Toxic Substances and Disease Registry priority list of hazardous substances.[7]

Aerobic and anaerobic cometabolic biodegradation processes of CF have been described.[8] However, CF cometabolic degradation is restricted by several environmental factors such as the presence of other specific compounds that inhibit CF degradation, the availability of the substrate or the toxicity of derived metabolites.[8] Reductive dechlorination of CF via dehalorespiration by two *Dehalobacter* sp. strains (CF50 and UNSWDHB) and one *Desulfitobacterium* sp. strain (PR) has recently been described in laboratory studies[9−14] and proposed as anaerobic bioremediation strategy. However, this strategy is only applicable to contaminated sites in the absence of its parent compound, i.e. CT, which has been shown to strongly inhibit CF dehalorespiration in an enrichment culture containing *Dehalobacter* spp.[15] In turn, CF itself is a strong inhibitor of chlorinated ethene- or ethane-degrading cultures even when present at low concentrations.[16,17] These interdependencies make the remediation of sites contaminated with

several chlorinated compounds particularly challenging so that multiple-stage remediation strategies are warranted in which inhibitors like chloromethanes are removed upfront.

Abiotic reactions bear potential to accomplish such an initial removal. Naturally occurring iron-bearing minerals like goethite and iron sulfide under low-redox environments have been demonstrated to be involved in the reductive dechlorination of CF.[18] However, due to the very restricted natural attenuation conditions for CF and its complex distribution in the subsurface as a dense nonaqueous phase liquid (DNAPLs), more efficient engineered remediation strategies have been proposed to increase CF removal in the environment. As a result of the high oxidation state of carbon in CF, its degradation by in situ chemical oxidation (ISCO) is in general much less effective than for chlorinated ethenes using common oxidants such as permanganate, iron-activated persulfate (PS), ozone, hydrogen peroxide, or Fenton's Reagent.[19] However, thermally activated PS was recently shown to be a better option for efficient CF oxidation with the advantage that under thermal activation, the strongly oxidizing sulfate radical and other reactive intermediates (i.e., hydroxyl radicals, or reducing radicals such as superoxide radicals, $O_2^{\bullet-}$) can be generated at neutral pH.[20−23]

Alternatively, CF alkaline hydrolysis has recently been proposed as a remediation technology based on its occurrence in drainage trenches filled with concrete-based construction wastes.[24] For the sustainable use of this new remediation strategy, identifying and assessing the performance of CF degradation reaction by alkaline hydrolysis, as well as understanding the underlying mechanism, is important.

Finally, CF reductive dechlorination by zerovalent metals has been studied only at laboratory scale.[25−29] Nevertheless, this remediation strategy has been successfully proven at field sites contaminated by chlorinated ethenes using permeable reactive barriers with micro/macro-scale Fe(0)[30,31] or Fe(0) nanoparticle injection.[32,33]

Improved methods are needed to delineate the relative efficacy of the above-mentioned CF remediation approaches in the field. During the last decades, compound-specific isotope analysis (CSIA) has evolved as a tool to monitor transformation reactions and to quantify the progress of natural and enhanced remediation of organic contaminants.[34,35] Molecules with light isotopes in the reactive position typically react slightly faster than molecules containing the heavy ones leading to a kinetic isotope effect (KIE). As a consequence, the heavier isotopes (e.g., ^{13}C and ^{37}Cl) usually become enriched in the remaining substrate. For a given reaction, quantification of the extent of contaminant transformation based on stable isotope ratios requires the experimental determination of isotopic fractionation (ε, see Materials and Methods).[36]

Isotopic fractionation values for transformation reactions need to be known for very practical reasons: (i) to understand what changes in isotope values can be expected in the field at all, and whether this holds promise to qualitatively detect degradation; (ii) to understand what mechanism lies behind the isotope effect, in order to subsequently chose an appropriate ε value for quantification in the field.

In order to gain insight into the underlying reaction mechanism, apparent kinetic isotope effects (AKIEs) can be derived from determined ε values taking into account which of the atoms in the target molecule are expected to be present at the reactive position. Comparison of the observed AKIEs to the theoretical maximum KIEs ("semiclassical Streitwieser Limits") associated with breakage of chemical bonds, enables interpretation of occurring transition state(s) of a bond cleavage in terms of (i) primary isotope effects affecting the atoms present in the reacting bond, (ii) secondary isotope effects affecting atoms located adjacent to the reacting position.[37,38] Often, however, it is uncertain whether additional factors exert an influence on observable isotope fractionation such as (iii) masking due to rate-limitation in mass transfer, and (iv) superimposed isotope effects of multiple reaction steps typical of enzyme catalysis or multistep chemical reactions.[39−42] When observable isotope fractionation of a single element varies between experiments, it is, therefore, often uncertain whether this is due to a different mechanism, or whether these other factors are responsible. Dual-element isotope plots, that is, graphs in which changes in isotope values of one element are plotted against those of a second offer a more reliable distinction between reaction mechanisms than ε values alone.[35,39,43−50]

Such information can be highly valuable in field situations. Nondestructive abiotic natural processes, such as sorption, volatilization or diffusion strongly affect concentrations of a contaminant, but generally do not cause significant isotopic fractionation.[51−57] Temporal or spatial shifts in isotope ratios, in contrast, are highly indicative of degradation and can, therefore, better monitor the success of remediation strategies at contaminated sites than mass balances alone.[58] Dual (or multi) isotope patterns, finally, can even be used to derive the relative contribution of different reaction mechanisms and then to quantify the efficiency of each of them in the field—provided that ε values of these processes have previously been characterized in laboratory experiments.[59−64]

Reported carbon isotope effects during CF transformation are, however, scarce in the literature. Chan et al.[11] reported a carbon isotope fractionation value of $-27.5 \pm 0.9‰$ during dehalorespiration of CF by a mixed culture containing *Dehalobacter* sp. strain CF50. In comparison, a much lower ε_C value of $-4.3 \pm 0.4‰$ was reported by Lee et al.[29] for the same dechlorination reaction by a mixed consortium containing another *Dehalobacter* sp. strain, UNSWDHB, whereas isotope fractionation in CF abiotic reductive dechlorination by microsized Fe(0) was found to be indistinguishable from that of the first experiment ($-29 \pm 2‰$). Significantly, larger carbon isotopic fractionation was observed for CF alkaline hydrolysis at pH ranging from 11.8 to 12.7 ($-53 \pm 3‰$).[24] To the best of our knowledge, chlorine isotope fractionation during any CF transformation mechanism has not been reported so far. Specifically, understanding whether different reaction mechanisms lead to characteristic patterns in dual C−Cl isotope plots is still limited even for chlorinated ethenes[46,47,62] and, to our knowledge, is currently nonexistent for chlorinated methanes. Hence, there is a need to explore dual element CSIA for defined reactions under controlled laboratory conditions to pave the path for the interpretation of isotope data in field studies.

Therefore, the goal of this study was to determine carbon and, for the first time, chlorine isotope fractionation patterns for different transformation processes of CF in important abiotic engineered reactions in order to explore the ability of CSIA to identify these processes at field sites. The selected chemical reactions were: oxidative C−H bond cleavage by radicals produced from PS activation, alkaline hydrolysis of chloroform at pH 12 and C−Cl bond cleavage in reductive dechlorination by cast milli-sized Fe(0).
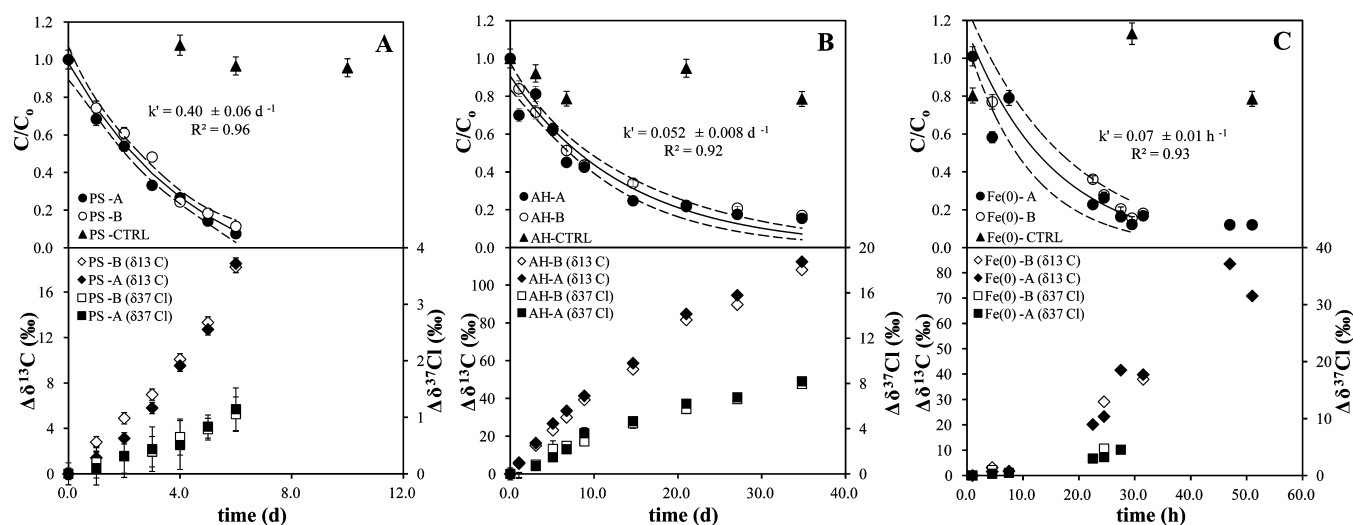
Figure 1. CF degradation kinetics (upper panels) and changes in C and Cl isotope ratios (lower panels) during oxidation by thermally activated PS with an initial PS/CF molar ratio of 40/1 (A), alkaline hydrolysis (B) and dechlorination by Fe(0) (C). Data from duplicate experiments (A and B parallel series) and from control (CTRL) experiments are shown. In the upper panels, the error bars show the uncertainty in of C/C_0, calculated by error propagation including uncertainty in concentration measurements. In some cases, error bars are smaller than the symbols. k′ values were obtained from curve fittings according to eq SI4 (see Figure S1). Fits were conducted with liner regressions in Sigma Plot 10.0 for Windows. Dashed lines represent 95% CI of regression. For CF dechlorination with Fe(0), k′ was calculated omitting data after 30 days when the disappearance of CF almost stopped. In the lower panels, error bars of individual data points indicate standard deviations of the measurements. In most cases, error bars are smaller than the symbols.

2. MATERIAL AND METHODS

2.1. Experimental Setup. All the experiments were conducted in duplicate using glass vials completely filled with aqueous solution without headspace to avoid partitioning of chlorinated volatile compounds into the gas phase. For the experiments with heat-activated PS and alkaline hydrolysis, 21 mL vials sealed with PTFE-coated rubber stoppers and aluminum crimp seals were used, whereas the Fe(0) experiments were performed using 42 mL clear glass vials capped with PTFE-coated rubber stoppers and plastic screw caps. A list of chemicals and additional experiment details is available in the Supporting Information (SI).

For the thermally activated PS experiments, the vials were filled with a pH 7 buffer solution and 0.5 mL of solutions with variable concentrations of PS were added to achieve initial PS-to-CF-molar ratios of 5/1, 10/1, or 40/1. The vials were placed in a thermostatic water bath at 50.0 ± 0.5 °C and the reaction was initiated by the addition of 0.5 mL of an aqueous CF (99%, Sigma-Aldrich) stock solution containing 2100 mg L^{-1} to achieve initial concentrations of 50 mg L^{-1}. The experiments lasted for 10 h and samples for analysis were collected at different time intervals. At each sampling time, the vials were removed from the water bath and immediately placed in an ice bath to quench the reaction by chilling. Samples were stored in the dark at 4 °C until analysis. Losses of CF due to volatilization and/or sorption were accounted for in control experiments set up in an identical manner except for the addition of PS.

CF alkaline hydrolysis experiments were performed at room temperature (~25 °C) in a pH 12 buffer solution and the vials were covered with aluminum foil to avoid photocatalyzed oxidation of CF. The reaction was initiated by the addition of 0.5 mL of the CF (99%, Sigma-Aldrich) stock solution to reach initial theoretical concentrations of 50 mg L^{-1}. The experiments started at different times to achieve reaction times varying from 0 to 35 days. After 35 days from the earliest prepared vials, all

the vials were sacrificed at the same time. An appropriate volume of 0.1 M acetic acid was added to the vials to neutralize the solution to pH 6 and quench the alkaline hydrolysis reaction. Samples were stored in the dark at 4 °C until analysis. Control experiments with unbuffered deionized water were also performed.

For the Fe(0) experiments, 2 g of milli-sized cast iron (1.624 ± 0.007 m^2 g^{-1}) were added to each 42 mL vial to reach a surface concentration of 77 m^2 L^{-1}. Afterward the vials were filled with a pH 6.6 buffer solution and the reaction was initiated by the addition of the CF pure phase (99%, Alfa Aesar) to reach initial theoretical concentrations of 100 mg L^{-1}. The vials were covered with aluminum foil to avoid photocatalyzed oxidation of CF and were rotated on a horizontal shaker (IKA KS 260 BASIC, Stanfen, Germany) at 200 rpm. Control experiments without iron were also carried out. The experiments were performed at room temperature (~25 °C) and they lasted 51 h. Reactions were stopped by filtration through 0.2 μm filters at different time intervals and samples for analysis were stored frozen in 10 mL vials covered with aluminum foil.

2.2. Analytical Methods. Detailed descriptions of analytical methods are available in the SI. Briefly, concentration measurements of chlorinated compounds were performed by headspace (HS) using GC/MS as explained elsewhere,[24] except for the samples from Fe(0) experiments for which GC/TOF/MS was used. Chloride anion concentrations were analyzed by high-performance liquid chromatography. Carbon isotope analyses of CF and some detectable volatile daughter products were performed using two different GC/IRMS systems located at the University of Neuchâtel (GC/IRMS-1)[50] and at the Scientific and Technological Centers of the University of Barcelona (GC/IRMS-2).[24] Chlorine isotope CF analyses were performed using a GC/qMS system from the University of Neuchâtel as explained elsewhere[66] or a GC/IRMS system from the Institute of Groundwater Ecology of the Helmholtz
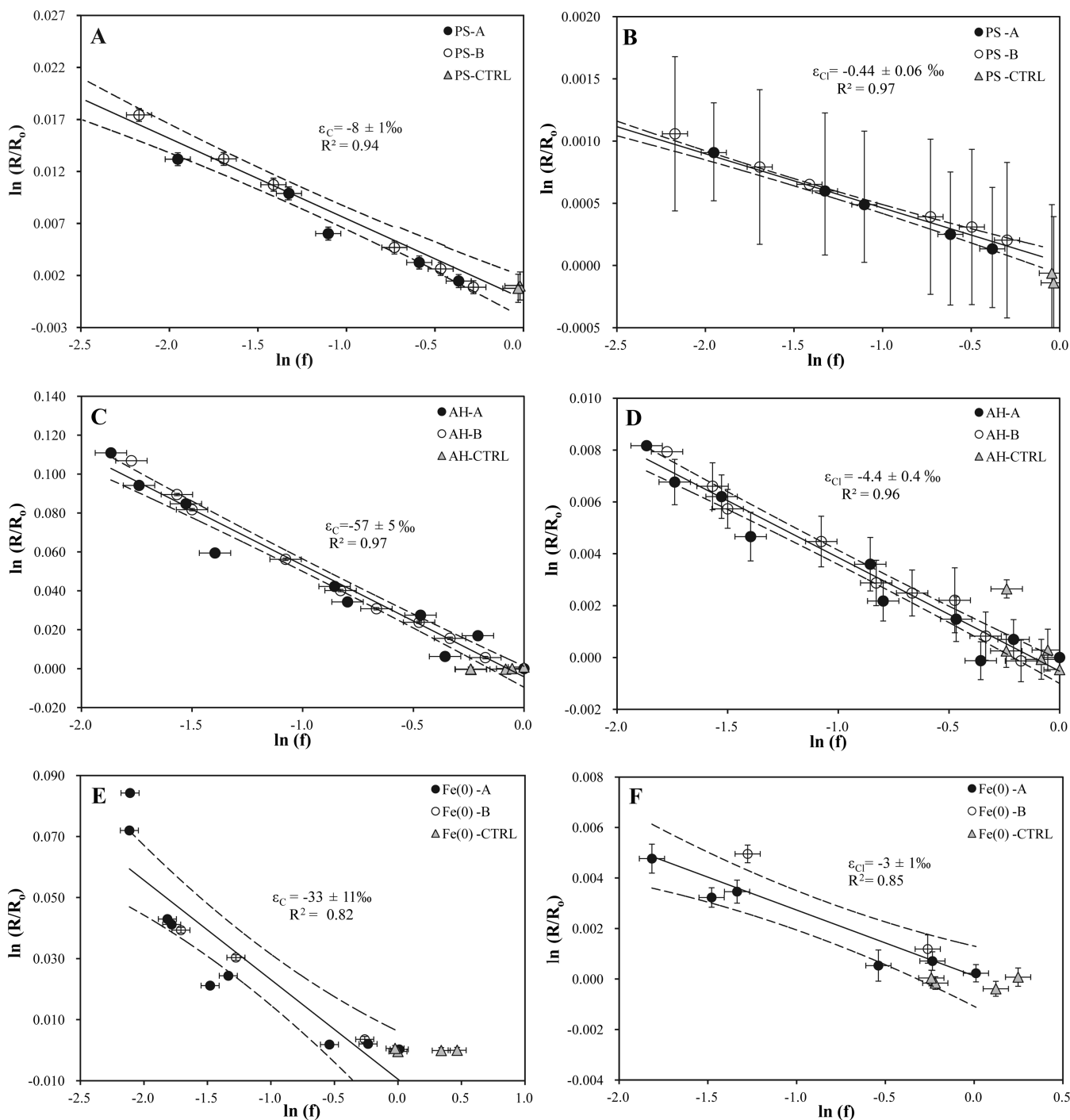
Figure 2. Logarithmic plots according to Rayleigh eq (eq 1) of carbon (left panels) and chlorine (right panels) isotope ratios during CF oxidation by thermally activated PS (A and B), alkaline hydrolysis (C and D) and dechlorination by Fe(0) (E and F). Data from duplicate experiments were used for estimating ε_C and ε_{Cl}. Dashed lines represent 95% CI of the linear regression. Error bars display the uncertainty calculated by error propagation including uncertainties in concentration and isotope measurements. In some cases, error bars are smaller than the symbols.

Zentrum München (GC/IRMS-3). An interlaboratory comparison demonstrating excellent agreement between the two analytical methods is provided in Heckel et al.[67]

2.3. Isotope Data Evaluation. Bulk carbon and chlorine ε values were obtained from the slope of the linearized Rayleigh equation for a closed system:[36]

$$\ln\left(\frac{\delta_t + 1}{\delta_0 + 1}\right) = \varepsilon \times \ln f \tag{1}$$

where δ_0 and δ_t are isotope values in the beginning (0) and at a given time (t), respectively, and f is the fraction of substrate remaining at time t. Isotope signatures were reported in per mil (‰) using the delta notation relative to international standards, that is, Vienna PeeDee Belemnite for carbon ($\delta^{13}C_{VPDB}$) and the international Standard Mean Ocean Chloride (SMOC) for chlorine ($\delta^{37}Cl_{SMOC}$):

$$\delta(\text{in‰}) = (R/R_{std} - 1) \tag{2}$$

where R and R_{std} are the isotope ratios of the sample and the standard, respectively.

Errors given for ε values are the 95% confidence intervals (CI) of the slope of the regression line in the Rayleigh plots.

The apparent kinetic isotope effects (AKIEs) were calculated to evaluate the intrinsic isotope effect of the bond cleavage (see equations in the SI).

For dual C−Cl isotope plots, the slope of the correlation trend was determined by linear regression and the uncertainty corresponds to the 95% CI.

3. RESULTS AND DISCUSSION

3.1. Carbon and Chlorine Isotope Fractionation.
Changes in CF concentration and C and Cl isotope ratios of CF during degradation by the three different mechanisms are shown in Figure 1. No CF degradation was observed in the experimental controls (without adding PS, Fe(0) or at neutral pH in the case of the hydrolysis reaction) for any of the three studied reactions. Measured concentrations in all the samples from the control experiments were always higher than 80% of the initial CF concentration (Figure 1). Accordingly, no significant changes in $\delta^{13}C$ and $\delta^{37}Cl$ isotope values were detected in the control experiments. In the rest of the experiments, a normal isotope effect was observed for both carbon and chlorine. The isotope results of combined experimental replicates, which were highly consistent for each experimental system, were used to derive C and Cl isotope fractionation values by the use of Rayleigh plots (Figure 2 and SI Figure S3). Further details on kinetics data evaluation, comparison with previous studies and product yields are provided in the SI.

PS Oxidation. The initial carbon and chlorine isotope composition remained constant ($-42 \pm 1‰$ and $-3.1 \pm 0.2‰$, respectively, both $n = 4$) in the control experiments (SI Figure S3A, B). Around 90% of CF removal was observed after 6 days in the PS experiments with an initial PS/CF molar ratio of 40/1 (Figure 1A). In contrast, only 30% and 20% of CF degradation were accomplished after 7 days with initial molar ratios of 10/1 and 5/1, respectively (SI Figure S1). Therefore, isotope ratios were determined only in those samples from the experiments with an initial PS to CF molar ratio of 40/1. Carbon isotope fractionation during oxidation with PS has been shown to be independent of the PS/contaminant molar ratio for chlorinated ethenes and 1,1,1-trichloroethane.[68,69] Carbon isotope composition exhibited an enrichment of $^{13}C/^{12}C$ up to $\delta^{13}C$ values of $-23.8 \pm 0.5‰$, which resulted in an ε_C value of $-8 \pm 1‰$ (Figure 2A). Compared to carbon, a much smaller shift in $^{37}Cl/^{35}Cl$ was observed (Figure 1A), resulting in $\delta^{37}Cl$ values up to $-1.9 \pm 0.4‰$ (SI Figure S3AB). An ε_{Cl} of $-0.44 \pm 0.06‰$ was obtained (Figure 2B). Neither carbon nor chlorine isotope fractionation associated with this reaction have been reported so far. The pH was kept at circumneutral values (7.0 ± 0.2) during the course of the experiment. This reaction followed pseudo-first-order kinetics with a k′ of 0.40 ± 0.06 d^{-1} ($R^2 = 0.96$, SI Figure S1). Neither PS consumption nor sulfate production were monitored along the experiments. Chloride concentrations released into solution were measured at the end of the experiment and accounted for between 95% and 110% of the total theoretical CF dechlorination yield, which was calculated assuming release of all the three chlorine atoms. Neither products nor intermediates were detected by headspace GC/MS analysis during the course of the experiments.

Alkaline Hydrolysis. Carbon and chlorine isotope values remained constant ($-41.8 \pm 0.5‰$ and $-2.6 \pm 0.4‰$, respectively, both $n = 5$) in control vials at neutral pH. Under alkaline conditions (the pH remained constant 11.84 ± 0.03 over the duration of the experiment), a 85% decrease in CF concentration within approximately 35 days was observed (Figure 1B). Alkaline hydrolysis induced a significant isotope effect, resulting in $\delta^{13}C$ and $\delta^{37}Cl$ values up to $+70.6 \pm 0.3‰$ and $+5.7 \pm 0.4‰$, respectively, after 85% CF removal (SI Figure S3C, D). An ε_C of $-57 \pm 5‰$ (Figure 2C) and ε_{Cl} of $-4.4 \pm 0.4‰$ (Figure 2D) were determined. So far, the only reported carbon isotope fractionation value for CF alkaline hydrolysis was $-53 \pm 3‰$ at a pH range from 11.9 to 12.7,[24] which is comparable, within uncertainty, to that obtained in the present study. Carbon isotope fractionation is therefore independent of the pH in the tested range (from 11.8 to 12.7). To our knowledge chlorine isotope fractionation for this reaction has not been reported up to now. The reaction followed pseudo-first-order kinetics ($R^2 = 0.92$, SI Figure S1) with a k′ of 0.052 ± 0.008 d^{-1}, which is in agreement with a previously reported rate constant of 0.047 ± 0.004 d^{-1} obtained at a similar pH 11.9 ± 0.1.[24] No particular attempts were made to identify potential products of CF degradation, such as carbon monoxide (CO), formate (HCO$_2^-$), and chloride (Cl$^-$). In our previous work, excellent chlorine balances were achieved in similar experiments, indicating that CF was completely dehalogenated without accumulation of chlorinated intermediates.[24]

Fe(0) Dechlorination. CF in the controls without Fe(0) at pH 6.3 ± 0.2 did not show any changes in carbon and chlorine isotope composition ($\delta^{13}C = -47.8 \pm 0.5‰$, $n = 4$ and $\delta^{37}Cl = -3.2 \pm 0.2‰$, $n = 6$, respectively). In the presence of milli-sized Fe(0), CF isotope signatures of both elements showed significant changes leading up to values of $\delta^{13}C = +35.9 \pm 0.5‰$ and $\delta^{37}Cl = +1.7 \pm 0.1‰$, respectively, after 84% CF removal (SI Figure S3E, F). Isotope fractionation values of $\varepsilon_C = -33 \pm 11‰$ and $\varepsilon_{Cl} = -3 \pm 1‰$ were determined (Figure 2E and F). The obtained ε_C was not significantly different from ε_C of $-29 \pm 2‰$ reported recently after 50% of CF dechlorination by commercial microsized Fe(0).[29] Chlorine isotope fractionation associated with this reaction has not been reported yet. The pH did not vary significantly over the duration of the experiment (6.2 ± 0.2). The degradation kinetics followed a pseudo-first-order rate law at the beginning of the reaction but after 30 h the disappearance of CF almost stopped (Figure 1C). For Fe(0)-mediated dechlorination of chlorinated ethenes, iron surface passivation due to reactive site saturation by iron hydroxide precipitates has been suggested as the cause of increased reaction half-lives and deviations from pseudo-first-order kinetics at later stages of a reaction.[70] The obtained k′ was 0.07 ± 0.01 h^{-1} ($R^2 = 0.93$, SI Figure S1), which corresponds to a k$_{SA}$ of $2.1 \pm 0.4 \times 10^{-2}$ L m^{-2} d^{-1} (see SI).

DCM and free chloride were detected as final products in Fe(0) experiments, whereas no compounds different from CF appeared in the control experiments without iron. The yield of DCM, defined as the moles of product formed per mole of CF transformed (DCM$_t$/(CF$_0$ − CF$_t$)), where subscripts 0 and t indicate initial time and different sampling times, respectively) ranged from 0 to 2.4% over time, showing that accumulation of DCM only accounted for a small fraction of the initial CF. DCM was depleted in ^{13}C compared to the initial isotopic composition of the substrate (CF). DCM showed a trend toward higher $\delta^{13}C$ values, reflecting the enrichment trend of

Table 1. Carbon and Chlorine Isotope Fractionation (ε_C and ε_{Cl}, Respectively), Apparent Kinetic Isotope Effects (AKIE$_C$ and AKIE$_{Cl}$, Respectively) and Dual Isotope Slopes ($\Lambda = \Delta\delta^{13}C/\Delta\delta^{37}Cl$) Values Obtained for the Three Studied CF Transformation Pathways: Oxidation with Thermally-Activated PS, Alkaline Hydrolysis and Fe(0)-Based Reductive Dechlorination[a]

experiment	reaction mechanism	ε_{bulkC} (‰)	R^2	AKIE$_C$	ε_{bulkCl} (‰)	R^2	AKIE$_{Cl}$	Λ
persulfate	oxidative C−H bond cleavage	−8 ± 1	0.94	1.008 ± 0.001	−0.44 ± 0.06	0.97	1.00045 ± 0.00004[b]	17 ± 2
alkaline hydrolysis	E1$_{CB}$ elimination	−57 ± 5	0.97	1.061 ± 0.006	−4.4 ± 0.4	0.96	1.0133 ± 0.0004	13.0 ± 0.8
Fe(0)	reductive dechlorination by C−Cl bond cleavage	−33 ± 11	0.82	1.034 ± 0.012	−3 ± 1	0.85	1.008 ± 0.001	8 ± 2

[a]The uncertainty of ε, AKIE and Λ values corresponds to the 95% CI. In all cases, AKIE$_C$ was calculated using $x = z = 1$ in eq SI6. For both alkaline hydrolysis and dechlorination by Fe(0), AKIE$_{Cl}$ was calculated using $x = z = 3$ as all C−Cl bonds are equivalent and compete for reaction. For oxidation with PS, as there is not primary chlorine isotopic effect, the secondary AKIE$_{Cl}$ was also calculated by eq SI6 using in this case $x = 3$ and $z = 1$ because no specific bond containing Cl is broken, and there is, therefore, no intramolecular competition for this bond. [b]secondary isotope effect.

the CF from which it was formed (SI Figure S3E). The DCM-related isotope fractionation $\varepsilon^C_{substrate \rightarrow product}$ was estimated as −19 ± 3‰ using the fitting parameter, D(δ^{13}C) = +13 ± 2‰ (R^2 = 0.62) (see equations in the SI). This discrepancy between the product-related and the substrate-related isotope fractionations ($\varepsilon^C_{CF \rightarrow DCM}$ = −19 ± 3‰ vs ε_C = −33 ± 11‰) is likely attributable to the formation of other products including isotope-sensitive branching from the parent compound or intermediates, such as a dichloromethyl radical (SI Figure S4), to DCM.[71] However, due to the lack of DCM isotope signatures at early stages of reaction, such interpretations must be conducted with caution.

3.2. Mechanistic Considerations. For further elucidation of the reaction mechanism, AKIE values were calculated using eq SI6, to characterize the isotope effect of the cleavage of the chemical bond at the reactive positions. Table 1 summarizes the obtained results and proposed reaction pathways for the three studied reactions are shown in Figure 3 and discussed in detail in the SI.

The AKIE$_C$ for the oxidation reaction was 1.008 ± 0.001, which is within the range of reported carbon AKIEs for oxidative C−H bond cleavage for both abiotic (1.008−1.015) and microbial oxidation reactions (1.001−1.044) (SI Table S2), indicating that the observed fractionation was dominated by the KIE associated with oxidative cleavage of a C−H bond. A similar AKIE$_C$ value (1.008) was obtained for 1,1,1-TCA oxidation by thermally activated PS[65] from which it was suggested that the first reaction step was the rupture of the C−H bond and the abstraction of the hydrogen atom from the molecule by the attack of any of the radicals formed after persulfate activation.[65,72,73] The secondary AKIE$_{Cl}$ estimated in the present experiments (1.00045 ± 0.00004) also points to an oxidative reaction, where there is not initial C−Cl bond cleavage and thus a primary chlorine kinetic isotope effect is not expected. A reaction pathway involving the cleavage of the C−H as the rate-limiting step is proposed (Figure 3A and SI). In order to track more confidently the proposed mechanism, hydrogen isotope fractionation during CF oxidation with thermally activated PS might be further measured.

During alkaline hydrolysis, CF is abiotically dechlorinated to carbon monoxide and formate.[74,75] A stepwise elimination mechanism (E1$_{CB}$) has been proposed for this reaction.[24,74,76,77] This mechanism consists of the rapid, reversible, base-catalyzed deprotonation of the molecule with the formation of a trichloromethyl carbanion (:CCl$_3^-$), followed by the rate-determining unimolecular loss of a chloride ion to produce the reactive intermediate dichlorocarbene (CCl$_2$), which is then rapidly transformed into carbon monoxide and formate (SI Figure S4). If this is the case, as the deprotonation
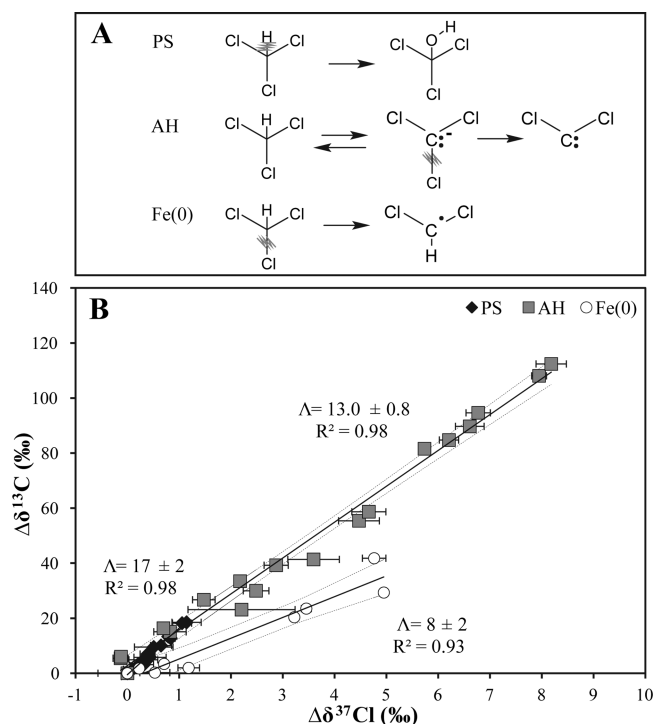
Figure 3. (A) Proposed reaction pathways for CF degradation by the three studied reactions. More details are given in the SI. (B) Dual C−Cl isotope plot for CF degradation by the three studied pathways: oxidation by thermally activated PS (PS), alkaline hydrolysis (AH) and dechlorination by Fe(0) (Fe(0)). Data from duplicate experiments were combined. Lines are linear regressions of the data sets with 95% CI (dashed lines). Error bars show uncertainty in isotope measurements. Note that error bars of δ^{13}C values are smaller than the symbols.

step is reversible and the loss of a chloride ion is the rate-determining step, both carbon and chlorine primary isotope effects in the CF molecule are expected during this process. In the present experiments, an AKIE$_C$ of 1.061 ± 0.006 was obtained for alkaline hydrolysis, which is consistent with the Streitwieser limit for a primary carbon KIE in C−Cl bonds (1.057, SI Table S2)[37,78] and is equivalent, within the given 95% CI, to the value previously found by Torrentó et al.[24] (1.056 ± 0.003). The AKIE$_{Cl}$ was calculated as 1.0133 ± 0.0004, which is equal to the maximum expected KIE$_{Cl}$ for cleavage of a C−Cl bond (1.013, SI Table S2),[37] indicating the involvement of a C−Cl bond. In principle, the Cl kinetic isotope effect estimated in the present study is, therefore, consistent with the occurrence of a carbanion mechanism

(Figure 3A) but also with a C−Cl bond cleavage via a concerted one-step S_N2 nucleophilic substitution mechanism. Nevertheless, based on energy considerations, the E1$_{CB}$ mechanism seems more plausible for this reaction (see the SI for further discussion). Further deuterium-exchange experiments might be performed to confirm the existence of a carbanion intermediate as a way to further corroborate the occurrence of the stepwise elimination mechanism.[79]

In the case of reductive dechlorination by Fe(0), an AKIE$_C$ of 1.034 ± 0.012 was obtained, which is similar to the value of 1.030 ± 0.007 obtained by Lee et al.[29] and within the AKIE$_C$ range for the reductive cleavage of C−Cl bonds reported in the literature (1.003−1.060) (SI Table S2). In fact, most AKIE$_C$ values for reductive dehalogenation fall in the range of 1.027 and 1.033, which corresponds to about 50% bond cleavage when considering a Streitwieser limit for a C−Cl bond of 1.057 for complete bond cleavage in an infinitely late transition state.[80] Regarding AKIE$_{Cl}$, a value of 1.008 ± 0.001 was calculated, which is also about 50% of the Streitwieser limit for KIE$_{Cl}$ in C−Cl bonds (1.013).[37] Similar AKIE$_{Cl}$ values, ranging from 1.008 to 1.016 for abiotic reductive dechlorination and from 1.004 to 1.011 for biotic reductive dechlorination, have been previously reported for chlorinated methanes, ethenes and ethanes (SI Table S2). Therefore, both C and Cl-AKIEs pointed to cleavage of a C−Cl bond in the first rate-limiting step, which is compatible with the two-step pathway that is commonly hypothesized for this reaction (see SI). The first step may, for example, involve the transfer of a single electron from the metal surface causing the removal of a chlorine atom and the formation of a dichloromethyl radical ($\cdot$CHCl$_2$) (Figure 3A).

3.3. Dual Element Isotope Plot. Figure 3B shows the dual C−Cl isotope plot for the reactions of this study. A linear correlation between $\Delta\delta^{13}C$ and $\Delta\delta^{37}Cl$ was observed for the three studied transformation mechanisms (r² ≥ 0.92). A comparison of the slopes ($\Lambda = \Delta\delta^{13}C/\Delta\delta^{37}Cl$) for the regression lines was performed by analysis of covariance (ANCOVA). Statistical significance was accepted at the $p < 0.05$ level. There is no significant statistical difference between oxidation by thermally activated persulfate (17 ± 2) and alkaline hydrolysis (13.0 ± 0.8) slopes (ANCOVA, $p = 0.2$). In contrast, these results differ significantly (ANCOVA, $p < 0.0001$) from the slope observed during CF reductive dechlorination by Fe(0) (8 ± 2).

Hence, although different mechanisms are involved in CF degradation by oxidation by thermally activated PS (cleavage of a C−H bond) and by alkaline hydrolysis (cleavage of a C−Cl bond), the obtained Λ values for both degradation reactions are not significantly different. This may be explained by considerations for carbon and chlorine isotope effects. *Carbon.* As expected, the obtained AKIE$_C$ value for CF degradation by oxidation with heat-activated PS is smaller than for alkaline hydrolysis. The higher the mass of the bonding partner, the greater is typically the primary kinetic isotope effects.[37] Hence it can be explained that carbon isotope fractionation associated with C−Cl bond cleavage is greater than in C−H bond cleavage since the carbon atom is bound to a heavier atom (chlorine vs hydrogen). *Chlorine.* This difference, however, is matched by similar differences in chlorine isotope fractionation. On the one hand, C−Cl bond cleavage involves a primary AKIE$_{Cl}$, which is clearly greater than a secondary AKIE$_{Cl}$ next to a reacting C−H bond. On the other hand, this primary AKIE$_{Cl}$ is "diluted" in ε_{Cl} due to the intramolecular competition

between three chemically equivalent C−Cl bonds (z = 3 in eq SI6), whereas the simultaneous secondary AKIE$_{Cl}$ of three Cl atoms are not diluted (z = 1). By coincidence, the interplay of these factors results in a similar reduction of carbon as of chlorine isotope fractionation so that similar Λ are obtained. This unexpected result restrains the use of C−Cl isotope plots for distinguishing these reactions in the field and highlights the need to apply this approach with precaution and using complementary tools for identification of degradation mechanisms in the field (e.g., complementary hydrogen isotope analysis).

4. ENVIRONMENTAL SIGNIFICANCE

Carbon and chlorine isotope fractionation of CF during oxidation with heat-activated PS, by alkaline hydrolysis and by reductive dechlorination with Fe(0) was studied in batch experiments in order to explore the potential of CSIA for the identification of reaction mechanisms in the monitoring of remediation strategies at contaminated sites. For the first time, carbon isotope fractionation values (for heat-activated PS) and chlorine isotope fractionation values (for the three reactions) were determined. These new ε values increase the options of using CSIA for estimating the extent of contaminant degradation at field sites where remediation strategies are implemented that rely on induced abiotic transformations of CF. Based on the obtained ε values, it is likely that changes in isotope values in the field may be larger than 2‰ for carbon and 0.4‰ (for GC/IRMS instruments) or 2‰ (for GC/qMS instruments) for chlorine - these are the significant levels that have been suggested as reliable indicators of degradation.[34,81] Even with the relatively small carbon fractionation obtained for CF oxidation by PS (−8 ± 1‰) and chlorine isotope fractionation observed for Fe(0)-mediated reductive dechlorination (−3 ± 1‰), shifts in CF isotopic composition will be already detectable with a reasonable accuracy if the substrate is degraded by 20% and 25−50%, respectively.

Although only the reductive dechlorination showed significantly statistically different C−Cl isotope slope compared with the other two reactions (oxidation and alkaline hydrolysis), the dual isotope approach might still be used to identify different CF degradation mechanisms in the field, which would (or not necessarily) take place at the same time. For example, the coupling of two common treatments—ISCO and in situ bioremediation— has been shown not only to be feasible, but in many cases also to be able to provide a more efficient and extensive cleanup of contaminated sites.[82] In the case of PS, the anaerobic environment that is created following the consumption of the oxidant is ideal for CF microbial dehalogenation under sulfate reduction conditions to be enhanced. Enhanced CF bioremediation has also been observed when combining Fe(0) and methanogens that use the cathodic hydrogen generated by iron corrosion for cometabolic degradation of CF[83−85] or even better by dehalorespiring bacteria which are not inhibited at certain concentrations of CF.[29] Therefore, there would be an increasing number of case studies, where CF degradation due to PS application or Fe(0) barriers should be distinguished from biotic reductive dechlorination in the field. Although chlorine isotope fractionation during biotic CF dechlorination remains to be evaluated in detail, as well as the effect in CF degradation of Fe(0) aging or the presence of Fe(0) impurities such as graphite,[86] the dual C−Cl slopes obtained in the present work sets the grounds for the potential application of this approach

for assessing if CF abiotic reductive dechlorination performed by Fe(0)-PRB or naturally occurring iron-bearing minerals would be or not distinguishable from microbial reductive dechlorination.

Although CF anaerobic biodegradation has been reported to occur mainly via cometabolic dechlorination or by dehalorespiration,[8] an alternative pathway was suggested in the presence of cobalamins and involving CF hydrolysis.[87,88] The mechanism of this reaction is not well-known, but it presumably involves the cobalamin-catalyzed conversion of CF to a monochlorocarbene, which would be subsequently hydrolyzed to formaldehyde. The produced formaldehyde could then be oxidized to CO or formate and finally to CO_2. The abiotic alkaline hydrolysis reaction characterized in the present study might be used as a reference system for this suggested CF biotic hydrolysis in future dual isotope-CSIA studies.

Finally, due to the significant difference between the C−Cl isotope slope of CF oxidation and reductive dechlorination, the dual isotope approach might be in addition useful for distinguishing between aerobic and anaerobic CF biodegradation pathways. CF aerobic biodegradation only occurs during oxidative cometabolism with other primary substrates such as methane, butane or toluene by oxygenase-expressing microorganisms.[8] The pathway of CF cooxidation starts by insertion of one oxygen atom into the molecule via H abstraction with phosgene as intermediate and final mineralization to chloride and CO_2. The chemical mechanism of CF oxidation is variable among the various existent monooxygenases, but the rate-limiting step is expected to be the cleavage of the C−H bond.

In conclusion, our study established an expedient base with carbon and chlorine isotope fractionation during three abiotic CF transformation mechanisms. Further research is needed in order to explore if other CF natural degradation pathways (for example naturally occurring iron-bearing minerals as well as aerobic and anaerobic degraders) might be similar to or different from the patterns generated in this study. Such information will allow connecting dual-plot slopes to known reaction mechanisms with the aim to distinguish different degradation processes in the field. This distinction would be important for better monitoring the success of remediation strategies at contaminated sites.

■ ASSOCIATED CONTENT

ⓢ Supporting Information

The Supporting Information is available free of charge on the ACS Publications website at DOI: 10.1021/acs.est.7b00679.

> Chemicals; analytical methods; further discussion in kinetics; calculation of AKIE values; calculation of isotope trend for DCM in the Fe(0) experiment; carbon and chlorine isotope fractionation patterns; further discussion in reaction pathways; comparison of ε and AKIE values for C and Cl isotopes in different studies (PDF)

■ AUTHOR INFORMATION

Corresponding Author

*Phone: +41 32 718 26 49; fax: +41 32 718 26 03; e-mail: clara.torrento@unine.ch.

ORCID ⓘ

Clara Torrentó: 0000-0003-1480-2744
Jordi Palau: 0000-0001-9492-7306
Diana Rodríguez-Fernández: 0000-0002-2515-9945
Mònica Rosell: 0000-0003-1563-8595
Martin Elsner: 0000-0003-4746-9052

Notes

■ ACKNOWLEDGMENTS

■ REFERENCES

(1) Laturnus, F.; Haselmann, K. F.; Borch, T.; Gron, C. Terrestrial natural sources of trichloromethane (chloroform, CHCl3) - An overview. *Biogeochemistry* **2002**, *60*, 121−139.

(2) Albers, C. N.; Jacobsen, O. S.; Flores, E. M. M.; Pereira, J. S. F.; Laier, T. Spatial variation in natural formation of chloroform in the soils of four coniferous forests. *Biogeochemistry* **2011**, *103*, 317−334.

(3) Hunkeler, D.; Laier, T.; Breider, F.; Jacobsen, O. S. Demonstrating a natural origin of chloroform in groundwater using stable carbon isotopes. *Environ. Sci. Technol.* **2012**, *46*, 6096−6101.

(4) Rossberg, M.; Lendle, W.; Pfleiderer, G.; Tögel, A.; Torkelson, T. R.; Beutel, K. K. *Chloromethanes. Ullmann's Encyclopedia of Industrial Chemistry*, 2011.

(5) Zogorski, J. S.; Carter, J. M.; Ivahnenko, T.; Lapham, W. W.; Moran, M. J.; Rowe, B. L.; Squillace, P. J.; Toccalino, P. L. *The Quality of Our Nation'S Waters - Volatile Organic Compounds in the Nation'S Ground Water and Drinking-Water Supply Wells*; U.S. Geological Survey Circular 1292, 2006.

(6) Dobrzyńska, E.; Pośniak, M.; Szewczyńska, M.; Buszewski, B. Chlorinated volatile organic compounds: Old, however, actual analytical and toxicological problem. *Crit. Rev. Anal. Chem.* **2010**, *40*, 41−57.

(7) Agency for toxic substances and disease registry (ATSDR). Priority List of Hazardous Substances 2015, .http://www.atsdr.cdc.gov/spl/index.html.

(8) Cappelletti, M.; Frascari, D.; Zannoni, D.; Fediet, S. Microbial degradation of chloroform. *Appl. Microbiol. Biotechnol.* **2012**, *96*, 1395−1409.

(9) Grostern, A.; Duhamel, M.; Dworatzek, S.; Edwards, E. A. Chloroform respiration to dichloromethane by a *Dehalobacter* population. *Environ. Microbiol.* **2010**, *12*, 1053−1060.

(10) Lee, M.; Low, A.; Zemb, O.; Koenig, J.; Michaelsen, A.; Manefield, M. Complete chloroform dechlorination by organochlorine respiration and fermentation. *Environ. Microbiol.* **2012**, *14*, 883−894.

(11) Chan, C. C. H.; Mundle, S. O. C.; Eckert, T.; Liang, X.; Tang, S.; Lacrampe-Couloume, G.; Edwards, E. A.; Sherwood-Lollar, B. Large carbon isotope fractionation during biodegradation of chloroform by *Dehalobacter* cultures. *Environ. Sci. Technol.* **2012**, *46*, 10154−10160.

(12) Tang, S.; Edwards, E. A. Identification of *Dehalobacter* reductive dehalogenases that catalyse dechlorination of chloroform, 1,1,1-trichloroethane and 1,1-dichloroethane. *Philos. Trans. R. Soc., B* **2013**, *368*, 20120318.

(13) Deshpande, N. P.; Wong, Y. K.; Manefield, M.; Wilkins, M. R.; Lee, M. Genome sequence of *Dehalobacter* UNSWDHB, a chloroform dechlorinating bacterium. *Genome Announc.* **2013**, *1*, e00720−13.

(14) Ding, C.; Zhao, S.; He, J. A *Desulfitobacterium* sp. strain PR reductively dechlorinates both 1,1,1-trichloroethane and chloroform. *Environ. Microbiol.* **2014**, *16*, 3387−3397.

(15) Justicia-Leon, S. D.; Higgins, S.; Mack, E. E.; Griffiths, D. R.; Tang, S.; Edwards, E. A.; Löffler, F. E. Bioaugmentation with distinct *Dehalobacter* strains achieves chloroform detoxification in microcosms. *Environ. Sci. Technol.* **2014**, *48*, 1851−1858.

(16) Duhamel, M.; Wehr, S. D.; Yu, L.; Rizvi, H.; Seepersad, D.; Dworatzek, S.; Cox, E. E.; Edwards, E. A. Comparison of anaerobic dechlorinating enrichment cultures maintained on tetrachloroethene, trichloroethene, cis-dichloroethene and vinyl chloride. *Water Res.* **2002**, *36*, 4193−4202.

(17) Maymó-Gatell, X.; Nijenhuis, I.; Zinder, S. H. Reductive dechlorination of cis-1,2-dichloroethene and vinyl chloride by *Dehalococcoides ethenogenes*. *Environ. Sci. Technol.* **2001**, *35*, 516−521.

(18) Kenneke, J. F.; Weber, E. J. Reductive dehalogenation of halomethanes in iron- and sulfate-reducing sediments. 1. Reactivity pattern analysis. *Environ. Sci. Technol.* **2003**, *37*, 713−720.

(19) Huling, S. G.; Pivetz, B. E. *In Situ Chemical Oxidation-Engineering Issue*, EPA/600/R-06/072; U.S. Environmental Protection Agency Office of Research and Development, National Risk Management Research Laboratory: Cincinnati, OH, 2006.

(20) Huang, K. C.; Zhao, Z.; Hoag, G. E.; Dahmani, A.; Block, P. A. Degradation of volatile organic compounds with thermally activated persulfate oxidation. *Chemosphere* **2005**, *61*, 551−560.

(21) Waldemer, R. H.; Tratnyek, P. G.; Johnson, R. L.; Nurmi, J. T. Oxidation of chlorinated ethenes by heat-activated persulfate: Kinetics and products. *Environ. Sci. Technol.* **2007**, *41*, 1010−1015.

(22) Tsitonaki, A.; Petri, B.; Crimi, M.; Mosbaek, H.; Siegrist, R. L.; Bjerg, P. L. In situ chemical oxidation of contaminated soil and groundwater using persulfate: a review. *Crit. Rev. Environ. Sci. Technol.* **2010**, *40*, 55−91.

(23) Zhu, X.; Du, E.; Ding, H.; Lin, Y.; Long, T.; Li, H.; Wang, L. QSAR modeling of VOCs degradation by ferrous-activated persulfate oxidation. *Desalin. Water Treat.* **2016**, *57*, 1−15.

(24) Torrentó, C.; Audí-Miró, C.; Bordeleau, G.; Marchesi, M.; Rosell, M.; Otero, N.; Soler, A. The use of alkaline hydrolysis as a novel strategy for chloroform remediation: feasibility of using urban construction wastes and evaluation of carbon isotopic fractionation. *Environ. Sci. Technol.* **2014**, *48*, 1869−1877.

(25) Gillham, R. W.; OHannesin, S. F. Enhanced reduction of halogenated aliphatics by zero-valent iron. *Groundwater* **1994**, *32*, 958−967.

(26) Matheson, L. J.; Tratnyek, P. G. Reductive dehalogenation of chlorinated methanes by iron metal. *Environ. Sci. Technol.* **1994**, *28*, 2045−2053.

(27) Johnson, T. L.; Scherer, M. M.; Tratnyek, P. G. Kinetics of halogenated organic compound reduction by iron metal. *Environ. Sci. Technol.* **1996**, *30*, 2634−2640.

(28) Feng, J.; Lim, T.-T. Pathways and kinetics of carbon tetrachloride and chloroform reductions by nano-scale Fe and Fe/Ni particles: comparison with commercial micro-scale Fe and Zn. *Chemosphere* **2005**, *59*, 1267−1277.

(29) Lee, M.; Wells, E.; Wong, Y. K.; Koenig, J.; Adrian, L.; Richnow, H. H.; Manefield, M. Relative contributions of *Dehalobacter* and zerovalent Iron in the degradation of chlorinated methanes. *Environ. Sci. Technol.* **2015**, *49*, 4481−4489.

(30) O'Hannesin, S. F.; Gillham, R. W. Long-term performance of an in Situ "iron wall" for remediation of VOCs. *Groundwater* **1998**, *36*, 164−170.

(31) Wilkin, R. T.; Acree, S. D.; Ross, R. R.; Puls, R. W.; Lee, T. R.; Woods, L. L. Fifteen-year assessment of a permeable reactive barrier for treatment of chromate and trichloroethylene in groundwater. *Sci. Total Environ.* **2014**, *468−469*, 186−194.

(32) Zhang, W.-X. Nanoscale iron particles for environmental remediation: An overview. *J. Nanopart. Res.* **2003**, *5*, 323−332.

(33) Elsner, M.; Lacrampe-Couloume, G.; Mancini, S. A.; Burns, L.; Sherwood Lollar, B. Carbon isotope analysis to evaluate nanoscale

Fe(0) treatment at a chlorohydrocarbon contaminated site. *Groundwater Monit. Rem.* **2010**, *30*, 79−95.

(34) Meckenstock, R. U.; Barbara Morasch, B.; Griebler, C.; Richnow, H. H. Stable isotope fractionation analysis as a tool to monitor biodegradation in contaminated aquifers. *J. Contam. Hydrol.* **2004**, *75*, 215−255.

(35) Elsner, M. Stable isotope fractionation to investigate natural transformation mechanisms of organic contaminants: principles, prospects and limitations. *J. Environ. Monit.* **2010**, *12*, 2005−2031.

(36) Mariotti, A.; Germon, J. C.; Hubert, P.; Kaiser, P.; Letolle, R.; Tardieux, A.; Tardieux, P. Experimental determination of nitrogen kinetic isotope fractionation: Some principles; illustration for the denitrification and nitrification processes. *Plant Soil* **1981**, *62*, 413−430.

(37) Elsner, M.; Zwank, L.; Hunkeler, D.; Schwarzenbach, R. P. A new concept linking observable stable isotope fractionation to transformation pathways of organic pollutants. *Environ. Sci. Technol.* **2005**, *39*, 6896−6916.

(38) Hofstetter, T. B.; Berg, M. Assessing transformation processes of organic contaminants by compound-specific stable isotope analyses. *TrAC, Trends Anal. Chem.* **2011**, *30*, 618−627.

(39) Mancini, S. A.; Hirschorn, S. K.; Elsner, M.; Lacrampe-Couloume, G.; Sleep, B. E.; Edwards, E. A.; Sherwood Lollar, B. Effects of trace element concentration on enzyme controlled stable isotope fractionation during aerobic biodegradation of toluene. *Environ. Sci. Technol.* **2006**, *40*, 7675−7681.

(40) Penning, H.; Cramer, C. J.; Elsner, M. Rate-dependent carbon and nitrogen kinetic isotope fractionation in hydrolysis of isoproturon. *Environ. Sci. Technol.* **2008**, *42*, 7764−7771.

(41) Renpenning, J.; Keller, S.; Cretnik, S.; Shouakar-Stash, O.; Elsner, M.; Schubert, T.; Nijenhuis, I. Combined C and Cl isotope effects indicate differences between corrinoids and enzyme (*Sulfurospirillum multivorans* PceA) in reductive dehalogenation of tetrachloroethene, but not trichloroethene. *Environ. Sci. Technol.* **2014**, *48*, 11837−11845.

(42) Renpenning, J.; Rapp, I.; Nijenhuis, I. Substrate hydrophobicity and cell composition influence the extent of rate limitation and masking of isotope fractionation during microbial reductive dehalogenation of chlorinated ethenes. *Environ. Sci. Technol.* **2015**, *49*, 4293−4301.

(43) Tobler, N. B.; Hofstetter, T. B.; Schwarzenbach, R. P. Carbon and hydrogen isotope fractionation during anaerobic toluene oxidation by *Geobacter metallireducens* with different Fe(III) phases as terminal electron acceptors. *Environ. Sci. Technol.* **2008**, *42*, 7786−7792.

(44) Vogt, C.; Cyrus, E.; Herklotz, I.; Schlosser, D.; Bahr, A.; Herrmann, S.; Richnow, H. H.; Fischer, A. Evaluation of toluene degradation pathways by two-dimensional stable isotope fractionation. *Environ. Sci. Technol.* **2008**, *42*, 7793−7800.

(45) Abe, Y.; Aravena, R.; Zopfi, J.; Shouakar-Stash, O.; Cox, E.; Roberts, J. D.; Hunkeler, D. Carbon and chlorine isotope fractionation during aerobic oxidation and reductive dechlorination of vinyl chloride and cis-1,2-dichloroethene. *Environ. Sci. Technol.* **2009**, *43*, 101−107.

(46) Audí-Miró, C.; Cretnik, S.; Otero, N.; Palau, J.; Shouakar-Stash, O.; Soler, A.; Elsner, M. Cl and C isotope analysis to assess the effectiveness of chlorinated ethene degradation by zero-valent iron: Evidence from dual element and product isotope values. *Appl. Geochem.* **2013**, *32*, 175−183.

(47) Cretnik, S.; Thoreson, K. A.; Bernstein, A.; Ebert, K.; Buchner, D.; Laskov, C.; Haderlein, S.; Shouakar-Stash, O.; Kliegman, S.; McNeill, K.; Elsner, M. Reductive dechlorination of TCE by chemical model systems in comparison to dehalogenating bacteria: Insights from dual element isotope analysis ($^{13}C/^{12}C$, $^{37}Cl/^{35}Cl$). *Environ. Sci. Technol.* **2013**, *47*, 6855−6863.

(48) Kuder, T.; van Breukelen, B. M.; Vanderford, M.; Philp, P. 3D-CSIA: Carbon, chlorine, and hydrogen isotope fractionation in transformation of TCE to ethene by a *Dehalococcoides* culture. *Environ. Sci. Technol.* **2013**, *47*, 9668−9677.

(49) Badin, A.; Buttet, G.; Maillard, J.; Holliger, C.; Hunkeler, D. Multiple dual C−Cl isotope patterns associated with reductive

dechlorination of tetrachloroethene. *Environ. Sci. Technol.* **2014**, *48*, 9179−9186.

(50) Palau, J.; Cretnik, S.; Shouakar-Stash, O.; Höche, M.; Elsner, M.; Hunkeler, M. C and Cl isotope fractionation of 1,2-dichloroethane displays unique $\delta^{13}C/\delta^{37}Cl$ patterns for pathway identification and reveals surprising C−Cl bond involvement in microbial oxidation. *Environ. Sci. Technol.* **2014**, *48*, 9430−9437.

(51) Poulson, S. R.; Drever, J. I. Stable isotope (C, Cl, and H) fractionation during vaporization of trichloroethylene. *Environ. Sci. Technol.* **1999**, *33*, 3689−3694.

(52) Slater, G. F.; Ahad, J. M. E.; Sherwood Lollar, B.; Allen-King, R. M.; Sleep, B. E. Carbon isotope effects resulting from equilibrium sorption of dissolved VOCs. *Anal. Chem.* **2000**, *72*, 5669−5672.

(53) Wang, Y.; Huang, Y. S. Hydrogen isotopic fractionation of petroleum hydrocarbons during vaporization: Implications for assessing artificial and natural remediation of petroleum contamination. *Appl. Geochem.* **2003**, *18*, 1641−1651.

(54) Bouchard, D.; Hohener, P.; Hunkeler, D. Carbon isotope fractionation during volatilization of petroleum hydrocarbons and diffusion across a porous medium: a column experiment. *Environ. Sci. Technol.* **2008**, *42*, 7801−7806.

(55) Kuder, T.; Philp, P.; Allen, J. Effects of volatilization on carbon and hydrogen isotope ratios of MTBE. *Environ. Sci. Technol.* **2009**, *43*, 1763−1768.

(56) Jeannottat, S.; Hunkeler, D. Chlorine and carbon isotopes fractionation during volatilization and diffusive transport of trichloroethene in the unsaturated zone. *Environ. Sci. Technol.* **2012**, *46*, 3169−3176.

(57) Wanner, P.; Hunkeler, D. Carbon and chlorine isotopologue fractionation of chlorinated hydrocarbons during diffusion in water and low permeability sediments. *Geochim. Cosmochim. Acta* **2015**, *157*, 198−212.

(58) Hunkeler, D.; Meckenstock, R. U.; Sherwood Lollar, B.; Schmidt, T.; Wilson, J.; Schmidt, T.; Wilson, J. *A Guide for Assessing Biodegradation and Source Identification of Organic Ground Water Contaminants Using Compound Specific Isotope Analysis (CSIA)*, PA 600/R-08/148; US EPA: 2008; www.epa.gov/ada.

(59) Van Breukelen, B. M. Extending the Rayleigh equation to allow competing isotope fractionating pathways to improve quantification of biodegradation. *Environ. Sci. Technol.* **2007**, *41*, 4004−4010.

(60) Hunkeler, D.; Abe, Y.; Broholm, M. M.; Jeannottat, S.; Westergaard, C.; Jacobsen, C. S.; Aravena, R.; Bjerg, P. L. Assessing chlorinated ethene degradation in a large scale contaminant plume by dual carbon-chlorine isotope analysis and quantitative PCR. *J. Contam. Hydrol.* **2011**, *119*, 69−79.

(61) Wiegert, C.; Aeppli, C.; Knowles, T.; Holmstrand, H.; Evershed, R.; Pancost, R. D.; Macháčková, J.; Gustafsson, O. Dual carbon-chlorine stable isotope investigation of sources and fate of chlorinated ethenes in contaminated groundwater. *Environ. Sci. Technol.* **2012**, *46*, 10918−10925.

(62) Audí-Miró, C.; Cretnik, S.; Torrentó, C.; Rosell, M.; Shouakar-Stash, O.; Otero, N.; Palau, J.; Elsner, M.; Soler, A. C, Cl and H compound-specific isotope analysis to assess natural versus Fe(0) barrier-induced degradation of chlorinated ethenes at a contaminated site. *J. Hazard. Mater.* **2015**, *299*, 747−754.

(63) Badin, A.; Broholm, M. M.; Jacobsen, C. S.; Palau, J.; Dennis, P.; Hunkeler, D. Identification of abiotic and biotic reductive dechlorination in a chlorinated ethene plume after thermal source remediation by means of isotopic and molecular biology tools. *J. Contam. Hydrol.* **2016**, *192*, 1−19.

(64) Palau, J.; Jamin, P.; Badin, A.; Vanhecke, N.; Haerens, B.; Brouyère, S.; Hunkeler, D. Use of carbon-chlorine dual isotope analysis to assess the degradation pathways of 1,1,1-trichloroethane in groundwater. *Water Res.* **2016**, *92*, 235−243.

(65) Palau, J.; Shouakar-Stash, O.; Hunkeler, D. Carbon and chlorine isotope analysis to identify abiotic degradation pathways of 1,1,1-trichloroethane. *Environ. Sci. Technol.* **2014**, *48*, 14400−14408.

(66) Breider, F.; Hunkeler, D. Investigating chloroperoxidase-catalyzed formation of chloroform from humic substances using stable chlorine isotope analysis. *Environ. Sci. Technol.* **2014**, *48*, 1592−1600.

(67) Heckel, B.; Rodríguez-Fernández, D.; Torrentó, D.; Meyer, A.; Palau, J.; Domènech, C.; Rosell, M.; Soler, A.; Hunkeler, D.; Elsner, D. Compound-specific chlorine isotope analysis of tetrachloro-methane and trichloromethane by GC-IRMS vs. GC-qMS: Method development and evaluation of precision and trueness. *Anal. Chem.* **2017**, *89*, 3411−3420.

(68) Marchesi, M.; Aravena, R.; Sra, K. S.; Thomson, N. R.; Otero, N.; Soler, A.; Mancini, S. Carbon isotope fractionation of chlorinated ethenes during oxidation by Fe2+ activated persulfate. *Sci. Total Environ.* **2012**, *433*, 319−322.

(69) Marchesi, M.; Thomson, N. R.; Aravena, R.; Sra, K. S.; Otero, N.; Soler, A. Carbon isotope fractionation of 1,1,1-trichloroethane during base-catalyzed persulfate treatment. *J. Hazard. Mater.* **2013**, *260*, 61−66.

(70) Farrell, J.; Kason, M.; Melitas, N.; Li, T. Investigation of the long-term performance of zero-valent iron for reductive dechlorination of trichloroethylene. *Environ. Sci. Technol.* **2000**, *34*, 514−521.

(71) Neumann, A.; Hofstetter, T. B.; Skarpeli-Liati, M.; Schwarzenbach, R. P. Reduction of polychlorinated ethanes and carbon tetrachloride by structural Fe(II) in smectites. *Environ. Sci. Technol.* **2009**, *43*, 4082−4089.

(72) Gu, X. G.; Lu, S. G.; Li, L.; Qiu, Z. F.; Sui, Q.; Lin, K. F.; Luo, Q. S. Oxidation of 1,1,1-trichloroethane stimulated by thermally activated persulfate. *Ind. Eng. Chem. Res.* **2011**, *50*, 11029−11036.

(73) Xu, M. H.; Gu, X. G.; Lu, S. G.; Qiu, Z. F.; Sui, Q. Role of reactive oxygen species for 1,1,1-trichloroethane degradation in a thermally activated persulfate system. *Ind. Eng. Chem. Res.* **2014**, *53*, 1056−1063.

(74) Hine, J. Carbon dichloride as an intermediate in the basic hydrolysis of chloroform. A mechanism for substitution reactions at a saturated carbon atom. *J. Am. Chem. Soc.* **1950**, *72*, 2438−2445.

(75) Fells, I.; Moelwyn-Hughes, E. A. The kinetics of the hydrolysis of the chlorinated methanes. *J. Chem. Soc.* **1959**, 398−409.

(76) Hine, J.; Ehrenson, S. J. The effect of structure on the relative stability of dihalomethylenes. *J. Am. Chem. Soc.* **1958**, *80*, 824−830.

(77) Valiev, M.; Garrett, B. C.; Tsai, M.-K.; Kowalski, K.; Kathmann, S. M.; Schenter, G. K.; Dupuis, M. Hybrid approach for free energy calculations with high-level methods: Application to the S_N2 reaction of $CHCl_3$ and OH^- in water. *J. Chem. Phys.* **2007**, *127*, 051102−1−4.

(78) Aelion, C. M.; Hohëner, P.; Hunkeler, D.; Aravena, R. *Environmental Isotopes in Biodegradation and Bioremediation*; CRC Press: Boca Raton, FL, 450 p, 2010.

(79) Skell, P. S.; Hauser, C. R. The mechanism of beta-elimination with alkyl halides. *J. Am. Chem. Soc.* **1945**, *67*, 1661−1661.

(80) Zwank, L.; Elsner, M.; Aeberhard, A.; Schwarzenbach, R. P. Carbon isotope fractionation in the reductive dehalogenation of carbon tetrachloride at iron (hydr)oxide and iron sulfide minerals. *Environ. Sci. Technol.* **2005**, *39*, 5634−5641.

(81) Bernstein, A.; Shouakar-Stash, O.; Ebert, K.; Laskov, C.; Hunkeler, D.; Jeannottat, S.; Sakaguchi-Sader, K.; Laaks, J.; Jochmann, M. A.; Cretnik, S.; Jager, J.; Haderlein, S. B.; Schmidt, T. C.; Aravena, R.; Elsner, M. Compound-specific chlorine isotope analysis: A comparison of gas chromatography/isotope ratio mass spectrometry and gas chromatography/quadrupole mass spectrometry methods in an interlaboratory study. *Anal. Chem.* **2011**, *83*, 7624−7634.

(82) Sutton, N. B.; Grotenhuis, J. T. C.; Langenhoff, A. A. M.; Rijnaarts, H. H. M. Efforts to improve coupled in situ chemical oxidation with bioremediation: a review of optimization strategies. *J. Soils Sediments* **2011**, *11*, 129−140.

(83) Weathers, L. J.; Parkin, G. F.; Alvarez, P. J. Utilization of cathodic hydrogen as electron donor for chloroform cometabolism by a mixed, methanogenic culture. *Environ. Sci. Technol.* **1997**, *31*, 880−885.

(84) Novak, P.; Daniels, L.; Parkin, G. Enhanced dechlorination of carbon tetrachloride and chloroform in the presence of elemental iron

and *Methanosarcina barkeri, Methanosarcina thermophila,* or *Methanosaeta concillii. Environ. Sci. Technol.* **1998**, *32*, 1438−1443.

(85) Gregory, K. B.; Mason, M. G.; Picken, H. D.; Weathers, L. J.; Parkin, G. F. Bioaugmentation of Fe (0) for the remediation of chlorinated aliphatic hydrocarbons. *Environ. Eng. Sci.* **2000**, *17*, 169−181.

(86) Támara, M. L.; Butler, E. C. Effects of iron purity and groundwater characteristics on rates and products in the degradation of carbon tetrachloride by iron metal. *Environ. Sci. Technol.* **2004**, *38*, 1866−1876.

(87) Becker, J. G.; Freedman, D. L. Use of cyanocobalamin to enhance anaerobic biodegradation of chloroform. *Environ. Sci. Technol.* **1994**, *28*, 1942−1949.

(88) Guerrero-Barajas, C.; Field, J. A. Riboflavin- and cobalamin-mediated biodegradation of chloroform in a methanogenic consortium. *Biotechnol. Bioeng.* **2005**, *89*, 539−550.

Supporting Information

Carbon and chlorine isotope fractionation patterns associated with different engineered chloroform transformation reactions

Clara Torrentó[†‡*], Jordi Palau[†‡], Diana Rodríguez-Fernández[‡], Benjamin Heckel[§], Armin Meyer[§], Cristina Domènech[‡], Mònica Rosell[‡], Albert Soler[‡], Martin Elsner[§], Daniel Hunkeler[†]

[†]Centre for Hydrogeology and Geothermics, Université de Neuchâtel, 2000 Neuchâtel, Switzerland.

[‡]Grup de Mineralogia Aplicada i Geoquímica de Fluids, Departament de Mineralogia, Petrologia i Geologia Aplicada, Facultat de Ciències de la Terra, Martí Franques s/n, Universitat de Barcelona (UB), 08028 Barcelona, Spain.

[§]Institute of Groundwater Ecology, Helmholtz Zentrum München, 85764 Neuherberg, Germany.

Corresponding Author:
*Clara Torrentó Phone: +41 32 718 26 49; Fax: +41 32 718 26 03, e-mail: clara.torrento@unine.ch

Total number of pages (including cover): 25

Figures: 4

Tables: 2

CHEMICALS

Dibasic anhydrous sodium phosphate (Na_2HPO_4, Panreac AppliChem, Barcelona, Spain) and sodium hydroxide (NaOH, Baker, Phillipsburg, NJ, USA) were used to prepare a solution buffered at pH 12 consisting of 0.05 M Na_2HPO_4 and 0.1 M NaOH. A pH 7 phosphate-buffer solution was prepared from 0.2 M potassium dihydrogen phosphate (KH_2PO_4, Merck kGaA, Darmstadt, Germany) and 0.2 M Na_2HPO_4 solutions. Sodium peroxodisulfate ($Na_2S_2O_8$, Sigma-Aldrich, St Louis, MO, USA) solutions of different concentrations (i.e. 88, 176 and 704 mM) were prepared less than three hours before starting the experiments. A 1 M acetic acid solution was prepared from glacial acetic acid (CH_3CO_2H, Sigma-Aldrich). A 0.2 mM HEPES (99.5%, Sigma-Aldrich) pH 6.6 buffer solution was also prepared.

A saturated CF solution was prepared by adding pure chloroform (99%, Sigma-Aldrich) to distilled water in a concentration exceeding its solubility at room temperature and stirring upside down overnight in amber glass bottles without headspace. An aqueous CF stock solution containing 2100 mg L^{-1} was prepared from the saturated solution and preserved at 4 °C until use. For the experiments with Fe(0), pure CF (99%, Alfa Aesar, Ward Hill, MA, USA) was used.

The cast iron (92% purity) was obtained from Gotthart Maier Metallpulver GmbH (Rheinfelden, Germany). To reduce the oxidized coating on the iron surface, prior to the experiments the iron was acid-cleaned and dried under anoxic conditions inside a chamber containing a gas mixture of 90% N_2 and 10% H_2. During acid cleaning, the Fe was soaked in degassed 1 M hydrochloric acid solution (HCl, 32 wt. %, Sigma-Aldrich) for 1 h, then rinsed five times with degassed deionized water, and dried overnight (Matheson and Tratnyek, 1994; Dayan et al., 1999; Slater et al., 2002). The iron was weighed before and after the treatment to verify its dryness. The specific surface area was measured by N_2 gas adsorption (Brunauer-Emmett-Teller, BET method) (Brunauer et al., 1938) before (1.00±0.01 m^2g^{-1}) and after (1.624±0.007 m^2g^{-1}) the acid cleaning indicating that this procedure increased the potential reactive surface. The particle size distribution of the iron particles was determined using a particle size analyzer (Beckman Coulter, Inc., Fullerton, CA, USA) and by photon correlation spectroscopy (Beckman Coulter, model N5) as between 0.4 to 2.0 mm, where the average diameter was 1.2 mm. Hence it is considered to be milli-sized ZVI and, therefore, compared to micro-sized rather than to nano-sized iron throughout the paper.

ANALYTICAL METHODS

Chemical analyses

Concentration measurements of chlorinated compounds were performed by headspace (HS) using GC/MS or GC/TOF/MS. The GC/MS system, located in the Scientific and Technological Centers of the University of Barcelona (CCiTUB), consisted of a FOCUS Gas Chromatograph (GC) coupled with a DSQ II Mass Spectrometer (MS, Thermo Fisher Scientific, Waltham, MA, USA). Compounds were separated in a DB-624 column (60 m × 0.32 mm × 1.8 μm, Agilent, Palo Alto, CA, USA) with helium as the carrier gas (flow of 1.8 mL min^{-1}). The column was initially held at 60 °C for 2 min, ramped at 8 °C min^{-1} to 220°C and held at 220 °C for 5 min. The HS procedure was conducted for 30 min at 80 °C in 20 mL headspace vials containing 15 mL of sample. For the experiments of CF oxidation by PS, the agitation was performed at room temperature in order to avoid heat-activation of PS and CF degradation in the agitator unit. A headspace volume of 0.75 mL was injected in split mode (22:1 split ratio) at 220 °C through a split/splitless injector using a Triplus headspace autosampler (Thermo Fisher Scientific). The interface and the ionization source were set to 260 °C and 200 °C, respectively and MS (EI, 70 eV) was performed in full scan mode between 35 and 350 amu. Concentration calculations were performed using seven point calibration curves. The error based on replicate measurements was around 5% for all the compounds. For the experiments with Fe(0), a GC/TOF/MS system from the Institute of Groundwater Ecology of the Helmholtz Zentrum München was used, which consisted of a Dani Master 10115004 GC coupled to a time-of-flight (TOF) and an Agilent 5975C MS. Compounds were separated in a VOCOL column (30 m × 0.25 mm × 1.5 μm, Supelco) with helium as the carrier gas (flow 1.4 mL min^{-1}). The column was initially held at 60 °C for 2 min, ramped at 8 °C min^{-1} to 165°C, then ramped at 25 °C min^{-1} to 220°C and finally held at 220 °C for 1 min. The HS procedure was conducted for 5 min at 40 °C in 10 mL headspace vials containing 1 mL of sample. A headspace volume of 1 mL was injected in split mode (10:1 split ratio) at 250 °C through a split/splitless injector using a Combi Pal autosampler (CTC Analytics). Concentration calculations were performed using seven point calibration curves. The error based on replicate measurements was around 5% for all the compounds. In addition, chloride anions concentrations were analyzed by high-performance liquid chromatography (HPLC) using a WATERS 515 HPLC pump with IC-PAC Anion column and WATERS mod 432 detector and pH evolution was monitored using a Labor-pH-Meter Lab 850 Messparameter (SI-Analytics GmbH, Mainz, Germany).

Stable Isotope Ratio Measurements

Carbon isotope analyses of CF and some detectable volatile daughter products were performed using two different GC/IRMS systems. The GC/IRMS-1, located in the University of Neuchâtel, consisted of a 7890A GC (Agilent, Santa Clara, CA, USA) coupled to an Isoprime^{TM} 100 isotope ratio mass spectrometer (IRMS) via an Isoprime^{TM} GC5 combustion interface set to 970 °C (Isoprime Ltd., Manchester, UK). Aqueous samples and standards were prepared in 42-mL VOC vials without headspace and preconcentrated with a Stratum purge & trap system (Teledyne Tekmar Dohrmann, Mason, OH, US) connected to a cryogenic trap (Teledyne Tekmar Dohrmann). A 25 mL sample volume was purged with N$_2$ at 40 mL min^{-1} for 10 min and the degassed compounds were retained on a VOCARB 3000 trap (Supelco, Bellefonte, PA, US) at room temperature. After desorption from the trap at 250 °C, the compounds were condensed in the cryogenic unit at -80 °C, released by heating to 180 °C and injected by splitless mode into the GC. The GC was equipped with a DB-VRX column (60m x 0.32 mm x 1.8 μm) (Agilent, Santa Clara, CA, US). Helium was used as carrier gas at 1.7 mL min^{-1} and the oven temperature was initially held at 40°C for 6 min, increased to 130 °C at 10 °C min^{-1} (0.1 min)

and increased to 220°C at 20°C min^{-1} and held for 1 min at 220°C. Aqueous samples and isotopic standards interspersed along the sequence were diluted to a similar concentration and one of every three samples was analyzed twice as a quality control. The analytical uncertainty 2σ of carbon isotopic measurements with the GC/IRMS-1 was ±0.3‰ obtained from a total of 11 standard injections along the analyzing period.

For the experiments with Fe(0), the GC/IRMS-2 available in the CCiTUB was used as described elsewhere (Torrentó et al., 2014). The system consisted of a Thermo Finnigan Trace GC Ultra instrument coupled via a GC-Isolink interface to a Delta V Advantage IRMS (Thermo Scientific GmbH, Bremen, Germany). This GC was equipped with a Supelco SPB-624 column (60 m × 0.32 mm × 1.8 μm, Bellefonte, PA, USA). The oven temperature program was kept at 60 °C for 5 min, heated to 165 °C at a rate of 8 °C min^{-1}, heated to 220 °C at 25 °C min^{-1} and finally held at 220 °C for 1 min. The injector was set to split mode with a split ratio of 1:5 at a temperature of 250 °C. Helium was used as a carrier gas (2.2 mL min^{-1}). The VOCs were extracted from the aqueous samples by automated headspace solid-phase micro-extraction (HS-SPME) using a 75-μm Carboxen-PDMS fiber (Supelco, Bellefonte, PA, USA). The 20-mL vials filled with 10-mL aqueous samples were placed in a TriPlusTM Autosampler equipped with a SPME holder (Thermo Fisher Scientific, Waltham, USA). Samples were extracted for 20 minutes at 40 °C and constant agitation (600 rpm) and the SPME fibers were desorbed for 5 min at 250 °C. To correct slight carbon isotopic fractionation induced by the HS-SPME preconcentration technique (Palau et al., 2007), the samples delta values obtained with the GC/IMRS-2 were corrected by daily values of calibrated in-house standards of known C isotope ratios, prepared at the same concentration range than the samples and that were previously determined using a Flash EA1112 (Carlo-Erba, Milano, Italy) elemental analyzer (EA) coupled to a Delta C isotope ratio mass spectrometer (Thermo Fisher Scientific, Bremen, Germany) through a Conflo III interface (Thermo Finnigan, Bremen, Germany) using four international reference materials (USGS 40, IAEA 600, IAEA CH6, IAEA CH7) with respect to the Vienna Pee Dee Belemnite (VPDB) standard, according to Coplen et al. (2006). The analytical uncertainty 2σ of carbon isotopic measurements with the GC/IRMS-2 was ±0.5‰ obtained from a total of 16 standard injections along the analyzing period.

Chlorine isotope CF analyses were performed using a GC/qMS system from the University of Neuchâtel or a GC/IRMS system from the Institute of Groundwater Ecology of the Helmholtz Zentrum München (GC/IRMS-3). An interlaboratory comparison of the two analytical methods can be found in Heckel et al. (2017). The GC/qMS system consisted of a 7890A GC coupled to a 5975C qMS (Agilent, Santa Clara, CA, US). Samples were prepared in 20-mL HS vials filled with 15 mL of solution. After incubating at 60 °C for 2 min, headspace samples of 1 mL were injected in the split/splitless injector (1:20 split ratio) at 250 °C using a CombiPal autosampler (CTC Analytics, Zwingen, Switzerland). For the experiment of CF oxidation by PS, the extraction was performed at room temperature in order to avoid heat-activation of PS and CF degradation in the agitator unit. The GC was equipped with a DB-5 column (30 m x 0.25 mm x 0.25 μm, Agilent, Santa Clara, CA, US). The He flow rate was 1.2 mL min^{-1} and the temperature program was 70 °C (2 min), followed by a ramp of 20 °C min^{-1} to 230 °C. A dwell time of 50 msec was defined for all measurements and positive electron impact ionization at 70 eV was used.

For chlorine isotope CF analyses of the samples for the Fe(0) experiment, the GC/IRMS-3, located in the Institute of Groundwater Ecology of the Helmholtz Zentrum München, was used. It consisted of a Trace GC coupled to a MAT 253 IRMS with dual inlet system via a heated transfer line. The GC was equipped with a VOCOL column (30 m × 0.25 mm × 1.5 μm, Supelco) with Helium as the carrier gas

(flow 1.4 mL min^{-1}). The column was initially held at 60 °C for 2 min, ramped at 8 °C min^{-1} to 165 °C, then ramped again at 25 °C min^{-1} to 220°C and finally held at 220 °C for 1 min. The HS procedure was conducted for 5 min at 40 °C in 10 mL headspace vials containing 1 mL of sample. A headspace volume of 1 mL was injected in split mode (1:10 split ratio) at 220 °C through a split/splitless injector.

For the GC/qMS, average δ^{37}Cl values were determined on the basis of ten injections of each sample while two external working standards were interspersed along the sequence. Raw values were determined by referencing versus one of the external working standard according to Eq. 1. Precision 2σ of chlorine isotopic measurements using this system was in all the cases below ±0.5‰ based on replicate measurements. In the GC/IRMS-3, six measurements of the external working standards were performed at the beginning, two during and four at the end of each sequence. Pure CF was used as monitored gas and three reference gas peaks were run at the beginning and at the end of each analysis run. Raw δ^{37}Cl values were determined by automatic evaluation of selected CF ion peaks against the reference gas peaks. The analytical uncertainty 2σ of chlorine isotopic measurements using the GC/IRMS-3 was ±0.2‰. The peak intensities of the two most abundant fragment ions (m/z 83 and 85) were measured by GC/qMS whereas two fragment ions (m/z 47 and 49) were used for the GC/IRMS-3 measurements. These ion couples correspond to the isotopologue pairs ($[^{35}Cl_2{}^{12}C^1H]^+$ and $[^{35}Cl^{37}Cl^{12}C^1H]^+$) and ($[^{35}Cl^{12}C]^+$ and $[^{37}Cl^{12}C]^+$), respectively. The isotope ratio was obtained from the ratio of these isotopologues according to Eq. SI2 (Elsner and Hunkeler, 2008).

$$R = \frac{^{37}Cl}{^{35}Cl} = \frac{^{37}p}{^{35}p} = \frac{k}{(n-k+1)} \cdot \frac{^{37}Cl_{(k)}{}^{35}Cl_{(n-k)}}{^{37}Cl_{(k-1)}{}^{35}Cl_{(n-k+1)}} = \frac{1}{2} \cdot \frac{^{85}I}{^{83}I} = \frac{^{49}I}{^{47}I} \tag{SI2}$$

where ^{37}p and ^{35}p are the probabilities of encountering ^{37}Cl and ^{35}Cl, n is the number of Cl atoms, k is the number of ^{37}Cl isotopes, ^{37}Cl(k) ^{35}Cl(n−k) and ^{37}Cl(k−1) ^{35}Cl(n−k+1) represent the isotopologues containing k and (k−1) heavy isotopes, respectively, and I indicates the ion peak intensities. In both cases, the conversion to delta values relative to the SMOC was performed by an external two-point calibration analyzing two external working standards according to Bernstein et al (2011) (CF-F, 99.5% Fluka; CF-A, 99% Alfa Aesar), with δ^{37}Cl$_{SMOC}$ values of -3.0±0.2‰ (n=17) and -5.4±0.3‰ (n=8), respectively. The isotope composition of these standards was determined in Waterloo (Isotope Tracer Technologies Inc., Waterloo, Canada) by IRMS after conversion of CF to CH$_3$Cl using the method developed by Holt et al. (1997).

KINETICS

Data for aqueous concentrations of CF versus time were fit to a pseudo-first-order rate model:

$$dC/dt = -k'C \qquad \text{(SI3)}$$

where C is the chlorinated target compound concentration, t is time and k' is the pseudo-first-order rate constant. The k' was obtained using the integrated form of Eq. SI3:

$$\ln C = \ln C_0 - k't \qquad \text{(SI4)}$$

where C_0 is the initial concentration of the chlorinated compound. Uncertainty was obtained from 95% confidence intervals (CI).

For CF reductive dechlorination with Fe(0), a surface-area-normalized reaction rate constant (k_{SA}) was calculated for comparison with other studies. Dechlorination can be described by Eq. SI5 (Matheson and Tratnyek, 1994; Johnson et al., 1996):

$$dC/dt = -k'C = -k_{SA}\, a_S\, \rho_m\, C \qquad \text{(SI5)}$$

where α_S is the specific surface area of metal and ρ_m is the mass concentration of Fe(0).

<u>PS oxidation.</u> This reaction followed pseudo-first-order kinetics with a k' of 0.40±0.06 d^{-1} (R^2= 0.96, Fig S1). Kinetics of the experiments with initial molar ratios of 10/1 and 5/1 are shown in Fig S2. Kinetics of CF oxidation by thermally-activated PS were not described so far as Huang et al. (2005) found no degradation of CF after 72 h reaction with 5 g L^{-1} of sodium PS activated at 40°C in a mixture of 59 VOCs. Our k' is similar to the values (0.1 and 0.2 d^{-1}) reported by Zhu et al. (2015) for CF oxidation with PS activated by Fe(II) at a PS/CF molar ratio much higher (12400/1). Reaction with UV-activated PS at a PS/CF molar ratio of 290/1 resulted in higher k' values (between 30 and 300 d^{-1}, Jung et al., 2015).

<u>Alkaline hydrolysis.</u> The reaction followed pseudo first order kinetics (R^2= 0.92, Fig S1) with a k' of 0.052±0.008 d^{-1}, which is in agreement with a previously reported rate constant of 0.047±0.004 d^{-1} obtained at a similar pH 11.9±0.1 (Torrentó et al., 2014).

<u>Fe(0) dechlorination.</u> The obtained k' was 0.07±0.01 h^{-1} (R^2= 0.93, Fig S1), which corresponds to a k_{SA} of 2.1±0.4x10^{-2} L m^{-2} d^{-1}. Milli-sized Fe(0) particles were used in the present experiments. The normalized CF degradation rate constant (k_{SA}) obtained here is within a comparable range of values reported previously for CF reductive dechlorination at pH 5-8 with micro-sized iron (between 0.8 and 12.5 x10^{-2} L m^{-2} d^{-1}) (Johnson et al., 1996; Feng and Lim, 2005; Song and Carraway, 2006; Lee et al., 2015) and with nano-sized iron (between 1.2 and 125 x10^{-2} L m^{-2} d^{-1}) (Choe et al., 2001; Feng and Lim, 2005; Song and Carraway, 2006). Mass-transfer control is assumed as limitation affecting the rate constant, according to Arnold et al. (1999). Significant variations among k_{SA} data for a given compound, with over an order of magnitude differences, have been already reported and attributed to variability of the specific surface area (α) of Fe(0) due to iron treatment, differences in grain size distribution and the differences between physical surface area and reactive real surface area (Johnson et al., 1996). The effect of mixing speed on reaction rate constant have been studied to demonstrate the possibility of mass transfer limitations in batch systems for zero-valent iron

reactions, exhibiting a linear relationship of rate constant with respect to $(rpm)^{0.5}$ (Agrawal and Tratnyek, 1996). Even though the $(rpm)^{0.5}$ of the present study (14.2) is higher than in some of the referred experiments (4.5-11), the decrease of thickness of concentration boundary layers (increasing fluid velocity relative to the particles) with higher mixing speed is achieved up to a point (Arnold et al., 1999). In spite of the hypothetical lack of control of mixing speed on observed reaction rate, the rate limiting step also may represent either mass transfer to the surface or reaction at the surface (Arnold et al., 1999). External (geometric) surface area of the particles is preferred by some studies rather than the measured BET surface area and the comparison of k_{obs} to surface-area normalized mass transfer coefficients ($k_L a$) as a diagnostic for mass transfer control is recommended (Arnold et al., 1999). Moreover, used cast iron had a prismatic habitus and there is an uncertainty in $k_L a$ associated with particle sphericity and roughness (Roberts et al., 1985). To sum up, mass-transfer control is assumed as limitation affecting the rate constant, according to Arnold et al. (1999), and therefore exhaustive comparison of the obtained k_{SA} with the published values is not performed.

Two degradation pathways have been proposed for CF dechlorination by Fe(0): a reductive elimination pathway to form methane (CH_4) as final product and hydrogenolysis to form dichloromethane (DCM, CH_2Cl_2). CF reduction by micro-sized iron has been reported to occur predominantly via hydrogenolysis producing DCM as the final product (Matheson and Tratnyek, 1994; Feng and Lim, 2005; Song and Carraway, 2006), although the combination of both hydrogenolysis and the elimination pathway to methane has also been shown in studies with micro-sized iron (Feng and Lim, 2005; Li and Farrell, 2000; Támara and Butler, 2004; Lee et al., 2015). In the case of CF reduction with nano-sized iron, the elimination pathway has been reported as the dominant one, yielding to preferential production of methane over DCM (Choe et al., 2001; Feng and Lim, 2005; Song and Carraway, 2006). Lien and Zhang (1999) reported, however, preferential production of DCM with nano-sized iron.

In the present experiments, the yield of DCM, defined as the moles of product formed per mole of CF transformed ($DCM_t/(CF_0 - CF_t)$), where subscripts 0 and t indicate initial time and different sampling times, respectively) ranged from 0 to 2.4% over time, showing that accumulation of DCM accounted for only a small part of the initial CF. Similarly, low DCM yields have been previously reported (Choe et al., 2001; Feng and Lim, 2005; Nurmi et al., 2005; Song and Carraway, 2006; Lee et al., 2015). Lee et al. (2015) observed approximately 10% yield of DCM, whereas methane and formic acid accounted for approximately 12% and 5% of the lost CF, respectively, giving a low carbon mass balance of 29%. In the present experiments, analysis of other potential intermediate or end products, such as formic acid, methane or other hydrocarbons, were not performed and mass balance calculations are therefore difficult. Low Cl mass recovery was also observed: after 51 h of experiment, 88% of CF was not anymore in solution, but free chloride and DCM-chlorine only accounted for 35% and 2% of the initial CF-chlorine, respectively. Low mass recoveries during dechlorination of chlorinated ethenes and methanes have been attributed to adsorption of the parent compounds to nonreactive sites of the iron surface (Burris et al., 1995, 1998; Song and Carraway, 2006) or to adsorption of a substantial proportion of produced hydrocarbons intermediates (Hardy and Gillham, 1996; Lee et al., 2015). Compounds in the sorbed phase were in the present experiments not subject to exhaustive extraction for analysis and quantification.
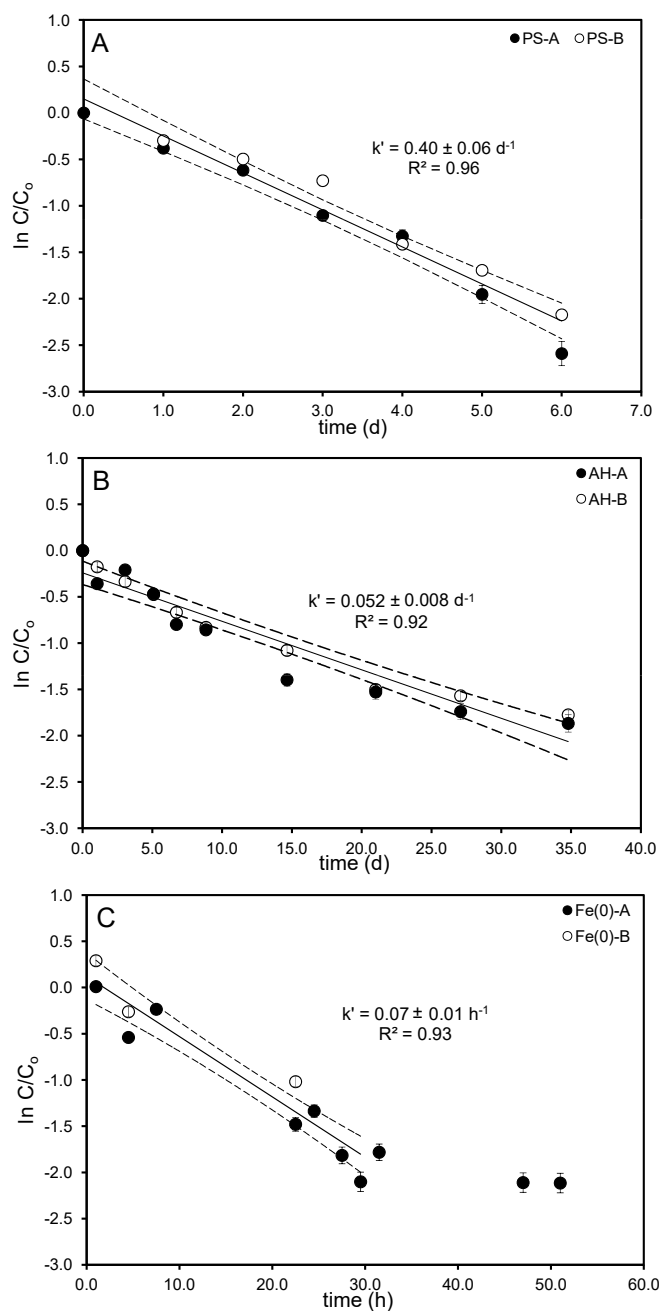
Figure S1. Semi-logarithmic plot of kinetics of CF degradation by oxidation by thermally-activated PS (A), alkaline hydrolysis (B) and dechlorination by Fe(0) (C). Data from the duplicated experiments are shown (i.e. filled and empty symbols). The error bars show the uncertainty in the natural logarithm of C/C_o, calculated by error propagation including uncertainty in concentration measurements. Note that in some cases error bars are smaller than the marker size. Pseudo-first-order rate constants (k') were extracted from curve fittings according to Eq. SI4. Dotted lines represent 95% CI of linear regression. For CF dechlorination with Fe(0), pseudo-first-order rate constant was calculated omitting data after 30 days, after when the disappearance of CF almost stopped.
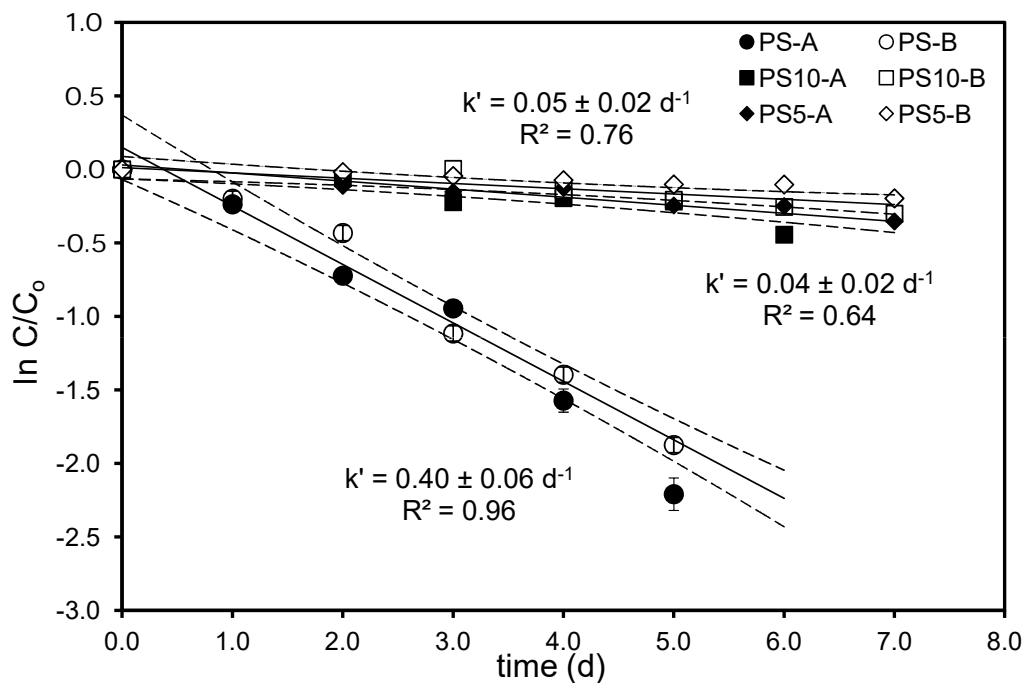
Figure S2. Semi-logarithmic plot of kinetics of CF oxidation with thermally-activated PS with initial PS to CF molar ratios of 5/1 (PS5), 10/1 (PS10) and 40/1 (PS). Data from duplicate experiments (A and B) are shown. Dotted lines represent 95% CI of linear regressions. The uncertainty in the natural logarithm of C/C_o was calculated by error propagation using uncertainty in concentration measurements. In some cases, error bars are smaller than the symbols.

CALCULATION OF APPARENT KINETIC ISOTOPE EFFECTS (AKIE)

Carbon and chlorine AKIE values were calculated by Eq. SI6 (Elsner et al., 2005)

$$\text{AKIE} = \frac{1}{1 + \left(\dfrac{z\, n}{x} \varepsilon_{bulk} \right)}$$

(SI6)

where n is the number of atoms of the considered element in the molecule, x is the number of these atoms located at the reactive site/s, z is the number of atoms located at the reactive site/s and being in intramolecular competition. The values for n, x, and z were chosen depending on the considered reaction mechanism (see "Mechanistic considerations" section in the main text and "Further discussion in reaction pathways" below). The uncertainty of the AKIE was estimated by error propagation in Eq. SI6.

PRODUCT CARBON ISOTOPE FRACTIONATION TRENDS

During a transformation reaction, the concentration weighted average C isotope ratio of all products ($\delta^{13}C_{P, average}$) can be obtained using an isotope mass-balance equation:

$$\delta^{13}C_{0,S} = f \times \delta^{13}C_S + (1-f) \times \delta^{13}C_{P, average} = f \times (\delta^{13}C_{0,S} + \varepsilon \ln f) + (1-f) \times \delta^{13}C_{P, average} \tag{SI7}$$

where $\delta^{13}C_{0,S}$ is the initial isotope ratio of the substrate. Rearrangement of Eq. SI7 leads to:

$$\delta^{13}C_{P,average} = \delta^{13}C_{0,S} - \frac{f \times \varepsilon_C}{1-f} \times \ln f \tag{SI8}$$

Using the parameter $D(\delta^{13}C)$ ($D(\delta^{13}C)=\delta^{13}C_P - \delta^{13}C_{P,average}$), which expresses how much a particular product isotope ratio deviates from the weighted average of all products (Elsner et al., 2008), Eq. SI9 can be derived:

$$\delta^{13}C_P = \left(\delta^{13}C_{0,S} + D(\delta^{13}C)\right) - \varepsilon_C \times \frac{f \times \ln f}{(1-f)} \tag{SI9}$$

where $\delta^{13}C_P$ is the isotope ratio of the product measured during the course of the reaction. As kinetic isotope effects of parallel pathways do not change during a reaction, $D(\delta^{13}C)$ also remains constant.

For the experiment with Fe(0), carbon isotope data of the reaction product (DCM) was evaluated using Eq. SI9. The DCM isotope trend was fitted in Sigma Plot according to Eq. SI9 with εC and $D(\delta^{13}C)$ as fitting parameters. The error of the parameter $D(\delta^{13}C)$ is given as the 95% CI of the regression.

The following fit equation was used in Sigma Plot.

f = a − ((k) × (x × ln(x))/(1 − x))

where f is fitted to the dependent variable ($\delta^{13}C_{DCM}$), the independent variable x corresponds to f (i.e. C/C_0), a is the coefficient from which $D(\delta^{13}C)$ is estimated, and the coefficient k is ε from DCM data. ε from DCM data is identical to ε for CF data, because all carbon isotopes are transferred from reactant to product so that the product isotope curve reflects the enrichment trend of the original atoms in the reactant.

Subsequently, the product-related isotope fractionation $\varepsilon^C_{substrate \rightarrow product}$ was calculated by Eq. SI10:

$$\varepsilon^C_{substrate \rightarrow product} = \delta^{13}C_{0,P} - \delta^{13}C_{0,S} = D(\delta^{13}C) + \varepsilon_C \tag{SI10}$$

where $\delta^{13}C_{0,P}$ represents the initial isotopic composition of the product. The uncertainty was estimated by error propagation. Eq. SI10 is solely based on isotope measurements of the substrate and a given product and therefore it allows the determination of $\varepsilon^C_{substrate \rightarrow product}$ even without knowledge of absolute reaction rates, product distribution, or closed molar balances (Elsner et al., 2008).
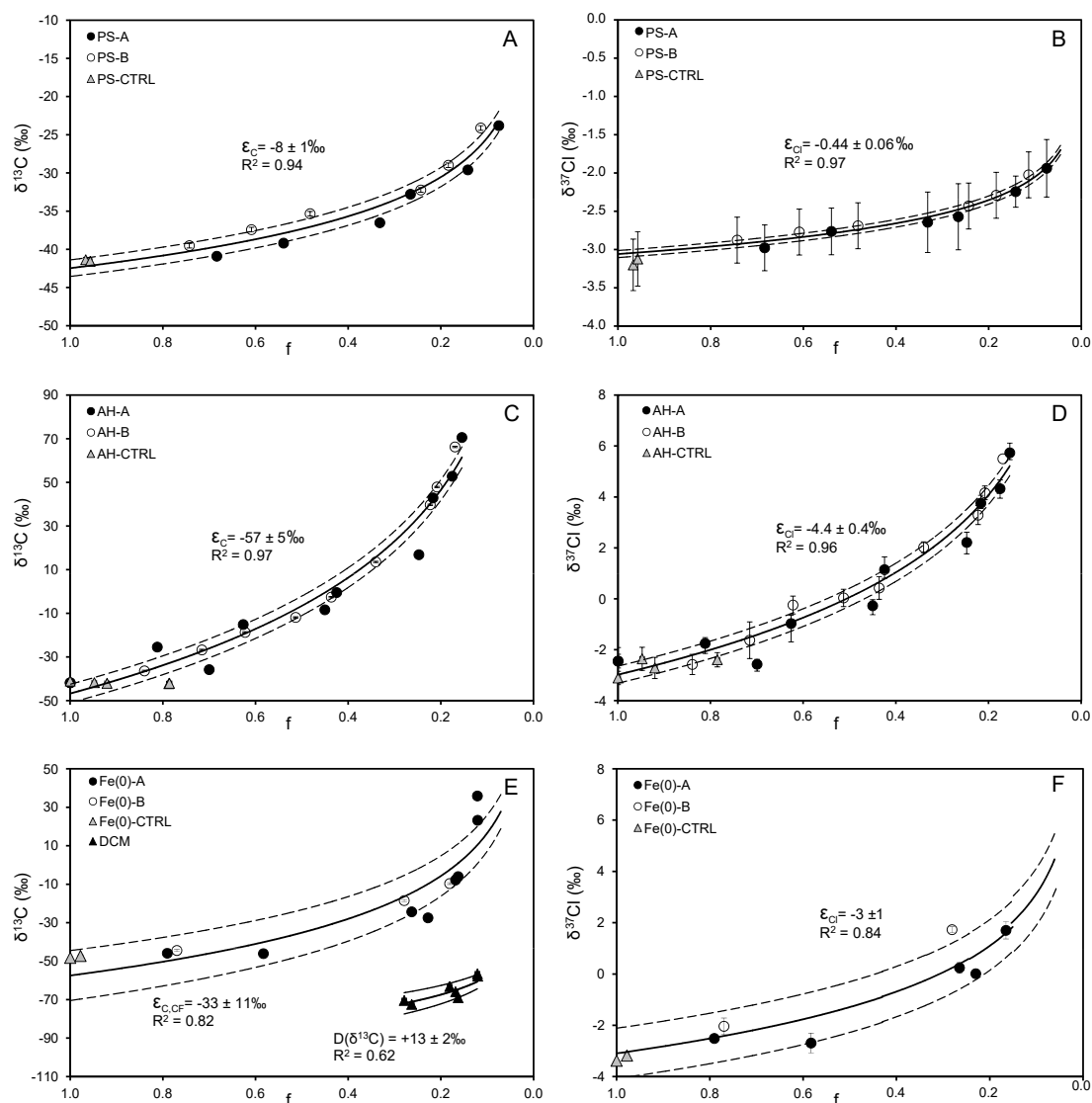
Figure S3. Isotope fractionation patterns in CF of $\delta^{13}C$ (left panels) and $\delta^{37}Cl$ (right panels) measured during oxidation by PS (A and B), degradation by alkaline hydrolysis (C and D) and dechlorination by Fe(0) (E and F). Isotopic fractionation values for both carbon and chlorine were extracted from curve fittings according to the Rayleigh equation (Eq. 1, see Fig 2 in the main text for the Rayleigh plots). Data from the duplicated experiments (i.e. filled and empty symbols) and from the control experiments are shown. Error bars of individual data points indicate standard deviations. For the experiment with Fe(0), the isotope fractionation pattern of DCM is also shown. The dashed curve shows the fit of the DCM isotope data according to Eq. SI9. The uncertainties for given ε are 95% CI.

FURTHER DISCUSSION IN REACTION PATHWAYS

Table S1 shows the obtained AKIE values for different mechanistic scenarios checked for each CF degradation experiment, as well as the comparison with the expected values. See also table S2 for typical C and Cl AKIE values estimated in different studies.

TABLE S1

Table S1. Derived C and Cl AKIE values assuming different reaction scenarios for CF degradation by PS, alkaline hydrolysis (AH) and Fe(0).

	Mechanistic scenario	C parameters	$AKIE_C$	Streitwieser limit KIE_C	typical $AKIE_C$	Cl parameters	$AKIE_{Cl}$	Streitwieser limit KIE_{Cl}	Typical $AKIE_{Cl}$	Scenario consistent
PS	Oxidative C-H bond cleavage	n=x=z=1	1.008 ± 0.001	1.021	1.00 to 1.03	n=x=3 z=1	1.00045± 0.00004	-	small secondary $AKIE_{Cl}$	yes
PS	C-Cl bond cleavage	n=x=z=1	1.008 ± 0.001	1.057	1.01 to 1.03	n=x=z=3	1.00134 ±0.00004	1.013	1.008 to 1.01	no
AH	E1$_{CB}$ elimination	n=x=z=1	1.061 ± 0.006	1.057		n=x=z=3	1.0133 ± 0.0004	1.013		yes
AH	S$_N$2 substitution	n=x=z=1	1.061 ± 0.006	1.057	1.03 to 1.09	n=x=z=3	1.0133 ± 0.0004	1.013	1.006 to 1.009	yes
Fe(0)	C-Cl bond cleavage	n=x=z=1	1.034 ± 0.012	1.057	1.027-1.033	n=x=z=3	1.008 ± 0.001	1.013		yes

PS oxidation. Initial C-H bond cleavage is the most plausible mechanistic scenario but initial C-Cl bond cleavage scenario was also checked. A primary KIE_{Cl} is only expected for the latter case, where x = z = 3 as the three C-Cl bonds are equivalent and compete for reaction. In the oxidative C-H bond cleavage scenario only a secondary KIE_C occurs. Thus, the following parameters for calculation of $AKIE_{Cl}$ have to be used: x = 3 and z = 1 since any of the three C-Cl bond is broken, and there is, therefore, no intramolecular competition between the three Cl atoms. The obtained C and Cl AKIEs are only consistent with an oxidative C-H bond cleavage mechanism. Therefore, it is proposed a reaction pathway involving the cleavage of the C-H as the rate-limiting step by abstraction of the hydrogen atom from the molecule by the attack of any of the radicals formed after persulfate activation. Although no intermediates were detected, it may be hypothesized that trichloromethanol (Cl_3COH) could form, which would rapidly undergo an elimination reaction to yield phosgene (CCl_2O) (Pohl et al., 1977) that would further hydrolyze to chloride and CO_2 (Pohl et al., 1977). In order to track more confidently the proposed mechanism, hydrogen isotope fractionation during CF oxidation with thermally-activated PS might be further measured.

Alkaline hydrolysis. During alkaline hydrolysis, the rate-limiting step is expected to be the cleavage of the C-Cl bond and thus only one $AKIE_{Cl}$ scenario is possible: x = z = 3 as the three C-Cl bonds are equivalent and compete for reaction. The obtained $AKIE_C$ and $AKIE_{Cl}$ values indicate the involvement of a C-Cl bond in the first rate-limiting step. In principle, the Cl kinetic isotope effect estimated in the present study is, therefore, consistent with the occurrence of a carbanion mechanism but also with a C-Cl bond cleavage via a concerted one-step S$_N$2 nucleophilic substitution mechanism. There is some

uncertainty in the literature whether a one-step S_N2 nucleophilic substitution mechanism could be a viable option for alkaline hydrolysis of CF in aqueous solution. This mechanism is thermodynamically favorable for gas-phase reaction of OH^- with CF (Borisov et al., 2001). For the reaction in aqueous solution, in contrast, Hine (1950), Valiev et al. (2007) and Kowalski and Valiev (2009) concluded that the S_N2 mechanism is unlikely to play a major role due to the high estimated reaction energy barriers based on experimental and computational chemical data. Since the $E1_{CB}$ mechanism, therefore, seems most plausible for this reaction, further deuterium-exchange experiments might be performed to confirm the existence of a carbanion intermediate as a way to further corroborate the occurrence of the stepwise elimination mechanism (Skell and Hauser, 1945).

<u>Fe(0) dechlorination.</u> The obtained $AKIE_C$ and $AKIE_{Cl}$ values point to cleavage of a C-Cl bond in the first rate-limiting step, which is compatible with the two-step pathway that is commonly hypothesized for this reaction. The first step involves the transfer of a single electron from the metal surface causing the removal of a chlorine atom and the formation of a dichloromethyl radical ($^\cdot CHCl_2$), which can undergo two parallel degradation pathways: (1) a reductive elimination pathway to form chloromethyl carbene ($^{\cdot\cdot}CHCl$), which can be further reduced to methane (CH_4) as final product, or can be hydrolyzed to give off HCl and carbon monoxide (CO) that can further be converted to formate ($HCOO^-$) and/or methane; (2) hydrogenolysis to form dichloromethane (DCM, CH_2Cl_2), the latter being the dominant pathway for micro-sized iron (Matheson and Tratnyek, 1994; Feng and Lim, 2005; Song and Carraway, 2006). In all the cases, cleavage of a C-Cl bond is expected to be the first rate-limiting step.

FIGURE S4
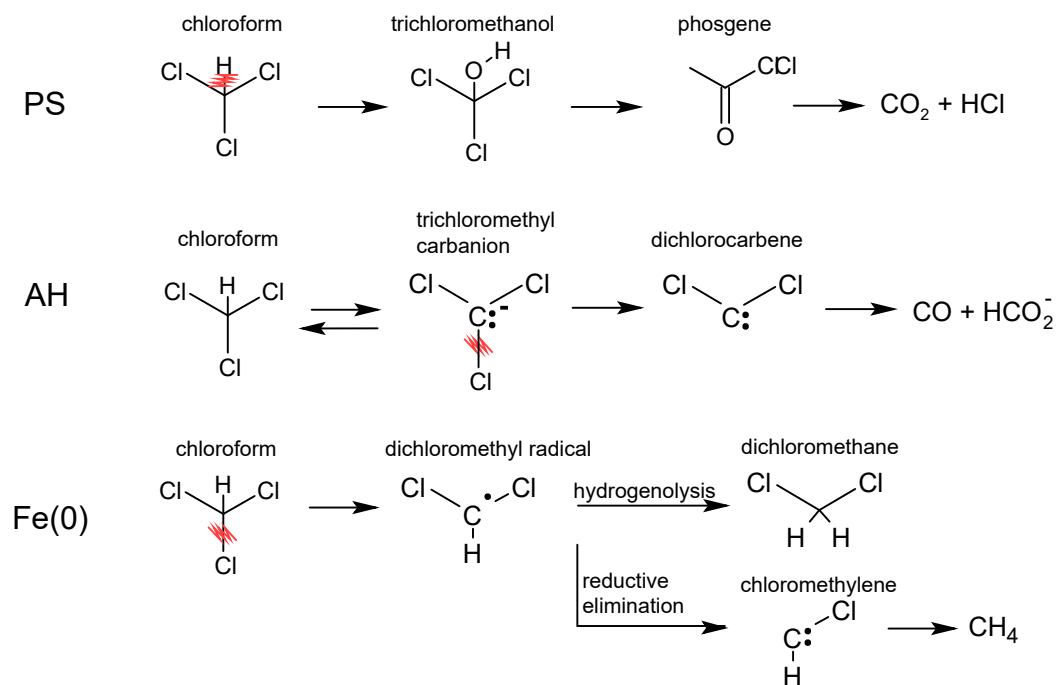
Figure S4. Proposed reaction pathways for chloroform degradation by oxidation with PS (upper scheme), alkaline hydrolysis (middle scheme) and reductive dechlorination with milli-sized Fe(0) (lower scheme).

TABLE S2

Table S2. Comparison of ε and AKIE values for C and Cl isotopes in different studies. Selected examples involving oxidative C-H bond cleavage, the $E1_{CB}$ mechanism, nucleophilic substitution reactions (S_N2-type) and C-Cl bond cleavage are shown.

Compound	Degradation pathway	Type	Conditions	ε_{bulkC} (‰) ± 95%CI	n_C	x_C	z_C	$AKIE_C$	ε_{bulkCl} (‰) ± 95%CI	n_{Cl}	x_{Cl}	z_{Cl}	$AKIE_{Cl}$	$\Lambda \approx \varepsilon C/\varepsilon Cl$	Reference
Oxidative C-H bond cleavage	Streitwieser limit KIE_C = 1.02 (Elsner et al., 2005)														
CF	oxidation with thermally-activated PS	abiotic	laboratory	-8 ± 1	1	1	1	1.008 ± 0.001	-0.44 ± 0.06	3	3	1	1.00045± 0.00004[a]	17 ± 2	this study
1,1,1-TCA	oxidation with thermally-activated PS	abiotic	laboratory	-4.0 ± 0.2	2	1	1	1.0081 ± 0.0002	0					∞	Palau et al. (2014a)
1,2-DCA	aerobic oxidation	biotic (*Pseudomonas* sp.)	laboratory	-3.0 ± 0.2	2	2	2	1.006	NM					NM	Hirschorn et al. (2004)
1,2-DCA	aerobic oxidation	biotic (*Pseudomonas* sp. DCA1)	laboratory	-3.5 ± 0.1	2	2	2	1.0070 ± 0.0002	-3.8 ± 0.2	2	2	1	1.0038 ± 0.0002[a]	0.78 ± 0.03	Palau et al. (2014b)
TBNPA	oxidation with H_2O_2/nCuO	abiotic	laboratory	-2.4 ± 0.3	5	4	4	1.012 ± 0.0015	NAP					NAP	Kozell et al. (2015)
Ethylbenzene	oxidation with t-BuOOH	abiotic	laboratory	NA	NA	NA	NA	1.015	NAP					NAP	Merrigan et al. (1999)
Toluene	aerobic oxidation	biotic	laboratory	-0.4 to -3.3	7	5	5	1.000 to 1.030	NAP					NAP	Elsner et al. (2005) ; Vogt et al. (2008)
Toluene	anaerobic oxidation	biotic	laboratory	-0.8 to -6.2	7	1	1	1.006 to 1.044	NAP					NAP	Meckenstock et al. (1999); Vogt et al. (2008); Hermann et al. (2009); Dorer et al. (2016)
MTBE	aerobic oxidation	biotic (Methylibium petroleiphilum PM1)	laboratory	-2.0 to -2.4				1.008-1.012	NAP					NAP	Hunkeler et al. (2001); Gray et al. (2002)
MTBE	aerobic oxidation	biotic (Methylibium sp.)	laboratory	-0.28 to -2.3				1.001-1.011	NAP					NAP	Rosell et al. (2007)
MTBE	aerobic oxidation	biotic (different pure cultures)	laboratory	-1.4 to -2.6				NA	NAP					NAP	Rosell et al. (2010)
MTBE	aerobic oxidation	biotic (US3-M mixed culture)	laboratory	-2.2 to -2.3				1.011	NAP					NAP	Bastida et al. (2010)
atrazine	oxidative N-dealkylation	biotic (*Rhodococcus* NI86/21)	laboratory	-4.0 ± 0.2				1.0040 ± 0.0002	NM					NM	Meyer et al. (2014)
isoproturon	hydroxylation	biotic (Phoma cf. eupyrena Gr61)	laboratory	-1.0 ± 0.2				1.01	NAP					NAP	Penning et al. (2010)
nitrobenzene	dioxygenation	biotic (*Escherichia coli*, purified NBO)	laboratory	-3.5 to -3.7	2	2	2	1.021 to 1.023	NAP					NAP	Pati et al. (2014)

Compound	Reaction	System	Setting	ε_C				KIE_C	ε_{Cl}				KIE_{Cl}	Λ	Reference
nitrobenzene	dioxygenation	biotic (*Comamonas* JS765)	laboratory	-3.9 ± 0.09	2	2	2	1.024 ± 0.0005	NAP					NAP	Hofstetter et al. (2008)
Stepwise elimination reaction (E1$_{CB}$)		**Streitwieser limit C–Cl bond cleavage KIE$_C$ = 1.057 (Elsner et al., 2005; Aelion et al., 2010)**							**Streitwieser limit C–Cl cleavage KIE$_{Cl}$ = 1.013 (Elsner et al., 2005)**						
CF	Alkaline degradation	abiotic (alkaline hydrolysis)	laboratory	-57 ± 5	1	1	1	1.061 ± 0.006	-4.4 ± 0.4	3	3	3	1.0133 ± 0.0004	13.0 ± 0.8	this study
CF	Alkaline degradation	abiotic (alkaline hydrolysis)	laboratory	-53 ±3	1	1	1	1.056 ± 0.003	NM					NM	Torrentó et al. (2014)
Nucleophilic substitution reactions (S$_N$2-Type)		**Typical range KIE$_C$ = 1.03 to 1.09 (Elsner et al., 2005)**							**Theoretical range KIE$_{Cl}$ = 1.006 to 1.009 (for CH$_3$Cl, Dybala-Defratyka et al., 2004)**						
TBNPA	Alkaline degradation	abiotic (alkaline hydrolysis)	laboratory	-10.4 ± 1.6	5	3	3	1.052 ± 0.008	NAP					NAP	Kozell et al. (2015)
DCM	Aerobic oxidation	biotic (MC8b culture)	laboratory	-42.4 ± 1.5	1	1	1	1.044	-3.8 ± 0.3					11,2	Heraty et al. (1999)
CH$_3$Cl	Aerobic oxidation	biotic (IMB-1, MB-2 and CC495 cultures)	laboratory	-42 to -48	1	1	1	1.044 to 1.050	NM					NM	Miller et al. (2001)
1,2-DCA	Hydrolytic dehalogenation	biotic (*X. autotrophicus* GJ10 and *A. aquaticus* AD20)	laboratory	-29.5 to -32.3	2	2	2	1.060 to 1.068	-4.2 to -4.4	2	2	2	1.0087 ±0.0002	7.7 ±0.2	Hirschorn et al. (2004); Abe et al. (2009); Palau et al. (2014b)
Reductive dechlorination by C–Cl bond cleavage		**Streitwieser limit KIE$_C$ = 1.057 (Elsner et al., 2005; Aelion et al., 2010)**							**Streitwieser limit KIE$_{Cl}$ = 1.013 (Elsner et al., 2005)**						
CF	Reductive dechlorination	abiotic (Fe(0))	laboratory	-33 ± 11	1	1	1	1.034 ± 0.012	-3 ± 1	3	3	3	1.008 ± 0.001	8 ± 2	this study
CF	Reductive dechlorination	abiotic (Fe(0))	laboratory	-30 ± 2	1	1	1	1.03 ± 0.07	NM					NM	Lee et al. (2015)
CF	Reductive dechlorination	biotic (*Dehalobacter* sp. CF50 consortium)	laboratory	-27.5 ± 0.9	1	1	1	1.028± 0.002	NM					NM	Chan et al. (2012)
CF	Reductive dechlorination	biotic (*Dehalobacter* sp.UNSWDHB consortium)	laboratory	-4.3 ± 0.5	1	1	1	1.004	NM					NM	Lee et al. (2015)
CT	Reductive dechlorination	abiotic (goethite, magnetite, lepidocrocite, hematite, siderite)	laboratory	-26 to -32	1	1	1	1.027 to 1.033	NM					NM	Zwank et al. (2005); Elsner et al. (2004)
CT	Reductive dechlorination	abiotic (mackinawite)	laboratory	-10.9 to -15.9	1	1	1	1.011 to 1.016	NM					NM	Zwank et al. (2005); Neumann et al. (2009)
CT	Reductive dechlorination	abiotic (Zn(0))	laboratory	-10.8 ± 0.7	1	1	1	1.01	NM					NM	VanStone et al. (2008)
1,1,1-TCA	Reductive dechlorination	abiotic (Cr(II), Fe0 and Cu and Fe mixtures)	laboratory	-16 to -14	2	1	1	1.027 ± 0.002	NM					NM	Elsner et al. (2007)
1,1,1-TCA	Reductive dechlorination	abiotic (Fe(0))	laboratory	-7.8 ± 0.4	2	1	1	1.0158 ± 0.0008	-5.2 ±0.2	3	3	3	1.0160 ± 0.0006	1.5 ± 0.1	Palau et al. (2014a)
1,1,1-TCA	Reductive	abiotic (hydrolysis/	laboratory	-1.6 ± 0.2	2	1	1	1.0033 ±	-4.7 ±0.1	3	3	3	1.0145 ±	0.33	Palau et al. (2014a)

Compound	Reaction	Type	Setting	ε_C				α_C	ε_H				α_H	Λ	Reference
	dechlorination	dehydrohalogenation)						0.0004					0.0003	±0.04	
1,1,1-TCA	Reductive dechlorination	biotic	laboratory	-1.8 to -1.5	2	1	1	1.0036 ±0.0006	NM					NM	Sherwood Lollar et al. (2010)
1,2-DCA	Reductive dechlorination	abiotic (Zn(0))	laboratory	-29.7 ± 1.5	2	2	1	1.03	NM					NM	VanStone et al. (2008)
TCE	Reductive dechlorination	abiotic (Fe(0))	laboratory	-13 ± 2	2	1	1	1.0275	-2.6 ±0.1	3	1	1	1.008 ± 0.001	5.2 ±0.3	Audí-Miró et al. (2013)
TCE	Reductive dechlorination	abiotic (Fe(0))	field	-12	2	1	1	1.0254	-3.0	3	1	1	1.009	4.2	Lojkasek-Lima et al. (2012)
TCE	Reductive dechlorination	abiotic (FeS)	laboratory	-27.9 to -33.4	2	1	1	1.059 to 1.072	NM					NM	Liang et al. (2007)
TCE	Reductive dechlorination	abiotic (corrinoids)	laboratory	-15.0 to -18.5					-3.2 to -4.2					0.3 to 0.8	Renpenning et al. (2014)
TCE	Reductive dechlorination	abiotic (vitamin B12)	laboratory	-16.7 to -17.2	2	1	1	1.034 to 1.036							Slater et al. (2003)
TCE	Reductive dechlorination	abiotic (cyanocobalamin)	laboratory	-16.1 ±0.9	2	1	1	1.03	-4.0 ±0.2	3	1	1	1.01	3.9 ± 0.2	Cretnik et al. (2013)
TCE	Reductive dechlorination	biotic	laboratory	-8.8 ± 0.2	2	1	1	1.0179	-3.5 ± 0.5	3	1	1	1.0106	2.7 ± 0.1	Wiegert et al. (2013)
TCE	Reductive dechlorination	biotic (KB-1 consortium)	laboratory	-2.5 to -13.8	2	1	1	1.005 to 1.028	NM						Bloom et al. (2000): Slater et al. (2001)
TCE	Reductive dechlorination	biotic (*S. multivorans*, *D. michiganesis* BB1 and BD1 mixed *Dehaloc.* consortium)	laboratory	-4.1 to -15.3	2	1	1	1.008 to 1.0315	NM					NM	Liang et al. (2007)
TCE	Reductive dechlorination	biotic (*S. multivorans*)	laboratory	-20.0 to -20.2					-3.7 to -3.9					5.0 to -5.3	Renpenning et al. (2014)
TCE	Reductive dechlorination	biotic (*G. lovleyi* SZ, *D. hafniense* Y51)	laboratory	-9.1 to -12.2	2	1	1	1.02	-2.7 to -3.6	3	1	1	1.01	3.4 ± 0.2	Cretnik et al. (2013)
TCE	Reductive dechlorination	biotic (mixed *Dehaloc.* consortium)	laboratory	-16.4 ± 0.4	2	2	1	1.017 ± 0.000	-3.6 ± 0.3	3	3	1	1.004 ± 0.000	4.7	Kuder et al. (2013)
PCE	Reductive dechlorination	abiotic (corrinoids)	laboratory	-22.4 -25.3					-3.4 to -4.8					4.6 to 7.0	Renpenning et al. (2014)
PCE	Reductive dechlorination	abiotic (vitamin B12)	laboratory	-15.8 to -16.5	2	2	2	1.033 to 1.034							Slater et al. (2003)
PCE	Reductive dechlorination	abiotic (FeS)	laboratory	-24.6 to -30.2	2	2	2	1.052 to 1.064	NM					NM	Liang et al. (2007)
PCE	Reductive dechlorination	biotic (*Desulfitobacterium*)	laboratory	-5.6 ± 0.7	2	2	2	1.0113	-2.0 ± 0.5	4	4	4	1.0081	2.5 ± 0.8	Wiegert et al. (2013)
PCE	Reductive dechlorination	biotic (*Desulfitobacterium* Viet1)	laboratory	-19.0 ±0.9	2	2	2	1.019	-5.0 ±0.1	4	4	4	1.005	3.8 ± 0.2	Cretnik et al. (2014)
PCE	Reductive dechlorination	biotic (*Sulfurospirillum*, PceATCE)	laboratory	-3.6 ± 0.2	2	2	2	1.007	-1.2 ± 0.1	4	4	4	1.005	2.7 ± 0.3	Badin et al. (2014)

PCE	Reductive dechlorination	biotic (*Sulfurospirillum*, PceADCE)	laboratory	-0.7 ± 0.1	2	2	2	1.001	-0.9 ±0.1	4	4	4	1.004	0.7 ± 0.2	Badin et al. (2014)
PCE	Reductive dechlorination	biotic (*S. multivorans*)	laboratory	-1.3 to -1.4					-0.4 to -0.6					2.2 to 2.8	Renpenning et al. (2014)
PCE	Reductive dechlorination	biotic (*S. multivorans, D. michiganesis* BB1 and BD1 mixed *Dehaloc.* consortium)	laboratory	-1.3 to -7.1	2	2	2	1.003 to 1.0415	NM					NM	Liang et al. (2007)
PCE	Reductive dechlorination	biotic	field	NA					NA	NA				NA	0.42 to 1.12	Wiegert et al. (2012)

[a] secondary isotope effect; NM: not measured; NA: not available; NAP: not applicable

References

Abe, Y.; Aravena, R.; Zopfi, J.; Shouakar-Stash, O.; Cox, E.; Roberts, J.D.; Hunkeler, D. Carbon and chlorine isotope fractionation during aerobic oxidation and reductive dechlorination of vinyl chloride and cis-1,2-dichloroethene. *Environ. Sci. Technol.* **2009**, 43, 101-107

Agrawal, A.; Tratnyek, P.G. Reduction of nitro aromatic compounds by zero-valent iron metal. *Environ. Sci. Technol.* **1996**, 30, 153-160

Arnold, W.A; Ball, W.P.; Roberts, A.L. Polychlorinated ethane reaction with zero-valent zinc: pathways and rate control. *J. Contam. Hydrol.* **1999**, 40, 183-200

Audí-Miró, C.; Cretnik, S.; Otero, N.; Palau, J.; Shouakar-Stash, O.; Soler, A.; Elsner, M. Cl and C isotope analysis to assess the effectiveness of chlorinated ethene degradation by zero-valent iron: Evidence from dual element and product isotope values. *Appl. Geochem.* **2013**, 32, 175-183

Badin, A.; Buttet, G.; Maillard, J.; Holliger, C.; Hunkeler, D. Multiple dual C–Cl isotope patterns associated with reductive dechlorination of tetrachloroethene. *Environ. Sci. Technol.* **2014**, 48, 9179-9186

Bastida, F.; Rosell, M.; Franchini, A. G.; Seifert, J.; Finsterbusch, S.; Jehmlich, N.; Jechalke, S.; von Bergen, M.; Richnow, H.H. Elucidating MTBE degradation in a mixed consortium using a multidisciplinary approach. *FEMS Microbiol. Ecol.* **2010**, 73, 370-384

Bernstein, A.; Shouakar-Stash, O.; Ebert, K.; Laskov, C.; Hunkeler, D.; Jeannottat, S.; Sakaguchi-Söder, K.; Laaks, J.; Jochmann, M.A.; Cretnik, S.; Jager, J.; Haderlein, S.B.; Schmidt, T.C.; Aravena, R.; Elsner, M. Compound-specific chlorine isotope analysis: A comparison of gas chromatography/isotope ratio mass spectrometry and gas chromatography/quadrupole mass spectrometry methods in an interlaboratory study. *Anal. Chem.* **2011**, 83, 7624-7634

Bloom, Y.; Aravena, R. ; Hunkeler, D. ; Edwards, E. ; Frape, S.K. Carbon isotope fractionation during microbial dechlorination of trichloroethene, cis-1,2-dichloroethene, and vinyl chloride: Implications for assessment of natural attenuation. *Environ. Sci. Technol.* **2000**, 34, 2768-2772

Borisov, Y.A.; Arcia, E.E.; Mielke, S.L.; Garrett, B.C.; Dunning, T.H. A systematic study of the reactions of OH- with chlorinated methanes. 1. Benchmark studies of the gas-phase reactions. *J. Phys. Chem. A* **2001**, 105, 7724-7736

Brunauer, S.; Emmet, P.H.; Teller, E. Adsorption of gases on multimolecular layers. *J. Am. Chem. Soc.* **1938**, 60, 309-319

Burris, D.R.; Campbell, T.J.; Manoranjan, V.S. Sorption of trichloroethylene and tetrachloroethylene in a batch reactive metallic iron-water system. *Environ. Sci. Technol.* **1995**, 29, 2850-2855

Burris, D.R.; Allen-King R.M.; Manoranjan, V.S.; Campbell, T.J.; Loraine, G.A.; Deng, B. Chlorinated ethane reduction by cast iron: Sorption and mass transfer. *J. Environm. Eng.-ASCE* **1998**, 124, 1012-1019

Chan, C.C.H.; Mundle, S.O.C.; Eckert, T.; Liang, X.; Tang, S.; Lacrampe-Couloume, G.; Edwards, E.A.; Sherwood Lollar, B. Large carbon isotope fractionation during biodegradation of chloroform by Dehalobacter cultures. *Environ. Sci. Technol.* **2012**, 46, 10154-10160

Choe, S.; Lee, S.H.; Chang, Y.Y.; Hwang, K.Y.; Khim, J. Rapid reductive destruction of hazardous organic compounds by nanoscale Fe-0. *Chemosphere* **2001**, 42, 367-372.

Coplen, T.B.; Brand, W.A.; Gehre, M.; Gröning, M.; Meijer, H.A.J.; Toman, B.; Verkouteren, R.M. After two decades a second anchor for the VPDB $\delta^{13}C$ scale. *Rapid Commun. Mass Spectrom.* **2006**, 20, 3165-3166

Cretnik, S.; Thoreson, K.A.; Bernstein, A.; Ebert, K.; Buchner, D.; Laskov, C.; Haderlein, S.; Shouakar-Stash, O.; Kliegman, S.; McNeill, K.; Elsner, M. Reductive dechlorination of TCE by chemical model systems in comparison to dehalogenating bacteria: Insights from dual element isotope analysis ($^{13}C/^{12}C$, $^{37}Cl/^{35}Cl$). *Environ. Sci. Technol.* **2013**, 47, 6855-6863

Cretnik, S.; Bernstein, A.; Shouakar-Stash, O.; Löffler, F.; Elsner, M. Chlorine isotope effects from isotope ratio mass spectrometry suggest intramolecular C-Cl bond competition in trichloroethene (TCE) reductive dehalogenation. *Molecules* **2014**, 19, 6450-6473

Dayan, H.; Abrajano, T.; Sturchio, N.C.; Winsor, L. Carbon isotopic fractionation during reductive dehalogenation of chlorinated ethenes by metallic iron. *Org. Geochem.* **1999**, 30, 755-763

Dorer, C.; Vogt, C.; Neu, T.R.; Kleinsteuber, S.; Stryhanyuk, H.; Richnow, H.-H. Characterization of toluene and ethylbenzene biodegradation under nitrate-, iron(III)- and manganese(IV)-reducing conditions by compound-specific isotope analysis. *Environ. Pollut.* **2016**, 211, 271-281

Dybala-Defratyka, A.; Rostkowski, M.; Matsson, O.; Westaway, K.C.; Paneth, P. A new interpretation of chlorine leaving group kinetic isotope effects; A theoretical approach. *J. Org. Chem.* **2004**, 69, 4900-4905

Elsner, M.; Chartrand, M.; VanStone, N.; Lacrampe-Couloume, G.; Sherwood Lollar, B. Identifying abiotic chlorinated ethene degradation: Characteristic isotope patterns in reaction products with nanoscale zero-valent iron. *Environ. Sci. Technol.* **2008**, 42, 5963-5970

Elsner, M.; Cwiertny, D.M.; Roberts, A.L.; Sherwood Lollar, B. 1,1,2,2-tetrachloroethane reactions with OH^-, Cr(II), granular iron, and a copper-iron bimetal: Insights from product formation and associated carbon isotope fractionation. *Environ. Sci. Technol.* **2007**, 41, 4111-4117

Elsner, M.; Haderlein, S.B.; Kellerhals, T.; Luzi, S.; Zwank, L.; Angst, W.; Schwarzenbach, R.P. Mechanisms and products of surface-mediated reductive dehalogenation of carbon tetrachloride by Fe(II) on goethite. *Environ. Sci. Technol.* **2004**, 38, 2058-2066

Elsner, M.; Hunkeler, D. Evaluating chlorine isotope effects from isotope ratios and mass spectra of polychlorinated molecules. *Anal. Chem.* **2008**, 80, 4731-4740

Elsner, M.; Zwank, L.; Hunkeler, D.; Schwarzenbach, R.P. A new concept linking observable stable isotope fractionation to transformation pathways of organic pollutants. *Environ. Sci. Technol.* **2005**, 39, 6896-6916

Feng, J.; Lim, T.-T. Pathways and kinetics of carbon tetrachloride and chloroform reductions by nano-scale Fe and Fe/Ni particles: comparison with commercial micro-scale Fe and Zn. *Chemosphere* **2005**, 59, 1267-1277

Gray, J.R.; Lacrampe-Couloume, G.; Gandhi, D.; Scow, K.M.; Wilson, R.D.; Mackay, D.M.; Sherwood Lollar, B. Carbon and hydrogen isotopic fractionation during biodegradation of methyl tertbutyl ether. *Environ. Sci. Technol.* **2002**, 36, 1931-1938

Hardy, L.I.; Gillham, R.W. Formation of hydrocarbons from the reduction of aqueous CO_2 by zero-valent iron. *Environ. Sci. Technol.* **1996**, 30, 57-65

Heckel, B.; Rodríguez-Fernández, D.; Torrentó, D.; Meyer, A.; Palau, J.; Domènech, C.; Rosell, M.; Soler, A.; Hunkeler, D.; Elsner, D. Compound-specific chlorine isotope analysis of tetrachloro-methane and trichloromethane by GC-IRMS vs. GC-qMS: Method development and evaluation of precision and trueness. *Anal. Chem.* **2017**, 89, 3411-3420

Heraty, L.J.; Fuller, M.E.; Huang, L.; Abrajano, T.; Sturchio, N. C. Isotope fractionation of carbon and chlorine by microbial degradation of dichloromethane. *Org. Geochem.* **1999**, 30, 793-799

Herrmann, S.; Vogt, C.; Fischer, A.; Kuppardt, A.; Richnow, H.-H. Characterization of anaerobic xylene biodegradation by two-dimensional isotope fractionation analysis. *Environ. Microbiol. Rep.* **2009**, 1, 535-544

Hine, J. Carbon dichloride as an intermediate in the basic hydrolysis of chloroform. A mechanism for substitution reactions at a saturated carbon atom. *J. Am. Chem. Soc.* **1950**, 72, 2438-2445

Hirschorn, S.K.; Dinglasan, M.J.; Elsner, M.; Mancini, S.A.; Lacrampe-Couloume, G. ; Edwards,‖E.A.; Sherwood Lollar, B. Pathway dependent isotopic fractionation during aerobic biodegradation of 1,2-dichloroethane. *Environ. Sci. Technol.* **2004**, 38, 4775-4781

Hofstetter, T.B.; Spain, J.C.; Nishino, S.F.; Bolotin, J.; Schwarzenbach, R.P. Identifying competing aerobic nitrobenzene biodegradation pathways using compound-specific isotope analysis. *Environ. Sci. Technol.* **2008**, 42, 4764-4770

Holt, B.D.; Sturchio, N.C.; Abrajano, T.A.; Heraty, L.J. Conversion of chlorinated volatile organic compounds to carbon dioxide and methyl chloride for isotopic analysis of carbon and chlorine. *Anal. Chem.* **1997**, 69, 2727-2733

Huang, K.C.; Zhao, Z.; Hoag, G.E.; Dahmani, A.; Block, P.A. Degradation of volatile organic compounds with thermally activated persulfate oxidation. *Chemosphere* **2005**, 61, 551-560

Hunkeler, D.; Butler, B.J.; Aravena, R.; Barker, J.F. Monitoring biodegradation of methyl tert-butyl ether (MTBE) using compoundspecific carbon isotope analysis. *Environ. Sci. Technol.* **2001**, 35, 676-681

Johnson, T.L.; Scherer, M.M.; Tratnyek, P.G. Kinetics of halogenated organic compound reduction by iron metal. *Environ. Sci. Technol.* **1996**, 2634-2640

Jung, J.-G.; Do, S.-H.; Kwon, Y.-J.; Kong, S.-H. Degradation of multi-DNAPLs by a UV/persulphate/ethanol system with the additional injection of a base solution. *Environ. Technol.* **2015**, 36, 1044-1049

Kowalski, K.; Valiev, M. Extensive regularization of the coupled cluster methods based on the generating functional formalism: Application to gas-phase benchmarks and to the S_N2 reaction of $CHCl_3$ and OH^- in water. *J. Chem. Phys.* **2009**, 131, 234107

Kozell, A.; Yecheskel, Y.; Balaban, N.; Dror, I.; Halicz, L.; Ronen, Z.; Gelman, F. Application of dual carbon−bromine isotope analysis for investigating abiotic transformations of tribromoneopentyl alcohol (TBNPA). *Environ. Sci. Technol.* **2015**, 49, 4433-4440

Kuder, T.; van Breukelen, B.M.; Vanderford, M.; Philp, P. 3D-CSIA: Carbon, chlorine, and hydrogen isotope fractionation in transformation of TCE to ethene by a *Dehalococcoides* culture. *Environ. Sci. Technol.* **2013**, 47, 9668-9677

Lee, M.; Wells, E.; Wong, Y.K.; Koenig, J.; Adrian, L.; Richnow, H.H.; Manefield, M. Relative contributions of *Dehalobacter* and zerovalent iron in the degradation of chlorinated methanes. *Environ. Sci. Technol.* **2015**, 49, 4481-4489

Li, T.; Farrell, J. Reductive dechlorination of trichloroethene and carbon tetrachloride using iron and palladized-iron cathodes. *Environ. Sci. Technol.* **2000**, 34, 173-179

Liang, X.; Dong, Y.; Kuder, T.; Krumholz, L.R.; Philp, R.P.; Butler, E.C. Distinguishing abiotic and biotic transformation of tetrachloroethylene and trichloroethylene by stable carbon isotope fractionation. *Environ. Sci. Technol.* **2007**, 41, 7094-7100

Lien, H.-L.; Zhang, W.-X. Transformation of chlorinated methanes by nanoscale iron particles. J. *Environ. Eng.* **1999**, 125, 1042-1047

Lojkasek-Lima, P.; Aravena, R.; Shouakar-Stash, O.; Frape, S.K.; Marchesi, M.; Fiorenza, S.; Vogan, J. Evaluating TCE abiotic and biotic degradation pathways in a permeable reactive barrier using compound specific isotope analysis. *Ground Water Monit. Remediat.* **2012**, 32, 53-62

Matheson, L.J.; Tratnyek, P.G. Reductive dehalogenation of chlorinated methanes by iron metal. *Environ. Sci. Technol.* **1994**, 2045-2053

Meckenstock, R.U.; Morasch, B.; Warthmann, R.; Schink, B.; Annweiler, E.; Michaelis, W.; Richnow, H.H. C-13/C-12 isotope fractionation of aromatic hydrocarbons during microbial degradation. *Environ Microbiol.* **1999**, 1, 409-414

Merrigan, S.R.; Le Gloahec, V.N.; Smith, J.A.; Barton, D.H.R.; Singleton, D.A. Separation of the primary and secondary kinetic isotope effects at a reactive center using starting material reactivities. Application to the FeCl$_3$-catalyzed oxidation of C-H bonds with tertbutyl hydroperoxide. *Tetrahedron Lett.* **1999**, 40, 3847-3850

Meyer, A.H.; Dybala-Defratyka, A.; Alaimo, P.J.; Geronimo, I.; Sanchez, A.D.; Cramer, C.J.; Elsner, M. Cytochrome P450-catalyzed dealklyation of atrazine by *Rhodococcus* sp. strain NI86/21 involves hydrogen atom transfer rather than single electron transfer. *Dalton Trans.* **2014**, 43, 12111-12432

Miller, L.G.; Kalin, R.M.; McCauley, S.E.; Hamilton, J.T.G.; Harper, D.B.; Millet, D.B.; Oremland, R.S.; Goldstein, A.H. Large carbon isotope fractionation associated with oxidation of methyl halides by methylotrophic bacteria. *Proc. Natl. Acad.Sci. U.S.A.* **2001**, 98, 5833-5837

Neumann, A.; Hofstetter, T.B.; Skarpeli-Liati, M.; Schwarzenbach, R.P. Reduction of polychlorinated ethanes and carbon tetrachloride by structural Fe(II) in smectites. *Environ. Sci. Technol.* **2009**, 43, 4082-4089

Nurmi, J.T.; Tratnyek, P.G.; Sarathy, V.; Amonette, J.E.; Pecher, K.; Wang, C.; Linehan, J.C.; Matson, D.W.; Penn, R.L.; Driessen, M.D. Characterization and properties of metallic iron nanosized particles: Spectroscopy, electrochemistry, and kinetics. *Environ. Sci. Technol.* **2005**, 39, 1221-1230

Palau, J.; Soler, A.; Teixidor, P.; Aravena, R. Compound-specific carbon isotope analysis of volatile organic compounds in water using solid-phase microextraction. *J. Chromatogr.* A **2007**, 1163, 260-268

Palau, J.; Shouakar-Stash, O.; Hunkeler, D. Carbon and chlorine isotope analysis to identify abiotic degradation pathways of 1,1,1-trichloroethane. *Environ. Sci. Technol.* **2014a**, 48, 14400-14408

Palau, J; Cretnik, S.; Shouakar-Stash, O.; Höche, M.; Elsner, M.; Hunkeler, M. C and Cl isotope fractionation of 1,2-dichloroethane displays unique $\delta^{13}C/\delta^{37}Cl$ patterns for pathway identification and reveals surprising C–Cl bond involvement in microbial oxidation. *Environ. Sci. Technol.* **2014b**, 48, 9430-9437

Pati, S.G.; Kohler, H.-P.E.; Bolotin, J.; Parales, R.E.; Hofstetter, T.B. Isotope effects of enzymatic dioxygenation of nitrobenzene and 2−nitrotoluene by nitrobenzene dioxygenase. *Environ. Sci. Technol.* **2014**, 48, 10750-10759

Penning, H.; Sorensen, S.R.; Meyer, A.H.; Aamand, J.; Elsner, M. C, N, and H isotope fractionation of the herbicide isoproturon reflects different microbial transformation pathways. *Environ. Sci. Technol*. **2010**, 44, 2372-2378

Pohl, L.R.; Bhooshan, B.; Whittaker, N.F.; Krishna, G. Phosgene: a metabolite of chloroform. *Biochem. Bioph. Res. Co.* **1977**, 79, 684-691

Renpenning, J.; Keller, S.; Cretnik, S.; Shouakar-Stash, O.; Elsner, M.; Schubert, T.; Nijenhuis, I. Combined C and Cl isotope effects indicate differences between corrinoids and enzyme

(*Sulfurospirillum multivorans* PceA) in reductive dehalogenation of tetrachloroethene, but not trichloroethene. *Environ. Sci. Technol.* **2014**, 48, 11837-11845

Roberts, P.V.; Cornel, P.; Summers, R.S. External mass-transfer rate in fixed-bed adsorption. *J. Environ. Eng.* **1985**, 111, 891-905

Rosell, M.; Barcelo, D.; Rohwerder, T.; Breuer, U.; Gehre, M.; Richnow, H.H. Variations in $^{13}C/^{12}C$ and D/H enrichment factors of aerobic bacterial fuel oxygenate degradation. *Environ. Sci. Technol.* **2007**, 41, 2036-2043

Rosell, M.; Finsterbusch, S.; Jechalke, S.; Hübschmann, T.; Vogt, C.; Richnow, H.H. Evaluation of the effects of low oxygen concentration on stable isotope fractionation during aerobic MTBE biodegradation. *Environ. Sci. Technol.* **2010**, 44, 309-315

Sherwood Lollar, B.; Hirschorn, S.; Mundle, S.O.C.; Grostern, A.; Edwards, E.A.; Lacrampe-Couloume, G. Insights into enzyme kinetics of chloroethane biodegradation using compound specific stable isotopes. *Environ. Sci. Technol.* **2010**, 44, 7498-7503

Skell, P.S.; Hauser, C.R. The mechanism of beta-elimination with alkyl halides. *J. Am. Chem. Soc.* **1945**, 67, 1661-1661

Slater, G.F.; Sherwood Lollar, B.; Sleep, B.E.; Edwards, A.E. Variability in carbon isotopic fractionation during biodegradation of chlorinated ethenes: Implications for field applications. *Environ. Sci. Technol.* **2001**, 35, 901-907

Slater, G.F.; Sherwood Lollar, B.; King, A.; O'Hannesin, S. Isotopic fractionation during reductive dechlorination of trichloroethene by zero-valent iron: influence of surface treatment. *Chemosphere* **2002**, 49, 587-596

Slater, G.F.; Sherwood Lollar, B.; Lesage, S.; Brown, S. Carbon isotope fractionation of PCE and TCE during dechlorination by vitamin B12. *Ground Water Monit. Remediat.* **2003**, 23, 59-67

Song, H.H.; Carraway, E.R. Reduction of chlorinated methanes by nano-sized zero-valent iron. Kinetics, pathways, and effect of reaction conditions. *Environ. Eng. Sci.* **2006**, 23, 272-284

Támara, M.; Butler, E.C. Effects of iron purity and groundwater characteristics on rates and products in the degradation of carbon tetrachloride by iron metal. *Environ. Sci. Technol.* **2004**, 38, 1866-1876

Torrentó, C.; Audí-Miró, C.; Bordeleau, G.; Marchesi, M.; Rosell, M.; Otero, N.; Soler, A. The use of alkaline hydrolysis as a novel strategy for chloroform remediation: feasibility of using urban construction wastes and evaluation of carbon isotopic fractionation. *Environ. Sci. Technol.* **2014**, 48, 1869-1877

Valiev, M.; Garrett, B.C.; Tsai, M.-K.; Kowalski, K.; Kathmann, S.M.; Schenter, G.K.; Dupuis, M. Hybrid approach for free energy calculations with high-level methods: Application to the S_N2 reaction of $CHCl_3$ and OH^- in water. *J. Chem. Phys.* **2007**, 127, 051102-1-4

VanStone, N.; Elsner, M.; Lacrampe-Couloume, G.; Mabury, S.; Sherwood Lollar, B. Potential for identifying abiotic chloroalkane degradation mechanisms using carbon isotopic fractionation. *Environ. Sci. Technol.* **2008**, 42, 126-132

Vogt, C.; Cyrus, E.; Herklotz, I.; Schlosser, D.; Bahr, A.; Herrmann, S.; Richnow, H.-H.; Fischer, A. Evaluation of toluene degradation pathways by two-dimensional stable isotope fractionation. *Environ. Sci. Technol.* **2008**, 42, 7793-7800

Wiegert, C.; Aeppli, C.; Knowles, T.; Holmstrand, H.; Evershed, R.; Pancost, R.D. ; Macháčková, J.; Gustafsson, O. Dual carbon-chlorine stable isotope investigation of sources and fate of chlorinated ethenes in contaminated groundwater. *Environ. Sci. Technol.* **2012**, 46, 10918-10925

Wiegert, C.; Mandalakis, M.; Knowles, T.; Polymenakou, P.; Aeppli, C.; Machackova, J.; Holmstrand, H.; Evershed, R.P.; Pancost, R.; Gustafsson, O. Carbon and chlorine isotope fractionation during microbial degradation of tetra- and trichloroethene. *Environ. Sci. Technol.* **2013**, 47, 6449-6456

Zhu, X.; Du, E.; Ding, H.; Lin, Y.; Long, T.; Li, H.; Wang, L. QSAR modeling of VOCs degradation by ferrous-activated persulfate oxidation. *Desalin. Water Treat.* **2015**, 1-15

Zwank, L.; Elsner, M.; Aeberhard, A.; Schwarzenbach, R.P. Carbon isotope fractionation in the reductive dehalogenation of carbon tetrachloride at iron (hydr)oxide and irons minerals. *Environ. Sci. Technol.* **2005**, 39, 5634-5641

Annex D. Article 3. Abiotic chlorinated methanes degradation

Rodríguez-Fernández, D., Heckel, B, Torrentó, C., Meyer, A., Elsner, M., Hunkeler,D., Soler, A., Rosell, M, Domènech, C. 2018. Dual element (C-Cl) isotope approach to characterize abiotic reactions of chlorinated methanes by Fe(0) and by Fe(II) on iron minerals at neutral and alkaline pH. Chemosphere, 206, 447-456, doi: 10.1016/j.chemosphere.2018.05.036

Dual element (C–Cl) isotope approach to distinguish abiotic reactions of chlorinated methanes by Fe(0) and by Fe(II) on iron minerals at neutral and alkaline pH

Diana Rodríguez-Fernández [a, *], Benjamin Heckel [b], Clara Torrentó [c], Armin Meyer [b], Martin Elsner [b], Daniel Hunkeler [c], Albert Soler [a], Mònica Rosell [a], Cristina Domènech [a]

[a] Grup MAiMA, Mineralogia Aplicada, Geoquímica i Geomicrobiologia, Departament de Mineralogia, Petrologia i Geologia Aplicada, Facultat de Ciències de la Terra, Martí Franquès s/n, Universitat de Barcelona (UB), 08028 Barcelona, Spain
[b] Institute of Groundwater Ecology, Helmholtz Zentrum München, 85764 Neuherberg, Germany
[c] Centre d'hydrogéologie et de géothermie, Université de Neuchâtel, Neuchâtel 2000, Switzerland

HIGHLIGHTS

- Carbon tetrachloride (CT) and chloroform (CF) C and Cl isotope fractionation study.
- CT and CF abiotic reactions with Fe(0), FeCl$_2$, pyrite and magnetite were assessed.
- Unlike at pH 12, at pH 7 only CT degradation by Fe(0) and pyrite was detected.
- Different C–Cl plots for CT hydrogenolysis and CT hydrolytic or thiolytic reduction.
- Reactions with Fe(0) and pyrite showed similar Λ for each compound regardless pH.

GRAPHICAL ABSTRACT
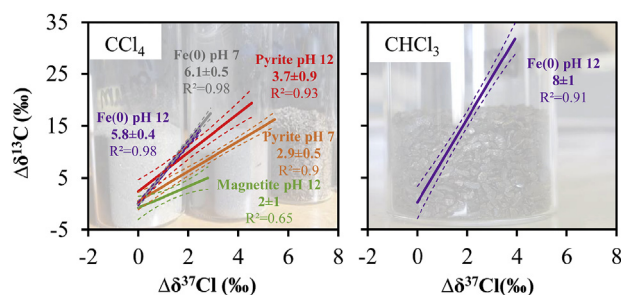
ARTICLE INFO

ABSTRACT

A dual element C–Cl isotopic study was performed for assessing chlorinated methanes (CMs) abiotic transformation reactions mediated by iron minerals and Fe(0) to further distinguish them in natural attenuation monitoring or when applying remediation strategies in polluted sites. Isotope fractionation was investigated during carbon tetrachloride (CT) and chloroform (CF) degradation in anoxic batch experiments with Fe(0), with FeCl$_2$(aq), and with Fe-bearing minerals (magnetite, Mag and pyrite, Py) amended with FeCl$_2$(aq), at two different pH values (7 and 12) representative of field and remediation conditions. At pH 7, only CT batches with Fe(0) and Py underwent degradation and CF accumulation evidenced hydrogenolysis. With Py, thiolytic reduction was revealed by CS$_2$ yield and is a likely reason for different Λ value ($\Delta\delta^{13}C/\Delta\delta^{37}Cl$) comparing with Fe(0) experiments at pH 7 (2.9 ± 0.5 and 6.1 ± 0.5, respectively). At pH 12, all CT experiments showed degradation to CF, again with significant differences in Λ values between Fe(0) (5.8 ± 0.4) and Fe-bearing minerals (Mag, 2 ± 1, and Py, 3.7 ± 0.9), probably evidencing other parallel pathways (hydrolytic and thiolytic reduction). Variation of pH did not significantly affect the Λ values of CT degradation by Fe(0) nor Py.

CF degradation by Fe(0) at pH 12 showed a Λ (8 ± 1) similar to that reported at pH 7 (8 ± 2), suggesting CF hydrogenolysis as the main reaction and that CF alkaline hydrolysis (13.0 ± 0.8) was negligible.

---

* Corresponding author.
  E-mail address: diana.rodriguez@ub.edu (D. Rodríguez-Fernández).

Our data establish a base for discerning the predominant or combined pathways of CMs natural attenuation or for assessing the effectiveness of remediation strategies using recycled minerals or Fe(0).

1. Introduction

Chloroform (CF, $CHCl_3$) and carbon tetrachloride (CT, CCl_4) are chlorinated volatile organic compounds (VOCs) from the group of chlorinated methanes (CMs). Both are toxic and predicted to be carcinogenic substances (IARC, 1999). They are found in groundwater as a consequence of releases from chemical manufacturing processes or accidental spills (Zogorski et al., 2006), although CF can also be naturally formed (Cappelletti et al., 2012; Hunkeler et al., 2012; Breider et al., 2013).

Abiotic CMs degradation in groundwater mainly proceeds under anoxic conditions. The main CT degradation pathway is hydrogenolysis to CF, although CT reduction followed by hydrolytic or thiolytic substitution of dechlorinated intermediates to CO, CO_2 or CS_2 is also possible (He et al., 2015). Abiotic CF degradation processes under anoxic conditions include hydrogenolysis to DCM and reductive elimination to CH_4 (Song and Carraway, 2006; He et al., 2015). Bioremediation strategies for CMs are scarce (Penny et al., 2010; Cappelletti et al., 2012; Koenig et al., 2015). Thus, although both compounds can be biotically (Penny et al., 2010; Cappelletti et al., 2012) or abiotically degraded, they are considered recalcitrant compounds requiring targeted remediation strategies in groundwater.

In situ chemical oxidation is not an effective treatment for CT and CF due to the highly oxidized state of carbon (Huang et al., 2005; Huling and Pivetz, 2006). Alkaline hydrolysis (AH) has been studied for CF at laboratory and field scale as a new and effective remediation strategy (Torrentó et al., 2014) but CT hydrolysis is pH independent and extremely slow (Jeffers et al., 1989). Fortunately, zero-valent metals and Fe-bearing minerals have proven to mediate the transformation of CF and CT at laboratory scale (e.g. Matheson and Tratnyek, 1994; Támara and Butler, 2004; Feng and Lim, 2005; Zwank et al., 2005; He et al., 2015; Lee et al., 2015). Fe(0) has been commonly used in permeable reactive barriers (PRBs) since it is a strong reducing agent, cheaper and less harmful than other zero-valent metals (Vodyanitskii, 2014). Micro-sized Fe(0) has been used in long-functioning PRBs, while nano-sized Fe(0) injections have been recently used to renew PRBs in highly polluted sites (Obiri-Nyarko et al., 2014). Some minerals such as magnetite (Fe_3O_4, Mag hereafter) can be formed in Fe(0) PRBs reducing their efficiency (Vodyanitskii, 2014), while others, such as FeS, can promote CT degradation (Obiri-Nyarko et al., 2014). Since long-term evolution of PRBs is still not fully understood (Obiri-Nyarko et al., 2014) and Fe-bearing minerals such as pyrite (FeS_2, Py hereafter), green rusts or Mag are naturally ubiquitous in anoxic aquifers and/or in transition zones (Ferrey et al., 2004; Scheutz et al., 2011), it is interesting to assess their influence on CMs degradation.

Detection of CMs natural attenuation or monitoring of the above-mentioned remediation strategies can be challenging when relying on only by-products, since these daughter products can be further degraded, are difficult to quantify in the field (e.g. gases), could come from other parent compounds or stem from a secondary source (i.e. CF). In such cases, compound specific isotope analysis (CSIA) has been developed and matured into a widely applied method allowing the investigation of VOCs transformation reactions and the associated isotopic fractionation values (ε)

(Renpenning and Nijenhuis, 2016). The occurrence of limiting steps prior to the reaction step that mask the real magnitude of the ε has been shown when mineral phases are involved in abiotic degradation processes (Elsner et al., 2007). Controlled laboratory studies are thus required to confine the ranges of possible ε values and determine conservative estimates of quantification of CMs degradation extent in the field. The concept of dual element (C−Cl) isotope plots featuring slopes ($\Lambda = \Delta\delta^{13}C/\Delta\delta^{37}Cl$) that are characteristic of different reaction mechanism, holds promise to provide information on the manner and order of chemical bond cleavage for organohalides (Nijenhuis et al., 2016) and this, in turn, may help to distinguish potential competing processes and to assess their individual effectiveness as field remediation strategies (Van Breukelen, 2007). Although some abiotic Λ values for CF were recently published (Heckel et al., 2017a; Torrentó et al., 2017), neither Λ for CT abiotic reactions nor field demonstrations are available.

In a multiple-compound polluted site in Òdena (Catalonia) (Palau et al., 2014), shifts in carbon isotopic composition of CF were attributed to AH (Torrentó et al., 2014) since alkaline conditions (pH ~12) were generated in recharge water concrete-based interception trenches. In contrast, detected shifts in the carbon isotopic composition of CT could not be explained by AH but here, reduction by Fe-bearing materials from the construction wastes used in the trenches could have played an important role (Torrentó et al., 2014). The presence of surficial iron patinas growths and of variable iron amounts in concrete-based aggregates obtained from one of the boreholes was confirmed by Scanning Electron Microscopy with X-ray microanalysis (SEM-EDS) and X-ray fluorescence (XRF) (data not published), but specific mineral phases are still under study.

In order to close this knowledge gap on isotopic data of abiotic CMs reactions and, therefore, to allow better field interpretations such as in the case of Òdena, this study aims at providing dual element isotope data on abiotic degradation of CT and CF by Fe(0) and Fe-bearing minerals with $FeCl_2$(aq) under anoxic conditions at pH 7 and 12. Characterization is based on monitoring the carbon and chloride isotopic composition ($\delta^{13}C$ and $\delta^{37}Cl$) of CF and CT, as well as on detecting volatile dissolved by-products to identify the existence of parallel reaction pathways. Nano-sized Fe(0) was used for CT experiments because it is more reactive than micro-sized Fe(0) (Song and Carraway, 2006). CF experiments at pH 12 were performed with milli-sized Fe(0) to compare the pH effect with published pH 7 experiments (Torrentó et al., 2017). Py and Mag were chosen as Fe-bearing minerals because they involve different potential redox species for reaction with CMs (Fe(II), and S_2^{2-} in Py, according to Kriegman-King and Reinhard (1994) and represent widespread oxidation products of Fe(0) in PRBs (He et al., 2015) and mining or industrial wastes, which are potential recyclable materials for remediation.

2. Materials and methods

2.1. Experimental setup

Experiments were prepared in an anaerobic chamber and performed in 42 mL VOA/EPA glass vials capped with PTFE-coated rubber stoppers and plastic screw caps. A summary of

experiment nomenclature, amendments and concentrations, incubation parameters representative of typical environmental conditions and performed analyses is provided in Table 1, together with data from already published CF experiments with milli-sized Fe(0) at pH 7 (Torrentó et al., 2017) for the sake of comparison. After the addition of the solid phase, vials were completely filled with buffered aqueous solution (at pH 7 or 12) without headspace, except for CT experiments with nano-sized Fe(0), for which the vials contained 21 mL liquid phase and 21 mL gas phase. For Mag and Py batches, $FeCl_2(aq)$ was also added to the buffered solution to better mimic field conditions, and because it is thought that CT degradation reactions can be surface-mediated by Fe(II) sorbed to solid phases (Scherer et al., 1998; Amonette et al., 2000; Pecher et al., 2002; Elsner et al., 2004). Bottles with 0.6 mM of $FeCl_2(aq)$ and without Fe-minerals (named as 'aq') were prepared as reactive controls for the potential of $FeCl_2(aq)$ for CMs degradation. Controls (CO) with only buffered solution at the corresponding pH were prepared to observe losses or effects of the pH itself on CF transformation. The reaction started with the addition of pollutant pure phase to reach the initial theoretical concentration. Vials were placed in horizontal shakers at room temperature until sampling.

Replicates (n vials) were prepared for each experiment and reaction vials were sacrificed at appropriate time intervals. The CT experiments with nano-sized Fe(0) were conducted in triplicate and headspace samples were taken from each single vial at appropriate time intervals. Concentration and C and Cl isotope ratios of parent compounds and potential by-products were monitored over time. The used analytical methods are included in Table 1.

Although Eh could not be monitored, it would be assumed below 0 V, postulated as the boundary for anoxic conditions (Morris et al., 2003; Hosono et al., 2011). At these Eh conditions, Fe(0) (and Py to a lesser extent) is not stable at pH 7 neither 12 (Fig. S1). Thermodynamically, Fe(0) oxidation should occur and electron release should be expected. More details about chemicals, minerals and Fe(0) preparation and characterization, sampling, samples preservation and analytical methods are available in the Supplementary Information (SI).

3. Results and discussion

In the following sections, isotope results for CF and CT degradation by the Fe(0), Mag, Py and $FeCl_2(aq)$ are presented (Table 2)

Table 1
Summary of performed experiments nomenclature, conditions, procedure and analyses. The equipment used for each analysis is specified. n.u = not used in the experiment, n.a. = not analyzed.

Pollutant	pH	Name	Pollutant concentration (mM)	Fe(0)/ mineral loading (m²/L)	FeCl₂ (mM)	n vials	Incubation temperature (°C)	Incubation time (days)	Shaker	By-products analyses	δ¹³C analyses of parent compounds and by-products	δ³⁷Cl analyses of parent compounds	Ref.
CT	7	CT_Fe_7	2.6	28	n.u	1	25 ± 2	0.1	Horizontal[a] 300 rpm	VOCs HS-GC-qMS-1[d] as described in Heckel et al. (2017b)	HS-GC-IRMS-2[d] as described in Cretnik et al. (2013)	HS-GC-IRMS-2[d] as described in Heckel et al. (2017b)	This study
	12	CT_Fe_12				1	25 ± 2	0.1	Horizontal[a] 300 rpm				
	7	CT_aq_7	0.3	n.u	0.6	9	17.4 ± 0.3*	11	Horizontal[b] 100 rpm	VOCs, CS₂ HS-GC-MS[e] as described in Torrentó et al. (2017)	SPME-HS-GC-IRMS-1[e] as described in Martín-González et al. (2015)	HS-GC-qMS-2[f] as described in Heckel et al. (2017b) (n.a. for CT_Mag_7)	
	12	CT_aq_12				11	19.2 ± 0.4*	9					
						5	20 ± 2*	0.9					
	7	CT_Mag_7	0.3	17	0.6	20	15 ± 3*	11					
	12	CT_Mag_12			0.6	20	20 ± 2*	9					
	7	CT_Py_7	0.3	59	0.6	20	18.7 ± 0.3*	4					
	12	CT_Py_12			0.6	19	20 ± 1*	7					
						20	20.2 ± 0.1*	1					
CF	7	CF_CO_7	0.9	n.u.	n.u	6	25 ± 2	2	Horizontal[c] 200 rpm	VOCs HS-GC-TOF-MS[d] as described in Torrentó et al. (2017)	SPME-HS-GC-IRMS-1[e] as described in Martín-González et al. (2015)	HS-GC-IRMS-2[d] as described in Heckel et al. (2017b)	Torrentó et al. (2017)
	12	CF_CO_12	0.4	n.u	n.u	12	25 ± 2	9					This study
	7	CF_Fe_7	0.9	77	n.u	20	25 ± 2	2					Torrentó et al. (2017)
	12	CF_Fe_12	0.4			20	25 ± 2	9					This study
	7	CF_aq_7	0.4	n.u	0.6	9	17.4 ± 0.5*	8	Horizontal[b] 100 rpm	VOCs, CS₂ HS-GC-MS[e] as described in Torrentó et al. (2014)		HS-GC-qMS-2[f] as described in Heckel et al. (2017b)	
	12	CF_aq_12				10	17.2 ± 0.7*	23					
	7	CF_Mag_7	0.4	17	0.6	19	17.0 ± 0.5*	21				n.a.	
	12	CF_Mag_12				20	17.0 ± 0.6*	23					
	7	CF_Py_7	0.4	59	0.6	19	18 ± 1*	21				HS-GC-qMS-2[f] as described in Heckel et al. (2017b)	
	12	CF_Py_12				20	17.4 ± 0.5*	22				n.a.	

Equipment abbreviations correspond to headspace (HS)-gas chromatography (GC)- mass spectrometry (MS); HS-GC coupled to a time-of-flight (TOF) MS; GC quadrupole MS (GC-qMS); GC coupled to a isotope ratio mass spectrometer (GC-IRMS).
*Spot measurement when sampling.
[a] R1000 ROTH.
[b] Denlay Instruments LTD nº 941157.
[c] IKA KS 260 BASIC.
[d] In Institute of Groundwater Ecology of *Helmholtz Zentrum (München)*.
[e] In *Universitat de Barcelona*.
[f] In *Université de Neuchâtel*.

Table 2
Summary of isotope results, identified by-products and hypothesized degradation pathways. Uncertainty of ε, AKIE and Λ ($\Delta\delta^{13}C/\Delta\delta^{37}Cl$) values corresponds to the 95% confidence intervals. AKIEs were calculated assuming C—Cl bond cleavage in the first rate-limiting reaction step. $AKIE_C$ values for CT and CF were calculated with $z = x = n = 1$ and $AKIE_{Cl}$ values with $z = x = n = 4$ for CT and of $z = x = n = 3$ for CF (Calculations in SI). Question marks indicate hypothesized pathways not proved in this research.

Experiment	By-products*	ε (‰)	AKIE	Λ	Removal (%)	Proposed pathway
CT_Fe_7	CF	$\varepsilon C = -3.7 \pm 0.1$ $R^2 = 0.995$ $\varepsilon Cl = -0.58 \pm 0.04$ $R^2 = 0.98$	$AKIE_C = 1.0037 \pm 0.0001$ $AKIE_{Cl} = 1.00233 \pm 0.00004$	6.1 ± 0.5 $R^2 = 0.98$	99	Hydrogenolysis
CT_Fe_12	CF	$\varepsilon C = -3.4 \pm 0.1$ $R^2 = 0.993$ $\varepsilon Cl = -0.55 \pm 0.03$ $R^2 = 0.98$	$AKIE_C = 1.0034 \pm 0.0001$ $AKIE_{Cl} = 1.00220 \pm 0.00003$	5.8 ± 0.4 $R^2 = 0.98$	99	Hydrogenolysis
CT_aq_7	n.d.	no degradation				
CT_aq_12	CF	$\varepsilon C = -3 \pm 3$ $R^2 = 0.50$	$AKIE_C = 1.003 \pm 0.003$	High confidence interval	87	Hydrogenolysis
CT_Mag_7	n.d.	no degradation				
CT_Mag_12	CF	$\varepsilon C = -2 \pm 1$ $R^2 = 0.70$ $\varepsilon Cl = -0.8 \pm 0.2$ $R^2 = 0.93$	$AKIE_C = 1.002 \pm 0.001$ $AKIE_{Cl} = 1.0032 \pm 0.0002$	2 ± 1 $R^2 = 0.65$	98	Hydrogenolysis ± hydrolytic reduction?
CT_Py_7	CF, CS_2	$\varepsilon C = -5 \pm 2$ $R^2 = 0.70$ $\varepsilon Cl = -1.5 \pm 0.4$ $R^2 = 0.8$	$AKIE_C = 1.005 \pm 0.002$ $AKIE_{Cl} = 1.0060 \pm 0.0004$	2.9 ± 0.5 $R^2 = 0.9$	99	Hydrogenolysis and thiolytic reduction
CT_Py_12	CF, CS_2	$\varepsilon C = -4 \pm 1$ $R^2 = 0.87$ $\varepsilon Cl = -0.9 \pm 0.4$ $R^2 = 0.84$	$AKIE_C = 1.004 \pm 0.001$ $AKIE_{Cl} = 1.0036 \pm 0.0004$	3.7 ± 0.9 $R^2 = 0.93$	99	Hydrogenolysis and thiolytic reduction
CF_CO_7	n.d.	no degradation				
CF_CO_12	n.d.	n.c.	n.c			Partly by AH±reductive elimination?
CF_Fe_7[a]	DCM	$\varepsilon C = -33 \pm 11$ $R^2 = 0.82$ $\varepsilon Cl = -3 \pm 1$ $R^2 = 0.85$	$AKIE_C = 1.034 \pm 0.012$ $AKIE_{Cl} = 1.008 \pm 0.001$	8 ± 2 $R^2 = 0.93$	84	Hydrogenolysis ± reductive elimination?
CF_Fe_12	DCM	$\varepsilon C = -20 \pm 9$ $R^2 = 0.62$ $\varepsilon Cl = -2 \pm 1$ $R^2 = 0.64$	$AKIE_C = 1.020 \pm 0.009$ $AKIE_{Cl} = 1.006 \pm 0.001$	8 ± 1 $R^2 = 0.92$	85	Hydrogenolysis ± reductive elimination?
CF_aq_7	n.d.	no degradation				
CF_aq_12	n.d.	$\varepsilon C = -16 \pm 13$ $R^2 = 0.70$	$AKIE_C = 1.02 \pm 0.01$	$\delta^{37}Cl$ values n.a.	60	Partly by AH ± reductive elimination?
CF_Mag_7	n.d.	no degradation				
CF_Mag_12	n.d.	$\varepsilon C = -16 \pm 9$ $R^2 = 0.65$	$AKIE_C = 1.016 \pm 0.009$	$\delta^{37}Cl$ values n.a.	80	Partly by AH ± reductive elimination?
CF_Py_7	n.d.	no degradation				
CF_Py_12	DCM	$\varepsilon C = -20 \pm 7$ $R^2 = 0.85$	$AKIE_C = 1.020 \pm 0.007$	$\delta^{37}Cl$ values n.a.	62	Hydrogenolysis ± reductive elimination and partly by AH?

*Potential gas by-products such as CO, CO_2, CH_4 or formate were not analyzed. n.c. = not calculated, n.d. = not detected; n.a. = not analyzed.
[a] From Torrentó et al. (2017).

and compared with literature data. Concentrations were lower than expected in some experiments probably due to sorption on non-reactive sites of initial or newly formed solid phases as observed by other authors (Burris et al., 1995, 1998; Kim and Carraway, 2000; Song and Carraway, 2006). pH was constant for all experiments (SD < 0.5) except for CF_Mag_12, CF_Py_12, CT_aq_7, CT_Mag_7 (Fig. S2) where higher fluctuations might be attributable to iron corrosion processes and $Fe(OH)_3$(am) formation.

3.1. Degradation study by Fe(0)

At both pH 7 and 12, CT concentration decrease below the detection limit in experiments with nano-sized Fe(0) was achieved before 4 h (Fig. 1A) and followed a pseudo-first-order kinetic law with rate constant values k_{SA} of $(4.9 \pm 0.6) \times 10^{-2}$ and $(4.4 \pm 0.1) \times 10^{-2}$ $Lm^{-2}h^{-1}$, respectively (Table S1). pH effect on k_{SA} was minimal as expected by thermodynamics, since E^0 of Fe(0) transformation to Fe(II) does not depend on pH.

Significant shifts in $\delta^{13}C_{CT}$ and $\delta^{37}Cl_{CT}$ were detected after 99.4% and 98.6% of CT removal at pH 7 and 12, respectively (Fig. 1B and C), resulting in very similar εC_{CT} (-3.7 ± 0.1, $R^2 = 0.995$ and -3.4 ± 0.1,

$R^2 = 0.993$, respectively, see Eq. S4 and Fig. S3) and εCl_{CT} values (-0.58 ± 0.04, $R^2 = 0.98$ and -0.55 ± 0.03, $R^2 = 0.98$, respectively). Calculated $AKIE_C$ values (Eq. S5) were therefore also similar at pH 7 (1.0037 ± 0.0001) and 12 (1.0034 ± 0.0001) as for $AKIE_{Cl}$ values (1.0023 ± 0.0004 and 1.00220 ± 0.00003, respectively) (Table S2). These similarities regardless of pH confirmed that pH affects primarily intermediate [$\cdot CCl_3$] radical reactions rather than the initial rate-limiting step (Zwank et al., 2005). AKIEs values were below 50% of the Streitwieser limit for a C—Cl bond cleavage ($KIE_C = 1.057$, $KIE_{Cl} = 1.013$) (Elsner et al., 2005) and also below all reported values for abiotic and biotic reductive dechlorination of chlorinated compounds (Table S2), indicating significant mass transfer masking effects. CT is rapidly reduced when contacting a strong reducing agent like Fe(0) and, thus, the rate-limiting step of the reaction might be the diffusion of CT through the solution to the Fe(0) surface rather than the C—Cl bond cleavage (Arnold et al., 1999). In our experiments, this diffusion control could have been enhanced by the low concentration of CT (2.6 mM) compared to Fe(0) loading (28 m^2/L), but further research would be needed to confirm this hypothesis.

The use of HEPES in the pH 7 experiments might constrain exact

CT EXPERIMENTS
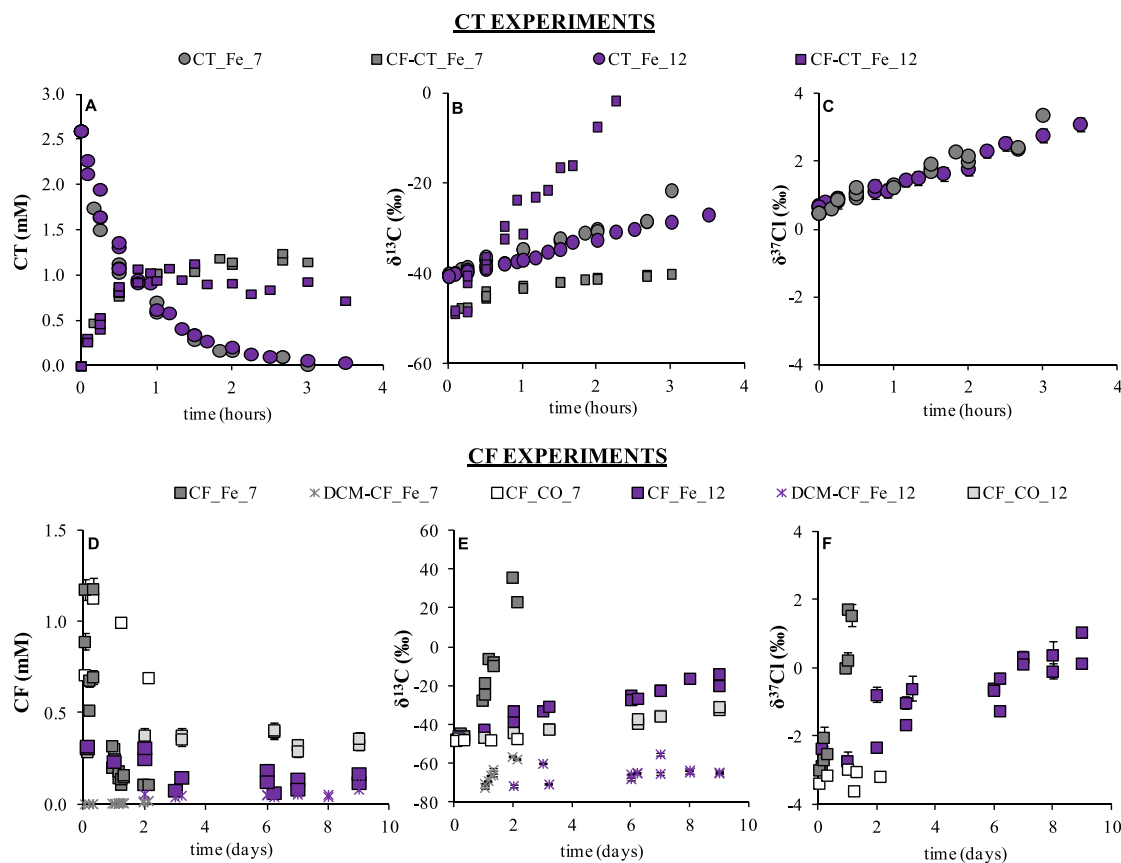
CF EXPERIMENTS

Fig. 1. Concentration (A, D), carbon (B, E) and chlorine (C, F) isotope composition (δ^{13}C and δ^{37}Cl, ‰) over time in the CT (upper panels) and CF (lower panels) experiments at pH 7 and 12 with Fe(0) and control CF experiments (CO). CF_Fe_7 and CF_CO_7 data from Torrentó et al. (2017), and concentration and δ^{13}C evolution of CF and DCM as CT and CF by-products, respectively, are also shown. δ^{37}Cl data of by-products are not available. Error bars are smaller than symbols.

quantitative by-product distribution as it appears to alter by-product formation acting as possible H• radical donor and favoring CF formation (Elsner et al., 2004; Danielsen et al., 2005). However, by-product distribution study was not the aim of this work and by-products different from VOCs such as CH$_4$, CO, CO$_2$ (Lien and Zhang, 1999; Choe et al., 2001; Song and Carraway, 2006), were not analyzed. CF (45—56%) and DCM (up to 0.3% of initial CT) were detected as by-products at pH 7 and 12, after 99% of CT degradation, similarly to what was reported previously (Helland et al., 1995; Támara and Butler, 2004; Song and Carraway, 2006; Lien et al., 2007; Feng et al., 2008), which confirms CT and CF hydrogenolysis. Isotopic mass balances showed a maximum $\Delta\delta^{13}$C$_{SUM}$ (defined as final δ^{13}C$_{SUM}$, Eq. S6, with respect to initial δ^{13}C$_{SUM}$ considering, CT and by-product CF data) of only +1.5‰ at pH 7, compared to +35‰ at pH 12. Thus, at pH 7, CF degradation to other by-product different from DCM was insignificant in the present experimental conditions and duration (3.5 h). At pH 12, however, important further CF degradation (and a possible formation of other CT by-products) was evidenced by $\Delta\delta^{13}$C$_{SUM}$, $\Delta\delta^{13}$C and more enriched δ^{13}C$_{CF}$ values than those δ^{13}C$_{CT}$ values of the parental CT (Fig. 1B).

As carbon and chlorine CT isotope fractionation is affected to the same extent by the above-mentioned masking effects, in a C—Cl dual plot these effects cancel out. As shown in Fig. 2A, Λ values obtained at pH 7 and 12 are similar (6.1 ± 0.5, R^2 = 0.98 and 5.8 ± 0.4, R^2 = 0.98, respectively), and indicative of CT hydrogenolysis attending to CF formation. The above-mentioned closed mass balances in CT_Fe_7 and the similar Λ at both pH revealed that CT hydrogenolysis by Fe(0) might also be the main pathway at

pH 12. Moreover, if CT parallel pathways occur at pH 12, they should involve one C—Cl bond cleavage as hydrogenolysis does (Scheme S1). The obtained Λ values for CT degradation by Fe(0) show no statistically significant difference (with statistical significance at the p < 0.05 level, ANCOVA, p = 0.8) to that reported for biotically-mediated CT anaerobic degradation detected in field-derived microcosms (6.1 ± 0.5) (Rodríguez-Fernández et al., 2018).

The CF_Fe_12 experiments were carried out to complement existing data at pH 7 with milli-sized Fe(0) (Torrentó et al., 2017) (CF_Fe_7 in Table 1) and to provide, thereby, a more comprehensive picture of isotope effects in CF reduction by Fe(0). The corresponding control experiment without Fe(0) (CF_CO_12) showed certain variation in CF concentration (Fig. 1D) and although no VOCs by-products were detected, a significant δ^{13}C$_{CF}$ shift of +17.6‰ was shown after 9 days (Fig. 1E). Since no isotopic changes occurred in previously reported CF_CO_7 (Torrentó et al., 2017), the results of CF_CO_12 experiment suggest that CF was degraded by AH. Assuming this was the only degradation fractionation process, the CF transformation extent by AH in CF_CO_12 was estimated to be 27 ± 7% using Eq. S7 and the ϵ_C of −57 ± 5‰ obtained by Torrentó et al. (2017). This extent of degradation fits well with the reported CF hydrolysis rates (Torrentó et al., 2014, 2017).

In the CF_Fe_12 experiment, CF degradation was also evidenced. CF concentration decreased with some fluctuations (Fig. 1D) causing poor correlation in rate constant k_{SA} ((1.4 ± 0.6) × 10^{-3} Lm^{-2}d^{-1}, R^2 = 0.67, Table S1) and ϵ calculations (ϵC$_{CF}$ = −20 ± 9 R^2 = 0.62 and ϵCl$_{CF}$ = −2±1, R^2 = 0.64) (Fig. S4). Hence, comparison to CF_Fe_7 and literature data was based on evaluation of Λ values.
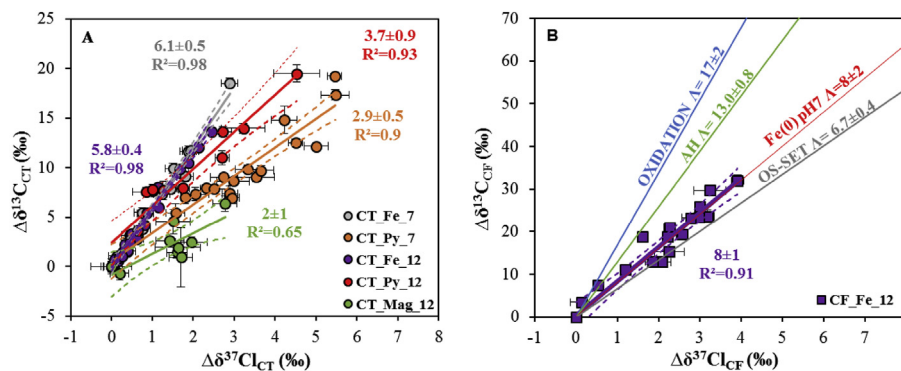
Fig. 2. Dual C–Cl isotope plot for CT (A) and CF (B) abiotic experiments. Same coloured solid and dashed lines correspond to linear regressions of the data sets of this study and 95% CI, respectively. Error bars show uncertainty in duplicate isotope measurements except for CT_Fe_7 and CT_Fe_12 experiments, where 0.5‰ and 0.2‰ were considered for $\delta^{13}C$ and $\delta^{37}Cl$, respectively. In some cases, error bars are smaller than symbols. Solid slopes in B correspond to CF abiotic degradation reference systems: oxidation by thermally-activated persulfate (blue), alkaline hydrolysis, AH (green), dechlorination by Fe(0) at pH 7 (red) (Torrentó et al., 2017) and reductive outer-sphere electron transfer by CO_2 radical anions, OS-SET (grey) (Heckel et al., 2017a). (For interpretation of the references to colour in this figure legend, the reader is referred to the Web version of this article.)

In this experiment, a moderated DCM accumulation was detected as by-product ($\leq 0.3\%$ yield after 9 days). This, together with the slower CF consumption in CF_Fe_12 compared to CF_Fe_7 (Fig. 1D), could be explained by Fe(0) surface passivation due to Fe-oxyhydroxides precipitation, enhanced at alkaline pH (Farrell et al., 2000; Támara and Butler, 2004). Low $\Delta\delta^{13}C_{DCM}$ was measured at pH 12 ($+16‰$ after 85% of CF removal) (Fig. 1E) similar to pH 7 ($+15‰$, after 87% of CF removal, Torrentó et al., 2017). The $\Delta\delta^{13}C_{SUM}$ (taking into account CF and DCM data) at pH 12 was only around $+10‰$, which might suggest an isotope-branching from CF or its intermediates (Zwank et al., 2005), that might have produced the low DCM carbon isotope fractionation observed for both pH.

The Λ value for CF_Fe_12 was 8 ± 1 ($R^2 = 0.91$), not significantly different from that of Torrentó et al. (2017) for CF_Fe_7 ($p = 0.05065$) (Fig. 2B). Combining the data at pH 7 and 12, the Λ value is not significantly different from that of CF reaction in model systems for outer-sphere single electron transfer (OS-SET) ($p = 0.1056$) (Heckel et al., 2017a), suggesting a concerted C–Cl bond cleavage, involving OS-SET in the first rate-limiting step. For CF-Fe_7, Torrentó et al. (2017) postulated two parallel CF dechlorination pathways (hydrogenolysis and reductive elimination) as reported for other CF reduction studies with micro-sized Fe(0) (Matheson and Tratnyek, 1994; Feng and Lim, 2005; Song and Carraway, 2006). In the present experiments, CF reductive elimination related by-products (e.g. CH_4, CO and $HCOO^-$) were not analyzed, and thus, further conclusions are limited. The similar Λ values for Fe(0) are far from the $\Lambda = 13.0 \pm 0.8$ for CF AH (Torrentó et al., 2017), indicating that AH in CF_Fe_12 was negligible. Accordingly, negligible contribution of AH was evidenced by assessing the distribution (F) of AH and dechlorination by Fe(0) to the total CF degradation following Van Breukelen (2007) and using Eq (S8) and ε data from Torrentó et al. (2017).

3.2. Degradation study by FeCl2(aq) and Mag

Despite concentration fluctuations (Fig. 3A), no significant $\delta^{13}C_{CT}$ shifts over time were observed in the CT_aq_7 and CT_Mag_7 experiments ($-41.9 \pm 0.5‰$, $n = 9$ and $-41.4 \pm 0.5‰$, $n = 6$, respectively, Fig. 3B) and no VOCs by-products were detected. CT degradation therefore does not seem to occur in these experiments. In fact, the analogous experiments with CF at pH 7 neither showed also significant changes in $\delta^{13}C_{CF}$ ($-49.2 \pm 0.2‰$, $n = 5$, and $-49.0 \pm 0.6‰$, $n = 7$, for CF_Mag_7 and CF_aq_7 experiments, respectively) (Fig. 3B). This agrees with the decrease in the degradation efficiency of aged Fe(0) PRBs when Mag is formed through

corrosion (Vodyanitskii, 2014). However, CT degradation by Mag has been previously reported in the literature under different experimental conditions (Zwank et al., 2005; Hanoch et al., 2006; Maithreepala and Doong, 2007; Vikesland et al., 2007). Further discussion about this discrepancy can be found in the SI.

In contrast, at pH 12, CT degradation occurred and kinetics of CT_Mag_12 and CT_aq_12 followed a pseudo-first-order rate law with a k_{SA} of $(8 \pm 5) \times 10^{-2} Lm^{-2}d^{-1}$ and k' of $0.3 \pm 0.2 d^{-1}$, respectively (Table S3). CT degradation was confirmed by significant $\Delta\delta^{13}C_{CT}$ (Fig. 3E) and $\Delta\delta^{37}Cl_{CT}$ (Fig. 3F) after 87 and 98% CT removal in the CT_aq_12 and CT_Mag_12 experiments, respectively, obtaining $\varepsilon C_{CT} = -2\pm1‰$ ($R^2 = 0.7$) and $\varepsilon Cl_{CT} = -0.8 \pm 0.2‰$ ($R^2 = 0.93$) for CT_Mag_12 (Fig. S6) and $\varepsilon C_{CT} = -2\pm3‰$ for CT_aq_12, but with poor linear regression ($R^2 = 0.5$) (Fig. S7). AKIE$_C$ (1.002 ± 0.0001) and AKIE$_{Cl}$ (1.0032 ± 0.0002) values of CT_Mag_12 were well below 50% of the Streitwieser limit for a C–Cl bond cleavage (Elsner et al., 2005) and also below the reported values for abiotic and biotic reductive dechlorination of chlorinated compounds (Table S2), suggesting significant mass transfer masking effects as for Fe(0). A maximum CF yield of $+38\%$ and $+26\%$ in CT_Mag_12 and CT_aq_12, respectively (Fig. S5), evidenced CT hydrogenolysis. $\delta^{13}C$ enrichment in the produced CF was detected. To further study CF degradation, analogous experiments with CF at pH 12 were performed and showed a CF concentration decrease to values down to $0.2–0.1$ mM after 23 days (Fig. 3D). Obtained pseudo-first-order rate constants had poor correlation ($k' = (6 \pm 3) \times 10^{-2}$ d^{-1}, $R^2 = 0.6$, for CF_aq_12 and $k_{SA} = (6 \pm 2) \times 10^{-3} Lm^{-2}d^{-1}$, $R^2 = 0.7$, for CF_Mag_12, Table S3). In both experiments at pH 12, degradation was confirmed by $\delta^{13}C$ shifts (Fig. 3E). Comparing with the absence of CF degradation in the pH 7 analogous experiments, AH could be assumed as the main degradation pathway in these experiments (Torrentó et al., 2017). However, despite poor regression, the obtained values of εC_{CF} for CF_Mag_12 ($-16 \pm 9‰$, $R^2 = 0.65$) and CF_aq_12 ($-16 \pm 13‰$, $R^2 = 0.70$) (Fig. S6, S7) are in the range for CF reductive dechlorination studies (Table S2) and far away from the reported values for CF AH at pH 12 ($-57 \pm 5‰$) (Torrentó et al., 2017). These results suggest the occurrence of additional parallel pathways (such as CF reductive elimination to CH_4) (Scheme S1). Since nor CF Cl isotope ratios neither other non-chlorinated potential by-products were measured in these experiments, further conclusions cannot be drawn.

The calculated Λ value for CT_aq_12 (2 ± 3, $R^2 = 0.67$) was discarded due to its wide confidence interval, while that for CT_Mag_12 (2 ± 1, $R^2 = 0.65$) (Fig. 2A) was, despite its poor linear
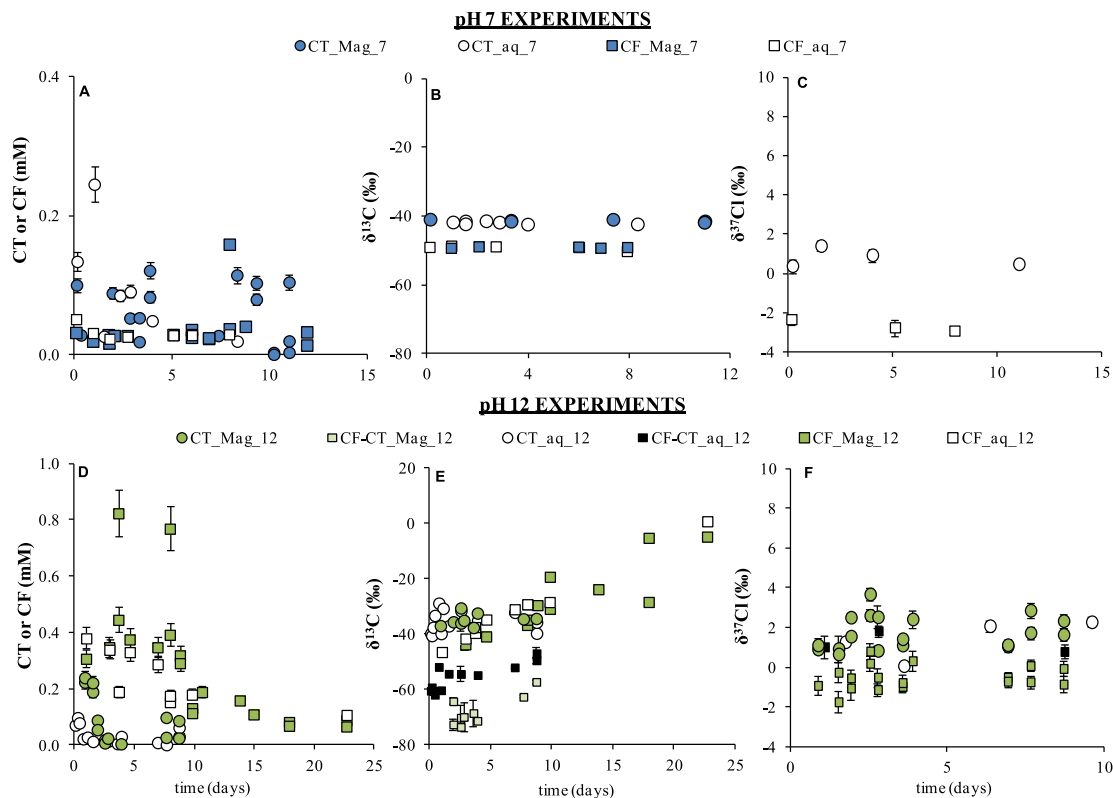
Fig. 3. Concentration (A, D) and carbon (B, E) and chlorine (C, F) isotope composition (δ^{13}C and δ^{37}Cl, ‰) over time in the CT and CF experiments at pH 7 (upper panels) and 12 (lower panels) with magnetite and FeCl$_2$(aq)(Mag) and FeCl$_2$(aq)alone (aq). Isotope data of by-products of each experiment are also shown and named as 'by-product-experiment name' to distinguish them from experiments where those compounds are parental compounds. In some cases, error bars are smaller than symbols.

regression, highly statistically different (p < 0.0001) from those of CT_Fe_7 and CT_Fe_12. It suggests that although CF was formed as by-product in both Fe(0) and Mag CT experiments, parallel pathways other than hydrogenolysis could have occurred in CT_Mag_12. Also, a different first rate-determining step between reactions such as that producing CF or CO (hypothesized by-product by CT hydrolytic reduction according to Danielsen and Hayes (2004) might have occurred. That case would question whether branching in trichloromethyl free radical [·CCl$_3$] or trichlorocarbanion [:CCl$_3^-$] intermediates (Scheme S1) were responsible for by-products distribution (Danielsen and Hayes, 2004; Elsner et al., 2004; Zwank et al., 2005) because intermediates branching alone would have not affected CT isotope fractionation and Λ would have been similar. Differences in Λ value might be also explained by a change in transition states in mineral surfaces (Elsner et al., 2004).

The absence of CT degradation at pH 7 compared to pH 12, might be attributed to the control that pH exerts on Mag reactivity (see SI for further discussion). Under our experimental conditions, CT degradation by FeCl$_2$(aq) and Mag was only feasible under alkaline conditions. Although further field research would be required, Mag might be responsible of δ^{13}C$_{CT}$ fractionation detected in the alkaline trenches of the Òdena field site (Torrentó et al., 2014) given that Mag is an ubiquitous mineral, commonly present in construction wastes.

3.3. Degradation study by Py

CT concentrations in CT_Py_7 and CT_Py_12 decreased quickly, especially at pH 12 where they reached 0.01 mM after 4 h (Fig. 4A, D). Although poor correlated, degradation followed a pseudo-first-

order rate law for CT_Py_7 (k_{SA}=(1.6 ± 0.6) × 10^{-2} Lm^{-2}d^{-1}, R^2 = 0.72) and CT_Py_12 ((2 ± 1) × 10^{-2} Lm^{-2}d^{-1}, R^2 = 0.6), (Table S3). CT degradation was confirmed at both pH by enrichment in ^{13}C and ^{37}Cl (Fig. 4). Calculated εC$_{CT}$ and εCl$_{CT}$ values were −5±2‰ (R^2 = 0.7) and −1.5 ± 0.4‰ (R^2 = 0.8), respectively for CT_Py_7 (Fig. S8), and −4±1‰ (R^2 = 0.87) and −0.9 ± 0.4‰ (R^2 = 0.84), respectively for CT_Py_12 (Fig. S9). Corresponding AKIE$_C$ (1.005 ± 0.002 and 1.004 ± 0.001, respectively) and AKIE$_{Cl}$ values (1.0060 ± 0.0004 and 1.0036 ± 0.0004, respectively) indicate significant mass transfer masking effects for the same reasons than for Fe(0) and Mag experiments. Poor correlation in CT_Py_7 might be linked to the low pH reached (4.7 ± 1.1, Fig. S2) that might have caused changes in Py surface (Bonnissel-Gissinger et al., 1998) affecting CT degradation.

In both experiments, the formation of by-products CF and CS$_2$ was observed (Fig. S5) agreeing with literature (Kriegman-King and Reinhard, 1994; Devlin and Muller, 1999). Analogous experiments with Py and CF as parent compound demonstrated no CF degradation at pH 7 (δ^{13}C$_{CF}$ = −49.1 ± 0.3‰, δ^{37}Cl$_{CF}$ = −3.1 ± 0.3‰, n = 7). At pH 12, however, CF degradation was evidenced by a clear CF concentration decrease (k_{SA}=(2 ± 1) × 10^{-2} Lm^{-2}d^{-1}, R^2 = 0.6), a significant carbon isotope enrichment (εC$_{CF}$ = −20 ± 7‰, R^2 = 0.85) (Fig. S9) and up to a 6% DCM yield (Fig. S5). Py oxidation at pH 12 by CF is an unknown process but, by analogy to CT (Kriegman-King and Reinhard, 1992, 1994), it would follow Eq. (1), with an overall reaction potential higher at pH 12 (0.7 V) than at pH 7 (0.5 V).

$$FeS_2 + CHCl_3 + 8H_2O \rightarrow Fe^{2+} + 2SO_4^{2-} + CH_2Cl_2 + Cl^- + 15H^+ + 12e^-$$

(1)
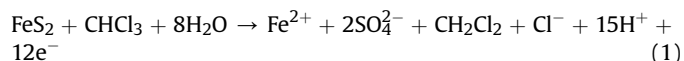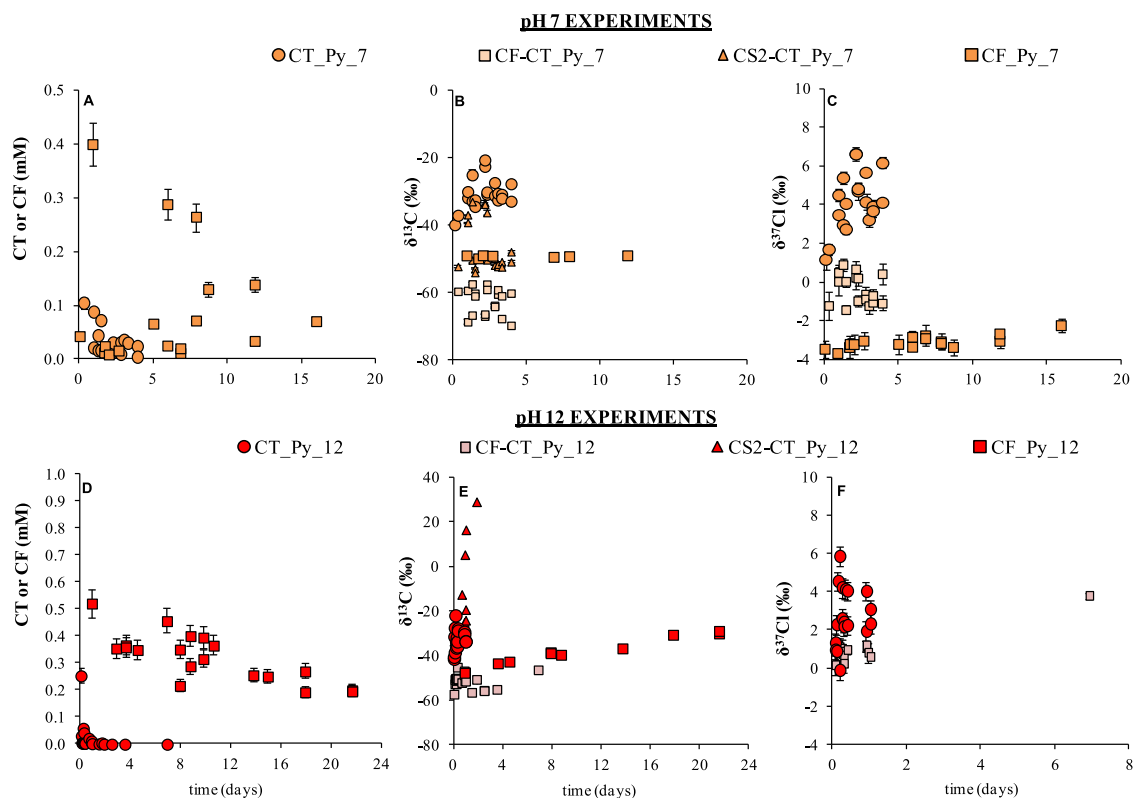
Fig. 4. Concentration (A, D) and carbon (B, E) and chlorine (C, F) isotope composition ($\delta^{13}C$ and $\delta^{37}Cl$, ‰) over time in the CT and CF experiments at pH 7 (upper panels) and 12 (lower panels) with pyrite (Py) and FeCl$_2$(aq). Isotope data of by-products of each experiment are also shown and named as 'by-product-experiment name' to distinguish them from experiments where those compounds are parental compounds. In some cases, error bars are smaller than symbols.

The accumulation of DCM (Fig. S5) suggests that hydrogenolysis together with AH might be responsible for CF carbon isotope fractionation. Since $\delta^{37}Cl$ was not measured in this experiment, quantification of each pathway following Eq. (S8) is not possible.

The detected CS$_2$ in the CT experiments with Py (Fig. S5) may form via aqueous or adsorbed HS$^-$ (Kriegman-King and Reinhard, 1992) or via S$_2^{2-}$ sites on Py surface acting as electron donor (Kriegman-King and Reinhard, 1994). Despite fluctuations, shifts in $\delta^{13}C_{CS2}$ values (Fig. 4B) and non-closed isotopic mass balance calculations at pH 7 ($\delta^{13}C_{SUM}$ range from −44 to −59‰) might reveal further CS$_2$ degradation since, as mentioned above, these shifts in $\delta^{13}C_{SUM}$ cannot be attributed to CF degradation. At pH 12, CS$_2$ degradation was confirmed by the much enriched $\delta^{13}C_{CS2}$ values (+28.8‰) with respect to the initial $\delta^{13}C_{CT}$ after 46 h (Fig. 4E). CS$_2$ degradation might occur through hydrolysis mediated by hydroxide ions at these alkaline conditions (11.8 ± 0.2). CS$_2$ alkaline hydrolysis has been proven at laboratory scale (Svoronos and Bruno, 2002) with rate constants at 25 °C ranging between 10^{-4} and 10^{-3} M^{-1}s^{-1}, equivalent to half-lifes of 1–13 days at pH 11.8. According to literature (Peyton et al., 1976; Adewuyi and Carmichael, 1987; Kriegman-King and Reinhard, 1992, 1994; McGeough et al., 2007), CS$_2$ is stable to hydrolysis within the pH range of 4–10, suggesting Py mediation in the potentially occurring CS$_2$ degradation at pH 7, as Fe(0) involvement has also been reported (McGeough et al., 2007). Further research is needed to clarify this point. In any case, it follows that the previously proposed CF:CS$_2$ mass ratio for distinguishing CT transformations reactions (Devlin and Muller, 1999; Davis et al., 2003) is inappropriate.

The obtained Λ values for CT_Py_7 (2.9 ± 0.5, R^2 = 0.9) and CT_Py_12 experiments (3.7 ± 0.9, R^2 = 0.93) are similar to each other and to that of CT_Mag_12 (p = 0.2302), but they are

statistically different from that of CT hydrogenolysis by Fe(0) experiments at both pH values (p < 0.0001) (Fig. 2A). CT thiolytic reduction evidenced by CS$_2$ formation is thus supported by means of C−Cl Λ. Moreover, since the obtained Λ values in CT_Mag_12 and in CT experiments with Py were similar, a comparable contribution of initial parallel reaction mechanisms for both reactions is hypothesized (hydrolytic and thiolytic reduction, respectively Scheme S1).

4. Conclusions

CT and CF degradation by Fe(0) occurs at pH 7 and 12, with similar C−Cl Λ values at both pH values for each compound (8 ± 2 and 8 ± 1 for CF; 6.1 ± 0.5 and 5.8 ± 0.4 for CT, respectively), pointing in both cases to a hydrogenolysis pathway. Accumulation of recalcitrant DCM in this pathway should be taken into consideration in remediation strategies by PRBs.

Isotope fractionation proved that under our experimental conditions, FeCl$_2$(aq), Mag and Py are effective reducing agents for CT at pH 12, whereas at pH 7 only Py was able to degrade CT. CF was detected as by-product in all CT-degrading experiments, while CS$_2$ was only detected with Py. The occurrence of parallel CT hydrogenolysis and hydrolytic or thiolytic reduction pathways was also evidenced by the dual-plot approach, showing CT experiments with FeCl$_2$(aq) and Mag at pH 12 (2 ± 1) and with Py (2.9 ± 0.5 and 3.7 ± 0.9 at pH 7 and 12) Λ values different than that for hydrogenolysis alone with Fe(0) (6.1 ± 0.5 at pH 7). Further CF and CS$_2$ degradation at pH 12 was confirmed through isotopic tracking, reaffirming that by-products are not always traceable to confirm parent compound degradation. Mag and Py are thus effective minerals for abiotic CT remediation strategies, especially under

alkaline conditions, where the accumulation of harmful by-products is avoided by further degradation. On the contrary, under aquifer conditions, recycling these minerals for cost-effective PRB-building requires ensuring subsequent CF and CS_2 elimination. The studied CMs degradation reactions might be diffusion-controlled under natural field conditions, as it was previously reported (Elsner et al., 2007; Thullner et al., 2013). Thus, due to this isotope masking by rate-limitations in mass transfer, the highest reported ε value should be used for a conservative assessment of CMs degradation extent (Elsner, 2010; Thullner et al., 2012). However, if these minerals or Fe(0) were used as remediation techniques, where a high contaminant/mineral ratio is normally used, the C–Cl bond cleavage might be the rate-limiting step. Nevertheless, further research would be needed to confirm this hypothesis.

To sum up, all the data provided in this dual element C–Cl isotopic approach – especially first-time-published abiotic CT Λ values – in combination with earlier data for CF abiotic (Heckel et al., 2017a; Torrentó et al., 2017) and CT and CF biotic transformation reactions (Rodríguez-Fernández et al., 2018), improve considerably the isotopic database of CMs reactions. This information could be further applied in field studies for discerning the predominant pathway or the contribution of combined pathways in CMs natural attenuation following Van Breukelen (2007) or assessing the effect of remediation treatments over time.

Acknowledgements

Appendix A. Supplementary data

Supplementary data related to this article can be found at https://doi.org/10.1016/j.chemosphere.2018.05.036.

References

Adewuyi, Y.G., Carmichael, G.R., 1987. Kinetics of hydrolysis and oxidation of carbon disulfide by hydrogen peroxide in alkaline medium and application to carbonyl sulfide. Environ. Sci. Technol. 21, 170–177. https://doi.org/10.1021/es00156a602.

Amonette, J.E., Workman, D.J., Kennedy, D.W., Fruchter, J.S., Gorby, Y.A., 2000. Dechlorination of carbon tetrachloride by Fe (II) associated with goethite. Environ. Sci. Technol. 34, 4606–4613. https://doi.org/10.1021/es9913582.

Arnold, W.A., Ball, W.P., Roberts, A.L., 1999. Polychlorinated ethane reaction with zero-valent zinc: pathways and rate control. J. Contam. Hydrol. 40, 183–200. https://doi.org/10.1016/S0169-7722(99)00045-5.

Bonnissel-Gissinger, P., Alnot, M., Ehrhardt, J.J., Behra, P., 1998. Surface oxidation of pyrite as a function of pH. Environ. Sci. Technol. 32, 2839–2845. https://doi.org/10.1021/es980213c.

Breider, F., Albers, C.N., Hunkeler, D., 2013. Assessing the role of trichloroacetyl-containing compounds in the natural formation of chloroform using stable carbon isotopes analysis. Chemosphere 90, 441–448. https://doi.org/10.1016/j.chemosphere.2012.07.058.

Burris, D.R., Campbell, T.J., Manoranjan, V.S., 1995. Sorption of trichloroethylene and tetrachloroethylene in a batch reactive metallic iron-water system. Environ. Sci. Technol. 29, 2850–2855. https://doi.org/10.1021/es00011a022.

Burris, D.R., Allen-King, R.M., Manoranjan, V.S., Campbell, T.J., Loraine, G.A., Deng, B., 1998. Chlorinated ethene reduction by cast iron: sorption and mass transfer. J. Environ. Eng. 124, 1012–1019. https://doi.org/10.1061/(ASCE)0733-9372(1998)124:10(1012).

Cappelletti, M., Frascari, D., Zannoni, D., Fedi, S., 2012. Microbial degradation of chloroform. Appl. Microbiol. Biotechnol. 96, 1395–1409. https://doi.org/10.1007/s00253-012-4494-1.

Choe, S., Lee, S.H., Chang, Y.Y., Hwang, K.Y., Khim, J., 2001. Rapid reductive destruction of hazardous organic compounds by nanoscale Fe^0. Chemosphere 42, 367–372. https://doi.org/10.1016/S0045-6535(00)00147-8.

Cretnik, S., Thoreson, K.A., Bernstein, A., Ebert, K., Buchner, D., Laskov, C., Haderlein, S., Shouakar-stash, O., Kliegman, S., McNeill, K., Elsner, M., 2013. Reductive dechlorination of TCE by chemical model systems in comparison to dehalogenating bacteria: insights from dual element isotope analysis ($^{13}C/^{12}C$, $^{37}Cl/^{35}Cl$). Environ. Sci. Technol. 47, 6855–6863. https://doi.org/10.1021/es400107n.

Danielsen, K.M., Hayes, K.F., 2004. pH dependence of carbon tetrachloride reductive dechlorination by magnetite. Environ. Sci. Technol. 38, 4745–4752. https://doi.org/10.1021/es0496874.

Danielsen, K.M., Gland, J.L., Hayes, K.F., 2005. Influence of amine buffers on carbon tetrachloride reductive dechlorination by the iron oxide magnetite. Environ. Sci. Technol. 39, 756–763. https://doi.org/10.1021/es049635e.

Davis, A., Fennemore, G.G., Peck, C., Walker, C.R., McIlwraith, J., Thomas, S., 2003. Degradation of carbon tetrachloride in a reducing groundwater environment: implications for natural attenuation. Appl. Geochem. 18, 503–525. https://doi.org/10.1016/S0883-2927(02)00102-6.

Devlin, J.F., Muller, D., 1999. Field and laboratory studies of carbon tetrachloride transformation in a sandy aquifer under sulfate reducing conditions. Environ. Sci. Technol. 33, 1021–1027. https://doi.org/10.1021/es9806884.

Elsner, M., Haderlein, S.B., Kellerhals, T., Luzi, S., Zwank, L., Angst, W., Schwarzenbach, R.P., 2004. Mechanisms and products of surface-mediated reductive dehalogenation of carbon tetrachloride by Fe(II) on goethite. Environ. Sci. Technol. 38, 2058–2066. https://doi.org/10.1021/es034741m.

Elsner, M., Zwank, L., Hunkeler, D., Schwarzenbach, R.P., 2005. A new concept linking observable stable isotope fractionation to transformation pathways of organic pollutants. Environ. Sci. Technol. 39, 6896–6916. https://doi.org/10.1021/es0504587.

Elsner, M., Cwiertny, D.M., Roberts, A.L., Sherwood Lollar, B., 2007. 1,1,2,2-Tetrachloroethane reactions with OH⁻, Cr(II), granular iron, and a copper-iron bimetal: insights from product formation and associated carbon isotope fractionation. Environ. Sci. Technol. 41, 4111–4117. https://doi.org/10.1021/es072046z.

Elsner, M., 2010. Stable isotope fractionation to investigate natural transformation mechanisms of organic contaminants: principles, prospects and limitations. J. Environ. Monit. 12, 2005–2031. https://doi.org/10.1039/c0em00277a.

Farrell, J., Kason, M., Melitas, N., Li, T., 2000. Investigation of the long-term performance of zero-valent iron for reductive dechlorination of trichloroethylene. Environ. Sci. Technol. 34, 514–521. https://doi.org/10.1021/es990716y.

Feng, J., Lim, T.T., 2005. Pathways and kinetics of carbon tetrachloride and chloroform reductions by nano-scale Fe and Fe/Ni particles: comparison with commercial micro-scale Fe and Zn. Chemosphere 59, 1267–1277. https://doi.org/10.1016/j.chemosphere.2004.11.038.

Feng, J., Zhu, B.-W., Lim, T.T., 2008. Reduction of chlorinated methanes with nano-scale Fe particles: effects of amphiphiles on the dechlorination reaction and two-parameter regression for kinetic prediction. Chemosphere 73, 1817–1823. https://doi.org/10.1016/j.chemosphere.2008.08.014.

Ferrey, M.L., Wilkin, R.T., Ford, R.G., Wilson, J.T., 2004. Nonbiological removal of cis-dichloroethylene and 1,1-dichloroethylene in aquifer sediment containing magnetite. Environ. Sci. Technol. 38, 1746–1752. https://doi.org/10.1021/es0305609.

Hanoch, R.J., Shao, H., Butler, E.C., 2006. Transformation of carbon tetrachloride by bisulfide treated goethite, hematite, magnetite, and kaolinite. Chemosphere 63, 323–334. https://doi.org/10.1016/j.chemosphere.2005.07.016.

He, Y.T., Wilson, J.T., Su, C., Wilkin, R.T., 2015. Review of abiotic degradation of chlorinated solvents by reactive iron minerals in aquifers. Groundw. Monit. Remed. 35, 57–75. https://doi.org/10.1111/gwmr.12111.

Heckel, B., Cretnik, S., Kliegman, S., Shouakar-Stash, O., McNeill, K., Elsner, M., 2017a. Reductive outer-sphere single electron transfer is an exception rather than the rule in natural and engineered chlorinated ethene dehalogenation. Environ. Sci. Technol. 51, 9663–9673. https://doi.org/10.1021/acs.est.7b01447.

Heckel, B., Rodríguez-Fernández, D., Torrentó, C., Meyer, A., Palau, J., Domènech, C., Rosell, M., Soler, A., Hunkeler, D., Elsner, M., 2017b. Compound-specific chlorine isotope analysis of tetrachloromethane and trichloromethane by gas chromatography-isotope ratio mass spectrometry vs gas chromatography-quadrupole mass spectrometry: method development and evaluation of precision and trueness. Anal. Chem. 89, 3411–3420. https://doi.org/10.1021/acs.analchem.6b04129.

Helland, B.R., Alvarez, P.J.J., Schnoor, J.L., 1995. Reductive dechlorination of carbon tetrachloride with elemental iron. J. Hazard Mater. 41, 205–216. https://doi.org/10.1016/0304-3894(94)00111-S.

Hosono, T., Nakano, T., Shimizu, Y., Onodera, S. ichi, Taniguchi, M., 2011. Hydrogeological constraint on nitrate and arsenic contamination in Asian metropolitan groundwater. Hydrol. Process. 25, 2742–2754. https://doi.org/10.1002/hyp.8015.

Huang, K.C., Zhao, Z., Hoag, G.E., Dahmani, A., Block, P.A., 2005. Degradation of volatile organic compounds with thermally activated persulfate oxidation. Chemosphere 61, 551–560. https://doi.org/10.1016/j.chemosphere.2005.02.032.

Huling, S.G., Pivetz, B.E., 2006. In-situ Chemical Oxidation-engineering Issue. EPA/

600/R-06/072. U.S. Environmental Protection Agency Office of Research and Development, National Risk Management Research Laboratory, Cincinnati, OH.

Hunkeler, D., Laier, T., Breider, F., Jacobsen, O.S., 2012. Demonstrating a natural origin of chloroform in groundwater using stable carbon isotopes. Environ. Sci. Technol. 46, 6096–6101. https://doi.org/10.1021/es204585d.

IARC, 1999. IARC Monographs on the Evaluation of Carcinogenic Risks to Humans, vol. 71, pp. 319–335.

Jeffers, P.M., Ward, L.M., Woytowltch, L.M., Wolfe, N.L., 1989. Homogeneous hydrolysis rate constants for selected chlorinated methanes, ethanes, ethenes, and propanes. Environ. Sci. Technol. 23, 965–969. https://doi.org/10.1021/es0066a006.

Kim, Y.H., Carraway, E.R., 2000. Dechlorination of pentachlorophenol by zero valent iron and modified zero valent irons. Environ. Sci. Technol. 34, 2014–2017. https://doi.org/10.1021/es991129f.

Koenig, J., Lee, M., Manefield, M., 2015. Aliphatic organochlorine degradation in subsurface environments. Rev. Environ. Sci. Bio/Technol. 14, 49–71. https://doi.org/10.1007/s11157-014-9345-3.

Kriegman-King, M.R., Reinhard, M., 1992. Transformation of carbon tetrachloride in the presence of sulfide, biotite, and vermiculite. Environ. Sci. Technol. 26, 2198–2206. https://doi.org/10.1021/es00035a019.

Kriegman-King, M.R., Reinhard, M., 1994. Transformation of carbon tetrachloride by pyrite in aqueous solution. Environ. Sci. Technol. 28, 692–700. https://doi.org/10.1021/es00053a025.

Lee, M., Wells, E., Wong, Y.K., Koenig, J., Adrian, L., Richnow, H.H., Manefield, M., 2015. Relative contributions of Dehalobacter and zerovalent iron in the degradation of chlorinated methanes. Environ. Sci. Technol. 49, 4481–4489. https://doi.org/10.1021/es5052364.

Lien, H.L., Zhang, W.X., 1999. Transformation of chlorinated methanes by nanoscale iron particles. J. Environ. Eng. 125, 1042–1047. https://doi.org/10.1061/(ASCE)0733-9372(1999)125:11(1042).

Lien, H.-L., Jhuo, Y.-S., Chen, L.-H., 2007. Effect of heavy metals on dechlorination of carbon tetrachloride by iron nanoparticles. Environ. Eng. Sci. 24, 21–30. https://doi.org/10.1089/ees.2007.24.21.

Maithreepala, R.A., Doong, R., 2007. Dechlorination of carbon tetrachloride by ferrous ion associated with iron oxide nano particles. In: Proceedings of the Fourth Academic Sessions 2007.

Martín-González, L., Mortan, S.H., Rosell, M., Parladé, E., Martínez-Alonso, M., Gaju, N., Caminal, G., Adrian, L., Marco-Urrea, E., 2015. Stable carbon isotope fractionation during 1,2-dichloropropane-to-propene transformation by an enrichment culture containing Dehalogenimonas strains and a dcpA gene. Environ. Sci. Technol. 49, 8666–8674. https://doi.org/10.1021/acs.est.5b00929.

Matheson, L.J., Tratnyek, P.G., 1994. Reductive dehalogenation of chlorinated methanes by iron metal. Environ. Sci. Technol. 28, 2045–2053. https://doi.org/10.1021/es00061a012.

McGeough, K.L., Kalin, R.M., Myles, P., 2007. Carbon disulfide removal by zero valent iron. Environ. Sci. Technol. 41, 4607–4612. https://doi.org/10.1021/es062936z.

Morris, B.L., Lawrence, A.R.L., Chilton, P.J.C., Adams, B., Calow, C.R., Klinck, B.A., 2003. Groundwater and its Susceptibility to Degradation: a Global Assessment of the Problem and Options for Management. Early Warning and Assessment Report Series, RS. 03–3. United Nations Environment Programma, Nairobi, Kenya. https://doi.org/10.1d017/CBO9781107415324.004.

Nijenhuis, I., Renpenning, J., Kümmel, S., Richnow, H.H., Gehre, M., 2016. Recent advances in multi-element compound-specific stable isotope analysis of organohalides: achievements, challenges and prospects for assessing environmental sources and transformation. Trends Environ. Anal. Chem. 11, 1–8. https://doi.org/10.1016/j.teac.2016.04.001.

Obiri-Nyarko, F., Grajales-Mesa, S.J., Malina, G., 2014. An overview of permeable reactive barriers for in situ sustainable groundwater remediation. Chemosphere 111, 243–259. https://doi.org/10.1016/j.chemosphere.2014.03.112.

Palau, J., Marchesi, M., Chambon, J.C.C., Aravena, R., Canals, À., Binning, P.J., Bjerg, P.L., Otero, N., Soler, A., 2014. Multi-isotope (carbon and chlorine) analysis for fingerprinting and site characterization at a fractured bedrock aquifer contaminated by chlorinated ethenes. Sci. Total Environ. 475, 61–70. https://doi.org/10.1016/j.scitotenv.2013.12.059.

Pecher, K., Haderlein, S.B., Schwarzenbach, R.P., 2002. Reduction of polyhalogenated methanes by surface-bound Fe(II) in aqueous suspensions of iron oxides. Environ. Sci. Technol. 36, 1734–1741. https://doi.org/10.1021/es011191o.

Penny, C., Vuilleumier, S., Bringel, F., 2010. Microbial degradation of tetrachloromethane: mechanisms and perspectives for bioremediation. FEMS Microbiol. Ecol. 74, 257–275. https://doi.org/10.1111/j.1574-6941.2010.00935.x.

Peyton, T.O., Steel, R.V., Mabey, W.R., 1976. Carbon Disulfide, Carbonyl Sulfide: Literature Review and Environmental Assessment (EPA-600/9-78-009). Washington, DC.

Renpenning, J., Nijenhuis, I., 2016. Evaluation of the microbial reductive dehalogenation reaction using Compound-Specific Stable Isotope Analysis (CSIA). In: Adrian, L., Löffler, E.F. (Eds.), Organohalide-respiring Bacteria. Springer Berlin Heidelberg, Berlin, pp. 429–453. https://doi.org/10.1007/978-3-662-49875-0_18.

Rodríguez-Fernández, D., Torrentó, C., Guivernau, M., Viñas, M., Hunkeler, D., Soler, A., Domènech, C., Rosell, M., 2018. Vitamin B$_{12}$ effects on chlorinated methanes-degrading microcosms: dual isotope and metabolically active microbial populations assessment. Sci. Total Environ. 621, 1615–1625. https://doi.org/10.1016/j.scitotenv.2017.10.067.

Scherer, M.M., Balko, B.A., Tratnyek, P.G., 1998. The role of oxides in reduction reactions at the metal-water interface. In: T, G. (Ed.), Kinetics and Mechanisms of Reactions at the Mineral/water Interface. ACS Symposium Series, Division of Geochemistry, Washington, DC, pp. 301–322.

Scheutz, C., Durant, N.D., Hansen, M.H., Bjerg, P.L., 2011. Natural and enhanced anaerobic degradation of 1,1,1-trichloroethane and its degradation products in the subsurface - a critical review. Water Res. 45, 2701–2723. https://doi.org/10.1016/j.watres.2011.02.027.

Song, H., Carraway, E.R., 2006. Reduction of chlorinated methanes by nano-sized zero-valent iron. Kinetics, pathways and effect of reaction conditions. Environ. Eng. Sci. 23, 272–284. https://doi.org/10.1089/ees.2006.23.272.

Svoronos, P.D.N., Bruno, T.J., 2002. Carbonyl Sulfide: a review of its chemistry and properties. Ind. Eng. Chem. Res. 41, 5321–5336. https://doi.org/10.1021/ie020365n.

Támara, M.L., Butler, E.C., 2004. Effects of iron purity and groundwater characteristics on rates and products in the degradation of carbon tetrachloride by iron metal. Environ. Sci. Technol. 38, 1866–1876. https://doi.org/10.1021/es0305508.

Thullner, M., Centler, F., Richnow, H.H., Fischer, A., 2012. Quantification of organic pollutant degradation in contaminated aquifers using compound specific stable isotope analysis - review of recent developments. Org. Geochem. 42, 1440–1460. https://doi.org/10.1016/j.orggeochem.2011.10.011.

Thullner, M., Fischer, A., Richnow, H.-H., Wick, L.Y., 2013. Influence of mass transfer on stable isotope fractionation. Appl. Microbiol. Biotechnol. 97, 441–452. https://doi.org/10.1007/s00253-012-4537-7.

Torrentó, C., Audí-Miró, C., Bordeleau, G., Marchesi, M., Rosell, M., Otero, N., Soler, A., 2014. The use of alkaline hydrolysis as a novel strategy for chloroform remediation: the feasibility of using construction wastes and evaluation of carbon isotopic fractionation. Environ. Sci. Technol. 48, 1869–1877. https://doi.org/10.1021/es403838t.

Torrentó, C., Palau, J., Rodríguez-Fernández, D., Heckel, B., Meyer, A., Domènech, C., Rosell, M., Soler, A., Elsner, M., Hunkeler, D., 2017. Carbon and chlorine isotope fractionation patterns associated with different engineered chloroform transformation reactions. Environ. Sci. Technol. 51, 6174–6184. https://doi.org/10.1021/acs.est.7b00679.

Van Breukelen, B.M., 2007. Extending the Rayleigh equation to allow competing isotope fractionating pathways to improve quantification of biodegradation. Environ. Sci. Technol. 41, 4004–4010. https://doi.org/10.1021/es0628452.

Vikesland, P.J., Heathcock, A.M., Rebodos, R.L., Makus, K.E., 2007. Particle size and aggregation effects on magnetite reactivity toward carbon tetrachloride. Environ. Sci. Technol. 41, 5277–5283. https://doi.org/10.1021/es062082i.

Vodyanitskii, Y.N., 2014. Effect of reduced iron on the degradation of chlorinated hydrocarbons in contaminated soil and ground water: a review of publications. Eurasian Soil Sci. 47, 119–133. https://doi.org/10.1134/S1064229314020136.

Zogorski, J.S., Carter, J.M., Ivahnenko, T., Lapham, W.W., Moran, M.J., Rowe, B.L., Squillace, P.J., Toccalino, P.L., 2006. The Quality of Our Nation's Waters - Volatile Organic Compounds in the Nation's Groundwater and Drinking-water Supply Wells. U.S. Geological Survey Circular 1292.

Zwank, L., Elsner, M., Aeberhard, A., Schwarzenbach, R.P., 2005. Carbon isotope fractionation in the reductive dehalogenation of carbon tetrachloride at iron (hydr)oxide and iron sulfide minerals. Environ. Sci. Technol. 39, 5634–5641. https://doi.org/10.1021/es0487776.

Supplementary Information

Dual element (C-Cl) isotope approach to distinguish abiotic reactions of chlorinated methanes by Fe(0) and by Fe(II) on iron minerals at neutral and alkaline pH

Diana Rodríguez-Fernández[†], Benjamin Heckel[§], Clara Torrentó[‡], Armin Meyer[§], Martin Elsner[§], Daniel Hunkeler[‡], Albert Soler[†], Mònica Rosell[†], Cristina Domènech[†]

[†]Grup MAiMA, Mineralogia Aplicada, Geoquímica i Geomicrobiologia, Departament de Mineralogia, Petrologia i Geologia Aplicada, Facultat de Ciències de la Terra, Martí Franques s/n, Universitat de Barcelona (UB), 08028 Barcelona, Spain.

[§]Institute of Groundwater Ecology, Helmholtz Zentrum München, 85764 Neuherberg, Germany.

[‡]Centre for Hydrogeology and Geothermics, Université de Neuchâtel, 2000 Neuchâtel, Switzerland.

Corresponding author: Diana Rodríguez-Fernández (diana.rodriguez@ub.edu)

Total number of pages (including cover):23

Scheme: 1

Figures: 9

Tables: 3

1. Chemicals

HEPES buffer (99.5%, Sigma-Aldrich) was used to prepare the buffer at pH 7 (0.2 mM). 10 mM sodium hydroxide (NaOH, Baker) was used to prepare the buffer at pH 12. For the CF_Fe_12 and CF_CO_12 experiments, pure CF (99.5%, Fluka) was used. Pure CF (99%, Merck) was used for the CF Mag, Py and aqueous $FeCl_2$ experiments and corresponding controls, since they were performed in different laboratories. For all the CT experiments, pure CT (99%, Panreac) was used. A solution of 0.6 mM $FeCl_2$ (99.99%, purity, Sigma-Aldrich) was prepared for the CF_aq_7, CF_aq_12, CT_aq_7, CT_aq_12 and experiments with Mag and Py. Milli-sized iron (92% purity) from Gotthart Maier Metallpulver GmbH was used in the CF_Fe_12 experiments. Nano-sized iron (99%, Sigma-Aldrich) was used for the CT_Fe_7 and CT_Fe_12 experiments. 1 M acetic acid solution was prepared from glacial acetic acid (CH_3CO_2H, Sigma-Aldrich) to quenching pH 12 solution in order to avoid further CF alkaline hydrolysis in the pH 12 experiments concerning this compound.

2. Minerals and Fe(0) preparation and characterization

Natural Py and Mg crystals were obtained from sedimentary deposits in Navajún (Logroño, Spain) and from a retrograding skarn from Mina Cala (Huelva, Spain), respectively. The X-ray diffraction patterns confirmed they were Py and Mag and showed no significant evidence of any other mineral phase, although some impurities (Ca, Al, Mn in Py and Ca and Ti in Mag) were identified with scanning electron microscopy with energy-dispersive X-ray spectroscopy (SEM-EDS). Minerals were crushed with a tungsten carbide mill (94% tungsten carbide and 6% cobalt, Retsch model RS100) and sieved to a maximum diameter of 106 μm with a Retsch AS 200 sieve. The resulting particle size distribution ranged from 1 to 160 μm with an average diameter of 40 μm for Mag and from 0.1 to 400 μm (due to the formation of particle aggregates) with an average diameter of 111 μm for Py. Particle size distribution of the cast Fe(0) (92% purity, Gotthart Maier Metallpulver GmbH) ranged from 0.4 to 2.0 mm, with an average diameter of 1.2 mm. According to the provider the particle size distribution for nano-sized Fe(0) (99%, Sigma-Aldrich) ranged from 40 to 60 nm. The milli-sized Fe(0), nano-sized Fe(0) and micro-sized Fe-bearing minerals were acid-cleaned to increase surface area, dissolve any unreactive oxide or organic coating (Matheson and Tratnyek, 1994; Slater et al., 2002) and obtain a reproducible surface (Kriegman-King and Reinhard, 1994). Milli-sized Fe(0) and minerals were soaked in degassed 0.1 M hydrochloric solution (HCl, 32 wt %, Sigma-Aldrich) for 1 h, while for nano-sized Fe(0), soaking was done for 5 min. All the solids were rinsed five times with degassed deionized water and dried overnight (Matheson and Tratnyek, 1994; Slater et al., 2002). Py and Mag samples were dried in an oven (Technopyro model PR4T) at 100 ºC in closed serum bottles and lyophilized afterwards (Telstar Cryodos-45 2001 nº376) to remove remaining water. Specific surface area was measured

by BET for milli-sized Fe(0), Py and Mag before (1.00 ± 0.01, 0.830 ± 0.005, 0.62 ± 0.01 m^2/g, respectively) and after acid cleaning (1.624 ± 0.007, 2.47 ± 0.02, 0.698 ± 0.003 m^2/g, respectively). For nano-sized Fe(0), it was only measured before cleaning (11.16 ± 0.09 m^2/g).

3. Sampling and preservation

Except for the nano-sized Fe(0) experiments, reactions were stopped by filtration with 0.2 μm-filters Mille-LG PTFE LCR (Merck Millipore) at different time intervals. Small aliquots were taken for pH measurements before filtration. At pH 12, the filtered solution was neutralized by acetic acid for quenching the alkaline hydrolysis reaction. Samples were held at 4 ºC until analysis in 12-mL glass vials covered with aluminum foil (Elsner et al., 2006) for the milli-sized Fe(0) experiments; and in 12-mL vials amber glass vials for the Mag and Py experiments. In the case of the nano-sized Fe(0) experiments, 0.1 mL of headspace were taken from each single 42-mL vial for measuring CT and CF concentrations and carbon and chlorine isotope analyses by direct injection in the equipment. For concentration estimation, calculations of total mM in the liquid phase considering Henry's law constant at 24 °C (Staudinger and Roberts, 2001) were performed.

4. Analytical methods

pH measurements

pH evolution was monitored using a Crison pH2001 nº6037 (Crison, Spain) in the experiments with Py and Mag and by using a Labor-pH-Meter Lab 850 Messparameter (SI-Analytics, Germany) in the Fe experiments.

BET

Specific surface areas were determined by the BET (Brunauer–Emmett–Teller) gas adsorption method with a TriStar 3000 V6.04 micromeritics surface area analyzer using 5-point N$_2$ adsorption isotherms (Brunauer et al., 1938) in *Centres científics i tecnològics de la Universitat de Barcelona* (CCiT-UB).

Particle size distribution

Milli-sized iron, Py and Mag particle size distribution was determined using a particle size analyzer by photon correlation spectroscopy (Beckman Coulter, model N5) between 0.04 to 2000 μm in *Laboratori de Sedimentologia* (UB).

Unaltered and crushed Py and Mag were studied with a scanning electron microscope Quanta 200 FEI XTE 325/D8395 coupled with Energy-dispersive X-ray spectroscopy Genesi (EDAX) in CCiT-UB.

X-ray analyses

X-ray powder diffraction measurements were performed in CCiT-UB on homogenized sample aliquots using a Bragg–Brentano $\theta/2\theta$ PANalytical X'Pert PRO MPD Alpha1 powder diffractometer (radius = 240 mm) with Cu $K\alpha_1$ radiation, selected by means of a Focalizing Ge (111) primary monochromator. Experimental conditions: sample spinning at 2 revolutions per second; variable automatic divergence slit to get an illuminated length in the beam direction of 10 millimetres; mask defining a length of the beam over the sample in the axial direction of 12 millimetres; diffracted beam of 0.04 radians *Soller* slits; X'Celerator Detector with Active length of 2.122 °. The starting and the final 2θ angles were 4° and 80°, respectively. The step size was 0.017° 2θ and the measuring time, 150 s per step. Mineral identification was made using the X´Pert HighScore software (Degen et al., 2014).

5. Experimental conditions
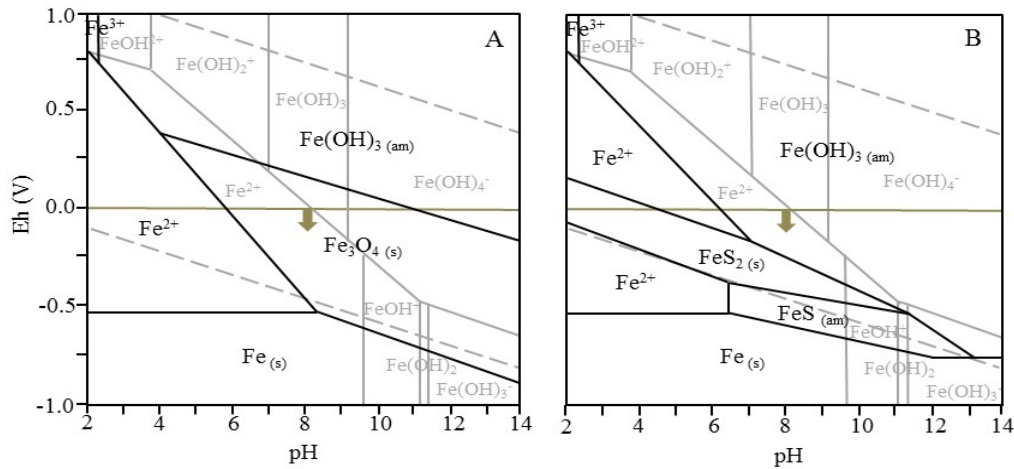
Fig. S1. Eh-pH predominance diagrams of Fe-Cl-H_2O (A) and Fe-Cl-S-H_2O (B) systems. Fe_3O_4 (Mag) is not allowed to form in B. Calculations were performed using the code MEDUSA (Puigdomènech, 2010) and with [Cl⁻]$_{tot}$: 1.2 mM, [Fe^{2+}]$_{tot}$: 0.6 mM and [SO_4^{2-}]$_{tot}$:10 μM. In grey, aqueous species are represented. The arrow indicates assumed Eh experimental conditions and the dashed lines, water stability field.

6. Degradation pathways
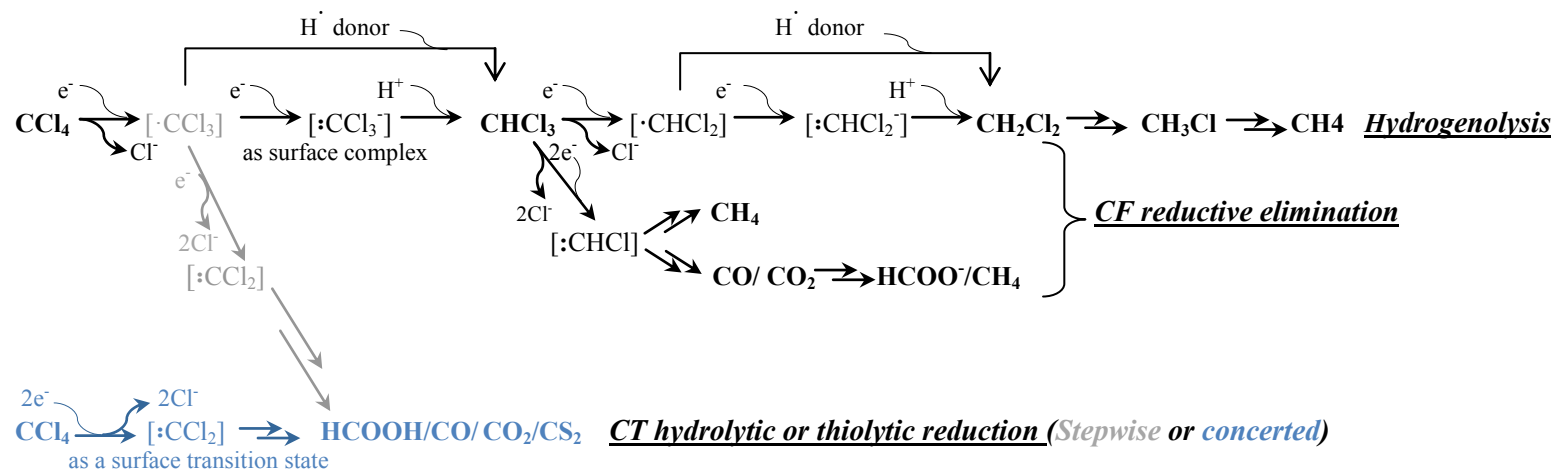
Scheme S1. Discussed CT and CF abiotic reductive degradation pathways. The double arrow indicates omitted intermediate steps for simplification

7. pH evolution

In the CT experiments at pH 7, acidic conditions occurred during the first days, especially in the case of the CT_Py_7 experiment, for which pH remained acidic during all the experimental period (4.7±1.1) (Fig. S2). In the presence of Py at pH 12, however, the pH was kept constant (11.8±0.2) during the course of the experiment (Fig. S2). This different behavior between pH values in homologous experiments is consistent with previous studies, which concluded that in all Py oxidizing systems, pH tends to reach more acidic values but when pH is higher than 11, the pH decrease is much slower than at neutral pH values (Bonnissel-Gissinger et al., 1998). However, this pH decrease was not observed in CF_Py_7 experiment, which suggested low Py oxidizing capacity towards CF.
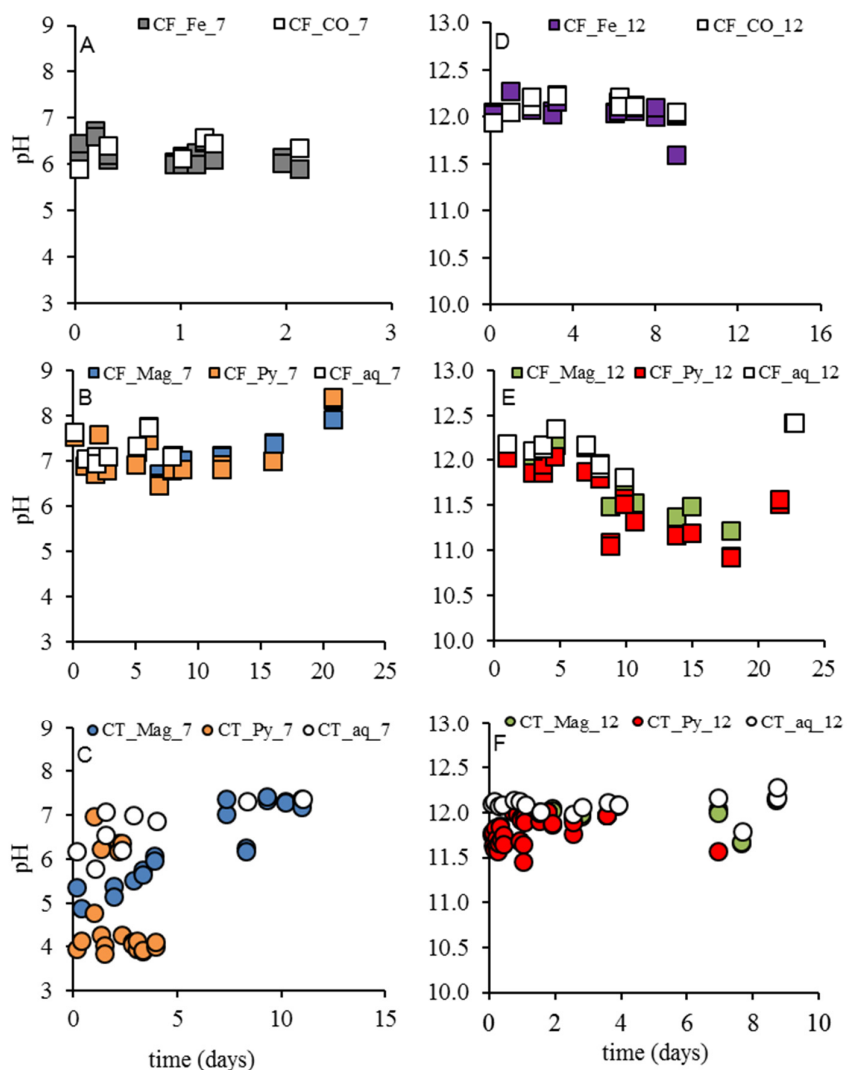
Fig. S2. pH evolution over time in the pH 7 experiments (left): CF_Fe_7 and CF_CO_7 (A, from Torrentó et al., 2017); CF_Mag_7, CF_Py_7 and CF_aq_7 (B); CT_Mag_7, CT_Py_7 and CT_aq_7 (C); and in the pH 12 experiments (right): CF_Fe_12 and CF_CO_12 (D); CF_Mag_12, CF_Py_12 and CF_aq_12 (E) CT_Mag_12, CT_Py_12 and CT_aq_12 (F). Error bars are smaller than the symbols.

8. Degradation study by Fe(0)

Kinetics of Fe(0) experiments

Assuming that all the removal of CT or CF is due to a degradation process, data for CT and CF aqueous concentration versus time can be fitted to a pseudo-first-order rate model following Eq. S1, in order to compare kinetics among pH 7 and pH 12 and to those from the literature (Table S1, S3).

$$dC/dt = -k'C \qquad (S1)$$

C is the target chlorinated compound concentration in $\mu mol/L$, t is time in hours and k' is the pseudo-first-order rate constant (h^{-1}). The k' was obtained using the integrated form of Eq. S1, as shown in Eq. S2, where C_0 is the initial concentration of the chlorinated compound ($\mu mol/L$). Uncertainty was obtained from 95% confidence intervals (CI).

$$\ln f = \ln C/C_0 = k't \qquad (S2)$$

When possible, a surface-area-normalized reaction rate constant (k_{SA}, L m^{-2} h^{-1}) was calculated for comparison with other studies (Table S1, S3) as described by Eq. S3 (Matheson and Tratnyek, 1994; Johnson et al., 1996):

$$dC/dt = -k'C = -k_{SA} \, a_S \, \rho_m C \qquad (S3)$$

where a_S is the specific surface area of metal and ρ_m is the mass concentration of Fe(0).

The k_{SA} values for CT_Fe_7 and CT_Fe_12 experiments are within the range of some values reported in literature (Table S1) for CT degradation by Fe(0) or by FeS, but there are discrepancies with other types of Fe(0) or Fe-bearing minerals (He et al., 2015). Similarly, the k_{SA} values for CF_Fe_7 and CF_Fe_12 experiments are lower than for nano-sized experiments (Table S1). This confirms, as stated by Johnson et al. (1996), that variability in pollutant disappearance rates despite surface area normalization is high, being attributable to different Fe(0) pre-treatment, 'non-reactive' sites amount and experimental conditions (Noubactep, 2009).

Table S1. Degradation products, pseudo first-order rate constants (k') and surface area normalized rate constants (k_{SA}) of abiotic degradation of chlorinated methanes by Fe(0) under anoxic conditions. n.m. =not measured.

Pollutant	Fe(0)	Conditions	Degradation product	k' (h^{-1})	k_{SA} (Lm^{-2}·h^{-1})	Reference
CT	Nano: 11.2 m^2/g 40-60 nm	pH 7	CF	1.4±0.2 $R^2 = 0.95$	(4.9±0.6)×10^{-2}	This study
		pH 12	CF	1.24±0.04 $R^2 = 0.99$	(4.4±0.1)×10^{-2}	This study
CT	Nano 27.9 m^2/g	Buffered pH 7.5	CF, DCM, CH$_4$	5.0±0.4	1.1±0.1	Song and Carraway (2006)
		Unbuffered		2.2±0.1	0.48±0.04	
		Unbuffered		2.2±0.1	0.49±0.04	
CT	2.4 m^2/g ~10 μm	pH 7.7, 1g Fe(0)	CF, DCM	0.30-0.45	2.8-4.1×10^{-2}	Helland et al. (1995)
		pH 7.7, 10g Fe(0)		1.72-2.21	1.9-2.5×10^{-2}	
CT	0.09±0.03 m^2/g	pH 7	CF	0.47±0.06	(4.2±0.5)×10^{-4}	Támara and Butler (2004)
	0.20±0.02 m^2/g,	pH 7		0.6±0.1	(2.3±0.4)×10^{-3}	
	7.4±0.2 m^2/g	pH 7		0.12±0.04	(4.0±1.4)×10^{-3}	
	1.79±0.07 m^2/g	pH 7		0.4±0.1	(2.6±0.9)×10^{-2}	
		pH 12		0.04±0.01	(1.6±0.4)×10^{-4}	
CT	<100 nm	-	CF, DCM,CH$_4$	0.5-2.2	5.4×10^{-4}-1.01	Lien and Zhang (1999)
CT	Micro: 0.22 m^2/g	EDTA (organic ligand) pH 3.5-7.5	CF, DCM	0.843-0.280	(6.5-2.1)×10^{-3}	Zhang et al. (2011)
		pH 3.5-7.5		0.021-0.005	(1.7-0.4)×10^{-4}	
CT	Nano 26 m^2/g 100 nm	Ultrapure water	Not studied	6±1	9.60±1.92×10^{-2}	Feng et al. (2008)
		Humic acid (50-1000 mg/L)		5-3	6.92-4.12×10^{-2}	
		Surfactant SDS (1-2.4mM)		1-2	1.82-2.46×10^{-2}	
		Surfactant CTAB (0.1-10mM)		10-9	14.7-14.5×10^{-2}	
		Surfactant NPE (0.02-1mM)		5-7	7.95-10.9×10^{-2}	
CF	Milli 77 m^2/L (1.00±0.01) m^2/g	pH 12.1±0.1	DCM	(4.6±1.9) ×10^{-3} $R^2 = 0.67$	(5.9±2.5)×10^{-5}	This study
CF	Milli (1.00±0.01) m^2/g	pH 6.3±0.2	DCM	(7±1)×10^{-2} $R^2 = 0.93$	(9±2)×10^{-4}	Torrentó et al. (2017)
CF	Nano 26 m^2/g 100 nm	Ultrapure water	Not studied	(1.3±0.3)×10^{-2}	1.9±0.5×10^{-4}	Feng et al. (2008)
		Humic acid (50-1000 mg/L)		2-32×10^{-2}	3-50×10^{-4}	
		Surf. SDS (1-2.4mM)		2-8×10^{-2}	3-13×10^{-4}	
		Surf. CTAB (0.1-10mM)		2-4×10^{-2}	2-5×10^{-4}	
		Surf. NPE (0.02-1mM)		2-1×10^{-2}	2-5×10^{-4}	
CF	Nano 27.9 m^2/g	Buffered pH 7.5	DCM, CH$_4$	1.9±0.2	4.2±0.5	Song and Carraway (2006)
		unbuffered		1.4±0.1	3.1±0.3	
		Equilibrated (unbuffered)		1.5±0.1	3.3±0.3	

Isotopic fractionation of Fe(0) experiments

The extent of a contaminant transformation for a defined reaction in terms on stable isotope ratios can be determined by its isotopic fractionation (ε) following the Rayleigh approach (Eq. S4), where δ_0 and δ_t are isotope values in the beginning (0) and at a given time (t), respectively, and f is the fraction of substrate remaining at time t.

Isotope signatures are usually reported in per mil (‰) using the delta notation relative to international standards, i.e. Vienna PeeDee Belemnite for carbon ($\delta^{13}C_{VPDB}$) and the international Standard Mean Ocean Chloride (SMOC) for chlorine ($\delta^{37}Cl_{SMOC}$).

$$\ln\left(\frac{\delta_t + 1}{\delta_0 + 1}\right) = \varepsilon \times \ln f \qquad (S4)$$
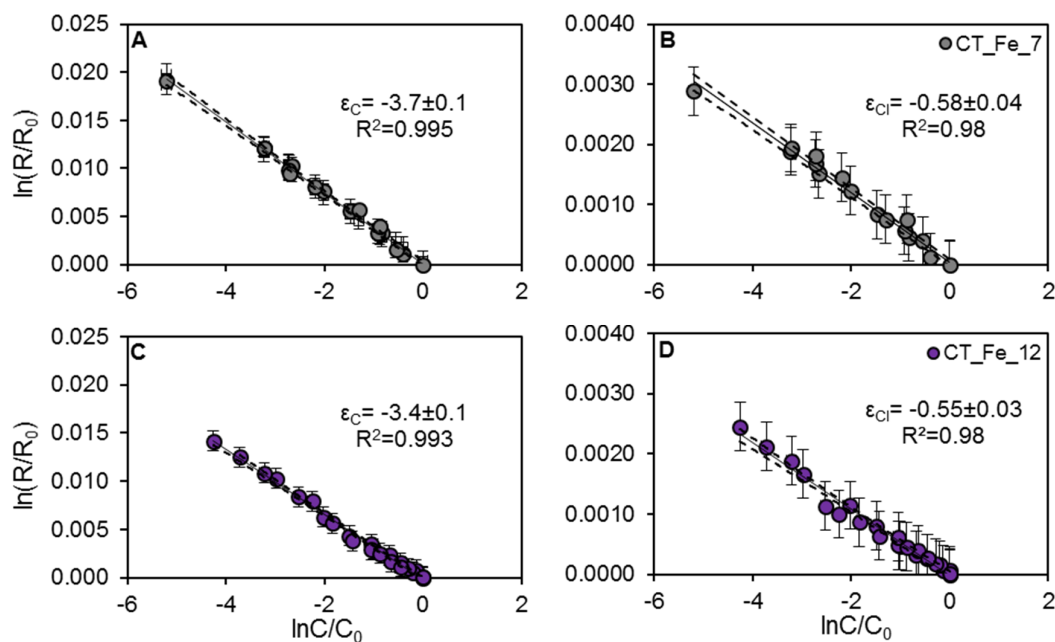
Fig. S3. Logarithmic plots according to Rayleigh equation (Eq. S4) of carbon (A, C panels) and chlorine (B, D panels) isotope ratios during CT reductive dechlorination by Fe(0) at pH 7 (upper panels) and at pH 12 (lower panels). ƐC and ƐCl values are given. Dashed lines represent 95% CI of the linear regression. Error bars display the uncertainty calculated by error propagation including uncertainties in concentration (5%) and isotope measurements (0.5‰ for $\delta^{13}C$ and 0.2‰ for $\delta^{37}Cl$). In some cases, error bars are smaller than the symbols.
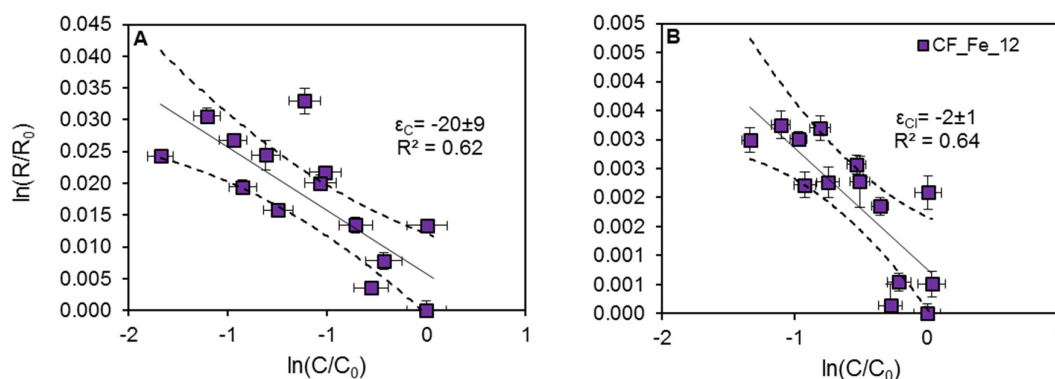
Fig. S4. Logarithmic plots according to Rayleigh equation (Eq. S4) of carbon (A) and chlorine (B) isotope ratios during CF reductive dechlorination by Fe(0) at pH 12. ƐC and ƐCl values are given. Dashed lines represent 95% CI of the linear regression. Error bars display the uncertainty calculated by error propagation including uncertainties in concentration (5%) and standard deviation of duplicates in isotope measurements. In some cases, error bars are smaller than the symbols.

<u>Calculation of Apparent Kinetic Isotope Effects (AKIE)</u>

Carbon and chlorine AKIE values were calculated following Eq. S5 (Elsner et al., 2005), where *n* is the number of atoms of the considered element in the molecule, *x* is the number of these atoms located at the reactive site/s, and *z* is the number of atoms located at the reactive site/s and being in intramolecular competition. $AKIE_C$ of CT in the CT_Fe_7 and CT_Fe_12 experiments was calculated using n=x=z=1, while for $AKIE_{Cl}$, n=x=z=4 was used. The uncertainty of the AKIE was estimated by error propagation in Eq. S7. The results of these experiments were compared to reductive dechlorination studies reported in literature in Table S2.

$$AKIE_E \approx \frac{1}{1+\left(\frac{z \times n}{x} \times \frac{\varepsilon}{1000}\right)} \tag{S5}$$

<u>Carbon isotopic mass balance</u>

Carbon isotopic mass balance ($\delta^{13}C_{SUM}$) was calculated following Eq. (S6) (Hunkeler et al., 1999; Aeppli et al., 2010) where x is the molar fraction of each compound relative to the total molar CMs mass from those isotopic values that are available in each experiment. The uncertainty of $\delta^{13}C_{SUM}$ was determined by error propagation in Eq. S6.

$$\delta^{13}C_{SUM} (‰) = x_{CT}\delta^{13}C_{CT} + x_{CF}\delta^{13}C_{CF} + x_{DCM}\delta^{13}C_{DCM} \tag{S6}$$

<u>The extent of degradation and pathway-specific contributions</u>

Assuming that only one degradation process occurs, the extent of degradation (D) can be estimated using the expression derived from the Rayleigh equation (Eq. S7), where δ_0 and δ_t are isotope values in the beginning (0) and at a given time (t), respectively and ε is the isotope fractionation of the transformation reaction under consideration.

$$D(\%) = \left[1 - \left(\frac{\delta_t + 1000}{\delta_0 + 1000}\right)^{\frac{1000}{\varepsilon}}\right] \times 100 \tag{S7}$$

Pathway-specific contributions to total degradation of a pollutant may be estimated using the expression derived by Van Breukelen (2007) (Eq. S8), where F is the distribution of pathways 1 and 2; εC and εCl are the C and Cl isotope fractionation values of the two pathways, respectively and Λ is the obtained dual C-Cl isotope slope for a target pollutant.

$$F = \frac{\Lambda \varepsilon_1^{Cl} - \varepsilon_1^C}{\left(\varepsilon_2^C - \varepsilon_1^C\right) - \Lambda\left(\varepsilon_2^{Cl} - \varepsilon_1^{Cl}\right)} \tag{S8}$$

Summary of Ɛ, AKIE and Λ values from studied and reported experiments

Table S2. Comparison of ε and AKIE values for C and Cl isotopes in different reductive dechlorination studies. n.m.: not measured; n.ap.: not available;

Compound	Degradation pathway	Type	Conditions	ε_{bulkC} (‰) ± 95%CI	n_C	x_C	z_C	$AKIE_C$	ε_{bulkCl} (‰) ± 95%CI	n_{Cl}	x_{Cl}	z_{Cl}	$AKIE_{Cl}$	$\Lambda \approx \varepsilon C/\varepsilon Cl$	Reference
Reductive dechlorination by C−Cl bond cleavage		**Streitwieser limit KIE_C = 1.057 (Elsner et al., 2005; Aelion et al., 2010)**							**Streitwieser limit KIE_{Cl} = 1.013 (Elsner et al., 2005)**						
CF	Reductive dechlorination	abiotic Fe(0) pH 7	laboratory	-33 ± 11	1	1	1	1.034 ± 0.012	-3 ± 1	3	3	3	1.008 ± 0.001	8 ± 2	Torrentó et al. (2017)
CF	Reductive dechlorination	abiotic Fe(0) pH 12	laboratory	-20 ± 9	1	1	1	1.020 ± 0.009	-2 ± 1	3	3	3	1.006±0.001	8 ± 1	This study
CF	Reductive dechlorination	abiotic Fe(0)	laboratory	-29.4 ± 2.1	1	1	1	1.030 ± 0.07	n.m.					n.m.	Lee et al. (2015)
CF	Reductive outer-sphere single electron transfer	CO_2 radical anions	laboratory	-17.7±0.8					-2.6±0.4					6.7 ±0.4	Heckel et al. (2017)
CF	Reductive dechlorination	biotic (*Dehalobacter* sp. CF50 consortium)	laboratory	-27.5 ± 0.9	1	1	1	1.028± 0.002	n.m.					n.m.	Chan et al. (2012)
CF	Reductive dechlorination	biotic (*Dehalobacter* sp.UNSWDHB consortium)	laboratory	-4.3 ± 0.5	1	1	1	1.004	n.m.					n.m.	Lee et al. (2015)
CF	Hydrogenolysis ± reductive elimination	Biotic (field slurry) with vitamin B_{12}	laboratory	-14 ± 4	1	1	1	1.014 ± 0.002	-2.4 ± 0.4	3	3	3	1.0072 ± 0.0004	7 ± 1	Rodríguez-Fernández et al. (2017)
CT	Reductive dechlorination	abiotic (goethite, magnetite, lepidocrocite, hematite, siderite)	laboratory	-26 to -32	1	1	1	1.027 to 1.033	n.m.					n.m.	Zwank et al., (2005); Elsner et al. (2004)
CT	Reductive dechlorination	abiotic (mackinawite)	laboratory	-10.9 to -15.9	1	1	1	1.011 to 1.016	n.m.					n.m.	Zwank et al. (2005); Neumann et al. (2009)
CT	Reductive dechlorination	abiotic (Zn(0))	laboratory	-10.8 ± 0.7	1	1	1	1.01	n.m.					n.m.	Vanstone et al. (2008)
CT	Hydrogenolysis	Nano-sized Fe(0) at pH 7 and pH 12	laboratory	-3.7 and -3.4	1	1	1	1.0037 and 1.0034	-0.58 and -0.55	4	4	4	1.00233 and 1.00220	5.8 ± 0.4 and 6.1±0.5	This study
CT	Hydrogenolysis	Aqueous $FeCl_2$ at pH 12	laboratory	-3 ± 3	1	1	1	1.003 ± 0.003							This study
CT	Hydrogenolysis and thiolytic reduction	Pyrite at pH 7	laboratory	-5 ± 2	1	1	1	1.005 ± 0.002	-1.5±0.4	4	4	4	1.0060 ± 0.0004	2.9 ± 0.5	This study
CT	Hydrogenolysis and thiolytic reduction	Pyrite pH 12	laboratory	-4 ± 1	1	1	1	1.004 ± 0.001	-0.9 ± 0.4	4	4	4	1.0036 ± 0.0004	3.7 ± 0.9	This study
CT	Hydrogenolysis and hydrolytic reduction?	Magnetite at pH 12	laboratory	-2 ± 1	1	1	1	1.002 ± 0.001	-0.8±0.2	4	4	4	1.0032±0.0002	2 ± 1	This study

Compound	Reaction	System	Type	ε				α	ε				α	Λ	Reference
CT	Hydrogenolysis among other reductions	Biotic (field slurry)	laboratory	-16 ± 6	1	1	1	1.016 ± 0.001	-6 ± 3	4	4	4	1.023 ± 0.003	6.1 ± 0.5	Rodríguez-Fernández et al. (2017)
CT	Reduction processes	Biotic (field slurry) with vitamin B$_{12}$	laboratory	-13 ± 2	1	1	1	1.013 ± 0.003	-4 ± 2	4	4	4	1.015 ± 0.002	5 ± 1	Rodríguez-Fernández et al. (2017)
1,1,1-TCA	Reductive dechlorination	abiotic (Cr(II), Fe0 and Cu and Fe mixtures)	laboratory	-16 to -14	2	1	1	1.027 ± 0.002	n.m.					n.m.	Elsner et al. (2007)
1,1,1-TCA	Reductive dechlorination	abiotic (Fe(0))	laboratory	-7.8 ± 0.4	2	1	1	1.0158 ± 0.0008	-5.2 ±0.2	3	3	3	1.0160 ± 0.0006	1.5 ± 0.1	Palau et al. (2014)
1,1,1-TCA	Reductive dechlorination	abiotic (hydrolysis/ dehydrohalogenation)	laboratory	-1.6 ± 0.2	2	1	1	1.0033 ± 0.0004	-4.7 ±0.1	3	3	3	1.0145 ± 0.0003	0.33 ± 0.04	Palau et al. (2014)
1,1,1-TCA	Reductive dechlorination	biotic	laboratory	-1.8 to -1.5	2	1	1	1.0036 ±0.0006	n.m.					n.m.	Sherwood Lollar et al. (2010)
1,2-DCA	Reductive dechlorination	abiotic (Zn(0))	laboratory	-29.7 ± 1.5	2	2	1	1.03	n.m.					n.m.	Vanstone et al. (2008)
TCE	Reductive dechlorination	abiotic (Fe(0))	laboratory	-13 ± 2	2	1	1	1.0275	-2.6 ±0.1	3	1	1	1.008 ± 0.001	5.2 ±0.3	Audí-Miró et al. (2013)
TCE	Reductive dechlorination	abiotic (Fe(0))	field	-12	2	1	1	1.0254	-3.0	3	1	1	1.009	4.2	Lojkasek-Lima et al. (2012)
TCE	Reductive dechlorination	abiotic (FeS)	laboratory	-27.9 to -33.4	2	1	1	1.059 to 1.072	n.m.					n.m.	Liang et al. (2007)
TCE	Reductive dechlorination	abiotic (corrinoids)	laboratory	-15.0 to -18.5					-3.2 to -4.2					0.3 to 0.8	Renpenning et al. (2014)
TCE	Reductive dechlorination	abiotic (vitamin B12)	laboratory	-16.7 to -17.2	2	1	1	1.034 to 1.036	n.m.						Slater et al. (2003)
TCE	Reductive dechlorination	abiotic (cyanocobalamin)	laboratory	-16.1 ±0.9	2	1	1	1.03	-4.0 ±0.2	3	1	1	1.01	3.9 ± 0.2	Cretnik et al. (2013)
TCE	Reductive dechlorination	biotic	laboratory	-8.8 ± 0.2	2	1	1	1.0179	-3.5 ± 0.5	3	1	1	1.0106	2.7 ± 0.1	Wiegert et al. (2013)
TCE	Reductive dechlorination	biotic (KB-1 consortium)	laboratory	-2.5 to -13.8	2	1	1	1.005 to 1.028	n.m.					n.m.	Bloom et al. (2000); Slater et al. (2001)
TCE	Reductive dechlorination	biotic (*S. multivorans*, *D. michiganesis* BB1 and BD1 mixed *Dehaloc.* consortium)	laboratory	-4.1 to -15.3	2	1	1	1.008 to 1.0315	n.m.					n.m.	Liang et al. (2007)
TCE	Reductive dechlorination	biotic (*S. multivorans*)	laboratory	-20.0 to -20.2					-3.7 to -3.9					5.0 to -5.3	Renpenning et al. (2014)
TCE	Reductive dechlorination	biotic (*G. lovleyi* SZ, *D. hafniense* Y51)	laboratory	-9.1 to -12.2	2	1	1	1.02	-2.7 to -3.6	3	1	1	1.01	3.4 ± 0.2	Cretnik et al. (2013)
TCE	Reductive dechlorination	biotic (mixed *Dehaloc.* consortium)	laboratory	-16.4 ± 0.4	2	2	1	1.017 ± 0.001	-3.6 ± 0.3	3	3	1	1.004 ± 0.000	4.7	Kuder et al. (2013)
PCE	Reductive dechlorination	abiotic (corrinoids)	laboratory	-22.4 to -25.3					-3.4 to -4.8					4.6 to 7.0	Renpenning et al., (2014)
PCE	Reductive dechlorination	abiotic (vitamin B12)	laboratory	-15.8 to -16.5	2	2	2	1.033 to 1.034	n.m.					n.m.	Slater et al. (2003)

Compound	Process	Type	Setting	ε_C				α_C	ε_H				α_H	Λ	Reference
PCE	Reductive dechlorination	abiotic (FeS)	laboratory	-24.6 to -30.2	2	2	2	1.052 to 1.064	n.m.					n.m.	Liang et al. (2007)
PCE	Reductive dechlorination	biotic (*Desulfitobacterium*)	laboratory	-5.6 ± 0.7	2	2	2	1.0113	-2.0 ± 0.5	4	4	4	1.0081	2.5 ± 0.8	Wiegert et al. (2013)
PCE	Reductive dechlorination	biotic (*Desulfitobacterium* Viet1)	laboratory	-19.0 ±0.9	2	2	2	1.019	-5.0 ±0.1	4	4	4	1.005	3.8 ± 0.2	Cretnik et al. (2014)
PCE	Reductive dechlorination	biotic (*Sulfurospirillum*, PceATCE)	laboratory	-3.6 ± 0.2	2	2	2	1.007	-1.2 ± 0.1	4	4	4	1.005	2.7 ± 0.3	Badin et al. (2014)
PCE	Reductive dechlorination	biotic (*Sulfurospirillum*, PceADCE)	laboratory	-0.7 ± 0.1	2	2	2	1.001	-0.9 ±0.1	4	4	4	1.004	0.7 ± 0.2	Badin et al. (2014)
PCE	Reductive dechlorination	biotic (*S. multivorans*)	laboratory	-1.3 to -1.4					-0.4 to -0.6					2.2 to 2.8	Renpenning et al.(2014)
PCE	Reductive dechlorination	biotic (*S. multivorans*, *D. michiganesis* BB1 and BD1 mixed *Dehaloc.* consortium)	laboratory	-1.3 to -7.1	2	2	2	1.003 to 1.0415	n.m.					n.m.	Liang et al. (2007)
PCE	Reductive dechlorination	biotic	field	n.ap.				n.ap.	n.ap.				n.ap.	0.42 to 1.12	Wiegert et al. (2012)

9. Degradation study by Fe-minerals and FeCl$_2$

Kinetics of Mag, Py and aq experiments

Table S3. Degradation products, pseudo first-order rate constants (k_{obs}) and surface area normalized rate constants (k_{SA}) of abiotic degradation of chlorinated methanes by iron minerals under anoxic conditions. n.m.=not measured; n.d.= not detected; n.a.=not available; n.ap.=not aplicable

Pollutant	Mineral phase	Conditions	Degradation product	k_{obs} (d^{-1})	k_{SA} (Lm^{-2}d^{-1})	Reference
CT	FeCl$_2$(aq)	pH 12.1±0.1	CF	0.3±0.2	n.ap.	This study
CT	Magnetite (17 m^2/L)	pH 12.0±0.1	CF	1.4±0.8	(8±5)×10^{-2} (R^2=0.8)	This study
CT	Pyrite	pH 4.7 ± 1.1	CF, CS$_2$	1.0±0.4	(1.6±0.6)×10^{-2} (R^2=0.72)	This study
CT	Pyrite	pH 11.8±0.2	CF, CS$_2$	1.2±0.4	(2±1)×10^{-2} (R^2=0.6)	This study
CT	Mackinawite (13 m^2/g)	pH 7.2	CF	n.a.	1.2±0.06	(Zwank et al., 2005)
CT	Mackinawite (77 m^2/g)	pH 7.2	CF	n.a.	(3.0±0.22)×10^{-2}	(Zwank et al., 2005)
CT	FeS (33 g/L)	pH 7.5	CF, C$_2$H$_4$, C$_2$H$_6$	(2.98±0.22) ×10^1	n.a.	(Choi and Lee, 2009)
CT	FeS (200 g/L)	pH 6.5	n.m.	(4.15±0.12) ×10^1	n.a.	(Lipczynska-Kochany et al., 1994)
CT	FeS$_2$ (200 g/L)	pH 6.5	n.m.	(4.15±0.19) ×10^1	n.a.	(Lipczynska-Kochany et al., 1994)
CT	FeS fresh (0.73 g/L)	pH 7-8	CF, CS$_2$	1.07	n.a.	(Devlin and Muller, 1999)
CT	FeS aged (0.73 g/L)	pH 7-8	CF, CS$_2$	1.24	n.a.	(Devlin and Muller, 1999)
CT	FeS (18g/L)	-	CF, DCM	9.7×10^1	n.a.	(Assaf-Anid and Lin, 2002)
CT	FeS (0.05 m^2/g). Freeze dried	pH 8.3	CF		5.2±0.62	(Butler and Hayes, 2000)
CT	FeS coating on 0.13 g/L Goethite and 0.20 g/L hematite	pH 8.0	CF	0.28±0.14 0.22±0.12	n.a.	(Hanoch et al., 2006)
CT	Py (0.01 m^2/g; 1.2-1.4 m^2/L)	pH 6.5	CF, CO$_2$, CS$_2$, formate		0.16	(Kriegman-King and Reinhard, 1994)
CT	Pyrite	Neutral pH	CF	0.22	n.a.	(Devlin and Muller, 1999)
CT	Pyrrhotite	Neutral pH	CF	0.91	n.a.	(Devlin and Muller, 1999)
CT	Magnetite	Neutral pH	CF, CH$_4$	n.a.	8.9×10^{-4}	(McCormick et al., 2002)
CT	Green rust	pH 8.0	CF	n.a.	6.23×10^{-3}	(Liang and Butler, 2010)
CT	Green rust (dodecanoate anions)	pH 8±2	CF, HCOOH, CO	1.56 to 2.64	n.a.	(Ayala-Luis et al., 2012)
CT	Magnetite	pH 7.0	CF, CO	n.a.	4.8×10^{-4}	(Danielsen and Hayes, 2004)
CT	Magnetite	pH 7.2	CF	n.a.	1.2×10^{-1}	(Zwank et al., 2005)
CT	Magnetite	pH 7.8	CF, CO	n.a.	2.2×10^{-2} 9.9×10^{-4}	(Vikesland et al., 2007)
CF	FeCl$_2$ (aq)	pH 12.1±0.1	n.d.	(6±3)×10^{-2} R^2=0.6	n.ap.	This study
CF	Magnetite	pH 11.8±0.4	n.d.	0.10±0.03 R^2=0.7	(6±2) ×10^{-3}	This study
CF	Pyrite	pH 11.5±0.4	DCM	(4±1)×10^{-2} R^2=0.6	(6±2) ×10^{-3}	This study
CF	FeS (0.14 m^2/g)	pH 7.8	n.m.	n.a.	6.1×10^1	(Kenneke and Weber, 2003)

By-products concentration of Mag, Py and aq experiments
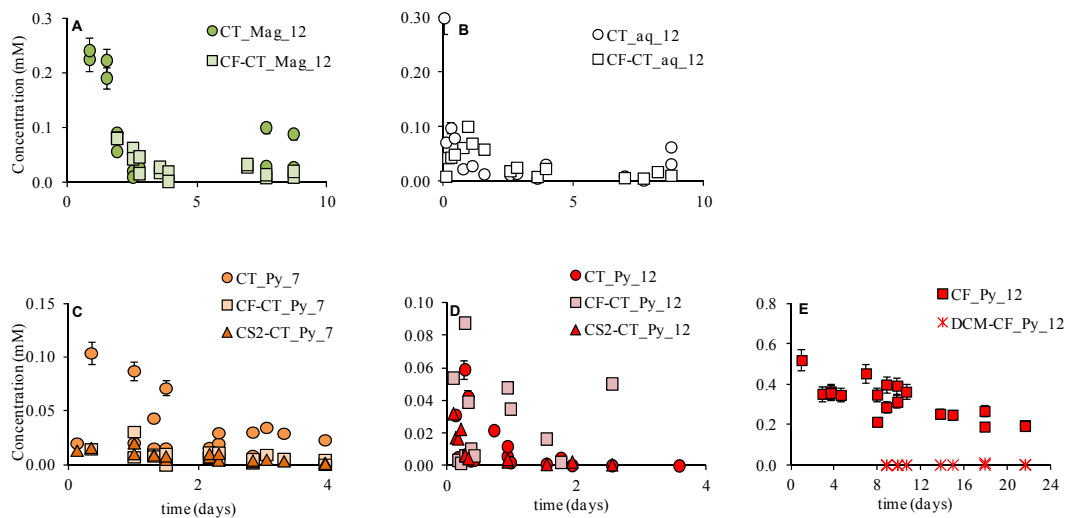
Fig. S5. Concentration (mM) of parent compound (CT or CF) and corresponding by-products (CF, CS_2 or DCM) of those Mag (A), $FeCl_2$ (B) and Py (C,D,E) experiments where by-products were detected.

Isotopic fractionation of Mag, Py and aq experiments
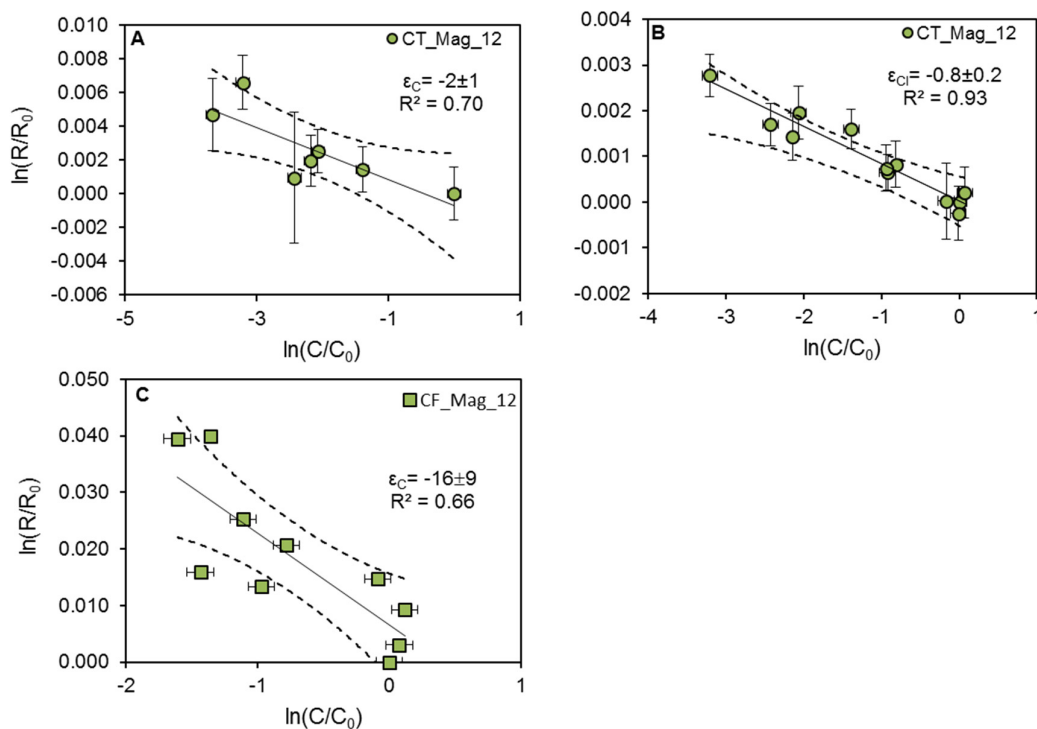
Fig. S6. Logarithmic plots according to Rayleigh equation (Eq. S4) of carbon (A) and chlorine (B) isotope ratios during CT reductive dechlorination by magnetite at pH 12 (upper panels) and carbon isotope ratios during CF reductive dechlorination by magnetite at pH 12 (C). εC and εCl values are given. Dashed lines represent 95% CI of the linear regression. Error bars display the uncertainty calculated by error propagation including uncertainties in concentration (5%) and standard deviation of duplicates in isotope measurements. In some cases, error bars are smaller than the symbols.
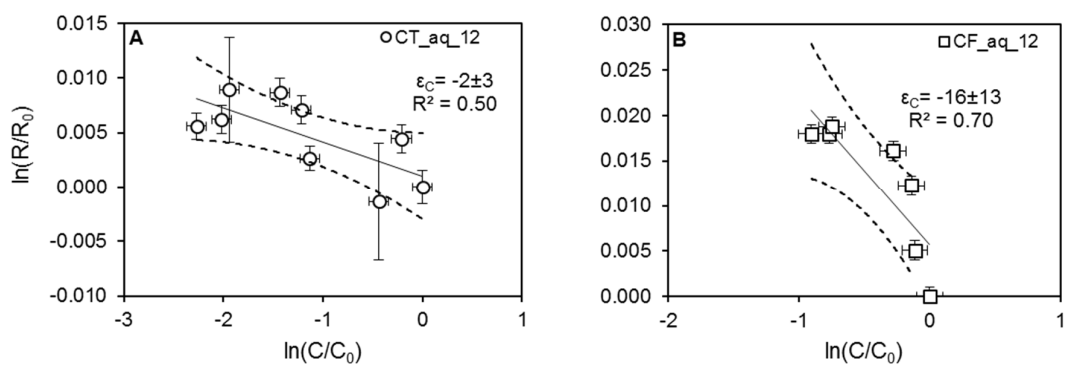
Fig. S7. Logarithmic plots according to Rayleigh equation (Eq. S4) of carbon isotope ratios during CT (A) and CF (B) reductive dechlorination by FeCl$_2$(aq) at pH 12. εC values are given. Dashed lines represent 95% CI of the linear regression. Error bars display the uncertainty calculated by error propagation including uncertainties in concentration (5%) and standard deviation of duplicates in isotope measurements. In some cases, error bars are smaller than the symbols.
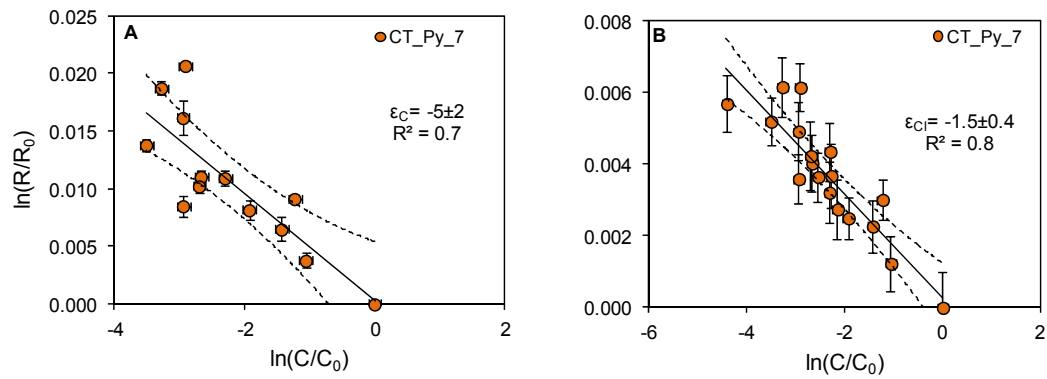
Fig. S8. Logarithmic plots according to Rayleigh equation (Eq. S4) of carbon (A) and chlorine (B) isotope ratios during CT reductive dechlorination by pyrite at pH 7. εC and εCl values are given. Dashed lines represent 95% CI of the linear regression. Error bars display the uncertainty calculated by error propagation including uncertainties in concentration (5%) and standard deviation of duplicates in isotope measurements. In some cases, error bars are smaller than the symbols.
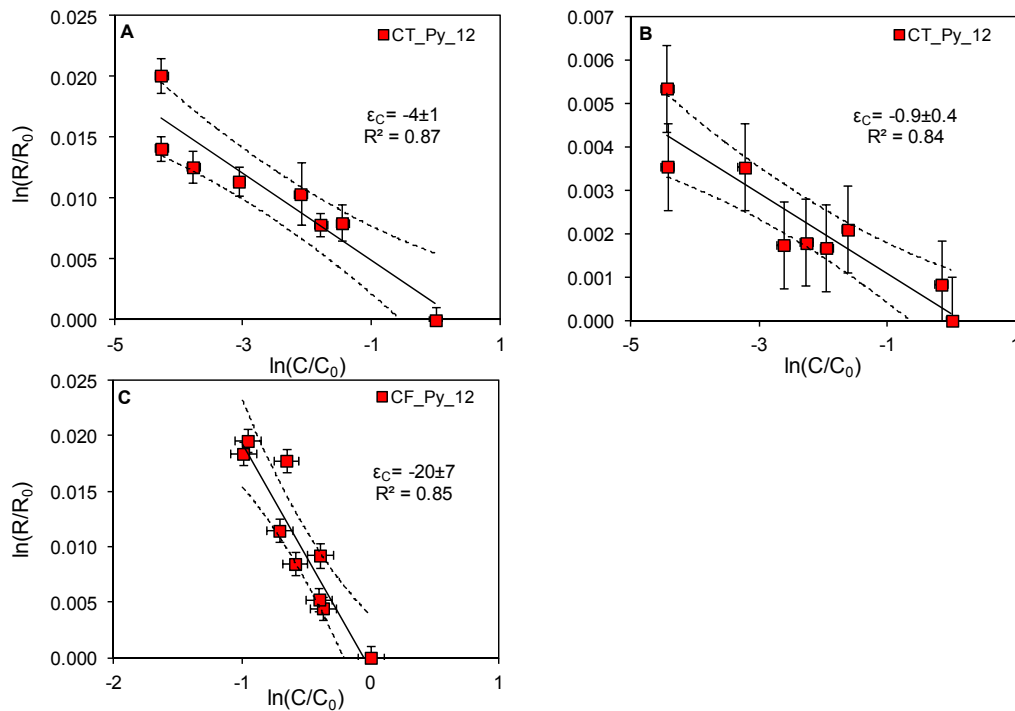
Fig. S9. Logarithmic plots according to Rayleigh equation (Eq. S4) of carbon (A, C) and chlorine (B) isotope ratios during CT (A,B) and CF (B) reductive dechlorination by pyrite at pH 12. εC values are given. Dashed lines represent 95% CI of the linear regression. Error bars display the uncertainty calculated by error propagation including uncertainties in concentration (5%) and standard deviation of duplicates in isotope measurements. In some cases, error bars are smaller than the symbols.

Discussion of CT degradation in Mag experiments at pH 7 and pH 12

Although CT degradation by Mag was not detected in CT_Mag_7 experiments, CT degradation by Mag has been previously reported in the literature. This discrepancy might be attributed to the use in the present experiments of micro-sized Mag in contrast to nano-sized Mag (Hanoch et al., 2006; Maithreepala and Doong, 2007; Vikesland et al., 2007); to the use of a lower Mag/CT ratio than in Zwank et al., (2005); or to the use of different minerals treatments (Hanoch et al., 2006) or different amounts of Fe(II) (Zwank et al., 2005; Vikesland et al., 2007). Total dissolved Fe(II) content was not measured in the present experiments (the theoretical added $FeCl_2$ amount was 0.6 mM) and thus comparison with previous studies is not straightforward. However, the added 0.6 mM of $FeCl_2$ was chosen to mimic field conditions since Fe(II) concentrations in anoxic groundwater usually range from 0.009 to 0.179 mM, reaching concentrations up to 0.896 mM (World Health Organization, 2003).

CT degradation with Mag is strongly pH dependent, being faster at higher pH because of the higher density of deprotonated sites at the mineral surface responsible of dechlorination (Danielsen and Hayes, 2004; Lin and Liang, 2013). However, Fe(II) sorption and surface precipitation of $Fe(OH)_3$(am) onto Mag or other precipitates like green rust are more stable under alkaline conditions and might also contribute on CT degradation (Klausen et al., 1995; Erbs et al., 1999; Liger et al., 1999). In addition, alkaline pH also enhances Fe(II) oxidation to Fe(III) aqueous species (Fig. S1), favoring the CT hydrogenolysis to CF as the overall reaction potential is 0.7 V, while it takes a value below or equal to zero at pH 7. Finally, it is also reported that in nano-sized Mag experiments particle aggregation is expected to decrease as the solution pH increases above or below the pH of isoelectric point (Vikesland et al., 2007), so the available surface to dechlorinate could be higher at pH 12 than at pH 7.

10. References

Aeppli, C., Hofstetter, T.B., Amaral, H.I.F., Kipfer, R., Schwarzenbach, R.P., Berg, M., 2010. Quantifying in situ transformation rates of chlorinated ethenes by combining compound-specific stable isotope analysis, groundwater dating, and carbon isotope mass balances. Environ. Sci. Technol. 44, 3705–3711. doi:10.1021/es903895b

Assaf-Anid, N., Lin, K.-Y., 2002. Carbon tetrachloride reduction by Fe^{2+}, S^{2-}, and FeS with vitamin B_{12} as organic amendment. J. Environ. Eng. 128, 94–99. doi:10.1061/(ASCE)0733-9372(2002)128:1(94)

Audí-Miró, C., Cretnik, S., Otero, N., Palau, J., Shouakar-Stash, O., Soler, A., Elsner, M., 2013. Cl and C isotope analysis to assess the effectiveness of chlorinated ethene degradation by zero-valent iron: Evidence from dual element and product isotope values. Appl. Geochemistry 32, 175–183. doi:10.1016/j.apgeochem.2012.08.025

Ayala-Luis, K.B., Cooper, N.G.A., Koch, C.B., Hansen, H.C.B., 2012. Efficient dechlorination of carbon tetrachloride by hydrophobic green rust intercalated with dodecanoate anions. Environ. Sci. Technol. 46, 3390–3397. doi:10.1021/es204368u

Badin, A., Buttet, G., Maillard, J., Holliger, C., Hunkeler, D., 2014. Multiple dual C-Cl isotope patterns associated with reductive dechlorination of tetrachloroethene. Environ. Sci. Technol. 48, 9179–9186. doi:10.1021/es500822d

Bloom, Y., Aravena, R., Hunkeler, D., Edwards, E., Frape, S.K., 2000. Carbon isotope fractionation during microbial dechlorination of trichloroethene, cis-1,2-dichloroethene, and vinyl chloride: implications for assessment of natural attenuation. Environ. Sci. Technol. 34, 2768–2772. doi:10.1021/es991179k

Bonnissel-Gissinger, P., Alnot, M., Ehrhardt, J.J., Behra, P., 1998. Surface oxidation of pyrite as a function of pH. Environ. Sci. Technol. 32, 2839–2845. doi:10.1021/es980213c

Brunauer, S., Emmett, P.H., Teller, E., 1938. Adsorption of gases in multimolecular layers. J. Am. Chem. Soc. 60, 309–319. doi:citeulike-article-id:4074706

Butler, E.C., Hayes, K.F., 2000. Kinetics of the transformation of halogenated aliphatic compounds by iron sulfide. Environ. Sci. Technol. 34, 422–429. doi:10.1021/es980946x

Chan, C.C.H., Mundle, S.O.C., Eckert, T., Liang, X., Tang, S., Lacrampe-Couloume, G., Edwards, E.A., Sherwood Lollar, B., 2012. Large carbon isotope fractionation during biodegradation of chloroform by *Dehalobacter* cultures. Environ. Sci. Technol. 46, 10154–10160. doi:10.1021/es3010317

Choi, K., Lee, W., 2009. Reductive dechlorination of carbon tetrachloride in acidic soil manipulated with iron(II) and bisulfide ion. J. Hazard. Mater. 172, 623–630. doi:10.1016/j.jhazmat.2009.07.041

Cretnik, S., Bernstein, A., Shouakar-Stash, O., Löffler, F., Elsner, M., 2014. Chlorine isotope effects from isotope ratio mass spectrometry suggest intramolecular C-Cl bond competition in trichloroethene (TCE) reductive dehalogenation. Molecules 19, 6450–6473. doi:10.3390/molecules19056450

Cretnik, S., Thoreson, K.A., Bernstein, A., Ebert, K., Buchner, D., Laskov, C., Haderlein, S., Shouakar-Stash, O., Kliegman, S., McNeill, K., Elsner, M., 2013. Reductive dechlorination of TCE by chemical model systems in comparison to dehalogenating bacteria: Insights from dual element isotope analysis ($^{13}C/^{12}C$, $^{37}Cl/^{35}Cl$). Environ. Sci. Technol. 47, 6855–6863. doi:10.1021/es400107n

Danielsen, K.M., Hayes, K.F., 2004. pH dependence of carbon tetrachloride reductive dechlorination by magnetite. Environ. Sci. Technol. 38, 4745–4752. doi:10.1021/es0496874

Degen, T., Sadki, M., Bron, E., König, U., Nénert, G., 2014. The HighScore suite. Powder Diffr. 29, S13–S18. doi:10.1017/S0885715614000840

Devlin, J.F., Muller, D., 1999. Field and laboratory studies of carbon tetrachloride transformation in a sandy aquifer under sulfate reducing conditions. Environ. Sci. Technol. 33, 1021–1027. doi:10.1021/es9806884

Elsner, M., Cwiertny, D.M., Roberts, A.L., Sherwood Lollar, B., 2007. 1,1,2,2-Tetrachloroethane reactions with OH⁻, Cr(II), granular iron, and a copper - iron bimetal: insights from product formation and associated carbon isotope fractionation. Environ. Sci. Technol. 41, 4111–4117. doi:10.1021/es072046z

Elsner, M., Haderlein, S.B., Kellerhals, T., Luzi, S., Zwank, L., Angst, W., Schwarzenbach, R.P., 2004. Mechanisms and products of surface-mediated reductive dehalogenation of carbon tetrachloride by Fe(II) on goethite. Environ. Sci. Technol. 38, 2058–2066. doi:10.1021/es034741m

Elsner, M., Lacrampe-Couloume, G., Sherwood Lollar, B., 2006. Freezing to preserve groundwater samples and improve headspace quantification limits of water-soluble organic contaminants for carbon isotope analysis. Anal. Chem. 78, 7528–7534. doi:10.1021/ac061078m

Elsner, M., Zwank, L., Hunkeler, D., Schwarzenbach, R.P., 2005. A new concept linking observable stable isotope fractionation to transformation pathways of organic pollutants. Environ. Sci. Technol. 39, 6896–6916. doi:10.1021/es0504587

Erbs, M., Christian, H., Hansen, B., Olsen, C.E., 1999. Reductive dechlorination of carbon tetrachloride using iron (II) iron (III) hydroxide sulfate (green rust). Environ. Sci. Technol. 33, 307–311. doi:doi:10.1021/es980221t

Feng, J., Zhu, B. wei, Lim, T.T., 2008. Reduction of chlorinated methanes with nano-scale Fe particles: Effects of amphiphiles on the dechlorination reaction and two-parameter regression for kinetic prediction. Chemosphere 73, 1817–1823. doi:10.1016/j.chemosphere.2008.08.014

Hanoch, R.J., Shao, H., Butler, E.C., 2006. Transformation of carbon tetrachloride by bisulfide treated goethite, hematite, magnetite, and kaolinite. Chemosphere 63, 323–334. doi:10.1016/j.chemosphere.2005.07.016

He, Y.T., Wilson, J.T., Su, C., Wilkin, R.T., 2015. Review of abiotic degradation of chlorinated solvents by reactive iron minerals in aquifers. Groundw. Monit. Remediat. 35, 57–75. doi:10.1111/gwmr.12111

Heckel, B., Cretnik, S., Kliegman, S., Shouakar-Stash, O., McNeill, K., Elsner, M., 2017. Reductive outer-sphere single electron transfer is an exception rather than the rule in natural and engineered chlorinated ethene dehalogenation. Environ. Sci. Technol. 51, 9663–9673. doi:10.1021/acs.est.7b01447

Helland, B.R., Alvarez, P.J.J., Schnoor, J.L., 1995. Reductive dechlorination of carbon tetrachloride with elemental iron. J. Hazard. Mater. 41, 205–216. doi:10.1016/0304-3894(94)00111-S

Hunkeler, D., Aravena, R., Butler, B.J., 1999. Monitoring microbial dechlorination of tetrachloroethene (PCE) using compound-specific carbon isotope ratios: Microcosms and

field experiments. Environ. Sci. Technol. 33, 2733−2738. doi:10.1021/es981282u

Johnson, T.L., Scherer, M.M., Tratnyek, P.G., 1996. Kinetics of halogenated organic compound degradation by iron metal. Environ. Sci. &Technology 30, 2634–2640. doi:S0013-936X(96)00090-9

Kenneke, J.F., Weber, E.J., 2003. Reductive dehalogenation of halomethanes in iron- and sulfate-reducing sediments. 1. Reactivity pattern analysis. Environ. Sci. Technol. 37, 713–720. doi:10.1021/es0205941

Klausen, J., Troeber, S.P., Haderlein, S.B., Schwarzenbach, R.P., 1995. Reduction of substituted nitrobenzenes by Fe(II) in aqueous mineral suspensions. Environ. Sci. Technol. 29, 2396–2404. doi:10.1021/es00009a036

Kriegman-King, M.R., Reinhard, M., 1994. Transformation of carbon tetrachloride by pyrite in aqueous solution. Environ. Sci. Technol. 28, 692–700. doi:10.1021/es00053a025

Kuder, T., Van Breukelen, B.M., Vanderford, M., Philp, P., 2013. 3D-CSIA: Carbon, chlorine, and hydrogen isotope fractionation in transformation of TCE to ethene by a *Dehalococcoides* culture. Environ. Sci. Technol. 47, 9668–9677. doi:10.1021/es400463p

Lee, M., Wells, E., Wong, Y.K., Koenig, J., Adrian, L., Richnow, H.H., Manefield, M., 2015. Relative contributions of *Dehalobacter* and zerovalent iron in the degradation of chlorinated methanes. Environ. Sci. Technol. 49, 4481–4489. doi:10.1021/es5052364

Liang, X., Butler, E.C., 2010. Effects of natural organic matter model compounds on the transformation of carbon tetrachloride by chloride green rust. Water Res. 44, 2125–2132. doi:10.1016/j.watres.2009.12.026

Liang, X., Dong, Y., Kuder, T., Krumholz, L.R., Philp, R.P., Butler, E.C., 2007. Distinguishing abiotic and biotic transformation of tetrachloroethylene and trichloroethylene by stable carbon isotope fractionation. Environ. Sci. Technol. 41, 7094–7100. doi:10.1021/es070970n

Lien, H.L., Zhang, W.X., 1999. Transformation of chlorinated methanes by nanoscale iron particles. J. Environ. Eng. 125, 1042–1047. doi:10.1061/(ASCE)0733-9372(1999)125:11(1042)

Liger, E., Charlet, L., van Cappellen, P., 1999. Surface catalysis of uranium(VI) reduction by iron(II). Geochim. Cosmochim. Acta 63, 2939–2955. doi:10.1016/S0016-7037(99)00265-3

Lin, Y.T., Liang, C., 2013. Carbon tetrachloride degradation by alkaline ascorbic acid solution. Environ. Sci. Technol. 47, 3299–3307. doi:10.1021/es304441e

Lipczynska-Kochany, E., Harms, S., Milbum, R., Sprah, G., Nadarajah, N., 1994. Degradation of carbon tetrachloride in the presence of iron and sulphur containing compounds. Chemosphere 29, 1477–1489.

Lojkasek-Lima, P., Aravena, R., Shouakar-Stash, O., Frape, S.K., Marchesi, M., Fiorenza, S., Vogan, J., 2012. Evaluating TCE abiotic and biotic degradation pathways in a permeable reactive barrier using compound specific isotope analysis. Ground Water Monit. Remediat. 32, 53–62. doi:10.1111/j1745

Maithreepala, R.A., Doong, R., 2007. Dechlorination of carbon tetrachloride by ferrous ion associated with iron oxide nano particles, in: Proceedings of the Fourth Academic Sessions 2007.

Matheson, L.J., Tratnyek, P.G., 1994. Reductive dehalogenation of chlorinated methanes by iron metal. Environ. Sci. Technol. 28, 2045–2053. doi:10.1021/es00061a012

McCormick, M.L., Bouwer, E.J., Adriaens, P., 2002. Carbon tetrachloride transformation in a model iron-reducing culture: Relative kinetics of biotic and abiotic reactions. Environ. Sci. Technol. 36, 403–410. doi:10.1021/es010923+

Neumann, A., Hofstetter, T.B., Skarpeli-Liati, M., Schwarzenbach, R.P., 2009. Reduction of polychlorinated ethanes and carbon tetrachloride by structural Fe(II) in smectites. Environ. Sci. Technol. 43, 4082–4089. doi:10.1021/es9001967

Noubactep, C., 2009. On the validity of specific rate constants (k_{SA}) in Fe^0/H_2O systems. J. Hazard. Mater. 164, 835–837. doi:10.1016/j.jhazmat.2008.08.074

Palau, J., Shouakar-Stash, O., Hunkeler, D., 2014. Carbon and chlorine isotope analysis to identify abiotic degradation pathways of 1,1,1-trichloroethane. Environ. Sci. Technol. 48, 14400–14408. doi:10.1021/es504252z

Puigdomènech, I., 2010. MEDUSA (Make Equilibrium Diagrams Using Sophisticated Algorithms) Windows interface to the MS-DOS versions of INPUT, SED and PREDOM (FORTRAN programs drawing chemical equilibrium diagrams).

Renpenning, J., Keller, S., Cretnik, S., Shouakar-stash, O., Elsner, M., Schubert, T., Nijenhuis, I., 2014. Combined C and Cl isotope effects indicate differences between corrinoids and enzyme (*Sulfurospirillum multivorans* PceA) in reductive dehalogenation of tetrachloroethene, but not trichloroethene. Environ. Sci. Technol 48, 11837–11845. doi:dx.doi.org/10.1021/es503306g

Rodríguez-Fernández, D., Torrentó, C., Guivernau, M., Viñas, M., Hunkeler, D., Soler, A., Domènech, C., Rosell, M., 2018. Vitamin B_{12} effects on chlorinated methanes-degrading microcosms: Dual isotope and metabolically active microbial populations assessment. Sci. Total Environ. 621, 1615–1625. doi:10.1016/j.scitotenv.2017.10.067

Sherwood Lollar, B., Hirschorn, S., Mundle, S.O.C., Grostern, A., Edwards, E.A., Lacrampe-Couloume, G., 2010. Insights into enzyme kinetics of chloroethane biodegradation using compound specific stable isotopes. Environ. Sci. Technol. 44, 7498–7503. doi:10.1021/es101330r

Slater, G.F., Sherdwood Lollar, B., Lesage, S., Brown, S., 2003. Carbon isotope fractionation of PCE and TCE during dechlorination by vitamin B_{12}. Ground Water Monit. Remediat. 23, 59–67. doi:10.1111/j.1745-6592.2003.tb00695.x

Slater, G.F., Sherwood Lollar, B., Allen King, R., O'Hannesin, S., 2002. Isotopic fractionation during reductive dechlorination of trichloroethene by zero-valent iron: influence of surface treatment. Chemosphere 49, 587–596. doi:10.1016/S0045-6535(02)00327-2

Slater, G.F., Sherwood Lollar, B., Sleep, B.E., Edwards, E.A., 2001. Variability in carbon isotopic fractionation during biodegradation of chlorinated ethenes: Implications for field applications. Environ. Sci. Technol. 35, 901–907. doi:10.1021/es001583f

Song, H., Carraway, E.R., 2006. Reduction of chlorinated methanes by nano-sized zero-valent iron. Kinetics, pathways and effect of reaction conditions. Environ. Eng. Sci. 23, 272–284. doi:10.1089/ees.2006.23.272

Staudinger, J., Roberts, P. V., 2001. A critical compilation of Henry's law constant temperature dependence relations for organic compounds in dilute aqueous solutions. Chemosphere 44, 561–576. doi:10.1016/S0045-6535(00)00505-1

Támara, M.L., Butler, E.C., 2004. Effects of iron purity and groundwater characteristics on rates and products in the degradation of carbon tetrachloride by iron metal. Environ. Sci. Technol. 38, 1866–1876. doi:10.1021/es0305508

Torrentó, C., Palau, J., Rodríguez-Fernández, D., Heckel, B., Meyer, A., Domènech, C., Rosell, M., Soler, A., Elsner, M., Hunkeler, D., 2017. Carbon and chlorine isotope fractionation patterns associated with different engineered chloroform transformation reactions. Environ. Sci. Technol. 51, 6174–6184. doi:10.1021/acs.est.7b00679

Van Breukelen, B.M., 2007. Extending the Rayleigh equation to allow competing isotope fractionating pathways to improve quantification of biodegradation. Environ. Sci. Technol. 41, 4004–4010. doi:10.1021/es0628452

Vanstone, N., Elsner, M., Lacrampe-Couloume, G., Mabury, S., Sherwood Lollar, B., 2008. Potential for identifying abiotic chloroalkane degradation mechanisms using carbon isotopic fractionation. Environ. Sci. Technol. 42, 126–132. doi:10.1021/es0711819

Vikesland, P.J., Heathcock, A.M., Rebodos, R.L., Makus, K.E., 2007. Particle size and aggregation effects on magnetite reactivity toward carbon tetrachloride. Environ. Sci. Technol. 41, 5277–5283. doi:10.1021/es062082i

Wiegert, C., Aeppli, C., Knowles, T., Holmstrand, H., Evershed, R., Pancost, R.D., Macháčková, J., Gustafsson, Ö., 2012. Dual carbon-chlorine stable isotope investigation of sources and fate of chlorinated ethenes in contaminated groundwater. Environ. Sci. Technol. 46, 10918–10925. doi:10.1021/es3016843

Wiegert, C., Mandalakis, M., Knowles, T., Polymenakou, P.N., Aeppli, C., Macháčková, J., Holmstrand, H., Evershed, R.P., Pancost, R.D., Gustafsson, O., 2013. Carbon and chlorine isotope fractionation during microbial degradation of tetra- and trichloroethene. Environ. Sci. Technol. 47, 6449–6456. doi:10.1021/es305236y

World Health Organization, 2003. Iron in drinking-water. WHO Guidelines for drinking-water quality, WHO/SDE/WSH/03.04/08. Geneva.

Zhang, X., Deng, B., Guo, J., Wang, Y., Lan, Y., 2011. Ligand-assisted degradation of carbon tetrachloride by microscale zero-valent iron. J. Environ. Manage. 92, 1328–1333. doi:10.1016/j.jenvman.2010.12.020

Zwank, L., Elsner, M., Aeberhard, A., Schwarzenbach, R.P., 2005. Carbon isotope fractionation in the reductive dehalogenation of carbon tetrachloride at iron (hydr)oxide and iron sulfide minerals. Environ. Sci. Technol. 39, 5634–5641. doi:10.1021/es0487776

Annex E. Preliminary microcosms experiments

Experimental setup

Following Fennell et al. (2001) procedure, preliminary microcosm assays were performed. In order to assess natural dechlorinating activity and to evaluate the impact of different biostimulation strategies on the indigenous microbial community composition of the Òdena site first microcosm experiments were set up in batch (Figure E1) by directly using slurry collected in June 2012 from the bottom of S3, the most anoxic well containing the original pollutant mixture. Losses during sampling and preparation were avoided. No flushing was done. Experiments were monitored during 197 days (t_6) (and in some cases up to 348 days, t_7).

Three treatments with different electron donors were tested (lactate (LA), methanol (ME) and acetate (AC)), all with and without vitamin B_{12} (B). Two types of controls were also performed: live controls, to evaluate natural dechlorinating activity and heat-killed controls, to discard abiotic processes. Each experiment was performed in triplicate.

Figure E1. Preliminary batch experiments set up in 2012

120 mL-bottles (Figure E1) were filled with 100 mL of slurry, 1 mg/L resazurin as redox indicator9, 3 mM of the corresponding electron donor (Fennell et al., 2001) and 10 µM of vitamin B_{12} (Shan et al., 2010). Bottles were crimped inside an anoxic glovebox filled with N_2(g).

The microcosms were incubated statically in the dark at room temperature and regularly monitored. Eight 3mL-samples from liquid phase were extracted periodically and kept frozen until analysis for concentration and isotopic fractionation (when possible) of the main pollutants. Two replicates of each treatment were sacrificed after 197 days of incubation (t_6), except all LAB bottles which were sacrificed by mistake after 58 days (t_3). Initial and final measurements of relevant geochemical parameters and microbial community composition assessment were done. The third replicates kept on going and some of them were analyzed after 348 days (t_7).

Although pink colour of resazurin indicated certain amount of oxygen during the preparation of all bottles, (see KI in Figure E1), all live incubations became quickly colorless or black after one day indicating O_2 consumption. Bottles kept strictly anoxic along the 8 sampling times.

Analytical methods

<u>DGGE</u>. DNA extracts from different microcosms samples (t_0; LA_t_3; COB_t_6; CO_t_6; LAB_t_3; MEB_t_6; ME_t_6; ACB_t_6; AC_t_6) were analysed by performing eubacterial and archaeal DGGE profiling. Three primer sets selectively amplified eubacterial (F341GC/R907) and

archaeal (ArchF0025/ArchR1517; nested ArchF344/ArchR915GC) 16S rRNA gene fragments. The PCR amplification of hypervariable V3-V5 region from the 16S rRNA gene of both domains and the DGGE profiles and sequencing were performed as previously reported by Palatsi et al. (2010). The sequences were chimera-checked by using Bellerephon on-line tool (DeSantis et al., 2006), and aligned against GenBank database by using the alignment tool comparison software BLASTn and RDP. Sequences were submitted to the Genbank (NCBI) with the accession numbers (KY921703-KY921707).

Real Time PCR (qPCR). Several target genes were selected and quantified by quantitative real time PCR (qPCR) technique. Aliquots from well S3 without any treatment and microcosms samples were filtered by using 0.22µm cellulose acetate filters in Swinnex supports (Millipore) and extracted with Power Soil DNA Isolation Kit (MoBio) in triplicate. The analyses were fulfilled by using Brilliant II qPCR Master Mix (Stratagene), with or without SYBR ®Green in a Real Time PCR System MX3000P (Stratagene, La Jolla, CA). gBlocks® Gene Fragments (IDT, Integrated DNA Technologies) were used for the standard curve of each target gene. Ten-fold serial dilutions from synthetic genes were subjected to qPCR assays in duplicate showing a linear range between 10^1 and 10^8 gene copies per reaction to generate standard curves. qPCR reactions were under quality standards: efficiencies were between 90-110% and R^2 above 0.985. All results were processed by MxPro™ QPCR Software (Stratagene, La Jolla, CA) and were treated statistically.

Dehalorespiring bacteria were assessed by chloroethene-reductive dehalogenases encoding genes (*bvcA*, *vcrA* and *tceA*) and the specific 16S rRNA *Dehalococcoides* gene (*Dhc*). Primers and probes were described in Ritalahti et al. (2006) as well as the qPCR protocol. Analyses were performed by using Double Quenched PrimeTime® Probes (IDT, Integrated DNA Technologies). An important organohalide-respiring bacteria (OHRB) as *Dehalobacter* sp. was quantified by CF reductive dehalogenase catalytic subunit A (*cfrA* gene) as described in Tang and Edwards (2013). 16S rRNA gene from eubacterial population and *mcrA* gene from methanogenic archaea were measured as previously reported in Prenafeta-Boldú et al. (2016). Ammonia oxidizing archaea (AOA) were studied by ammonia monooxygenase α-subunit encoding genes (*amoA*_AOA gene). A new combination of primers, previously described at Pelissari et al. (2017), was performed in order to match the known *amoA*-related AOA lineages (group I.1a: *Nitrosopumilus* cluster; group I.1a-associated: *Nitrosotalea* cluster; group I.1b: *Nitrososphaera* cluster; and *ThAOA* group: *Nitrosocaldus* cluster).

Results

The original amounts of the pollutants present in the field (CMs, chlorinated ethenes and ethanes, BTEXs, and traces of pesticides (Torrentó et al., 2014) remained unchanged in these preliminary microcosm assays. These preliminary microcosm assays served to prove the natural attenuation of CMs, which was accelerated with the addition of 10 µM of B_{12}.

Some problems in determining certain VOCs concentration were arisen, probably due to volatilization losses generated by the freezing-out effect (higher concentration in the headspace over frozen solutions) according to Raoult's law, as was also detected by Elsner et al. (2006). These problems prevented the authors to extract strict quantitative conclusions based only on concentrations (some results are provided for comparison purposes) or to quantify fractionation (ε). In contrast to concentration results, isotope values could be taken into consideration as it was demonstrated the absence of significant carbon isotope fractionation during freezing Elsner et al. (2006).

Table E1. Initial aqueous concentration (in µg/L) at initial time (t_0) and relative aqueous concentration after 197 days (t_6) (as C_{t6}/C_{t0} (%)) of the main pollutants (chlorinated ethenes: tetrachloroethene (PCE), trichloroethene (TCE) and cis-dichloroethene (cDCE); chlorinated methanes: carbon tetrachloride (CT), chloroform (CF) and dichloromethane (DCM); carbon disulphide (CS_2) and toluene representing BTEXs compounds) for all the treatments (live control (CO), lactate (LA), methanol (ME), acetate (AC), heat-killed controls (KI)). B is vitamin B_{12}. Replicates 1 and 2 are shown. % consumption of added e-donor is also shown.

	Sample	PCE	TCE	cDCE	CT	CF	DCM	CS_2	toluene	Consumed added e-donor
µg/L	t_0	318	5539	1873	1324	17838	6217	41	555	
	CO1-t_6	99	76	100	25	104	81	109	90	
	CO2-t_6	100	79	103	19	109	82	104	94	No e-donor added
	CO1B-t_6	113	84	106	<8	38	93	308	97	
	CO2B-t_6	78	56	81	<8	6	88	433	72	
	LA1-t_6	92	70	94	22	85	76	100	99	89%
	LA2-t_6	108	80	97	22	90	81	110	97	
	LAB	Sacrificed at t_3								
C_{t6}/C_{t0} (%)	ME1-t_6	111	82	103	31	95	81	114	105	54%
	ME2-t_6	91	71	96	46	88	74	103	93	
	ME1B-t_6	117	85	111	<8	26	112	591	114	99%
	ME2B-t_6	107	80	106	<8	2	107	723	106	
	AC1-t_6	128	95	113	61	107	85	117	126	6%
	AC2-t_6	112	85	104	53	99	78	118	112	
	AC1B-t_6	109	76	95	<8	12	91	497	103	84%
	AC2B-t_6	113	80	103	<8	3	118	735	112	
	KI1-t_6	111	85	101	156	105	83	105	100	
	KI2-t_6	69	51	75	81	79	63	94	71	No e-donor added
	KI1B-t_6	99	79	96	118	103	79	136	96	
	KI2B-t_6	77	59	77	69	82	63	102	80	

The addition and consumption of the selected electron donors (Table E1) did not show any apparent biostimulating effect on the degradation of any of the analysed compounds, in comparison to the natural potential of the indigenous microbial community (live controls).

Despite concentration problems, carbon isotope enrichment showed that CF was only significantly degraded in live treatments in presence of B_{12} (Table E1, Figure E2). CT was degraded with and without the addition of B_{12}, although degradation was faster in the presence of B_{12}. CT isotope fractionation results could be only obtained by comparing initial and final values of bottles without B_{12} due to the low CT concentrations along the incubation (sampled volume was not sufficient for its isotope determination) (Table E2). CS_2 accumulation was only observed in B_{12} treatments although it only represented a maximum of 11% of the initial CT concentration. No apparent DCM accumulation was detected in any case and it could not be checked by isotope analyses (Table E1).

The decrease in CF concentration and the increase of more than 2‰ in $\delta^{13}C$ of trichloroethene (TCE) after 348 days (Table E2) proved TCE degradation in the live control, and in the acetate and methanol B_{12} amended treatments. Low concentrations of PCE in the solution did not allow PCE carbon isotope measurements.
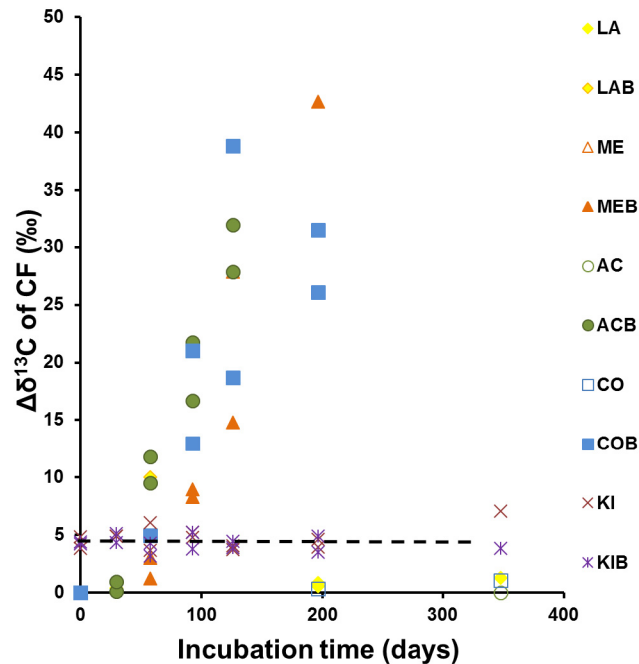
Figure E2. Variation of carbon isotope composition of CF ($\Delta\delta^{13}C$, ‰) over time for all treatments. Killed controls showed a carbon isotopic enrichment (dashed line) from initial $\delta^{13}C_{CF}$ value probably due to autoclaving process.

For microbial community assessment of both eubacterial and archaeal population, DNA extraction for further 16S rRNA (DNA-based) DGGE analysis of the V3-V5 hypervariable region was performed at initial time, at 58 days (t_3) for LAB and at 197 days (t_6) for the rest of live treatments. Sequencing of 16S rRNA (DNA-based) and functional genes related to dechlorination of chlorinated ethenes (*tceA, bvcA* and *vcrA*) or CF (*cfrA*), to methanogenic archaea (*mcrA*) and to ammonia oxidizing archaea (*amoA, AOA)* were also done.

16S rRNA (DNA-based) DGGE results revealed a stable microbial community related to halomethane biodegradation with the presence of both eubacterial (Pseudomonadaceae, Rhodobacteraceae and Porphyromonadaceae) and archaeal (Nitrosopumilaceae and Nitrososphaeraceae) population (Figure A3, Table E3). Neither *Dehalococcoides* spp. nor their functional genes (*tceA, bvcA* and *vcrA*) were detected. The abundance of *cfrA* gene (Tang and Edwards, 2013) might prove the presence of *Dehalobacter* spp. with CF reductive dehalogenase. *cfrA* gene was detected with a concentration of 10^3 copies/mL sample, four orders of magnitude beneath the total eubacterial population of 10^7 16S rRNA copies/mL sample (Figure A4). However, DGGE results did not show any *Dehalobacter* spp. (Figure E3) given that they could be below the detection limit which depends on the species or the specific strain (Ercolini, 2004). *cfrA* gene was DNA-based measured in this preliminary microcosms, whereas for Article 4, its activity was studied by RNA.
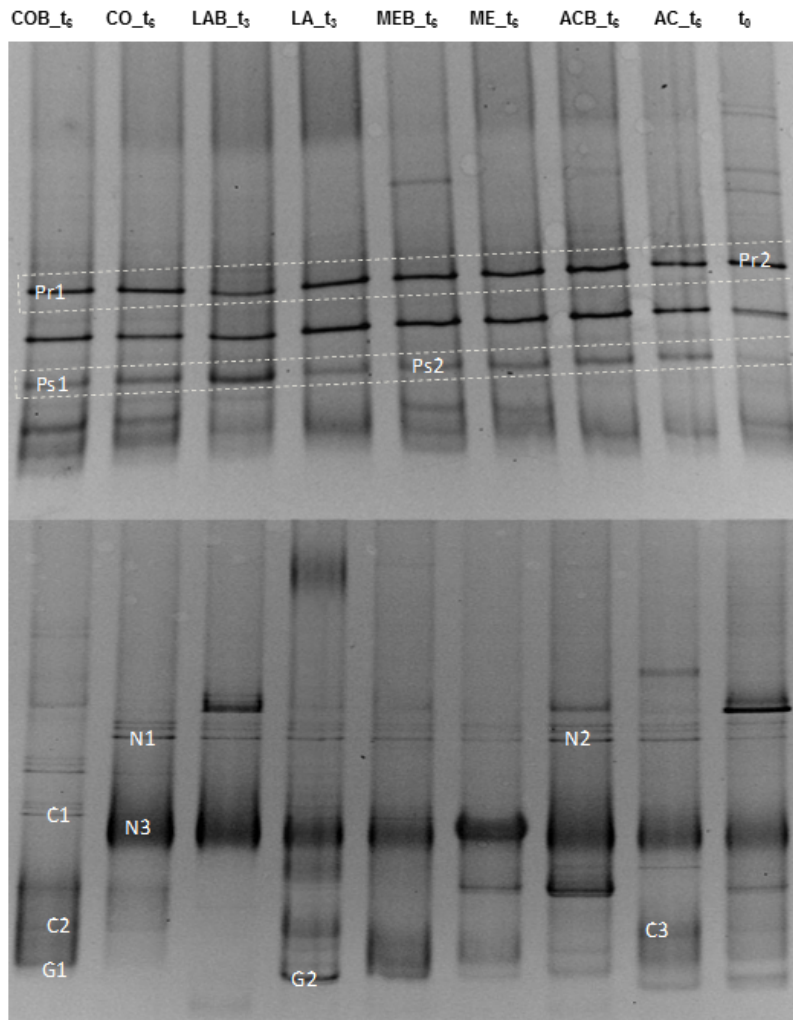
Figure E3. Eubacterial (above) and archaeal (below) DGGE results of 16S rRNA (DNA-based) V3-V5 hypervariable region.

Table E2. Evolution of carbon isotope composition ($\delta^{13}C$ expressed in ‰) of some key VOCs in microcosms experiments with respect the initial $\delta^{13}C$ after 197 days (replicates 1 and 2) and after 348 days (replicate 3) of incubation for all treatments: Live control (CO), lactate (LA), methanol (ME), acetate (AC), heat-killed controls (KI)). B is vitamin B_{12}. In bold, values differing more than 2‰ from the initial value. nm is not measured and bdl, below detection limit.

	Time (days)	TCE	CT	CF	toluene
Live average $\delta^{13}C_{t0}$ (‰)	0	*-10.5*	*-12.5*	*-26.1*	*-26.2*
CO1	197	-10.3	nm	-25.7	-26.2
CO2	197	-10.6	nm	-26.2	-25.8
CO3	348	-9.0	**+9.4**	-25.0	-25.8
CO1B	197	-9.8	nm	**+5.4**	-26.1
CO2B	197	-9.4	bdl	nm	-26.1
CO3B	348	**-7.4**	bdl	nm	-25.8
LA1	197	-10.5	nm	-25.5	-26.4
LA2	197	-10.6	nm	-25.2	-26.6
LA3	348	-9.1	**+4.0**	-24.8	-26.0
ME1	197	-10.6	nm	-25.9	-26.5
ME2	197	-10.7	nm	nm	-26.2
ME3	348	-9.3	**+2.5**	**-29.3**	-25.9
ME1B	197	-9.4	nm	**+16.6**	-26.5
ME2B	197	-9.2	bdl	nm	-26.5
ME3B	348	**-7.9**	bdl	nm	-25.5
AC1	197	-10.5	nm	-27.3	-26.4
AC2	197	-10.2	nm	-27.3	-26.4
AC3	348	-9.1	**+3.5**	-26.1	-26.0
AC1B	197	-9.2	nm	nm	-26.1
AC2B	197	-8.8	bdl	nm	-26.5
AC3B	348	**-7.2**	bdl	nm	-25.5
Killed average $\delta^{13}C_{t0}$ (‰)	0	*-10.6*	*-12.5*	*-21.7*	*-25.6*
KI1	197	-10.5	nm	-21.5	-26.1
KI2	197	-10.5	nm	-22.1	-26.0
KI3	348	-9.2	-11.7	**-19.0**	-25.6
KI1B	197	-10.4	nm	-22.6	-26.3
KI2B	197	-10.8	nm	-21.1	-26.5
KI3B	348	-9.9	**-6.4**	-22.3	-26.0

Table E3. DGGE band description, designations, and levels of similarity to closest related organisms in GenBank.

Band	Accession Number	Closest type strain in GenBank	Similarity (%)	Phylogenetic group
Pr1, Pr2	KY921706	*Proteiniphilum* sp. S2 (KP178480)	97.5	p_ Bacteroidetes; f_ Porphyromonadaceae
Ps1, Ps2	KY921707	*Pseudomonas pseudoalcaligenes* (KJ586277)	99.2	p_ Proteobacteria; f_ Pseudomonadaceae
C1,C2,C3	KY921703	Ca. *Nitrosocosmicus franklandus* (KU290365)	100	p_Thaumarchaeota; f_Nitrososphaeraceae
		Ca. *Nitrocosmicus oleophilus* (CP012850)	100	
N1,N2,C3	KY921704	Ca. *Nitrosoarchaeum koreensis* MY1 (HQ331116)	100	p_Thaumarchaeota; f_Nitrosopumilaceae
G1, G2	KY921705	Ca. *Nitrososphaera gargensis* Ga9.2 (CP002408)	99.9	p_Thaumarchaeota; f_Nitrososphaeraceae
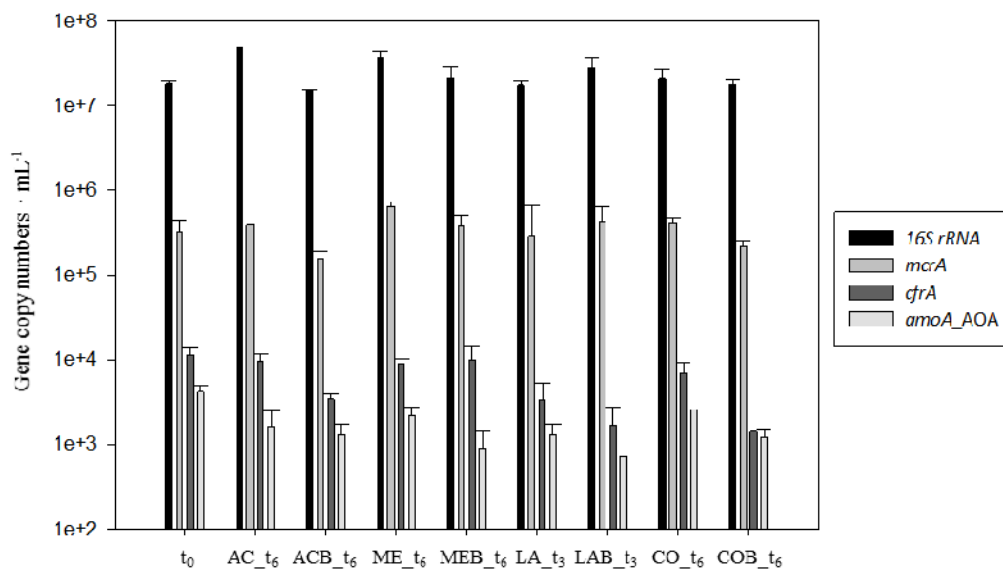
Figure E4. qPCR results of *16SrRNA*, *mcrA*, *cfrA* and *amoA_AOA*: copy numbers at initial time (t_0) and after 58 days (t_3) for LA and LAB treatments and after 197 days (t_6), for the rest.

References Annex E

DeSantis, T.Z., Hugenholtz, P., Larsen, N., Rojas, M., Brodie, E.L., Keller, K., Huber, T., Dalevi, D., Hu, P., Andersen, G.L., 2006. Greengenes, a chimera-checked 16S rRNA gene database and workbench compatible with ARB. Appl. Environ. Microbiol. 72, 5069–5072. doi:10.1128/AEM.03006-05

Elsner, M., Lacrampe-Couloume, G., Sherwood Lollar, B., 2006. Freezing to preserve groundwater samples and improve headspace quantification limits of water-soluble organic contaminants for carbon isotope analysis. Anal. Chem. 78, 7528–7534. doi:10.1021/ac061078m

Ercolini, D., 2004. PCR-DGGE fingerprinting: Novel strategies for detection of microbes in food. J. Microbiol. Methods 56, 297–314. doi:10.1016/j.mimet.2003.11.006

Fennell, D.E., Carroll, A.B., Gossett, J.M., Zinder, S.H., 2001. Assessment of indigenous reductive dechlorinating potential at a TCE-contaminated site using microcosms, polymerase chain reaction analysis, and site data. Environ. Sci. Technol. 35, 1830–1839. doi:10.1021/es0016203

Palatsi, J., Illa, J., Prenafeta-Boldú, F.X., Laureni, M., Fernandez, B., Angelidaki, I., Flotats, X., 2010. Long-chain fatty acids inhibition and adaptation process in anaerobic thermophilic digestion: Batch tests, microbial community structure and mathematical modelling. Bioresour. Technol. 101, 2243–2251. doi:10.1016/j.biortech.2009.11.069

Pelissari, C., Guivernau, M., Viñas, M., de Souza, S.S., García, J., Sezerino, P.H., Ávila, C., 2017. Unraveling the active microbial populations involved in nitrogen utilization in a vertical subsurface flow constructed wetland treating urban wastewater. Sci. Total Environ. 584–585, 642–650. doi:10.1016/j.scitotenv.2017.01.091

Prenafeta-Boldú, F.X., Fernández, B., Viñas, M., Lizardo, R., Brufau, J., Owusu-Asiedu, A., Walsh, M.C., Awati, A., 2016. Effect of *Bacillus* spp. direct-fed microbial on slurry characteristics and gaseous emissions in growing pigs fed with high fibre-based diets. Animal 14, 1–10. doi:10.1017/S1751731116001415

Ritalahti, K.M., Amos, B.K., Sung, Y., Wu, Q., Koenigsberg, S.S., Löffler, F.E., 2006. Quantitative PCR targeting 16S rRNA and reductive dehalogenase genes simultaneously monitors multiple *Dehalococcoides* strains. Appl. Environ. Microbiol. 72, 2765–2774. doi:10.1128/AEM.72.4.2765-2774.2006

Shan, H., Kurtz, H.D., Freedman, D.L., 2010. Evaluation of strategies for anaerobic bioremediation of high concentrations of halomethanes. Water Res. 44, 1317–1328. doi:10.1016/j.watres.2009.10.035

Tang, S., Edwards, E.A., 2013. Identification of *Dehalobacter* reductive dehalogenases that catalyse dechlorination of chloroform, 1,1,1-trichloroethane and 1,1-dichloroethane. Phil. Trans. R. Soc. B 368, 20120318. doi:10.1098/rstb.2012.0318

Torrentó, C., Audí-Miró, C., Bordeleau, G., Marchesi, M., Rosell, M., Otero, N., Soler, A., 2014. The use of alkaline hydrolysis as a novel strategy for chloroform remediation: The feasibility of using construction wastes and evaluation of carbon isotopic fractionation. Environ. Sci. Technol. 48, 1869–1877. doi:10.1021/es403838t.

Annex F. Article 4. Biotic chlorinated methanes degradation

Rodríguez-Fernández, D., Torrentó, C., Guivernau, M., Viñas, M., Hunkeler, D., Soler, A., Domènech, C., Rosell, M., 2018. Vitamin B_{12} effects on chlorinated methanes-degrading microcosms: Dual isotope and metabolically active microbial populations assessment. Sci. Total Environ. 621, 1615–1625. doi:10.1016/j.scitotenv.2017.10.067.

Vitamin B$_{12}$ effects on chlorinated methanes-degrading microcosms: Dual isotope and metabolically active microbial populations assessment

Diana Rodríguez-Fernández [a],*, Clara Torrentó [b], Miriam Guivernau [c], Marc Viñas [c], Daniel Hunkeler [b], Albert Soler [a], Cristina Domènech [a], Mònica Rosell [a]

[a] Grup de Mineralogia Aplicada i Geoquímica de Fluids, Departament de Mineralogia, Petrologia i Geologia Aplicada, Facultat de Ciències de la Terra, Universitat de Barcelona (UB), c/Martí Franquès s/n, 08028 Barcelona, Spain
[b] Centre d'hydrogéologie et de géothermie, Université de Neuchâtel, Rue Emile-Argand 11, Neuchâtel 2000, Switzerland
[c] GIRO Joint Research Unit IRTA-UPC, IRTA, Torre Marimon, Caldes de Montbui E-08140, Spain

HIGHLIGHTS

- B$_{12}$ catalyzed CT and CF anaerobic biodegradation in field-derived microcosms
- C-Cl CSIA and active microbial community used for CMs degradation assessment
- Distinct C-Cl isotope slope (Λ) for B$_{12}$-amended vs. unamended CT-treatments
- Λ for CF biodegradation with B$_{12}$ similar to reported abiotic CF reduction by Fe(0)
- Higher activity of *P. stutzeri* and *Ancylobacter* in treatments with B$_{12}$

GRAPHICAL ABSTRACT
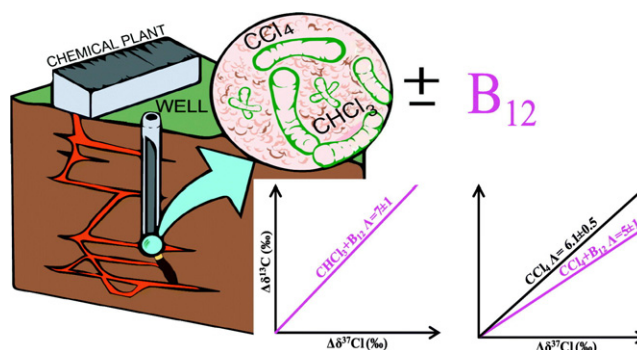
ARTICLE INFO

ABSTRACT

Field-derived anoxic microcosms were used to characterize chloroform (CF) and carbon tetrachloride (CT) natural attenuation to compare it with biostimulation scenarios in which vitamin B$_{12}$ was added (B$_{12}$/pollutant ratio of 0.01 and 0.1) by means of by-products, carbon and chlorine compound-specific stable-isotope analysis, and the active microbial community through 16S rRNA MiSeq high-throughput sequencing. Autoclaved slurry controls discarded abiotic degradation processes. B$_{12}$ catalyzed CF and CT biodegradation without the accumulation of dichloromethane, carbon disulphide, or CF. The carbon isotopic fractionation value of CF (εC_{CF}) with B$_{12}$ was -14 ± 4‰, and the value for chlorine (εCl_{CF}) was -2.4 ± 0.4‰. The carbon isotopic fractionation values of CT (εC_{CT}) were -16 ± 6 with B$_{12}$, and -13 ± 2‰ without B$_{12}$; and the chlorine isotopic fractionation values of CT (εCl_{CT}) were -6 ± 3 and -4 ± 2‰, respectively. *Acidovorax*, *Ancylobacter*, and *Pseudomonas* were the most metabolically active genera, whereas *Dehalobacter* and *Desulfitobacterium* were below 0.1% of relative abundance. The dual C-Cl element isotope slope ($\Lambda = \Delta\delta^{13}C/\Delta\delta^{37}Cl$) for CF biodegradation (only detected with B$_{12}$, 7 ± 1) was similar to that reported for CF reduction by Fe(0) (8 ± 2). Several reductive pathways might be competing in the tested CT scenarios, as evidenced by the lack of CF accumulation when B$_{12}$ was added, which might be linked to a major activity of *Pseudomonas stutzeri*; by different chlorine apparent kinetic isotope effect values and Λ which was statistically different with and without B$_{12}$ (5 ± 1 vs 6.1 ± 0.5), respectively. Thus, positive B$_{12}$ effects such as CT and CF degradation catalyst were quantified for the first time in isotopic terms, and confirmed with the major activity of species potentially capable of their degradation. Moreover, the indirect benefits

* Corresponding author.
  E-mail address: diana.rodriguez@ub.edu (D. Rodríguez-Fernández).

of B_{12} on the degradation of chlorinated ethenes were proved, creating a basis for remediation strategies in multi-contaminant polluted sites.

1. Introduction

The chlorinated methanes (CMs) carbon tetrachloride (CT) and chloroform (CF) are volatile organic compounds (VOCs) commonly found in groundwater. Although natural sources of CT and CF have been reported (Penny et al., 2010; Cappelletti et al., 2012), anthropogenic sources are more relevant given their use in many industrial activities (Doherty, 2000; Cappelletti et al., 2012). Both are considered possibly carcinogenic substances (Group 2B) by the International Agency for Research on Cancer and Disease Registry (2016).

There are no known organisms that metabolically degrade CT under neither oxic nor anoxic conditions (Penny et al., 2010). Under anoxic conditions, microbial CT degradation appears to be a non-specific co-metabolic reaction involving electron shuttles produced by facultative or strictly anaerobic bacteria and methanogenic Archaea (Penny et al., 2010). CT reduction is the predominant reaction mechanism which is either abiotically mediated by iron minerals and/or metals or biotically catalyzed (Lewis and Crawford, 1995). As seen in Scheme 1, in the CT reductive hydrogenolysis (pathway 1, Scheme 1), the first step involves an electron transfer leading to CF, while in other reduction processes two electrons are initially transferred, followed by hydrolytic substitution producing CO, formate, and CO_2 (hydrolytic reduction, pathway 2), or by thiolytic substitution leading to CS_2 (thiolytic reduction, pathway 3). Finally, CT reduction by the *Pseudomonas stutzeri* strain KC leads to CO_2 as the main product without CF formation, but with phosgene and thiophosgene as toxic intermediates (pathway 4).

CF biodegradation has been described under both oxic and anoxic conditions (Cappelletti et al., 2012). Under anoxic conditions, the following pathways are reported in the literature: CF dehalorespiration and co-metabolic reductive dechlorination to DCM (pathway 1, Scheme 1), CF reductive elimination to CH_4 (pathway 1a), and a first reduction followed by hydrolysis and final oxidation to CO and CO_2 (pathway 2). The mentioned anaerobic CF pathways were also described abiotically (He et al., 2015).

Redox active corrinoids such as vitamin B_{12}, a cofactor for some dehalogenase enzymes (Banerjee and Ragsdale, 2003), catalyze the reductive biodegradation of CT to CO, CO_2, or CS_2, which suggests degradation through pathways 2 and 3 (Scheme 1), whereas toxic CF (though pathway 1, Scheme 1) becomes a minor product, possibly

because B_{12} stimulates further CF degradation (via pathway 1a or 2) (Cappelletti et al., 2012). However, it is unknown in which proportion these CMs degradation pathways take place in complex mixed cultures, and if they happen biotic or abiotically depending on the media composition. It is also unknown how different B_{12}/pollutant ratios impact this pathway selection, because the available data to date is only in terms of consumption rates or the characterization of by-products (Becker and Freedman, 1994; Hashsham et al., 1995; Workman et al., 1997; Zou et al., 2000; Guerrero-Barajas and Field, 2005a, 2005b; Shan et al., 2010). Hence, isotope and microbiological tools are proposed hereafter to better assess the natural attenuation and changes of CMs caused by B_{12} in field-derived anoxic microcosms.

Compound specific isotope analysis (CSIA) allows one to confirm degradation when monitoring of the concentration of parental or by-products is not conclusive (Elsner, 2010). The calculation of the extent of isotopic fractionation (ε) in the laboratory follows a Rayleigh approach (Elsner et al., 2005) through Eq. (1) in which δ_0 and δ_t are the isotope values (in per mil units, ‰, relative to international standards) of C or Cl at the initial start and after a given time (t) respectively, and f is the fraction of substrate remaining at time t. This calculation affords knowledge about whether degradation will be qualitatively detected in the studied field, and provides information about the reaction mechanism which is occurring by comparing the apparent kinetic isotope effects (AKIEs) to those reported in the literature and to the theoretical kinetic isotope effects (KIEs) (Elsner et al., 2005).

$$\ln \frac{\delta_t + 1000}{\delta_0 + 1000} = \frac{\varepsilon}{1000} \ln f \tag{1}$$

This approach however, has some limitations, since different AKIEs values for reactions undergoing the same bond cleavage can be obtained due to masking by rate limiting steps, or by secondary or superimposed isotope effects (Nijenhuis and Richnow, 2016). Thus, dual element isotope plots (2D-CSIA) allow a better distinction within different reactions, since slopes (e.g. $\Lambda = \Delta\delta^{13}C/\Delta\delta^{37}Cl$) are expected to be reaction-specific (Cretnik et al., 2013) and non-masked because both elements are affected to the same extent (Elsner et al., 2005). To our knowledge, only one study has explored Λ values for abiotic CF engineered transformation reactions (Torrentó et al., 2017), and no Λ

1. CT or CF hydrogenolysis
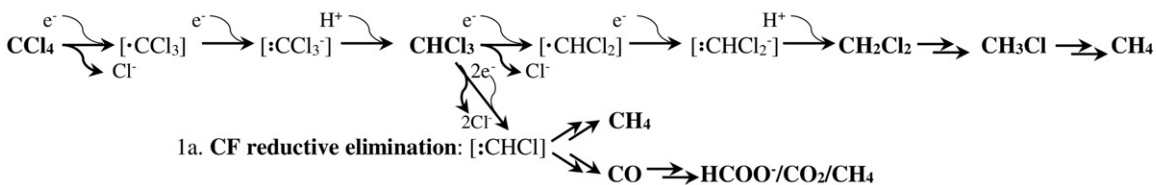
2. CT or CF hydrolytic reduction
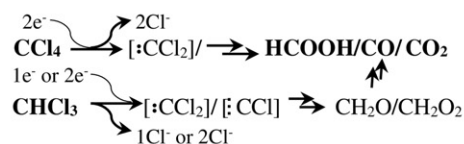
3. CT thiolytic reduction
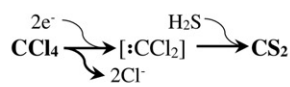
4. CT reduction by *Pseudomonas stutzeri*
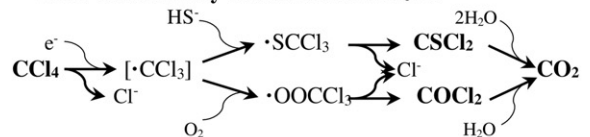
Scheme 1. Hypothetical CT (carbon tetrachloride) and CF (chloroform) reductive pathways according to Lewis and Crawford (1995), Field and Sierra-Alvarez (2004), Song and Carraway (2006), Penny et al. (2010), Cappelletti et al. (2012), and Torrentó et al. (2017).

values for biotic CF, or for abiotic or biotic CT degradation reaction models exist yet. Due to the limited Λ values of reference reactions, linking AKIE and Λ information with the activity of potential CT and CF microbial degraders can be worthwhile to gain insights into the natural attenuation and changes of CMs on the microbial population produced during bioremediation. RNA-based analyses provide more insight into active biologic processes than physiologic or genetic capability alone (Yargicoglu and Reddy, 2015). Next-Generation Sequencing (NGS) technologies, such as Miseq, have prompted a shift towards high-throughput methods for characterizing both total and metabolically active (16S rRNA from active ribosomes and total RNA, analyzed from synthesized cDNA) microbial communities (Pelissari et al., 2017).

The main aim of the present study was to characterize the anaerobic CT and CF biodegradation potential of indigenous microbiota from the monitored contaminated Òdena site (Barcelona, Spain) (Palau et al., 2014; Torrentó et al., 2014), and also to characterize the effects of vitamin B_{12}, as a bioremediation strategy, on the microbial community and on degradation pathways, for further field applications. B_{12} amended and unamended microcosm batch experiments were used for (1) monitoring the concentration of parental and by-product compounds and $\delta^{13}C$ and $\delta^{37}Cl$ to evidence degradation; (2) characterizing the active microbial community by RNA-based NGS to assess the effect of B_{12} addition on the microbial populations; and (3) determining the εC, εCl, the corresponding AKIEs and Λ of each compound and treatment to study the degradation pathways.

2. Material and methods

2.1. Experimental set-up

Following the Fennell et al. (2001) procedure, preliminary microcosm assays were performed with homogeneous slurry (groundwater and sediments) collected in June 2012 from the bottom portion (17 m.b.g.s.) of an iron-reducing well at the Òdena site (Palau et al., 2014). The original amounts of the pollutants present in the field (chlorinated methanes, ethenes and ethanes, BTEXs, and traces of pesticides (Torrentó et al., 2014)) remained unchanged in these preliminary microcosm assays. These preliminary microcosm assays served to prove the natural attenuation of CMs, which was accelerated with the addition of 10 μM of B_{12} (data not shown).

For studying the effect of different amounts of B_{12} on the degradation of CMs in detail, a new slurry was collected from the same well in February 2014. The slurry was flushed with $N_2(g)$ during two hours inside an anoxic $N_2(g)$-filled glovebox to remove the large original concentrations of VOCs and to add known amounts of CF and CT. According to Guerrero-Barajas and Field (2005a, 2005b), three scenarios exist for each target compound: (i) without the addition of vitamin B_{12}, called "pollutant without B_{12} treatment" abbreviated as CFw/oB or CTw/oB; (ii) with a molar ratio of vitamin B_{12}/pollutant of 0.01, called "0.01B/pollutant treatment"; and (iii) with a molar ratio of 0.1, called "0.1B/pollutant treatment"; the pollutant being CT (99% Panreac) or CF (99% Merck) depending on the case. Live treatments were run in quintuplicate using 120 mL-serum bottles filled with 100 mL of slurry, which were inoculated with a theoretical pollutant concentration of 200 μM, referred to as the liquid volume, and with the corresponding B_{12} volume (0, 2, or 20 μL). The bottles were filled-up inside an anoxic glove box and sealed with grey PTFE stoppers. Parallel series with triplicate heat-killed (KI) controls were performed to discard abiotic processes. KI controls were filled with 100 mL of slurry and sealed inside the glovebox prior to autoclaving in three cycles of 20 min at 121 °C. The same amounts of pollutant and B_{12} in comparison to the equivalent live treatment were subsequently added by using N_2-purged sterile syringes. KI controls were started 43 h after the live samples. Static incubation in darkness at room temperature was performed for all treatments during the 376 days long experimental period (t_{10}).

2.2. Sampling

Samples for chemical and isotopic analyses were periodically taken using sterilized syringes and filtered through 0.2 μm-nylon sterilized filters (Millipore) from three of the replicate bottles and kept refrigerated at 4 °C in 2.5 mL crimped vials. A sample from the flushed slurry without amendments was taken for VOCs concentration analysis and DNA was extracted for studying the total bacterial population present at the initial time (t_0) by DGGE and 16S rRNA MiSeq high-throughput sequencing. In addition, when the degradation of significant target contaminants was detected (at 85 days, t_3, from all B_{12} amended bottles, and at t_{10} from all live treatments), samples were taken from one of the two untouched replicates for total RNA extraction (then retrotranscripted to cDNA) for further DGGE and 16S rRNA MiSeq high-throughput sequencing. The concentrations of VOCs, $\delta^{13}C_{CT}$, and $\delta^{13}C_{CF}$ were also measured in these replicates just before the extraction (M_S bottles in the figures).

2.3. Chemical analyses

Due to volume limitations, the concentration of VOCs and C and Cl isotope analyses of CT and CF were prioritized. The concentration of VOCs was measured in the *Centres Científics i Tecnològics de la Universitat de Barcelona* (CCiT-UB) by headspace (HS)-gas chromatography (GC) - mass spectrometry (MS) as explained in Torrentó et al. (2014). The error based on replicate measurements was below 10% for all compounds.

To compare the concentration decrease kinetics among the treatments and the literature, aqueous concentration data of CT and/or CF versus time was fitted to a pseudo-first-order rate model according to Eq. (2), where C is the target chlorinated compound concentration in μM, t is the time in days, and k′ is the pseudo-first-order rate constant ($days^{-1}$), assuming that all the removal of CT and CF was due to a degradation process.

$$dC/dt = -k'C \qquad (2)$$

The k′ was obtained using the integrated form of Eq. (2), shown in Eq. (3) where C_0 is the initial concentration of the chlorinated compound (μmol/L).

$$lnf = lnC/C_0 = k't \qquad (3)$$

Uncertainty was obtained from 95% confidence intervals (CI).
Temperature, pH, and anions and cation concentrations were measured when possible (see SI for further details).

2.4. Isotope analyses

Due to volume limitations, $\delta^{13}C$ and $\delta^{37}Cl$ were measured in different replicates of the same treatment and incubation time. $\delta^{13}C$ analyses were performed in CCiT-UB by HS - solid-phase micro-extraction (SPME)-GC-isotope ratio MS (IRMS), as explained in Martín-González et al. (2015). According to the standard deviation of the daily standards of each compound (SD ≤ 0.5, n = 24), a total instrumental uncertainty (2σ) of ± 0.5‰ was considered (Sherdwood Lollar et al., 2007), given that volume limitation prevented duplication of the measurements. $\delta^{37}Cl$ analyses were performed in the University of Neuchâtel using a HS-GC-quadrupole MS (qMS), as explained in Heckel et al. (2017). Each $\delta^{37}Cl$ value and its analytical uncertainty (2σ, in all cases below ± 0.5%) were determined on the basis of ten injections, and the working standards were interspersed along the sequence.

Isotopic mass balances were calculated following Eq. (4), where *x* is the molar fraction of each compound relative to the total molar mass of CMs from which isotopic values are available at each time. The equation assumes only the hydrogenolysis pathway with the available isotopic

data from CMs, since potential gas products (CH$_4$, CO, CO$_2$, formate, phosgene, and tiophosgene) were not measured.

$$\delta^{13}C_{SUM}(‰) = x_{CT}\delta^{13}C_{CT} + x_{CF}\delta^{13}C_{CF} + x_{DCM}\delta^{13}C_{DCM} \qquad (4)$$

For AKIE calculations, carbon and chloride ε values determined by the Rayleigh approach (Eq. (1)) were used according to Eq. (5), where n is the total number of the atoms of the considered element (E) in the target molecule, x the number of atoms located at the reactive site, and z the number of atoms in intramolecular isotopic competition.

$$AKIE_E \approx \frac{1}{1 + \left(\frac{n \times z}{x} \times \frac{\varepsilon}{1000}\right)} \qquad (5)$$

AKIE$_C$ was calculated using $n = x = z = 1$ for both compounds, while AKIE$_{Cl}$ was calculated using $n = x = z = 4$ for CT and $n = x = z = 3$, for CF.

2.5. Microbial community abundance and diversity analyses

2.5.1. DNA-based study at the initial time

To have a sample representative of the initial time (t_0), a slurry was sampled after flushing and before the addition of target compounds and B$_{12}$. This sample was used for studying the total bacterial population through DNA extraction by following the same procedure detailed in the subsequent sections for RNA.

2.5.2. Total genomic DNA and RNA extraction

15 mL of slurry from microcosms at different incubation times were collected in triplicate and centrifuged at 4000 g/30′ and 4 °C. The supernatants were removed and the pellets were stored immediately at −80 °C until further analysis. Total RNA and DNA were extracted in triplicate from known weights of each sample with the PowerMicrobiome™ RNA Isolation Kit, Catalog #26000-50 (MoBio Laboratories Inc., Carlsbad, CA, USA), according to the manufacturer's instructions. Purified total RNA was obtained by the removal of the co-extracted DNA with DNase I (provided by the kit) at 25 °C for 10 min, and the subsequent inactivation of DNase I with EDTA 50 mM (Thermo Scientific Fermentas, USA) at 75 °C for 5 min. Reverse transcription polymerase chain reaction (RT-PCR) for cDNA synthesis from the obtained mRNA was performed using the PrimeScript™ RT Reagent Kit (Takara Bio Inc., Japan). The reaction was carried out in a volume of 30 μL, which contained 15 μL of purified mRNA, 6 μL of PrimeScript™ buffer, 1.5 μL of the enzyme mix, 1.5 μL of Random 6 mers, and 6 μL of RNase Free dH$_2$O.

2.5.3. DGGE analyses

Three primer sets selectively amplified bacterial (F341GC/R907) and archaeal (ArchF0025/ArchR1517; nested ArchF344/ArchR915GC) 16S rRNA gene fragments. The PCR amplification of the hypervariable V3-V5 region from the 16S rRNA gene of both domains, and the DGGE profiles and sequencing were performed as previously reported by Palatsi et al. (2010). The sequences were chimera-checked by using the Bellerephon on-line tool (DeSantis et al., 2006), and aligned against the GenBank database by using the BLASTn and RDP alignment tool comparison software. The sequences were submitted to Genbank (NCBI) with the accession numbers (KY921708-KY921709).

2.5.4. cfrA gene expression

In order to detect the presence and activity of *Dehalobacter* sp., *cfrA* encoding gene of the CF reductive dehalogenase alpha subunit (Chan et al., 2012; Tang and Edwards, 2013) was assessed by the qPCR technique as described in Tang and Edwards (2013). For the standard curve, it was designed a synthetic gene by using gBlocks® Gene Fragments (IDT, Integrated DNA Technologies). The *cfrA* sequence belongs to *Dehalobacter* sp. enrichment culture clone rdhA01 (GenBank

sequence database: JX282329.1). Ten-fold serial dilutions from synthetic genes were subjected to qPCR assays in duplicate showing a linear range between 10^1 and 10^8 gene copy numbers per reaction to generate standard curves. qPCR reactions fitted quality standards: efficiencies were between 90 and 110% and R^2 above 0.985. All results were processed by MxPro™ QPCR Software (Stratagene, La Jolla, CA) and were treated statistically.

2.5.5. 16S rRNA Illumina-sequencing of the active microbial populations

A deep microbial diversity assessment of the metabolically active populations was performed by means of 16S rRNA (RNA-based) Illumina (MiSeq) high-throughput sequencing, targeting the bacterial 16S rRNA V1-V3 region, by utilizing the Illumina MiSeq sequencing platform. The obtained DNA reads were compiled in FASTq files for further bioinformatic processing. Trimming of the 16S rRNA barcoded sequences into libraries was carried out using QIIME software version 1.8.0 (Caporaso et al., 2010a). Quality filtering of the reads was performed at Q25, prior to the grouping into Operational Taxonomic Units (OTUs) at a 97% sequence homology cutoff. The following steps were performed using QIIME: Denoising using Denoiser (Reeder and Knight, 2010); reference sequences for each OTU (OTU picking up) were obtained via the first method of the UCLUST algorithm (Edgar, 2010); for sequence alignment and chimera detection the algorithms PyNAST (Caporaso et al., 2010b) and ChimeraSlayer (Haas et al., 2011) were used. OTUs were then taxonomically classified using RDP Naïve Bayesian Classifier (2.2) with a bootstrap cutoff value of 80%, and compiled to each taxonomic level (Wang et al., 2007). To evaluate the alpha diversity of the samples, the number of OTUs, the inverted Simpson index, Shannon index, Goods coverage, and Chao1 richness estimators were calculated using the Mothur software v.1.35.9 (http://www.mothur.org) (Schloss et al., 2009). All the alpha-diversity estimators were normalized to 70,000 (the lower number of contigs among the different samples). Data from the MiSeq NGS assessment were submitted to the Sequence Read Archive (SRA) of the National Center for Biotechnology Information (NCBI) under the study accession number SRP090228.

3. Results and discussion

3.1. Biodegradation evidence

The elimination of VOCs by N$_2$ flushing of the slurry was not complete, as CT was much more efficiently flushed than CF (Table 1), although the remaining CF represented around a 10–20% of the total initial CF concentration in the CF treatments. The measured initial CT concentrations (Table 1) were four times smaller than the expected, likely due to the sorption of the slurry, while CF agreed better with the expected values, consistent with its lower tendency to sorb (Cappelletti et al., 2012).

Table 1

The average concentrations of VOCs (n measurements specified in parentheses) for the initial slurry after N$_2$ flushing (t_0) and live and heat-killed controls for all treatments of each parental compound (including together with and without B$_{12}$) in the first sampling (live treatments: 90 min after starting; heat-killed controls: 60 min after starting) expressed as μM at the liquid phase of the experimental bottle.

	Slurry t_0	CT treatments		CF treatments	
		Live	Heat-killed	Live	Heat-killed
CT	2	40 ± 17 (12)	26 ± 10 (15)	8 ± 5 (8)	4.5 ± 0.4 (9)
CF	26	<2	<2	132 ± 10 (9)	189 ± 37 (9)
DCM	0.4	<4	<4	<4	<4
CS$_2$	0.7	<0.7	<0.7	<0.7	<0.7
PCE	0.4	<2	<2	<2	<2
TCE	5	<2	<2	<2	<2
cDCE	9	2 ± 2 (8)	1.4 ± 0.1 (9)	10.0 ± 0.8 (3)	3.2 ± 0.2 (3)

Fluctuations in CF and CT concentration were observed in all the KI controls (Fig. 1), but they were not accompanied by an increase in the concentration of the expected metabolites neither by shifts in carbon nor in chlorine isotopic signatures ($\delta^{13}C_{CF} = -41.7 \pm 0.3‰$, n = 9; $\delta^{37}Cl_{CF} = -2.6 \pm 0.1‰$, n = 3; $\delta^{13}C_{CT} = -40.4 \pm 0.8‰$, n = 19; $\delta^{37}Cl_{CT} = -0.8 \pm 0.1‰$, n = 4) (Fig. 2). This would suggest that degradation is not occurring. The observed fluctuations in concentration could be due to sorption-desorption processes (Riley et al., 2010). This lack of CF degradation in the KI controls was consistent with results obtained in heat-killed controls amended with cobalamins performed by Guerrero-Barajas and Field (2005a), but not in the case of CT KI controls conducted by Guerrero-Barajas and Field (2005b). Guerrero-Barajas and Field (2005b) and Egli et al. (1990) pointed to CT and CF degradation by heat-killed cells, leading to DCM or CO_2, but at a markedly reduced rate compared to live treatments. The absence of CT degradation in our KI controls is also contrary to other studies (Hashsham et al., 1995; Puigserver et al., 2016). These degradation differences could be partially attributed to different slurry compositions, which may differ in the potential presence of reducing agents, such as sulfide or iron minerals, capable of supplying electrons for the abiotic reduction of CMs, which were not measured in any case.

The CT and CF concentration behaviour in triplicates of the same treatment were quite reproducible over time (Fig. A1), which permitted $\delta^{13}C$ and $\delta^{37}Cl$ analyses in different replicates. CF biodegradation only occurred in the presence of B_{12}. In the CFw/oB treatment, the CF concentration fluctuated (Fig. 1A), but $\delta^{13}C_{CF}$ did not vary significantly ($-40.8 \pm 0.8‰$, n = 7) (Fig. 2A). On the other hand, in the presence of B_{12} in the 0.01B/CF treatment, a CF concentration decrease (Fig. 1B) was accompanied by significant enrichment of the heavy isotopes for both C and Cl ($\Delta\delta$, 23 and 3‰, respectively, at t_{10}), indicative of normal isotope effects (Fig. 2A, B). In the 0.1B/CF treatment, CF was completely consumed before 72 days (Fig. 1C) which did not allow isotope measurements in the samples. No CS_2 accumulation (Fig. A2) was detected in any CF treatment, and significant transient DCM accumulation only occurred for the 0.01B/CF treatment after around 200 days (Fig. A3B).

CT degradation occurred both without and with B_{12}, being accelerated in the latter. The decrease of the CT concentration in the CTw/oB treatment (Fig. 1D) was accompanied by significant $\Delta\delta^{13}C$ and $\Delta\delta^{37}Cl$ (up to 32‰ and 6‰, at t_{10}, respectively, Fig. 2C), indicating natural biodegradation. CTw/oB treatments showed a change in the CT isotope enrichment trend after 211 days (Fig. 2C, D), a change that was also observed in the CT degradation rates (Fig. A4). CF was yielded as a by-product in the CTw/oB treatment, and its concentration increased over time (Fig. 1D). The $\delta^{13}C_{CF}$ depletion pattern during the first 200 days was probably due to the combined effect of both the produced and background CF isotopic signature (Fig. 2E, F). In addition, the least CF isotopic fractionation observed (Fig. 2E, F) could be explained by isotopically-sensitive branching (Zwank et al., 2005): CF might be formed in parallel with other non-analyzed products (as evidenced by non-closed isotopic mass balance, data not shown), and the enrichment effect of further CF degradation was discarded without B_{12}.

Complete CT consumption was observed in the 0.01B/CT and 0.1B/CT treatments after 110 and 72 days, respectively (Fig. 1E–F). Both treatments showed significant and similar carbon and chlorine isotopic enrichment trends (Fig. 2C, D). In the 0.01B/CT treatment, the CF concentration increased over time as a by-product (Fig. 1E), whereas in the 0.1B/CT treatment, a decrease in the CF concentration was detected (Fig. 1F). CF (hypothetical yield ± background) underwent isotopic enrichment, which was more significant once parental CT was totally consumed (Fig. 2C–F). This suggested that the 0.1B/CT ratio could be an eligible proportion to degrade both the parental CT and their degradation by-product (CF), if applied in the field site at the studied well. There was an absence of significant DCM or CS_2 accumulation in all the CT treatments (Fig. A2, A3).

Pseudo-first rate constant values of concentration removal kinetics (k', Fig. A4) confirmed the catalytic effect of B_{12} (e.g. $k' = 0.003 \pm 0.001$ d^{-1} for 0.01B/CF and $k' = 0.08 \pm 0.06$ d^{-1} for 0.1B/CF). These values cannot be directly compared to those reported in similar microcosm studies (Guerrero-Barajas and Field, 2005a, 2005b), since they
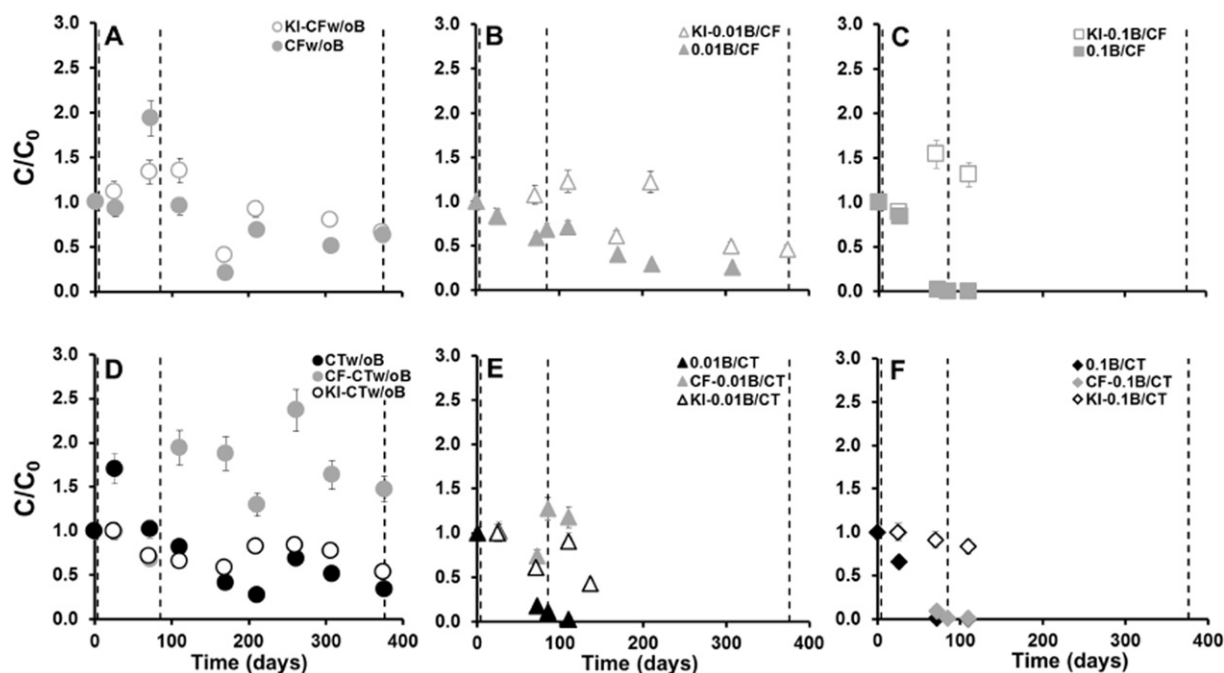
Fig. 1. Evolution of CF (grey) and CT (black) concentration (in C/C_0) in replicate 1 (from which C-CSIA measurements were done) of the CF (upper panels) and CT (lower panels) treatments: CFw/oB (A), 0.01B/CF (B), 0.1B/CF (C), CTw/oB (D), 0.01B/CT (E), and 0.1B/CT (F). C/C_0 were calculated from the total μmol in the bottle taking into account Henry's law constant at 24 °C according to Staudinger and Roberts (2001). CF evolution, as a potential product in the CT treatments, is also shown in D, E, and F. The evolution of parental compounds in replicate 1 from the corresponding heat-killed control (KI) experiments are shown for each treatment (empty symbols). No significant changes in the background CF were detected in CT-KI along the incubation time (data not shown). Dashed lines show the sampling times of the microbial analyses (t_0, t_3, and t_{10}). The error bars show the uncertainty in the concentration measurements. When not visible, error bars are smaller than the symbols.
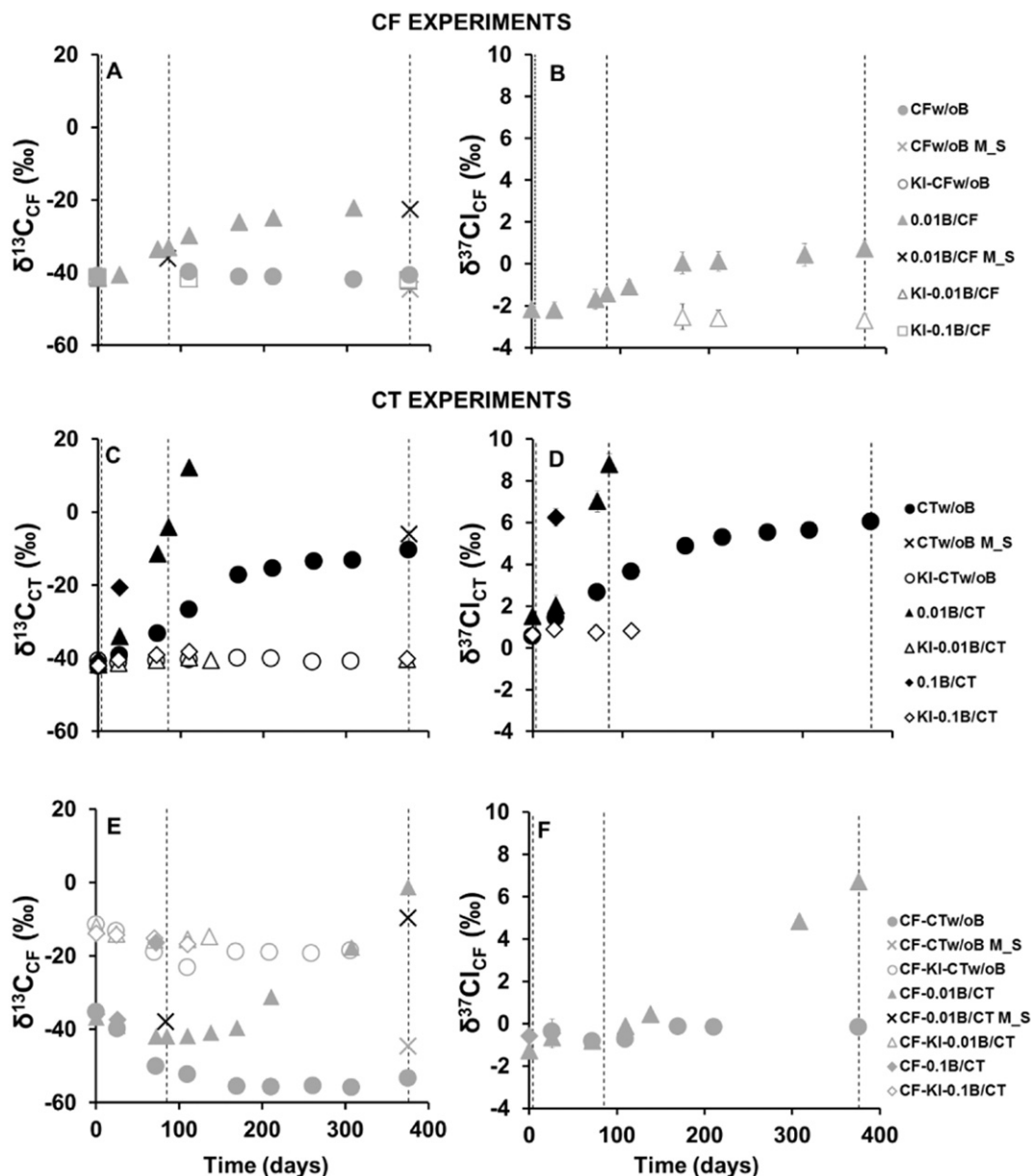
Fig. 2. The evolution of the CF and CT carbon (left panels), and chlorine (right panels) isotope composition (‰) over time, measured in replicates 1 and 2, respectively, of each treatment with CF (A, B) and CT (C, D) as target compounds, and CF (E, F) as a CT by-product. CF concentrations in the 0.1B/CF treatment decreased rapidly, and were therefore too low for isotopic measurements (no data points). The cross shaped symbol corresponds to carbon isotope data of the replicates (M_S bottles) used for microbial sampling (indicated in dashed lines). CT in 0.01B/CT and CT and CF, as a by-product, in the 0.1B/CT treatments were below the detection limit for carbon isotopic measurements (no data points) in replicates for microbial sampling. When not visible, error bars are smaller than the symbols.

were performed at different temperatures and with a different sludge composition. However, the ratios obtained for CT ($k'_{0.1B/CT}$ to $k'_{CTw/oB}$) were indeed similar (6 to 12) to Guerrero-Barajas and Field (2005b) (see Table A1). The k' for the CTw/oB treatment changed from 0.010 ± 0.003 d^{-1} towards a value of 0.005 ± 0.002 d^{-1} after 211 days. This half reduction of the kinetics might be due to CT inhibition by CF yield, redox mediators, and/or the consumption of other required nutrients (Chan et al., 2012; Lima and Sleep, 2010).

Low DCM amounts prevented the obtainment of its isotopic composition, and isotopic mass balances calculated with CF and CT did not close in those treatments where degradation was proved (all except the KI controls and CFw/oB), with a maximum difference, $\Delta(\delta_{sum} - \delta_{initial})$, of 40‰ in the case of the 0.1B/CT treatment. This is evidence of the degradation of further products or/and the existence of parallel pathways producing non-analyzed gas products (CH$_4$, CO, CO$_2$, formate, phosgene, and tiophosgene).

$\Delta\delta^{13}$C of the background PCE and cDCE was detected in the 0.1B/pollutant experiments (up to 11.6 and 5.3‰, respectively), when the CT and CF concentrations decreased to levels under the detection limit, while δ^{13}C$_{PCE}$ remained constant (-26.6 ± 0.1‰), if CF was still in solution in the 0.1B/CF treatment (Fig. 3). These inhibition effects of CMs on the degradation of chlorinated ethenes were previously reported in the literature (Bagley et al., 2000; Duhamel et al., 2002; Futagami et al., 2006), but never proved by isotopic data.

3.2. Active microbial populations assessment

Samples for DGGE and NGS analyses taken at t_0, t_3, and t_{10} were representative of different degradation stages in each treatment (detailed in 'Microbial assessment section', SI). The results of NGS revealed a metabolically active microbial diversity greater than that observed for DGGE (Fig. A5, Table A2), and allowed the identification of active species
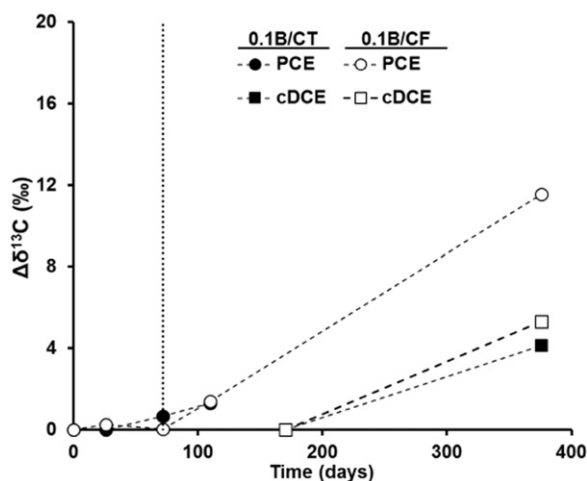
Fig. 3. PCE and cDCE carbon isotope composition variation (‰) over time in the 0.1B/CT and 0.1B/CF treatments. The vertical line shows the time when the concentrations of target compounds (CT and CF) in both treatments decreased below the detection limit.

within the autochthonous community (Table 2). Well-known organohalide-respiring bacteria (OHRB) according to Adrian and Löffler, 2016 such as *Dehalococcoides*, *Sulfurospirillum*, *Geobacter*, *Desulfosporosinus*, *Dehalobacter*, and *Desulfitobacterium* spp. (the last two with known CF reductive dehalogenases, Tang and Edwards, 2013; Ding et al., 2014), were not metabolically active (<0.1% relative abundance, RA) at any of the sampled times, and were not present at the initial time using DNA-based analyses (Table 2). In addition, the dehalogenase encoding *cfrA* gene was below the detection limit (<10^2 *cfrA* copies mL^{-1}, data not shown) in all t_3 samples, confirming the low metabolic activity of *Dehalobacter* spp. at this time. The low or non-existent presence and activity of OHRB could be connected with the well-known antagonistic effects of co-contaminants such as CMs against these TCE/PCE degrading bacteria (Futagami et al., 2006; Cappelletti et al., 2012; Tang et al., 2016); with the reported CT

inhibition of CF respiration by *Dehalobacter* (Lee et al., 2015), or with the competition with other active microbial populations from the phylum Proteobacteria (mentioned below), which would require further investigation.

In all treatments, the greatest represented phylum was Proteobacteria (RA > 80%) (Table 2, Fig. A6), and this phylum is described in better detail hereafter. In the CTw/oB treatment at t_{10}, the predominantly active genus was the facultatively anaerobic *Acidovorax* (53%) (Table 2, Fig. A7, Table A3), being more abundant than in the CT treatments with B_{12} (23 to 27%). *Acidovorax* sp. 2AN has been described as capable of anoxic Fe(II)-oxidation-enhanced chemotrophic growth coupled to NO_3^- reduction (Chakraborty et al., 2011), and an average NO_3^- concentration of 40 ± 12 μM (n = 16) (Table A6) in the parental CT treatments would support its growth. Lima and Sleep (2010) reported inhibition of the microbial activity related to CT degradation by 0.2–0.4 μM of CF. The authors observed a decrease in the number of bacterial species, including *Acidovorax*, under iron-limiting conditions. In the present study, the initial CF concentrations (Table 1) were close to those considered inhibitory in the reported study by Lima and Sleep (2010), which supports that the lowering of $\delta^{13}C_{CT}$ enrichment after 211 days in the CTw/oB treatment (Fig. 2C, D) might be due to the toxic effects of CF accumulation (Fig. 1D) on CT dechlorinating microorganisms. This might proceed through a general inhibition of the metabolic processes (Cappelletti et al., 2012) rather than by enzyme competition. Since bacterial community diversity was examined only at time t_0 and time t_{10} (after 376 days), this hypothesis cannot be confirmed in terms of changes in the bacterial population.

The genus *Pseudomonas* presented two predominantly active OTUs in all analyzed samples, belonging to *Pseudomonas lingynensis* (6–57% RA, similarity of 99.6%) and *Pseudomonas stutzeri* (1–10% RA, similarity of 99–100%) (Table A4). *P. stutzeri* constituted 9–10% RA (Table 2) in the B_{12}-amended CT treatments at t_3, whereas it represented only around 1% RA in the CTw/oB treatment at t_{10}, suggesting a relationship between this species and B_{12}. The *P. stutzeri* strain KC is able to denitrificate and to co-metabolically transform CT to CO_2 and non-volatile products (pathway 4, Scheme 1) by excreting a siderophore related to Fe chelation, enabling extracellular CT dehalogenation. Since

Table 2
Biodiversity of bacterial populations expressed as the relative abundance (RA, in %) at the Phylum/Family/Genus level according to the RDP Bayesian Classifier database (at the genus level with a bootstrap confidence above 80%), obtained from the M_S bottles. The most abundant phyla (above 1% of the RA in at least one sample) as well as striking genera and/or species are shown. Detailed abundances for all the detected genera are shown in the SI (Table A4). The remainder of the phyla up to 100% are included in "Others". The initial sample (t0_DNA) was direct 16S rRNA (DNA-based) analysis of the flushed slurry without amendments, while the remaining samples are 16S rRNA (RNA-based) extracted from the different CF and CT selected treatments and sampling points (t). Diversity, richness, and coverage indexes are shown in Table A5.

Phylum	Family	Genus/species	DNA t_0	CTw/oB t_{10}	0.01B/CT t_3	0.1B/CT t_3	0.01B/CF t_3
Total contigs 478,204)			70,705	113,413	98,700	88,726	106,660
Total OTUs (1087)			843	476	533	476	482
Proteobacteria (%)			25.75	83.46	83.10	85.64	94.13
	Comamonadaceae	*Acidovorax*	6.79	53.28	26.67	22.70	7.17
		Hydrogenophaga	0.07	7.73	1.17	2.50	1.01
		Variovorax	0.06	1.46	0.37	0.06	0.03
	Pseudomonadaceae	*Pseudomonas*	7.63	11.53	26.51	36.63	62.84
		Pseudomonas stutzeri	1.07	1.67	10.17	8.64	4.85
		Pseudomonas lingynensis	6.35	9.56	15.94	27.62	57.08
	Xanthobacteraceae	*Ancylobacter*	0.14	0.75	14.97	13.84	14.41
	Rhizobiaceae	*Rhizobium*	0.17	0.80	2.97	1.98	2.94
	Desulfovibrionaceae	*Desulfovibrio*	0.03	0.07	0.97	0.51	0.39
	Campylobacteraceae	*Sulfurospirillum*	0.05	0.09	<0.01	<0.01	<0.01
	Geobacteraceae	*Geobacter*	0.03	<0.01	<0.01	<0.01	<0.01
	Methylophilaceae	*Methylotenera*	5.52	0.35	1.25	0.64	0.23
Chloroflexi (%)			9.18	11.29	2.55	1.64	2.07
	Dehalococcoidacea	*Dehalococcoides*	<0.01	<0.01	<0.01	<0.01	<0.01
Deferribacteres (%)			0.09	1.32	1.13	0.82	0.09
	Deferribacteraceae	*Denitrovibrio*	0.08	1.31	1.12	0.82	0.09
Firmicutes (%)			10.87	0.27	0.16	0.60	0.12
	Peptococcaceae	*Dehalobacter*	<0.01	<0.01	<0.01	<0.01	0.02
		Desulfitobacterium	<0.01	<0.01	<0.01	<0.01	<0.01
		Desulfosporinus	0.06	0.05	0.27	0.01	0.17
Other (Phyla) (%)			54.10	3.66	13.06	11.30	3.60
		Others (Genera)	79.54	24.95	20.82	11.28	22.78

bioaugmentation with *P. stutzeri* has been successfully used in pilot-scale studies for the remediation of CT-contaminated sites (Penny et al., 2010), the key finding of the natural occurrence of this species and its RA increase by the addition of B_{12} makes *P. stutzeri*-mediated remediation strategies promising for the Òdena site.

The *Ancylobacter* genus (classified as *A. dichloromethanicus* or *A. aquaticus*, Table A2) was detected in greater RA (up to 15%, t_3) in the presence of B_{12} than in the absence of B_{12} (1%, t_{10}) (Table 2), suggesting a correlation with B_{12} addition. *A. dichloromethanicus* is an aerobic facultative methylotroph capable of DCM degradation (Firsova et al., 2010). In the CTw/oB treatment, the CF produced was not further degraded to DCM, preventing the proliferation of this species. In contrast, in the 0.01B/CF treatment, the only treatment with significant DCM detection, *Ancylobacter* exhibited 14% RA at t_3 (Table 2), supporting the hypothesis of DCM production and further DCM consumption (pathway 1, Scheme 1). *Ancylobacter* might also be linked to the degradation of structurally closed substrates in the absence of dihalomethanes (Firsova et al., 2010).

As aerobic or facultative-anaerobic bacteria were present in the microcosm, oxygen availability as a co-substrate could be explained by: (i) the occurrence of nitrite-driven processes that would supplement molecular oxygen to monooxygenase activity (Ettwig et al., 2010) as well as to the cometabolism for the degradation of halomethanes; ii) the availability of O_2 from chlorite dismutase activity in *P. stutzeri* (Cladera et al., 2006; Schaffner et al., 2015); iii) in the presence of L-2-haloacid dehalogenases, known to obtain an oxygen atom of the solvent water, in detected species including *A. aquaticus* (Kumar et al., 2016), *P. stutzeri* (Wang et al., 2015), and *Rhizobium sp. RC1* (Adamu et al., 2016) (the last genus with 1–3% RA in all analyzed samples).

3.3. Mechanistic insights

CT and CF reduction involves one or two C—Cl bond cleavages in the first rate-limiting step (Elsner et al., 2004; Chan et al., 2012; Lee et al., 2015). For AKIE calculations one C—Cl bond cleavage was assumed and the determined ε values ($R^2 \geq 0.9$) were used (Table 3, Fig. A8). The $AKIE_C$ for the 0.01B/CF (1.014 ± 0.002) and for the CTw/oB and 0.01B/CT treatments (1.016 ± 0.003 and 1.013 ± 0.001, respectively) were much below the Streitwieser limit of KIE_C for complete C—Cl bond cleavage (1.057) (Table A7), and the realistic value of 50% bond cleavage (1.029) (Elsner et al., 2005), making C-Cl cleavage feasible as the rate-limiting step, but showing important masking effects. $AKIE_C$ was slightly greater in the CTw/oB treatment. The obtained $AKIE_C$ values are within the range of those obtained for CF microbial reductive dechlorination (1.004–1.028), and below or within the range of those obtained for abiotic CT and CF reductive dechlorination (1.01–1.033 and 1.030–1.034, respectively) (Table A7).

The $AKIE_{Cl}$ of the 0.01B/CF treatment (1.0072 ± 0.0004) was lower than the Streitwieser limit for KIE_{Cl} (1.013) for a C—Cl bond cleavage, and also lower than the theoretical revised value (1.019) (Paneth, 1992), but it was closer to 50% of the Streitwieser limit (1.0065)

(Elsner et al., 2005), in contrast to the $AKIE_C$. Since both elements should be affected by masking to the same extent, this discrepancy suggests chlorine secondary isotopic effects that, in turn, are also masked. Moreover, although there are no $AKIE_{Cl}$ values of biotic CF degradation in the literature to compare, the value obtained here was consistent with abiotic CF hydrogenolysis ± the reductive elimination (pathway 1 ± 1a, Scheme 1) by Fe(0) (1.008 ± 0.001) (Torrentó et al., 2017) (Table A7).

For the CTw/oB treatment, the $AKIE_{Cl}$ (1.023 ± 0.003) was much above both the theoretical maximum expected KIE_{Cl} on a C—Cl bond cleavage (1.013) (Elsner et al., 2005) and the revised value (1.019) (Paneth, 1992). This could be associated with significant secondary isotopic effects (Świderek and Paneth, 2012), with the experimental values exceeding these established theoretical values, as it was also considered for PCE (Badin et al., 2014), or by the cleavage of two C—Cl bonds ($KIE = 1.013^2 = 1.026$) simultaneously or not to only one C—Cl bond cleavage (Elsner et al., 2004). In contrast, the $AKIE_{Cl}$ of CT biodegradation with B_{12} (1.015 ± 0.002) was similar to the expected KIE_{Cl} values for a C—Cl bond cleavage, probably with a small chlorine secondary isotopic effect or/and only the rare occurrence of two C—Cl bond cleavages, confirming the small differences observed between the CT treatments by $AKIE_C$. Thus, mechanistic differences were revealed by the $AKIE_{Cl}$ among the CT natural attenuation and B_{12} catalyzed reactions. These differences could be related to the fact that the derived $AKIE_{Cl}$ of CT is a weighted average of the kinetic effects of different proportions of competing parallel mechanisms in each case (i.e. one vs two C—Cl bond cleavages, leading to $\cdot CCl_3$ vs $:CCl_2$ respectively, Scheme 1), an aspect that is typical from mixed cultures which contain several species capable of pollutant degradation (Nijenhuis and Richnow, 2016). These detected $AKIE_{Cl}$ differences between CT natural attenuation and that mediated by B_{12} might also be partially uncovering dissimilarities in rate-determining steps preceding C—Cl bond cleavage related to rate limitations in biological reactions (Nijenhuis and Richnow, 2016). In fact, an extracellular catalyst of CT transformation affected by chemical reductants and the presence of transition metals was identified in *P. stutzeri* (Lee et al., 1999; Lewis et al., 2001). Since greater activity of *P. stutzeri* was observed in the presence of B_{12}, these extracellular processes might have induced rate-limiting effects, reducing the AKIEs.

3.4. Biodegradation pathways discussion

The non-existence or low accumulation of chlorinated by-products such as CF and DCM in all B_{12} live treatments, where degradation was confirmed, could highlight two non-excluding hypothesized pathways: 1) the formation of these products and their subsequently rapid consumption following a hydrogenolysis pathway combined or not with the reductive elimination (pathway 1 and 1a, Scheme 1); and/or 2) the reduction of CT or CF ultimately to CO_2 with minor or the inexistent accumulation of CMs (pathway 2, 4). CT thiolytic reduction (pathway 3, Scheme 1) was not confirmed due to the absence of CS_2 accumulation in the main microcosms, although this could also be

Table 3
Carbon and chlorine isotopic fractionation (ε_C and ε_{Cl}, respectively) and the corresponding apparent kinetic isotope effect ($AKIE_C$ and $AKIE_{Cl}$), dual C-Cl isotope slope (Λ), the dominant metabolically active genus (in relative abundance, RA, %), and the hypothesized pathway for each live treatment. Values from both CT treatments with B_{12} were used together for the Λ calculations. t_1, t_3, and t_{10} represent after 26, 85, and 376 days, respectively. n.m. = not measured since only two data points were available.

Treatment	CFw/oB	0.01B/CF	0.1B/CF	CTw/oB	0.01B/CT	0.1B/CT
ε_C (‰) ± 95% CI	No degradation detected	-14 ± 4	Concentration b.d.l. after t_1	-16 ± 6	-13 ± 2	n.m.
$AKIE_C$		1.014 ± 0.002		1.016 ± 0.001	1.013 ± 0.003	
ε_{Cl} (‰) ± 95% CI		-2.4 ± 0.4		-6 ± 3	-4 ± 2	
$AKIE_{Cl}$		1.0072 ± 0.0004		1.023 ± 0.003	1.015 ± 0.002	
Λ		7 ± 1		6.1 ± 0.5	5 ± 1	
Dominant genus (RA, %)		*Pseudomonas* (57), t_3		*Acidovorax* (53), t_{10}	*Acidovorax* (27), *Pseudomonas* (27), t_3	*Pseudomonas* (37), t_3
Hypothesized pathway		Hydrogenolysis ± reductive elimination		Hydrogenolysis among other possible reductions	Different simultaneous reduction processes	

further degraded (Cox et al., 2013). For further pathway conclusions, $\Delta\delta^{13}C$ and $\Delta\delta^{37}Cl$ of the same treatment and incubation time but measured in different replicates (since similar CT and CF evolution was detected in replicate bottles, Fig. A1) were plotted to obtain the CT and CF Λ values (Fig. 4). For both C and Cl, linear trends ($R^2 \geq 0.95$) were observed. An integrating overview of the different live treatments is shown in Table 3.

The Λ for the 0.01B/CF treatment (7 ± 1) was statistically similar (ANCOVA, p = 0.4) to the abiotic CF reduction by Fe(0) (8 ± 2) (Torrentó et al., 2017) (Fig. 4), which supports CF hydrogenolysis ± the reductive elimination (pathway 1 and 1a, Scheme 1) as the dominant pathways. CF hydrogenolysis is substantiated by only punctual DCM accumulation after 200 days, and the detection of species capable of DCM dechlorination (e.g. Ancylobacter dichloromethanicus). In addition, B_{12} might have stimulated CF reductive elimination to CO and CO_2 as reported previously (Cappelletti et al., 2012). Moreover, Λ was significantly different (ANCOVA, p < 0.0001) from the CF abiotic hydrolysis or oxidation (13.0 ± 0.8, 17 ± 2) (Torrentó et al., 2017), discarding CF hydrolytic reduction (pathway 2, Scheme 1), assuming the Λ of the reported CF abiotic hydrolysis as a reference system with a C—Cl bond cleavage as a rate-limiting step (Torrentó et al., 2017) and corroborating the absence of oxidation processes.

There was no significant statistical difference between Λ from the 0.01B/CT and 0.1B/CT treatments (Fig. A9) (n = 6) (ANCOVA, p = 0.23), thus data points from both treatments were plotted together (Fig. 4). The slopes of CT biodegradation with and without B_{12} were similar in terms of the 95% CI: 5 ± 1 (n = 6) and 6.1 ± 0.5 (n = 9), respectively, although ANCOVA analysis showed a significant statistical difference (p = 0.02), as evidenced by Λ flattening with the addition of B_{12} (Fig. 4). This difference was also suggested by CF accumulation only in the CTw/oB treatment, non-closed isotopic balances, and mechanistic insights results. Metabolically active P. stutzeri is capable of readily degrading CT to CO_2 without CF accumulation (pathway 4, Scheme 1) together with the presence of metabolically active species capable of DCM dechlorination (Ancylobacter dichloromethanicus). This supports the coexistence of different reduction pathways when B_{12} is present. In order to better understand and quantify the contribution of different CT reaction mechanisms with and without B_{12}, further research is extremely needed to obtain Λ representative of CT transformation models.

4. Conclusions

The anaerobic CT natural attenuation potential was confirmed in Òdena site-derived anoxic microcosms, as well as the B_{12} catalysing effects on both CT and CF biodegradation. An RNA-based NGS approach showed the metabolically active members (Acidovorax, Pseudomonas, and Ancylobacter) that could be related to the biodegradation of target compounds, that otherwise would be difficult to estimate by means of DNA-based strategies. The dual C-Cl element isotope slope coincidence of CF biodegradation with B_{12} and CF abiotic chemical models confirmed the CF hydrogenolysis (± the reductive elimination) pathway, which spurred the use of complementary tools for CF abiotic/biotic hydrogenolysis distinction in future study sites. In addition, the detected differences in CT product distribution, $AKIE_{Cl}$, and Λ in B_{12}-amended and unamended treatments were also consistent with the major relative activity of P. stutzeri when B_{12} was added, whose natural occurrence is a key finding for effective Òdena remediation. The discretized tracking of by-products was not always conclusive, because some by-products were missed due to further degradation (such as CF or DCM). However, the combination of the isotopic approach and the study of the active indigenous community became of relevant usefulness for evidencing degradation processes. The outcomes of this study create a basis for application of this combined approach in further CMs degradation studies. The 2D-CSIA is a tool to rapidly uncover changes in the field related to the application of CMs remediation strategies, and for pathway identification, although a further thorough assessment of reference Λ which is representative of different CMs reaction mechanisms is necessary. This study is a striking example of the benefits of B_{12} in the remediation of complex multi-contaminant polluted sites, which requires a sequential treatment strategy to minimize CF inhibition issues by inducing its transformation. Further feasibility upscaling studies are needed to estimate the required amount of B_{12}, to find cheaper B_{12} sources, and to elucidate the possible inhibition effects of B_{12}-related intermediates (phosgene, thiophosgene) on the degradation of CMs. Furthermore, since the co-deposition of nitrate and VOCs is widespread in soils and groundwater worldwide (Squillace et al., 2002), the presence of metabolically active denitrifying genera (Pseudomonas, Rhizobium, or Acidovorax) which are linked to CT and CF biodegradation in the present experiments, raises interest in the study of the co-metabolism of both pollutants as a potential bioremediation strategy.
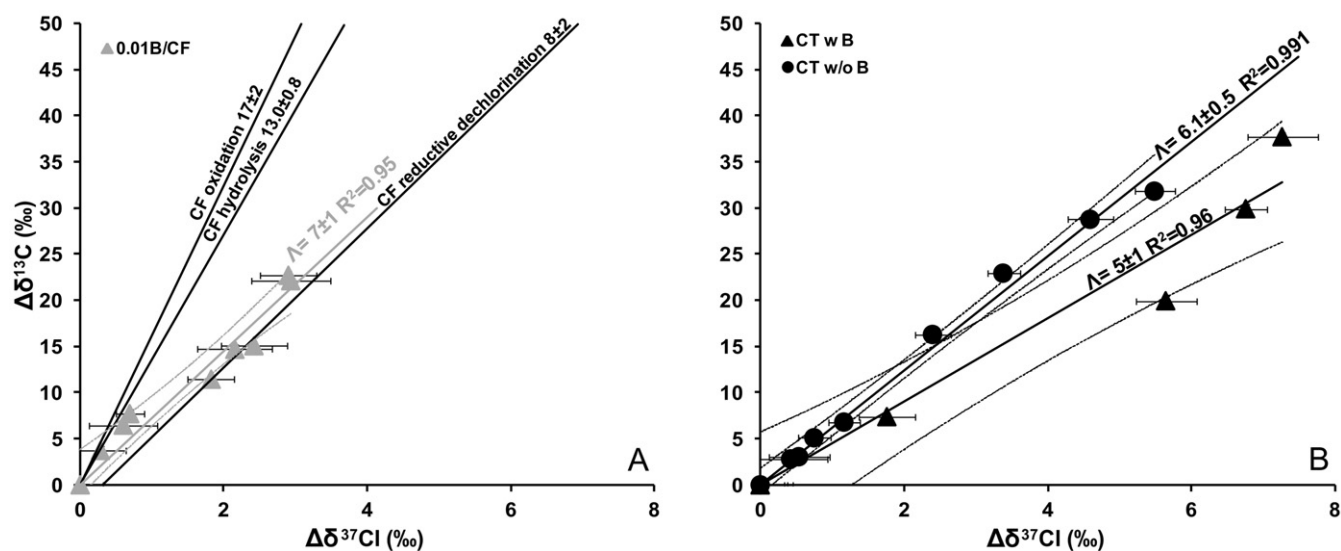
Fig. 4. Dual C-Cl isotope plot for CF (A) and CT (B) biodegradation data observed in the microcosms. Solid grey in A and black lines in B correspond to linear regressions of the data sets obtained in this study with 95% CI (dashed lines). Error bars show uncertainty in duplicate isotope measurements. Note that the error bars of the $\Delta\delta^{13}C$ values are smaller than the symbols. The CF oxidation by thermally-activated persulphate, CF alkaline hydrolysis, and CF reductive dechlorination by Fe(0) slopes in A (black lines) correspond to the CF abiotic degradation reference systems (Torrentó et al., 2017).

Author contributions

The manuscript was written through contributions of all authors. All authors have given approval to the final version of the manuscript.

Acknowledgements

Appendix A. Supplementary data

Supplementary data to this article can be found online at https://doi.org/10.1016/j.scitotenv.2017.10.067.

References

Adamu, A., Wahab, R.A., Huyop, F., 2016. L-2-Haloacid dehalogenase (DehL) from *Rhizobium* sp. RC1. Spring 5, 695. https://doi.org/10.1186/s40064-016-2328-9.

Adrian, L., Löffler, E.F. (Eds.), 2016. Organohalide-respiring Bacteria. Springer, Berlin Heidelberg https://doi.org/10.1007/978-3-662-49875-0.

Badin, A., Buttet, G., Maillard, J., Holliger, C., Hunkeler, D., 2014. Multiple dual C-Cl isotope patterns associated with reductive dechlorination of tetrachloroethene. Environ. Sci. Technol. 48:9179–9186. https://doi.org/10.1021/es500822d.

Bagley, D.M., Lalonde, M., Kaseros, V., Stasiuk, K.E., Sleep, B.E., 2000. Acclimation of anaerobic systems to biodegrade tetrachloroethene in the presence of carbon tetrachloride and chloroform. Water Res. 34:171–178. https://doi.org/10.1016/S0043-1354(99)00121-9.

Banerjee, R., Ragsdale, S.W., 2003. The many faces of vitamin B₁₂: catalysis by cobalamin-dependent enzymes. Annu. Rev. Biochem. 72:209–247. https://doi.org/10.1146/annurev.biochem.72.121801.161828.

Becker, J.G., Freedman, D.L., 1994. Use of cyanocobalamin to enhance anaerobic biodegradation of chloroform. Environ. Sci. Technol. 28:1942–1949. https://doi.org/10.1021/es00060a027.

Caporaso, J., Bittinger, K., Bushman, F.D., Desantis, T.Z., Andersen, G.L., Knight, R., 2010a. PyNAST: a flexible tool for aligning sequences to a template alignment. Bioinformatics 26:266–267. https://doi.org/10.1093/bioinformatics/btp636.

Caporaso, J., Kuczynski, J., Stombaugh, J., Bittinger, K., Bushman, F.D., Costello, E.K., Fierer, N., Peña, A.G., Goodrich, J.K., Gordon, J.I., Huttley, G.A., Kelley, S.T., Knights, D., Koenig, J.E., Ley, R.E., Lozupone, C.A., Mcdonald, D., Muegge, B.D., Pirrung, M., Reeder, J., Sevinsky, J.R., Turnbaugh, P.J., Walters, W.A., Widmann, J., Yatsunenko, T., Zaneveld, J., Knight, R., 2010b. QIIME allows analysis of high-throughput community sequencing data intensity normalization improves color calling in SOLiD sequencing. Nat. Publ. Gr. 7:335–336. https://doi.org/10.1038/nmeth0510-335.

Cappelletti, M., Frascari, D., Zannoni, D., Fedi, S., 2012. Microbial degradation of chloroform. Appl. Microbiol. Biotechnol. 96:1395–1409. https://doi.org/10.1007/s00253-012-4494-1.

Chakraborty, A., Roden, E.E., Schieber, J., Picardal, F., 2011. Enhanced growth of *Acidovorax* sp. strain 2AN during nitrate-dependent Fe(II) oxidation in batch and continuous-flow systems. Appl. Environ. Microbiol. 77:8548–8556. https://doi.org/10.1128/AEM.06214-11.

Chan, C.C.H., Mundle, S.O.C., Eckert, T., Liang, X., Tang, S., Lacrampe-Couloume, G., Edwards, E.A., Sherwood Lollar, B., 2012. Large carbon isotope fractionation during biodegradation of chloroform by *Dehalobacter* cultures. Environ. Sci. Technol. 46: 10154–10160. https://doi.org/10.1021/es3010317.

Cladera, A.M., García-Valdés, E., Lalucat, J., 2006. Genotype versus phenotype in the circumscription of bacterial species: the case of *Pseudomonas stutzeri* and *Pseudomonas chloritidismutans*. Arch. Microbiol. 184:353–361. https://doi.org/10.1007/s00203-005-0052-x.

Cox, S.F., McKinley, J.D., Ferguson, A.S., O'Sullivan, G., Kalin, R.M., 2013. Degradation of carbon disulphide (CS₂) in soils and groundwater from a CS₂-contaminated site. Environ. Earth Sci. 68:1935–1944. https://doi.org/10.1007/s12665-012-1881-y.

Cretnik, S., Thoreson, K.A., Bernstein, A., Ebert, K., Buchner, D., Laskov, C., Haderlein, S., Shouakar-Stash, O., Kliegman, S., McNeill, K., Elsner, M., 2013. Reductive dechlorination of TCE by chemical model systems in comparison to dehalogenating bacteria: insights from dual element isotope analysis (¹³C/¹²C, ³⁷Cl/³⁵Cl). Environ. Sci. Technol. 47:6855–6863. https://doi.org/10.1021/es400107n.

DeSantis, T.Z., Hugenholtz, P., Larsen, N., Rojas, M., Brodie, E.L., Keller, K., Huber, T., Dalevi, D., Hu, P., Andersen, G.L., 2006. Greengenes, a chimera-checked 16S rRNA gene database and workbench compatible with ARB. Appl. Environ. Microbiol. 72: 5069–5072. https://doi.org/10.1128/AEM.03006-05.

Ding, C., Zhao, S., He, J., 2014. A *Desulfitobacterium* sp. strain PR reductively dechlorinates both 1,1,1-trichloroethane and chloroform. Environ. Microbiol. 16:3387–3397. https://doi.org/10.1111/1462-2920.12387.

Doherty, R., 2000. A history of the production and use of carbon tetrachloride, tetrachloroethylene, trichloroethylene and 1,1, 1-trichloroethane in the United States: part 1 – historical background; carbon tetrachloride and tetrachloroethylene. Environ. Forensics 1, 175.

Duhamel, M., Wehr, S.D., Yu, L., Rizvi, H., Seepersad, D., Dworatzek, S., Cox, E.E., Edwards, E.A., 2002. Comparison of anaerobic dechlorinating enrichment cultures maintained on tetrachloroethene, trichloroethene, cis-dichloroethene and vinyl chloride. Water Res. 36:4193–4202. https://doi.org/10.1016/S0043-1354(02)00151-3.

Edgar, R.C., 2010. Search and clustering orders of magnitude faster than BLAST. Bioinformatics 26:2460–2461. https://doi.org/10.1093/bioinformatics/btq461.

Egli, C., Stromeyer, S., Cook, A.M., Leisinger, T., 1990. Transformation of tetra- and trichloromethane to CO₂ by anaerobic bacteria is a non-enzymic process. FEMS Microbiol. Lett. 68, 207–212.

Elsner, M., 2010. Stable isotope fractionation to investigate natural transformation mechanisms of organic contaminants: principles, prospects and limitations. J. Environ. Monit. 12:2005–2031. https://doi.org/10.1039/c0em00277a.

Elsner, M., Haderlein, S.B., Kellerhals, T., Luzi, S., Zwank, L., Angst, W., Schwarzenbach, R.P., 2004. Mechanisms and products of surface-mediated reductive dehalogenation of carbon tetrachloride by Fe(II) on goethite. Environ. Sci. Technol. 38:2058–2066. https://doi.org/10.1021/es034741m.

Elsner, M., Zwank, L., Hunkeler, D., Schwarzenbach, R.P., 2005. A new concept linking observable stable isotope fractionation to transformation pathways of organic pollutants. Environ. Sci. Technol. 39, 6896–6916.

Ettwig, K.F., Butler, M.K., Le Paslier, D., Pelletier, E., Mangenot, S., Kuypers, M.M.M., Schreiber, F., Dutilh, B.E., Zedelius, J., de Beer, D., et al., 2010. Nitrite-driven anaerobic methane oxidation by oxygenic bacteria. Nature 464:543–548. https://doi.org/10.1038/nature08883.

Fennell, D.E., Carroll, A.B., Gossett, J.M., Zinder, S.H., 2001. Assessment of indigenous reductive dechlorinating potential at a TCE-contaminated site using microcosms, polymerase chain reaction analysis, and site data. Environ. Sci. Technol. 35:1830–1839. https://doi.org/10.1021/es0016203.

Field, J.A., Sierra-Alvarez, R., 2004. Biodegradability of chlorinated solvents and related chlorinated aliphatic compounds. Rev. Environ. Sci. Biotechnol. 3:185–254. https://doi.org/10.1007/s11157-004-4733-8.

Firsova, J.E., Doronina, N.V., Trotsenko, Y.A., 2010. Analysis of the key functional genes in new aerobic degraders of dichloromethane. Mikrobiologiya 79:72–78. https://doi.org/10.1134/S0026261710010091.

Futagami, T., Yamaguchi, T., Nakayama, S.I., Goto, M., Furukawa, K., 2006. Effects of chloromethanes on growth of and deletion of the *pce* gene cluster in dehalorespiring *Desulfitobacterium hafniense* strain Y51. Appl. Environ. Microbiol. 72:5998–6003. https://doi.org/10.1128/AEM.00979-06.

Guerrero-Barajas, C., Field, J.A., 2005a. Riboflavin- and cobalamin-mediated biodegradation of chloroform in a methanogenic consortium. Biotechnol. Bioeng. 89:539–550. https://doi.org/10.1002/bit.20379.

Guerrero-Barajas, C., Field, J.A., 2005b. Enhancement of anaerobic carbon tetrachloride biotransformation in methanogenic sludge with redox active vitamins. Biodegradation 16:215–228. https://doi.org/10.1007/s10532-004-0638-z.

Haas, B.J., Gevers, D., Earl, A.M., Feldgarden, M., Ward, D.V., Giannoukos, G., Ciulla, D., Tabbaa, D., Highlander, S.K., Sodergren, E., Methé, B., DeSantis, T.Z., The Human Microbiome Consortium, Petrosino, J.F., Knight, R., Birren, B.W., 2011. Chimeric 16S rRNA sequence formation and detection in Sanger and 454-Pyrosequenced PCR amplicons. Genome Res. 21:494–504. https://doi.org/10.1101/gr.112730.110.Freely.

Hashsham, S.A., Scholze, R., Freedman, D.L., 1995. Cobalamin-enhanced anaerobic biotransformation of carbon tetrachloride. Environ. Sci. 29, 2856–2863.

He, Y.T., Wilson, J.T., Su, C., Wilkin, R.T., 2015. Review of abiotic degradation of chlorinated solvents by reactive iron minerals in aquifers. Groundw. Monit. Remediat. 35:57–75. https://doi.org/10.1111/gwmr.12111.

Heckel, B., Rodríguez-Fernández, D., Torrentó, D., Meyer, A., Palau, J., Domènech, C., Rosell, M., Soler, A., Hunkeler, D., Elsner, D., 2017. Compound-specific chlorine isotope analysis of tetrachloromethane and trichloromethane by GC-IRMS vs. GC-qMS: method development and evaluation of precision and trueness. Anal. Chem. 89:3411–3420. https://doi.org/10.1021/acs.analchem.6b04129.

International Agency for Research on Cancer, 2016. IARC Monographs on the Evaluation of Carcinogenic Risks to Humans. [WWW Document]. http://monographs.iarc.fr/ENG/Classification/latest_classif.php (accessed 5.24.16).

Kumar, A., Pillay, B., Olaniran, A.O., 2016. L-2-Haloacid dehalogenase from *Ancylobacter aquaticus* UV5: sequence determination and structure prediction. Int. J. Biol. Macromol. 83:216–225. https://doi.org/10.1016/j.ijbiomac.2015.11.066.

Lee, C.H., Lewis, T.A., Paszczynski, A., Crawford, R.L., 1999. Identification of an extracellular catalyst of carbon tetrachloride dehalogenation from *Pseudomonas stutzeri* strain KC as pyridine-2, 6-bis(thiocarboxylate). Biochem. Biophys. Res. Commun. 261: 562–566. https://doi.org/10.1006/bbrc.1999.1077.

Lee, M., Wells, E., Wong, Y.K., Koenig, J., Adrian, L., Richnow, H.H., Manefield, M., 2015. Relative contributions of *Dehalobacter* and zerovalent iron in the degradation of chlorinated methanes. Environ. Sci. Technol. 49:4481–4489. https://doi.org/10.1021/es5052364.

Lewis, T.A., Crawford, R.L., 1995. Transformation of carbon tetrachloride via sulfur and oxygen substitution by *Pseudomonas* sp. strain KC. J. Bacteriol. 177, 2204–2208.

Lewis, T.A., Paszczynski, A., Gordon-Wylie, S.W., Jeedigunta, S., Lee, C.H., Crawford, R.L., 2001. Carbon tetrachloride dechlorination by the bacterial transition metal chelator

pyridine-2,6-bis(thiocarboxylic acid). Environ. Sci. Technol. 35:552–559. https://doi.org/10.1021/es001419s.

Lima, G. da P., Sleep, B.E., 2010. The impact of carbon tetrachloride on an anaerobic methanol-degrading microbial community. Water Air Soil Pollut. 212:357–368. https://doi.org/10.1007/s11270-010-0350-z.

Martín-González, L., Mortan, S.H., Rosell, M., Parladé, E., Martínez-Alonso, M., Gaju, N., Caminal, G., Adrian, L., Marco-Urrea, E., 2015. Stable carbon isotope fractionation during 1,2-dichloropropane-to-propene transformation by an enrichment culture containing *Dehalogenimonas* strains and a *dcpA* gene. Environ. Sci. Technol. 49: 8666–8674. https://doi.org/10.1021/acs.est.5b00929.

Nijenhuis, I., Richnow, H.H., 2016. Stable isotope fractionation concepts for characterizing biotransformation of organohalides. Curr. Opin. Biotechnol. 41:108–113. https://doi.org/10.1016/j.copbio.2016.06.002.

Palatsi, J., Illa, J., Prenafeta-Boldú, F.X., Laureni, M., Fernandez, B., Angelidaki, I., Flotats, X., 2010. Long-chain fatty acids inhibition and adaptation process in anaerobic thermophilic digestion: batch tests, microbial community structure and mathematical modelling. Bioresour. Technol. 101:2243–2251. https://doi.org/10.1016/j.biortech.2009.11.069.

Palau, J., Marchesi, M., Chambon, J.C.C., Aravena, R., Canals, À., Binning, P.J., Bjerg, P.L., Otero, N., Soler, A., 2014. Multi-isotope (carbon and chlorine) analysis for fingerprinting and site characterization at a fractured bedrock aquifer contaminated by chlorinated ethenes. Sci. Total Environ. 475:61–70. https://doi.org/10.1016/j.scitotenv.2013.12.059.

Paneth, P., 1992. How to measure heavy atom isotope effects: general principles. In: Buncel, E., Saunders, W.H.J. (Eds.), Isotopes in Organic Chemistry. Elsevier, New York, p. 1992.

Pelissari, C., Guivernau, M., Viñas, M., de Souza, S.S., García, J., Sezerino, P.H., Ávila, C., 2017. Unraveling the active microbial populations involved in nitrogen utilization in a vertical subsurface flow constructed wetland treating urban wastewater. Sci. Total Environ. 584–585:642–650. https://doi.org/10.1016/j.scitotenv.2017.01.091.

Penny, C., Vuilleumier, S., Bringel, F., 2010. Microbial degradation of tetrachloromethane: mechanisms and perspectives for bioremediation. FEMS Microbiol. Ecol. 74:257–275. https://doi.org/10.1111/j.1574-6941.2010.00935.x.

Puigserver, D., Nieto, J.M., Grifoll, M., Vila, J., Cortés, A., Viladevall, M., Parker, B.L., Carmona, J.M., 2016. Temporal hydrochemical and microbial variations in microcosm experiments from sites contaminated with chloromethanes under biostimulation with lactic acid. Bioremediat. J. 20:54–70. https://doi.org/10.1080/10889868.2015.1124061.

Reeder, J., Knight, R., 2010. Rapidly denoising pyrosequencing amplicon reads by exploiting rank-abundance distributions. Nat. Methods 7:668–669. https://doi.org/10.1038/nmeth0910-668b.

Riley, R.G., Szecsody, J.E., Sklarew, D.S., Mitroshkov, A.V., Gent, P.M., Brown, C.F., Thompson, C.J., 2010. Desorption behaviour of carbon tetrachloride and chloroform in contaminated low organic carbon aquifer sediments. Chemosphere 79:807–813. https://doi.org/10.1016/j.chemosphere.2010.03.005.

Schaffner, I., Hofbauer, S., Krutzler, M., Pirker, K.F., Furtmüller, P.G., Obinger, C., 2015. Mechanism of chlorite degradation to chloride and dioxygen by the enzyme chlorite dismutase. Arch. Biochem. Biophys. 574:18–26. https://doi.org/10.1016/j.abb.2015.02.031.

Schloss, P.D., Westcott, S.L., Ryabin, T., Hall, J.R., Hartmann, M., Hollister, E.B., Lesniewski, R.A., Oakley, B.B., Parks, D.H., Robinson, C.J., Sahl, J.W., Stres, B., Thallinger, G.G., Van Horn, D.J., Weber, C.F., 2009. Introducing mothur: open-source, platform-independent, community-supported software for describing and comparing microbial communities. Appl. Environ. Microbiol. 75:7537–7541. https://doi.org/10.1128/AEM.01541-09.

Shan, H., Kurtz, H.D., Freedman, D.L., 2010. Evaluation of strategies for anaerobic bioremediation of high concentrations of halomethanes. Water Res. 44:1317–1328. https://doi.org/10.1016/j.watres.2009.10.035.

Sherdwood Lollar, B., Hirschorn, S.K., Chartrand, M.M.G., Lacrampe-Couloume, G., 2007. An approach for assessing total instrumental uncertainty in compound-specific isotope analysis: implications for environmental remediation studies. Anal. Chem. 79: 3469–3475. https://doi.org/10.1021/ac062299v.

Song, H., Carraway, E.R., 2006. Reduction of chlorinated methanes by nano-sized zero-valent iron. Kinetics, pathways and effect of reaction conditions. Environ. Eng. Sci. 23, 272–284.

Squillace, P.J., Scott, J.C., Moran, M.J., Nolan, B.T., Kolpin, D.W., 2002. VOCs, pesticides, nitrate, and their mixtures in groundwater used for drinking water in the United States. Environ. Sci. Technol. 36:1923–1930. https://doi.org/10.1021/es015591n.

Staudinger, J., Roberts, P.V., 2001. A critical compilation of Henry's law constant temperature dependence relations for organic compounds in dilute aqueous solutions. Chemosphere 44:561–576. https://doi.org/10.1016/S0045-6535(00)00505-1.

Świderek, K., Paneth, P., 2012. Extending limits of chlorine kinetic isotope effects. J. Organomet. Chem. 77:5120–5124. https://doi.org/10.1021/jo300682f.

Tang, S., Edwards, E.A., 2013. Identification of *Dehalobacter* reductive dehalogenases that catalyse dechlorination of chloroform, 1,1,1-trichloroethane and 1,1-dichloroethane. Philos. Trans. R. Soc. B 368, 20120318. https://doi.org/10.1098/rstb.2012.0318.

Tang, S., Wang, P.H., Higgins, S.A., Löffler, F.E., Edwards, E.A., 2016. Sister *Dehalobacter* genomes reveal specialization in organohalide respiration and recent strain differentiation likely driven by chlorinated substrates. Front. Microbiol. 7:1–14. https://doi.org/10.3389/fmicb.2016.00100.

Torrentó, C., Audí-Miró, C., Bordeleau, G., Marchesi, M., Rosell, M., Otero, N., Soler, A., 2014. The use of alkaline hydrolysis as a novel strategy for chloroform remediation: the feasibility of using construction wastes and evaluation of carbon isotopic fractionation. Environ. Sci. Technol. 48:1869–1877. https://doi.org/10.1021/es403838t.

Torrentó, C., Palau, J., Rodríguez-Fernández, D., Heckel, B., Meyer, A., Domènech, C., Rosell, M., Soler, A., Elsner, M., Hunkeler, D., 2017. Carbon and chlorine isotope fractionation patterns associated with different engineered chloroform transformation reactions. Environ. Sci. Technol. 51:6174–6184. https://doi.org/10.1021/acs.est.7b00679.

Wang, Q., Garrity, G.M., Tiedje, J.M., Cole, J.R., 2007. Naive Bayesian classifier for rapid assignment of rRNA sequences into the new bacterial taxonomy. Appl. Environ. Microbiol. 73 (16), 5261–5267.

Wang, Y., Xin, Y., Cao, X., Xue, S., 2015. Enhancement of L-2-haloacid dehalogenase expression in *Pseudomonas stutzeri* DEH138 based on the different substrate specificity between dehalogenase-producing bacteria and their dehalogenases. World J. Microbiol. Biotechnol. 31:669–673. https://doi.org/10.1007/s11274-015-1817-2.

Workman, D.J., Woods, S.L., Gorby, Y.A., Fredrickson, J.K., Truex, M.J., 1997. Microbial reduction of vitamin B12 by *Shewanella alga* strain BrY with subsequent transformation of carbon tetrachloride. Environ. Sci. Technol. 31:2292–2297. https://doi.org/10.1021/es960880a.

Yargicoglu, E.N., Reddy, K.R., 2015. Review of biological diagnostic tools and their applications in geoenvironmental engineering. Rev. Environ. Sci. Biotechnol. 14:161–194. https://doi.org/10.1007/s11157-014-9358-y.

Zou, S., Stensel, H.D., Ferguson, J.F., 2000. Carbon tetrachloride degradation: effect of microbial growth substrate and vitamin B_{12} content. Environ. Sci. Technol. 34: 1751–1757. https://doi.org/10.1021/es990930m.

Zwank, L., Elsner, M., Aeberhard, A., Schwarzenbach, R.P., 2005. Carbon isotope fractionation in the reductive dehalogenation of carbon tetrachloride at iron (hydr)oxide and iron sulfide minerals. Environ. Sci. Technol. 39, 5634–5641.

Supplementary Information

Vitamin B$_{12}$ effects on chlorinated methanes-degrading microcosms: carbon-chlorine isotope and metabolically active microbial populations' assessment

Diana Rodríguez-Fernández[1*], Clara Torrentó[2], Miriam Guivernau[3], Marc Viñas[3], Daniel Hunkeler[2], Albert Soler[1], Cristina Domènech[1], Mònica Rosell[1]

[1] Grup de Mineralogia Aplicada i Geoquímica de Fluids. Departament de Mineralogia, Petrologia i Geologia Aplicada, Facultat de Ciències de la Terra, Universitat de Barcelona (UB), c/Martí i Franquès s/n, 08028 Barcelona, Spain.

[2] Centre d'hydrogéologie et de géothermie, Université de Neuchâtel, Rue Emile-Argand 11, Neuchâtel 2000, Switzerland

[3] GIRO Joint Research Unit IRTA-UPC, IRTA, Torre Marimon, Caldes de Montbui E-08140 Spain

Corresponding Author:

*Diana Rodríguez-Fernández Phone: +34 93 403 90 74; Fax: +34 93 402 13 40, e-mail: diana.rodriguez@ub.edu

Total number of pages (including cover): 20

Figures: 9

Tables: 7

INDEX

1. METHODOLOGIES

1.1. pH, total elements, cations and anions concentration

pH evolution was monitored using a pH meter Crison 6037. Aliquots of samples were preserved in nitric acid to measure concentrations of S, Fe, Ca and Na by inductively coupled plasma-optic emission spectrometry (ICP-OES) by using an Optima 3200 RL spectrometer and by inductively coupled plasma mass spectrometry (ICP-MS) by using an Elan 6000 spectrometer from the *Centres Científics i Tecnològics de la Universitat de Barcelona* (CCiT-UB) (Spain). For NH_4^+ determination no sample preservation was conducted and ionic chromatography (DIONEX, Model IC5000) was used with IonPac® CS16 cation-exchange column (5×250 mm) with the CG Guard column (5×50 mm) in the *Serveis Científics i Tècnics* (SCT) de *l'Institut Català de Recerca de l'Aigua* (ICRA) (Spain). NO_3^-, Cl^- and SO_4^{2-} concentrations were analyzed by high-performance liquid chromatography (HPLC) using a WATERS 515 HPLC pump with IC-PAC Anion column and a WATERS mod 432 detector in CCiT-UB. For ClO_2^- and ClO_3^-, ion chromatography was used with a DIONEX, Model IC5000 with IonPac® AS18 anion-exchange column (4×250 mm) with a AG Guard column (4×50 mm) and a Chromeleon 6.8 data processor in ICRA.

2. RESULTS

2.1. Detailed CT, CF and by-products concentration over time for individual replicates
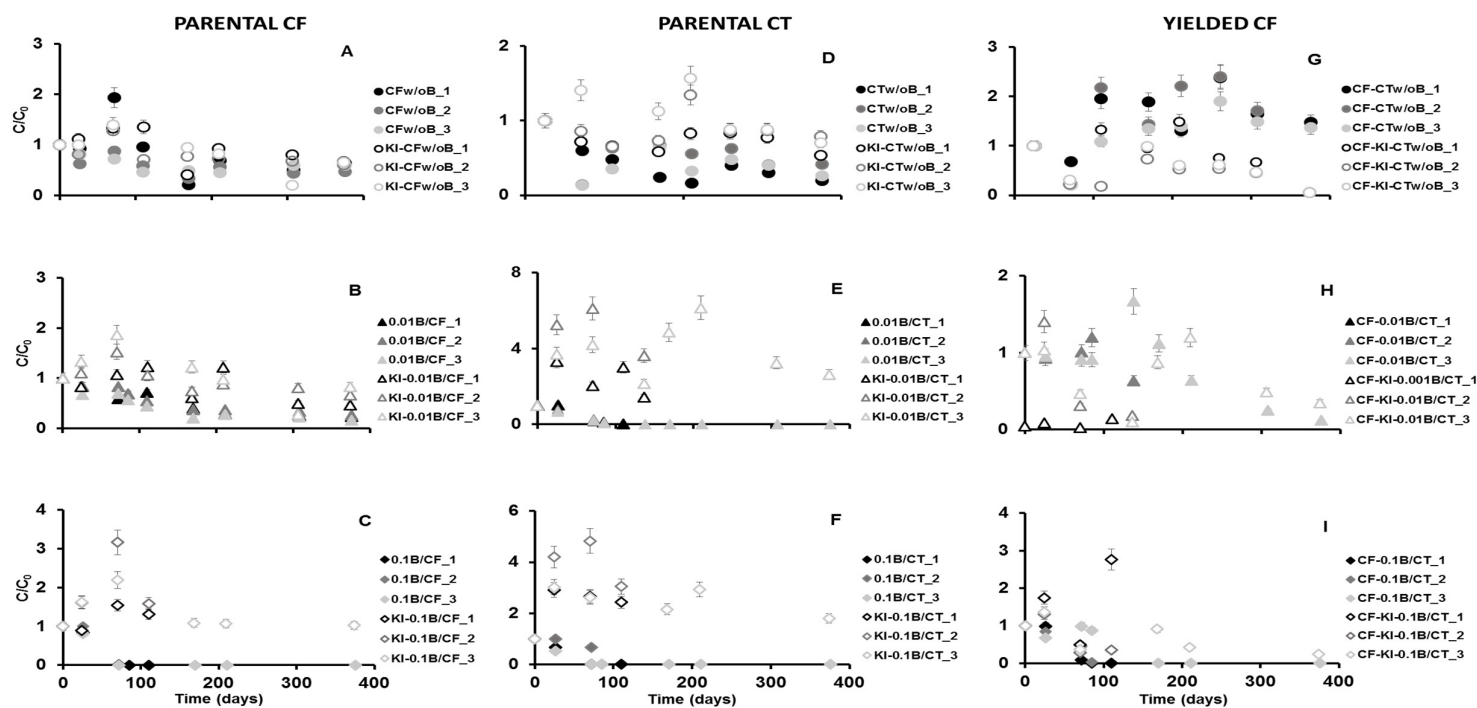
Fig.A1. Changes in concentration of CF and CT (C/C$_0$) calculated from total μmol in the bottle taking into account Henry's law constant at 24°C according to Staudinger and Roberts (2001) for the three replicates of each treatment: CFw/oB (A), 0.01B/CF (B) and 0.1B/CF (C), CTw/oB (D), 0.01B/CT (E), 0.1B/CT (F) and the evolution of yielded CF of CT treatments (G,H,I) Corresponding heat-killed controls (KI) are also shown. Error bars show the uncertainty in concentration measurements. In some cases, error bars are smaller than the symbols.
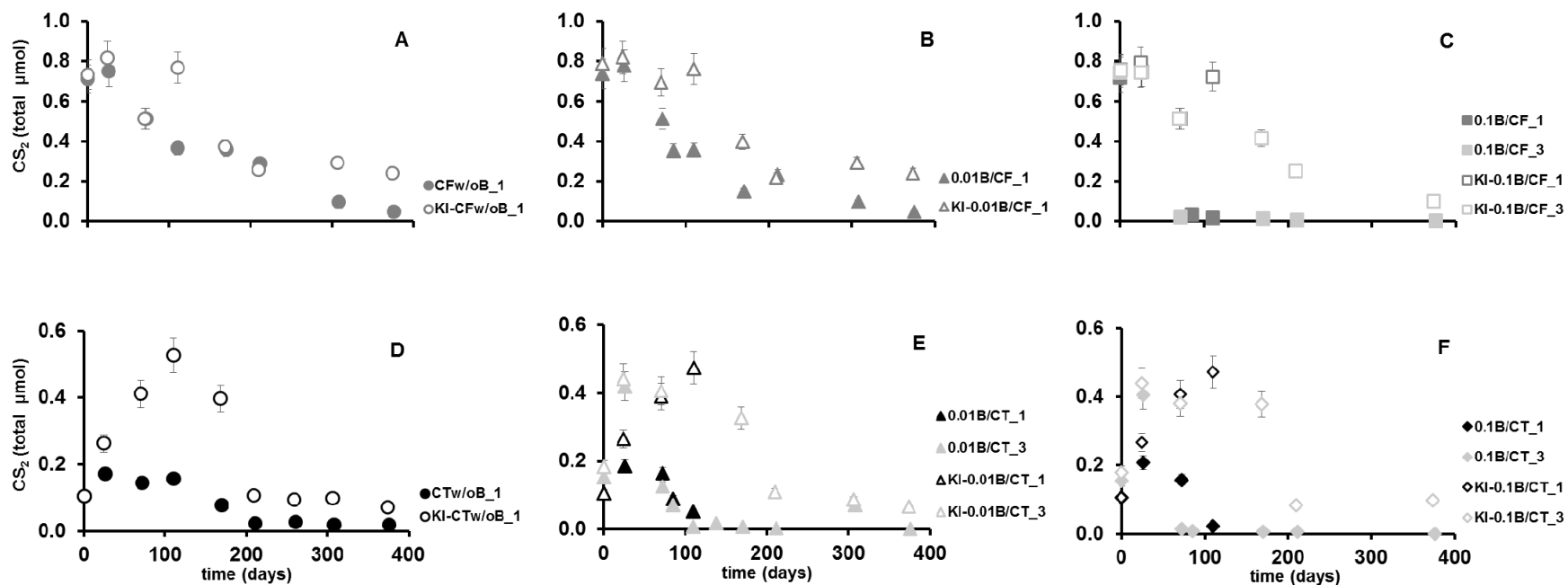
Fig. A2. CS$_2$ concentration (calculated from total µmol in the bottle by Henry's law constant (H$_i$) at 24 °C according to Staudinger and Roberts (2001) over time in one (replicate 1) or two replicates (as specified) for live microcosms and heat-killed controls (KI) of each treatment: CFw/oB (A), 0.01B/CF (B), 0.1B/CF (C), CTw/oB (D), 0.01B/CT (E) and 0.1B/CT (F). The error bars show the uncertainty in concentration measurements. In some cases, error bars are smaller than the symbols.

5
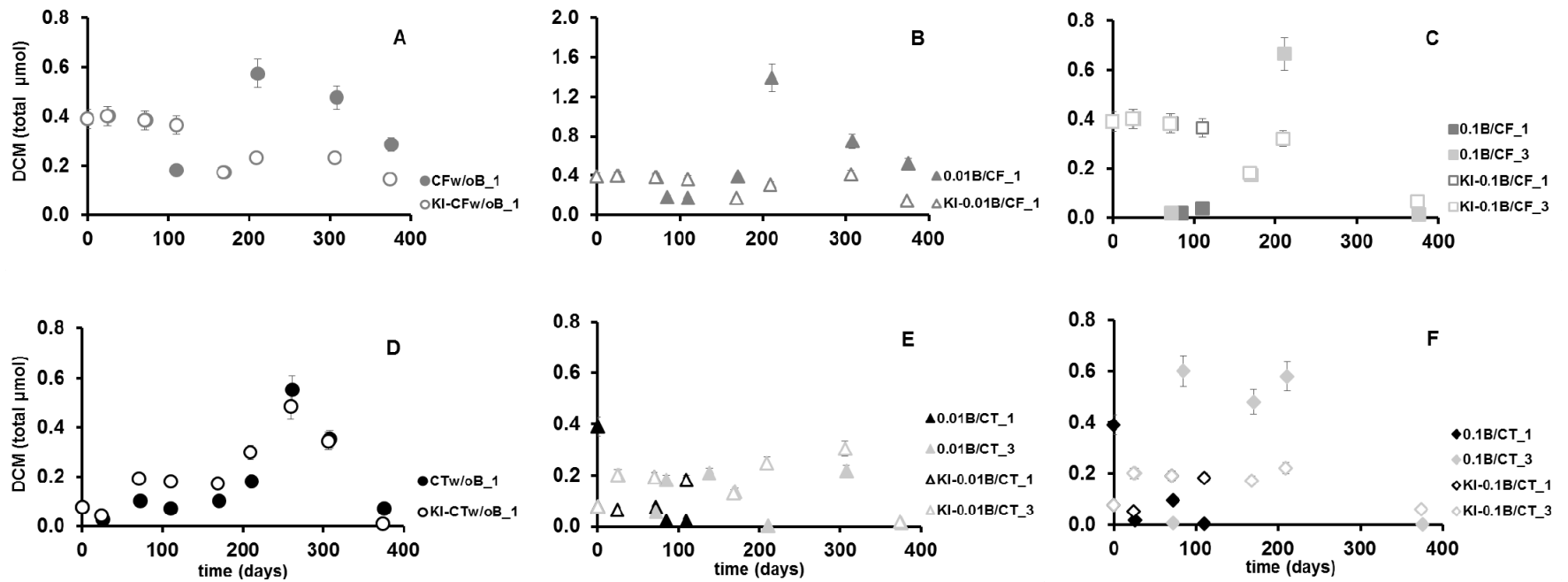
Fig. A3. DCM concentration (calculated from total μmol in the bottle by Henry's law constant at 24°C according to Staudinger and Roberts (2001) over time in one (replicate 1) or two replicates (as specified) for live microcosms and heat-killed controls (KI) of each treatment: CFw/oB (A), 0.01B/CF (B), 0.1B/CF (C), CTw/oB (D), 0.01B/CT (E) and 0.1B/CT (F). The error bars show the uncertainty in concentration measurements. In some cases, error bars are smaller than the symbols.

2.2. Pseudo-first order rate constant results
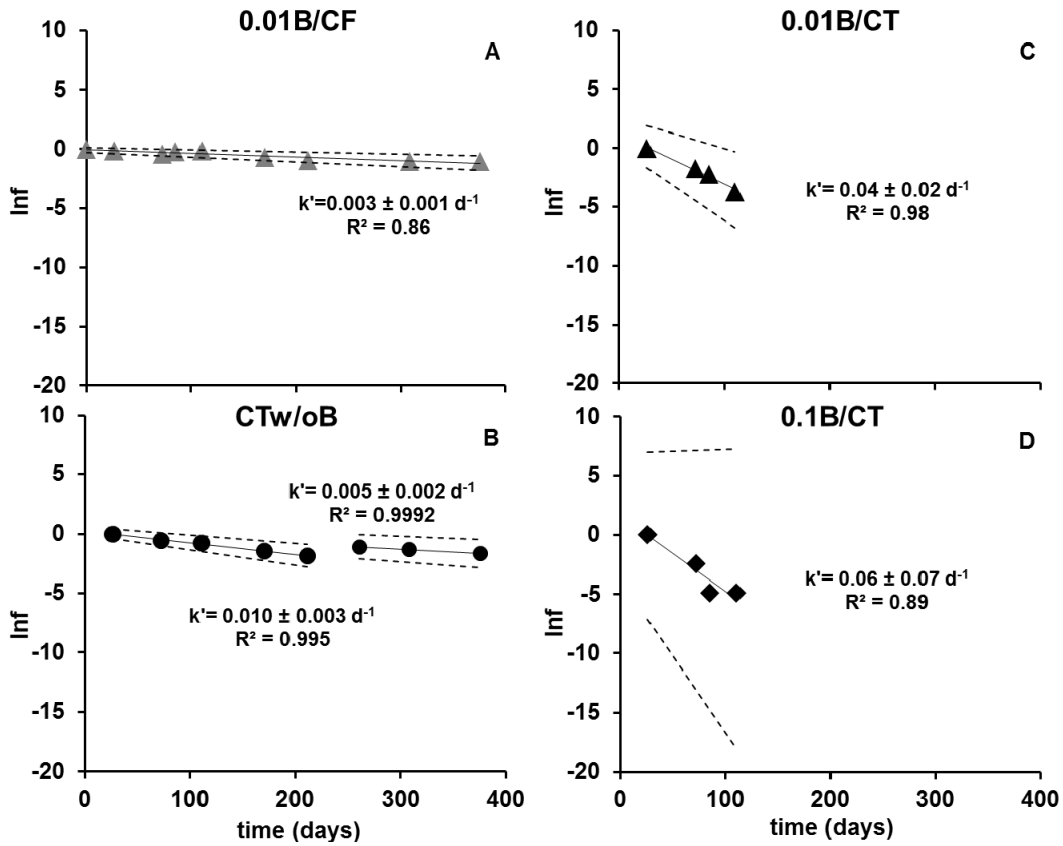
Fig. A4. Semi-logarithmic plot of kinetics of CF and CT removal for the 0.01B/CF (A), CTw/oB (B), 0.01B/CT (C) and 0.1B/CT (D) treatments. No degradation was detected in CFw/oB treatment. The error bars of the uncertainty in the natural logarithm of f (i.e. C/C_0), calculated by error propagation including uncertainty in concentration measurements bars, are smaller than the symbol size. Pseudo-first-order rate constants (k') were extracted from curve fittings according to Eq. (3). Dashed lines represent 95% CI of linear regression. Pseudo-first-order rate constant in CTw/oB treatment (B) was calculated for two different intervals due to a change in the kinetics after 211 days.

Table A1. Summary of pseudo-first-order rate constants (days^{-1}) of CF and CT removal with B$_{12}$ in comparison with the literature. pH and T of the experiments are also listed for sake of comparison. na: not applicable

Experiment	k' (d^{-1}) Eq. (A1)	CI 95 (%)	k'/k'$_{w/oB}$	pH ± SD	T ($^{\circ}$C)	References
CFw/oB					23 ±2	not degraded in this study
0.01B/CF	0.026	0.008	7	buffer pH 7	32	Guerrero-Barajas and Field (2005a)
0.01B/CF	0.003	0.001	no degradation w/o B$_{12}$	7.6 ± 0.2	23 ±2	this study
0.1B/CF	0.17	0.06	43	buffer pH 7	32	Guerrero-Barajas and Field (2005a)
0.1B/CF	0.08	0.06	no degradation w/o B$_{12}$	8.0 ± 0.5	23 ±2	this study
CTw/oB	0.19	0.04	na	buffer pH 7	32	Guerrero-Barajas and Field (2005b)
CTw/oB	0.010	0.003	na	8.1 ± 0.1	23 ±2	0 to 211 days, this study
	0.005	0.002	na	8.1 ± 0.1	23 ±2	211 to 376 days, this study
0.1B/CT	1.05	0.06	6	buffer pH 7	32	Guerrero-Barajas and Field (2005b)
0.1B/CT	0.06	0.07	6 to 12	7.92 ± 0.03	23 ±2	this study

2.3. Microbial assessment

Samples for DGGE (Fig. A5) and NGS (Fig. A6) taken in three different times (t$_0$, t$_3$ and t$_{10}$) represented different degradation stages in each treatment. Samples from t$_0$, from the initial flushed slurry before adding the extra amendments, represented the total predominant microbial community (Fig. A6). Samples from t$_3$ were taken at this time because significant degree of biodegradation of the parental compounds in the 0.01B/pollutant treatments was proved by isotope enrichment and because parental compounds in the 0.1B/pollutant treatments were already consumed. All collected samples from t$_3$ were also analysed by NGS (Fig. A6), except for 0.1B/CF since CF was already fast degraded without product accumulation, making its study meaningless at this time. Samples at t$_{10}$ were taken from all live treatments at final time when parental compounds were long over (0.1B/CF, 0.1B/CT and 0.01B/CT) and thus the activity information might be more connected to biodegradation of by-products or when degradation of the parental compounds became slower but was still active, stagnant or not significant (CTw/oB,

0.01B/CF and CFw/oB treatments, respectively). At t_{10} only CTw/oB was analysed by NGS since only in this treatment changes in CT isotope ratios were still observed.

DGGE analyses were performed as a preliminary approach to detect global population changes. Results showed few phylotypes belonging to families, genus and species with a homology higher than 90 % (Fig. A5, Table A2). DGGE profile of initial groundwater is different from the rest of treatments; however, it should be considered that all treatments are related to RNA analysis, which microbial activity is expressed, unlike initial groundwater sample (DNA based analysis). By DGGE only two phylotypes were depicted with 100% of sequence homology belonging to the organohalide respiring bacteria genera (OHR) (Fig. A5, Table A2): aerobic *Ancylobacter* spp., with ubiquitous activity in different treatments (*A. aquaticus* strain NBRC 102453, NR 114097, and *A. dichloromethanicus* strain DM16, NR 116379) and *Sulfurospirillum* spp., which were only well detected in CTw/oB treatment at t_{10} (*S. halorespirans* DSM 13726, CP017111, and *S. multivorans* DSM 12446, CP007201).
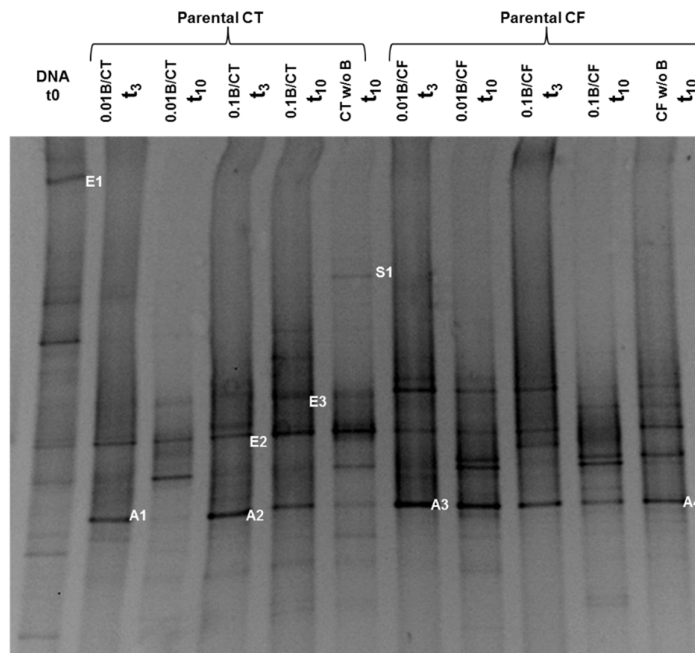
Fig. A5. Bacterial 16S rRNA DGGE (region V3-V5) from samples of different treatments and experiment times. DNA-based for initial slurry (t_0) and RNA-based for the rest of treatments.

Table A2. DGGE band description, designations, and levels of similarity to closest related organisms in GenBank. E1, E2 and E3 from Fig. A5 are not conclusive.

Band	Accession Number	Closest type strain in GenBank	Similarity (%)	Phylogenetic group
A1,A2,A3,A4	KY921708	*Ancylobacter aquaticus* strain NBRC 102453 (NR_114097)	100	p_Alphaproteobacteria; f_Xantobacteraceae
		Ancylobacter dichloromethanicus strain DM16 (NR_116379)	100	
S1	KY921709	*Sulfurospirillum halorespirans* DSM 13726 (CP017111)	100	p_Epsilonproteobacteria; f_Campylobacteraceae
		Sulfurospirillum multivorans DSM 12446 (CP007201)	100	
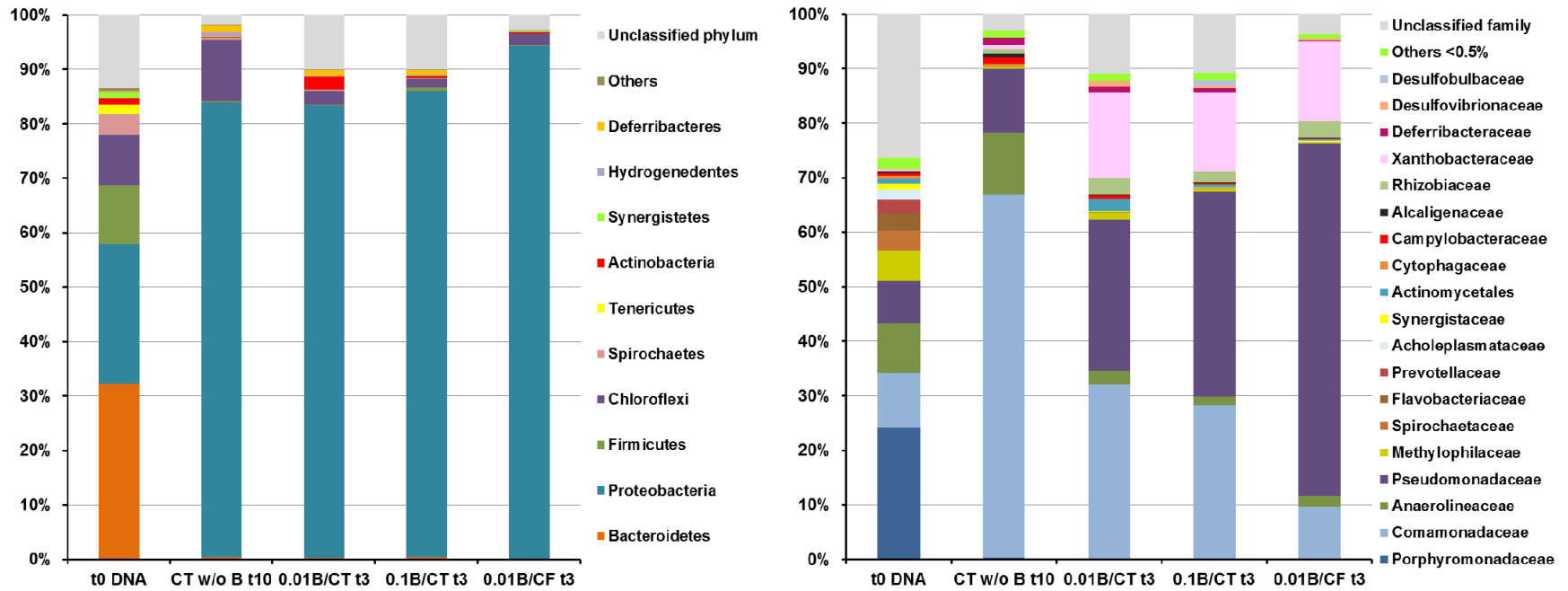
Fig. A6. Biodiversity of metabolically active bacterial populations expressed as the relative OTUs abundance (in %) according to the RDP Bayesian Classifier database at phylum (left panel) and family level (right panel), with a bootstrap confidence above 80%. Taxa with an abundance lower than 0.5% is grouped as "others". The initial sample (t_0) was based on direct DNA-based analysis while the remaining ones are RNA-based.
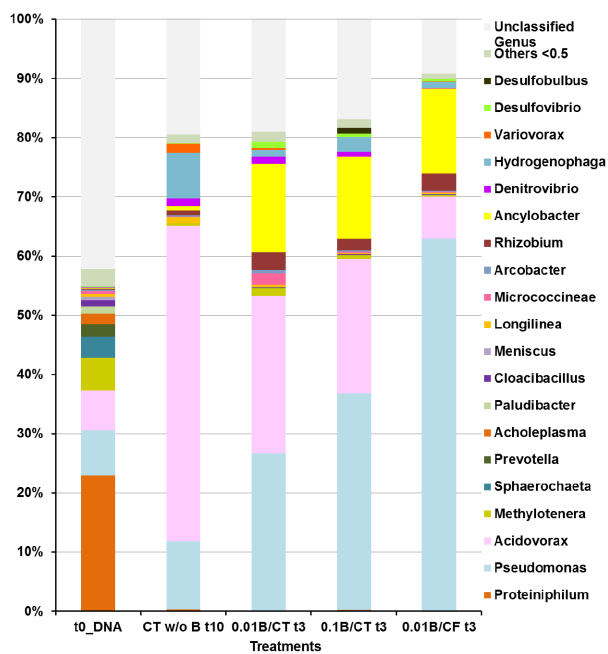
Fig. A7. Biodiversity of metabolically active bacterial populations expressed as the relative OTUs abundance (in %) according to the RDP Bayesian Classifier database (at the genus level with a bootstrap confidence above 80%) obtained from the M_S bottles. The initial sample (t0_DNA) was based on direct DNA-based analysis of flushed slurry without amendments while the remaining ones are RNA-based extracted from the different CF and CT selected treatments and sampling points (t). Taxa with an abundance lower than 0.5% is grouped as "others".

Table A3. Relative abundance (%) at genus level. Initial time (t_0) is DNA-based analysis whereas the rest of sampling times are RNA-based. RDP (Bayesian Classifier) database. "Others" includes genera < 0.5% in all treatments.

Genus	DNA t_0	CTw/oB t_{10}	0.01B/CT t_3	0.1B/CT t_3	0.01B/CF t_3
Proteiniphilum	22.94	0.32	0.16	0.18	0.10
Pseudomonas	7.63	11.53	26.51	36.63	62.84
Acidovorax	6.79	53.28	26.67	22.70	7.17
Methylotenera	5.52	0.35	1.25	0.64	0.23
Sphaerochaeta	3.54	0.02	0.05	0.02	0.02
Prevotella	2.12	<0.01	0.01	<0.01	<0.01
Acholeplasma	1.73	<0.01	0.01	<0.01	<0.01
Paludibacter	1.27	<0.01	<0.01	0.01	<0.01
Cloacibacillus	0.98	0.02	0.02	0.11	0.11
Meniscus	0.63	0.01	<0.01	<0.01	<0.01
Longilinea	0.49	1.08	0.46	0.16	0.23
Micrococcineae	0.43	0.09	1.92	0.27	0.15
Arcobacter	0.25	0.20	0.59	0.24	0.14
Rhizobium	0.17	0.80	2.97	1.98	2.94
Ancylobacter	0.14	0.75	14.97	13.84	14.41
Denitrovibrio	0.08	1.31	1.12	0.82	0.09
Hydrogenophaga	0.07	7.73	1.17	2.50	1.01
Variovorax	0.06	1.46	0.37	0.06	0.03
Desulfovibrio	0.03	0.07	0.97	0.51	0.39
Desulfobulbus	0.02	0.01	0.01	1.01	0.03
Others	2.91	1.48	1.71	1.47	0.98
Unclassified Genera	42.21	19.48	19.03	16.86	9.13

Table A4. Relative abundance (%) of *Pseudomonas* OTUs for Miseq Illumina. Initial time (t_0) is DNA-based analysis whereas the rest of sampling times are RNA-based. RDP (Bayesian Classifier) database.

OTU	Homology %	Assignment	DNA t_0	CTw/oB t_{10}	0.01B/CT t_3	0.1B/CT t_3	0.01B/CF t_3
1	99.6	*P. lingynensis* (NR_117838.1*)*	6.35	9.56	15.94	27.62	57.08
8	98.6	*P. stutzeri (*CP007441.1)	0.69	1.30	8.45	7.13	4.46
14	99.6	*P. stutzeri (*KF863235.1)	0.38	0.37	1.72	1.51	0.39
158	98.6	*P. putida (*KT792731.1)	0.09	0.06	0.06	0.05	0.07
40	99.6	*P. sp.* (CP018420.1)	0.07	0.16	0.04	0.03	0.34
520	99.8	*P. sp. (*JX177697.1)	0.04	0.03	0.06	0.09	0.26
941	96.2	*P. sp. (*KR012325.1)	0.02	0.05	0.24	0.20	0.24
863	99.1	*P. sp.* (KU601279.1)	<0.001	<0.001	0.01	<0.001	<0.001
	Total Pseudomonas		7.63	11.53	26.51	36.63	62.84

Table A5: Diversity, richness and coverage indexes for bacterial community analyses in the different treatments (mean ± standard deviation).

Index	DNA t_0	CTw/oB t_{10}	0.01B/CT t_3	0.1B/CT t_3	0.01B/CF t_3
Total of contigs (478204)	70705	113413	98700	88726	106660
OTUs[1]	843±1	423±6	487±6	447±5	410±7
Coverage[1]	0.9999±0.0001	0.998±0.0001	0.998±0.001	0.998±0.0001	0.998±0.0001
Inv Simpson[1]	17.04±0.01	3.15±0.01	7.31±0.02	6.27±0.01	2.683±0.008
Shannon[1]	3.737±0.001	2.217±0.005	2.765±0.004	2.533±0.003	1.869±0.004
Chao1[1]	887±3	517±22	597±22	605±26	577±33
ACE[1]	869±1	524±16	610±17	604±23	625±65

[1]Data normalized to the sample with the lowest number of contigs (70705 from DNA t0). Values calculated with MOTHUR at the 3% distance level.

2.4. pH, total elements, cations and anions concentration evolution with time

Samples for temperature, pH and anions and cations concentrations were obtained at initial time and at t_5= 138 days by sacrificing replicates 1 and 2 of the monitored triplicates of 0.1B/CT, 0.1B/CF, 0.01B/CT treatments and their corresponding heat-killed controls (KI) and at t_{10}=376 days in monitored triplicates (or in the resting third replicate bottle for the three treatments already sacrificed at 139 days) in order to compare them to initial flushed slurry without amendments (Table A6).

Table A6. Average of pH, anions and cations concentrations of different sampling times n (specified in parentheses for each treatment). ClO_3^- was analysed but it was in all cases below the detection limit (0.2 mM); n.a. (not analysed). SD calculated with different replicates and different sampling points over time except for ClO_2^-, which are replicates for only one time (after 376 days).

Treatment	pH	NO_3^- (μM)	NO_2^- (μM)	Cl^- (mM)	SO_4^{2-} (mM)	NH_4^+ (μM)	ClO_2^- (μM)	S_{total} (mM)	Fe_{total} (μM)	Ca_{total} (mM)	Na_{total} (mM)
Initial value	n.a.	33	16	46	10	200	n.a.	n.a.	n.a.	n.a.	n.a.
CTw/oB	7.6±0.2 (2)	54±9 (2)	8±5 (2)	43±6 (2)	8.8±0.5 (2)	200±70 (2)	0.8±0.1 (1)	10.0±0.1 (2)	213±75 (2)	9.8±0.6 (2)	33±87 (2)
KI-CTw/oB	7.54±0.02 (2)	41±2 (2)	10±4 (2)	45.4±0.2 (2)	8.8±0.4 (2)	234±4 (2)	0.31±0.01 (1)	9.90±0.02 (2)	2.1±0.3 (2)	8.0±0.1 (2)	36.3±0.4 (2)
0.01B/CT	8.1±0.1 (2)	27±9 (3)	13±4 (3)	44±3 (3)	8.9±0.6 (3)	250±20 (3)	1.1 (1)	9.7±0.4 (2)	4±2 (2)	89±1 (2)	35.7±0.6 (2)
KI-0.01B/CT	8.0±0.4 (3)	30±9 (3)	14±4 (3)	45.6±0.7 (3)	9.1±0.2 (3)	260±20 (3)	0.3 (1)	10.0±0.1 (3)	2.2±0.5 (3)	8.0±0.1 (3)	35.9±0.7 (3)
0.1B/CT	8.1±0.4 (3)	37±6 (3)	17±4 (3)	42±7 (3)	8.9±0.5 (3)	220±50 (3)	0.9 (1)	9.7±0.2 (3)	7±5 (3)	10±2 (3)	26±9 (3)
KI-0.1B/CT	8.0±0.4 (3)	27±11 (3)	14±3 (3)	45.46±0.07 (3)	9.0±0.6 (1)	250±20 (2)	0.4 (1)	10.08±0.02 (3)	66±110 (3)	8.6±0.9 (3)	36.2±0.2 (3)
CFw/oB	7.8 ±0.2 (2)	39.1±10 (2)	6±6 (2)	31.8±0.8 (2)	10.7±0.6 (2)	160±30 (2)	0.7±0.4 (1)	10.1±0.2 (2)	212±153 (2)	10.7±0.2 (2)	20.6±0.3 (2)
KI-CFw/oB	7.64±0.02 (2)	40 ±2 (2)	10±4 (2)	45.4±0.4 (2)	9.6±0.3 (2)	239±2 (2)	0.36±0.04 (1)	10.0±0.2 (2)	2.4±0.1 (2)	7.92±0.03 (2)	36.3±0.5 (2)
0.01B/CF	7.92±0.03 (2)	20±20 (2)	6±6 (2)	32.7±0.1 (2)	9.2±0.4 (2)	163±2 (2)	0.92±0.07 (1)	9.6±0.1 (2)	38±4 (2)	10.7±0.1 (2)	20.6±0.2 (2)
KI-0.01B/CF	7.57±0.04 (2)	39.2±0.8 (2)	10±4 (2)	45.2±0.2 (2)	9.0±0.4 (2)	237±3 (2)	0.33±0.01 (1)	10.1±0.1 (2)	2.1±0.2 (2)	8.0±0.1 (2)	35.9±0.7 (2)
0.1B/CF	8.0±0.5 (3)	27±14 (3)	12±7 (3)	32.7±0.4 (3)	9.5±0.2 (3)	170±10 (3)	1.1 (1)	9.8±0.4 (3)	83±100 (3)	10.2±0.6 (3)	29±8 (3)
KI-0.1B/CF	8.0±0.4 (3)	28±11 (3)	14±3 (3)	45.3±0.2 (3)	9.3±0.8 (3)	260±10 (3)	0.4 (1)	10.0±0.4 (3)	11±13 (3)	9±2 (3)	31±9 (3)

2.5. Fractionation and mechanistic insights
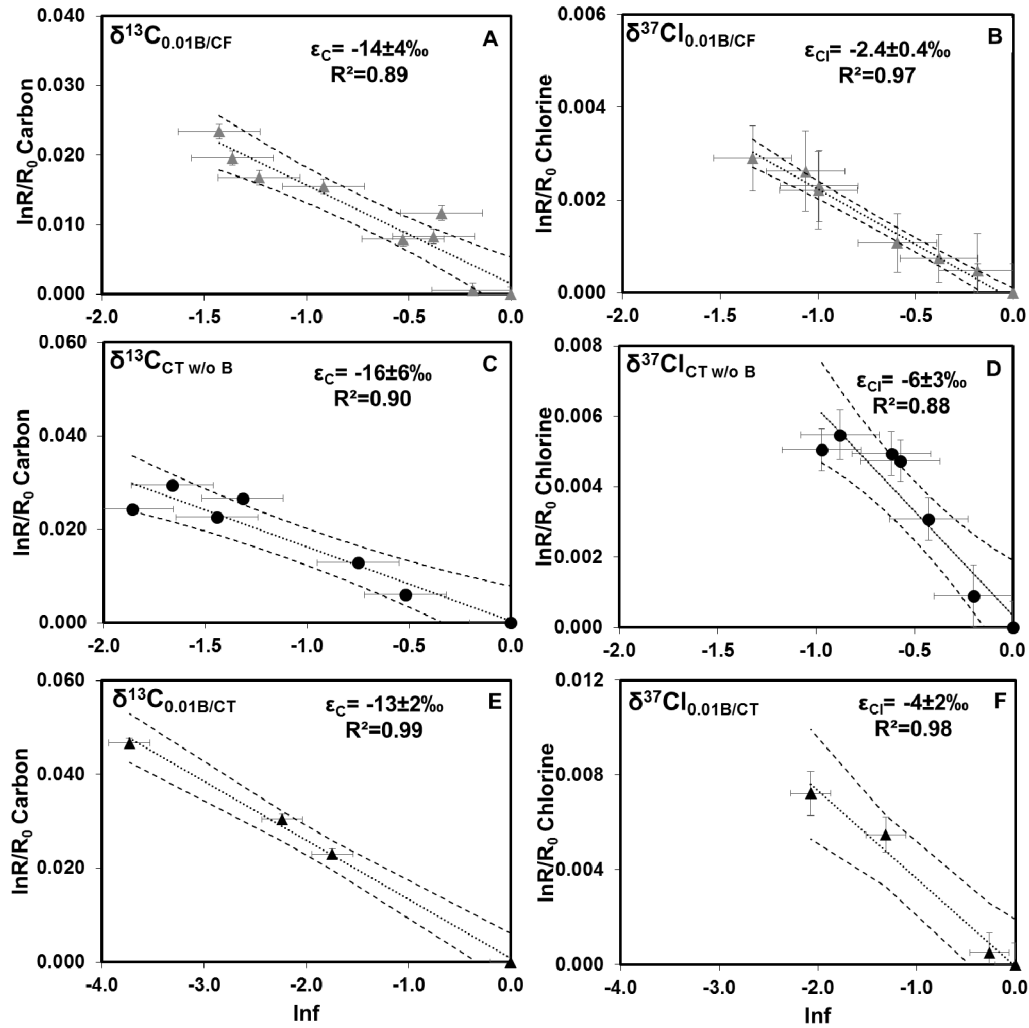
Fig. A8. Logarithmic plots according to Rayleigh equation (Eq. 1) of carbon (left panels) and chlorine (right panels) isotope ratios of treatments: 0.01B/CF (A and B), CTw/oB treatment (C and D) and 0.01B/CT (E and F). Dashed lines represent 95% CI of linear regression. Error bars display the error calculated by error propagation including uncertainties in concentration and isotope measurements. In some cases, error bars are smaller than symbols.

16

Table A7. Summary of ε, AKIE and Λ values for C and Cl isotopes for chlorinated methanes reported in different studies.

Compound	Degradation pathway	Type	Conditions	ε_{bulkC} (‰) ± 95% CI	$n_C=x_C=z_C$	$AKIE_C$	ε_{bulkCl} (‰) ± 95% CI	n_{Cl}	x_{Cl}	z_{Cl}	$AKIE_{Cl}$	$\Lambda≈\varepsilon C/\varepsilon Cl$	Reference
	Reductive dechlorination by C−Cl bond cleavage			**Streitwieser limit C-Cl bond cleavage KIE_C = 1.057 (Elsner et al. (2005); Aelion et al. (2010))**			**Streitwieser limit C-Cl bond cleavage KIE_{Cl} = 1.013 (Elsner et al. (2005))**						
CF	Reductive dechlorination	abiotic (Fe(0))	laboratory	-33±11	1	1.034± 0.012	-3±1	3	3	3	1.008±0.001	8±2	Torrentó et al.(2017)
CF	Reductive dechlorination	abiotic (Fe(0))	laboratory	-30±2	1	1.03± 0.07	NM					NM	Lee et al.(2015)
CF	Reductive dechlorination	biotic (*Dehalobacter* sp. CF50 consortium)	laboratory	-27.5±0.9	1	1.028± 0.002	NM					NM	Chan et al.(2012)
CF	Reductive dechlorination	biotic (*Dehalobacter* sp.UNSWDHB consortium)	laboratory	-4.3	1	1.004	NM					NM	Lee et al.(2015)
CF	Reductive dechlorination	biotic + vitamin B$_{12}$	laboratory	-14±4	1	1.014± 0.002	-2.4±0.4	3	3	3	1.0072±0.0004	7±1	This study
CT	Reductive dechlorination	abiotic (goethite, magnetite, lepidocrocite, hematite, siderite)	laboratory	-26 to -32	1	1.027 to 1.033	NM					NM	Zwank et al.(2005) Elsner et al.(2004)
CT	Reductive dechlorination	abiotic (mackinawite)	laboratory	-10.9 to -15.9	1	1.011 to 1.016	NM					NM	Zwank et al.(2005) Neumann et al.(2009)
CT	Reductive dechlorination	abiotic (Zn(0))	laboratory	-10.8±0.7	1	1.01	NM					NM	VanStone et al. (2008)
CT	Reductive dechlorination	biotic	laboratory	-16±6	1	1.016± 0.001	-6±3	4	4	4	1.023±0.003	6.1±0.5	This study
CT	Reductive dechlorination	biotic + vitamin B$_{12}$	laboratory	-13±2	1	1.013± 0.003	-4±2	4	4	4	1.015±0.002	5±1	This study
	Stepwise elimination reaction (E1CB)			**Streitwieser limit C-Cl bond cleavage KIE_C = 1.057 (Elsner et al.(2005); Aelion et al.(2010))**			**Streitwieser limit C-Cl bond cleavage KIE_{Cl} = 1.013 (Elsner et al.(2005))**						
CF	Alkaline degradation	abiotic (alkaline hydrolysis)	laboratory	-57±5	1	1.061± 0.006	-4.4±0.4	3	3	3	1.013±0.0004	13.0±0.8	Torrentó et al. (2017)
CF	Alkaline degradation	abiotic (alkaline hydrolysis)	laboratory	-53±3	1	1.056± 0.003	NM					NM	Torrentó et al.(2017)
	Nucleophilic substitution reactions (S$_N$2-Type)			**Typical range KIE_C = 1.03 to 1.09 (Elsner et al.(2005))**			**Theoretical maximum KIE_{Cl} = 1.019-1.020 (Paneth (1992); Dybała-Defratyka et al. (2004))**						
DCM	Aerobic oxidation	biotic (MC8b culture)	laboratory	-42.4±1.5	1	1.044	-3.8±0.3					11.2	Heraty et al.(1999)
CM	Aerobic oxidation	biotic (IMB-1, MB-2 and CC495 cultures)	laboratory	-42 to -48	1	1.044 to 1.050	NM					NM	Miller et al.(2001)

2.6. Dual C-Cl isotope plot for CT treatmetns
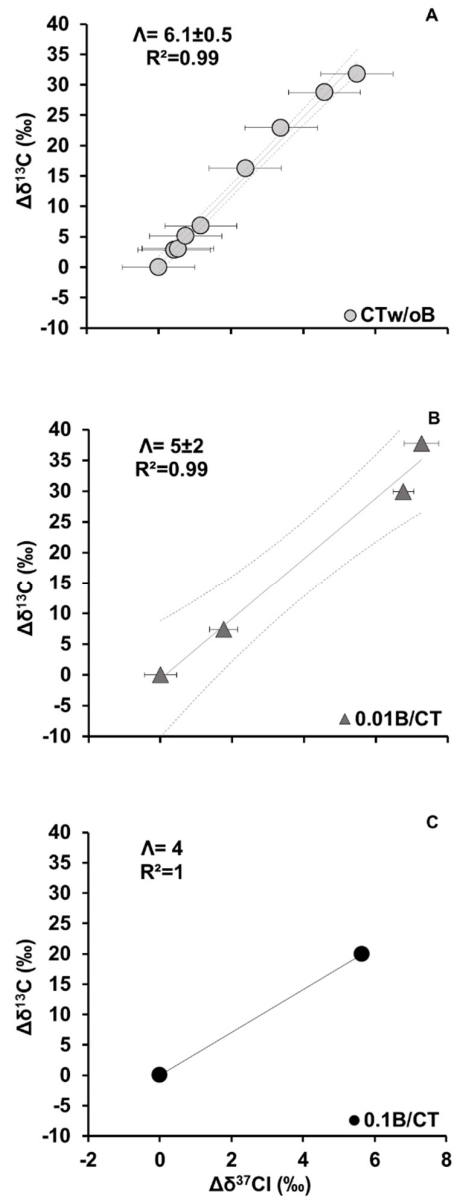
Fig. A9. Dual C-Cl isotope plot for CT for treatments CTw/oB (A), 0.01B/CT (B) and 0.1B/CT (C) (last one with only two available points for plotting). Lines are linear regressions of the data sets with 95% CI (dashed lines). Error bars show uncertainty in isotope measurements. Note that error bars of $\delta^{13}C$ values are smaller than the symbols.

3. <u>REFERENCES</u>

Aelion, C.M.; Hohëner, P.; Hunkeler, D.; Aravena, R., 2010. Environmental isotopes in biodegradation and bioremediation. CRC Press, Boca Raton, FL.

Chan, C.C.H., Mundle, S.O.C., Eckert, T., Liang, X., Tang, S., Lacrampe-Couloume, G., Edwards, E.A., Sherwood Lollar, B., 2012. Large carbon isotope fractionation during biodegradation of chloroform by *Dehalobacter* cultures. Environ. Sci. Technol. 46, 10154–10160. doi:10.1021/es3010317

Dybała-Defratyka, A., Rostkowski, M., Matsson, O., Westaway, K.C., Paneth, P., 2004. A new interpretation of chlorine leaving group kinetic isotope effects ; A theoretical approach. J. Org. Chem. 69, 4900–4905.

Elsner, M., Haderlein, S.B., Kellerhals, T., Luzi, S., Zwank, L., Angst, W., Schwarzenbach, R.P., 2004. Mechanisms and products of surface-mediated reductive dehalogenation of carbon tetrachloride by Fe(II) on goethite. Environ. Sci. Technol. 38, 2058–2066. doi:10.1021/es034741m

Elsner, M., Zwank, L., Hunkeler, D., Schwarzenbach, R.P., 2005. A new concept linking observable stable isotope fractionation to transformation pathways of organic pollutants. Environ. Sci. Technol. 39, 6896–6916.

Guerrero-Barajas, C., Field, J.A., 2005a. Riboflavin- and cobalamin-mediated biodegradation of chloroform in a methanogenic consortium. Biotechnol. Bioeng. 89, 539–550. doi:10.1002/bit.20379

Guerrero-Barajas, C., Field, J.A., 2005b. Enhancement of anaerobic carbon tetrachloride biotransformation in methanogenic sludge with redox active vitamins. Biodegradation 16, 215–228. doi:10.1007/s10532-004-0638-z

Heraty, L.J., Fuller, M.E., Huang, L., Abrajano, T.A., Sturchio, N.C., 1999. Isotopic fractionation of carbon and chlorine by microbial degradation of dichloromethane. Org. Geochem. 30, 793–799.

Lee, M., Wells, E., Wong, Y.K., Koenig, J., Adrian, L., Richnow, H.H., Manefield, M., 2015. Relative contributions of *Dehalobacter* and zerovalent iron in the degradation of chlorinated methanes. Environ. Sci. Technol. 49, 4481–4489. doi:10.1021/es5052364

Miller, L.G., Kalin, R.M., McCauley, S.E., Hamilton, J.T.G., Harper, D.B., Millet, D.B., Oremland, R.S., Goldstein, A.H., 2001. Large carbon isotope fractionation associated with oxidation of methyl halides by methylotrophic bacteria. Proc. Natl. Acad. Sci. U. S. A. 98, 5833–5837.

Neumann, A., Hofstetter, T.B., Skarpeli-Liati, M., Schwarzenbach, R.P., 2009. Reduction of polychlorinated ethanes and carbon tetrachloride by structural Fe(II) in smectites. Environ. Sci. Technol. 43, 4082–4089. doi:10.1021/es9001967

Paneth, P., 1992. How to measure heavy atom isotope effects: general principles., in: Buncel, E., Saunders, W.H.J. (Eds.), Isotopes in Organic Chemistry. Elsevier, New York, p. 1992.

Staudinger, J., Roberts, P. V., 2001. A critical compilation of Henry's law constant temperature dependence relations for organic compounds in dilute aqueous solutions. Chemosphere 44, 561–576. doi:10.1016/S0045-6535(00)00505-1

Torrentó, C., Palau, J., Rodríguez-Fernández, D., Heckel, B., Meyer, A., Domènech, C., Rosell, M., Soler, A., Elsner, M., Hunkeler, D., 2017. Carbon and chlorine isotope fractionation patterns associated with different engineered chloroform transformation reactions. Environ. Sci. Technol. 51, 6174–6184. doi:10.1021/acs.est.7b00679

Vanstone, N., Elsner, M., Lacrampe-Couloume, G., Mabury, S., Sherwood Lollar, B., 2008. Potential for identifying abiotic chloroalkane degradation mechanisms using carbon isotopic fractionation. Environ. Sci. Technol. 42, 126–132. doi:10.1021/es0711819

Zwank, L., Elsner, M., Aeberhard, A., Schwarzenbach, R.P., 2005. Carbon isotope fractionation in the reductive dehalogenation of carbon tetrachloride at iron (hydr)oxide and iron sulfide minerals. Environ. Sci. Technol. 39, 5634–5641.

Erratum of <u>Rodríguez-Fernández, D</u>., Torrentó, C., Guivernau, M., Viñas, M., Hunkeler, D., Soler, A., Domènech, C., Rosell, M., 2018. Vitamin B$_{12}$ effects on chlorinated methanes-degrading microcosms: Dual isotope and metabolically active microbial populations assessment. Sci. Total Environ. 621, 1615–1625. doi:10.1016/j.scitotenv.2017.10.067.

In the references Caporaso et al. 2010a should be:
Caporaso, J., Kuczynski, J., Stombaugh, J., Bittinger, K., Bushman, F.D., Costello, E.K., Fierer, N., Peña, A.G., Goodrich, J.K., Gordon, J.I., Huttley, G.A., Kelley, S.T., Knights, D., Koenig, J.E., Ley, R.E., Lozupone, C.A., Mcdonald, D., Muegge, B.D., Pirrung, M., Reeder, J., Sevinsky, J.R., Turnbaugh, P.J.,Walters,W.A.,Widmann, J., Yatsunenko, T., Zaneveld, J., Knight, R., 2010a. QIIME allows analysis of high-throughput community sequencing data intensity normalization improves color calling in SOLiD sequencing. Nat. Publ. Gr. 7:335–336. https://doi.org/10.1038/nmeth0510-335.

And Caporaso et al. 2010b should be:
Caporaso, J., Bittinger, K., Bushman, F.D., Desantis, T.Z., Andersen, G.L., Knight, R., 2010b. PyNAST: a flexible tool for aligning sequences to a template alignment. Bioinformat- ics 26:266–267. https://doi.org/10.1093/bioinformatics/btp636.

Annex G. Article 5. Chlorinated methanes degradation: field study

Rodríguez-Fernández, D., Torrentó, C., Palau, J., Marchesi, M., Soler, A., Hunkeler, D., Domènech, C., Rosell, M. Unraveling long-term source removal effects and chlorinated methanes natural attenuation processes by C and Cl stable isotopic patterns at a complex site. Submitted to Sci. Total Environ.

Graphical abstract
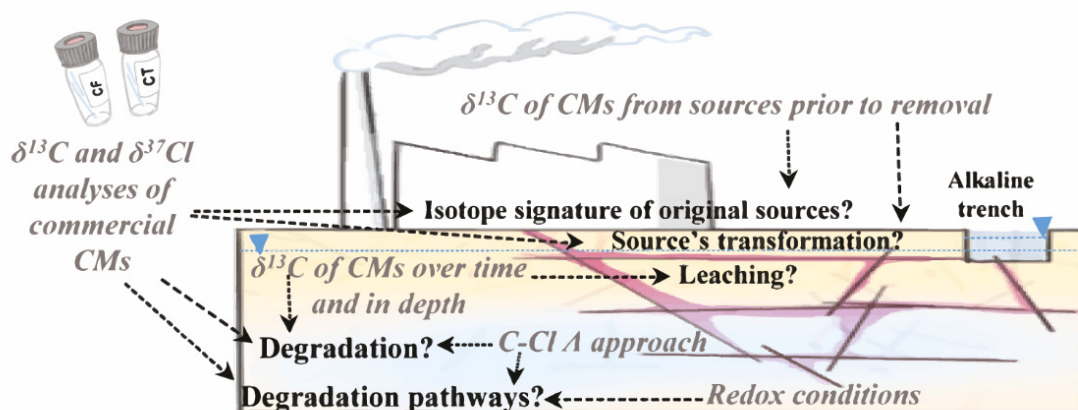
Highlights

- Long-term $\delta^{13}C$ monitoring of chlorinated methanes (CMs) after source removal
- CMs concentration and $\delta^{13}C$ study enabled detection of still active CMs sources
- Assessment of CT and CF field degradation processes by dual C-Cl isotope approach
- CF oxidation or/and alkaline hydrolysis in pit and CT reduction in tank zone
- CT thiolytic reduction in wastewater pipe is combined with hydrogenolysis

1 # Unravelling long-term source removal effects and

2 # chlorinated methanes natural attenuation processes by

3 # C and Cl stable isotopic patterns at a complex field site

4 Diana Rodríguez-Fernández[1], Clara Torrentó[2,1], Jordi Palau[2, 3, 1], Massimo Marchesi[1,4], Albert

5 Soler[1], Daniel Hunkeler[2], Cristina Domènech[1], Mònica Rosell[1]

6 [1] Grup MAiMA, Mineralogia Aplicada, Geoquímica i Geomicrobiologia, Departament de Mineralogia, Petrologia i

7 Geologia Aplicada, Facultat de Ciències de la Terra, Universitat de Barcelona (UB), C/Martí i Franquès s/n, 08028

8 Barcelona, Spain.

9 [2] Centre for Hydrogeology and Geothermics, University of Neuchâtel, 2000 Neuchâtel, Switzerland

10 [3] Institute of Environmental Assessment and Water Research (IDAEA), CSIC, Jordi Girona 18-26, 08034 Barcelona,

11 Spain; Associated Unit: Hydrogeology Group (UPC-CSIC), Barcelona, Spain.

12 [4] Politecnico di Milano, Dept. of Civil and Environmental Engineering (DICA), Piazza L. Da Vinci, 32, 20133 Milano,

13 Italy

14 **Corresponding Author:**

15 *Diana Rodríguez-Fernández Phone: +34 93 403 90 74; Fax: +34 93 402 13 40, e-mail:

16 diana.rodriguez@ub.edu

17 **Science of the Total Environment**

18 Total number of pages (including cover): 27

19 Figures: 5

20 Tables: 1

21

22   **ABSTRACT**

23   The effects of contaminant sources removal in 2005 (i.e. barrels, wastewater tank, disposal pit

24   and wastewater pipe) on carbon tetrachloride (CT) and chloroform (CF) concentration in

25   groundwater were assessed at several areas of a multi-contaminant aquifer (Òdena, Spain) over a

26   long-term period (2010-2014). Changes in redox conditions, in these chlorinated methanes (CMs)

27   concentration and in their carbon isotopic compositions ($\delta^{13}C$) were monitored in multilevel wells.

28      $\delta^{13}C$ values were compared to those obtained from the sources (2002-2005) and commercial

29   solvents samples. Additionally, CMs natural attenuation processes were identified by C-Cl

30   isotope slopes (Λ).

31   Analyses revealed the downstream migration of the pollutant focus and an efficient removal of

32   DNAPLs in the pit source's influence area. However, the removal of the tank and wastewater

33   pipe sources was uncompleted as active leaching from unsaturated zone was proved.

34   Nevertheless, significant CMs degradation was detected close to all sources and Λ values pointed

35   to different reactions. For CT in the tank area, Λ value fitted with hydrogenolysis pathway

36   although other possible reduction processes were also uncovered. Near the wastewater pipe area,

37   thiolytic reduction combined with hydrogenolysis was derived. The highest CT degradation

38   extent accounted for these areas was 72±11% and 84±6%, respectively. For CF, the Λ value in

39   the pit source's area was consistent with oxidation and/or with transport of CF affected by alkaline

40   hydrolysis from upstream interception trenches. In contrast, isotope data evinced CF reduction in

41   the tank and wastewater pipe influence areas, although the observed Λ slightly deviates from the

42   reference values, likely due to the continuous leaching from the non-saturated zone of distinctly

43   degraded CF.

44   Keywords: carbon tetrachloride, chloroform, 2D-CSIA, case study, Òdena site

1. INTRODUCTION

Carbon tetrachloride (CT) and chloroform (CF) are volatile organic compounds (VOCs) from the chlorinated methanes (CMs) group, considered toxic pollutants by the USEPA (2014). Identifying sources and tracing their evolution over time is crucial to set up effective decontamination strategies (Penny et al., 2010; Cappelletti et al., 2012).

In groundwater, CT degradation only occurs under anoxic conditions. CT can be reduced biotically or by Fe(II) sorbed on iron oxy/hydroxides surfaces to CF and then to dichloromethane (DCM), chloromethane and CH_4 following a hydrogenolysis pathway. In addition, CT hydrolytic reduction (e.g. by magnetite) leads to formate, CO and CO_2 while CT thiolytic reduction produces CS_2 being mediated either by Fe(II)-sulfides or by bacteria (Field and Sierra-Alvarez, 2004; Penny et al., 2010; Koenig et al., 2012; He et al., 2015). CT reduction by *Pseudomonas stutzeri* also produces CO_2 as the final product, with transient accumulation of toxic phosgene and tiophosgene (Lewis and Crawford, 1995).

CF degradation occurs under oxic and anoxic conditions. Under oxic conditions, cometabolic microbial reactions transform CF to CO_2 (Cappelletti et al., 2012). Abiotic reactions like oxidation (e.g. by persulfate) and CF alkaline hydrolysis have been proved as efficient CF remediation strategies (Torrentó et al., 2014; 2017). Under anoxic conditions, direct or indirect hydrolytic reduction of CF to CO_2 and cometabolic hydrogenolysis are described, the latter being associated to methanogens, fermenting bacteria and sulfate reducers (Cappelletti et al., 2012). Finally, *Dehalobacter* and *Desulfitobacterium* genus are able to dechlorinate CF to DCM by dehalorespiration (Grostern et al., 2010; Chan et al., 2012; Lee et al., 2012; Deshpande et al., 2013; Tang and Edwards, 2013; Ding et al., 2014).

CT and CF inhibit mutual biodegradation (Grostern et al., 2010; Lima and Sleep, 2010; Justicia-Leon et al., 2014) and also microbial respiration of chlorinated ethanes and ethenes by *Dehalococcoides* and *Desulfitobacterium* species (Bagley et al., 2000; Weathers and Parkin, 2000; Maymó-Gatell et al., 2001; Duhamel et al., 2002; Futagami et al., 2006, 2013), and this hinders natural attenuation and bioremediation strategies in complex sites impacted by mixtures of chlorinated compounds.

According to the European Environment Agency (EEA, 2014), *ex situ* physical and/or chemical treatments represent 37% of the techniques used in groundwater decontamination. Monitored Natural Attenuation (MNA) is an alternative cost-effective treatment, although it requires appropriate quantification and evaluation over time (Wiegert et al., 2012). There are only few MNA case studies of CT and CF in polluted sites, mainly based on the detection and quantification of by-products (Devlin and Muller, 1999; Davis et al., 2003; Puigserver et al., 2013). However,

monitoring parental and by-product compounds concentration as an indicator of (bio)degradation has some limitations, such as i) long periods of time are often necessary to detect a significant decrease in concentrations, especially at highly polluted sites or when sources have not been removed; and ii) no clear conclusions can be drawn when a given compound appears as both parent and by-product; when a by-product originates from multiple parent compounds; or when the target by-product is further degraded.

To overcome these limitations, compound specific isotope analysis (CSIA) is increasingly used for source apportionment and *in situ* assessment of chlorinated ethenes and ethanes MNA (Wiegert et al., 2012, 2013; Kuder et al., 2013; Badin et al., 2014, 2016; Kaown et al., 2014; Palau et al., 2014, 2016; Audí-Miró et al., 2015). Moreover, dual isotopic studies (2D-CSIA) with carbon and chlorine isotope analyses have allowed more precise identification of pollutants' origin and fate as dual isotope slopes (Λ) reflect ongoing degradation mechanisms and can be compared with characteristic slopes from laboratory studied reactions (Hunkeler et al., 2009). However, an aged source of contamination would have undergone fractionation processes in the unsaturated zone distinctly or not to those occurred in the saturated zone (Jeannottat and Hunkeler, 2012, 2013) and, thus, it would hamper reliable degradation processes discrimination. Therefore, if the original pure phase is not available, the study and comparison of isotope values from wells located in source areas (Wiegert et al., 2012) to those of commercial solvents (Imfeld et al., 2008; Palau et al., 2014) is strongly advisable. To our knowledge, there are only few field CSIA studies dedicated to CMs. These studies are mainly based on carbon isotope measurements to confirm CT degradation in the non-saturated zone (Kirtland et al., 2003), to characterise the very depleted $\delta^{13}C$ of CT and CF industrially produced from methane (Nijenhuis et al., 2013), to confirm CF degradation, along with concentration data, in a multi-contaminant polluted aquifer (Hunkeler et al., 2005) and/or to evaluate CF remediation treatment by alkaline hydrolysis in Òdena site (Spain) (Torrentó et al., 2014). New methods for chlorine isotope analyses of CMs and reference Λ values have only became available recently (Heckel et al., 2017a,b; Torrentó et al., 2017; Rodríguez-Fernández et al., 2018a,b).

In this research, we combine the identification and quantification of by-products with $\delta^{13}C$ and redox shifts monitoring over time aiming at studying the long-term effect in CMs behaviour of the removal of the identified pollutant sources and natural attenuation processes in the monitored contaminated site at Òdena (Spain). This research includes comparison of CMs isotope values from sources with those of CMs commercial solvents and with groundwater samples to identify potential aging of these sources and uncovering CMs active leaching zones. In addition, dual C-Cl isotope plots are compared with data from literature and from recent microcosms studies performed with Òdena site slurry (Rodríguez-Fernández et al., 2018a) for evaluating the potential

114 of this 2D-CSIA approach to identify CMs degradation pathways in complex fractured systems
115 with multi-contaminant spills.

116 **2. MATERIAL AND METHODS**
117 **2.1. Site description**

118 The studied site is an unconfined bedrock aquifer located in Òdena (NE Spain) (Palau et al., 2014;
119 Torrentó et al., 2014). The aquifer is mainly composed of low permeability fractured limestone.
120 Groundwater pollution was attributed to three main potential contaminant sources (i.e.,
121 abandoned barrels, a disposal pit and a wastewater tank) of a former chemical plant working from
122 1978 to 1985 (Fig.1), although some other spills were detected and mentioned as potential
123 chlorinated ethenes contamination sources (Palau et al., 2014). In 2005, contaminated soil of the
124 tank and pit areas was removed (Palau et al., 2014; Torrentó et al., 2014) and the barrels and the
125 wastewater pipe system were dismantled. The tank and pit excavated areas in the non-saturated
126 zone (hereafter called trenches) were filled with concrete-based construction wastes aiming to
127 induce alkaline conditions (pH ~12) and, thus, promote CF degradation through alkaline
128 hydrolysis (Torrentó et al., 2014).
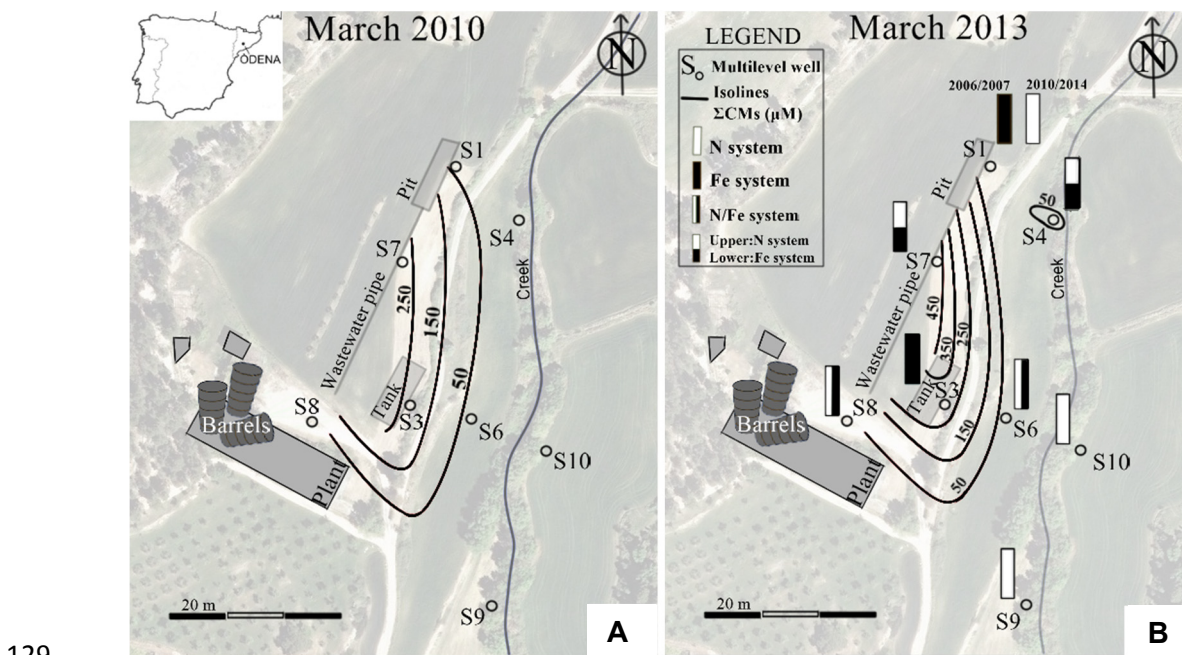
130 Figure 1. Òdena site map and groundwater monitoring wells network (S1-10). Groundwater flow system from Palau et
131 al. (2014) was used to draw a simplified contamination CMs plume evolution (sum of molar concentrations of CT, CF
132 and DCM at the most contaminated level for each well) from A) March 2010 to B) March 2013. The barrels from
133 chemical plant, the tank, pit and the wastewater pipe were all removed in 2005 but are shown in the map for a better
134 understanding. Rectangles in B represent the well's Eh-controlling system from 2006 to 2014, determined after
135 analysing the Eh-pH diagrams (Fig. A1), calculated with data from field samples over time (Table A1). Changes in
136 depth and over time are also specified, if occurred.

2.2. Sample collection

During the 2002-2005 period, the barrels and the tank and/or pit areas were sampled for CT, CF and DCM concentration and $\delta^{13}C$ analyses. In June 2006, June 2007, September 2007, January 2008, March and November 2010 (Mar-10 and Nov-10 hereafter), March 2013 (Mar-13) and November 2014 (Nov-14) samples from 8 multilevel wells (S1, S3, S4, S6, S7, S8, S9 and S10, Fig. 1) were taken for pH and Eh measurements and total Ca, Na, Fe, Cl^-, HCO_3^-, NO_3^- and SO_4^{2-} concentration analyses. $\delta^{34}S$ and $\delta^{18}O$ analyses of dissolved sulfate were done in June 2006 and Mar-13 campaigns. In Mar-10, Nov-10, Mar-13 and Nov-14 VOCs concentration and isotopic measurements ($\delta^{13}C$) were also done. $\delta^{37}Cl$ measurements were only performed in Mar-13 for CF and in Nov-14 for CT and CF. In addition, different commercial CT and CF solvents were analysed to complete the range of $\delta^{13}C$ and $\delta^{37}Cl$ reported in the literature for CMs.

2.3. Analytical methods

pH and Eh were monitored in field samples using a pH-meter (Crison 6037) and a redox sensor (SenTix® ORP 900), respectively. Aliquots of samples were preserved with nitric acid to measure total concentrations of Fe, Ca and Na by inductively coupled plasma-optic emission spectrometry (ICP-OES, Optima 3200 RL) and by inductively coupled plasma-mass spectrometry (ICP-MS, Elan 6000) at the *Centres Científics i Tecnològics de la Universitat de Barcelona* (CCiT-UB). HCO_3^- was determined by titration (METROHM 702SM Titrino). NO_3^-, Cl^- and SO_4^{2-} concentrations were analyzed by high-performance liquid chromatography (HPLC) using a WATERS 515 HPLC pump with an IC-PAC anion column and a WATERS detector (mod 432) at the CCiT-UB. To identify the predominant equilibrium system controlling the Eh, Eh-pH predominance diagrams were drawn with the MEDUSA code (Puigdomènech, 2010).

VOCs concentration measurements were done by headspace (HS) - gas chromatography (GC) - mass spectrometry (MS) at the CCiT-UB (Torrentó et al., 2014). The uncertainty based on replicate measurements was below 10% for all the compounds.

For the SO_4^{2-} isotopic analysis, the dissolved SO_4^{2-} was precipitated as $BaSO_4$ according to (Dogramaci et al., 2001). $\delta^{34}S$-SO_4^{2-} and $\delta^{18}O$-SO_4^{2-} were analysed at the CCiT-UB as performed by Puig et al. (2013), except that a Finnigan Delta XP Plus IRMS was used for $\delta^{34}S$ determination. Notation is expressed in terms of δ (‰) relative to the international standard VSMOW (Vienna Standard Mean Oceanic Water) for $\delta^{18}O$ and VCDT (Vienna Canyon Diablo Troillite) for $\delta^{34}S$. The reproducibility (1σ) of the samples was ±0.2‰ for $\delta^{34}S$-SO_4^{2-} and ±0.5‰ for $\delta^{18}O$-SO_4^{2-}.

Carbon isotope analyses of CMs ($\delta^{13}C_{CT}$, $\delta^{13}C_{CF}$ and $\delta^{13}C_{DCM}$) were also performed at the CCiT-UB by headspace (HS)-solid phase microextraction (HS-SPME) coupled to GC-isotope ratio mass spectrometry (IRMS) (Torrentó et al., 2014; Martín-González et al., 2015). Notation is expressed

171   in terms of δ (‰) relative to VPDB (Vienna Pee Dee Belemnite). Total instrumental uncertainty

172   (2σ) was considered as the standard deviation of duplicate measurements.

173   CT and CF chlorine isotope analyses ($\delta^{37}Cl_{CT}$ and $\delta^{37}Cl_{CF}$) were performed by HS-GC-

174   quadrupole mass spectrometry (qMS) at the University of Neuchâtel (Heckel et al., 2017b). The

175   averaged $\delta^{37}Cl$ values were determined on the basis of ten injections of the same sample corrected

176   by two-point calibration with known working standards interspersed along the sequence. Notation

177   is expressed in terms of δ (‰) relative to VSMOC (Vienna Standard Mean Oceanic Chlorine).

178   The analytical uncertainty (2σ) of $\delta^{37}Cl$ measurements was in all cases below ±0.5‰ (n=10 per

179   sample). $\delta^{37}Cl_{CF}$ measurements were only performed for the samples collected on Mar-13 and

180   Nov-14 and $\delta^{37}Cl_{CT}$ for those obtained on Nov-14.

181   For all these isotopic measurements, several international and laboratory standards have been

182   interspersed among the analytical batches for normalization of analyses according to Coplen et

183   al. (2011).

184   For a given compound, the extent of degradation (D, %) was estimated following Eq.(1), derived

185   from the Rayleigh distillation equation, where εC is the carbon isotopic fractionation of the

186   selected degradation pathway and $\delta^{13}C_t$ and $\delta^{13}C_0$ are, respectively, the most positive value and

187   the assumed to be the most similar to the original value found in the field site.

188
$$D\ (\%) = \left[1 - \left(\frac{\delta^{13}C_t + 1000}{\delta^{13}C_0 + 1000}\right)^{\frac{1000}{\varepsilon C}}\right] \times 100 \tag{1}$$

189   Changes in both carbon and chlorine isotope values in the field should be greater than 2‰ so that

190   the degradation is considered significant (Hunkeler et al., 2008; Bernstein et al., 2011).

191

192   **3. RESULTS AND DISCUSSION**

193   **3.1. $\delta^{13}C$ data of CMs in sources prior to their removal**

194    $\delta^{13}C_{CT}$ values in the contamination sources were only available for the wastewater tank source.

195   They shifted significantly from -16.1±0.9‰ in 2003 to -11.31±0.04‰ in 2004 (Table 1) and they

196   were well above the range of available commercial CT (-54.4 to -37.0‰) (Table A2). The barrels

197    $\delta^{13}C_{CF}$ value (-46.2±0.4‰) was within the range of commercial CF (-63.7 to -43.2‰) (Table 1).

198   Important volatilization processes from neat volume of the abandoned barrels, which would have

199   produced an inverse isotopic effect on $\delta^{13}C_{CF}$ (Baertschi et al., 1953; Hunkeler and Aravena,

200   2000), can be discarded. $\delta^{13}C_{CF}$ values found in the tank and pit sources were more enriched than

201   those in the barrels and commercial solvents (Table 1). This fact may suggest that CMs

202 fractionation processes have started during the industrial process and/or in the tank and pit sources

203 in some point between the industrial activity period (1978 -1985) and 2003, especially for CT.

204 For DCM, the $\delta^{13}C_{DCM}$ in the tank (-36±3‰) was also enriched relative to that of the barrels (-

205 42.1±0.5‰), although in this case both values are within or very close to the upper limit of

206 available commercial DCM range (Table 1). Thus, since the residual CMs source had already

207 underwent C isotope fractionation before source's removal took place, isotope information from

208 these aged sources should be taken with caution as their CMs isotopic signature might not be

209 representative of the original solvent which has been released into the aquifer.

210 Table 1. CT, CF and DCM carbon isotopic composition ($\delta^{13}C$, ‰) from the abandoned barrels, the wastewater tank

211 and the disposal pit of the Òdena site sampled between 2002 and 2005 (Palau et al., 2014). $\delta^{13}C$ ranges of commercial

212 CMs from different suppliers (see Table A2 in SI for details) are also shown. b.d.l.: below detection limit.

	$\delta^{13}C$ (‰)				
Compound	Abandoned barrels (2002)	Wastewater tank		Disposal pit (2005)	Commercial CMs
		(2003)	(2004)		
CT	b.d.l.	-16.1±0.9	-11.30±0.04	b.d.l.	-54.4 to -37.0
CF	-46.2±0.4	-29.9±0.1	-34.0±0.6	-36.7±0.6	-63.7 to -43.2
DCM	-42.1±0.5	-36±3	b.d.l.	b.d.l.	-40.9 to -34.2

213

3.2. Source removal effects and evidences of CT and CF natural attenuation

215 Given the above-mentioned site complexity and in order to study the sources' removal efficiency,

216 values representative of the original sources were searched in wells located in sources' influence

217 areas for assessing long-term effect on CMs natural attenuation. As suggested by groundwater

218 flow paths (Palau et al., 2014) (Fig.1), wells S1 and S4 and wells S3 and S6 were selected as

219 representative of the pit and tank areas, respectively. Wells S8 and S7 (Fig.1) were also chosen

220 as zones vulnerable to pollution around the industrial plant building (where the barrels were

221 found) and the wastewater pipe circuit, respectively. Moreover, wells S9 and S10, located further

222 downstream and on the other side of the creek, respectively (Fig.1), were studied as overall outer

223 controls of the contaminated site.

3.2.1.Pit source's influence area

225 In S1 well, located exactly in the former pit source (Fig.1), the most abundant CM was CF during

226 all campaigns (up to 97% out of total molar CMs concentration) (Fig.2). Total CMs concentration

227 decreased with time at all depths with no significant variation in CMs distribution with depth

228 (Fig.2). The CT content decreased by nearly one order of magnitude between Mar-10 and Nov-

229 14 and DCM and CS_2 were always <0.2 μM (Table A3).

230   Due to low concentrations, $\delta^{13}C_{CT}$ values could only be measured twice in S1 (Fig.3A), being that

231   of Mar-10 (-30.0±0.5‰) the most depleted value observed for CT within all sampling wells and

232   campaigns. This value is, respectively, 20‰ and 19‰ lighter than the most enriched $\delta^{13}C_{CT}$ value

233   found in S3 (Fig.3C) and the value measured in the tank source (Table 1), which, in turn, was

234   already considered degraded as discussed above. Thus, this CT might have reached the aquifer

235   before being affected by significant degradation. Both $\delta^{13}C_{CT}$ values (-30.0±0.5‰ and -

236   21.7±0.5‰) and also the $\delta^{37}Cl_{CT}$ in Nov-14 were clearly above the CT commercial values (Table

237   1, Fig.3A, Table A4), suggesting transformation. Therefore, the $\delta^{13}C_{CT}$ value from Mar-10 in S1

238   could be more representative of the original CT than those values measured in the tank source

239   between 2003 and 2004 (Table 1). This hypothesis was also supported by a difference < 2‰

240   between the most depleted $\delta^{13}C_{CT}$ values in S1, S4 and S8 wells (Fig.3E), being the latter located

241   near the industrial plant and upstream of any remediation action (Fig.1). However, since C isotope

242   fractionation of CT in trenches was detected in previous studies (Torrentó et al., 2014), certain

243   influence of CT coming from the upstream trench cannot be excluded in the enriched $\delta^{13}C_{CT}$ value

244   found in S1 (Mar-13).
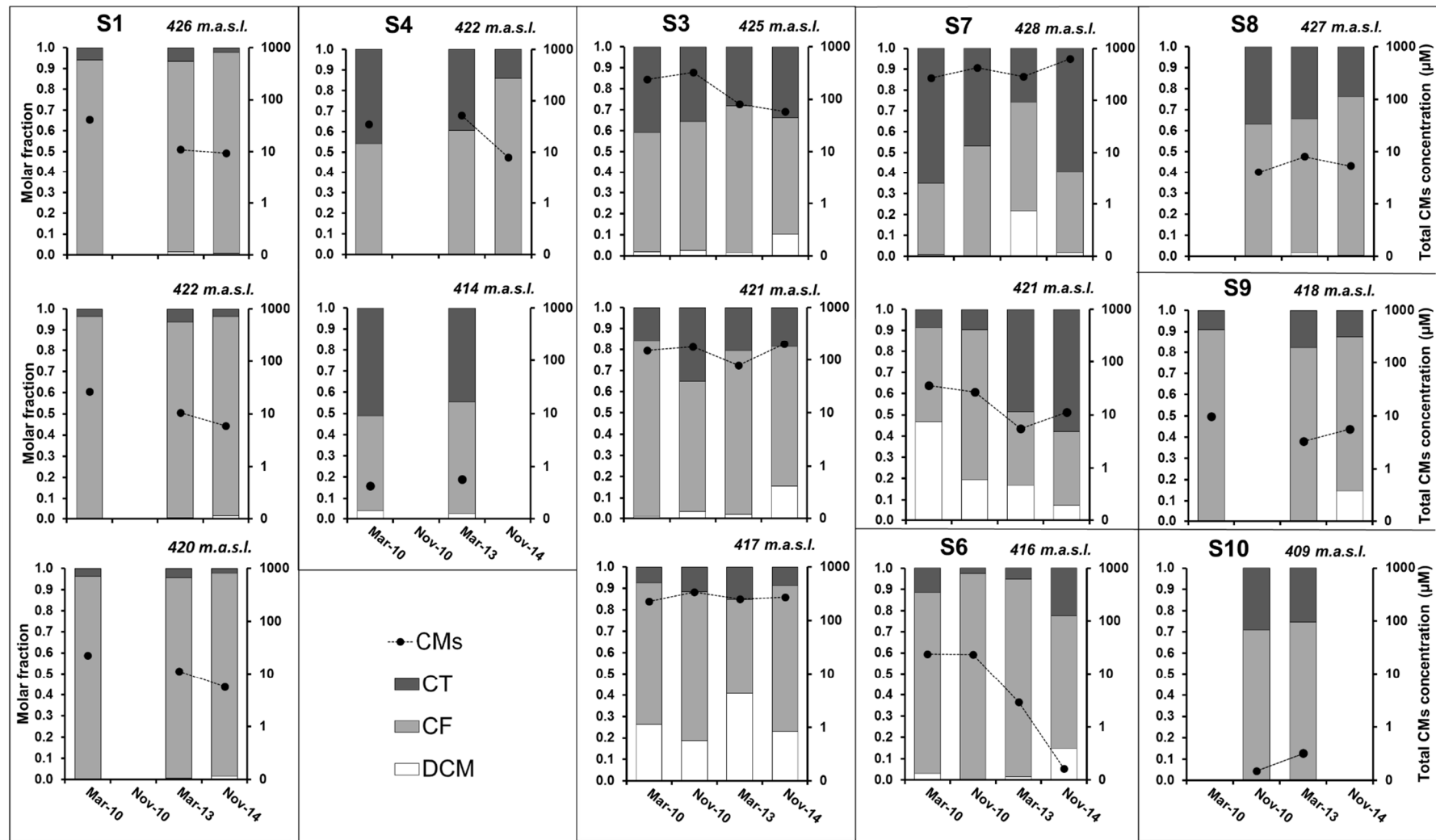
Figure 2. Total CMs molar concentration (µM, dots), in logarithmic scale, and molar fraction distribution (bars) for Mar-10, Nov-10, Mar-13 and Nov-14 campaigns in wells S1, S4, S3, S7, S6, S8, S9 and S10. Different sampling depths for each well are represented when possible (in meters above sea level, m.a.s.l.).
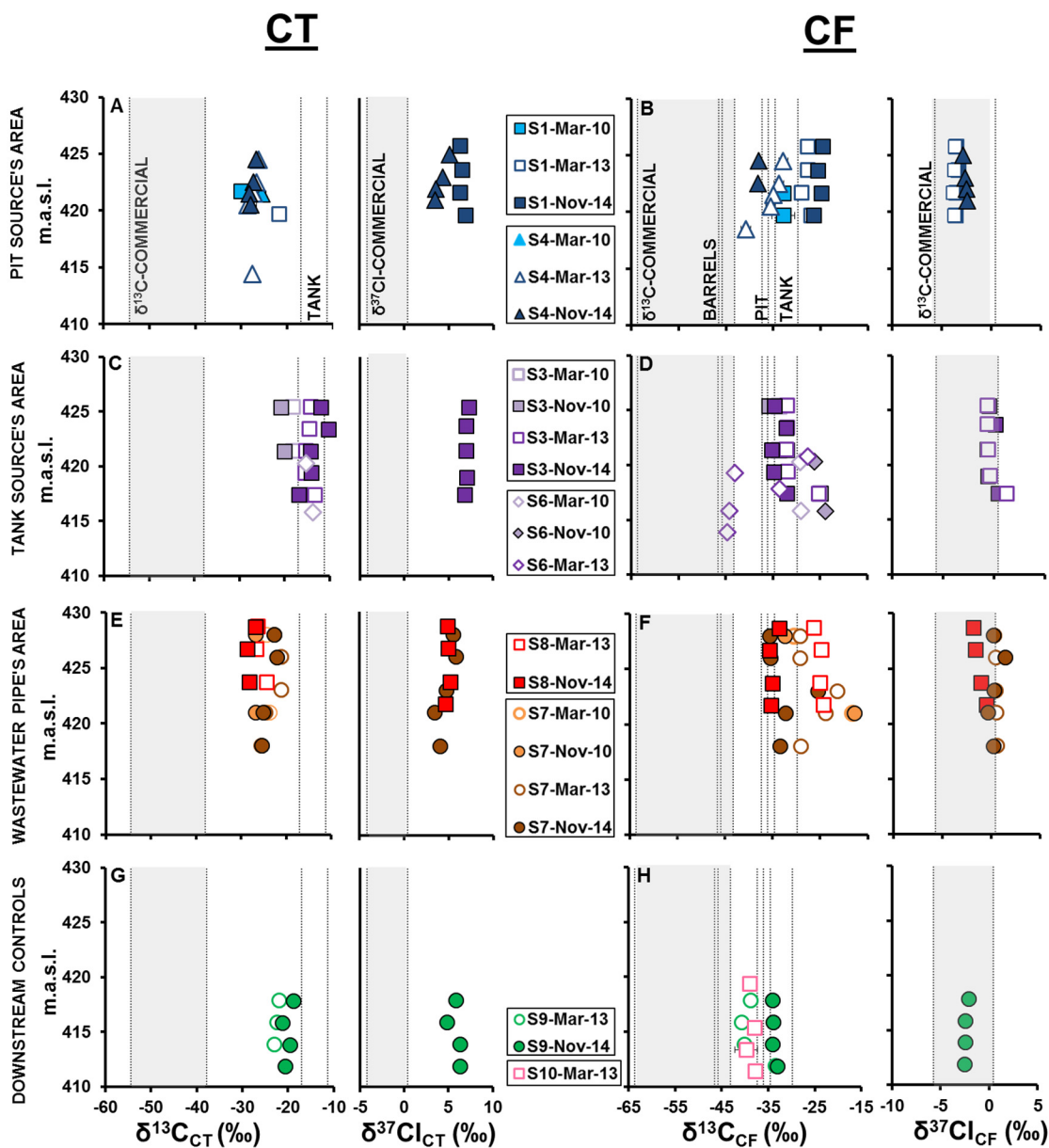
Figure 3. Carbon and chlorine isotopic composition of CT (left panels) and CF (right panels) for wells S1 and S4 (A, B), S3 and S6 (C, D), S7 and S8 (E, F), and S9 and S10 (G, H) at different depths (m.a.s.l.) and campaigns. The dashed lines show the $\delta^{13}C_{CT}$ and $\delta^{13}C_{CF}$ range of commercial CT and CF (shaded areas), barrels, tank and pit sources, when available. In most cases, error bars are smaller than the symbols.

For CF in S1, $\delta^{13}C_{CF}$ values in Mar-10 (-33±2 and -32.8±0.3‰) were slightly more enriched than those from the pit source and much more than those from the barrels or available commercial CF (Fig. 3B), evidencing CF fractionation processes. Over time, $\delta^{13}C_{CF}$ values increased at all depths, which, agreeing with the decrease in CMs concentration (Fig.2), suggest either CF *in situ* degradation or arrival of CF degraded by alkaline hydrolysis from the upstream trench (Torrentó et al., 2014). In contrast, $\delta^{37}Cl_{CF}$ remained almost constant between Mar-13 (with an average of -3.8±0.5‰) and Nov-14 (with an average of -3.5±0.3‰) without any clear trend in depth (Fig.3B).

260 These values, which are within the available range for commercial CF, were the most depleted

261 $\delta^{37}Cl_{CF}$ values measured for all the wells at the site.

262 In S4 well, located downstream of S1 well (Fig.1), samples from the deepest part showed much

263 lower CMs concentrations than those from the upper part (Fig.2), as was also the case for

264 chlorinated ethenes (Table A3). The CT and CF molar fractions were quite similar in Mar-10 and

265 Mar-13 and also for the different depths, although the fraction of CF increased in Nov-14 at the

266 upper part, while total CMs concentration decreased (Fig.2). However, $\delta^{13}C_{CT}$ and $\delta^{37}Cl_{CT}$ of S4

267 did not significantly change compared to S1 during the monitored period (Fig.3A), indicating that

268 observed changes in CT and CF molar fractions could not be attributed to *in situ* CT degradation,

269 but to the previously proved degradation in the unsaturated zone. This result agrees with the low

270 concentrations of DCM and CS_2 in this well (up to 0.04 and 0.03 μM in Mar-13, respectively,

271 Table A3).

272 For CF in S4, the most enriched $\delta^{13}C_{CF}$ (-32.9±0.4, 425 m.a.s.l., Mar-13) and the most depleted

273 $\delta^{13}C_{CF}$ (-40.8±0.1‰, 419 m.a.s.l., Mar-13) values were 4‰ higher and 3‰ lower than $\delta^{13}C_{CF}$ in

274 the pit source, respectively (Table 1). Since CT isotopic composition remained quite stable for all

275 depths during the studied period, these depleted $\delta^{13}C_{CF}$ values cannot be linked to CT degradation.

276 $\delta^{13}C_{CF}$ enrichment might suggest CF degradation or influx of already fractionated CF, at the upper

277 parts of S4 where the redox state was governed by the N system (Fig.1).

278 Higher total CMs concentrations and CT proportion in S4 than in S1 (Fig.1, 2 and Table A3) point

279 out the detachment of the plume downgradient from S1 towards S4 through the fracture network.

280 In addition, the isotopic compositions of CT and CF in S4 showed, in general, more depleted ^{13}C

281 and ^{37}Cl values than in S1 (Fig.3A,B), suggesting a lower extent of degradation for both

282 compounds downstream. Differences in C and Cl isotope ratios between S1 and S4 are

283 particularly evident for $\delta^{13}C_{CF}$. CMs moving downstream in the pit source's influence area might

284 inhibit chlorinated ethenes biodegradation (Bagley et al., 2000), explaining the results previously

285 reported by Palau et al. (2014).

286   **3.2.2. Tank source's influence area**

287 One of the most polluted wells at the site, S3, is located in the former wastewater tank (Fig.1).

288 CMs concentration clearly decreased over time in the upper part of the well, while fluctuated

289 without a clear trend at the middle and deepest points. A maximum value close to 350 μM was

290 reached at the deepest part in Nov-10 (Fig.2). CF was the most abundant CM in all the studied

291 campaigns, especially at the deepest parts, where it was almost an order of magnitude higher than

292 CT (Fig.2). High DCM contents were observed along all S3 levels, especially at the deepest part

293 (up to 102 μM in Mar-13, the 41% of the CMs molar fraction) (Fig.2). In addition, CS_2 values up

294 to 0.8 μM were found (Table A3).

295 For CT in S3, $\delta^{13}C_{CT}$ values were very far from the isotopic composition range of commercial CT

296 and were fluctuating around the tank source range with offsets of up to +6.0‰ and -5.0‰

297 (Fig.3C). $\delta^{13}C_{CT}$ and $\delta^{37}Cl_{CT}$ values in S3, up to -10.3±0.3‰ and +7.3±0.3‰ (Fig.3C),

298 respectively, were the most enriched values of all wells and campaigns. $\delta^{37}Cl_{CT}$ values from the

299 single available campaign (Nov-14, Fig. 3C) did not show changes with depth. Enrichments in

300 $\delta^{13}C_{CT}$ were observed in S3 over time, as well as from top to bottom in Mar-10 and Nov-10

301 (maximum difference of +5.2‰). However, the opposite trend was observed in Nov-14, with up

302 to a +6.5‰ difference (Fig.3C). These opposite trends could be explained by the occurrence in

303 parallel of different processes: 1) CT degradation inducing isotopic enrichment in ^{13}C, more

304 evident in the deepest parts and supported by a steady Eh controlled by Fe-system; and 2) new

305 CT incomings leading to depleted $\delta^{13}C_{CT}$ values in the upper parts, especially in the early

306 campaigns.

307 For CF in S3, $\delta^{13}C_{CF}$ fluctuated over time within the limits of the tank and pit sources ranges

308 (Fig.3D), except at the deepest part, where $\delta^{13}C_{CF}$ values were over a 5‰ more enriched than the

309 rest of the well (Fig.3D). As the same isotope pattern was observed for $\delta^{37}Cl_{CF}$ values in Mar-13

310 and Nov-14, with an enrichment of up to 1.9‰ (Fig.3D), CF degradation processes in the deepest

311 part of the well can be assumed. At shallower depths, $\delta^{13}C_{CF}$ probably reflects a mixture of isotope

312 effects associated with CF degradation and the continuous input of CF, as by-product of proved

313 CT degradation and/or as incoming pollution.

314 In S3, only $\delta^{13}C_{DCM}$ values from the deepest levels of Mar-13 and Nov-14 campaigns were

315 available (from -41±1 to -36±1‰, Table A3). They were in a range similar to that of those of the

316 barrels and tank sources (from -42.1±0.5 to -36±3‰, respectively) (Table 1). Nevertheless, this

317 similar isotope range may have resulted from DCM coming from CF degradation. Thus, although

318 high DCM concentrations at deep levels of S3 were detected comparing with the other wells

319 (Fig.3), $\delta^{13}C_{DCM}$ shifts did not support unequivocal evidences of DCM origin or fate during the

320 studied period.

321 In well S6, situated downstream from the tank source, total CMs concentration was much lower

322 than in S3 for all campaigns (Fig.2) and decreased over time. CF was the most abundant

323 compound (up to 51 μM), frequently showing concentrations an order of magnitude higher than

324 those of CT. DCM and CS_2 were also detected, with maximum concentrations of 0.7 μM and 0.02

325 μM, respectively (Table A3). Due to the low CT concentration, $\delta^{13}C_{CT}$ was only measured for few

326 samples and no data for $\delta^{37}Cl_{CT}$ was obtained (Fig.3C). Determined $\delta^{13}C_{CT}$ values (-15.2±0.5‰

327 and -13.8±0.4‰) are within the S3 and tank source values range. This fact hindered the

328   identification of i) CT degradation and ii) whether the observed isotope ratios were the result of

329   enriched CT transported from the former tank or latter degradation in S3 or S6. For CF in S6,

330    $\delta^{13}C_{CF}$ values in Mar-10 were 16‰ more enriched than latter in Mar-13 when the most negative

331   values for all sampling wells and campaigns (-44.6±0.5‰ Fig.3D) were found. This latter value

332   was within the range of the barrels and commercial CF (Fig.3D) but it could also represent a CF

333   by-product from a completely degraded CT with an isotopic signature similar to CT from

334   commercial brands and barrels. Moreover, in Mar-13, $\delta^{13}C_{CF}$ values increased from this depleted

335   value at the bottom to a value similar to those found in previous campaigns at the top (Fig.3D).

336   Since new entrances of non-degraded CF from upstream areas seem improbable (attending to the

337   enriched $\delta^{13}C_{CF}$ values of S3 well over time, Fig.3D), this behaviour might be explained by

338   extensive CT degradation in S3-S6 area. Although the decrease in concentration and the Eh value

339   controlled by Fe and N systems (Fig.1) would support this hypothesis, it cannot be confirmed by

340    $\delta^{37}Cl_{CF}$ or any CT isotope data.

3.2.3. Wastewater pipe area

342   The S8 well, located upstream of the tank source at the point where the wastewater pipe was

343   connected to the chemical plant (Fig.1), showed low CMs concentrations with a maximum of 8

344   μM at 427 m.a.s.l. in Mar-13 (Fig.2). In general, CF was more abundant than CT. CMs

345   concentration did not clearly decrease during the monitored period (Fig.2), although in Nov-10

346   and Mar-13, CT and CF concentrations fell with depth down three orders of magnitude (Table

347   A3). DCM and CS_2 were present also in low concentrations (up to 0.1 μM and 0.04 μM,

348   respectively). $\delta^{13}C_{CT}$ values were depleted with respect to the tank source values (>10‰) but

349   enriched compared to the range for commercial CT. As already mentioned, $\delta^{13}C_{CT}$ values of S8

350   in Nov-14 (Fig.3E), were similar to those found in S4 (Mar-13 and Nov-14) or in S1 (Mar-10,

351   Fig.3A); but S8 cannot be affected by any interception trench because it is located upstream the

352   trenches. As a maximum $\delta^{13}C_{CT}$ decrease of 4‰ was measured at the upper part (424 m.a.sl.)

353   between Mar-13 and Nov-14 (Fig.3E), leaching processes could be suggested. $\delta^{37}Cl_{CT}$ values

354   (Nov-14) did not show a relevant enrichment in depth (Fig. 3E). For CF, $\delta^{13}C_{CF}$ underwent more

355   than a 10‰ decrease from Mar-13 to Nov-14 (Fig. 3F). The depleted $\delta^{13}C_{CF}$ values of Nov-14

356   were close to the pit and tank values, but enriched with respect to the range determined for the

357   barrels and commercial CF (Fig.3F). $\delta^{37}Cl_{CF}$ data were only available for Nov-14 (Fig.3F) with

358   slight enrichment in depth ($\Delta\delta^{37}Cl_{CF}$=+1.3‰).

359   For the well S7, CMs concentrations in the upper part of S7 were always much higher than those

360   of its deepest part and the rest of the wells (Fig.2). Moreover, at 428 m.a.s.l., CMs concentration

361   increased up to 632 μM in Nov-14 (Fig.2), consistently with the increase revealed in previous

362   Nov-10 campaign. CT and CF molar ratios presented similar values at the upper part of S7, except

363 in Mar-2013 when the molar ratio of DCM became significant and a decrease in total CMs

364 concentration was observed. At depth, DCM and CF molar fractions decreased over time (Fig.2).

365 CS_2 concentration values were only analysed for Mar-13 (up to 0.04 µM), preventing us to define

366 if CS_2 was yielded as a by-product.

367 Determined $\delta^{13}C_{CT}$ values in S7 were, similarly to the results obtained for S8, between those from

368 the tank source and those for commercial CT (Fig.3E). The values fluctuated over campaigns with

369 an enrichment of around 5‰ from the bottom to the top during Mar-13 and Nov-14 (Fig.3E),

370 which accompanied by a 2‰ enrichment of $\delta^{37}Cl_{CT}$ values (Fig.3E), may suggest reliable CT

371 degradation at the upper part during the studied period. For CF in S7, $\delta^{13}C_{CF}$ also fluctuated over

372 time and showed the most depleted values in Nov-14, close to pit and tank values (Fig.3F). In

373 contrast to CT, the strongest enrichment in $^{13}C_{CF}$ was observed at the middle part (around 420

374 m.a.s.l). The $\delta^{13}C_{CF}$ and $\delta^{37}Cl_{CF}$ measured in 2010 (-17.9±0.7 and +1.6±0.5‰, respectively)

375 (Fig.3F, Table A5) were the most enriched values in all campaigns and wells. Therefore, despite

376 the contribution of active leaching arriving from the unsaturated zone trough the fracture network,

377 the meaningful isotopic enrichment at the middle part along with the high DCM molar fractions

378 and the decrease of Eh values with depth (Fig.1, Fig.A1) evinced the occurrence of CMs natural

379 attenuation processes in this area.

3.2.4. Downstream controls

381 The S9 well, the furthest well downstream from the chemical plant and the highly affected area

382 (Fig.1), serves as outer control to establish if authorities should implement additional remediation

383 measures. CMs concentrations were low (up to 10 µM, Fig.2) and did not show a clear trend over

384 time or in depth during the monitored period. CF was always more abundant than CT, and in the

385 last campaign both concentrations (up to 4 and 0.9 µM, respectively) (Table A3), exceeded the

386 European Union (EU) limits of 0.08 and 0.02 µM, respectively (2008/105/CE). DCM also

387 exceeded the EU limits (0.2 µM) showing a maximum of 0.8 µM in Nov-14. CS_2 concentrations

388 were low (e.g 0.04 µM in Nov-14); nevertheless this compound is not regulated. The most

389 negative S9 $\delta^{13}C_{CT}$ value (-22.97±0.02, Mar-13, Fig.3G) was 7‰ more depleted than the most

390 negative value of the tank source (Table 1), but very enriched compared to the range obtained for

391 commercial CT. These results suggest once again the occurrence of CT isotope fractionation

392 during the industrial process. CMs degradation processes would also have affected the tank only

393 after certain original CMs pollution had already reached the saturated zone downstream,

394 explaining the high CT fractionation detected in 2003 and 2004 source's sampling in comparison

395 to some depleted CT values in wells. On the other hand, the most enriched S3 $\delta^{13}C_{CT}$ value (-

396 19±1‰, Nov-14, Fig.3G) was ~11‰ more enriched than the most negative value found in the

397 site (corresponding to S1). Thus, CT from S9 had undergone degradation processes upstream this

well, but without reaching values as high as those of the tank in 2003 and 2004 or of S3 in the last campaigns. For CF, $\delta^{13}C_{CF}$ values in Nov-14 were around those of the tank source and, from Mar-13 to Nov-14, they enriched up to 6‰ in almost all the depths (Fig.3H), pointing to CF degradation. In Nov-14, $\delta^{13}C$ or $\delta^{37}Cl$ values of CT and CF were not significantly different in depth.

The S10 well was located downstream of S6, at the other side of the creek (Fig.1). In this well, the highest concentrations of CMs were found in Mar-13, with up to 0.1 μM CT and 0.3 μM CF, both slightly above the EU limits. Measured CS_2 contents were low (≤0.01 μM). Thus, pollution has not strongly affected the groundwater eastbound moving far beyond this well. Low concentration of CMs did not allow for $\delta^{13}C_{CT}$ analyses but $\delta^{13}C_{CF}$ values from -42.0 to -37.8‰ were measured in Mar-13. These values were similar to those obtained from S9 and ranged between former sources and commercial CF (Fig.3H).

Thus, despite surpassing legal concentration threshold values, CT and CF natural attenuation processes are proved in the field site.

3.3. Degradation pathways study

Figure 4 shows the $\delta^{13}C$ vs $\delta^{37}Cl$ data of CT and CF obtained in Mar-13 and Nov-14 campaigns and stablishes the origin of C-Cl Λ values, being all these data plotted together with values from sources prior to their removal as well as respect to commercial solvents. Moreover, statistical comparison of the obtained C-Cl Λ values from wells with those of different degradation mechanisms or pathways already reported in literature is also included in this section.

16

418
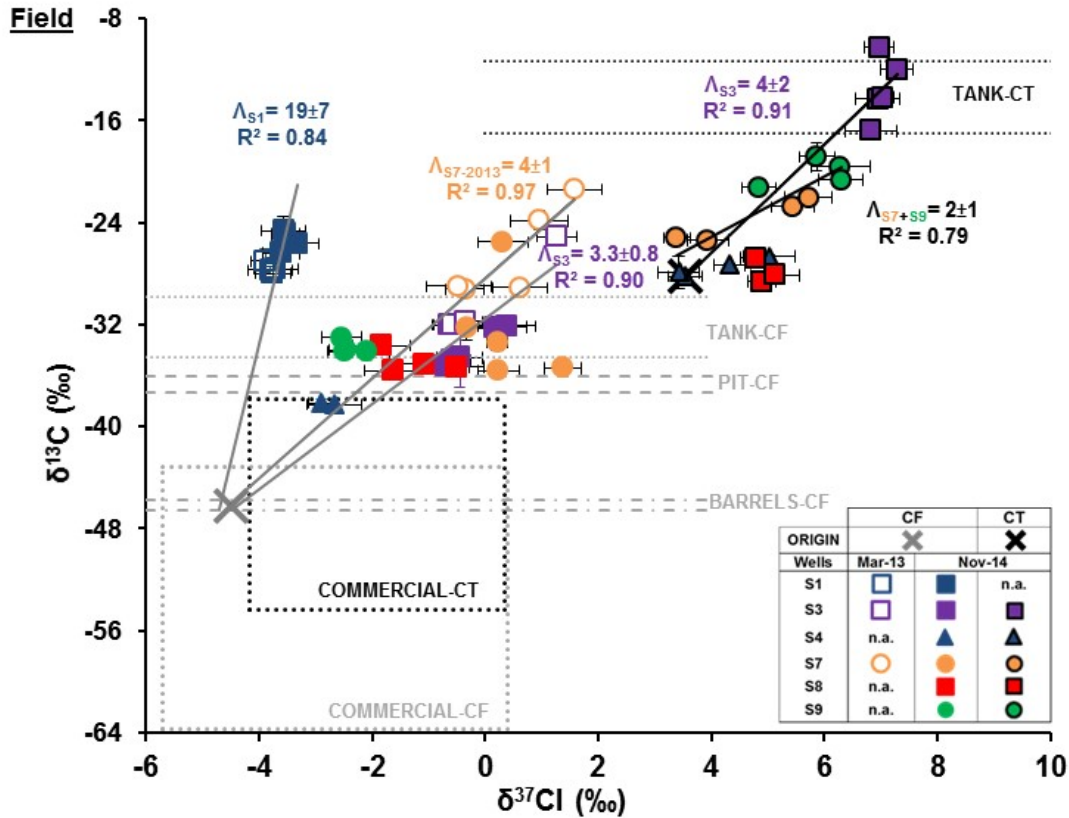
Figure 4. Dual C-Cl isotope plot for CT and CF data from sampling wells (S-number) in Mar-13 and Nov-14 campaigns
(n.a.= data not available). Error bars show uncertainty in $\delta^{13}C$ and $\delta^{37}Cl$ values. $\delta^{13}C$ of the sources (barrels, pit and
tank) sampled prior to their removal and $\delta^{13}C$ and $\delta^{37}Cl$ of commercial compounds are represented in black and grey
dashed lines and boxes for CT and CF, respectively. Upper plots show: CF (left) reference slopes of oxidation (OX),
alkaline hydrolysis (AH) and hydrogenolysis + reductive elimination (Fe(0)) from Torrentó et al. (2017); outer-sphere
single electron transfer (OS-SET) from Heckel et al. (2017a); and CF inferred pathways from biodegradation with
vitamin B_{12} (BIO+B_{12}) (Rodríguez-Fernández et al., 2018a); as well as CT (right) reference slopes of hydrogenolysis
(Fe(0), Rodríguez-Fernández, 2018b) and inferred pathways from biodegradation with vitamin B_{12} from microcosms
(BIO and +B_{12}, Rodríguez-Fernández et al., 2018a) and from degradation by pyrite (Py) and by magnetite (Mag) at pH
12, Rodríguez-Fernández, 2018b). The CT and CF slopes (Λ_{well}) are shown relative to the most depleted isotope values
detected in the field (referred as 'Origin' in legend).

The CT dual C-Cl isotope plot (Fig.4) supports that CT in S4 and S8 wells, despite the distance
between the wells (Fig.1), likely comes from the same spilled CT. Similar CMs carbon isotopic
mass balance values ($\delta^{13}C_{SUM}$, see Eq. A1) for the tank, before its removal, and for S3 and S7 over
time, especially in the shallowest parts, might also point out to a single mixture of original spilled

17

434   CMs in all over Òdena site (Fig.A2). CT in S8 and S4 showed negligible $\delta^{13}C$ variation but certain

435    $\delta^{37}Cl$ enrichment (Fig.4). This might be attributable to Cl isotope fractionation processes in the

436   unsaturated zone, such as diffusion-controlled vaporization, inasmuch as normal isotope effects

437   of both reactive and non-reactive processes that might occur in the unsaturated zone accumulate

438   for chlorine (Jeannottat and Hunkeler, 2012). Thus, since there are not available barrel values

439   (Table 1), the most depleted S4 values (+3.5‰ for $\delta^{37}Cl$ and -28.2‰ for $\delta^{13}C$) could be considered

440   as origin for slope calculations.

441   CT samples in Figure 4 showed a general C and Cl enrichment trend confirming CT degradation

442   processes. If S3, S7 and S9 values are considered together with the above-mentioned origin, the

443   obtained Λ value (4±1, R^2= 0.82) is statistically similar (ANCOVA $p>0.05$) to that found in

444   laboratory experiments for CT hydrogenolysis combined with CT thiolytic reduction (Py in Fig.4,

445   Rodríguez-Fernández et al. 2018b). Despite this general observation, we also provide a separate

446   study of each well, as we consider it interesting to discern different contributions of these

447   pathways under each wells' conditions given the complexity of the site.

448   In this sense, CT samples of S3 show a Λ value (4±2, R^2=0.91) statistically similar to the reference

449   slope for net hydrogenolysis (Fe(0) reaction in Fig.4 with Λ= 5.8±0.4, Rodríguez-Fernández et

450   al. 2018b). The obtained Λ value for S3 is also consistent i) with an OS-SET mechanism (Heckel

451   et al., 2017a) (6.7±0.4); ii) with biodegradation obtained in microcosms experiments using

452   sediment slurry from this well (6.1±0.5, Rodríguez-Fernández et al., 2018a), and iii) with a

453   reductive pathway involving *Pseudomonas stutzeri,* obtained when vitamin B$_{12}$ was added in the

454   slurry (5±1, Rodríguez-Fernández et al., 2018a). This result confirmed *in situ* CT anaerobic

455   reduction in S3, consistently with the steady Eh controlled by the Fe-system during the studied

456   period (Fig.A1). Nevertheless, due to the relatively high CS_2 amount detected in S3, in

457   comparison to the rest of the wells, a certain contribution of thiolytic CT reduction mediated by

458   iron sulfides like pyrite (Davis et al., 2003; Rodríguez-Fernández et al. 2008b) or biotically-

459   mediated by sulfate-reducing bacteria (Koenig et al., 2012) cannot be excluded. This hypothesis

460   is supported by the decrease in total dissolved iron and sulfate concentrations and by a $\delta^{34}S$

461   enrichment in SO_4^{2-} (from +14±0.2 to +22±0.2‰) with depth in S3 (Table A1). Therefore,

462   although the dual slope revealed hydrogenolysis as the main pathway, little involvement of

463   thiolytic or hydrolytic reduction might be possible (Py and Mag reactions, respectively in Fig.4,

464   Rodríguez-Fernández et al. 2018b) as it is also suggested by enriched $\delta^{13}C_{SUM}$ in the shallowest

465   parts of S3 in Nov-10 campaign when dual plot is not available (see Isotopic mass balance section

466   in SI).

467   Assuming reductive biodegradation as the main CT degradation process, the maximum extent

468   D(%) in S3 would be 72±11%, which is estimated following Eq.(1), using ϵC_{CT} from S3

18

469   microcosm experiments (-16±6‰) (Rodríguez-Fernández et al., 2018a), the most positive value

470   for CT in S3 as $\delta^{13}C_t$ (-10.3±0.3‰), and the most depleted value found in the field as $\delta^{13}C_0$ (-

471   30.0±0.5‰). The extent of CT biodegration in S3 is probably a conservative estimate due to the

472   fact that leaching of less-degraded CT from the unsaturated zone could mask $\delta^{13}C$ values (see

473   further discussion in Isotopic mass balance section in SI).

474   Since S7 and S9 showed similar slopes, isotope data of CT from these wells were combined. The

475   resulting Λ (2±1, R^2=0.79) is statistically similar to that inferred from laboratory experiments

476   with Py, suggesting that both CT hydrogenolysis with CT thiolytic reduction might occur (Py in

477   Fig.4, Rodríguez-Fernández et al., 2018b). Although both pathways were also inferred for CT,

478   the contribution of CT thiolytic reduction is revealed higher in S7 and S9 than in S3, attending to

479   2D-CSIA approach and as it was also confirmed by $\delta^{13}C_{SUM}$ comparison between S3 and S7 in

480   Nov-10 (see further discussion in Isotopic mass balance section in SI). CT reduction pathways

481   are consistent with the low Eh values measured in the deepest parts of S7 (Fig.A1). However, in

482   S9, Eh values are higher, consistent with the assumption that already degraded CT could have

483   migrated from upstream areas with stronger reducing conditions suitable for reductive

484   dechlorination processes. The maximum CT degradation extent would be 84±6% for S7 and

485   90±4% for S9 assuming a combination of hydrogenolysis and thiolytic reduction pathways (Fig.4)

486   and using a εC_{CT}=-5±2‰, (Py, Rodríguez-Fernández et al., 2018b), the most enriched values for

487   CT in S7 and S9 as $\delta^{13}C_t$ (-21.0±0.3‰ and -19±1‰, respectively), and the most depleted value

488   found in the field as $\delta^{13}C_0$ (-30.0±0.5‰).

489   The interpretation of the determined dual C-Cl isotope trends for CF (Fig.4) should consider that

490   CF can also be produced by CT degradation besides being degraded, similarly to TCE or cisDCE

491   in other studies (Badin et al., 2016). Because of this, comparison with reported Λ values from

492   literature is not straightforward and should be done with caution. However, according to Hunkeler

493   et al. (2009), in a reaction where CF is a by-product, $\delta^{37}Cl_{CF}$ cannot be more depleted than the

494   initial $\delta^{37}Cl$ value of the parent compound CT (assuming no secondary isotopic effects). In Òdena,

495   all field $\delta^{37}Cl_{CF}$ values plotted in Figure 4 are more depleted than $\delta^{37}Cl_{CT}$ ones, confirming the

496   predominance of CF as a parent compound. Moreover, CF was present in the sources as a pure

497   phase in the barrels (Table 1) and represented more than 70% of the molar fraction among CMs

498   in the other sources. These two arguments support a predominance of CF as a parent compound

499   and suggest that, although some contribution of CF as by-product is undeniable, the obtained CF

500   Λ values are primarily controlled by CF degradation.

501   Values for S1 clearly plot in a different pattern than those from the rest of the wells (Fig. 4). This

502   well, together with S4, could only be influenced by the processes affecting the CMs in the pit

503   source area and, as argued previously for CT, a single original CMs mixture is therefore

504   considered and reactive processes that fractionate inversely are discarded for the interpretation of
505   the data since they have not been described yet. The isotopic composition of the contaminant
506   source might had shifted towards heavier $\delta^{37}Cl$ over time due to ageing, as it was observed for
507   CT. The most depleted $\delta^{37}Cl_{CF}$ value determined in the field site was (-3.9±0.6‰), which was
508   measured in S1 (422 m.a.s.l., Mar-13), consistent with the most depleted $\delta^{37}Cl_{CF}$ commercial
509   values. Since calculations for estimating the $\delta^{37}Cl_0$ of CF require the unavailable εCl of CF
510   diffusion in Òdena's soil, the SD of the most depleted $\delta^{37}Cl_{CF}$ value was considered for obtaining
511   the value used as origin for slope calculations, i.e. $\delta^{37}Cl_{CF}$ = -4.5‰. In the case of C, the most
512   depleted $\delta^{13}C_{CF}$ determined in the field site, the pure phase analysed in 2002 in barrels (-
513   46.2±0.4‰), which falls in the upper range of for commercial CF (Table 1, Fig.4), was considered
514   as the outset for the slope.

515   The different pattern of S1 data shows that processes affecting CF in S1 might be different than
516   those affecting CF in the other wells (Fig.4). Additionally, S1 data from Mar-13 and Nov-14
517   campaigns form a cluster while data of the other wells distribute along a clear trend. This different
518   behaviour could be related to the absence of CMs leaching in S1, while in the other wells, leaching
519   was proved. The obtained slope for S1 (Λ=19±7, R^2=0.84) was consistent with CF oxidation (OX,
520   Fig.4) or with CF alkaline hydrolysis (AH, Fig.4) (ANCOVA, p>0.05) (Torrentó et al., 2017). CF
521   oxidation in the pit source's influence area might be supported by an Eh evolution from Fe-
522   controlled conditions in 2006 and 2007 towards more oxidising conditions in the latter campaigns
523   (Fig.1, Fig.A1) as well as by the open air spills in the pit source occurred while the chemical plant
524   was active according to Palau et al. (2014). Alkaline hydrolysis might also be plausible, by
525   migration of degraded CF from the upstream trench, in which CF alkaline hydrolysis takes place,
526   given the hydraulic conductivity between the trench and the S1 well (Torrentó et al., 2014).
527   Further research with complementary tools would be necessary to distinguish between CF
528   oxidation and alkaline hydrolysis in the field giving the similarity of Λ values.

529   The CF dual C-Cl isotope slopes are only linear considering S3 and S7 wells, thus, wells S4, S8
530   and S9 were not included in Λ calculations. The dual C-Cl isotope slopes observed for CF in S3
531   (Mar-13 and Nov-14) and S7 (Mar-13) are Λ=3.3±0.8 (R^2=0.90) and 4±1 (R^2=0.97), respectively,
532   considering the same CF origin as for S1 well. Both Λ values are more similar to CF reduction
533   processes (Fe(0) and BIO+B12, Fig.4, Rodríguez-Fernández et al., 2018a,b) than to CF oxidation
534   or alkaline hydrolysis (OX and AH, Fig.4, Torrentó et al., 2017), in accordance with the redox
535   conditions (Fig.1) and with the presence of DCM indicative of hydrogenolysis, especially high in
536   S7 (Fig.2). The lack of statistical coincidence between CF Λ values of wells S3 and S7 and the
537   available reference values for reduction processes could be attributed to 1) mixing of degraded
538   CF with pollutant continuously being leached into the saturated zone that in turn, might be
539   continuously affected by fractionation processes (either reactive or non-reactive); 2) chlorine

540 isotope fractionation by a non-reactive processes, such as diffusion (Jeannottat and Hunkeler,

541 2012) that might explain lower S3 and S7 CF slopes regarding the reference slopes; 3) certain

542 influence of CF as by-product and/or 4) the existence of several CF reduction pathways for which

543 additional laboratory experiments to obtain further reference Λ values are needed.

544 **Conclusions**

545 Although Òdena is a complex polluted site, long-term monitoring of CMs concentration and

546 isotope ratios evidenced that in the pit source's influence area, the focus of CMs pollution was

547 detached downgradient and moved from S1 to S4 wells, confirming that the source removal was

548 effective and that no new CMs entered in this part of the plume. The same monitoring tools

549 disclosed that the removal of the tank and wastewater pipe sources was uncompleted since new

550 CMs incomings were still arriving at S3, S7 and S8 wells during the monitoring time and the

551 plume seemed still active. The S7 well was of special concern because of CMs prevailing

552 leaching, causing the highest CMs concentrations in the field site during the studied period. The

553 furthest well downstream from the chemical plant (S9) showed CMs concentration values that

554 surpassed the legal limits.

555 Important CT and CF isotope fractionation processes were identified in wells S1, S3 and S7,

556 located close to the former disposal areas. In particular, $\delta^{13}C$ long-term monitoring disclosed that

557 almost all samples from wells and sources were enriched in ^{13}C with respect to CT and CF

558 commercial values, suggesting the occurrence of C isotope fractionation processes during the

559 industrial process or/and *in situ* degradation. The more enriched $\delta^{13}C$ values of CMs in the tank

560 and pit sources before their removal (2002-2005) than in commercial values and, in the case of

561 CT, even more enriched than groundwater during the studied period (except for the highly

562 degraded CT in S3 well), revealed i) the occurrence of strong isotope fractionation processes

563 during industrial activities or during sources ageing in the unsaturated zone before their removal,

564 and ii) an important leaching to the saturated zone previous to that CMs isotope fractionation.

565 Thus, the most depleted isotope CMs values ever found in Òdena site (from S1 and S4 wells)

566 together with $\delta^{13}C_{CF}$ value from barrels in 2002 were considered as representative of the original

567 source CT and CF isotopic composition. It follows that values found in aged sources (like those

568 of pit and tank in this study) should be treated with caution to evaluate and quantify current field

569 degradation.

570 The dual element CSIA allowed degradation pathways differentiation among different areas at

571 the site. CT reductive pathways were confirmed in S3, S7 and S9 wells, and CT degradation

572 extents over 90% were estimated. CF oxidative degradation might have taken place at the former

573 pit source area (S1 well), congruently with open air spills documented in this area and with the

574 evolution towards more oxidising redox conditions after source removal. As the determined dual

isotope slope in this area was also fitting with CF alkaline hydrolysis taking place in groundwater arriving from the upstream remediation trench (Torrentó et al., 2014), complementary tools are needed for distinguishing both processes. For instance, hydrogen isotopes analysis (i.e., δ^2H), or active microbial population assessment (e.g. monooxygenase-encoding genes or species) would be useful for distinguishing between both pathways. CF degradation due to reductive processes might be possible in S3 and S7.

Hence, the study we have presented shows that in field sites with high heterogeneity, such as Òdena, an in-depth study of i) the areas impacted by different sources and ii) degradation processes occurring in distinct parts of the aquifer is critical to tailor the remediation strategy that should be applied to each contaminated area, and that the use of a single monitoring well as representative of the whole system leads to an incorrect evaluation of the site and the associated environmental and human risks. This study shows that 2D-CSIA is a valuable tool not only to assess source apportionment and *in situ* natural attenuation of CMs in different parts of the aquifer but also to satisfactorily monitor the effectiveness of remediation strategies at complex polluted field sites.

References

Audí-Miró, C., Cretnik, S., Torrentó, C., Rosell, M., Shouakar-Stash, O., Otero, N., Palau, J., Elsner, M., Soler, A., 2015. C, Cl and H compound-specific isotope analysis to assess natural versus Fe(0) barrier-induced degradation of chlorinated ethenes at a contaminated site. J Hazard Mater 299, 747–754. doi:10.1016/j.jhazmat.2015.06.052

Badin, A., Broholm, M.M., Jacobsen, C.S., Palau, J., Dennis, P., Hunkeler, D., 2016. Identification of abiotic and biotic reductive dechlorination in a chlorinated ethene plume after thermal source remediation by means of isotopic and molecular biology tools. J. Contam. Hydrol. doi:10.1016/j.jconhyd.2016.05.003

Badin, A., Buttet, G., Maillard, J., Holliger, C., Hunkeler, D., 2014. Multiple dual C-Cl isotope patterns associated with reductive dechlorination of tetrachloroethene. Environ. Sci.

Technol. 48, 9179–9186. doi:10.1021/es500822d

Baertschi, P., Kuhn, W., Kuhn, H., 1953. Fractionation of isotopes by distillation of some organic substances. Nature 171, 1018–1020.

Bagley, D.M., Lalonde, M., Kaseros, V., Stasiuk, K.E., Sleep, B.E., 2000. Acclimation of anaerobic systems to biodegrade tetrachloroethene in the presence of carbon tetrachloride and chloroform. Water Res. 34, 171–178. doi:10.1016/S0043-1354(99)00121-9

Bernstein, A., Shouakar-stash, O., Ebert, K., Laskov, C., Hunkeler, D., Jeannottat, S., Sakaguchi-Söder, K., Laaks, J., Jochmann, M.A., Cretnik, S., Jager, J., Haderlein, S.B., Schmidt, T.C., Aravena, R., Elsner, M., 2011. Compound-specific chlorine isotope analysis: a comparison of gas chromatography/isotope ratio mass spectrometry and gas chromatography/quadrupole mass spectrometry methods in an interlaboratory study. Anal. Chem. 83, 7624–7634. doi:dx.doi.org/10.1021/ac200516c

Cappelletti, M., Frascari, D., Zannoni, D., Fedi, S., 2012. Microbial degradation of chloroform. Appl. Microbiol. Biotechnol. 96, 1395–1409. doi:10.1007/s00253-012-4494-1.

Chan, C.C.H., Mundle, S.O.C., Eckert, T., Liang, X., Tang, S., Lacrampe-Couloume, G., Edwards, E.A., Sherwood Lollar, B., 2012. Large carbon isotope fractionation during biodegradation of chloroform by *Dehalobacter* cultures. Environ. Sci. Technol. 46, 10154–10160. doi:10.1021/es3010317

Coplen (2011). Guidelines and recommended terms for expression of stable-isotope-ratio and gas-ratio measurement results. Rapid Commun. Mass Spectrom. 2011, 25, 2538–2560

Davis, A., Fennemore, G.G., Peck, C., Walker, C.R., McIlwraith, J., Thomas, S., 2003. Degradation of carbon tetrachloride in a reducing groundwater environment: Implications for natural attenuation. Appl. Geochemistry 18, 503–525. doi:10.1016/S0883-2927(02)00102-6

Deshpande, N.P., Wong, Y.K., Manefield, M., Wilkins, M.R., Lee, M., 2013. Genome sequence of *Dehalobacter* UNSWDHB, a chloroform-dechlorinating bacterium. Genome Announc. 1, 1–2. doi:10.1186/1471-2105-11-485.7.

Devlin, J.F., Muller, D., 1999. Field and laboratory studies of carbon tetrachloride transformation in a sandy aquifer under sulfate reducing conditions. Environ. Sci. Technol. 33, 1021–1027. doi:10.1021/es9806884

Ding, C., Zhao, S., He, J., 2014. A *Desulfitobacterium* sp. strain PR reductively dechlorinates both 1,1,1-trichloroethane and chloroform. Environ. Microbiol. 16, 3387–3397. doi:10.1111/1462-2920.12387

Dogramaci, S.S., Herczeg, A.L., Schiff, S.L., Bone, Y., 2001. Controls on $\delta^{34}S$ and $\delta^{18}O$ of dissolved sulfate in aquifers of the murray basin, Australia and their use as indicators of flow processes. Appl. Geochemistry 16, 475–488. doi:10.1016/S0883-2927(00)00052-4

Duhamel, M., Wehr, S.D., Yu, L., Rizvi, H., Seepersad, D., Dworatzek, S., Cox, E.E., Edwards, E.A., 2002. Comparison of anaerobic dechlorinating enrichment cultures maintained on tetrachloroethene, trichloroethene, cis-dichloroethene and vinyl chloride. Water Res. 36, 4193–4202. doi:10.1016/S0043-1354(02)00151-3

European Union, 2008. Directive 2008/105/CE related to the rules of environmental quality within water policies, Official Journal of the European Union.

European Environment Agency (EEA), 2014. Progress in Management of Contaminated Sites (CSI 015) [WWW Document]. URL http://www.eea.europa.eu/data-and-maps/indicators/progress-in-management-of-contaminated-sites-3/assessment (accessed 4.18.17).

Field, J.A., Sierra-Alvarez, R., 2004. Biodegradability of chlorinated solvents and related chlorinated aliphatic compounds. Rev. Environ. Sci. Biotechnol. 3, 185–254. doi:10.1007/s11157-004-4733-8

Futagami, T., Yamaguchi, T., Nakayama, S.I., Goto, M., Furukawa, K., 2006. Effects of chloromethanes on growth of and deletion of the *pce* gene cluster in dehalorespiring *Desulfitobacterium hafniense* strain Y51. Appl. Environ. Microbiol. 72, 5998–6003. doi:10.1128/AEM.00979-06

Futagami, T., Fukaki, Y., Fujihara, H., Takegawa, K., Goto, M., Furukawa, K., 2013. Evaluation of the inhibitory effects of chloroform on ortho-chlorophenol- and chloroethene-dechlorinating *Desulfitobacterium* strains. AMB Express 3, 1–8. doi:10.1186/2191-0855-3-30

Grostern, A., Duhamel, M., Dworatzek, S., Edwards, E.A., 2010. Chloroform respiration to dichloromethane by a *Dehalobacter* population. Environ. Microbiol. 12, 1053–1060. doi:10.1111/j.1462-2920.2009.02150.x

He, Y.T., Wilson, J.T., Su, C., Wilkin, R.T., 2015. Review of abiotic degradation of chlorinated solvents by reactive iron minerals in aquifers. Groundw. Monit. Remediat. 35, 57–75. doi:10.1111/gwmr.12111

Heckel, B., Cretnik, S., Kliegman, S., Shouakar-Stash, O., McNeill, K., Elsner, M., 2017a. Reductive outer-sphere single electron transfer is an exception rather than the rule in natural and engineered chlorinated ethene dehalogenation. Environ. Sci. Technol. In press. doi:10.1021/acs.est.7b01447

Heckel, B., Rodríguez-Fernández, D., Torrentó, C., Meyer, A., Palau, J., Domènech, C., Rosell, M., Soler, A., Hunkeler, D., Elsner, M., 2017b. Compound-specific chlorine isotope analysis of tetrachloromethane and trichloromethane by gas chromatography-isotope ratio mass spectrometry vs gas chromatography-quadrupole mass spectrometry: method development and evaluation of precision and trueness. Anal. Chem. 89, 3411–3420. doi:10.1021/acs.analchem.6b04129

Hunkeler, D., Aravena, R., 2000. Determination of compound-specific carbon isotope ratios of chlorinated methanes, ethanes, and ethenes in aqueous samples. Environ. Sci. Technol. 34, 2839–2844. doi:10.1021/es991178s

Hunkeler, D., Aravena, R., Berry-Spark, K., Cox, E., 2005. Assessment of degradation pathways in an aquifer with mixed chlorinated hydrocarbon contamination using stable isotope analysis. Environ. Sci. Technol. 39, 5975–5981. doi:10.1021/es048464a

Hunkeler, D., Meckenstock, R.U., Lollar, B.S., Schmidt, T.C., Wilson, J.T., 2008. A Guide for assessing biodegradation and source identification of organic ground water contaminants using compound specific isotope analysis (CSIA), EPA.

Hunkeler, D., Van Breukelen, B.M., Elsner, M., 2009. Modeling chlorine isotope trends during sequential transformation of chlorinated ethenes. Environ. Sci. Technol. 43, 6750–6756. doi:10.1021/es900579z

722

723 Imfeld, G., Nijenhuis, I., Nikolausz, M., Zeiger, S., Paschke, H., Drangmeister, J., Grossmann,
724   J., Richnow, H.H., Weber, S., 2008. Assessment of in situ degradation of chlorinated
725   ethenes and bacterial community structure in a complex contaminated groundwater
726   system. Water Res. 42, 871–882. doi:10.1016/j.watres.2007.08.035

727 Jeannottat, S., Hunkeler, D., 2012. Chlorine and carbon isotopes fractionation during
728   volatilization and diffusive transport of trichloroethene in the unsaturated zone. Environ.
729   Sci. Technol. 46, 3169–3176. doi:10.1021/es203547p
730
731 Jeannottat, S., Hunkeler, D., 2013. Can soil gas VOCs be related to groundwater plumes based
732   on their isotope signature? Environ. Sci. Technol. 47, 12115–12122.
733   doi:10.1021/es4010703

734 Justicia-Leon, S.D., Higgins, S., Mack, E.E., Griffiths, D.R., Tang, S., Edwards, E.A., Löffler,
735   F.E., 2014. Bioaugmentation with distinct *Dehalobacter* strains achieves chloroform
736   detoxification in microcosms. Environ. Sci. Technol. 48, 1851–1858.
737   doi:10.1021/es403582f
738
739 Kaown, D., Shouakar-Stash, O., Yang, J., Hyun, Y., Lee, K.K., 2014. Identification of multiple
740   sources of groundwater contamination by dual isotopes. Groundwater 52, 875–885.
741   doi:10.1111/gwat.12130
742
743 Kirtland, B.C., Aelion, C.M., Stone, P.A., Hunkeler, D., 2003. Isotopic and geochemical
744   assessment of in situ biodegradation of chlorinated hydrocarbons. Environ. Sci. Technol.
745   37, 4205–4212. doi:10.1021/es034046e
746
747 Koenig, J.C., Lee, M.J., Manefield, M., 2012. Successful microcosm demonstration of a strategy
748   for biodegradation of a mixture of carbon tetrachloride and perchloroethene harnessing
749   sulfate reducing and dehalorespiring bacteria. J. Hazard. Mater. 219–220, 169–175.
750   doi:10.1016/j.jhazmat.2012.03.076
751
752 Kuder, T., Van Breukelen, B.M., Vanderford, M., Philp, P., 2013. 3D-CSIA: Carbon, chlorine,
753   and hydrogen isotope fractionation in transformation of TCE to ethene by a
754   *Dehalococcoides* culture. Environ. Sci. Technol. 47, 9668–9677. doi:10.1021/es400463p
755
756 Lee, M., Low, A., Zemb, O., Koenig, J., Michaelsen, A., Manefield, M., 2012. Complete
757   chloroform dechlorination by organochlorine respiration and fermentation. Environ.
758   Microbiol. 14, 883–894. doi:10.1111/j.1462-2920.2011.02656.x
759
760 Lewis, T.A., Crawford, R.L., 1995. Transformation of carbon tetrachloride via sulfur and oxygen
761   substitution by *Pseudomonas* sp. strain KC. J. Bacteriol. 177, 2204–2208.
762
763 Lima, G. da P., Sleep, B.E., 2010. The impact of carbon tetrachloride on an anaerobic methanol-
764   degrading microbial community. Water. Air. Soil Pollut. 212, 357–368.
765   doi:10.1007/s11270-010-0350-z
766
767 Martín-González, L., Mortan, S.H., Rosell, M., Parladé, E., Martínez-Alonso, M., Gaju, N.,
768   Caminal, G., Adrian, L., Marco-Urrea, E., 2015. Stable carbon isotope fractionation
769   during 1,2-dichloropropane-to-propene transformation by an enrichment culture
770   containing *Dehalogenimonas* strains and a *dcpA* gene. Environ. Sci. Technol. 49, 8666–
771   8674. doi:10.1021/acs.est.5b00929
772
773 Maymó-Gatell, X., Nijenhuis, I., Zinder, S.H., 2001. Reductive dechlorination of cis-1,2-

dichloroethene and vinyl chloride by *"Dehalococcoides ethenogenes."* Environ. Sci. Technol. 35, 516–521. doi:10.1021/es001285i

Nijenhuis, I., Schmidt, M., Pellegatti, E., Paramatti, E., Richnow, H.H., Gargini, A., 2013. A stable isotope approach for source apportionment of chlorinated ethene plumes at a complex multi-contamination events urban site. J. Contam. Hydrol. 153, 92–105. doi:10.1016/j.jconhyd.2013.06.004

Palau, J., Marchesi, M., Chambon, J.C.C., Aravena, R., Canals, À., Binning, P.J., Bjerg, P.L., Otero, N., Soler, A., 2014. Multi-isotope (carbon and chlorine) analysis for fingerprinting and site characterization at a fractured bedrock aquifer contaminated by chlorinated ethenes. Sci. Total Environ. 475, 61–70. doi:10.1016/j.scitotenv.2013.12.059

Palau J., Jamin P., Badin A., Vanhecke N., Haerens B., Brouyère S., Hunkeler D. 2016. Use of dual carbon-chlorine isotope analysis to assess the degradation pathways of 1,1,1-trichloroethane in groundwater. Water Res., 92, 235-243. doi: 10.1016/j.watres.2016.01.057

Penny, C., Vuilleumier, S., Bringel, F., 2010. Microbial degradation of tetrachloromethane: mechanisms and perspectives for bioremediation. FEMS Microbiol. Ecol. 74, 257–275. doi:10.1111/j.1574-6941.2010.00935.x

Puig, R., Folch, A., Menció, A., Soler, A., Mas-Pla, J., 2013. Multi-isotopic study (^{15}N, ^{34}S, ^{18}O, ^{13}C) to identify processes affecting nitrate and sulfate in response to local and regional groundwater mixing in a large-scale flow system. Appl. Geochemistry 32, 129–141. doi:10.1016/j.apgeochem.2012.10.014

Puigdomènech, I., 2010. MEDUSA (Make Equilibrium Diagrams Using Sophisticated Algorithms) Windows interface to the MS-DOS versions of INPUT, SED and PREDOM (FORTRAN programs drawing chemical equilibrium diagrams).

Puigserver, D., Carmona, J.M., Cortés, A., Viladevall, M., Nieto, J.M., Grifoll, M., Vila, J., Parker, B.L., 2013. Subsoil heterogeneities controlling porewater contaminant mass and microbial diversity at a site with a complex pollution history. J. Contam. Hydrol. 144, 1–19. doi:10.1016/j.jconhyd.2012.10.009

Rodríguez-Fernández, D., Torrentó, C., Guivernau, M., Viñas, M., Hunkeler, D., Soler, A., Domènech, C., Rosell, M., 2018a. Vitamin B$_{12}$ effects on chlorinated methanes-degrading microcosms: Dual isotope and metabolically active microbial populations assessment. Sci. Total Environ. 621, 1615–1625. doi:10.1016/j.scitotenv.2017.10.067

Rodríguez-Fernández, D., Heckel, B, Torrentó, C., Meyer, A., Elsner, M., Hunkeler, D., Soler, A., Rosell, M, Domènech, C. 2018b. Dual element (C-Cl) isotope approach to characterize abiotic reactions of chlorinated methanes by Fe(0) and by Fe(II) on iron minerals at neutral and alkaline pH. *Just accepted* in Chemosphere.

Tang, S., Edwards, E.A., 2013. Identification of *Dehalobacter* reductive dehalogenases that catalyse dechlorination of chloroform, 1,1,1-trichloroethane and 1,1-dichloroethane. Phil. Trans. R. Soc. B 368, 20120318. doi:10.1098/rstb.2012.0318

Torrentó, C., Audí-Miró, C., Bordeleau, G., Marchesi, M., Rosell, M., Otero, N., Soler, A., 2014. The use of alkaline hydrolysis as a novel strategy for chloroform remediation: The feasibility of using construction wastes and evaluation of carbon isotopic fractionation. Environ. Sci. Technol. 48, 1869–1877. doi:10.1021/es403838t

825

826 Torrentó, C., Palau, J., Rodríguez-Fernández, D., Heckel, B., Meyer, A., Domènech, C., Rosell,
827   M., Soler, A., Elsner, M., Hunkeler, D., 2017. Carbon and chlorine isotope fractionation
828   patterns associated with different engineered chloroform transformation reactions.
829   Environ. Sci. Technol. 51, 6174–6184. doi:10.1021/acs.est.7b00679

830

831 United states environmental protection agency (USEPA), 2014. Priority Pollutants [WWW
832   Document]. URL https://www.epa.gov/eg/toxic-and-priority-pollutants-under-clean-
833   water-act (accessed 4.18.17).

834

835 Weathers, L.J., Parkin, G.F., 2000. Toxicity of chloroform biotransformation to methanogenic
836   bacteria. Environ. Sci. Technol. 34, 2764–2767. doi:10.1021/es990948x

837

838 Wiegert, C., Aeppli, C., Knowles, T., Holmstrand, H., Evershed, R., Pancost, R.D., Macháčková,
839   J., Gustafsson, Ö., 2012. Dual carbon-chlorine stable isotope investigation of sources and
840   fate of chlorinated ethenes in contaminated groundwater. Environ. Sci. Technol. 46,
841   10918–10925. doi:10.1021/es3016843

842

843 Wiegert, C., Mandalakis, M., Knowles, T., Polymenakou, P.N., Aeppli, C., Macháčková, J.,
844   Holmstrand, H., Evershed, R.P., Pancost, R.D., Gustafsson, O., 2013. Carbon and
845   chlorine isotope fractionation during microbial degradation of tetra- and trichloroethene.
846   Environ. Sci. Technol. 47, 6449–6456. doi:10.1021/es305236y

2   # Unravelling long-term source removal effects and

3   chlorinated methanes natural attenuation processes by

4   C and Cl stable isotopic patterns at a complex site

5   Diana Rodríguez-Fernández[1], Clara Torrentó[2,1], Jordi Palau[2,3,1], Massimo Marchesi[1,4], Albert

6   Soler[1], Daniel Hunkeler[2], Cristina Domènech[1], Mònica Rosell[1]

7   [1]Grup MAiMA, Mineralogia Aplicada, Geoquímica i Geomicrobiologia, Departament de Mineralogia, Petrologia i
8   Geologia Aplicada, Facultat de Ciències de la Terra, Universitat de Barcelona (UB), C/Martí i Franquès s/n, 08028
9   Barcelona, Spain.

10   [2] Centre for Hydrogeology and Geothermics, University of Neuchâtel, 2000 Neuchâtel, Switzerland

11   [3] Institute of Environmental Assessment and Water Research (IDAEA), CSIC, Jordi Girona 18-26, 08034 Barcelona,
12   Spain; Associated Unit: Hydrogeology Group (UPC-CSIC), Barcelona, Spain.

13   [4] Politecnico di Milano, Dept. of Civil and Environmental Engineering (DICA), Piazza L. Da Vinci, 32, 20133
14   Milano, Italy

15   **Corresponding Author:**

16   *Diana Rodríguez-Fernández Phone: +34 93 403 90 74; Fax: +34 93 402 13 40, e-mail:
17   diana.rodriguez@ub.edu

18   Total number of pages (including cover): 12

19   Figures: 1

20   Tables: 5

21

Table A1. pH, Eh (mV), total Ca, Na, Fe, chloride, bicarbonate, nitrate, and sulfate concentrations (μM),
and $\delta^{34}S$ (‰) and $\delta^{18}O$ (‰) of dissolved sulfate measured at diferent depths (meters above sea level,
m.a.s.l.) of studied wells over time. SD in $\delta^{34}S$ corresponds to instrument uncertainty and in $\delta^{18}O$ to
uncertainty of duplicates. n.m.=not measured.

Samplig depth of well (masl)	Period	S1 426	S1 424	S1 422	S1 420	S3 425	S3 424	S3 421	S3 419	S3 417	S4 425	S4 423	S4 422	S4 421	S4 419	S4 417	S4 414	S6 421	S6 420	S6 419	S6 418	S6 416	S6 414
pH	June 2006	7	7	7	7	7	7	7	7	7	n.m.	n.m.	7	n.m.	n.m.	n.m.	7	7	n.m.	n.m.	n.m.	7	n.m.
Eh (mV)		116	124	95	84	152	169	146	188	151	n.m.	n.m.	294	n.m.	n.m.	n.m.	99	344	n.m.	n.m.	n.m.	249	n.m.
Ca (μM)		n.m.	16	16	n.m.	13	n.m.	13	n.m.	9	n.m.	n.m.	14	n.m.	n.m.	n.m.	11	14	n.m.	n.m.	n.m.	14	n.m.
Na (μM)		n.m.	14	14	n.m.	11	n.m.	11	n.m.	37	n.m.	n.m.	11	n.m.	n.m.	n.m.	206	13	n.m.	n.m.	n.m.	13	n.m.
Fe (μM)		n.m.	0.00	0.03	n.m.	0.02	n.m.	0.01	n.m.	0.01	n.m.	n.m.	0.001	n.m.	n.m.	n.m.	0.001	0.001	n.m.	n.m.	n.m.	0.001	n.m.
Cl^- (μM)		n.m.	27	26	n.m.	27	n.m.	24	n.m.	47	n.m.	n.m.	9	n.m.	n.m.	n.m.	259	26	n.m.	n.m.	n.m.	26	n.m.
HCO_3^- (μM)		n.m.	8	8	n.m.	12	n.m.	12	n.m.	13	n.m.	n.m.	6	n.m.	n.m.	n.m.	4	8	n.m.	n.m.	n.m.	9	n.m.
NO_3^- (μM)		n.m.	<0.3	0.2581	n.m.	<0.02	n.m.	<0.02	n.m.	<0.02	n.m.	n.m.	3	n.m.	n.m.	n.m.	0.07	1	n.m.	n.m.	n.m.	1	n.m.
SO_4^{2-} (μM)		n.m.	18	17	n.m.	11	n.m.	12	n.m.	10	n.m.	n.m.	18	n.m.	n.m.	n.m.	2	17	n.m.	n.m.	n.m.	18	n.m.
$\delta^{34}S$		n.m.	14.9	15.3	n.m.	15.2	n.m.	15.4	n.m.	19.5	n.m.	n.m.	17.8	n.m.	n.m.	n.m.	36.9	13.8	n.m.	n.m.	n.m.	14.1	n.m.
SD		n.m.	0.2	0.2	n.m.	0.2	n.m.	0.2	n.m.	0.2	n.m.	n.m.	0.2	n.m.	n.m.	n.m.	0.2	0.2	n.m.	n.m.	n.m.	0.2	n.m.
$\delta^{18}O$		n.m.	9.7	9.4	n.m.	8.9	n.m.	8.9	n.m.	10.7	n.m.	n.m.	10.4	n.m.	n.m.	n.m.	16.0	8.3	n.m.	n.m.	n.m.	8.8	n.m.
SD		n.m.	0.5	0.5	n.m.	0.5	n.m.	0.5	n.m.	0.5	n.m.	n.m.	0.5	n.m.	n.m.	n.m.	0.5	0.5	n.m.	n.m.	n.m.	0.5	n.m.
pH	June 2007	7	n.m.	n.m.	7	7	7	7	7	7	n.m.	n.m.	7	n.m.	n.m.	n.m.	7	n.m.	7	n.m.	7	7	7
Eh (mV)		168	n.m.	n.m.	110	141	129	130	79	77	n.m.	n.m.	270	n.m.	n.m.	n.m.	99	n.m.	158	n.m.	146	144	133
Ca (μM)		9	n.m.	n.m.	9	14	14	14	14	13	n.m.	n.m.	12	n.m.	n.m.	n.m.	11	n.m.	15	17	n.m.	15	16
Na (μM)		12	n.m.	n.m.	11	11	12	12	40	49	n.m.	n.m.	16	n.m.	n.m.	n.m.	251	n.m.	14	14	n.m.	13	15
Fe (μM)		0.04	n.m.	n.m.	0.04	0.5	0.5	0.6	1.5	2.4	n.m.	n.m.	0.08	n.m.	n.m.	n.m.	0.09	n.m.	0.2	0.2	n.m.	0.5	0.2
Cl^- (μM)		9	n.m.	n.m.	9	28	28	28	65	68	n.m.	n.m.	11	n.m.	n.m.	n.m.	292	n.m.	29	30	n.m.	30	36
HCO_3^- (μM)		3	n.m.	n.m.	3	12	12	12	14	16	n.m.	n.m.	7	n.m.	n.m.	n.m.	4	n.m.	11	11	n.m.	11	11
NO_3^- (μM)		n.m.	n.m.	n.m.	n.m.	n.m.	0.1	0.1	0.2	0.1	n.m.	n.m.	2	n.m.	n.m.	n.m.	n.m.	n.m.	n.m.	n.m.	n.m.	n.m.	n.m.
SO_4^{2-} (μM)		14	n.m.	n.m.	13	14	13	13	12	13	n.m.	n.m.	22	n.m.	n.m.	n.m.	8	n.m.	17	20	n.m.	18	19
pH	September 2007	n.m.	n.m.	n.m.	n.m.	n.m.	n.m.	n.m.	n.m.	n.m.	n.m.	n.m.	7	n.m.	n.m.	n.m.	7	n.m.	n.m.	n.m.	n.m.	n.m.	n.m.
Eh (mV)		n.m.	n.m.	n.m.	n.m.	n.m.	n.m.	n.m.	n.m.	n.m.	n.m.	n.m.	272	n.m.	n.m.	n.m.	78	n.m.	n.m.	n.m.	n.m.	n.m.	n.m.
Ca (μM)		8	n.m.	n.m.	9	16	n.m.	16	n.m.	11	n.m.	n.m.	13	n.m.	n.m.	n.m.	11	n.m.	12	n.m.	n.m.	13	n.m.
Na (μM)		10	n.m.	n.m.	13	12	n.m.	12	n.m.	48	n.m.	n.m.	10	n.m.	n.m.	n.m.	245	n.m.	11	n.m.	n.m.	12	n.m.
Fe (μM)		0.001	n.m.	n.m.	0.001	0.01	n.m.	0.01	n.m.	0.01	n.m.	n.m.	0.001	n.m.	n.m.	n.m.	0.00	n.m.	0.003	n.m.	n.m.	0.003	n.m.
Cl^- (μM)		11	n.m.	n.m.	12	42	n.m.	41	n.m.	65	n.m.	n.m.	10	n.m.	n.m.	n.m.	277	n.m.	20	n.m.	n.m.	22	n.m.
HCO_3^- (μM)		5	n.m.	n.m.	7	12	n.m.	12	n.m.	16	n.m.	n.m.	7	n.m.	n.m.	n.m.	4	n.m.	10	n.m.	n.m.	10	n.m.
NO_3^- (μM)		n.m.	n.m.	n.m.	n.m.	n.m.	n.m.	n.m.	n.m.	n.m.	n.m.	n.m.	n.m.	n.m.	n.m.	n.m.	n.m.	n.m.	n.m.	n.m.	n.m.	n.m.	n.m.
SO_4^{2-} (μM)		11	n.m.	n.m.	12	11	n.m.	11	n.m.	8	n.m.	n.m.	18	n.m.	n.m.	n.m.	6	n.m.	14	n.m.	n.m.	14	n.m.
pH	January 2008	n.m.	n.m.	n.m.	n.m.	7	n.m.	7	n.m.	7	n.m.	n.m.	8	n.m.	n.m.	n.m.	7	n.m.	n.m.	7	n.m.	7	n.m.
Eh (mV)		n.m.	n.m.	n.m.	n.m.	149	n.m.	152	n.m.	118	n.m.	n.m.	278	n.m.	n.m.	n.m.	125	n.m.	n.m.	50	n.m.	244	n.m.
Ca (μM)		n.m.	n.m.	n.m.	n.m.	15	n.m.	15	n.m.	10	n.m.	n.m.	13	n.m.	n.m.	n.m.	11	n.m.	n.m.	11	n.m.	11	n.m.
Na (μM)		n.m.	n.m.	n.m.	n.m.	12	n.m.	16	n.m.	56	n.m.	n.m.	42	n.m.	n.m.	n.m.	256	n.m.	n.m.	10	n.m.	10	n.m.
Fe (μM)		n.m.	n.m.	n.m.	n.m.	0.01	n.m.	0.01	n.m.	0.01	n.m.	n.m.	0.002	n.m.	n.m.	n.m.	0.001	n.m.	n.m.	0.002	n.m.	0.003	n.m.
Cl^- (μM)		n.m.	n.m.	n.m.	n.m.	37	n.m.	43	n.m.	70	n.m.	n.m.	46	n.m.	n.m.	n.m.	284	n.m.	n.m.	17	n.m.	19	n.m.
HCO_3^- (μM)		n.m.	n.m.	n.m.	n.m.	12	n.m.	13	n.m.	16	n.m.	n.m.	6	n.m.	n.m.	n.m.	4	n.m.	n.m.	9	n.m.	10	n.m.
NO_3^- (μM)		n.m.	n.m.	n.m.	n.m.	n.m.	n.m.	n.m.	n.m.	n.m.	n.m.	n.m.	0.1	n.m.	n.m.	n.m.	n.m.	n.m.	n.m.	n.m.	n.m.	n.m.	n.m.
SO_4^{2-} (μM)		n.m.	n.m.	n.m.	n.m.	n.m.	n.m.	n.m.	n.m.	n.m.	n.m.	n.m.	16	n.m.	n.m.	n.m.	6	n.m.	n.m.	13	n.m.	12	n.m.
pH	March 2010	7	n.m.	7	7	7	n.m.	7	n.m.	7	n.m.	n.m.	n.m.	7	n.m.	n.m.	8	n.m.	7	n.m.	n.m.	7	n.m.
Eh (mV)		289	n.m.	305	322	145	n.m.	141	n.m.	123	n.m.	n.m.	n.m.	390	n.m.	n.m.	106	n.m.	298	n.m.	n.m.	298	n.m.
Ca (μM)		9	n.m.	9	10	17	n.m.	17	n.m.	10	n.m.	n.m.	n.m.	14	n.m.	n.m.	13	n.m.	14	n.m.	n.m.	14	n.m.
Na (μM)		12	n.m.	13	16	6	n.m.	6	n.m.	85	n.m.	n.m.	n.m.	11	n.m.	n.m.	281	n.m.	14	n.m.	n.m.	14	n.m.
Fe (μM)		<0.0002	n.m.	<0.0002	<0.0002	0.1	n.m.	0.06	n.m.	0.2	n.m.	n.m.	n.m.	0.0009	n.m.	n.m.	n.m.	n.m.	0.0003	n.m.	n.m.	<0.0002	n.m.
Cl^- (μM)		10	n.m.	9	10	6	n.m.	5	n.m.	73	n.m.	n.m.	n.m.	11	n.m.	n.m.	261	n.m.	16	n.m.	n.m.	16	n.m.
HCO_3^- (μM)		4	n.m.	4	4	10	n.m.	10	n.m.	17	n.m.	n.m.	n.m.	6	n.m.	n.m.	3	n.m.	7	n.m.	n.m.	7	n.m.
NO_3^- (μM)		1	n.m.	1	1	0.04	n.m.	<0.04	n.m.	<0.04	n.m.	n.m.	n.m.	2	n.m.	n.m.	n.m.	n.m.	3	n.m.	n.m.	3	n.m.
SO_4^{2-} (μM)		12	n.m.	10	13	15	n.m.	13	n.m.	6	n.m.	n.m.	n.m.	17	n.m.	n.m.	n.m.	n.m.	15	n.m.	n.m.	16	n.m.
pH	November 2010	n.m.	n.m.	n.m.	n.m.	7	n.m.	7	n.m.	7	n.m.	n.m.	n.m.	n.m.	n.m.	n.m.	n.m.	n.m.	7	n.m.	n.m.	7	n.m.
Eh (mV)		n.m.	n.m.	n.m.	n.m.	n.m.	n.m.	n.m.	n.m.	n.m.	n.m.	n.m.	n.m.	n.m.	n.m.	n.m.	n.m.	n.m.	214	n.m.	n.m.	230	n.m.
Ca (μM)		n.m.	n.m.	n.m.	n.m.	16	n.m.	16	n.m.	44	n.m.	n.m.	n.m.	n.m.	n.m.	n.m.	n.m.	n.m.	n.m.	n.m.	n.m.	n.m.	n.m.
Na (μM)		n.m.	n.m.	n.m.	n.m.	12	n.m.	12	n.m.	463	n.m.	n.m.	n.m.	n.m.	n.m.	n.m.	n.m.	n.m.	n.m.	n.m.	n.m.	n.m.	n.m.
Fe (μM)		n.m.	n.m.	n.m.	n.m.	n.m.	n.m.	n.m.	n.m.	n.m.	n.m.	n.m.	n.m.	n.m.	n.m.	n.m.	n.m.	n.m.	n.m.	n.m.	n.m.	n.m.	n.m.
Cl^- (μM)		n.m.	n.m.	n.m.	n.m.	43	n.m.	49	n.m.	114	n.m.	n.m.	n.m.	n.m.	n.m.	n.m.	n.m.	n.m.	n.m.	n.m.	n.m.	n.m.	n.m.
CO_3^{2-} (μM)		n.m.	n.m.	n.m.	n.m.	n.m.	n.m.	n.m.	n.m.	n.m.	n.m.	n.m.	n.m.	n.m.	n.m.	n.m.	n.m.	n.m.	n.m.	n.m.	n.m.	n.m.	n.m.
NO_3^- (μM)		n.m.	n.m.	n.m.	n.m.	<0.04	n.m.	n.m.	n.m.	<0.04	n.m.	n.m.	n.m.	n.m.	n.m.	n.m.	n.m.	n.m.	n.m.	n.m.	n.m.	n.m.	n.m.
SO_4^{2-} (μM)		n.m.	n.m.	n.m.	n.m.	9	n.m.	14	n.m.	5	n.m.	n.m.	n.m.	n.m.	n.m.	n.m.	n.m.	n.m.	n.m.	n.m.	n.m.	n.m.	n.m.
pH	March 2013	7	7	7	7	7	7	7	7	7	7	7	7	7	7	7	7	7	n.m.	7	7	7	7
Eh (mV)		261	293	318	361	175	168	160	118	80	n.m.	388	372	367	417	-29	-25	206	n.m.	236	226	190	217
Ca (μM)		10	10	10	10	12	12	12	13	6	14	14	14	14	13	10	10	11	n.m.	11	11	8	11
Na (μM)		8	7	7	7	8	8	7	30	84	9	9	9	9	9	126	191	11	n.m.	11	12	20	11
Fe (μM)		0.001	0.001	0.001	0.001	0.3	0.2	0.2	0.2	0.3	0.001	0.001	0.001	0.001	0.04	0.004	0.01	0.002	n.m.	0.05	0.02	0.02	0.05
Cl^- (μM)		5	5	4	4	8	8	8	51	87	7	7	8	7	7	138	216	18	n.m.	18	19	20	19
HCO_3^- (μM)		3	3	3	3	10	10	10	14	17	6	6	6	6	6	5	4	10	n.m.	10	10	10	9
NO_3^- (μM)		0.4	0.4	0.4	0.4	0.04	0.04	0.08	0.1	<0.04	0.92	0.99	0.98	0.80	<0.04	<0.04	<0.04	0.03	n.m.	0.01	0.01	0.01	<0.04
SO_4^{2-} (μM)		14	14	16	15	12	12	12	9	7	18	19	20	18	13	5	5	13	n.m.	13	13	13	13
$\delta^{34}S$ (‰)		n.m.	n.m.	n.m.	n.m.	13.5	13.6	13.5	14.4	21.5	15.5	n.a	n.a	15.4	n.a	45.4	44.0	n.m.	n.m.	n.m.	n.m.	n.m.	n.m.
SD		n.m.	n.m.	n.m.	n.m.	0.2	0.2	0.2	0.2	0.2	0.2	n.a	n.a	0.2	n.a	0.2	0.2	n.m.	n.m.	n.m.	n.m.	n.m.	n.m.
$\delta^{18}O$ (‰)		n.m.	n.m.	n.m.	n.m.	11.6	10.4	10.2	11.1	11.7	11.1	n.a	n.a	n.a	n.a	18.5	18.6	n.m.	n.m.	n.m.	n.m.	n.m.	n.m.
SD		n.m.	n.m.	n.m.	n.m.	0.6	0.4	0.7	0.2	0.2	0.7	n.a	n.a	n.a	n.a	0.5	0.7	n.m.	n.m.	n.m.	n.m.	n.m.	n.m.
pH	Nov. 14	n.m.	n.m.	7.7	n.m.	n.m.	n.m.	n.m.	n.m.	n.m.	n.m.	7	n.m.	n.m.	n.m.	n.m.	n.m.	n.m.	n.m.	n.m.	n.m.	7	n.m.
Eh (mV)		n.m.	n.m.	276	n.m.	n.m.	n.m.	n.m.	n.m.	n.m.	n.m.	201	n.m.	n.m.	n.m.	n.m.	n.m.	n.m.	n.m.	n.m.	n.m.	69	n.m.

Table A1. (cont.)

Samplig depth of well (masl)		S7					S8					S9						S10					
		428	426	423	421	418	429	427	424	422	420	418	416	414	412	410	408	419	417	415	413	411	409
pH	June 2006	7	n.m.	n.m.	7	n.m.	n.m.	7	n.m.	n.m.	8	n.m.	n.m.	n.m.	n.m.	n.m.	7	7	n.m.	n.m.	n.m.	n.m.	7
Eh (mV)		337	n.m.	n.m.	224	n.m.	n.m.	367	n.m.	n.m.	244	n.m.	n.m.	n.m.	n.m.	n.m.	282	422	n.m.	n.m.	n.m.	n.m.	393
Ca (μM)		13	n.m.	n.m.	9	n.m.	n.m.	8	n.m.	n.m.	5	n.m.	n.m.	n.m.	n.m.	n.m.	6	10	n.m.	n.m.	n.m.	n.m.	9
Na (μM)		22	n.m.	n.m.	47	n.m.	n.m.	9	n.m.	n.m.	40	n.m.	n.m.	n.m.	n.m.	n.m.	16	12	n.m.	n.m.	n.m.	n.m.	6
Fe (μM)		n.m.	n.m.	n.m.	n.m.	n.m.	n.m.	n.m.	n.m.	n.m.	n.m.	n.m.	n.m.	n.m.	n.m.	n.m.	0.00	0.0002	n.m.	n.m.	n.m.	n.m.	0.0002
Cl^- (μM)		14	n.m.	n.m.	23	n.m.	n.m.	9	n.m.	n.m.	41	n.m.	n.m.	n.m.	n.m.	n.m.	14	16	n.m.	n.m.	n.m.	n.m.	8
HCO_3^- (μM)		7	n.m.	n.m.	7	n.m.	n.m.	7	n.m.	n.m.	8	n.m.	n.m.	n.m.	n.m.	n.m.	6	6	n.m.	n.m.	n.m.	n.m.	6
NO_3^- (μM)		0.3	n.m.	n.m.	<0.01	n.m.	n.m.	1	n.m.	n.m.	0.9	n.m.	n.m.	n.m.	n.m.	n.m.	0.2	1	n.m.	n.m.	n.m.	n.m.	2
SO_4^{2-} (μM)		27	n.m.	n.m.	27	n.m.	n.m.	12	n.m.	n.m.	8	n.m.	n.m.	n.m.	n.m.	n.m.	11	15	n.m.	n.m.	n.m.	n.m.	12
$\delta^{34}S$		13.0	n.m.	n.m.	12.3	n.m.	n.m.	16.6	n.m.	n.m.	17.4	n.m.	n.m.	n.m.	n.m.	n.m.	13.4	14.3	n.m.	n.m.	n.m.	n.m.	n.m.
SD		0.2	n.m.	n.m.	0.2	n.m.	n.m.	0.2	n.m.	n.m.	0.2	n.m.	n.m.	n.m.	n.m.	n.m.	0.2	0.2	n.m.	n.m.	n.m.	n.m.	n.m.
$\delta^{18}O$		6.4	n.m.	n.m.	6.4	n.m.	n.m.	10.2	n.m.	n.m.	10.3	n.m.	n.m.	n.m.	n.m.	n.m.	8.6	9.0	n.m.	n.m.	n.m.	n.m.	n.m.
SD		0.5	n.m.	n.m.	0.5	n.m.	n.m.	0.5	n.m.	n.m.	0.5	n.m.	n.m.	n.m.	n.m.	n.m.	0.5	0.5	n.m.	n.m.	n.m.	n.m.	n.m.
pH	June 2007	7	n.m.	n.m.	7	n.m.	n.m.	8	n.m.	n.m.	8	7	n.m.	n.m.	n.m.	n.m.	7	n.m.	n.m.	n.m.	n.m.	n.m.	n.m.
Eh (mV)		304	n.m.	n.m.	190	n.m.	n.m.	321	n.m.	n.m.	321	248	n.m.	n.m.	n.m.	n.m.	210	n.m.	n.m.	n.m.	n.m.	n.m.	n.m.
Ca (μM)		11	n.m.	n.m.	8	n.m.	n.m.	7	n.m.	n.m.	5	10	n.m.	n.m.	n.m.	n.m.	6	n.m.	n.m.	n.m.	n.m.	n.m.	n.m.
Na (μM)		12	n.m.	n.m.	85	n.m.	n.m.	8	n.m.	n.m.	68	6	n.m.	n.m.	n.m.	n.m.	17	n.m.	n.m.	n.m.	n.m.	n.m.	n.m.
Fe (μM)		0.06	n.m.	n.m.	0.04	n.m.	n.m.	0.03	n.m.	n.m.	0.03	0.03	n.m.	n.m.	n.m.	n.m.	0.03	n.m.	n.m.	n.m.	n.m.	n.m.	n.m.
Cl^- (μM)		8	n.m.	n.m.	58	n.m.	n.m.	8	n.m.	n.m.	57	6	n.m.	n.m.	n.m.	n.m.	13	n.m.	n.m.	n.m.	n.m.	n.m.	n.m.
HCO_3^- (μM)		7	n.m.	n.m.	7	n.m.	n.m.	8	n.m.	n.m.	7	6	n.m.	n.m.	n.m.	n.m.	n.m.	n.m.	n.m.	n.m.	n.m.	n.m.	n.m.
NO_3^- (μM)		0	n.m.	n.m.	n.m.	n.m.	n.m.	1	n.m.	n.m.	0.04	2	n.m.	n.m.	n.m.	n.m.	0.4	n.m.	n.m.	n.m.	n.m.	n.m.	n.m.
SO_4^{2-} (μM)		21	n.m.	n.m.	30	n.m.	n.m.	12	n.m.	n.m.	15	15	n.m.	n.m.	n.m.	n.m.	14	n.m.	n.m.	n.m.	n.m.	n.m.	n.m.
pH	September 2007	7	n.m.	n.m.	7	n.m.	n.m.	7	n.m.	n.m.	8	7	n.m.	n.m.	n.m.	n.m.	8	7	n.m.	n.m.	n.m.	n.m.	7
Eh (mV)		261	n.m.	n.m.	143	n.m.	n.m.	281	n.m.	n.m.	150	371	n.m.	n.m.	n.m.	n.m.	369	271	n.m.	n.m.	n.m.	n.m.	271
Ca (μM)		13	n.m.	n.m.	7	n.m.	n.m.	8	n.m.	n.m.	5	9	n.m.	n.m.	n.m.	n.m.	6	9	n.m.	n.m.	n.m.	n.m.	9
Na (μM)		15	n.m.	n.m.	76	n.m.	n.m.	9	n.m.	n.m.	68	5	n.m.	n.m.	n.m.	n.m.	17	10	n.m.	n.m.	n.m.	n.m.	7
Fe (μM)		0.001	n.m.	n.m.	0.001	n.m.	n.m.	n.m.	n.m.	n.m.	n.m.	0.001	n.m.	n.m.	n.m.	n.m.	0.001	0.001	n.m.	n.m.	n.m.	n.m.	0.001
Cl^- (μM)		12	n.m.	n.m.	55	n.m.	n.m.	9	n.m.	n.m.	58	5	n.m.	n.m.	n.m.	n.m.	11	14	n.m.	n.m.	n.m.	n.m.	10
HCO_3^- (μM)		7	n.m.	n.m.	7	n.m.	n.m.	7	n.m.	n.m.	7	6	n.m.	n.m.	n.m.	n.m.	7	7	n.m.	n.m.	n.m.	n.m.	6
NO_3^- (μM)		0.1	n.m.	n.m.	n.m.	n.m.	n.m.	1	n.m.	n.m.	n.m.	1	n.m.	n.m.	n.m.	n.m.	0.4	0.3	n.m.	n.m.	n.m.	n.m.	1
SO_4^{2-} (μM)		24	n.m.	n.m.	24	n.m.	n.m.	12	n.m.	n.m.	12	11	n.m.	n.m.	n.m.	n.m.	11	12	n.m.	n.m.	n.m.	n.m.	11
pH	January 2008	7	n.m.	n.m.	8	n.m.	n.m.	7	n.m.	n.m.	7	n.m.	n.m.	n.m.	n.m.	n.m.	7	n.m.	n.m.	n.m.	n.m.	n.m.	8
Eh (mV)		260	n.m.	n.m.	197	n.m.	n.m.	324	n.m.	n.m.	252	n.m.	355	n.m.	n.m.	n.m.	353	n.m.	n.m.	n.m.	n.m.	n.m.	338
Ca (μM)		13	n.m.	n.m.	7	n.m.	n.m.	8	n.m.	n.m.	5	n.m.	9	n.m.	n.m.	n.m.	6	n.m.	n.m.	n.m.	n.m.	n.m.	8
Na (μM)		14	n.m.	n.m.	79	n.m.	n.m.	5	n.m.	n.m.	81	n.m.	5	n.m.	n.m.	n.m.	14	n.m.	n.m.	n.m.	n.m.	n.m.	10
Fe (μM)		0.001	n.m.	n.m.	0.001	n.m.	n.m.	0.0003	n.m.	n.m.	0.001	n.m.	0.0004	n.m.	n.m.	n.m.	0.001	n.m.	n.m.	n.m.	n.m.	n.m.	0.001
Cl^- (μM)		12	n.m.	n.m.	122	n.m.	n.m.	11	n.m.	n.m.	76	n.m.	7	n.m.	n.m.	n.m.	9	n.m.	n.m.	n.m.	n.m.	n.m.	13
HCO_3^- (μM)		7	n.m.	n.m.	6	n.m.	n.m.	7	n.m.	n.m.	7	n.m.	7	n.m.	n.m.	n.m.	7	n.m.	n.m.	n.m.	n.m.	n.m.	7
NO_3^- (μM)		n.m.	n.m.	n.m.	n.m.	n.m.	n.m.	0.4	n.m.	n.m.	n.m.	n.m.	n.m.	n.m.	n.m.	n.m.	n.m.	n.m.	n.m.	n.m.	n.m.	n.m.	0.2
SO_4^{2-} (μM)		23	n.m.	n.m.	44	n.m.	n.m.	12	n.m.	n.m.	11	n.m.	11	n.m.	n.m.	n.m.	11	n.m.	n.m.	n.m.	n.m.	n.m.	11
pH	March 2010	7	n.m.	n.m.	7	n.m.	n.m.	n.m.	n.m.	n.m.	n.m.	n.m.	n.m.	n.m.	n.m.	n.m.	n.m.	n.m.	n.m.	n.m.	n.m.	n.m.	n.m.
Eh (mV)		188	n.m.	n.m.	144	n.m.	n.m.	n.m.	n.m.	n.m.	n.m.	n.m.	n.m.	n.m.	n.m.	n.m.	n.m.	n.m.	n.m.	n.m.	n.m.	n.m.	n.m.
Ca (μM)		13	n.m.	n.m.	9	n.m.	n.m.	n.m.	n.m.	n.m.	n.m.	n.m.	n.m.	n.m.	n.m.	n.m.	n.m.	n.m.	n.m.	n.m.	n.m.	n.m.	n.m.
Na (μM)		11	n.m.	n.m.	100	n.m.	n.m.	n.m.	n.m.	n.m.	n.m.	n.m.	n.m.	n.m.	n.m.	n.m.	n.m.	n.m.	n.m.	n.m.	n.m.	n.m.	n.m.
Fe (μM)		<0.0002	n.m.	n.m.	<0.0002	n.m.	n.m.	n.m.	n.m.	n.m.	n.m.	n.m.	n.m.	n.m.	n.m.	n.m.	n.m.	n.m.	n.m.	n.m.	n.m.	n.m.	n.m.
Cl^- (μM)		12	n.m.	n.m.	66	n.m.	n.m.	n.m.	n.m.	n.m.	n.m.	n.m.	n.m.	n.m.	n.m.	n.m.	n.m.	n.m.	n.m.	n.m.	n.m.	n.m.	n.m.
HCO_3^- (μM)		7	n.m.	n.m.	6	n.m.	n.m.	n.m.	n.m.	n.m.	n.m.	n.m.	n.m.	n.m.	n.m.	n.m.	n.m.	n.m.	n.m.	n.m.	n.m.	n.m.	n.m.
NO_3^- (μM)		2	n.m.	n.m.	n.m.	n.m.	n.m.	n.m.	n.m.	n.m.	n.m.	n.m.	n.m.	n.m.	n.m.	n.m.	n.m.	n.m.	n.m.	n.m.	n.m.	n.m.	n.m.
SO_4^{2-} (μM)		17	n.m.	n.m.	18	n.m.	n.m.	n.m.	n.m.	n.m.	n.m.	n.m.	n.m.	n.m.	n.m.	n.m.	n.m.	n.m.	n.m.	n.m.	n.m.	n.m.	n.m.
pH	November 2010	7	n.m.	n.m.	7	n.m.	n.m.	7	n.m.	n.m.	7	7	n.m.	n.m.	n.m.	n.m.	7	n.m.	7	n.m.	n.m.	n.m.	7
Eh (mV)		204	n.m.	n.m.	145	n.m.	n.m.	182	n.m.	n.m.	101	275	n.m.	n.m.	n.m.	n.m.	201	n.m.	305	n.m.	n.m.	n.m.	323
Ca (μM)		n.m.	n.m.	n.m.	29	n.m.	n.m.	8	n.m.	n.m.	22	9	n.m.	n.m.	n.m.	n.m.	8	n.m.	12	n.m.	n.m.	n.m.	7
Na (μM)		n.m.	n.m.	n.m.	324	n.m.	n.m.	7	n.m.	n.m.	394	8	n.m.	n.m.	n.m.	n.m.	17	n.m.	12	n.m.	n.m.	n.m.	5
Fe (μM)		n.m.	n.m.	n.m.	0.0002	n.m.	n.m.	0.0002	n.m.	n.m.	0.003	0.0002	n.m.	n.m.	n.m.	n.m.	0.0001	n.m.	0.001	n.m.	n.m.	n.m.	0.0001
Cl^- (μM)		n.m.	n.m.	n.m.	109	n.m.	n.m.	6	n.m.	n.m.	73	5	n.m.	n.m.	n.m.	n.m.	11	n.m.	10	n.m.	n.m.	n.m.	5
HCO_3^- (μM)		n.m.	n.m.	n.m.	n.m.	n.m.	n.m.	n.m.	n.m.	n.m.	n.m.	1.48	n.m.	n.m.	n.m.	n.m.	1.38	n.m.	n.m.	n.m.	n.m.	n.m.	n.m.
NO_3^- (μM)		n.m.	n.m.	n.m.	<0.04	n.m.	n.m.	n.m.	n.m.	n.m.	<0.04	1.4	n.m.	n.m.	n.m.	n.m.	<0.04	n.m.	<0.04	n.m.	n.m.	n.m.	1
SO_4^{2-} (μM)		n.m.	n.m.	n.m.	23	n.m.	n.m.	14	n.m.	n.m.	13	14	n.m.	n.m.	n.m.	n.m.	6	n.m.	11	n.m.	n.m.	n.m.	10
pH	March 2013	7	7	8	7	8	8	11	7	7	8	7	8	8	8	8	8	7	7	7	7	7	7
Eh (mV)		314	259	353	83	-11	376	348	346	308	195	316	315	332	308	280	139	350	323	322	331	328	312
Ca (μM)		12	9	12	7	11	6	7	6	4	4	8	8	8	7	6	4	8	7	7	6	7	n.m.
Na (μM)		10	32	11	79	139	5	7	15	63	35	3	4	4	8	13	19	5	5	5	4	4	n.m.
Fe (μM)		0.001	0.002	0.01	0.02	0.02	0.0005	0.0005	0.001	0.012	0.0004	0.001	0.001	0.001	0.001	0.002	0.07	0.001	0.001	0.001	0.001	0.001	<0.0005
Cl^- (μM)		16	26	16	71	136	5	6	9	19	47	4	4	4	7	10	12	6	8	5	4	4	4
HCO_3^- (μM)		8	7	8	6	5	8	8	7	8	8	7	6	6	7	7	8	0	6	6	6	6	6
NO_3^- (μM)		1	1	<0.04	<0.04	<0.04	0.6	0.4	0.3	0.5	0.000	0.7	1	1	0.6	0.1	<0.04	1	0.8	1	1	1	1
SO_4^{2-} (μM)		21	21	25	26	26	12	13	12	16	15	12	9	10	10	10	9	10	10	9	9	9	9
$\delta^{34}S$ (‰)		n.m.	n.m.	n.m.	n.m.	n.m.	n.m.	n.m.	n.m.	n.m.	n.m.	n.m.	n.m.	n.m.	n.m.	n.m.	n.m.	n.m.	n.m.	n.m.	n.m.	n.m.	n.m.
SD		n.m.	n.m.	n.m.	n.m.	n.m.	n.m.	n.m.	n.m.	n.m.	n.m.	n.m.	n.m.	n.m.	n.m.	n.m.	n.m.	n.m.	n.m.	n.m.	n.m.	n.m.	n.m.
$\delta^{18}O$ (‰)		n.m.	n.m.	n.m.	n.m.	n.m.	n.m.	n.m.	n.m.	n.m.	n.m.	n.m.	n.m.	n.m.	n.m.	n.m.	n.m.	n.m.	n.m.	n.m.	n.m.	n.m.	n.m.
SD		n.m.	n.m.	n.m.	n.m.	n.m.	n.m.	n.m.	n.m.	n.m.	n.m.	n.m.	n.m.	n.m.	n.m.	n.m.	n.m.	n.m.	n.m.	n.m.	n.m.	n.m.	n.m.
pH	Nov. 14	n.m.	7	n.m.	n.m.	n.m.	n.m.	7	n.m.	n.m.	n.m.	7	n.m.	n.m.	n.m.	n.m.	n.m.	n.m.	n.m.	n.m.	n.m.	n.m.	n.m.
Eh (mV)		n.m.	138	n.m.	n.m.	n.m.	n.m.	349	n.m.	n.m.	n.m.	353	n.m.	n.m.	n.m.	n.m.	n.m.	n.m.	n.m.	n.m.	n.m.	n.m.	n.m.

29

Fig. A1. Eh-pH diagram of the systems Fe-S-C-H$_2$O and N-H$_2$O. Calculations were performed with [Ca^{2+}]$_{tot}$ =0.013 M, [Fe]$_{tot}$ = 2×10^{-5} M, [Na^{+}]$_{tot}$= 0.011 M; [CO$_3^{2-}$]$_{tot}$ = 0.012 M, [SO$_4^{2-}$]$_{tot}$ = 0.014 M; [Cl^{-}]$_{tot}$ = 0.03 M and [N]$_{tot}$ =5×10^{-5} M and using the code MEDUSA (Puigdomènech, 2010). The coloured areas represent the Eh and pH values measured in each well (S+number). The arrows show evolution with time or depth of the Eh-pH conditions in the studied wells.

35

36　Table A2. Carbon and chlorine isotopic composition values ($\delta^{13}C$ and $\delta^{37}Cl$, respectively, both in ‰) of different commercial carbon tetrachloride (CT), chloroform
37　(CF) and dichloromethane (DCM) suppliers.

Supplier	$\delta^{13}C$ (‰/PDB)	±1σ	n	Method*	Reference	$\delta^{37}Cl$ (‰/SMOC)	±1σ	n	Method*	Reference
CT										
Fluka	-54.3	0.09	4	EA-IRMS	this study	-4.11	0.07	2	GC-IRMS	Heckel et al. (2017)
unknown	-38.1	0.2	-	EA-IRMS	this study	-	-	-	-	-
Panreac	-40.5	0.1	2	EA-IRMS	this study	+0.27	0.08	2	GC-IRMS	Heckel et al. (2017)
unknown	-47.2	-	1	-	Holt et al. (1997)	-0.02	-	1	GC-IRMS	Holt et al. (1997)
unknown	-47.3	-	1	-	Holt et al. (1997)	-0.01	-	1	GC-IRMS	Holt et al. (1997)
CF										
Fluka	-48.7	0.1	4	EA-IRMS	this study	-3.0	0.2	17	GC-IRMS	Heckel et al. (2017)
Alfa	-47.88	0.08	5	-	Breider (2013)	-5.4	0.3	8	GC-IRMS	Breider (2013)
Acros	-48.6	0.3	5	-	Breider (2013)	-4.4	0.6	10	GC-qMs	Breider (2013)
Fisher	-51.5	0.22	3	-	Breider (2013)	-3.5	0.6	10	GC-qMs	Breider (2013)
Fisher	-53.23	0.09	4	EA-IRMS	this study	-	-	-	-	-
Sigma-Aldrich	-63.4	0.22	6	-	Breider (2013)	-	-	-	-	-
Sigma-Aldrich	-63.6	0.1	4	-	Breider (2013)	-	-	-	-	-
Acros	-49.8	0.08	4	EA-IRMS	this study	-	-	-	-	-
unknown	-51.7	0.4	2	-	Jendrzejewski et al. (2001)	+0.32	0.08	2	GC-IRMS	Jendrzejewski et al. (2001)
unknown	-43.2	-	1	-	Holt et al. (1997)	-1.5	-	1	GC-IRMS	Holt et al. (1997)
unknown	-43.3	-	1	-	Holt et al. (1997)	-1.5	-	1	GC-IRMS	Holt et al. (1997)
DCM										
unknown	-34.2	-	1	-	Holt et al. (1997)	+1.6	-	1	GC-IRMS	Holt et al. (1997)
unknown	-34.2	-	1	-	Holt et al. (1997)	+1.6	-	1	GC-IRMS	Holt et al. (1997)
unknown	-40.1	0.3	-	EA-IRMS	this study					
unknown	-40.4	0.5	4	-	Jendrzejewski et al. (2001)	-	-	-	-	-

38　*EA-IRMS= elemental analyzer coupled to an isotope ratio mass spectrometer, GC-qMS= gas cromatograph coupled to a quadrople mass spectometer; GC-IRMS= gas
39　cromatograph coupled to an isotope ratio mass spectrometer.

40

Table A3. Concentration (µM) of chlorinated ethenes (PCE, TCE, cDCE) and chlorinated methanes (CT, CF, DCM) over field campaings from wells S1, S3, S4, S6, S7, S8, S9 and S10 at different sampling depths (meters above sea level, m.a.s.l.). CS_2 concentration (µM) was only measured in Mar-13 and Nov-14 field campaigns. n.m.= not measured.

Well	Samplig depth of well (m.a.s.l.)	March 2010						November 2010						March 2013							November 2014						
		PCE	TCE	cDCE	CT	CF	DCM	PCE	TCE	cDCE	CT	CF	DCM	PCE	TCE	cDCE	CT	CF	DCM	CS₂	PCE	TCE	cDCE	CT	CF	DCM	CS₂
S1	426	3	49	0.1	2	38	0.04	n.m.	n.m.	n.m.	n.m.	n.m.	n.m.	3	27	0.3	0.7	10	0.2	0.03	0.4	8	2	0.2	9	0.1	n.m.
	424	n.m.	n.m.	n.m.	n.m.	n.m.	n.m.	n.m.	n.m.	n.m.	n.m.	n.m.	n.m.	3	31	0.2	0.5	9	0.2	0.02	0.2	6	1	0.1	6	0.1	n.m.
	422	2	36	0.1	1	25	0.04	n.m.	n.m.	n.m.	n.m.	n.m.	n.m.	3	33	0.2	0.7	10	0.1	0.03	0.02	6	1	0.2	6	0.1	n.m.
	420	2	45	0.1	0.8	21	0.02	n.m.	n.m.	n.m.	n.m.	n.m.	n.m.	3	27	0.2	0.5	11	0.1	0.02	0.2	6	1	0.1	5	0.1	n.m.
S3	425	37	104	11.3	98	139	4	22	145	55	117	203	8	40	68	39	23	56	1	0.3	6	25	84	20	32	6	n.m.
	423	n.m.	n.m.	n.m.	n.m.	n.m.	n.m.	n.m.	n.m.	n.m.	n.m.	n.m.	n.m.	44	70	42	24	61	2	0.2	4	22	70	62	55	16	0.2
	421	32	61	5	24	125	2	13	79	47	62	109	6	42	59	40	16	61	1	0.2	5	31	55	38	133	31	n.m.
	419	n.m.	n.m.	n.m.	n.m.	n.m.	n.m.	n.m.	n.m.	n.m.	n.m.	n.m.	n.m.	23	188	52	103	103	57	0.3	3	42	54	41	161	43	0.8
	417	5	64	19	17	151	60	19	103	93	40	236	64	13	150	39	38	111	102	0.2	2	37	30	23	187	63	n.m.
S4	425	n.m.	n.m.	n.m.	n.m.	n.m.	n.m.	n.m.	n.m.	n.m.	n.m.	n.m.	n.m.	14	41	0.4	27	39	0.04	0.01	16	60	<0.01	7	15	<0.01	n.m.
	423	n.m.	n.m.	n.m.	n.m.	n.m.	n.m.	n.m.	n.m.	n.m.	n.m.	n.m.	n.m.	18	51	0.3	30	32	0.02	<0.7	15	52	<0.01	7	12	<0.01	n.m.
	422	12	43	0.2	16	19	0.03	n.m.	n.m.	n.m.	n.m.	n.m.	n.m.	11	33	0.3	20	31	0.02	0.01	19	67	<0.01	1	7	<0.01	n.m.
	421	n.m.	n.m.	n.m.	n.m.	n.m.	n.m.	n.m.	n.m.	n.m.	n.m.	n.m.	n.m.	15	43	0.3	23	33	0.03	0.01	11	36	<0.01	1	5	<0.01	n.m.
	418	n.m.	n.m.	n.m.	n.m.	n.m.	n.m.	n.m.	n.m.	n.m.	n.m.	n.m.	n.m.	1	3	0.2	0.1	0.2	0.02	0.03	n.m.	n.m.	n.m.	n.m.	n.m.	n.m.	n.m.
	416	n.m.	n.m.	n.m.	n.m.	n.m.	n.m.	n.m.	n.m.	n.m.	n.m.	n.m.	n.m.	1	1	0.02	0.1	0.1	0.01	0.01	n.m.	n.m.	n.m.	n.m.	n.m.	n.m.	n.m.
	414	1	0	0.02	0.2	0.2	0.02	n.m.	n.m.	n.m.	n.m.	n.m.	n.m.	1	1	0.02	0.3	0.3	0.01	<0.7	n.m.	n.m.	n.m.	n.m.	n.m.	n.m.	n.m.
S6	421	n.m.	n.m.	n.m.	n.m.	n.m.	n.m.	n.m.	n.m.	n.m.	n.m.	n.m.	n.m.	2	6	41	0.2	4	<0.01	0.01	n.m.	n.m.	n.m.	n.m.	n.m.	n.m.	n.m.
	420	5	15	11	3	26	0.6	8	34	104	2	51	n.m.	n.m.	n.m.	n.m.	n.m.	n.m.	n.m.	n.m.	n.m.	n.m.	n.m.	n.m.	n.m.	n.m.	0.02
	419	n.m.	n.m.	n.m.	n.m.	n.m.	n.m.	n.m.	n.m.	n.m.	n.m.	n.m.	n.m.	3	7	65	0.2	5	0.03	<0.7	1	2	<0.01	0.03	0.2	0.1	0.02
	418	n.m.	n.m.	n.m.	n.m.	n.m.	n.m.	n.m.	n.m.	n.m.	n.m.	n.m.	n.m.	2	5	70	0.1	3	0.1	<0.7	2	2	<0.01	0.04	0.1	0.03	0.02
	416	3	12	9	3	20	0.7	4	18	80	0.6	23	n.m.	2	5	66	0.1	3	0.0	<0.7	2	2	<0.01	0.04	0.1	0.02	0.02
	414	n.m.	n.m.	n.m.	n.m.	n.m.	n.m.	n.m.	n.m.	n.m.	n.m.	n.m.	n.m.	2	5	53	0.1	1	0.0	<0.7	2	3	<0.01	0.1	0.3	0.05	0.02

46   Table A3. (cont.)

		μM																									
Samplig depth of well (m.a.s.l.)		March 2010						November 2010						March 2013							November 2014						
		PCE	TCE	cDCE	CT	CF	DCM	PCE	TCE	cDCE	CT	CF	DCM	PCE	TCE	cDCE	CT	CF	DCM	CS$_2$	PCE	TCE	cDCE	CT	CF	DCM	CS$_2$
S7	428	4	13	<0.01	176	92	2	3	22	0.1	200	227	<0.01	6	29	0.1	95	194	0.3	0.04	1	10	<0.5	376	245	11	n.m.
	426	n.m.	n.m.	n.m.	n.m.	n.m.	n.m.	n.m.	n.m.	n.m.	n.m.	n.m.	n.m.	4	21	0.1	199	298	0.4	0.02	<0.4	<0.5	<0.7	7	78	10	n.m.
	423	n.m.	n.m.	n.m.	n.m.	n.m.	n.m.	n.m.	n.m.	n.m.	n.m.	n.m.	n.m.	2	1	0.04	7	65	0.3	0.01	1	10	<0.5	449	255	11	n.m.
	421	1	1	0.02	3	16	17	1	0.4	<0.01	3	19	5	2	1	0.02	3	2	0.2	0.04	0.5	0.4	<0.04	7	4	0.8	n.m.
	418	n.m.	n.m.	n.m.	n.m.	n.m.	n.m.	n.m.	n.m.	n.m.	n.m.	n.m.	n.m.	3	1	0.03	8	2	0.02	0.04	0.8	0.5	<0.04	9	2	0.5	n.m.
S8	429	n.m.	n.m.	n.m.	n.m.	n.m.	n.m.	n.m.	n.m.	n.m.	n.m.	n.m.	n.m.	28	113	2	4	15	0.1	0.04	7	34	0.4	2	3	0.01	n.m.
	427	n.m.	n.m.	n.m.	n.m.	n.m.	n.m.	26	171	0.3	1	3	<0.01	36	165	0.7	3	5	0.02	0.04	9	42	0.4	1	4	0.03	n.m.
	424	n.m.	n.m.	n.m.	n.m.	n.m.	n.m.	n.m.	n.m.	n.m.	n.m.	n.m.	n.m.	27	161	0.8	2	6	0.02	0.02	6	43	0.4	2	5	0.05	n.m.
	422	n.m.	n.m.	n.m.	n.m.	n.m.	n.m.	n.m.	n.m.	n.m.	n.m.	n.m.	n.m.	9	129	1	0.2	6	0.1	0.01	2	35	0.3	1	3	0.07	n.m.
	420	n.m.	n.m.	n.m.	n.m.	n.m.	n.m.	1	32	0.3	<0.01	0.01	<0.01	3	60	7	0.04	0.1	0.01	0.01	n.m.	n.m.	n.m.	n.m.	n.m.	n.m.	n.m.
S9	418	6	51	7	0.9	9	n.m.	n.m.	n.m.	n.m.	n.m.	n.m.	n.m.	3	16	3	0.6	3	<0.01	<0.01	1	7	2	0.7	4	0.8	n.m.
	416	n.m.	n.m.	n.m.	n.m.	n.m.	n.m.	n.m.	n.m.	n.m.	n.m.	n.m.	n.m.	0.5	3	0.4	0.3	0.8	<0.01	<0.01	0.8	5	2	0.9	2	0.3	0.04
	414	n.m.	n.m.	n.m.	n.m.	n.m.	n.m.	n.m.	n.m.	n.m.	n.m.	n.m.	n.m.	0.6	3	0.4	0.3	0.7	<0.01	<0.01	2	<0.01	<0.01	0.8	2	0.2	0.02
	412	n.m.	n.m.	n.m.	n.m.	n.m.	n.m.	n.m.	n.m.	n.m.	n.m.	n.m.	n.m.	0.4	2	0.9	0.1	0.5	<0.01	<0.01	2	<0.01	<0.01	0.8	1	0.1	0.02
	410	n.m.	n.m.	n.m.	n.m.	n.m.	n.m.	n.m.	n.m.	n.m.	n.m.	n.m.	n.m.	0.1	0.6	1	0.03	0.1	<0.01	<0.01	n.m.	n.m.	n.m.	n.m.	n.m.	n.m.	n.m.
	408	0.5	3	1	0.03	0.03	n.m.	n.m.	n.m.	n.m.	n.m.	n.m.	n.m.	0.2	0.6	4	0.01	<0.01	<0.01	<0.01	n.m.	n.m.	n.m.	n.m.	n.m.	n.m.	n.m.
S10	419	n.m.	n.m.	n.m.	n.m.	n.m.	n.m.	n.m.	n.m.	n.m.	n.m.	n.m.	n.m.	0.1	1	2	0.1	0.3	<0.01	<0.01	n.m.	n.m.	n.m.	n.m.	n.m.	n.m.	n.m.
	417	n.m.	n.m.	n.m.	n.m.	n.m.	n.m.	0.1	3	11	0.02	0.07	<0.01	0.2	2	6	0.05	0.2	<0.01	<0.01	n.m.	n.m.	n.m.	n.m.	n.m.	n.m.	n.m.
	415	n.m.	n.m.	n.m.	n.m.	n.m.	n.m.	n.m.	n.m.	n.m.	n.m.	n.m.	n.m.	0.1	1	2	0.1	0.2	<0.01	<0.01	n.m.	n.m.	n.m.	n.m.	n.m.	n.m.	n.m.
	413	n.m.	n.m.	n.m.	n.m.	n.m.	n.m.	n.m.	n.m.	n.m.	n.m.	n.m.	n.m.	0.1	1	1	0.1	0.3	<0.01	0.01	n.m.	n.m.	n.m.	n.m.	n.m.	n.m.	n.m.
	411	n.m.	n.m.	n.m.	n.m.	n.m.	n.m.	n.m.	n.m.	n.m.	n.m.	n.m.	n.m.	0.1	1	1	0.1	0.2	<0.01	0.01	n.m.	n.m.	n.m.	n.m.	n.m.	n.m.	n.m.
	409	n.m.	n.m.	n.m.	n.m.	n.m.	n.m.	0.1	1	4	0.04	0.1	<0.01	0.1	1	1	0.1	0.2	<0.01	0.01	n.m.	n.m.	n.m.	n.m.	n.m.	n.m.	n.m.

47

48

Table A4. $\delta^{13}C$ (‰) of chlorinated methanes (CT, CF, DCM) over field campaigns from wells S1, S3, S4, S6, S7, S8, S9 and S10 at different sampling depths (meters above sea level, m.a.s.l.). SD corresponds to uncertainty of duplicates. n.d.= not detected; n.m.= not measured.

| | | $\delta^{13}C$ (‰) | | | | | | | | | | | | | | | | | | | | | |
| | Samplig depth of well (m.a.s.l.) | March 2010 | | | | | November 2010 | | | | | March 2013 | | | | | | November 2014 | | | | | |
		CT	SD	CF	SD	DCM	CT	SD	CF	SD	DCM	CT	SD	CF	SD	DCM	SD	CT	SD	CF	SD	DCM	SD
S1	426	n.m.		n.m.		n.m.	n.m.		n.m.		n.m.	n.d.		-27.6	0.1	n.d.		n.d.		-25	1	n.d.	
	424	n.m.		n.m.		n.m.	n.m.		n.m.		n.m.	n.d.		-27.7	0.3	n.d.		n.d.		-25.6	0.2	n.d.	
	422	-30.0	0.5	-32.8	0.3	n.m.	n.m.		n.m.		n.m.	n.d.		-29.0	0.1	n.d.		n.d.		-24.9	0.9	n.d.	
	420	n.m.		-33	2	n.m.	n.m.		n.m.		n.m.	-21.7	0.5	-27.0	0.5	n.d.		n.d.		-26.4	0.2	n.d.	
S3	425	-18.2	0.4	-33.8	0.2	n.m.	-20.9	0.9	-35.8	0.6		-14.2	0.4	-32.0	0.1	n.d.		-12.0	0.4	-35	2	n.d.	
	424	n.m.		n.m.		n.m.	n.m.		n.m.			-14.5	0.1	-32.0	0.1	n.d.		-10.3	0.3	-32.2	0.2	n.d.	
	421	-18.2	0.9	-34	1	n.m.	-20	1	-32.0	0.4		-15.30	0.10	-32.0	0.1	n.d.		-14.3	0.2	-35.3	0.7	n.d.	
	419	n.m.		n.m.		n.m.	n.m.		n.m.			-15.4	0.4	-31.8	0.1	-41	1	-14.2	0.1	-34.8	0.7	-36	1
	417	-14.7	0.8	-25.1	0.1	n.m.	-15.7	0.6	-24.9	0.3	n.m.	-13.3	0.4	-25.2	0.5	-40.1	0.2	-16.8	0.1	-32.1	0.3	-37.8	0.4
S4	425	n.m.		n.m.		n.m.	n.m.		n.m.		n.m.	-26.2	0.5	-32.9	0.4	n.d.		-26.7	0.1	-38.2	0.3	n.d.	
	423	n.m.		n.m.		n.m.	n.m.		n.m.		n.m.	-26.6	0.2	-33.8	0.6	n.d.		-27.3	0.1	-38.3	0.1	n.d.	
	422	n.m.		n.m.		n.m.	n.m.		n.m.		n.m.	-27.3	0.1	-35.0	0.2	n.d.		-28.2	0.3	n.d.		n.d.	
	421	n.m.		n.m.		n.m.	n.m.		n.m.		n.m.	-28.7	0.1	-35.6	0.2	n.d.		-28	1	n.d.		n.d.	
	419	n.m.		n.m.		n.m.	n.m.		n.m.		n.m.	n.d.		-40.8	0.1	n.d.		n.m.		n.m.		n.m.	
	414	n.m.		n.m.		n.m.	n.m.		n.m.		n.m.	-27.6	0.1	n.d.		n.d.		n.m.		n.m.		n.m.	
S6	421	n.m.		n.m.		n.m.	n.m.		n.m.		n.m.	n.d.		-27.5	0.5	n.d.		n.m.		n.m.		n.m.	
	420	-15.2	0.5	-29.1	0.2	n.m.	n.m.		-26.1	0.4		n.m.		n.m.		n.m.		n.m.		n.m.		n.m.	
	419	n.m.		n.m.		n.m.	n.m.		n.m.		n.m.	n.d.		-43.0	0.4	n.d.		n.m.		n.m.		n.m.	
	418	n.m.		n.m.		n.m.	n.m.		n.m.		n.m.	n.d.		-34	1	n.d.		n.m.		n.m.		n.m.	
	416	-13.8	0.4	-29.0	0.1	n.m.	n.m.		-23.8	0.3		n.d.		-44.2	0.5	n.d.		n.m.		n.m.		n.m.	
	414	n.m.		n.m.		n.m.	n.m.		n.m.		n.m.	n.d.		-44.6	0.5	n.d.		n.m.		n.m.		n.m.	
S7	428	-24.3	0.5	-30.5	0.5	n.m.	-26.9	0.6	-32.5	0.1	n.m.	-22.6	0.4	-29.2	0.3	n.d.		-22.7	0.1	-35.6	0.2	n.d.	
	426	n.m.		n.m.		n.m.	n.m.		n.m.		n.m.	-21.1	0.1	-29.1	0.1	n.m.		-22.0	0.1	-35.4	0.6	n.d.	
	423	n.m.		n.m.		n.m.	n.m.		n.m.		n.m.	-21.0	0.3	-21.4	0.2	n.d.		n.d.		-25.5	0.5	n.d.	
	421	-24	5	-18.3	0.5	n.m.	-26.8	0.6	-17.9	0.7	n.m.	-24.6	0.1	-23.8	0.7	n.d.		-25.2	0.4	-32	1	n.d.	
	418	n.m.		n.m.		n.m.	n.m.		n.m.		n.m.	-25.5	0.4	-29.0	0.1	n.d.		-25.4	0.1	-33.4	0.7	n.d.	
S8	429	n.m.		n.m.		n.m.	n.m.		n.m.		n.m.	-26.2	0.1	-26.3	0.4	n.d.		-26.8	0.5	-33.6	0.5	n.d.	
	427	n.m.		n.m.		n.m.	n.m.		n.m.		n.m.	-26.6	0.2	-24.7	0.1	n.d.		-28.6	0.5	-35.6	0.5	n.d.	
	424	n.m.		n.m.		n.m.	n.m.		n.m.		n.m.	-24.2	0.5	-25.0	0.4	n.d.		-28.1	0.5	-35.1	0.5	n.d.	
	422	n.m.		n.m.		n.m.	n.m.		n.m.		n.m.	n.d.		-24.3	0.1	n.d.		n.d.		-35.3	0.5	n.d.	
	420	n.m.		n.m.		n.m.	n.m.		n.m.		n.m.	n.d.		n.d.		n.d.		n.m.		n.m.		n.m.	
S9	418	n.m.		n.m.		n.m.	n.m.		n.m.		n.m.	-22.0	0.7	-38.8	0.2	n.d.		-19	1	-34.1	0.7	n.d.	
	416	n.m.		n.m.		n.m.	n.m.		n.m.		n.m.	-22.4	0.2	-40.7	0.5	n.d.		-21.3	0.4	-34.0	0.5	n.d.	
	414	n.m.		n.m.		n.m.	n.m.		n.m.		n.m.	-22.9	0.1	-40.1	0.5	n.d.		-19.6	0.5	-34.1	0.5	n.d.	
	412	n.m.		n.m.		n.m.	n.m.		n.m.		n.m.	n.d.		-33.5	0.3	n.d.		-20.6	0.6	-33.0	0.1	n.d.	
	410	n.m.		n.m.		n.m.	n.m.		n.m.		n.m.	n.d.		n.d.		n.d.		n.m.		n.m.		n.m.	
	408	n.m.		n.m.		n.m.	n.m.		n.m.		n.m.	n.d.		n.d.		n.d.		n.m.		n.m.		n.m.	
S10	419	n.m.		n.m.		n.m.	n.m.		n.m.		n.m.	n.d.		-38.9	0.3	n.d.		n.m.		n.m.		n.m.	
	415	n.m.		n.m.		n.m.	n.m.		n.m.		n.m.	n.d.		-37.9	0.1	n.d.		n.m.		n.m.		n.m.	
	413	n.m.		n.m.		n.m.	n.m.		n.m.		n.m.	n.d.		-40	2	n.d.		n.m.		n.m.		n.m.	
	411	n.m.		n.m.		n.m.	n.m.		n.m.		n.m.	n.d.		-38	1	n.d.		n.m.		n.m.		n.m.	
	409	n.m.		n.m.		n.m.	n.m.		n.m.		n.m.	n.d.		-38.7	0.1	n.d.		n.m.		n.m.		n.m.	

53   Table A5. $\delta^{37}Cl$ (‰) of CT and CF in March 2013 and November 2014 field campaings from wells S1,
54   S3, S4, S6, S7, S8 and S9 at different sampling depths (meters above sea level, m.a.s.l.). SD corresponds
55   to uncertainty of ten measurements to obtain each $\delta^{37}Cl$ value. n.d.= not detected; n.m.= not measured.

Samplig depth of well (m.a.s.l.)		March 2013			November 2014			
		CT	CF	SD	CT	SD	CF	SD
S1	426	n.a.	-3.7	0.5	6.2	0.4	-3.6	0.4
	424	n.a.	-3.8	0.5	6.4	0.5	-3.3	0.4
	422	n.a.	-3.9	0.6	6.2	0.4	-3.5	0.2
	420	n.a.	-3.8	0.5	6.8	0.4	-3.6	0.3
S3	425	n.a.	-0.6	0.3	7.3	0.3	-0.5	0.4
	424	n.a.	-0.6	0.1	7.0	0.3	0.2	0.6
	421	n.a.	-0.6	0.4	6.9	0.4	-0.7	0.4
	419	n.a.	-0.3	0.3	7.0	0.2	-0.6	0.3
	417	n.a.	1.3	0.3	6.8	0.5	0.4	0.5
S4	425	n.a.	n.a.		5.0	0.5	-2.9	0.2
	423	n.a.	n.a.		4.3	0.3	-2.7	0.5
	422	n.a.	n.a.		3.5	0.3	-2.5	0.5
	421	n.a.	n.a.		3.4	0.4	-2.5	0.4
S6	421	n.a.	n.a.		n.a.		n.a.	
	420	n.a.	n.a.		n.a.		n.a.	
	419	n.a.	n.a.		n.d.		n.d.	
	418	n.a.	n.a.		n.d.		n.d.	
	416	n.a.	n.a.		n.d.		n.d.	
	414	n.a.	n.a.		n.d.		n.d.	
S7	428	n.a.	-0.4	0.3	5.4	0.4	0.2	0.4
	426	n.a.	0.6	0.5	5.7	0.4	1.4	0.3
	423	n.a.	1.6	0.5	4.6	0.2	0.3	0.4
	421	n.a.	1.0	0.5	3.4	0.4	-0.3	0.4
	418	n.a.	-0.5	0.6	3.9	0.2	0.2	0.2
S8	429	n.a.	n.a.		4.8	0.3	-1.8	0.5
	427	n.a.	n.a.		4.9	0.2	-1.6	0.4
	424	n.a.	n.a.		5.1	0.4	-1.1	0.3
	422	n.a.	n.a.		4.6	0.4	-0.5	0.4
S9	418	n.a.	n.a.		5.9	0.3	-2.1	0.4
	416	n.a.	n.a.		4.8	0.3	-2.5	0.3
	414	n.a.	n.a.		6.3	0.5	-2.5	0.3
	412	n.a.	n.a.		6.3	0.4	-2.5	0.4

56

ISOTOPIC MASS BALANCE

58   Carbon isotopic mass balance ($\delta^{13}C_{SUM}$) was calculated from those CMs for which

59 isotopic values are available at each time following Eq.(A1) (Hunkeler et al., 1999; Aeppli et

60 al., 2010) in order to obtain the overall isotopic signature of the CMs in tank and in wells S3 and

61 S7 with high CMs concentrations which allow $\delta^{13}C$ measurements.

62 $$\delta^{13}C_{SUM} (‰) = \chi_{CT}\, \delta^{13}C_{CT} + \chi_{CF}\, \delta^{13}C_{CF} + \chi_{DCM}\, \delta^{13}C_{DCM} \tag{A1}$$

63   where χ is the molar fraction of each compound relative to the total molar CMs mass.

64 The uncertainty was determined by error propagation of Eq.(A1).

65   In order to investigate with more detail the processes controlling the isotopic composition

66 of CMs in S3 and S7 wells over time as well as to study CMs leaching processes during all the

67 studied campaigns, $\delta^{13}C_{SUM}$ was calculated and discussed in detail for both wells.

68   In S3, $\delta^{13}C_{SUM}$ was calculated using both available $\delta^{13}C_{CT}$ and $\delta^{13}C_{CF}$ data in the studied

69 campaigns. $\delta^{13}C_{DCM}$ data were only considered in the deepest level (417 m.a.s.l.) for Mar-13 and

70 Nov-14 due to data scarcity. $\delta^{13}C_{SUM}$ values of 425 and 421 m.a.s.l. reached similar values and

71 were relatively close to that of the tank (Fig. A2A). Moreover, in Mar-13, these values were also

72 similar to the $\delta^{13}C_{SUM}$ at 417 m.a.s.l. which included DCM, indicating the role of DCM as a by-

73 product of CT and CF degradation. However, in 2010, $\delta^{13}C_{SUM}$ values at 417 m.a.s.l. were more

74 enriched, suggesting the presence of DCM ($\delta^{13}C_{DCM}$ not available at that time) or other volatile

75 by-products not considered in the $\delta^{13}C_{SUM}$ calculation such as chloromethane, CO, CO_2, CH_4 or

76 CS_2. In contrast, in Nov-14, $\delta^{13}C_{SUM}$ values at 417 m.a.s.l. were more depleted than those of

77 Mar-13 and other levels (Fig.A2A), suggesting that less-degraded CMs leached from the

78 unsaturated zone might have reached the deepest parts of S3.

79   The lack of $\delta^{13}C_{CS2}$ and $\delta^{13}C_{DCM}$ values prevented their use for the $\delta^{13}C_{SUM}$ calculations

80 Eq.(A1) in S7, despite thiolytic reduction to CS_2 is expected to occur according to the obtained

81 Λ. $\delta^{13}C_{SUM}$ was calculated for those levels with $\delta^{13}C_{CT}$ and $\delta^{13}C_{CF}$ data for all the studied

82 campaigns (421 and 428 m.a.s.l). At 428 m.a.s.l., the $\delta^{13}C_{SUM}$ was quite stable during the

83 monitored time (-28±2‰). This value is within the range of $\delta^{13}C_{SUM}$ values for the upper part of

84 S3 well and relatively close to that of the tank before its removal (Fig.A2B). The similarity

85 between $\delta^{13}C_{SUM}$ values from S3, S7 and the tank could suggest both i) a similar compound

86 mixture of originally spilled CMs and ii) a relatively low fraction of other non-considered by-

87 products. In contrast, for the shallowest level (421 m.a.s.l.), in Mar-10, the $\delta^{13}C_{SUM}$ was 16‰

88 more enriched in ^{13}C compared to those at 428 m.a.s.l and in the tank source, whereas in Nov-14

89 a similar value was obtained.
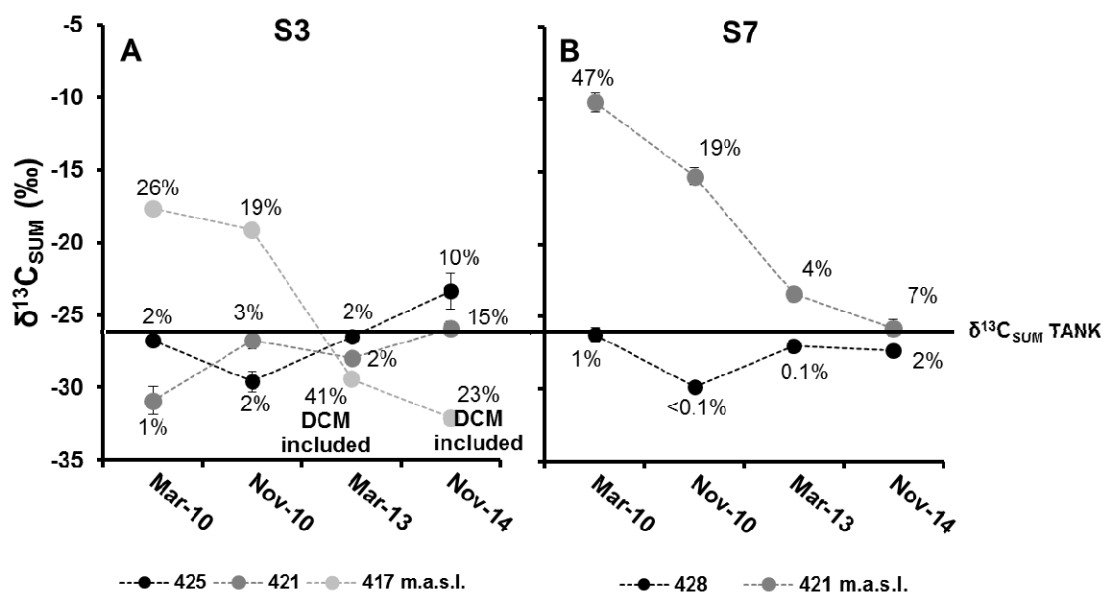
Figure A2. Carbon isotopic mass balance ($\delta^{13}C_{SUM}$) for S3 (A) and S7 (B) wells calculated at different sampling depths according to Eq.(A1). Due to the lack of $\delta^{13}C_{DCM}$ data, they were only included in S3 at 417 m.a.s.l. for Mar-13 and Nov-14 campaigns. The molar fraction of DCM (in percentage) is specified for each campaign and depth level. The horizontal black line represents the $\delta^{13}C_{SUM}$ measured in the tank source before its removal. In some cases, error bars are smaller than the symbols.

As for the same DCM percentage (19%, Nov-10) the $\delta^{13}C_{SUM}$ in S7 was more enriched than in S3, a higher proportion of other volatile compounds (e.g. CS_2), supporting the contribution of thiolytic reduction (Py, Fig.4) could be suggested. The clear trend towards lower values of DCM percentage and $\delta^{13}C_{SUM}$ over time suggests a continuous leaching of CT and CF mostly affecting the upper parts of S7 at the beginning and progressively reaching its deeper parts. This process is probably masking CMs degradation in S7 over time, which would be consistent with the concentrations evolution (Fig. 2).

The isotopic mass balance studies in these wells showed fluctuations over time which uncover different degradation and leaching processes.

REFERENCES

Aeppli, C., Hofstetter, T.B., Amaral, H.I.F., Kipfer, R., Schwarzenbach, R.P., Berg, M., 2010. Quantifying *in situ* transformation rates of chlorinated ethenes by combining compound-specific stable isotope analysis, groundwater dating, and carbon isotope mass balances. Environ. Sci. Technol. 44, 3705–3711. doi:10.1021/es903895b

Breider, F., 2013. Investigating the origin of chloroform in soils and groundwater using carbon and chlorine stable isotopes analysis. Thesis. Université de Neuchâtel (Switzerland).

Heckel, B., Rodríguez-Fernández, D., Torrentó, D., Meyer, A., Palau, J., Domènech, C., Rosell, M., Soler, A., Hunkeler, D., Elsner, D., 2017. Compound-specific chlorine isotope analysis of tetrachloromethane and trichloromethane by GC-IRMS vs. GC-qMS: Method development and evaluation of precision and trueness. Anal. Chem. 89, 3411–3420.

Holt, B.D., Sturchio, N.C., Abrajano, T.A., Heraty, L.J., 1997. Conversion of chlorinated volatile organic compounds to carbon dioxide and methyl chloride for isotopic analysis of carbon and chlorine. Anal. Chem. 69, 2727–2733. doi:10.1021/ac961096b

Hunkeler, D., Aravena, R., Butler, B.J., 1999. Monitoring microbial dechlorination of tetrachloroethene (PCE) using compound-specific carbon isotope ratios: Microcosms and field experiments. Environ. Sci. Technol. 33, 2733−2738. doi:10.1021/es981282u

Jendrzejewski, N., Eggenkamp, H.G.M., Coleman, M.L., 2001. Characterisation of chlorinated hydrocarbons from chlorine and carbon isotopic compositions: Scope of application to environmental problems. Appl. Geochemistry 16, 1021–1031. doi:10.1016/S0883-2927(00)00083-4

Puigdomènech, I., 2010. MEDUSA (Make Equilibrium Diagrams Using Sophisticated Algorithms) Windows interface to the MS-DOS versions of INPUT, SED and PREDOM (FORTRAN programs drawing chemical equilibrium diagrams).

Annex H. Other publications derived from this thesis

UNRAVELLING CHLORINATED METHANES DEGRADATION PROCESSES IN A COMPLEX POLLUTED AQUIFER BY ISOTOPIC AND MOLECULAR TOOLS

Diana Rodríguez-Fernández[1], Mònica Rosell[1], Clara Torrentó[1], Carme Audí-Miró[1], Massimo Marchesi[1,2], Miriam Guivernau[3], Marc Viñas[3], Neus Otero[1], Albert Soler[1]

1. Grup de Mineralogia Aplicada i Medi Ambient. Facultat de Geologia, Universitat de Barcelona, Barcelona, Spain.
2. Department of Earth & Environmental Sciences, University of Waterloo, Ontario, Canada.
3. GIRO Joint Research Unit IRTA-UPC, IRTA, Caldes de Montbuí, Spain

✉ diana.rodriguez@ub.edu ; monica.rosell@ub.edu

BACKGROUND and METHODOLOGY

Figure 1. A) Location map with target well (S3) in red B) S3 lithostratigraphic log and C) flow through cell sampling

A)
B)
C)

m.b.g.s

Anthropic refill of sand and gravel
Concrete

Brown sandstone
Brown limestone
Altered yellow marl and fine sand beds

Blue-grey limestone
Water table March 2013
Blue-grey limestone

Blue-grey marl
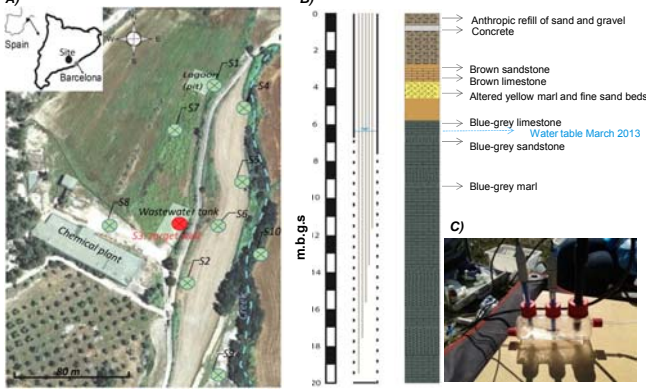
This study seeks to improve the understanding of chloroform (CF) and carbon tetrachloride (CT) degradation pathways in a fractured bedrock aquifer in Barcelona (Spain) contaminated with a complex mixture of chlorinated organic compounds due to the activity of a former chemical plant (1978-1985). This poster is focused in a highly contaminated hot spot (multilevel S3) located near the former wastewater tank which was removed in 2006.

In order to better understand the degradation processes affecting the complex mixture of VOCs in the field and to evaluate the impact of different biostimulation strategies on the indigenous microbial community composition, the following items were carried out:

METHODOLOGY
- Anaerobic microcosm experiments with slurry from the bottom of S3
- VOCs CSIA, concentration and geochemical data from 5 sampling depths of S3 during 3 sampling campaigns
- Microbial community analysis (DGGE and qPCR)
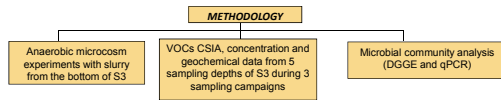
FIELD CAMPAINGS RESULTS

Figure 3. Redox conditions at five sampling depths from March 2013 field campaign (redox assignments criteria according to McMahon and Capelle, 2008)

S   SO₄²⁻   Mn   NO₃⁻   DO   Fe

Oxic-anoxic / sulfate reduction
Oxic-anoxic / sulfate reduction
Anoxic /nitrate and sulfate reduction
Anoxic /nitrate and sulfate reduction
Anoxic /sulfate reduction
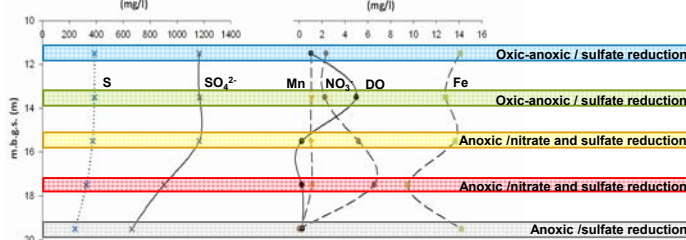
Figure 4. Variations in depth of CF and CT concentrations and $\delta^{13}C$ for the three sampling campaigns. DCM and CS₂ concentrations are included for November 2010 and March 2013. The biodegradation of the CF (*B_CF (%)) is calculated.

March 2010

CF Concentration (mg/l)   CT Concentration (mg/l)

$B_{CF}=0.3\%$
$B_{CF}=27\%$

November 2010

DCM (mg/l)	CS₂ (mg/l)
0.69	n.d.
0.47	n.d.
5.42	n.d.

$B_{CF}=9\%$
$B_{CF}=23\%$

March 2013

DCM (mg/l)	CS₂ (mg/l)
0.11	0.04
0.14	0.03
0.13	0.03
4.8	0.03
8.7	0.02

$B_{CF}=0.1\%$
$B_{CF}=0.1\%$
$B_{CF}=0.9\%$
$B_{CF}=21\%$
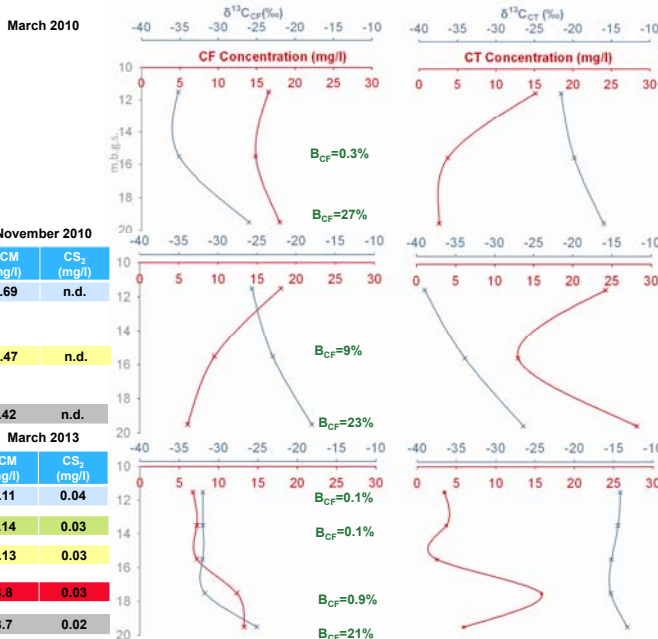
*B(%) represents the CF concentration decrease in depth assuming no mixing and the degradation process observed in the microcosm experiments (ε=-30‰). The initial $\delta^{13}C_{CF}$ value is assumed the most negative one at each sampling campaign.

n.d. means not determined

MICROCOSM EXPERIMENTS RESULTS

Microcosm experiments were set up in batch using a homogeneous slurry (groundwater and sediments from the bottom of S3 well) as inoculum. Three treatments were tested under anoxic conditions - (1) lactate, (2) methanol and (3) acetate-, together with two types of controls- (4) live control and (5) autoclaved control-, all of them with and without vitamin B₁₂ as bacterial corrinoid model compound or redox-active molecule (10 μM). The microcosms were incubated statically during 197 days, in the dark at room temperature and monitored regularly for concentration and carbon isotopic composition (when possible) of the main pollutants.

Figure 2. A) Mass balance for each treatment B) Chloroform carbon isotopic fractionation in live microcosms containing vitamin B₁₂ after 197 days

A)   Molar fraction vs. initial (%)

CS2
DCM
CF
CT

B)
CO2B-6
AC1B-6
ME1B-6
CO1B-6

$y = -0.03x - 0.0002$
$R^2 = 0.985$
$\varepsilon_{CF} = -30‰$

$\ln R_t/R_0$
$\ln C_t/C_0$
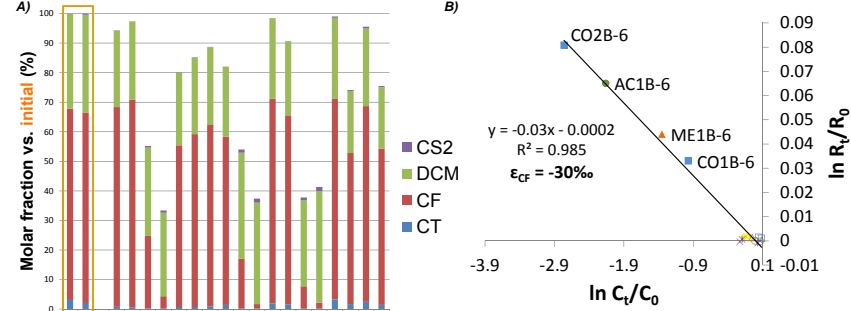
☞ Isotopic composition and concentration of chlorinated ethenes and toluene remained constant along the microcosm experiment.

PRELIMINARY MICROBIOLOGICAL RESULTS

Microbial community analysis in November 2010 revealed the presence of dehalorespiring bacteria (Desulfitobacterium and Dehalobacter genus) but the absence of Dehalococcoides-like bacteria neither its related reductive dehalogenases (vcrA, bvcA, tceA genes) in slurry from S3. In the microcosm experiments, relative amounts of eubacteria and archaeal were compared after 197 days in the different treatments versus the initial S3 pool (sampled in June 2012) by molecular tools (DGGE and qPCR).

Figure 5. 16SrRNA-based DGGE profile (V3-V5 region) A) Eubacterial population B) Archaeal population

A)

Porphyromonadaceae (Bacteroidia)
Unclassified bacteria
Pseudomonadaceae (g-Proteobacteria)
Rhodobacteraceae (α-Proteobacteria)

B)
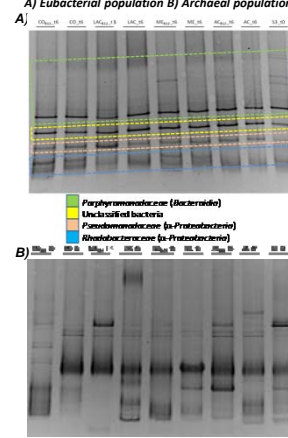
Figure 6. qPCR 16SrRNA gene of eubacterial population

C)   16SrRNA gene copies·ml⁻¹
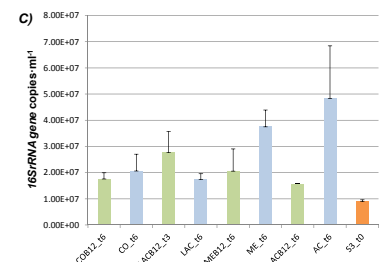
☞ The genes encoding the known reductive dehalogenases (vcrA, bvcA, tceA) of Dehalococcoides were not detected in any sample after 197 days.

☛ Pending tasks:
- Sequencing selected bands of the 16SrRNA-based DGGE
- Optimization of eubacterial DGGE in order to improve phylogenetic identification.
- qPCR of the CfrA gene (specific dehalogenase described for Dehalobacter sp. capable of CF dechlorination according to Tang and Edwards 2013)

CONCLUSIONS

- In microcosm experiments, the consumption of the added electron donors did not show any apparent biostimulating effect on the degradation of the target compounds.

- All live-cultures showed significant decrease of CT along the incubation accompanied of carbon isotopic fractionation (data not shown). Vitamin B₁₂ catalyzed CT conversion rate with consequent accumulation of high amounts of CS₂. In contrast, CF degradation only occurred in the presence of vitamin B₁₂. The observed fractionation of CF (-30‰) was similar to the one found recently by Chan et al., 2012 in Dehalobacter-containing cultures (-27.5‰). No apparent accumulation of other chlorinated intermediates (DCM) was observed in any experiment. Other studies reported that vitamin B₁₂ enhances the transformation of CF to CO and CO₂ (Becker and Freedman, 1994) and catalyzes CS₂ production from CT degradation under sulfate reducing conditions (Koenig et al., 2012).

- The number of Eubacterial 16SrRNA gene copies slightly increased in all the microcosms respect initial time. The different treatments seem to lead to significant changes in the archaeal composition, whereas the eubacterial community did not change significantly.

- At the deepest S3 sampling point, the most significant changes in the δ13C for CT and CF were observed among the three campaigns, coincidently with the most anoxic and sulfate reducing conditions and highest DCM concentrations. DCM accumulation might be related to CF dehalorespiration by Dehalobacter-like bacteria (Lee et al., 2012) or to CF cometabolic dechlorination (Cappelletti et al., 2012). The absence of DCM accumulation in the microcosm experiments could be explain by further DCM fermentation to H₂, CO₂ and acetate (Lee et al., 2012) although further research is needed.

- The presence of variable amounts of CS₂ at the studied well together with CT degradation evidences and sulfate reducing conditions are coherent with CT biodegradation under sulfate reducing conditions in presence of B₁₂ and ferric oxide described by Koenig et al., 2012.

REFERENCES

- Becker, J.G., Freedman, D.L., 1994. Use of cyanocobalamin to enhance anaerobic biodegradation of chloroform. Environ Sci Technol 28, 1942-1949
- Cappelletti, M., Frascari, D., Zannoni, D., Fedi, S., 2012. Microbial degradation of chloroform. Appl. Microbiol. Biotechnol. 96, 1395-1409.
- Chan, C.C., Mundle, S.O., Eckert, T., Liang, X., Tang, S., Lacrampe-Couloume, G., Edwards, E.A., Sherwood Lollar B., 2012. Large Carbon Isotope Fractionation during Biodegradation of Chloroform by Dehalobacter Cultures. Environ. Sci. Technol. 46 (18), 10154−10160.
- Koenig, J.C., Lee, M.J., Manefield, M., 2012. Successful microcosm demonstration of a strategy for biodegradation of a mixture of carbon tetrachloride and perchloroethene harnessing sulfate reducing and dehalorespiring bacteria. Journal of Hazardous Materials 219– 220, 169– 175.
- Lee, M., Low, A., Zemb, O., Koenig J., Michalsen A., Manefield, M. 2012. Complete chloroform dechlorination by organochlorine respiration and fermentation. Environ Microbiol , 14, 883-894.
- McMahon, P.B., Chapelle, F.H., 2008, Redox Processes and Water Quality of Selected Principal Aquifers, Ground Water, 46(2), 259-271.
- Tang, S., Edwards, E.A., 2013. Identification of Dehalobacter reductive dehalogenases that catalyze dechlorination of chloroform, 1,1,1-trichloroethane and 1,1-dichloroethane. Phil.Trans. R. Soc. B 368, 20120318

Acknowledgments

LONG-TERM MONITORING OF THE EVOLUTION OF THE CHLORINATED VOCs POLLUTION IN A FRACTURED BEDROCK AQUIFER USING CSIA

Diana Rodríguez-Fernández[1], Mònica Rosell[1], Clara Torrentó[1], Carme Audí-Miró[1], Massimo Marchesi[1, 2],
Jordi Palau [1,3], Neus Otero[1], Albert Soler[1]

1. Grup de Mineralogia Aplicada i Medi Ambient. Facultat de Geologia, Universitat de Barcelona, Barcelona, Spain.
2. Department of Earth & Environmental Sciences, University of Waterloo, Ontario, Canada.
3. Centre d'hydrogéologie et de géothermie, Université de Neuchâtel, Neuchâtel, Switzerland.

✉ diana.rodriguez@ub.edu

BACKGROUND

Figure 1. A) Location map with multilevel wells and the A-A' cross-section B) Sources removal works in 2006 C) Flow –through cell for water sampling

An unconfined fractured bedrock aquifer with low permeability and polluted with a complex mixture of chlorinated organic compounds is located in a former industrial area.

An underground wastewater tank and a disposal lagoon were identified as the main contaminant sources and were removed in 2006 as an early measure for contamination mitigation.

The A-A' cross section has been chosen as an example of the lithology, redox conditions and evolution of the plume in the studied site because it includes the well (S3) which was built in one of the pollution sources (the wastewater tank) and the only well (S10) located at the left side of the creek. Furthermore, homogeneous slurry (groundwater and sediments) from the bottom of S3 was used as an inoculum to perform batch microcosm experiments. Degradation of chloroform (CF) was observed and the calculated **fractionation of CF** (ε_{CF}:-30‰) was similar to the one found recently by Chan et al., 2012 in Dehalobacter-containing cultures (-27.5‰). CS_2 appeared as a by-product of the CT degradation. No chlorinated ethenes degradation was observed probably due to the inhibition caused by the toxic effects of carbon tetrachloride (CT) dechlorination products and free sulfide.

Figure 2. A) Redox conditions in A-A' cross section, S3 well includes $\delta^{34}S$-SO_4 (‰) data in italics B) Redox conditions at five sampling depths of S3 well in March as an example of redox assignments criteria according to McMahon and Capelle, 2008 C) A-A' lithostratigraphic cross-section along the groundwater flow system D) Microcosm experiments with S3 bottom slurry

ε_{CF} = -30‰

☞ For further information about the chlorinated methanes degradation: Rosell et al. talk (9:45 h, 27th Friday ORG-CONT session)

☞ **OBJECTIVES:** Assess the effectiveness of the sources removal as well as to shed light on natural attenuation processes

A long-term monitoring was performed from 2006 to 2013 distributed in seven field campaigns which included:

METHODOLOGY

- CSIA COUPLED WITH CONCENTRATION DATA OF VOCs
- CHEMICAL DATA (ANIONS, CATIONS, DOC, DIC)
- PHYSICOCHEMICAL PARAMETERS (TEMPERATURE, Eh, pH, CONDUCTIVITY, DO, WATER LEVEL)

COMPARING FIELD CAMPAIGNS RESULTS

The pollution derived from the manufacture of phytosanitary products and chemical compounds of a textile industry between 1978 and 1985. The main contaminants are a variety of chlorinated VOCs (chlorinated ethenes, ethanes, methanes and chlorobenzenes) with traces of BTEX and pesticides.

Figure 3. Chlorinated methanes concentration (µg/L) and isotopic data (δ13C;‰): evolution after three years in three selected wells. CF (chloroform), CT (carbon tetrachloride), DCM (dichloromethane). b.d.l. means below detection limit

| | \multicolumn{5}{c}{2010} | \multicolumn{5}{c}{2013} |
	CT	δ13C_CT	CF	δ13C_CF	DCM	CT	δ13C_CT	CF	δ13C_CF	DCM
S1-12	370	-32.9	45827	-33.3	3	108	b.d.l.	1199	-27.6	13
S1-13.5						81	b.d.l.	1100	-27.7	14
S1-15.5	149	-30.0	3002	-32.8	3	101	b.d.l.	1178	-29.0	5
S1-17.5	128	b.d.l.	2559	-32.8	2	75	-21.7	1278	-27.0	5
S3-11.5	15139	-18.2	16548	-33.8	380	3467	-14.2	6741	-32.0	113
S3-13.5						3717	-14.5	7244	-32.0	142
S3-15.5	3720	-18.2	14863	-33.8	134	2500	-15.3	7255	-32.0	126
S3-17.5						15827	-15.4	12312	-31.8	4802
S3-19.5	2619	-14.7	17984	-25.0	5103	5896	-13.3	13247	-25.2	8705
S6-9.5	397	-15.2	3125	-29.1	52	26	b.d.l.	435	-28.0	0
S6-11						18	b.d.l.	561	-43.0	3
S6-12.5						23	b.d.l.	354	-33.6	7
S6-14.5	3418	-13,8	2426	-29.0	60	11	b.d.l.	322	-44.2	4
S6-17.5						32	b.d.l.	155	-44.6	1

☞ The presence of diverse amounts of CS_2 in all samples might be explained as by-product related with chlorinated methanes degradation

Figure 4. Chlorinated methanes evolution from 2010 to 2013.
A) Red spots show CF concentration (µg/l) of the most polluted depth in each multilevel well in 2010 and its evolution in 2013. Isoconcentration lines show the sum of the average concentration (mM) of each chlorinated methane compound (CF, CT, DCM) in each multilevel well.
B) Transect A-A' with CF concentration and carbon isotopic data (δ13C CF) in italics along the plume for both 2010 and 2013, the depth is expressed in meters above sea level (m.a.s.l.).
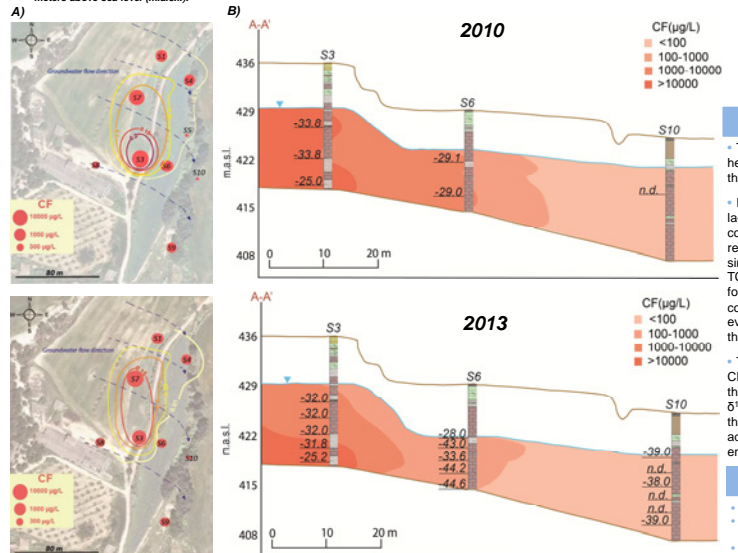

Figure 5. Chlorinated ethenes evolution from 2006 to 2013.
A) Green spots show TCE concentration (µg/l) of the most polluted depth in each multilevel well in 2006 and its evolution in 2013. Isoconcentration lines show the sum of the average concentration (mM) of each chlorinated ethene compound (PCE (perchloroethylene), TCE (trichloroethylene), cDCE (cis-dichloroethylene)) in each multilevel well.
B) Transect A-A' with TCE concentration and carbon isotopic data (δ13C_TCE) in italics along the plume for both 2006 and 2013.
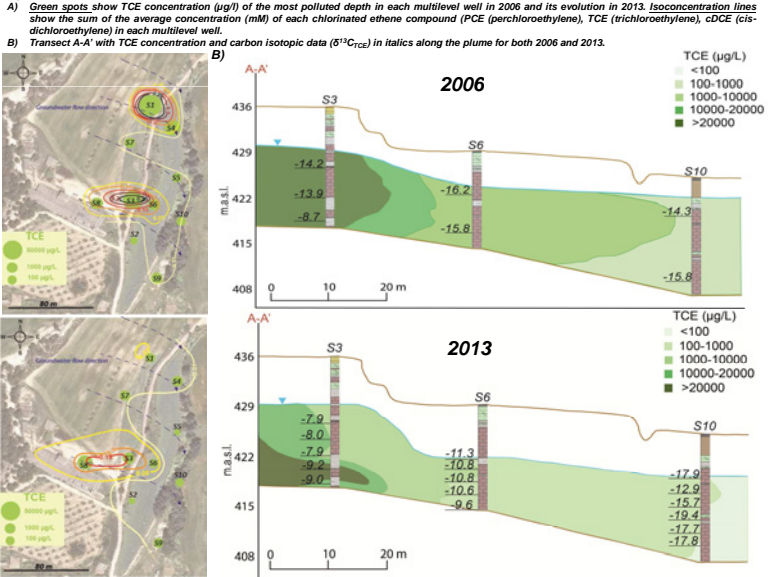
CONCLUSIONS

• The removal of the sources has produced a concentration decrease in most of the pollutants. Although the studied site has a complex heterogeneous nature, widespread shifts in carbon isotopic data (δ13C) along the time indicate also extensive natural attenuation processes. Few of the target pollutants increased throughout the time (e.g. DCM) probably due to the fact they are metabolites of different degradation pathways.

• Regarding the molar sum of chlorinated ethenes, an important reduction has been observed in all the target area, being more drastic in the former lagoon area (S1). The presence of higher amounts of CT and CF (well-known as ethenes inhibitors) in the ancient wastewater tank area (S3) in comparison with the lagoon (S1) might be the responsible of the differences between these zones. The PCE concentration and δ13C_PCE seem to remain quite constant along the time (data not shown), whereas the cross-section shows that TCE concentrations have been reduced along the plume since the source removal. Moreover, a significant enrichment in the δ13C_TCE in S3 and S6 wells from 2010 to 2013 indicates the degradation of the TCE. In turn, the TCE metabolite, cDCE, has also reduced its concentration over the time and slightly more positive values of δ13C_cDCE have been found in these two wells showing its further degradation (data not shown). The most δ13C_TCE negative values in S10 found after these 7 years might correspond to the initial TCE which reached the oxic fringe of the plume without much degradation. Taking all this into account, accompanied by the evolution of redox conditions across the studied A-A' cross-section, lead to suspect that reductive dechlorination processes are taking place closer to the former sources. To quantify the extent of these processes a site-specific isotopic fractionation for each chlorinated ethene involved is required.

• The molar sum of chlorinated methanes shows a decrease much less evident than the chlorinated ethenes. In addition, slight decreases in CT and CF are observed only in S3 and S6 wells, accompanied by a certain enrichment in δ13C_CT and δ13C_CF values. More negative δ13C_CF values in S6 throughout the time and also along the groundwater flow (S10) were observed. This fact might be explained by the influence of CT degradation on the δ13C of its metabolite, CF. Spatial and temporal accumulation of DCM is more obvious in S3 well, but its concentration decreased along the plume. All these data suggest also chlorinated methanes reductive dechlorination closer to the former source where the redox conditions are more favourable. In addition, significant amounts of CS_2 at the studied wells together with CT degradation evidences and sulphate reducing conditions (supported by enrichment of $\delta^{34}S_{SO4}$ in depth) are coherent with the results observed in our microcosm experiments and the ones found by Koenig et al., 2012.

REFERENCES

• Becker, J.G., Freedman, D.L., 1994. Use of cyanocobalamin to enhance anaerobic biodegradation of chloroform. Environ Sci Technol 28, 1942-1949
• Chan, C.C., Mundle, S.O., Eckert, T., Liang, X., Tang, S., Lacrampe-Couloume, G., Edwards, E.A., Sherwood Lollar B., 2012. Large Carbon Isotope Fractionation during Biodegradation of Chloroform by Dehalobacter Cultures. Environ. Sci. Technol. 46 (18), 10154–10160.
• Koenig, J.C., Lee, M.J., Manefield, M., 2012. Successful microcosm demonstration of a strategy for biodegradation of a mixture of carbon tetrachloride and perchloroethene harnessing sulfate reducing and dehalorespiring bacteria. Journal of Hazardous Materials 219– 220, 169– 175.
• McMahon, P.B., Chapelle, F.H., 2008, Redox Processes and Water Quality of Selected Principal Aquifers, Ground Water, 46(2), 259-271.

Acknowledgments

Evaluating potential chlorinated methanes degradation mechanisms and treatments in interception trenches filled with concrete-based construction wastes

Diana Rodríguez-Fernández[1], Clara Torrentó[1,2], Mònica Rosell[1], Carme Audí-Miró[1] and Albert Soler[1]

1. Grup de Mineralogia Aplicada i Medi Ambient. Facultat de Geologia, Universitat de Barcelona, Barcelona, Spain.
2. Centre d'hydrogéologie et de géothermie, Université de Neuchâtel, Neuchâtel, Switzerland.

✉ diana.rodriguez@ub.edu

STUDY OBJECTIVES

This study seeks:

✓ to improve the understanding of CT (and CF) degradation mechanisms/processes that are taking place in our field interception trenches filled with concrete-based construction wastes.

✓ to select between the two most effective chemical oxidation remediation treatments (persulfate and permanganate) taking into account their efficiency respect the chlorinated methanes removal, the generated acute toxicity and the applicability of the carbon isotopic fractionation as an indicator of the effectiveness of the future in situ remediation.

FIELD SITE BACKGROUND

A complex mixture of chlorinated organic compounds plume is located in an unconfined carbonated bedrock aquifer in a former industrial area next to Barcelona (NE Spain). The site exhibited an especially high complexity due to the presence of multiple contaminant sources, wide variety of pollutants (mainly chlorinated ethenes but also chlorinated methanes such as chloroform (CF) and carbon tetrachloride (CT)) and a low permeability matrix with conductive fractures and fissures.

In 2006, the sources were removed and, in their place, recycled concrete-based aggregates from a construction and demolition waste recycling plant were used for creating alkaline conditions (pH 11.6 ± 0.3) which could treat the accumulated contaminated recharge water before reaching the aquifer.

A) Location map with groundwater multilevel wells and the current trenches

B) Sampling wells installed in the trenches

C) Confirmed and hypothetical processes taking place in the trenches. * Experiments published in Torrentó et al. (2014).

STARTING POINT

Regarding isotopic results, negligible changes in δ13C values of TCE and PCE in the two trenches were found. However, δ13C-CT and CF values showed significant enrichment during two recharge periods in both trenches. CT transformation in the trenches is therefore occurring, especially in the tank trench. However, alkaline hydrolysis of CT, in contrast to CF, is theoretically extremely slow.

	by ALKALINE HYDROLYSIS	by Fe MINERALS
CT DEGRADATION	HYPOTHESIS DISCARDED* ⊠ high adsorption of CT on the concrete particles (73% after 50 days) with invariability of its δ13C values.	ONGOING HYPOTHESIS ?
CF DEGRADATION	HYPOTHESIS CONFIRMED* ☑ CF carbon isotopic fractionation εC (–53 ± 3‰).	ONGOING HYPOTHESIS ?

CT DEGRADATION HYPOTHESIS

Significant CT isotopic fractionation observed in the interception trenches could point out the occurrence of other degradation processes distinct than alkaline hydrolysis. Abiotic dehalogenation of CT by Fe(II) present at the surface of different iron minerals might take place.

PROVE 1: Geochemical speciation modelling using the code PHREEQC showed that water collected at the trenches is supersaturated with respect to several iron oxy-hydroxide.

H) Diagram of predominance area of Fe solid phases with the anion and cation data of the trench ([CO₃²⁻]total= 10μM; [Na⁺] total= 7.3 mM; [Ca²⁺]total= 7.5μM; [Cl⁻] total= 5.2 mM; [PO₄³⁻]total=9.8 mM; [SO₄²⁻]total=9.2 mM; [NO₃⁻]total=0.18 mM. In grey, if precipitation of goethite is not allowed. The solid circle indicates the trench conditions.
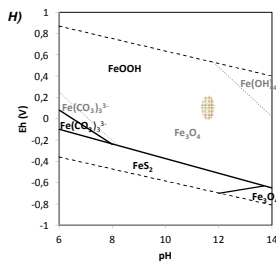
PROVE 2: The study of gravel samples by SEM-EDS shows presence of iron patinas growth on top of the gravel minerals surface as well as X-ray fluorescence (XRF) study of some gravel lithology shows variable iron amounts.

Calcite-Ankerite	Wt%	St error
CaO	79.69	0.09
Fe₂O₃	10.55	0.10
SiO₂	6.65	0.18
MgO	1.33	0.06
MnO	0.83	0.04
Others	0.86	
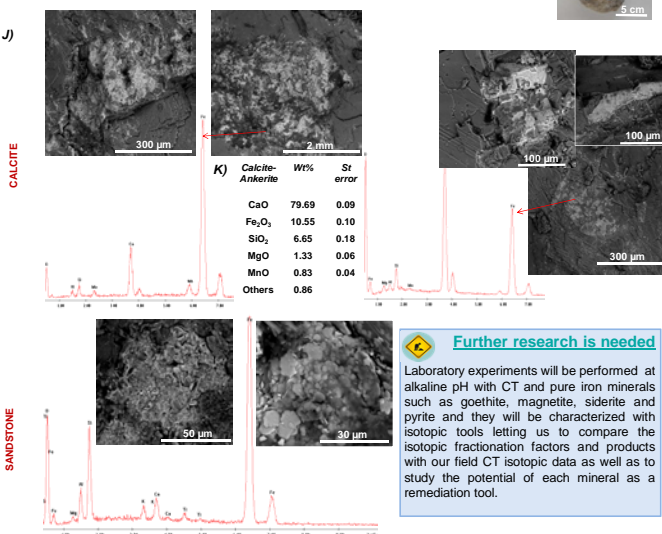
Further research is needed

Laboratory experiments will be performed at alkaline pH with CT and pure iron minerals such as goethite, magnetite, siderite and pyrite and they will be characterized with isotopic tools letting us to compare the isotopic fractionation factors and products with our field CT isotopic data as well as to study the potential of each mineral as a remediation tool.

I) Iron patina growth in a concrete gravel of the tank trench saturated zone.
J) SEM images of iron patinas in calcite-ankerite (above) and a sandstone (below) found among gravels and its qualitative elemental composition analysis by SEM-EDS. The brightest zones correspond to iron minerals.
K) Wt% compound of a calcite-ankerite as an example of lithology with high presence of iron analyzed by XRF.

INTERCEPTION TRENCHES

2006: sources removal and interception trenches filled with concrete-based recycled construction wastes

2010-2013: water trenches sampling and monitoring

D) Secuential images of pollution sources removal and construction of current trenches.

E) Schematic representation of proposed hydrogeological performance of the interception trenches. Rainwater lixiviates contaminants retained in the unsaturated zone and infiltrates to the trenches. The water table level of trenches represents the minimum level.
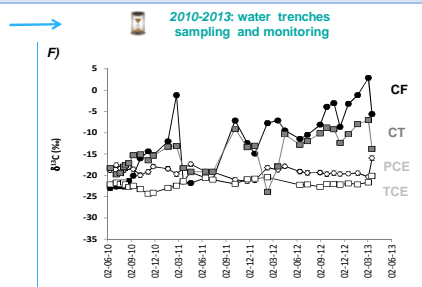
F) Evolution of δ13C-CSIA in the tank trench from 2010 to 2013

2014: gravel samples extraction to study CT degradation processes

G) Images of the bore hole performed on March 2014 in order to obtain gravel samples of the non-saturated and the saturated zone (the last ones were preserved into trench water). These samples are being characterized by SEM-EDS, XRF and X-ray diffraction with the aim of use the real material of the trenches in future lab experiments.

ISCO TO ENHANCE CHLOROMETHANES DEGRADATION?

Would the combination of alkaline conditions in trenches (pH 11.6 ± 0.3) with in situ chemical oxidation (ISCO) be able to remove the chloromethanes? Preliminary batch experiments were performed in our group to evaluate the feasibility of different chemical oxidation reactions (permanganate, persulfate, hydrogen peroxide and Fenton) on the complex contaminated recharge water which were, in general, more effective for degrading the chlorinated ethenes than for the chlorinated methanes (Torrentó et al. EGU 2012). Batch experiments at ambient temperature with trench water buffered by NaOH were performed at different oxidant concentration of potassium permanganate and sodium persulfate but it was found that only persulfate (in combination with alkaline hydrolysis, pH 13.19 ± 0.35) was able to degrade CF. None ISCO treatment neither alkaline hydrolysis has been found to enhance CT degradation.

PERMANGANATE+ alkaline hydrolysis			PERSULFATE+ alkaline hydrolysis		
MICROTOX colour corrected as Ashworth et al. (2010)			MICROTOX		
1 g/L	5 min (Equitox·m⁻³)	15 min (Equitox·m⁻³)	10 g/L	5 min (Equitox·m⁻³)	15 min (Equitox·m⁻³)
	301 ± 5	678 ± 68		No data	No data
5 g/L	5 min (Equitox·m⁻³)	15 min (Equitox·m⁻³)	20 g/L	5 min (Equitox·m⁻³)	5 min (Equitox·m⁻³)
	1468 ± 185	4397		287 ± 18	296 ± 22
Degradation (by Δδ13C)			Degradation (by Δδ13C)		
CF	⊠		CF	☑	
CT	⊠		CT	⊠	

L) The table shows the MICROTOX® (a standardized toxicity test system which employs the bioluminescent marine bacterium (Vibrio fischeri) as the test organism) values of each treatment after 22 days of experiment, the initial values are always below 15 Equitox · m-3. Above, it is shown the effectiveness of each treatment for CF and CT regarding the presence or not of significant isotopic shifts along time.

Effect of combination of alkaline hydrolysis and different concentrations of persulfate in chloroform degradation in trench water

CF degradation by a persulphate concentration of 20 g/L — CF degradation by a persulfate concentration of 10 g/L

$$\varepsilon_{CF-ISCO+ALK.HIDR.} = -24 ± 2 ‰$$
$$\varepsilon_{CF-ALK.HIDR.} = -32 ± 3 ‰$$

y = -0,0239x + 0,0005
R² = 0,9726

$$\varepsilon_{CF-ISCO+ALK.HIDR.} = -32 ± 2 ‰$$
$$\varepsilon_{CF-ALK.HIDR.} = -42 ± 2 ‰$$

y = -0,0323x + 0,0049
R² = 0,9677

If we compare the absolute fractionation value, we deduce that the combination of persulfate + alkaline hydrolysis (-24 to -32‰) is less selective and specific with the heaviest carbon isotope (13C) than only with alkaline hydrolysis process (calculated in control vials). A CF fractionation of -53‰ was obtained in batch experiments with concrete at pH ≈ 12 of Torrentó et al.(2014)

y = 1,0483e⁻⁰·⁰³¹ˣ
R² = 0,98819

y = 1,0285e⁻⁰·⁰⁴ˣ
R² = 0,9862

y = 1,0238e⁻⁰·⁰¹¹ˣ
R² = 0,995

y = 1,1566e⁻⁰·⁰¹⁶ˣ
R² = 0,9842

The combination of persulfate with alkaline hydrolysis slightly increases the CF degradation (7.6 ± 0.1% for 20 g/L of persulfate and 11.5 ± 0.4% for 10 g/L of persulfate). Clearly, we can observe in 10 g/L persulfate experiment that when pH reaches its highest value (pH 13.6 after 72 h) is when the combination of ISCO+alkaline hydrolysis improves CF degradation in relation to simple alkaline hydrolysis.

M) Above: Chloroform carbon isotopic fractionation in batch experiments of persulfate (at 10 and 20 g/L) with alkaline trench water adding NaOH as buffer. Below: Chloroform concentration over time in batch experiments of persulfate (at 10 and 20 g/L) in comparison to chloroform concentration in control vials (blue squares) which are representative of alkaline hydrolysis at obtained pH after adding the same amount of NaOH buffer in the experiments.

CONCLUSIONS

• Over time, the CT and CF isotopic composition increases in trench water at the field site. Alkaline hydrolysis degraded CF (Torrentó et al., 2014) but this process was not the responsible of CT isotopic shifts at field. The presence of iron minerals in gravels shed light on the hypothesis that reductive dechlorination due to superficial iron (specially Fe²⁺) could be the responsible of CT degradation. Thus, further investigation is needed with the aim of knowing the iron minerals potential as a remediation tool (as the conventional Fe⁰ is used).

• In batch experiments, the tested ISCO treatments were more effective for chloroethenes in trench water conditions, only persulfate slightly enhanced the role of alkaline hydrolysis in CF degradation, producing a less selective process. Moreover, persulfate was less toxic than permanganate. Liang, Wang and Bruell (2007) found out in experiments with persulfate and TCE that under basic conditions (pH 9) predominates hydroxyl radical (·OH) in contrast to the predominance of sulfate radical (SO₄·⁻) under acidic conditions. This fact would explain that the contribution to the CF degradation by the ·OH radicals from persulfate depends on the experimental pH and it was less selective (similar to Fenton reactions) and decrease the combined carbon isotopic effect.
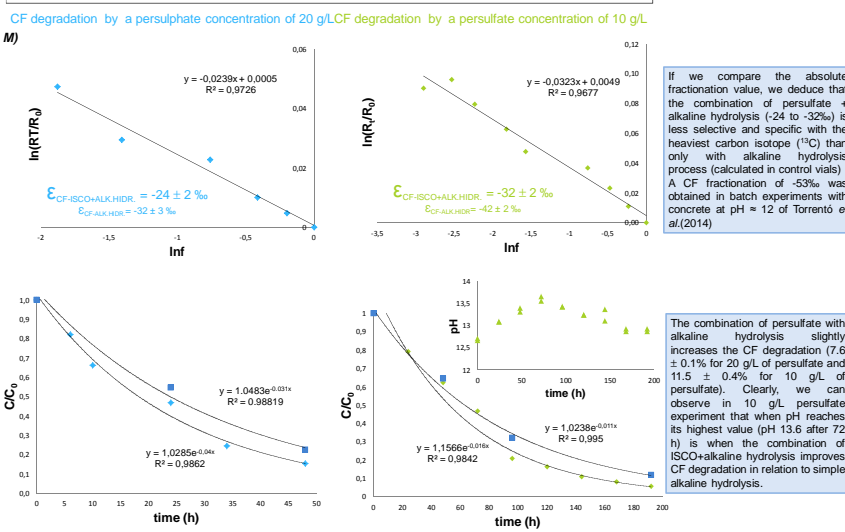
REFERENCES

• Torrentó, C.; Audí-Miró, C.; Bordeleau, G.; Marchesi, M.; Rosell, M.; Otero, N. and Soler, A. The Use of Alkaline Hydrolysis As a Novel Strategy for Chloroform Remediation: The Feasibility of Using Construction Wastes and Evaluation of Carbon Isotopic Fractionation. Environ. Sci. Technol. 2014. 48, 1869–1877.

• Ashworth, J; Nijenhuis, E.; Glowacka, B.; Tran, L.; Schenk-Watt, L. Turbidity and color correction in the Microtox™ Bioassay. The Open journal of Environmental Pollution & Toxicology Journal, 2010, 2, 1-7.

• Liang, C.; Wang, Z-S.; Bruell, C.J. Influence of pH on persulphate oxidation of TCE at ambient temperatures. Chemosphere, 2007, 66, 106-113.
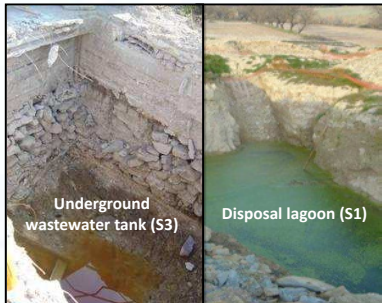
UNRAVELING MICROBIAL COMMUNITY INTERACTIONS IN A CHLORINATED VOCs POLLUTED AQUIFER HARBORING NATURAL ATTENUATION PROCESSES

Miriam Guivernau[1], Marc Viñas[1], Diana Rodríguez-Fernández[2], Clara Torrentó[2], Cristina Domènech[2], Albert Soler[2], Mònica Rosell[2]

1. GIRO Joint Research Unit IRTA-UPC, IRTA, Caldes de Montbui, Spain.
2. Grup de Mineralogia Aplicada i Medi Ambient. Facultat de Geologia, Universitat de Barcelona, Barcelona, Spain.

✉ miriam.guivernau@irta.cat; marc.vinas@irta.cat; monica.rosell@ub.edu

BACKGROUND

In a former industrial area, near Barcelona, a fractured bedrock aquifer was mainly polluted with a complex mixture of volatile organic compounds (VOCs). An underground wastewater tank and a disposal lagoon were identified as the main contaminant sources and were removed in 2006 as an early measure for contamination mitigation (Fig. 1). **Natural attenuation evidences** were observed in previous biogeochemical studies for chlorinated VOCs in 2006 (Palau *et al.*, 2014) and later campaigns (2010, 2013). Compound specific isotope analysis (CSIA) has revealed [13]C **enrichment** of residual trichloroethene (**TCE**), chloroform (**CF**) and carbon tetrachloride (**CT**) at the deepest zones of source well (S3) concomitant with a depletion of ^{13}C in dichloromethane (**DCM**). Although no significant isotopic fractionation of TCE was detected in the surroundings of the lagoon (S1) in 2006, this area has experimented along the time a more drastic decrease of chlorinated ethenes concentration than S3 zone which could be related to distinct source removal dilution effects or toxic effects of higher chlorinated methanes levels in S3.

✓ Former contamination sources as found in 2006 before their removal.

Biogeochemical characterization

A) Location map with multilevel wells and the A-A' cross-section, B) redox conditions there, S3 well includes δ34S-SO4 (‰) data and C) CF concentration and δ13C-CF in 2013.

Table 1. Concentration of main pollutants expressed in µg/L in the wells selected for microbial community assessment in 2012 just before the microcosm experiment.

Compounds	S1	S3	S9
[µg/L]	Wells (data from 2012)		
cisDCE	12	6985	145
CF	2494	6645	236
TCE	2890	4829	887
PCE	394	2841	288
CT	155	2240	70
1,2-DCB	bld	1176	14
Toluene	bld	762	10
DCM	2	737	2
1,2,4-TCB	bld	498	2
m+p-xylene	bld	249	3
Ethylbenzene	bld	213	2
1,3-DCB	bld	201	1
1,2,3-TCB	bld	171	bld
MCB	bld	89	bld
1,3,5-TMB	bld	64	0.2
1,1-DCE	2	63	0.5
o-xylene	bld	42	bld
transDCE	bld	27	0.3
Benzene	bld	20	bld
CS2	0.9	13	0.9
1,1,2-TCA	0.6	11	n.d.
1,1,1-TCA	0.3	5.5	0.1
naphthalene	bld	5.4	bld
n-propilbenzene	0.1	4.9	0.2
1,1-DCA	bld	4.6	bld

✓ From 2006 to 2013, redox conditions in **S1** have evolved from iron reducing to more oxidizing, whereas **S3** and **S9** maintain increasing reducing conditions in depth (from oxic to anoxic). In **S3**, δ34S-SO4 (‰) enrichment in depth might indicate **sulphate-reducing conditions**.

Microbial community assessment

·Eubacterial *16SrRNA* gene-based pyrosequencing

✓ Although previous qPCRs results showed low levels of *Dehalococcoides* and related functional genes in S1 and S9, detection by pyrosequencing was only confirmed in S9 (0.1%).

✓ **Peptococcaceae** is manly enriched in S3 by known dehalorespiring **Desulfitobacterium** and **Dehalobacter**.

✓ Marginal dehalorespiring bacteria was also enriched in S3 and S1 (such as *Geobacter*, *Anaeromyxobacter*, *Desulfovibrio*, *Desulfuromonas*, *Sulfospirillum* and *Dechloromonas*).

·Quantitative PCR Real-Time (qPCR) functional genes:

✓Potential for methanogenesis, denitrification and monoaromatic biodegradation.

MICROCOSM ASSAYS

Slurry from the bottom of S3 well was the inoculum for 197 days-microcosm experiments with and without vitamin B12 as a cofactor and different e-donors. Also, an abiotic control was set up with autoclaved/killed biomass (KI).

Chemical results: natural potential for CT/ CF degradation

Pollutants	PCE	TCE	cDCE	CT	CF	DCM	CS2	Toluene	
C_t0 (µg/L)	318	5539	1873	1324	6217	41	555		
	C_t6/C_t0 (%)								Consumed added e-donor
CO1-t6	99	76	100	25	104	81	109	90	No e-donor added
CO2-t6	100	79	103	19	109	82	104	94	
CO1B12-t6	113	84	106	<8	38	93	308	97	
CO2B-t6	78	56	81	<8	6	88	433	72	
LA1-t6	92	70	94	22	85	76	100	99	89% LACTATE
LA2-t6	108	80	97	22	90	81	110	97	
ME1-t6	111	82	103	31	95	81	114	105	54% METHANOL
ME2-t6	91	71	96	46	88	74	103	93	
ME1B12-t6	117	85	111	<8	26	112	591	114	99% METHANOL
ME2B-t6	107	80	106	<8	2	107	723	106	
AC1-t6	128	95	113	61	107	85	117	126	6% ACETATE
AC2-t6	112	85	104	53	99	78	118	112	
AC1B12-t6	109	76	95	<8	12	91	497	103	84% ACETATE
AC2B-t6	113	80	103	<8	3	118	735	112	
KI1-t6	111	85	101	156	105	83	105	100	No e-donor added
KI2-t6	69	51	75	81	79	63	94	71	
KI1B12-t6	99	79	96	118	103	79	136	96	
KI2B12-t6	77	59	77	69	82	63	102	80	

Each experiment was performed in duplicate (t6 = 197 days). CF was only degraded significantly in the **B12** presence, and no apparent DCM accumulation was observed.
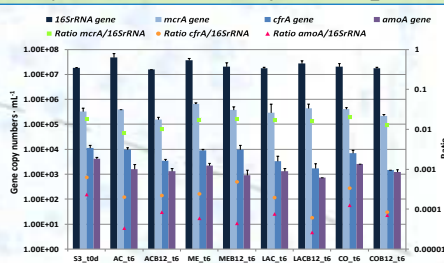
✓Degradation of CF was observed and the calculated C isotope **fractionation of CF (ε_CF=-30‰)** was similar to the one found recently by Chan *et al.*, 2012 in *Dehalobacter*-containing cultures (-27.5‰).

✓CS2 was produced as by-product of the CT degradation.

✓There was no chlorinated ethenes degradation probably due to the toxic effects of halomethanes.

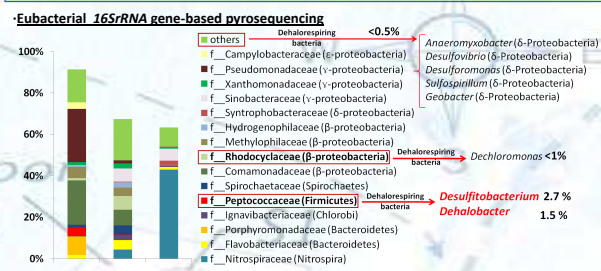### DGGE results: 16SrRNA V3-V5 hypervariable region

✓Microbial community structure was very stable during the microcosm assays.
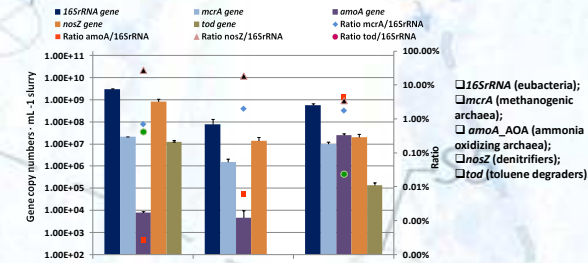
qPCR results: 16SrRNA, mcrA, cfrA and amoA_AOA

✓Neither *Dehalococcoides* nor their functional genes (*tceA*, *bvcA* and *vcrA*) were detected.

✓The abundance of *cfrA* gene (Tang & Edwards, 2013) might confirm the presence of *Dehalobacter spp.* with CF reductive dehalogenase.

CONCLUSIONS

Contaminated field:

▪An enrichment of dehalorespiring bacteria (*Desulfitobacterium* and *Dehalobacter*) was depicted in **well S3** concomitant to CSIA evidences of **natural attenuation** of chlorinated methanes and ethenes.

▪Archaeal community was represented in the three wells both by **methanogens** and **Ammonium Oxidizing Archaea** (AOA) such as *Nitrosopumilus* and *Nitrososphaera* genera suggesting the existence of microaerophilic environment, and a relevant role in the N cycle in the polluted site.

▪The presence of OTUs linked to **Commamonadaceae** and **Pseudomonadaceae**, specially in S3, could be related to **BTEX** presence.

▪The complexity of the microbial community encountered in **S3** linked to **potential reductive dehalogenation**, ammonia oxidation, denitrification and methanogenic processes could be explained by the complexity of the pollutant sources and by the **organic-N loads** linked to nearby agriculture activity upstream the polluted site.

Microcosm assays:

▪The addition of **vitamin B12** promotes **CF and CT biodegradation** processes with native alive biomass after 200 days of incubation in microcosm experiments.

▪The presence of *cfrA* gene, together with the **CF carbon isotopic** fractionation (ε_C= -30‰) and the pyrosequencing detection might indicate the role of *Dehalobacter* in CF degradation at this site.

▪Predominant **microbial community** structure (eubacteria and archaea) **did not change** throughout halomethane biodegradation.

▪No reductive dehalogenation genes related to *Dehalococcoides* were detected.

❖Further research is needed (i.e. at transcriptomic level) to better understand the role of dehalogenating bacteria in their interactions with the whole microbial community during reductive dehalogenation processes.

References

- Chan, C.C., Mundle, S.O., Eckert, T., Liang, X., Tang, S., Lacrampe-Couloume, G., Edwards, E.A., Sherwood Lollar B., (2012) *Environ. Sci. Technol.* 46 (18), 10154–10160.
- Palau, J., Marchesi, M., Chambon, J.C.C., Aravena, R., Canals, A., Binning P.J., Bjerg, P.L., Otero, N., Soler, A. (2014) *Sci. Total Environ.* 475, 61–70.
- Tang, S., Edwards, E.A. (2013) *Phil.Trans. R. Soc. B* 368, 20120318.

Caracterización hidrogeológica y modelización hidrodinámica del emplazamiento monitorizado de Òdena (Barcelona)

UNIVERSITAT POLITÈCNICA DE CATALUNYA
BARCELONATECH
UPC

Universitat de Barcelona

Albert Folch[1], Gemma Pijuan[1], Diana Rodríguez-Fernández[2], Mònica Rosell[2], Cristina Domènech[2], Daniel Fernàndez-Garcia[1], Albert Soler[2]

[1]*Grup d'Hidrologia Subterrània (UPC-CSIC), Departament d'Enginyeria del Terreny i Cartogràfica, Escola de Camins, Universitat Politècnica de Catalunya.*
[2]*Grup de Mineralogia Aplicada i Geoquímica de Fluids, Departament de Cristal·lografia, Mineralogia i Dipòsits Minerals, Fac. Geologia, Universitat de Barcelona.* ✉ albertsolergil@ub.edu

1. Problemática

El emplazamiento de Òdena (Barcelona) está siendo estudiado con el objetivo de utilizarlo como campo experimental para la **investigación in situ** de nuevas técnicas de **remediación** de la contaminación por *DNAPLs*.

Las principales características del acuífero son:
- *emplazado en medio fracturado no confinado;*
- *constituido por una serie sedimentaria Eocena de calizas, margas con intercalaciones de areniscas y microconglomerados cementados;*
- *contaminado por cloroetenos, clorometanos, cloroetanos, clorobencenos, BTEXs y trazas de pesticidas .*

Origen de la contaminación → infiltraciones de un tanque subterráneo de almacenaje de residuos y de una balsa de una antigua fábrica de productos fitosanitarios y textiles (1978-1985).

Tareas de remediación
- Extracción de las fuentes de contaminación y de 2000 t de suelo contaminado (2006)
- Construcción de dos zanjas de intercepción del agua de recarga en la zona no saturada rellenadas con residuos de construcción para la descontaminación mediante hidrólisis alcalina (Torrentó et al., 2014) .
- Construcción de 10 multi-piezómetros en el acuífero → 220 puntos de muestreo con los que seguir la evolución y atenuación natural de la pluma de contaminación en profundidad (Palau et al., 2014).

A pesar de los esfuerzos de seguimiento y monitorización hay algunas tendencias en la evolución de la concentración de contaminantes difíciles de explicar. Así, de cara a la aplicación de futuras estrategias de remediación, el objetivo de este trabajo es **una mejor caracterización hidrogeológica y una modelización** preliminar para entender la dinámica del sistema.

4. Modelización

El **modelo de transporte reactivo** considera la advección, la dispersión y la degradación anaeróbica en cadena de TCE hasta eteno. Se ha utilizado el código de diferencias finitas conocido como RT3D. A modo predictivo y con el objetivo de entender mejor el sistema, se han utilizado **dos hipótesis** distintas sobre la naturaleza del foco usando como base la concentración de TCE de 2007:
A. **Presencia de fase libre** (o aportes auxiliares de la zona no saturada/matriz) y, por tanto, aporte continuo de TCE a la fase disuelta en el tiempo;
B. **Solamente fase disuelta** en la zona saturada que actúa como aporte puntual.

Medidas
Concentración TCE (µg/L) a lo largo de 6 campañas de muestreo
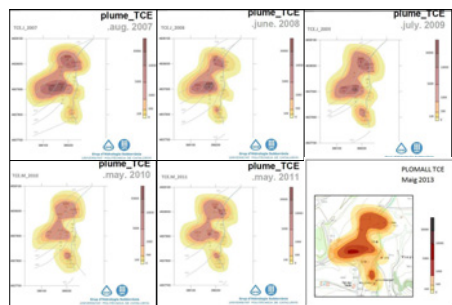
Predicción 6 años hipótesis A
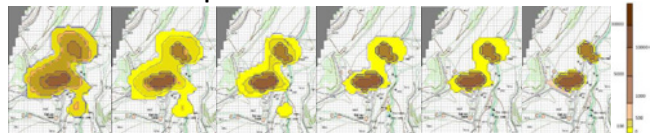
Predicción 6 años hipótesis B
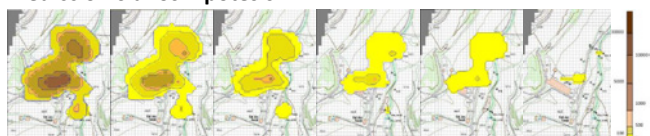
Referencias
- Palau, J.; Marchesi, M.: Chambon, J.: Aravena, R.; Canals, A.; Binning, P. J., Bjerg P. L.; Otero, N.; Soler, A. (2014) *Multi-isotope (carbon and chlorine) analysis for fingerprinting and site characterization at a fractured bedrock aquifer contaminated by chlorinated ethenes.* Science of the Total Environment, 475: 61-70.
- Torrentó, C.; Audí-Miró, C.; Bordeleau, G.; Marchesi, M.; Rosell, M.; Otero, N.; Soler, A. (2014) *The use of alkaline hydrolysis as a novel strategy for chloroform remediation: the feasibility of using urban construction wastes and evaluation of carbon isotopic fractionation.* Environ. Sci. Technol., 2014, 48 (3), pp 1869–1877.

2. Metodología

Datos previos
Litología, parámetros de campo, aniones, cationes y concentración de compuestos volátiles orgánicos (en este caso centrado en tricloroetileno, TCE) de 6 campañas de muestreo de agua subterránea de 2007 a 2013.

Caracterización hidrogeológica
FASE 1 (Nov. 2013): **Ensayo de bombeo** de larga duración en un pozo de gran diámetro (PCJ) midiendo en continuo con *divers* instalados en piezómetros cercanos, los cambios del nivel piezométrico inducidos por el bombeo para:
→ *estimar la transmisividad efectiva del macizo*
→ *establecer la conectividad hidráulica entre varios puntos de la zona.*
FASE 2 (Dic. 2013): Medidas puntuales de permeabilidad a través de ensayos de corta duración tipo **"slug tests"** (en algunos piezómetros) → *analizar la variabilidad espacial de la permeabilidad.*
Antes y después de 1 y 2: **Perfiles verticales de conductividad eléctrica** en los piezómetros de observación mediante descenso y ascenso manual de un *diver* (Mayo y septiembre 2013 vs. Enero y Febrero 2014).

➡️ *Todo ello para desarrollar un **modelo de flujo** para alimentar el **modelo de transporte reactivo** que simula la degradación en cadena de los compuestos organoclorados.*

3. Caracterización

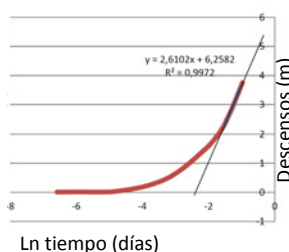### Medidas puntuales y globales de la permeabilidad

Ensayo de bombeo (28/11/2013)
Pozo Jorba (PCJ al límite del mapa), al SE de S9. Duración 8h. Caudal constante de 1,2 L/s. Medidas de descenso y ascenso del nivel piezométrico en PCJ, S9 y S10.

➡️ *Interpretación mediante el método de Jacob*
- Transmisividad → 1,4 - 14,9 m²/d
Coeficiente de almacenamiento → 0,0024 y 0,0009
➡️ Dan valor global representativo del acuífero y reflejan la permeabilidad del sistema debido a su fracturación

y = 2,6102x + 6,2582
R² = 0,9972

Descensos (m)

Ln tiempo (días)

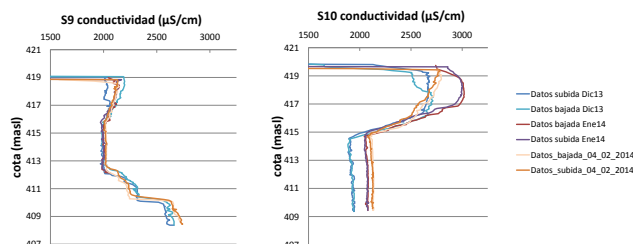|	ASSAIG BOMBAMENT		ASSAIG RECUP	SLUG
	T (m2/dia)	COEF EMM	T (m2/dia)	K (m/dia)
POU	3,24		1,6	
S3				0,0011
S5				0,0004
S6				0,0001
S9	5,8	0,0024	1,45	
S10	14,91	0,0009	4,8	0,0012

Ensayos tipos *Slug* (10/12/2013) en piezómetros S3, S5, S6 y S10.
- calculo de la permeabilidad en torno a los diferentes piezómetros
10⁻³ y 10⁻⁴ m/d,
➡️ valores muy bajos de permeabilidad que sólo reflejan el valor local del sondeo.

Perfiles verticales de conductividad eléctrica

Los perfiles de conductividad eléctrica en los piezómetros estudiados en diferentes épocas del año, así como antes y después de los ensayos de bombeo son bastante reproducibles y muestran **cambios significativos** de conductividad a lo largo del espesor saturado (ver S9 y S10). Estos cambios se podrían atribuir:
- A la influencia de los niveles más salinos que conforman la base del acuífero que concuerdan con las altas concentraciones de Na y Cl analizadas y/o,
- a la degradación de los contaminantes clorados (liberando Cl) en zonas donde se detectan valores de redox y $\delta^{34}S$ en el rango de la sulfato reducción.

S9 conductividad (µS/cm)

S10 conductividad (µS/cm)

cota (masl)

- Datos subida Dic13
- Datos bajada Dic13
- Datos bajada Ene14
- Datos subida Ene14
- Datos_bajada_04_02_2014
- Datos_subida_04_02_2014

5. Conclusiones preliminares

- Los ensayos hidráulicos hechos en la campaña de campo han permitido estimar la transmisividad global del emplazamiento entre 1 y 15 m²/d con valores puntuales de permeabilidad en los sondeos entre 10⁻³ y 10⁻⁴ m/d. Estos valores se atribuyen a un sistema de doble porosidad formado por materiales fisurados de baja permeabilidad y fracturas y/o estratos más permeables que canalizan la mayor parte del flujo.
- Se ha realizado un modelo de flujo en el emplazamiento y después de la calibración se ha conseguido un buen ajuste entre los valores calculados y los observados en la mayoría de los piezómetros y pozos del emplazamiento indicando la bondad del modelo (no mostrado). A pesar del buen ajuste logrado hay algunos puntos que no han podido ser calibrados debido a la heterogeneidad del sistema no representada por el modelo.
- El modelo de transporte reactivo sugiere que el foco de contaminación sigue activo, hecho atribuible a varios posibles mecanismos: (1) aún existe fase libre en la zona saturada; (2) posible lixiviación de contaminante durante la recarga por lluvia; (3) difusión en la matriz.
- Los perfiles de conductividad indican la presencia de estratos con distintas propiedades hidráulicas a escala métrica que puede dar lugar a flujos preferenciales. Dicha estructura debe incluirse en la mejora del modelo realizado.

Agradecimientos

11th Applied Isotope Geochemistry Conference, AIG-11 BRGM

C and Cl-CSIA for elucidating chlorinated methanes biotic and abiotic degradation at a polluted bedrock aquifer

Diana Rodríguez-Fernández[a]*, Mònica Rosell[a], Cristina Domènech[a], Clara Torrentó[b], Jordi Palau[b], Albert Soler[a]

[a] Grup de Mineralogia Aplicada i Geoquímica de Fluids, Departament de Cristal·lografia, Mineralogia i Dipòsits Minerals, Facultat de Geologia, Universitat de Barcelona (UB), C/ Martí i Franquès, s/n - 08028 Barcelona, Spain
[b]Centre d'hydrogéologie et de géothermie (CHYN), Université de Neuchâtel (UNINE), Rue Emile-Argand 11, Neuchâtel 2000, Switzerland

Abstract

In this study, concentration and δ^{13}C and δ^{37}Cl values of chloroform (CF) and carbon tetrachloride (CT) measured in groundwater samples are related to redox conditions to elucidate natural attenuation processes in a polluted site. Shifts in δ^{13}C and δ^{37}Cl of CF and CT were detected over time. δ^{13}C$_{CF}$ values found in the potential sources were -34.5 ± 0.6 ‰ (tank near S3 well), -37.3 ± 0.6 ‰ (in a fracture near S1 well) and -46.2± 0.4 ‰ (barrels) in 2004, whereas in later sampling campaigns, δ^{13}C$_{CF}$ enriched values such as -25.2 ± 0.5 ‰ were measured in S3 in 2013. 2D plots (δ^{13}C$_{CF}$ *vs* δ^{37}Cl$_{CF}$) showed different isotopic patterns in different wells and depths. δ^{37}Cl$_{CF}$ values let distinguish that the former sources evolved towards completely different isotopic signatures, whilst δ^{37}Cl$_{CF}$ values of +1.3 ± 0.3 ‰ were reached in 2013 for S3, S1 moved towards more depleted δ^{37}Cl$_{CF}$ values (down to -3.9 ± 0.6 ‰). These data indicate that different reductive dechlorination processes might occur.

© 2015 Published by Elsevier B.V. This is an open access article under the CC BY-NC-ND license
(http://creativecommons.org/licenses/by-nc-nd/4.0/).
Peer-review under responsibility of the scientific committee of AIG-11
Keywords: Compound-specific isotope analysis; Groundwater pollution; Environmental forensics; Chlorinated methanes

1. Introduction

Chlorinated methanes are persistent pollutants in groundwater compared with other volatile organic compounds. However, they have received less attention than other chlorinated compounds such as chlorinated ethenes or ethanes. CT has been used in fungicide formulation and as a commercial degreaser for almost 100 y[1]. CF was initially used as an anesthetic and as a chemical precursor to nowadays banned refrigerants. CT and CF are toxic and also considered possible carcinogenic substances[2]. In Europe, environmental water quality standards of 12 and 2.5 μg/L for CT and CF, respectively, have been established in the framework of water policy (Directive 2008/105/EC).

---

* Corresponding author. Tel.: +34 934 021 345; fax: +34 934 021 340.
E-mail address: diana.rodriguez@ub.edu

Up to now, microbial CT degradation is only known to occur by cometabolic reduction under anoxic conditions[3].Although CF and dichloromethane (DCM) are the most common detected metabolites of CT reduction, the presence of sulphate reducing bacteria and high sulphite systems leads to the biologically-mediated transformation of CT to carbon disulphide (CS_2) as main final product[4]. Regarding pure abiotic processes, several studies reported carbon isotopic fractionation associated with the reductive dechlorination of CT by Fe(II) sorbed onto iron minerals[5] or by Zn(0)[6]. Stable carbon isotopic fractionation values (εC) ranged from -10 to -32‰. CF biotic and abiotic reductive dechlorination occurs in anoxic environments[7]. However, CF biodegradation has been also described under oxic conditions[7]. Chan *et al.* (2012) obtained the first biotic carbon isotopic fractionation of CF (εC value of -27.5 ± 0.9‰) during dehalorespiration to DCM by *Dehalobacter* cultures[8]. In addition, CF could also be abiotically degraded by Fe-bearing minerals with slower dechlorination rates than CT[9]. For field studies, *in situ* abiotic reduction of CT has been proved based on the average ratio of CF:CS_2[10] and on CT metabolites and their spatial distribution to detect possible sources an comingling plumes[11]. However, little information about isotope effects on biotic or abiotic *in situ* degradation of CF and CT is currently available. Some C-CSIA measurements for CT are published in the vadose zone of a polluted site[12] but no data have been obtained for long-term field demonstrations of CT and CF degradation using 2D-CSIA.

The study site is an unconfined fractured bedrock aquifer with low permeability in Òdena (Barcelona, Spain) (Fig. 1). Contamination originated from a former chemical plant between 1978 and 1985[13]. The aquifer is contaminated by chlorinated volatile compounds (ethenes, methanes, aromatic hydrocarbons and ethanes), BTEX and traces of pesticides with the highest concentrations measured close to the former waste disposal areas: an underground wastewater tank (S3 well) and a disposal pit (S1 well) (Fig. 1). Both sources were removed in 2006 and the concentration of most pollutants decreased. Emptied space was filled with recycled aggregates from construction and demolition waste[14]. Ten multilevel nested wells leading to a total of 147 sampling points were installed in 2006[13].

Fig.1. Location map of the polluted area. Multilevel wells and A-A' transect are highlighted.

This study is focused on chlorinated methanes. CT and CF field isotope data is used to elucidate natural attenuation processes. In order to assess and predict the extent of the target compounds biodegradation due to indigenous microbial community, microcosm studies are being carried out in the laboratory. In addition, the role of Fe-bearing minerals in the abiotic dechlorination reactions of CT and CF is also being investigated. 2D-CSIA slopes obtained from field data will be compared with those determined in laboratory experiments.

2. Methods

2.1. Sampling

Above mentioned potential sources as well as abandoned barrels inside the factory were sampled in 2004 before their removal. Groundwater samples for plume characterization by concentration and isotopic measurements were collected from ten multilevel nested wells in four main campaigns (2006, 2010, 2013 and 2014). In some field campaigns, samples for analyzing redox sensitive compounds (NO_3^-, NO_2^-, dissolved Mn, dissolved Fe and SO_4^{2-}) were taken. Moreover, soil and groundwater samples impacted with CF, CT and DCM among other pollutants were collected from the bottom part of the well S3 (Fig. 1) in order to set up microcosms experiments.

2.2. Chlorinated methanes concentration and isotope data

Volatile organic compounds concentrations were determined by headspace (HS) analysis using a FOCUS gas chromatograph coupled with a DSQ II mass spectrometer (Thermo Fisher Scientific, Waltham, MA). For C-CSIA, the analyses were performed by headspace solid-phase microextraction (HS-SPME) in a Thermo Finnigan Trace GC Ultra instrument coupled via a GC-Isolink interface to a Delta V Advantage isotope ratio mass spectrometer (Thermo Scientific GmbH, Bremen, Germany). Volatile organic compounds concentrations and carbon isotope

measurements were performed in the Scientific and Technological Center of the University of Barcelona (CCiT-UB). The Cl-CSIA analyses were performed GC-qMS system (Agilent) located in the laboratories of the *Centre d'Hydrogéologie et Géothermie* (CHYN) from the University of Neuchâtel (UNINE) (Switzerland) according to the method of Sakaguchi-Söder *et al.* (2014)[15].

2.3. Biotic and abiotic laboratory-scale degradation experiments

To explore the feasibility of achieving CF and CT detoxification in the field as well as their associated isotopic fractionation patterns, anoxic microcosm experiments were conducted in batch with slurry material from the bottom of S3 well. Moreover, batch experiments were also performed to assess and determine the magnitude of carbon and chlorine isotopic fractionation of CT and CF due to abiotic dechlorination processes mediated with Fe-bearing minerals taking pyrite and magnetite in anoxic conditions as model systems.

3. Preliminary results

After the removal of the pollution sources in 2006, a significant decrease in CT and CF concentrations was detected accompanied by shifts in $\delta^{13}C$ values. In the case of CF, $\delta^{13}C_{CF}$ values found in the potential sources were -34.5 ± 0.6 ‰ (wastewater tank), -37.3 ± 0.6 ‰ (in a fracture near S1) and -46.2± 0.4 ‰ (barrels) in 2004, whereas in later sampling campaigns, $\delta^{13}C_{CF}$ enriched values were measured in zone S3 and S1, e.g. -25.2 ± 0.5 ‰ and -27.0 ± 0.5 ‰ respectively in 2013.
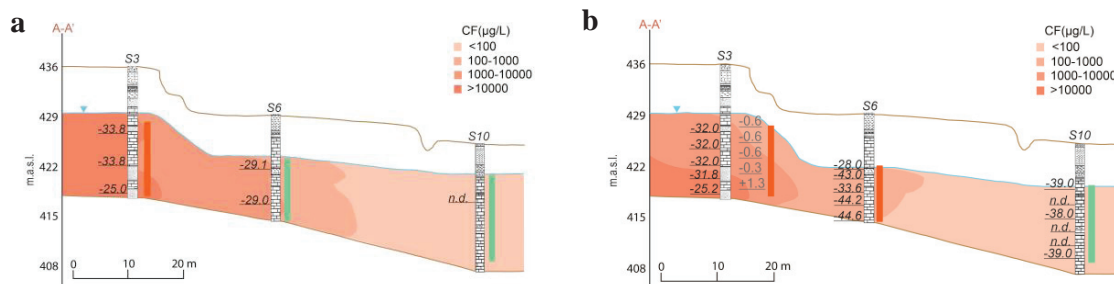
Fig. 2. Concentration of CF (μg/L), carbon ($\delta^{13}C$, ‰) isotopic data in italics and chlorine isotopic data ($\delta^{37}Cl$, ‰) in grey for samples of transect A-A' for both (a) 2010 and (b) 2013 campaigns. The depth is expressed in meters above sea level (m.a.s.l.). Bars indicates redox system is controlled by NO_3^--NO_2^--NH_4^+ (green) or by Fe(II)aq – Fe-oxyhydroxides equilibrium (orange).

The most negative $\delta^{13}C_{CF}$ values observed in S6 (-44.6 ± 0.5 ‰) are similar to those found in some solvent barrels stored in the factory (-46.2 ± 0.4 ‰). As a preliminary hypothesis, depleted $\delta^{13}C_{CF}$ values found in S6 and S10 wells might be explained as slightly degraded CF or due to mixing of CF from wastewater tank and pit areas (Fig. 2). A contribution of CT degradation in $\delta^{13}C_{CF}$ values should not be discarded. In S3, additionally to the enriched $\delta^{13}C_{CF}$ (-25.2 ± 0.5 ‰) and $\delta^{37}Cl_{CF}$ (+1.3 ± 0.3 ‰) values in the bottom part, high concentrations of CS_2 and a spatial and temporal accumulation of DCM were observed, suggesting that both CT and CF degradation may be occurring. $\delta^{37}Cl_{CF}$ values show differences among wells and let distinguish that the two main former sources (S1 and S3 zones) evolved towards completely different isotopic signatures: while $\delta^{37}Cl_{CF}$ values of +1.3 ± 0.3 ‰ could be reached in S3 in 2013, S1 moved towards more depleted $\delta^{37}Cl_{CF}$ values down to -3.9 ± 0.6 ‰ (Fig. 3). These differences might indicate that processes affecting CF in S1 are different than those of S3 and S7 (the wells with more positive values of $\delta^{37}Cl_{CF}$, Fig. 3) and may suggest that similar degradation processes are taking place in these last two wells. Moreover, S3 and S7 were those with higher dissolved Fe concentrations and whose redox system seems to be regulated totally or partially by equilibrium between Fe(II)$_{aq}$ and Fe-oxyhydroxides. The isotopic enrichment tendency observed in this 2D-CSIA plot for S3 and S7 will be compared with the slopes obtained in on-going laboratory scale experiments in order to see if it is possible to discriminate between biotic and abiotic degradation processes.
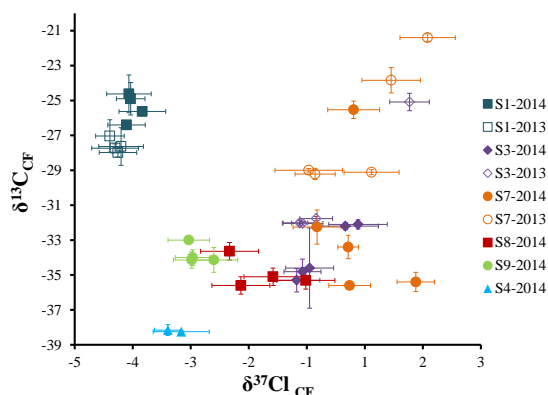
Fig. 3. $\delta^{13}C_{CF}$ *vs*. $\delta^{37}Cl_{CF}$ data from wells on March 2013 and November 2014. Error bars are related to standard deviation of the measurements.
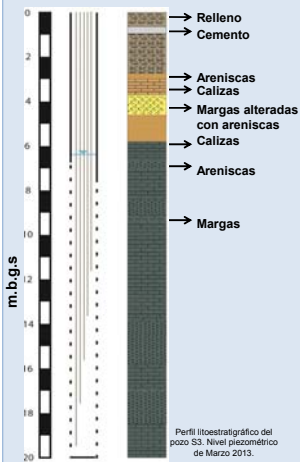
Acknowledgements

References

1. Morrison RD. Application of forensic techniques for age dating and source identification in environmental litigation. J. Environ. Forensics. 2000; **1**: 131-153.
2. Integrated Risk Information System (Iris): Toxicological Review of Chloroform (CAS no. 67-66-3); U.S. Environmental Protection Agency (EPA): Washington, DC; 2001.
3. Penny C, Vuilleumier S, Bringel F. Microbial degradation of tetrachloromethane: mechanisms and perspectives for bioremediation. FEMS Microbiol Ecol 2010; **74**: 257-275.
4. Koenig J, Lee M, Manefield M. Successful microcosm demonstration of a strategy for biodegradation of a mixture of carbon tetrachloride and perchloroethene harnessing sulfate reducing and dehalorespiring bacteria. Journal of Hazardous Materials 2012; **219– 220**: 169-175.
5. Zwank L, Elsner M, Aeberhard A, Schwarzenbach RP, Haderlein SB. Carbon isotope fractionation during reductive dehalogenation of carbon tetrachloride at iron hydroxide and iron sulfide minerals. Environ. Sci. Technol. 2005; **39**: 5634-5641.
6. Vanstone N, Elsner M, Lacrampe-Couloume G, Mabury S, Lollar BS. Potential for identifying abiotic chloroalkane degradation mechanisms using carbon isotopic fractionation. Environ. Sci. Technol. 2008; **42**(1): 126-132.
7. Cappelletti M, Frascari D, Zannonni D, Fedi S. Microbial degradation of chloroform. Appl. Microbiol. Biotechnol. 2012; **96**: 1395-1409
8. Chan C, Mundle S, Eckert T, Liang X, Tang S, Lacrampe-Couloume G, Edwards E, Lollar BS. Large carbon isotope fractionation during biodegradation of chloroform by Dehalobacter cultures. Environ. Sci. Technol. 2012; **46**: 10154-10160.
9. Maithreepala RA, Doong RA.Dechlorination of carbon tetrachloride by ferrous ion associated with iron oxide nano particles. Proceedings of the fourth academis sessions 2007; 197-205.
10. Davis A, Fennemore GG, Peck C, Walker CR, McIlwraith J, Thomas S. Degradation of carbon tetrachloride in a reducing groundwater environment: implications for natural attenuation. Appl. Geochem. 2003; **18**: 503-525.
11. Kaown D, Shouakar-Stash O, Yang J, Hyn Y, Lee K-K.Identification of multiple sources of groundwater contamination by dual isotopes. Groundwater 2014; **52**(6): 875-885.
12. Kirtland BC, Aelion CM, Stone PA, Hunkeler D. Isotopic and geochemical assessment of in situ biodegradation of chlorinated hydrocarbons. Environ. Sci. Technol. 2003; **37**:4205-4212.
13. Palau J, Marchesi M, Chambon J, Aravena R, Canals A, Binning P, Bjerg P, Otero N, Soler A. Multi-isotope (carbon and chlorine) analysis for fingerprinting and site characterization at a fractured bedrock aquifer contaminated by chlorinated ethenes. Science of the Total Environment 2014; **475**: 61–70.
14.Torrentó C, Audí-Miró C, Bordeleau G, Marchesi M, Rosell M, Otero N, Soler A. The use of alkaline hydrolisis as a novel strategy for chloroform remediation: the feasibility of using construction wastes and evaluation of carbon isotopic fractionation. Environ. Sci. Technol. 2014; **48** (3): 1869-1877.
15. Sakaguchi-Soder K, Jager J, Grund H, Matthaus F, Schuth, C. Monitoring and evaluation of dechlorination processes using compound-specific chlorine isotope analysis. Rapid Commun Mass Spectrom. 2007; **21**(18): 3077-3084.

CARACTERIZACIÓN HIDROGEOLÓGICA DEL ACUÍFERO FRACTURADO BAJO EL EMPLAZAMIENTO MONITORIZADO DE ÒDENA (BARCELONA, CATALUÑA)

Diana Rodríguez-Fernández[1], Albert Folch[2], Mahjoub Himi[3], Cristina Domènech[1], Mònica Rosell[1], Neus Otero[1], Raúl Lovera[3], Jordi Palau[1], Daniel Fernàndez-Garcia[2], Albert Casas[3], Albert Soler[1]

[1] Grup Mineralogia Aplicada i Geoquímica de Fluids (MAG), Dep. Cristal·lografia, Mineralogia i Dipòsits Minerals, Fac. Geologia, Universitat de Barcelona (UB).
[2] Grup d'Hidrologia Subterrània UPC-CSIC, Departament d'Enginyeria Civil i Ambiental, Universitat Politècnica de Catalunya, Jordi Girona, 1-3, 08034 Barcelona, Spain
[3] Grup Geologia Econòmica, Ambiental i Hidrologia, Dep. Geoquímica, Petrologia i Prospecció Geològica, Fac. Geologia, Universitat de Barcelona (UB)

INTRODUCCIÓN Y OBJETIVO

Perfil litoestratigráfico del pozo S3. Nivel piezométrico de Marzo 2013.

- Relleno
- Cemento
- Areniscas
- Calizas
- Margas alteradas con areniscas
- Calizas
- Areniscas
- Margas

El emplazamiento de Òdena (Barcelona) está contaminado por compuestos alifáticos clorados, aromáticos y pesticidas debido a infiltraciones de un tanque subterráneo de almacenaje de residuos y de una balsa de una antigua fábrica de productos fitosanitarios y textiles (1978-1985).

CARACTERÍSTICAS ACUÍFERO:
- Acuífero fracturado no confinado.
- Constituido por una serie sedimentaria Eocena de calizas, margas con intercalaciones de areniscas y microconglomerados cementados.

TAREAS DE REMEDIACIÓN:
- En 2006 se extrajeron 2000 Tm de suelo contaminado .
- Se construyeron dos zanjas de intercepción del agua de recarga para su descontaminación mediante hidrólisis alcalina (Torrentó et al., 2014).
- La monitorización del agua subterránea de este emplazamiento fue mejorada en 2006 con la construcción de 10 piezómetros con múltiples puntos de muestreo que permiten disponer de 220 localizaciones para seguir la evolución y atenuación natural de la contaminación en profundidad (Palau et al., 2014).

OBJETIVO: Caracterizar geológica e hidrogeológicamente el campo experimental para la futura investigación in situ de nuevas técnicas de remediación en episodios de contaminación por DNAPLs

Antigua balsa, actual zanja pequeña

Antiguo tanque de Infiltración, actual zanja grande

Bidones abandonados
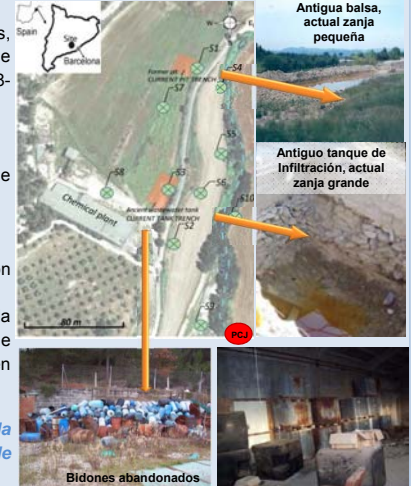
CARACTERIZACIÓN HIDROGEOLÓGICA E HIDROQUÍMICA

Medidas puntuales y globales de la permeabilidad

Ensayo de bombeo (28/11/2013)
Pozo Jorba (PCJ al límite del mapa), al SE de S9. Duración 8h con caudal constante de 1,2 L/s. Medidas de descenso y ascenso del nivel piezométrico en PCJ, S9 y S10.

Interpretación mediante el método de Jacob:
- Transmisividad → 1,4 – 14,9 m²/d
- Coeficiente de almacenamiento → 0,0024 y 0,0009
Dan valor global representativo del acuífero y reflejan la permeabilidad del sistema debido a su fracturación

Ensayos tipos *Slug* (10/12/2013)
En piezómetros S3, S5, S6 y S10.

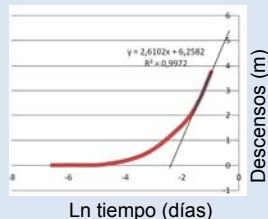- Cálculo de la permeabilidad en torno a los diferentes piezómetros: **10⁻³ y 10⁻⁴ m/d**

Valores muy bajos de permeabilidad que sólo reflejan el valor local del sondeo.

$y = 2,6102x + 6,2582$
$R^2 = 0,9972$

Descensos (m)

Ln tiempo (días)

	ASSAIG BOMBAMENT		ASSAIG RECUP	SLUG
	T (m2/dia)	COEF EMM	T (m2/dia)	K (m/dia)
POU	3,24		1,6	
S3				0,0011
S5				0,0004
S6				0,0001
S9	5,8	0,0024	1,45	
S10	14,91	0,0009	4,8	0,0012

Perfiles verticales de conductividad eléctrica

Se han realizado registros de conductividad eléctrica del agua subterránea (tomadas en descenso y ascenso manual de un *diver*) en distintos sondeos y diferentes épocas del año, antes y después de los ensayo de bombeo (28/11/2013). Se muestran dos a modo de ejemplo:

S9 Conductividad (µS/cm)
cota (masl)
- Datos bajada Dic13
- Datos subida Dic13
- Datos bajada Ene14
- Datos subida ene14
- Datos bajada 04_02_2014

S10 Conductividad (µS/cm)
- Datos subida Dic13
- Datos bajada Dic13
- Datos bajada Ene14
- Datos subida Ene14
- Datos bajada_04_02_2014
- Datos subida_04_02_2014

En general, se observan cambios significativos de conductividad eléctrica del agua subterránea. En algunos pozos se observa un aumento de la conductividad en la zona más superficial (ejemplo pozo S10). Por el contrario, los cambios más importantes se atribuyen a la influencia de los niveles más salinos que conforman la base del acuífero como lo indican los valores del orden de mS/cm detectados en el fondo de los pozos S8 (>5,5), S3 (>7) y S4 (>20), hecho que se empieza a insinuar en el pozo S9, atribuibles a las altas concentraciones de Na y Cl.
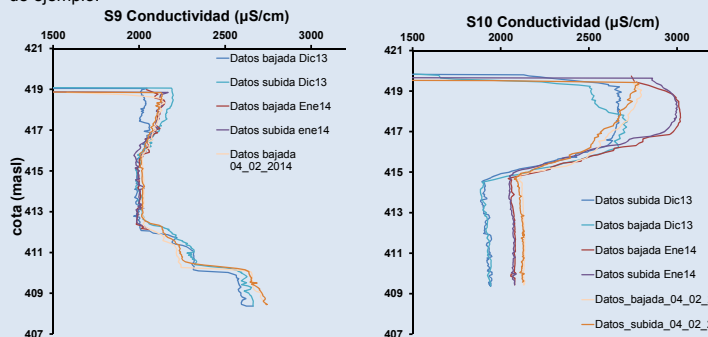
Tomografía eléctrica

Se han realizado un total de 10 perfiles de tomografía en dos periodos de tiempo diferentes (28/04/2014 y 18/12/2014). Han sido comparados con la litología de los sondeos y los perfiles de conductividad y representados en 3D para ver las relaciones de intersecciones entre éstas.
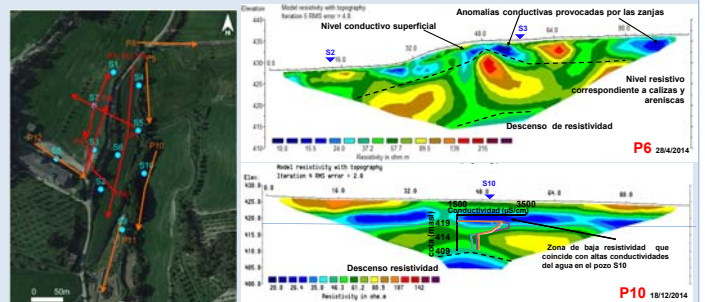
Ubicación de perfiles tomografía. En rojo, los realizados el 28/04/2014 y en naranja los de 18/12/2014. La nomenclatura P indica número perfil y S número pozo.

Anomalías conductivas provocadas por las zanjas
Nivel conductivo superficial
Nivel resistivo correspondiente a calizas y areniscas
Descenso de resistividad
P6 28/4/2014

Zona de baja resistividad que coincide con altas conductividades del agua en el pozo S10
Descenso resistividad
P10 18/12/2014

Perfiles de tomografía de los dos periodos de estudio. En perfil P6 se observan las anomalías causadas por las zanjas de intercepción. En el perfil P10 se ha superpuesto los perfiles de conductividad puntual realizados en diferentes épocas en S10 donde las bajadas de resistividad se corresponden con las subidas de conductividad.

Niveles conductivos de rellenos superficiales
Niveles resistivos de calizas y areniscas

CONCLUSIONES

Se ha estimado la transmisividad hidráulica global del emplazamiento entre 1 y 15 m²/día, con valores puntuales de permeabilidad en los sondeos entre 10⁻³ y 10⁻⁴ m/d. Esta variabilidad se atribuye a un sistema de doble porosidad formado por un medio fisurado de baja permeabilidad y fracturas y/o estratos más permeables que canalizan la mayor parte del flujo.
Los registros de conductividad eléctrica del agua subterránea indican la presencia de estratos con distintas propiedades hidráulicas a escala métrica que puede dar lugar a flujos preferenciales.
Las secciones de tomografía eléctrica han detectado heterogeneidades laterales en la distribución de la resistividad eléctrica del subsuelo que, de forma preliminar, se han atribuido a fracturas y/o cambios de facies a partir de la correlación con las litologías de los sondeos. Por otro lado, las variaciones en profundidad muestran valores relativamente bajos en superficie que se han correlacionado con rellenos antrópicos, y otros de resistividad eléctrica mucho menor, variando según la zona, que coinciden con altos valores de conductividad eléctrica del agua subterránea registrados en distintos pozos a diferentes tiempos. Las secciones de tomografía eléctrica revelan la presencia del efecto de las zanjas y su posible relación con el acuífero.
La caracterización hidrogeológica del emplazamiento permitirá la realización de modelos de flujo y de transporte reactivo que permitan utilizar este emplazamiento como campo experimental para la investigación in situ de nuevas técnicas de remediación de episodios de contaminación por DNAPLs.

BIBLIOGRAFÍA

Palau, J.; Marchesi, M.; Chambon, J.; Aravena, R.; Canals, A.; Binning, P. J.; Bjerg P. L.; Otero, N.; Soler, A. (2014) Multi-isotope (carbon and chlorine) analysis for fingerprinting and site characterization at a fractured bedrock aquifer contaminated by chlorinated ethenes. Science of the Total Environment, 475: 61-70.
Torrentó, C.; Audí-Miró, C.; Bordeleau, G.; Marchesi, M.; Rosell, M.; Otero, N.; Soler, A. (2014) The use of alkaline hydrolysis as a novel strategy for chloroform remediation: the feasibility of using urban construction wastes and evaluation of carbon isotopic fractionation. Environ. Sci. Technol., 2014, 48 (3), pp 1869–1877.

AGRADECIMIENTOS

ASSESSING CHLOROMETHANES ABIOTIC REDUCTIVE DECHLORINATION BY PYRITE AND MAGNETITE AT NEUTRAL AND ALKALINE CONDITIONS

Rodríguez-Fernández D.[1], García-Moliner D.[1], Bagaria-Rovira F.[1], Soler A.[1], Rosell M.[1] & Domènech C.*[1]

[1]Grup de Mineralogia aplicada i Geoquímica de fluids, Departament de Mineralogia, Petrologia i Geologia Aplicada, Facultat de Geologia, Universitat de Barcelona (UB), Spain

*Corresponding email: cristina.domenech@ub.edu

INTRODUCTION

Carbon tetrachloride (**CT**) and chloroform (**CF**) degradation was confirmed in Òdena field site (Barcelona, Spain) by:
- Shifts in $\delta^{13}C$ over time in the aquifer under **neutral** iron-reducing conditions (Rodríguez-Fernández et al., 2015).
- Shifts in $\delta^{13}C_{CF}$ under the alkaline conditions (~**pH 12**) generated in recharge water concrete-based interception trenches attributed to alkaline hydrolysis, but not for CT (Torrentó et al., 2014).

OBJECTIVE

To ascertain potential abiotic degradation of CT and CF by **pyrite (Py)** and **magnetite (Mag)** in comparison to **BK (without mineral)** by

Changes in concentration and $\delta^{13}C$ of parental pollutants

FRACTIONATION

'heavier' residual fraction, enriched $\delta^{13}C$ over time

PARENTAL COMPOUND

NEW PRODUCT 'lighter', depleted $\delta^{13}C$ until reaching initial of parental

Production and evolution of by-products

REDUCTIVE DECHLORINATION

REDUCTIVE OR ABIOTIC HYDROLYSIS

Fe(II) on oxide surfaces / Fe(0)

(CT) → (CF) → Dichloromethane (DCM)

Iron sulfides → $HCOO^-$, CO_2, CO, CS_2

(Davis et al., 2003)
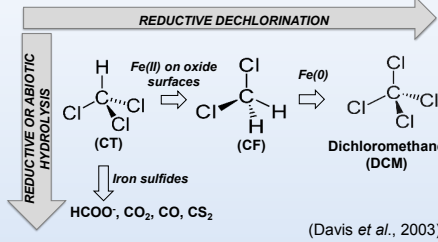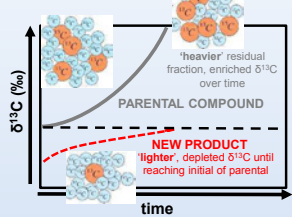
METHODOLOGY

	Py	Mag
Origin	Navajún (Spain)	Cala (Spain)
Treatment	Crushed, sieved (106μm), pretreated & dried	
Impurities	Marl	Rutile
BET area (m²/g)	2.47±0.02	0.699±0.003
Average particle size (μm)	105	32

No headspace — 42 mL

1 g of mineral powder — pH buffered solution — 1mM $FeCl_2$ — 1.3 or 1.4 µL of CT or CF

42 mL — 12 mL 12 mL 12 mL — 4°C stored

	pH7	pH12
CT + $FeCl_2$	BK	BK
	Mag	Mag
	Py	Py
CF + $FeCl_2$	BK	BK
	Mag	Mag
	Py	Py

- pH12 samples were neutralized with acetic acid.
- Volatile organic compounds (VOCs) concentration was measured by **HS-GC-MS**
- $\delta^{13}C$ of VOCs was measured by **HS-SPME-GC-IRMS**
- Remaining volumen was used for **pH** measurements

RESULTS AND DISCUSSION

pH 7

- pH not constant for CT-treatments
- Parental compounds lower than expected & without any clear trend
- Is CF decrease in CF-Py samples significant? Is there any pollutants adsorption process?
- CF and CS_2 production only in CT-Py

All except CT-Py

- No by-products detected
- No significant $\delta^{13}C$ shifts in 21 days
- Neither CT degradation by Mag nor $FeCl_2$
- Neither CF degradation by Mag nor Py or $FeCl_2$
- Mag coating → slow down chloromethanes degradation (Danielsen & Hayes, 2004)

CT-Py

- CF and CS_2 as by-products
- $\delta^{13}C$ shifts of parental CT and by-products from initial (-40‰) Is the reaction limited?
- Both reductive dechlorination and abiotic hydrolysis

pH 12

- pH more constant in CT than in CF-treatments
- Parental compounds concentration decreased
- DCM production in all treatments; CS_2 only in CT-Py

CT-Mag and BK

- CF as by-product
- $\delta^{13}C$ shifts of parental CT (spontaneous reaction?) and of by-product CF
- CT → reductive dechlorination by Mag or by only $FeCl_2$ (BK)
- CF → alkaline hydrolysis
- Mag and dissolved Fe(II) rapidly activated CT degradation in contrast with extremely slow CT alkaline hydrolysis (Jeffers et al., 1989)

- CF and CS_2 as by-products of CT-Py
- Sole CF production in CT-BK
- $\delta^{13}C$ shifts over time of parental CT and both by-products
- CT–Py → Both reductive dechlorination and abiotic hydrolysis
- Daughter CS_2 further degraded reaching more enriched $\delta^{13}C$ values than parental CT

All CF

- DCM yield as a by-product
- $\delta^{13}C_{CF}$ shifts over time
- CF degradation → only alkaline hydrolysis as comparable to Torrentó et al., 2014 (dashed line)
- Py might slowed down CF alkaline hydrolysis:

$$FeS_2 + 7/2O_2 + H_2O \leftrightarrow Fe^{2+} + 2SO_4^{2-} + 2H^+ \text{ (pH} \Downarrow)$$

$$Fe^{2+} \leftrightarrow Fe^{3+} + e^-$$

$$Fe^{3+} + 3H_2O \leftrightarrow Fe(OH)_3(aq) + 3H^+ \text{ (pH} \Downarrow)$$

REFERENCES
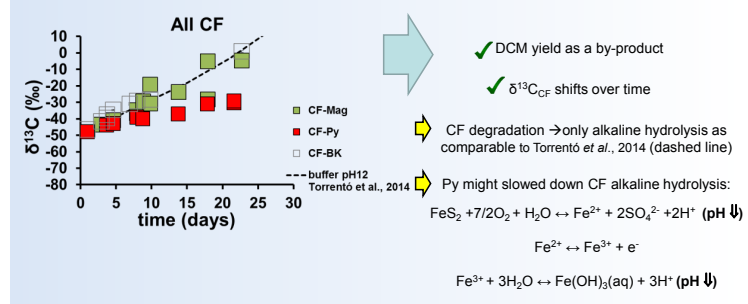
Danielsen et al. (2004): pH dependence of carbon tetrachloride reductive dechlorination by magnetite. Environ. Sci. Technol., 38, 4745-4752.

Davis et al. (2003): Degradation of carbon tetrachloride in a reducing groundwater environment: implications for natural attenuation. Appl. Geochem., 18, 503-525.

Jeffers et al. (1989): Homogeneous hydrolysis rate constants for selected chlorinated methanes, ethanes, ethenes and propanes. Environ. Sci. Technol., 23, 965-969.

Rodríguez-Fernández et al. (2015): C and Cl-CSIA for elucidating chlorinated methanes biotic and abiotic degradation at a polluted bedrock aquifer. Procedia Earth and Planetary Science, 13, 120 -123.

Torrentó et al. (2014): The use of alkaline hydrolysis as a novel strategy for chloroform remediation: feasibility of using urban construction wastes and evaluation of carbon isotopic fractionation. Environ. Sci. Technol., 48, 1869-1877.

ACKNOWLEDGEMENTS

Hydrogeological and Geophysical Characterization of Fractured Aquifer of Òdena (Barcelona, Catalunya)

M. Himi* (University of Barcelona), D. Rodríguez-fernández (University of Barcelona), A. Folch (Polytechnical University of Catalonia), C. Domènech (University of Barcelona), M. Rosell (University of Barcelona), N. Otero (University of Barcelona), (University of Barcelona), R. Lovera (University of Barcelona), J. Palau (University of Barcelona), D. Fernàndez-Garcia (University of Barcelona), A. Casas (University of Barcelona), L. Rivero (Universitu of Barcelona), A. Soler (University of Barcelona)

Summary

The results of the geophysical survey reflects the presence of heterogeneity distribution of electrical resistivity values. This allowed to delimit the geometry of the three layers, as indicated by borehole logging. At the same time, it has been possible to highlight several zones with low electrical resistivity values in the central part of some profiles. These have been considered as fractured areas. In many cases, these areas of low resistivity fractures coincide with areas where the wells have registered low values of the electrical conductivity. This fact reveals the effect as preferential flow areas that have these fractures throughout the circulation system of the contaminant.

Introduction

The identification of subsurface organic pollution, particularly by Dense Nonaqueous Phase Liquids (DNAPL) is one of the highest priorities and among the most difficult for remediation of many sites. DNAPLs are of concern at dissolved concentrations which are orders of magnitude lower than their solubility; they can migrate many metres vertically in soils within hours or days; they form pools at horizontal porosity and permeability boundaries; their migration is little affected by ground water flow or gradients, and there is no practical in situ method currently available to quantify DNAPL saturation. (Cardarelli and Di Filippo, 2009).

The physical, chemical and biological properties of DNAPLs render them difficult to detect and remediate, and lead to a high risk per unit mass. Separate-phase DNAPL is thought to be distributed in discontinuous stringers and globules and perhaps rarely in lenses or pools that are difficult to target by drilling alone.

Geophysical methods can be used for a variety of purposes in DNAPL investigations and remediation such as: Geological characterization, (lithology and thicknesses of strata, preferential flow pathways); Aquifer characterization (water table, water quality); Contaminant plume delineation when a dissolved DNAPL chemical is mixed with other contaminants with properties that can be distinguished by the geophysical method (e.g., conductive landfill leachate).

Over the years, ERT has become increasingly popular for monitoring a wide range of dynamic subsurface processes, including landfill leachate migration, groundwater flow patterns, salt-water intrusion, transport of saline tracers, recharge-induced contaminant plume behaviour, vadose zone water movement.

The main objective of this study is to characterize the state of the fractured aquifer of Ódena due to permeation from an underground waste storage tank (1978-1985).

Geological setting

Our research area is located in the municipality of Ódena, at 50 km NW of Barcelona (Fig. 1). The site exhibits a high complexity due to the presence of multiple sources of pollution related to the industrial activity registered between the years 1978 and 1985.

For the geological and hydrogeological characterization of the studies area, 10 rotational probes between 15 and 18 m depth and with continuous sample extraction were carried out. Two lithological facies can be differentiated (Fig. 1): a lower level formed by an Eocene blue-grey limestone alternating with sandstones and a higher level formed by quaternary deposits and anthropogenic fill with sand and gravel. The aquifer is unconfined and fractured. The water table is located at depths ranging between 3.2 and 11.7 m below ground surface.

Methodology

Resistivity methods have been widely used for obtaining information on discrete fractures and/or fracture density as electrolytic conduction in fractured rock is largely through the fractures (Robinson et al., 2013). Electrical resistivity Tomography (ERT) has also been exploited to monitor amendment treatments (Johnson et al., 2007) and capture indirect evidence of biodegradation.

The ERT surveys were performed in the area using a Syscal Pro 48 resistivity meter (Iris Instruments). A Schlumberger reciprocal configuration was selected. This array is less sensitive to noise than the dipole-dipole array (Dahlin and Zhoo, 2004). Twelve profiles distributed for covering the study area carried out. For achieving the required resolution, the spacing between adjacent electrodes was fixed of 2 m.
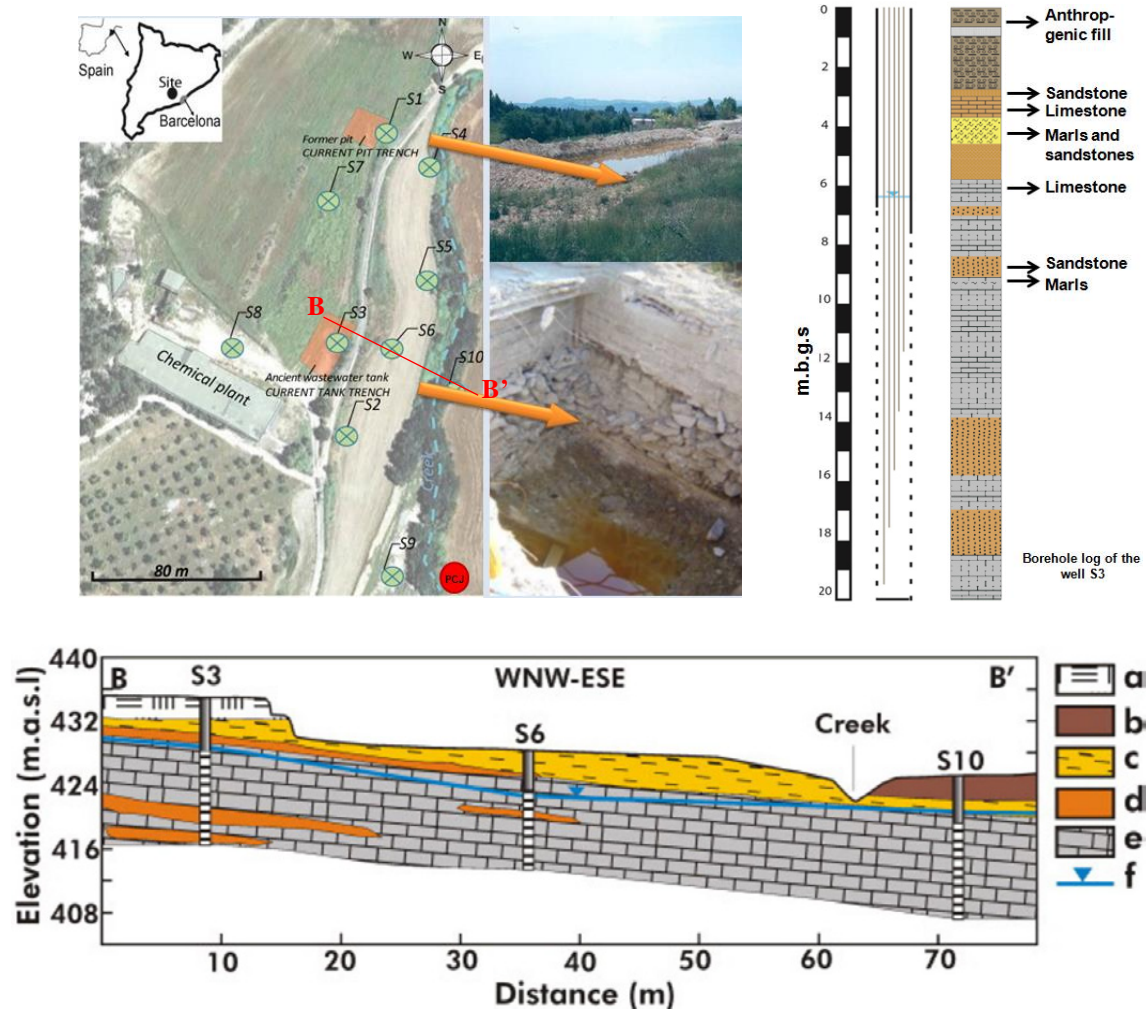
Figure 1 *Location of the study area with the borehole log and a geological cross-section B–B' (a. anthropogenic fill (sand and gravel), b. silt, c. marl, d. sandstone, e. limestone and f. water table). (Palau et al., 2014, modified).*

On the other side, the monitoring of groudwater was improved in 2006 with the construction of 10 wells with multiple sampling points that allow 220 locations to follow the evolution and natural attenuation of the contamination in depth (Palau et al., 2014).

Results

On November 28, 2013, a pumping test was carried out at the well (PCJ) for 8 hours and at a constant flow rate of 1.2 l/s. Water-table measurements were taken of descent and ascent in the same well and at the wells S9 and S10.

The interpretation by the Jacob method gives a transmissivity of between 1.4 and 14.9 m^2/day, while the coefficient of storage varies between $2.4 \cdot 10^{-3}$ and $9 \cdot 10^{-4}$. These results reflect the overall value of a highly fractured aquifer. Slug tests have been also conducted at the wells S3, S5, S6 and S10. The mean permeability varies between 10^{-3} and 10^{-4} m/day, these low values reflect local parameters around the wells.

The electrical conductivity of groundwater registered in the different wells show significant changes (Fig. 2). In some wells, it was observed an increase in the electrical conductivity of the groundwater at the top (well S10). On the contrary, the most important changes were observed in other wells in the deepest part (S3, S4, S8 wells). This effect can be attributed to the influence of high salinity layers (high concentration of Na and Cl) driving along chlorinated solvents (main pollutant in the area).
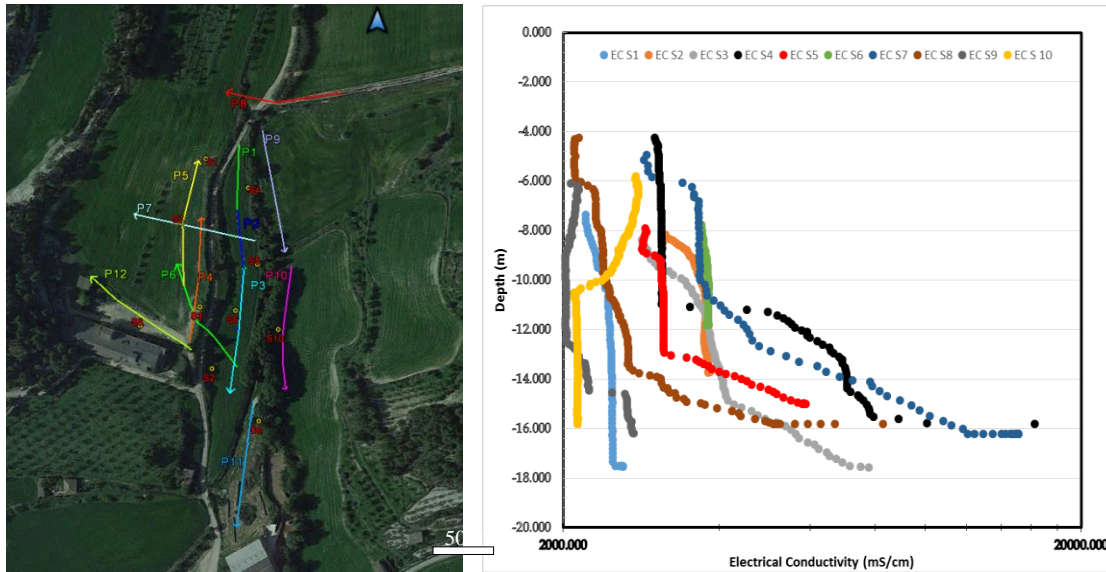
Figure 2 *Location of ERT profiles and the variation groundwater electrical conductivity with depth for the teen wells controlled in the studies area.*

The ERT cross-sections generally show a vertical variation of electrical resistivity values that can be grouped in three layers. (Profile 2): the upper layer with low resistivity values (less than 35 ohm.m), and with a thickness of less than 4 m, and corresponding to Quaternary deposits and anthropogenic fills; the intermediate layer with high resistivity values (more than 140 ohm.m) corresponding to limestone and sandstone and finally the deeper layer with relatively low values (less than 60 ohm.m) that appears in all profiles and correspond to marls.
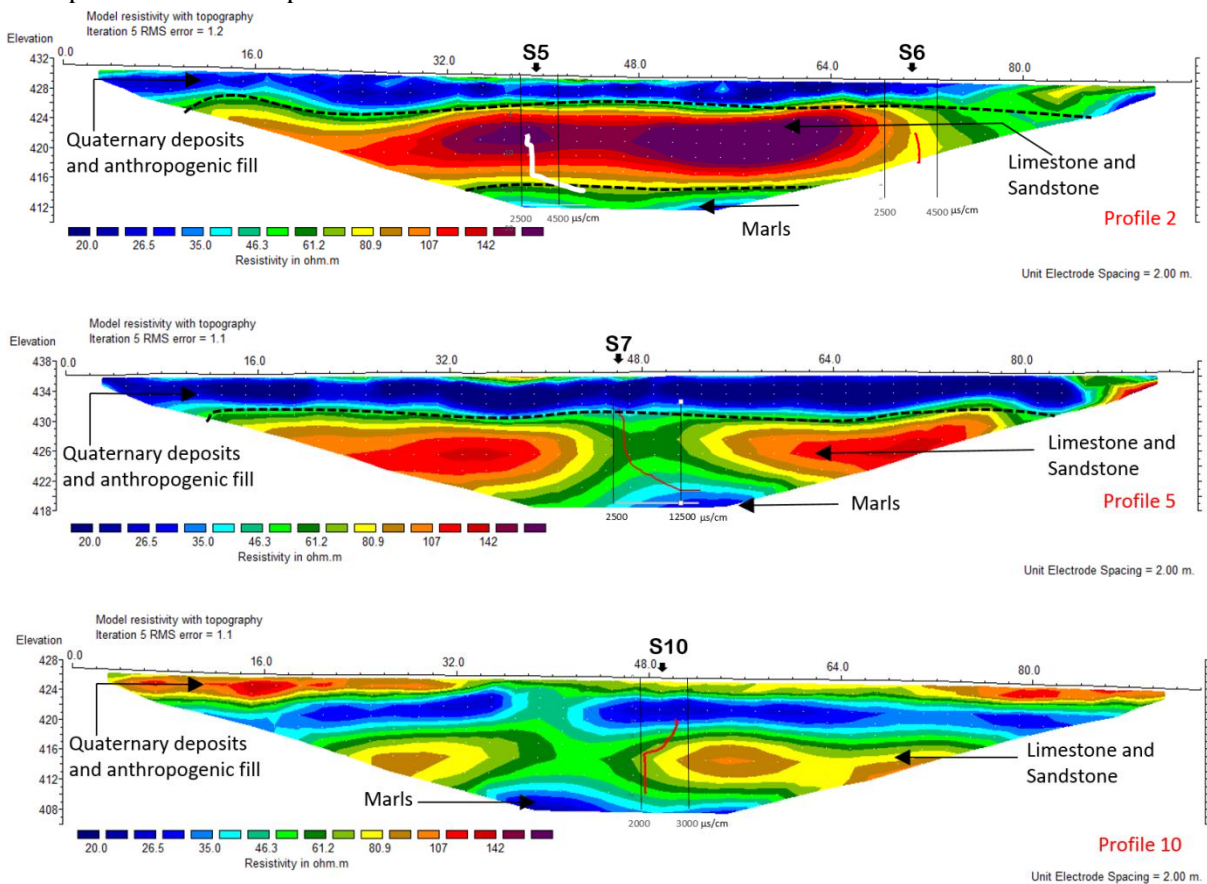
Figure 3 *ERT profiles and the variation of electrical conductivity of groundwater with depth for some wells.*

The electrical conductivities of groundwater recorded in well S6 (profile 2) and well S10 (profile 10), show relatively low values (below 3800 μS/cm) (Fig. 3). Conversely, the electrical conductivities recorded in well S7 (profile 5) show very high values exceeding 12500 μS/cm in the deepest part. The location of well S7 with high electrical conductivity coincides with the area of low resistivity in the intermediate layer. This indicates the presence of fractures in the limestone and sandstone layers which increases the preferential migration of the pollutants.

Conclusion

The estimated hydraulic transmissivity of around the study area ranges between 1 and 15 m^2/day, with punctual values of hydraulic permeability between 10^{-3} and 10^{-4} m/day. This variability is attributed to a system of low porosity, where the flow is mainly through fractures and fissures that control the most of the groundwater dynamics. Some of these fractures can lead to preferential dispersion of pollutants.

The electrical conductivity of groundwater recorded in 10 wells distributed through the area reflect a large variation. In some wells, high conductivity values are recorded at the deepest part of the well, while in other wells the highest electrical resistivity values are logged at the shallow part.

The results of the geophysical survey reflects the presence of heterogeneity distribution of electrical resistivity values. This allowed to delimit the geometry of the three layers, as indicated by borehole logging. At the same time, it has been possible to highlight several zones with low electrical resistivity values in the central part of some profiles. These have been considered as fractured areas. In many cases, these areas of low resistivity fractures coincide with areas where the wells have registered low values of the electrical conductivity. This fact reveals the effect as preferential flow areas that have these fractures throughout the circulation system of the contaminant.

Acknowledgements

References

Cardarelli, E. and Di Filippo, G. [2009] Electrical resistivity and induced polarization tomography in identifying the plume of chlorinated hydrocarbons in sedimentary formation: a case study in Rho (Milan – Italy). *Waste Management & Research*, **27**, 595-602.

Johansson, B., Jones, S., Dahlin, T. and Flyhammar, P. [2007] Comparisons of 2D- and 3D-inverted resistivity data as well as of resistivity- and IP-surveys on a landfill. Extended abstracts near surface 2007. *Proceedings of the 13th European Meeting of Environmental and Engineering Geophysics*. Istanbul.

Dahlin, T. and Zhoo, B. [2004] A numerical comparison of 2D resistivity imaging with 10 electrode arrays. *Geophysical Prospecting*, **52**(5), 379-398.

Palau, J., Marchesi, M., Chambon, J., Aravena, R., Canals, A., Binning, P.J., Bjerg, P.L., Otero, N. and Soler, A. [2014] Multi-isotope (carbon and chlorine) analysis for fingerprinting and site characterization at a fractured bedrock aquifer contaminated by chlorinated ethenes. *Science of the Total Environmen*t, **475**, 61-70.

Robinson, J., Slater, L., Johnson, T. and Binley, A. [2013]. Strategies for characterization of fractured rock using cross-borehole electrical tomography. *The Leading Edge*, **32**(7), 784-790.

Torrentó, C., Audí-Miró, C., Bordeleau, G., Marchesi, M., Rosell, M., Otero, N. and Soler, A. [2014] The use of alkaline hydrolysis as a novel strategy for chloroform remediation: the feasibility of using urban construction wastes and evaluation of carbon isotopic fractionation. *Environ. Sci. Technol.*, **48**(3), 1869–1877.

HYDROGEOLOGICAL AND GEOPHYSICAL CHARACTERIZATION OF FRACTURED AQUIFER OF ÒDENA (BARCELONA, CATALUNYA)

M. Himi[1], D. Rodríguez-Fernández[2], A. Folch[3], C. Domènech[2], M. Rosell[2], N. Otero[2], R. Lovera[1], J. Palau[2], D. Fernàndez-Garcia[2], A. Casas[1], L. Rivero[1], A. Soler[2]

[1] Grup Geologia Econòmica, Ambiental i Hidrologia, Dep. Mineralogia, Petrologia i Geologia Aplicada, Fac. Cie. Ter, Universitat de Barcelona (UB)
[2] Grup Mineralogia Aplicada i Geoquímica de Fluids (MAG), Dep. Mineralogia, Petrologia i Geologia aplicada, Fac. Geologia, Universitat de Barcelona (UB)
[3] Grup d'Hidrologia Subterrània UPC-CSIC, Departament d'Enginyeria Civil i Ambiental, Universitat Politècnica de Catalunya, Jordi Girona, 1-3, 08034 Barcelona

Introduction

The severity of the pollution problem by DNAPL

- Being denser than water, penetrate into the saturated zone.
- Having a very small viscosity, penetrate rapidly into the aquifer (Fig. 1).
- Having a low water / solvent surface tension, they very easily emerge in small fractures.
- Are poorly soluble in water so that the solvent persists for decades in the aquifer but is sufficiently soluble to generate a contamination problem.
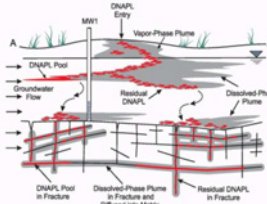- They degrade relatively little, having excessively long lifetimes.

Fig 1. Schematic illustration of contamination associated with a DNAPL release (NSCEP)

Geophysical methods are generally used to better understand the lithology and stratigraphy of a site and map preferential pathways. In rare cases they may be able to detect changes in the physical properties of the soil matrix caused by a DNAPL and steer an intrusive investigation to the area for further investigation.

Especially the electrical resistivity tomography:

- Has been demonstrated in the laboratory to be able to track DNAPL releases through soils.
- Has been used in the field to gage the progress of steam through the subsurface during a DNAPL remediation.
- Has found best use in observing changing conditions in the subsurface, not in locating DNAPLs directly or indirectly.

Geological setting and methodology

Our research area is located in the municipality of Òdena, at 50 km NW of Barcelona (Fig. 2). The site exhibits a high complexity due to the presence of multiple sources of pollution related to the industrial activity registered between the years 1978 and 1985.
For the geological and hydrogeological characterization of the studies area, 10 rotational probes between 15 and 18 m depth and with continuous sample extraction were carried out. Two lithological facies can be differentiated (Fig. 3): a lower level formed by an Eocene blue-grey limestone alternating with sandstones and a higher level formed by quaternary deposits and anthropogenic fill with sand and gravel. The aquifer is unconfined and fractured. The water table is located at depths ranging between 3.2 and 11.7 m below ground surface.

The monitoring of groundwater was improved in 2006 with the construction of 10 wells with multiple sampling points that allow 220 locations to follow the evolution and natural attenuation of the contamination in depth (Palau et al., 2014).
Resistivity methods have been widely used for obtaining information on discrete fractures and/or fracture density as electrolytic conduction in fractured rock is largely through the fractures (Robinson et al., 2013). Electrical resistivity Tomography (ERT) has also been exploited to monitor amendment treatments (Johnson et al., 2007) and capture indirect evidence of biodegradation.
The ERT surveys were performed in the area using a Syscal Pro 48 resistivity meter (Iris Instruments). A Schlumberger reciprocal configuration was selected. This array is less sensitive to noise than the dipole-dipole array (Dahlin and Zhoo, 2004). 12 profiles were carried out (Fig. 3) with a distance between adjacent electrodes of 2 m.

Fig 2. Geological map and location of the study area of Sant Llorenç de Montgai.
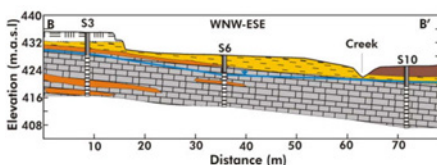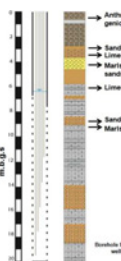

Fig. 3. The area of studies with the borehole log and a geological cross-section B–B' (a. anthropogenic fill (sand and gravel), b. silt, c. marl, d. sandstone, e. limestone and f. water table). (Palau et al., 2014, modified).

Results

Hydrological characterization

- Pumping test was carried out at the PCJ well for 8 hours and with a constant flow rate of 1.2 l/s.
- The measurement were taken of descent and ascent in the same well and at wells S9 and S10.
- Slugs tests were also carried out at wells S3, S5, S6 and S10.

- Transmissivity between 1.4 and 14.9 m²/day,
- Coefficient of storage varies between 2.4 .10⁻³ and 9.10⁻⁴,
- The mean permeability varies between 10⁻³ and 10⁻⁴ m/day.

These results reflect the overall value of a highly fractured aquifer.

The electrical conductivity of groundwater registered in the different wells show significant changes (Fig. 4). In some wells, an increase in conductivity is observed in the more superficial zone (well S10), while in other wells the most important changes are observed in the deep part (wells S3, S4, S8) and attributed to the influence of the saline levels (high concentration of Na and Cl) that accompany the circulation of the Chlorinated solvents (main pollutant in the area).
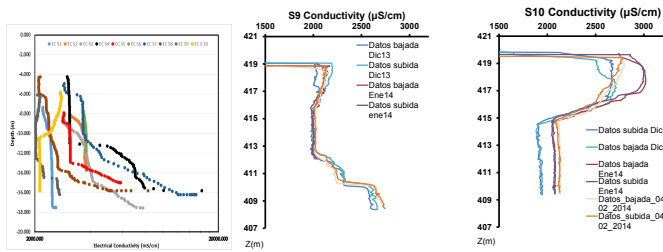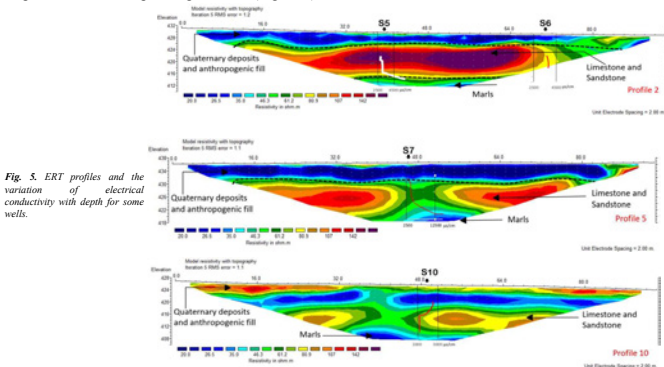

Fig. 4. Variation of electrical conductivity with depth for the teen wells controlled in the studies area

The ERT sections have generally registered a vertical variation of electrical resistivity values that can be grouped in three levels. (Profile 2): the upper level with low resistivity values (less than 35 ohm.m), and with a thickness of less than 4 m, corresponding to Quaternary deposits and anthropogenic fills; the intermediate level with high resistivity values (more than 140 ohm.m) corresponding to limestone and sandstone and finally the deeper level with relatively low values (less than 60 ohm.m) and appearing in all profiles and corresponding to marls (Fig. 5, 6).

Fig. 5. ERT profiles and the variation of electrical conductivity with depth for some wells.

The position of the well S7 with high electrical conductivity coincides with the area of low resistivity in the intermediate layer. This indicates the presence of fractures in the limestone and sandstone layer which favorite the circulation of the contaminated liquids.
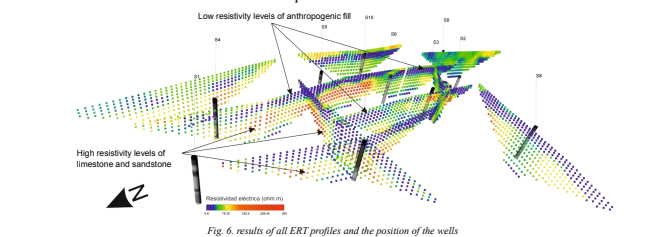

Fig. 6. results of all ERT profiles and the position of the wells

Conclusions

The estimated hydraulic transmissivity of the studies area has been between 1 and 15 m²/day, with punctual values of permeability between 10⁻³ and 10⁻⁴ m/day. This variability is attributed to a system of low porosity, where the circulation is mainly through fractures and fissures that control the most of the underground flow. Some of these fractures can lead to preferential flows of contaminants.

The electrical conductivity values recorder in the 10 wells distributed in the area of studies reflect a large variation. In some wells, high conductivity values are recorded in the deepest part of the well, while in other wells; high values are recorded in the most superficial part.

The ERT survey reflects the presence of heterogeneity distribution of electrical resistivity values. This allowed to delimit the geometry of the three layers, as indicated by borehole logging. At the same time, it has been possible to highlight several zones with low electrical resistivity values in the central part of some profiles. These have been considered as fractured areas. In many cases, these areas of low resistivity fractures coincide with areas where the wells have registered low values of the electrical conductivity. This fact reveals the effect as preferential flow areas that have these fractures throughout the circulation system of the contaminant.

References

Cardarelli, E. & Di Filippo, G. (2009) Electrical resistivity and induced polarization tomography in identifying the plume of chlorinated hydrocarbons in sedimentary formation: a case study in Rho (Milan – Italy). Waste Management & Research, 27: 595-602.
Dahlin, T. and Zhoo, B. [2004] A numerical comparison of 2D resistivity imaging with 10 electrode arrays. Geophysical Prospecting, 52(5), 379-398.
Palau, J.; Marchesi, M.: Chambon, J.: Aravena. R.; Canals, A.; Binning, P. J., Bjerg P. L.; Otero, N.; Soler, A. (2014) Multi-isotope (carbon and chlorine) analysis for fingerprinting and site characterization at a fractured bedrock aquifer contaminated by chlorinated ethenes. Science of the Total Environment, 475: 61-70.
Robinson, J.; Slater, L.; Johnson, T.; & Binley, A. (2013). Strategies for characterization of fractured rock using cross-borehole electrical tomography. The Leading Edge, 32(7), 784-790.
Torrentó, C.; Audi-Miró, C.; Bordeleau, G.; Marchesi, M.; Rosell, M.; Otero, N.; Soler, A. (2014) The use of alkaline hydrolysis as a novel strategy for chloroform remediation: the feasibility of using urban construction wastes and evaluation of carbon isotopic fractionation. Environ. Sci. Technol., 2014, 48 (3), pp 1869–1877.